Parabolic Dish Solar Thermal Power Annual Program Review Proceedings (December 8-10, 1981)

Parabolic Dish Solar Thermal Power Annual Program Review Proceedings (December 8-10, 1981)

ABSTRACT

These proceedings present the papers and a panel discussion given at the Parabolic Dish Solar Thermal Power Annual Program Review held in Atlanta, Georgia, from December 8-10, 1981. It was sponsored by the U.S. Department of Energy (DOE) and conducted by the Jet Propulsion Laboratory.

The primary objective of the review was to present the results of activities of the Parabolic Dish Technology and Applications Development element of DOE's Solar Thermal Energy Systems Program. Twenty-four papers were presented on the subjects of development and testing of concentrators, receivers, and power conversion units; system design and development for engineering experiments; economic analysis and marketing assessment; and advanced development activities. A panel discussion concerning industrial support sector requirements was also held.

ACKNOWLEDGMENT

CONTENTS

INTRODUCTION

The Parabolic Dish Solar Thermal Power Annual Program Review was held in Atlanta, Georgia, December 8-10, 1981. The three-day review was attended by approximately 100 representatives from industry, universities, national laboratories, the U.S. Department of Energy (DOE), and foreign research institutes.

Introductory remarks were made by Charles Stein, member of the technical staff at the Jet Propulsion Laboratory; Gerald Braun, director of the DOE Division of Solar Thermal Technology; and Dr. Vincent Truscello, manager of the Solar Thermal Power Systems Project at JPL.

Thirty papers were presented documenting the development and testing of concentrators, receivers, power conversion units, and system level engineering experiments. Also included were presentations on the development of point-focusing technology in France and Germany, a panel discussion on requirements of the industrial-support sector, and a session on the economic considerations of the parabolic dish program. Tours of the Georgia Institute of Technology Advanced Component Test Facility (ACTF) and the Solar Total Energy Project (STEP) at the Georgia Power Company site in Shenandoah took place on the final day.
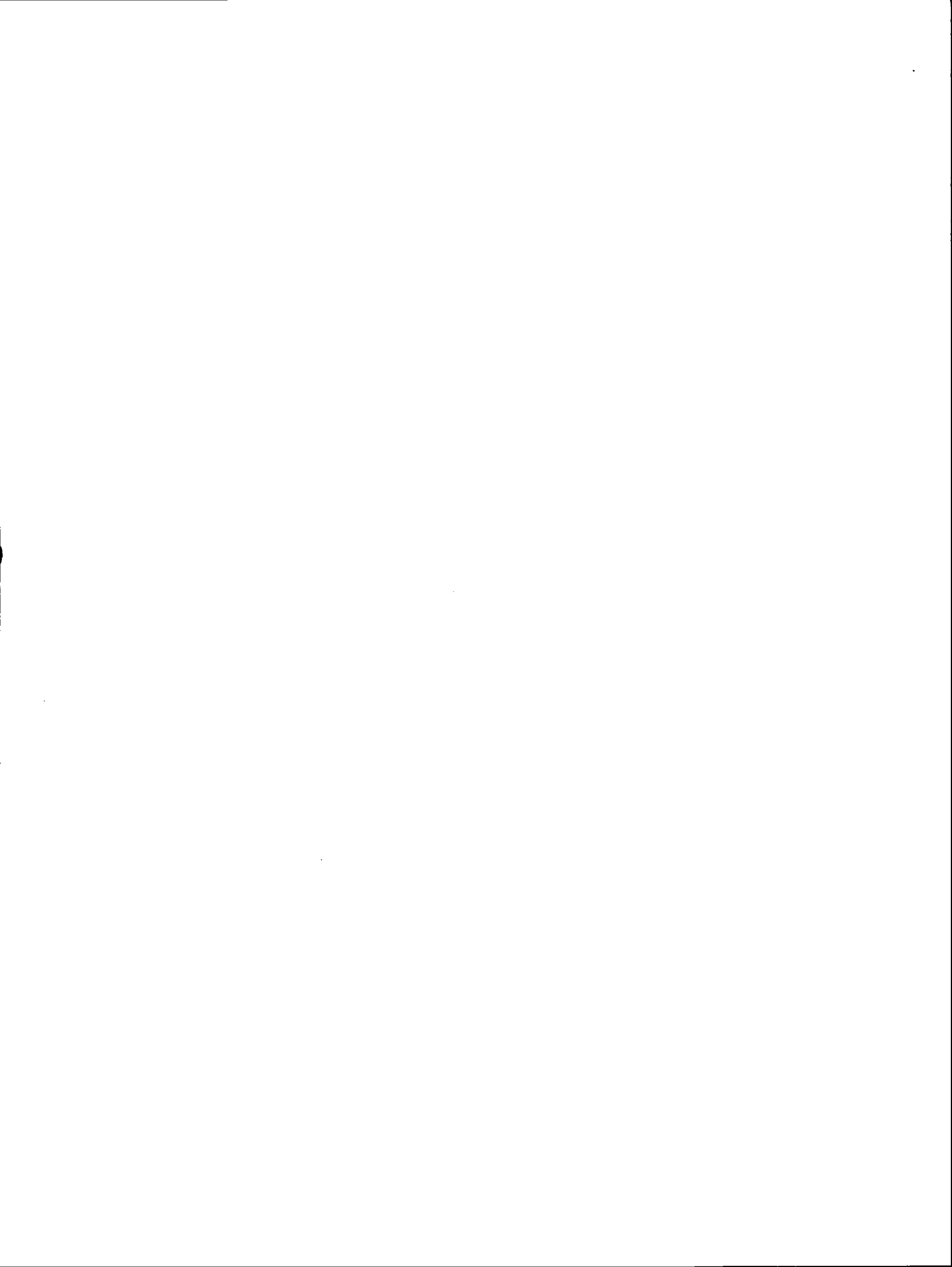
DEVELOPMENT STATUS OF THE PDC-1

PARABOLIC DISH CONCENTRATOR

I. F. Sobczak

R. L. Pons

Ford Aerospace & Communications Corp. (FACC)
Newport Beach, Calif.

T. Thostesen

Jet Propulsion Laboratory
Pasadena, Calif.

ABSTRACT

This paper summarizes the status of development of the 12 m. diameter parabolic
dish concentrator which is planned for use with the Small Community Solar Thermal
Power System under concurrent development by Ford Aerospace for the Jet
Propulsion Laboratory. The PDC-1 unit was designed by the General Electric Co.
and features the use of plastic reflector film bonded to structural plastic gores
supported by front-bracing steel ribs. An elevation-over-azimuth mount arrange-
ment is employed, with a conventional wheel-and-track arrangement; outboard
trunnions permit the dish to be stored in the face down position, with the added
advantage of easy access to the power conversion assembly. The PDC-1 unit will
be fabricated by Ford Aerospace under JPL contract, with JPL providing the
reflective panels and the control/tracking subsystem.

INTRODUCTION

The PDC-1 unit is shown in Figure 1; details of the General Electric design
were reported at previous Parabolic Dish Solar Thermal Power Annual Reviews
(Refs. 1 and 2). The General Electric effort was completed in mid-1981 and the
Aeronutronic Division of Ford Aerospace was subsequently selected by JPL to
fabricate and erect the first PDC-1 unit under an extension to the Small Commu-
nity Solar Experiment (SCSE) Contract. A team of carefully-selected vendors
will carry out the work; Table 1 shows the participating organizations and
their planned activities. A major procurement consists of the reflector
panels to be produced by DE-4 of Lebanon, Ohio under separate contract to JPL.
These panels, including a spare set, will be provided to Ford Aerospace as
GFE along with the sensors and other control equipment to be procured by JPL.
The PDC-1 program was initiated effective 1 December 1981 and is expected to be
completed in approximately twenty-five weeks as shown in Figure 2, the master
schedule. Installation will be at the JPL Parabolic Dish Test Site (PDTS) at
Edwards AFB, California. The activities of each vendor will be coordinated by
Ford Aerospace to assure timely execution of the program. The following para-
graphs summarize the current status of the major procurement elements of the
PDC-1 effort.

CONTROLS

The control system is comprised of a Central Computer (LSI 1123), a manual
control panel, a Concentrator Control Unit (CCU), two motor controllers, a
sun sensor, and two angular position resolvers. A manual control panel and
a CCU are shown in Figure 3. The system is designed for the simultaneous
control of several concentrators. A CCU is mounted on each concentrator and
all CCU's talk to the one Central Computer. Each CCU generates its own
ephemeris data. The CCU responds to commands from the Central Computer and
directs its concentrator to follow the desired action. Commandable actions
are:

> STOW - Go to stow
> COORD 1 & 2 - Go to either of two programmable fixed locations
> OFFSET TRACK -Track the sun offset by programmable azimuth and elevation
> angle offsets
> COARSE TRACK -Track the sun by ephemeris predictions
> FINE TRACK - Track the sun under sun sensor control
> DETRACK - Emergency motion in azimuth and elevation by predetermined
> amounts. Then stop and wait.

During tracking, the CCU monitors the resolver readings and makes a comparison with the ephemeris predictions. Depending upon the magnitude of any error found, the CCU will switch from fine track to coarse track or from coarse track to detrack.

The Central Computer can be commanded from any of three sources: a keyboard terminal, another (system) computer, or a manual control panel. The Parabolic Dish Test Site is an experimental facility and, therefore, a manual control panel is provided for each concentrator. The manual control panel enables inputting commands by pushbuttons. Lights in the pushbuttons indicate the mode under which the concentrator is operating. The manual control panel is also hardwired to the concentrator to allow display of resolver readings and to permit manual control or override of the central computer.

The system is set up so that a detrack can be implemented by the central computer, the CCU, the manual control panel, the system computer, or by any other source required. Detrack overrules all other modes and commands.

Developmental problems involving the JPL supplied central computer and operational system were encountered during the initial system integration tests but have been resolved. The control system for the prototype concentrator is currently at JPL and is being set up in preparation for final operational debugging and test.

PANELS

The reflective surface is an aluminized plastic film (Llumar) laminated to a plastic sheet which is then bonded to a molded fiberglass/balsa/sandwich panel substrate. Thirty-six (36) panels are arranged into three (3) concentric rows and are attached along their radial edges to 12 radial steel ribs. The ribs are located in front of the reflective panels.

Each of the 36 reflection panels is approximately 34 square feet in frontal area. The molding subcontractor, Design Evolution 4 of Lebanon, Ohio, completed fabrication and installation of the molding facility. Figure 4 shows the molding press and two of the three mold transfer tables. The press platten is 7' x 11-1/2' long and is raised by six air bags to provide a clamping force of 180 tons. This is one of the largest resin transfer presses in the United States.

System Resources of Boston, Massachusetts, fabricated tooling masters for each of the three panels. The middle panel master is shown in Figure 5. The master represents the desired panel laying on a curved surface; it has the proper front contour and thickness. DE 4 made a mold from each master. The bottom half of the outer panel mold is shown in Figure 6. The tubing manifold is used to control the mold temperature during cure of the panels. The complete middle panel mold is shown in Figure 7.

Panel substrates are fabricated by loading the mold bottom half with a mat of continuous strand glass fibers, a layer of end grain balsa blocks, and another mat. The mold is then closed and polyester resin flows throughout the cavity, filling the glass fiber mats and all gaps between the balsa blocks. Figure 8 shows all three panel substrates, arranged as a complete gore.

5

The reflective film laminate (Llumar on .060" Plexiglas DR) is bonded to the panel substrate using contact cement. The top layer of a folded separator film is pulled out from between the laminate and substrate and the laminate progressively pressed down onto the substrate, Figure 9. Two pieces of laminate are required to cover a panel. The laminate is protected by a strippable film, shown in Figure 10 being removed from an inner panel. The completed inner and middle first article panels are shown in Figure 11. All three first article panels were then shipped to JPL for optical testing. This completed GE's involvement in the Parabolic Dish Concentrator program.

OPTICAL TESTING

The first article panels were installed in a test fixture, Figure 12, which simulated two radial ribs. The panels were placed on the fixture face down, as is planned in the field installation, the clamp blocks installed along the radial edges of the panels, and the fixture inverted to the face-up orientation shown. The mating surface of the rib is simulated by a precision cut edge of a 1/2" plywood sheet. The plywood is bolted to an aluminum tubing truss.

The optical tests were performed in the JPL 25' diameter space simulator facility, Figure 13, using a single zenon arc lamp which acts as a 1 mr diameter source at 1400' distance. The reflected beam focused a few feet below the pulley wheels which are illuminated at the top of the chamber doorway.

The optical tests consisted of qualitative and diagnostic procedures. The light pattern at the focal plane was photographed for each individual panel and for all three combined. Figure 14 shows the pattern for a full gore. The concentrated light beam at the focal plane was also scanned using a photocell flux mapping device, yielding the data shown in Figure 15, the % intercepted versus the aperture diameter. Finally, a diagnostic optical system was set up consisting of a large lens at the panel focal point and a photographic target at the lens focus. Various sized apertures were introduced immediately in front of the lens. Figure 16 shows a pattern produced by a 5.6-inch diameter aperture for the inner panel. All light areas are reflecting light into the aperture while the dark areas have slope errors large enough to reflect light outside of the aperture.

The panels are considered adequate for Organic Rankine although the optical test did not simulate wind or gravity deflections when looking at the horizon. However, stiffening the middle and outer panels to reduce deflections appears to be beneficial. In addition, the method of bonding the laminate to the substrate using contact cement is being reviewed as it is suspected that adhesive thickness variations may be a major contributor to the observed slope errors.

REFERENCES

1. Zimmerman, J. J., 1st Generation Low Cost Point Focus Solar Concentrator, Pages 63-67, DOE/JPL 1060-33 (Proceedings of First Semi-Annual Distributed Receivers Systems Review - Lubbock, Texas, January 22-24, 1980).

2. Zimmerman, J. J., General Electric Point Focus Solar Concentrator Status, Pages 143-147, DOE/JPL 1060-46, (Parabolic Dish Solar Thermal Power Annual Program Review Proceedings - Pasadena, California, January 13-15, 1981).
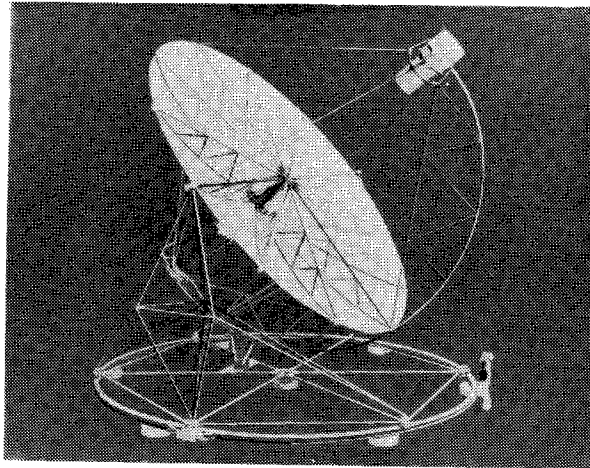
FIG. 1   PLASTIC/FILM PARABOLIC
         DISH CONCENTRATOR

TABLE 1 PDC-1 VENDOR ORGANIZATIONS

**Ford Aerospace &
Communications Corporation
Aeronutronic Division**
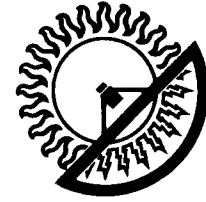
VENDOR	TASK
ALCO MACHINE CO., INC.	FAB COMPLETE STRUCTURE, FIXTURES AND SPARE RIBS, TRIAL ASSEMBLY, MATCH MARK, PAINT, CRATE AND SHIP
JAMES W. PRICE & ASSOCIATES	PROVIDE ARCHITECTURAL SUPPORT AND SUPERVISION OF FOUNDATION CONTRACTOR
ASHLAND CONSTRUCTION CO.	SITE PREPARATION, FOUNDATION AND RAIL INSTALLATION
VALLEY IRON	ERECTION, CABLING AND PAINT TOUCH-UP
RELIANCE ELECTRIC	PROVIDE MOTORS, CONTROLLERS AND ASSOCIATED HARDWARE
DESIGN EVOLUTION 4, INC.	PROVIDES REFLECTIVE PANELS TO JPL

*JPL WILL PROVIDE THE SUN SENSOR, RESOLVERS, CCU, LSI COMPUTER AND ASSOCIATED EQUIPMENT.

FIGURE 2. PDC-1 FABRICATION/INSTALLATION SCHEDULE

Ford

Ford Aerospace &
Communications Corporation
Aeronutronic Division

FIGURE 2. PDC-1 FABRICATION/INSTALLATION SCHEDULE

TASKS

1981 — D: 1 2 3 4 5 | J: 6 7 8 9 10 | 1982 — F: 11 12 13 14 | M: 15 16 17 18 | A: 19 20 21 22 | M: 23 24 25 26 27

STRUCTURE
- REVIEW DRWGS.
- FAB RAIL
- FAB STRUCTURE (RIBS)
- PANEL FIT CHECK
- SHOP ERECTION

FOUNDATION
- PREPARE SITE
- INSTALL PIERS
- INSTALL RAIL

ERECTION & CHECK-OUT
- RECEIVER COMPONENTS
- ERECT PDC-1
- VISUAL INSPECTION
- FUNCTIONAL CHECK

PROGRAM REVIEWS
- PROGRESS MTGS.
- FINAL REPORT

GFE ITEMS
- FINAL DOCUM. PCKG.
- REFLECTIVE PANELS   1st ART.
- POSITION SENSORS
- SUN SENSOR
- CONTROL COMPONENTS
- LSI COMPUTER

6

FIG. 3   MANUAL CONTROL PANEL AND
         CONCENTRATOR CONTROL UNIT
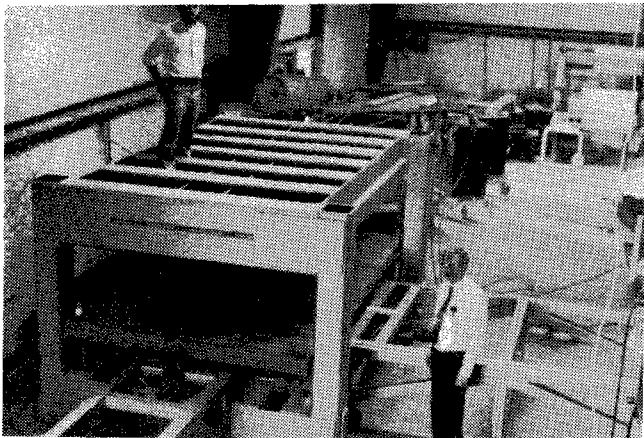
FIG. 4   AIR BAG RESIN TRANSFER
         MOLDING PRESS
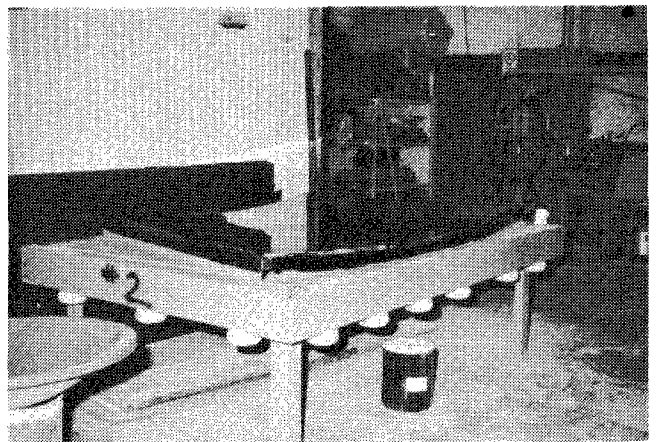
FIG. 5   MIDDLE PANEL TOOLING MASTER
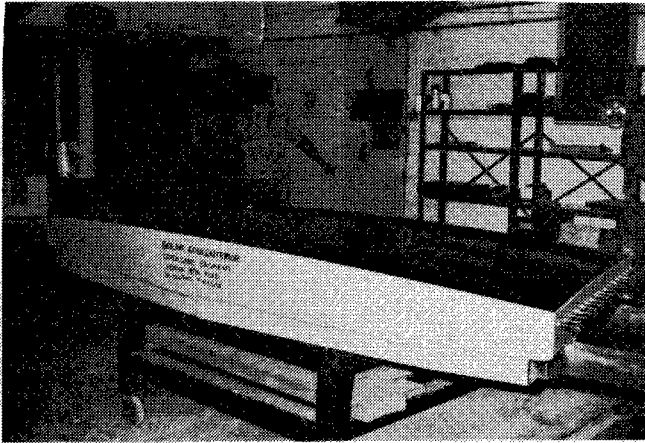
FIG. 6   BOTTOM HALF OF OUTER PANEL
         MOLD
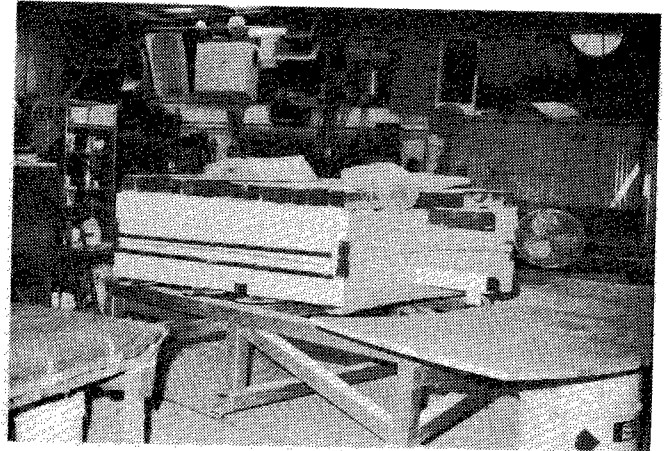
FIG. 7   MIDDLE PANEL MOLD
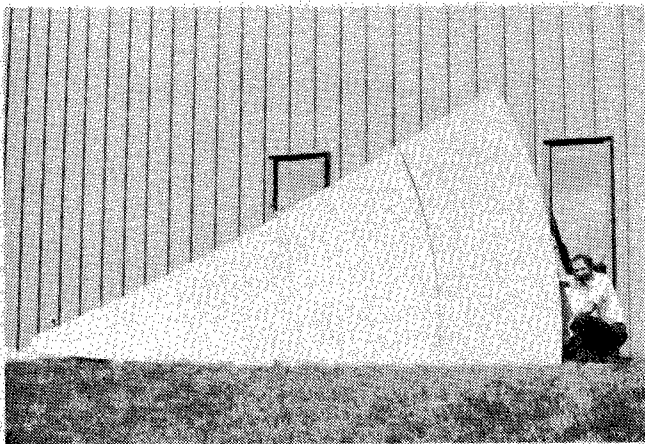
FIG. 8   THREE PANEL SUBSTRATES
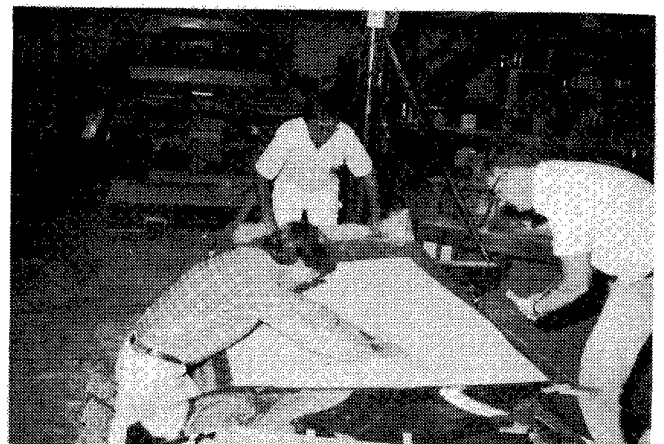
FIG. 9   BONDING REFLECTIVE LAMINATE
         TO OUTER PANEL SUBSTRATE

11
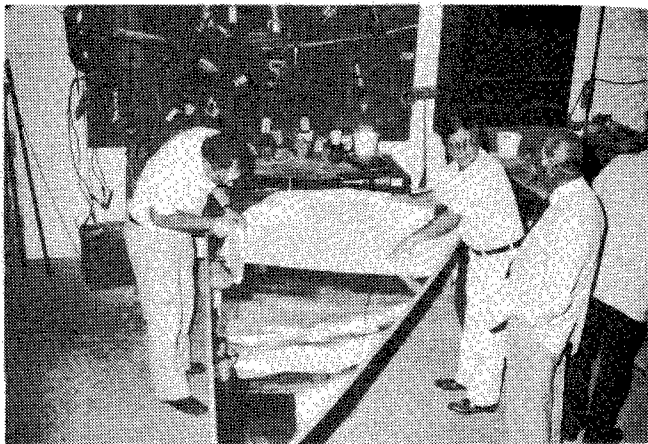
FIG. 10 REMOVING PROTECTIVE FILM
COVERING FROM REFLECTIVE
SURFACE OF INNER PANEL

FIG. 11 INNER AND MIDDLE FIRST
ARTICLE REFLECTIVE PANELS
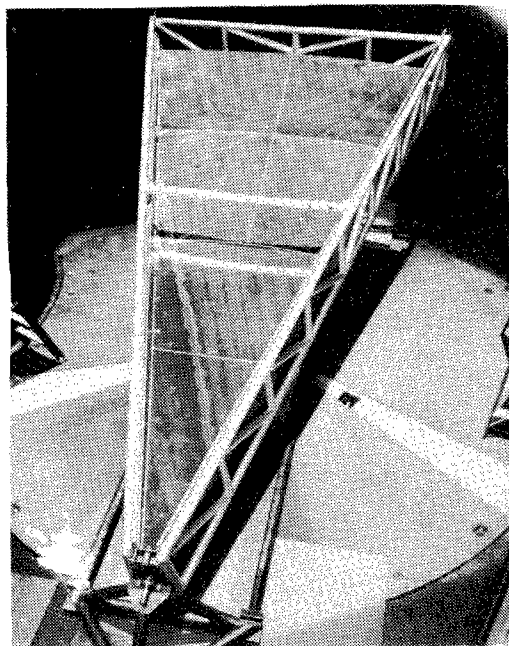
FIG. 12 FIRST ARTICLE PANELS MOUNTED IN
OPTICAL TEST FIXTURE
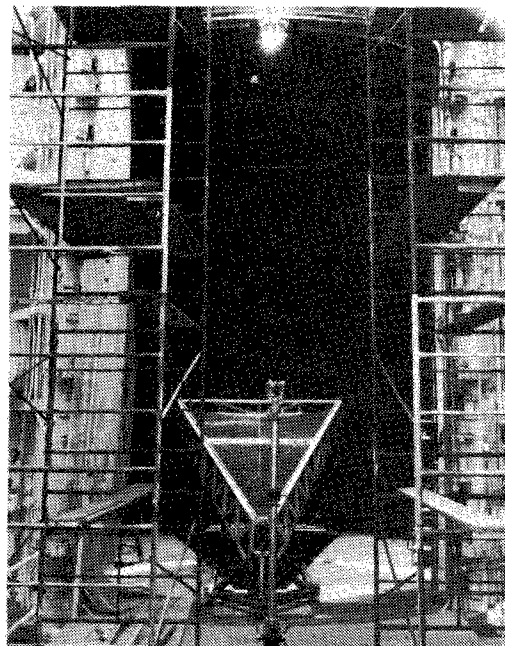
FIG. 13 OPTICAL TEST FIXTURE INSTALLED
IN JPL 25' DIA. SPACE SIMULATOR
FACILITY
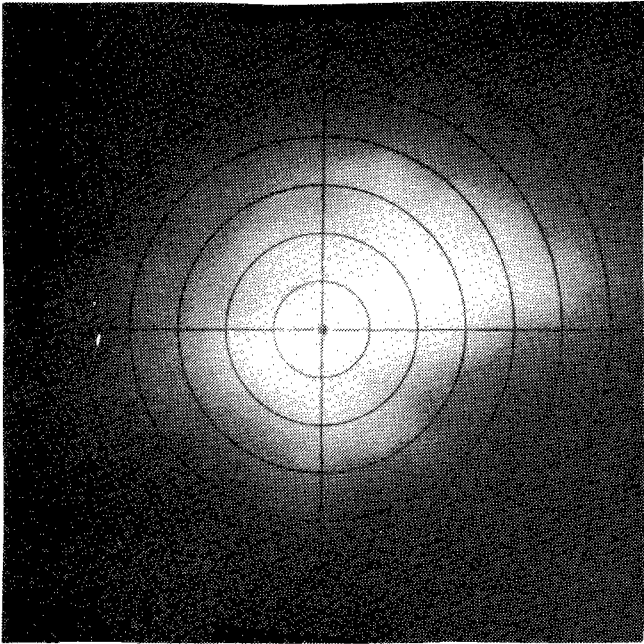
FIG. 14   BEAM PATTERN AT FOCAL PLANE FOR
ONE FULL GORE
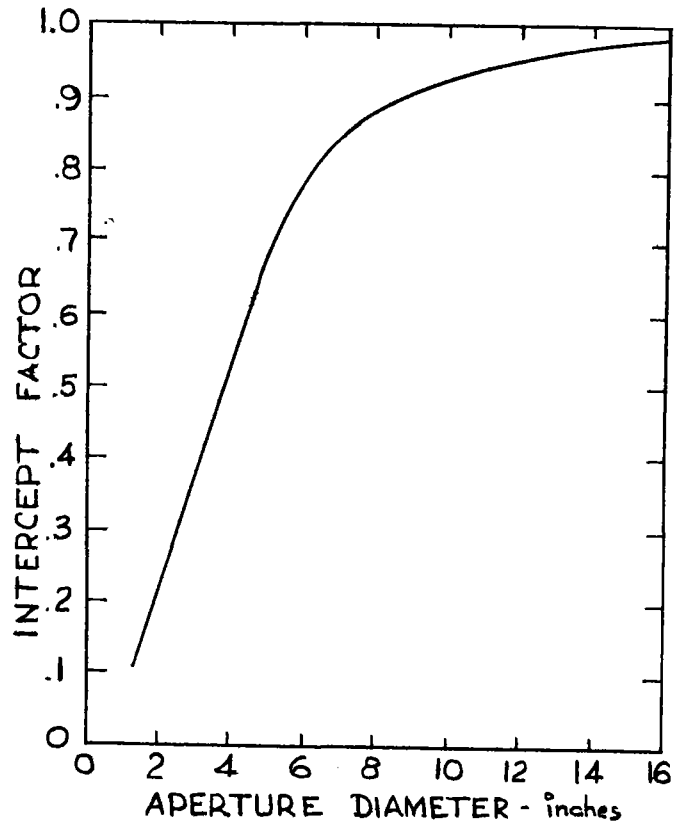
FIG. 15   INTERCEPT FACTOR VS APERTURE
DIAMETER FOR ONE FULL GORE
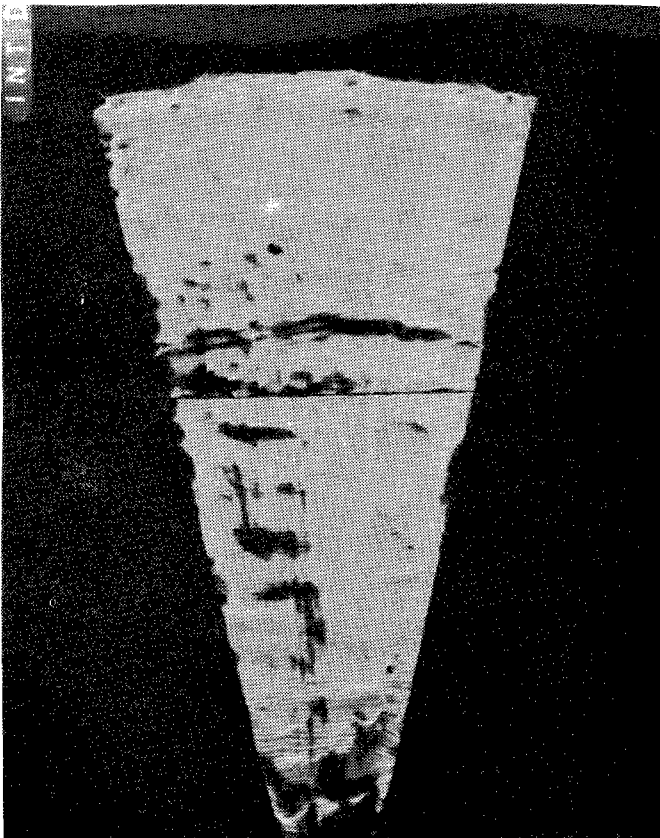
FIG. 16   DIAGNOSTIC PHOTOGRAPH OF INNER
PANEL SHOWING AREAS WHICH PUT
LIGHT THRU A 12" DIA. APERTURE

13

ACUREX PARABOLIC DISH CONCENTRATOR (PDC-2)

P. Overly
R. Bedard
Acurex Corporation
Mountain View, California

ABSTRACT

Acurex Corporation is under contract to the Jet Propulsion Laboratory (JPL) to design, fabricate, install, and test a cost-effective point-focus solar concentrator. The key to concentrator cost effectiveness is proper design of the reflector surface panels. The Low-Cost Concentrator reflective surface design is based on the use of a thin, backsilvered mirror glass reflector bonded to a molded structural plastic substrate. This combination of reflective panel material offers excellent optical performance at low cost. This paper briefly describes the design approach, rationale for the selected configuration, and the development status. Reflective panel development and demonstration results are also presented.

INTRODUCTION

The overall objective of the Low-Cost Concentrator project is to develop and demonstrate a state-of-the-art technology concentrator which is cost-effective in high-volume production and has a 30-year life under wide environmental extremes. The development project is structured into a three-phase effort. Phase I, completed in March 1979, encompassed the concept selection, preliminary design and cost assessment, and demonstration of the mass production reflective panel fabrication approach. The Phase II efforts, which began in September 1980 and were completed in July 1981, included detailed design and analysis and demonstration of the prototype reflective panel fabrication approach. Phase III, which encompasses fabrication, installation, and testing of three prototype concentrators, is scheduled to begin in December 1981 and will provide fully checked-out prototype units at the JPL, Edwards, California Test Site in December 1982.

DETAILED DESIGN SUMMARY

The design of the 11-meter diameter (95-m^2 gross aperture area) Low-Cost Concentrator is shown in Figure 1. The concentrator is a two-axis tracking system designed to interface with a 1,500-lb thermal receiver/power conversion unit package. Predicted performance of the
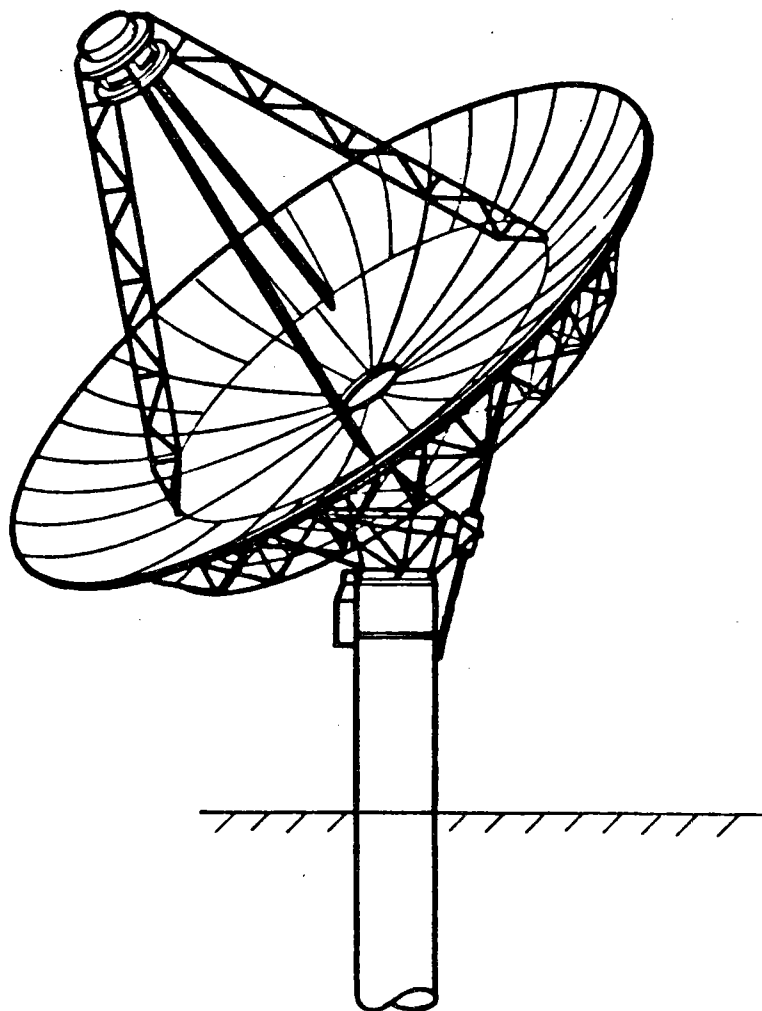
Figure 1. Design Description

concentrator is 63.9 kW through a 0.049-m^2 receiver aperture based on the following design conditions:

- 800 W/m^2 insolation
- 94 percent reflectance (clean mirror)
- 15 mph operating wind

A detailed design weight statement by major subassembly is as follows:

- Reflective panels   3,950 lb
- Support structure   7,000 lb
- Drives   2,050 lb
- Tracker control and electrical   500 lb
- Subtotal   13,500 lb
- Foundation   26,575 lb
- Total   40,075 lb

The major design features of each of the subassemblies of the concentrator are discussed in the following paragraphs. Prototype-specific modifications for the reflective panel subassembly are also presented.

Reflective Panel Subassembly

The reflective panel subassembly consists of inner and outer groups of gore-shaped panels forming a complete but physically discontinuous reflective surface. The subassembly consists of 40 outer and 24 inner panels. The reflective panels are a composite construction of thin (0.028 in.), backsilvered mirror glass with a sheet molding compound (SMC) supporting substrate. A thin glass reflector was chosen because of high performance and long life characteristics. In terms of performance, backsilvered mirror glass provides the highest practical solar hemispherical reflectance (0.94) and has excellent specularity. Glass is highly abrasion-resistant and environmentally durable. The reflective panel substrate is a compression-molded material generically referred to as SMC. SMC is a ready-to-mold polyester resin material with chopped fiberglass reinforcement processed in continuous sheet form. Parts of SMC are typically molded at 300°F and 1,000 psi in 3- to 5-min cycle times. SMC molding is a high-volume production process and offers the potential for low-cost reflective panel substrates. The reflective panel substrate design consists of a thin (0.15 in.) face sheet with an integrally molded rib structure. The glass mirror is bonded to the SMC substrate.

Two-foot square compression-molded SMC-mirror glass panels were fabricated and tested in the Phase I effort. Compliance with the requirements of the Low-Cost Concentrator were successfully demonstrated.

Support Structure Subassemblies

The three support structure subassemblies are:

- Panel support structure
- Receiver support structure
- Intermediate support structure

The lightweight space frame subassemblies feature welded-steel shop subassembly construction using standard size, commercially available steel tubing. Finite element analysis techniques were used to optimize the support structure for minimum weight.

Foundation and Drive Subassemblies

The foundation design features simple installation and adaptability to sloping or rough terrains. The foundation consists of a single steel pipe pedestal which is set in a cast-in-place, reinforced concrete pier. At the top of the pedestal is an azimuth turret mount. The single pedestal foundation was selected to minimize site preparation and foundation installation labor costs. Electric motor power units were selected for both the azimuth and elevation drive systems. The azimuth system uses a pinion/bullgear drive and the elevation system uses a ballscrew actuator/linear jack drive. All drive system components are commercially available items.

Tracking and Control System

A hybrid, two-axis, sun-tracking control system based on microprocessor technology, has been selected. Coarse synthetic tracking is achieved through a microcomputer-based control system to calculate sun position for transient periods of cloud cover as well as sundown and sunrise positioning. Accurate active tracking is achieved by two-axis optical sensors.

Reflective Panel Prototype Modifications

Prototype-specific modifications to the mass producible reflective panel design were made to reduce prototyping cost. The most significant modification is in the area of the compression-molded SMC substrate. The cost of a full-size mold is prohibitive for prototyping purposes. Prototype panels are fabricated by hand lay-up of glass-reinforced polyester (GRP) on a contoured epoxy tool. The panel face sheet is fabricated on this tool in a similar manner as boat hulls. The ribs are cut from GRP sheet stock, assembled, and bonded to the face sheet. The mirror glass is then bonded to the assembled substrate.

Prototype Reflective Panel Development and Demonstration

Subsize (24 by 48 in., rectangular) and full-size (33 in. max width by 91 in., gore-shaped) prototype engineering evaluation panels were fabricated and tested in the Phase II efforts. Compliance with the requirements has been successfully demonstrated with the one exception of torsional stiffness. A torsional-stiffness design inadequacy has been identified and will require a design-fabrication-testing iteraton to complete the demonstration of the prototype hand lay-up GRP-mirror glass reflective panel.

The primary objectives of the Phase II engineering evaluation panels were to:
- Develop and verify the prototype fabrication techniques
- Evaluate the optical quality, hail impact survivability, and temperature-humidity cycling effects
- Determine structural strength-deflection characteristics

Ten subsize panels and one full-size panel were fabricated.

The substrate face sheets were fabricated using two plies of style 7500 and four plies of style 2454 fiberglass-woven fabric. The resin was Polylite® 33-402 room-temperature polyester resin. The face sheet was laid up on an epoxy female tool cast from a male wooden master tool.

Flat stock for rib members was fabricated using four plies of style 2454 cloth and Polylite® 33-402 resin. Ribs were cut from the flat stock using templates and assembled and bonded in an egg-crate fashion using Epon® 828-Versamid® 140 two-part room temperature curing adhesive. The face sheet and rib subassemblies were bonded together using the face sheet tool as the assembly fixture.

Mirror glass was bonded to the completed substrate, again using the face sheet tool as the assembly fixture. The mirror glass was taped face down to the tool, and the volume between the mirror and the tool was evacuated forcing the glass into the desired curvature. After applying a mixture of Epon® 815 and Epon® 828 epoxy, the substrate was placed over the mirror glass and left in place until cured. The attachment pads were then bonded to the substrate, and the reflective panel was edged-sealed and painted.

The engineering unit panels were tested at both JPL and Acurex. A summary of the test results follows:

- Slope Error -- Measured slope error was approximately 1.5 mrad (std. dev.). Note that, due to inadequate torsional stiffness the panel was torsionally distorted. The slope error measurement result was obtained with the panel twisted and held in the best optical orientation (minimum image size).

- Hail Impact Survivability -- Survived six impacts of 3/4-in. diameter ice balls at 66 ft/sec (terminal velocity) with no structural damage observed.

- Temperature-Humidity Cycling -- Withstood 50 freeze-thaw cycles (-20 to +140°F, 0 to 100 percent relative humidity) with no damage or deterioration observed.

- Longitudinal Strength/Bending Stiffness -- Simulated most severe wind loading on panels with no structural damage observed. Structural deflections correlated with analytical predictions.

- Torsional Stiffness -- Torsional deflections did not correlate with analytical predictions. The cause of this problem was traced to a design inadequacy.

In our assessment, the hand lay-up GRP-mirror glass reflective panel concept provides a prototype panel low in cost due to a minimum tooling investment and capable of meeting all concentrator technical requirements. Torsional stiffness of the panel can be upgraded by diagonal rib bracing without significant weight penalty.

KEY RESULTS

The key results of this development project to date are:

- A state-of-the-art point-focus solar concentrator based on SMC-mirror glass reflective panels has been shown to be highly cost-effective in high-volume production

- A prototype of the high-volume production design based on hand lay-up GRP-mirror glass reflective panels has been shown to be cost-effective for producing prototype units

- SMC-mirror glass subsize reflective panels manufactured with the required precision have been demonstrated

- Prototype hand lay-up GRP-mirror glass panels have been demonstrated, with the one exception of torsional stiffness. A design-fabrication-testing iteration is required to complete the prototype demonstration.

The PKI Collector

by

Mark P. Rice
President
Power Kinetics, Inc.
Troy, New York

Introduction

The PKI solar collector system has undergone seven years of
development through construction of six generations of
prototypes to achieve an integrated system optimized for cost
performance tradeoffs, durability, ease of assembly, low
operating costs, maintainability, and safety.

This research and development effort has culminated in the
demonstration of the first production unit under JPL's EE3
experiment at Capitol Concrete Products in Topeka, Kansas, which
has been installed within the last month. It should be noted
that the EE3 experiment included manufacturing and installation
of two PKI collectors, as well as plant level design. System
level design was not included, although naturally improvement of
system design has been an ongoing process.

The experiment and preliminary results are presented
elsewhere in this review by Applied Concepts Corporation
personnel. Consequently, this paper will review system
characteristics, design improvements, and manufacturing
advances.

The PKI collector has three primary subsystems:
concentrator, receiver/fluid loop, and controls. Identical
curved reflective columns are utilized in a faceted Fresnel
design to support 864 one foot square flat inexpensive second-
surface, silvered glass mirrors. The columns are ganged
together and rotated through their centers of gravity to provide
elevation tracking. The concentrator is supported by a
lightweight spaceframe structure (composed of steel tubing
members and steel plate joints), which distributes all wind and
gravity loads to the base supports. The base of the structure
is a track (inverted to eliminate problems of dirt and ice
build-up) which rotates on wheels mounted on concrete piers.
Azimuthal tracking is accomplished by rotation of the entire
structure from east to west throughout the day.

A parallel tube steel heat exchanger is mounted at the
concentrator focal area in a well insulated, galvanized steel
housing. Two rows of vertical close-packed, staggered tubes

connect a mud header and a steam header. Level control switches connected to a solenoid valve in the feed line maintain a water level in the steam header. For this experiment, the system output is 40 pound saturated steam at a peak rate of about 200,000 BTU/hr.

Automatic two axis tracking and operational control is provided with a microprocessor based package. Concentrator-mounted shadowbands are the basis for active tracking. A software program provides azimuthal tracking during cloudy periods so that collection can begin immediately upon reappearance of the sun. The control package also includes a real time clock, digital display, and an integral digital voltmeter.

Design Improvements

One key feature of the PKI collector is its ability to operate in an unattended mode. This is a reflection of the safety features built into the system, microprocessor control, and overall system reliability. Controller initiated shut-down conditions include boiler overtemperature, low feedwater pressure, high winds, user initiated manual stow and controller failure. Collector initiated shut down conditions include AC power loss, low focus, and activation of the low limit switch on the elevation drive. The collector is protected to a reasonable degree from significant damage due to any system malfunction or dangerous environmental condition.

The system components most susceptible to critical failure are the controller, the feedwater supply, and the elevation and azimuth tracking drives. Controller failure initiates automatic stow of the mirrors and system shutdown. The feedwater system incorporates a maximum degree of simplicity. Control via the level switch/solenoid valve approach is external to the microprocessor. Monitoring of key parameters such as feedwater pressure and boiler temperature by the microprocessor provides protection in case of critical fluid loop malfunction. Azimuthal tracking employs a simple, reliable motor driven sprocket/roller chain approach. Because of the Fresnel design for the concentrator, the elevation drive involves more complexity than the azimuthal drive. A single drag link serves half of the mirror assemblies, and each drag link is driven by a single lead screw worm gear drive, both of which are mechanically connected to the elevation drive motor. Through modularity of design and careful quality control in manufacturing and assembly, the elevation drive system provides reliable elevation tracking.

Microprocessor control allows for automatic active tracking via shadowband sensors during sunny periods. Azimuthal tracking during cloudy periods is provided through computer memory. This feature permits the system to begin collection of energy after an extended cloudy period within 10 minutes of detection of a

22

threshold insolation level. An added advantage is the reduction in parasitic losses, since a large motor is not required in order to "catch up" to the sun position. As mentioned previously, fluid loop control is provided independently of the microprocessor. In conclusion, all control functions are automatic and do not require a human operator. Periodic inspection is naturally required to take care of maintenance and to resolve shutdowns.

It should be noted that reliability has been enhanced through recent design modifications which either reduce the number of parts or provide for additional standardization. For example, the fifth generation collector located on the roof of the RPI Science Center utilized four drag link assemblies. The new model utilizes two, thereby cutting in half the number of a majority of the parts incorporated in the elevation drive.

Significant design modifications have been incorporated to enhance ease of installation and maintenance. The space frame supporting structure incorporates platforms allowing safe and easy installation of mirror assemblies and the elevation drive package. The drag link assemblies are located behind the face of the collector, providing ready accessibility from the working platforms. An electric winch permits raising and lowering the boom for servicing the receiver.

Manufacturing Capabilities

One of PKI's primary concerns during the past year has been preparing the collector design and the company personnel for a production level operation. To that end as many components as possible have been designed to be off the shelf or readily manufactured by existing industries during this gearing up period. Figure 1F indicates current manufacturing capacity. The limiting component is in-house production of mirror drive and support assemblies. However, it is now clear that a considerable percentage of the components incorporated into this assembly could be sub-contracted out to reduce PKI's immediate responsibility to assembling those components.

At present PKI maintains over 3000 square feet of assembly and manufacturing space rented from Rensselaer Polytechnic Institute in Troy. PKI is one of about a dozen small high technology companies being nurtured in RPI's "incubator program," which is designed to promote companies which can participate in RPI's new Technology Center (modeled after the likes of Stanford Research Institute). A doubling of factory space is planned for early 1982. In any case we anticipate sales in 1982 of 10 to 100 units, and expect this to provide an opportunity to further gear up.

One primary benefit to PKI from involvement in JPL's EE3 experiment has been the experience gained from the requirement to grow beyond our strengths in research and development.

Manufacturing bottlenecks; quality control requirements; difficulties in installation, operation and maintenance at a distance from the factory; supplier-related problems; and demands for management and organization of production have all been experienced. These learning experiences have established a basis for building a manufacturing capability in-house.

In the initial phases of production, development of quality control systems for ensuring satisfactory performance of sub-contracted manufacturing will take top priority along with continuing to identify the best component suppliers. Only the most critical production elements will be reserved for closely controlled in-house manufacturing. As potential for cost savings warrant or quality control requires, additional manufacturing functions will be absorbed in-house. PKI will continue to provide R&D expertise for design and testing of renewable energy technologies. With these first steps towards a professional production capability, PKI is also carefully preparing itself to be able to meet the anticipated demand for its systems.

Thin Film Concentrator Panel Development

Donald K. Zimmerman
Boeing Engineering and Construction Company

SUMMARY

This study shows that a thin film reflective surface is acceptable for use on solar concentrators, including 816°C (1500°F) applications. In addition, it shows that a formed steel sheet substrate is a good choice for concentrator panels. The concept selected and described here uses a thin reflective film adhesively bonded to the structurally stiffened formed steel sheet substrate to form a concentrator gore. A description of the design, fabrication and evaluation of two test panels is presented. The work was performed under JPL Contract 955804; Dr. Edwin W. Dennison was JPL Technical Manager.

REFLECTOR PANEL CONCEPTUAL DESIGN

The objectives of the contract were to (1) identify candidate design concepts for thin-film reflector panels, (2) screen the panel concepts and (3) select an optimum panel concept for development in subsequent tasks. Table 1 lists the five most promising candidates along with comparative cost and technical data for each. The stiffened steel skin concept was the heaviest concept, but was among the lowest in material cost and bus bar energy cost and offered the lowest manufacturing complexity and technical risk. This concept is shown in Figure 1 and was selected for development.

The gore configuration selected consists of 22 gage (.76 mm) formed steel substrate, stiffened with radial and circumferential stiffeners as shown in Figure 1. The steel sheet is primed with epoxy prior to bonding the acrylic overcoated, aluminized polyester film (3M-YS91A).

CONCENTRATOR CONCEPTUAL DESIGN

The primary emphasis of this program was to identify and develop a low cost thin film concentrator panel. To provide a basis for panel design and evaluation, a representative concentrator was conceptually defined. Figure 2 shows the concentrator concept description and features. The concentrator reflective surface consists of 45 gore shaped panels, 15 inner and 30 outer. The weights of the receiver and concentrator are balanced and the azimuth-elevation drive actuators are located at the center of gravity. The concentrator design allows for inverted stowage for environmental protection. Reflective panel supports are located behind the gores, and the receiver support structure is aligned with the slot in the dish to eliminate blocking of the solar energy.

CONCENTRATOR PERFORMANCE

Computer simulations of the concentrator optics were run using the selected reflector panel design. Experimentally determined values for reflector surface specularity and reflectivity along with dimensional data were used in

the analysis. The simulations provided intercept factor and net energy into the aperture as a function of aperture size for different surface errors and pointing errors.

Figures 3 and 4 are example results of analyses for a 12 meter diameter concentrator with 1000 W/m^2 insolation. Inputs to the analyses included sun shape, hemispherical reflectance and specularity experimentally determined in coupon tests, small scale roughness (orange peel), and a receiver temperature of 816°C (1500°F). Four curves are provided on each plot showing the effects of surface error on performance. Cases with lower receiver temperatures were also analyzed.

The curves suggest that a surface error of 2 mrad or less will be required to capture the desired 80 kW of thermal energy. As the surface errors increase, the net energy rapidly drops off. Analysis results not shown indicate that larger surface errors could be tolerated on lower temperature systems. For example, at 815°C a peak energy of about 82 kW would be achieved with a 2 milliradian surface error, while at 370°C, 82 kW would be achieved with about 7 mrad surface error.

Figure 4 shows that surface errors of 1 mrad would add a few percent to the energy collected, provided the aperture diameter is reduced from .25 m (the optimum for 2 mrad surface error) to 0.175 m. However, the effects of pointing error and structural deflections also should be considered. At a 2 mrad pointing error, the 2 mrad surface error/.25 m aperture drops to 76 kW, but the 1 mrad surface error/.175 m aperture drops even more to 73 kW. Selecting the larger aperture not only permits more surface error but is also less sensitive to other errors. Allowing .5 mrad of the 1.52 mrad budgeted for environmental effects for gravity and temperature deflections, the manufactured panel error budget should be reduced to 1.5 mrad to achieve a 2 mrad total. Variable deflections due to wind loads will further degrade performance. For the average wind speed in the study (about 3 m/s) the equivalent panel surface error will be negligible. At higher wind speeds the concentrator truss deflection will have a significant effect on optical performance. This effect is not shown, but it can be concluded that losses would be lower at larger aperture sizes.

Based on these factors it is concluded that (1) achieving panel optical performance suitable for a Brayton cycle would also meet the needs for lower temperature applications, (2) a budget of 1.5 mrad RMS surface error or less for panel manufacturing tolerances is acceptable, and (3) the aperture diameter should be at least .25 m to reduce sensitivity to other errors.

TEST PANEL FABRICATION

The test panel design shown in Figure 5 represents a section of a full size parabolic gore reflector panel. The same stiffener configuration is used and the spherical radius of curvature closely matches the parabolic curvature midway on the full size panel. The overall dimensions of the test panel match dimensions of the JPL glass/foamglas Test Bed Concentrator panels.

The test panels were fabricated using the techniques and processes resulting from the coupon development work. Square steel sheet blanks were bulge formed

to the desired radius of curvature. The blanks were then cleaned and painted with zinc-rich two part epoxy primer and baked. Stiffener shapes were fabricated by brake forming. The curvatures were formed on a mechanical press and roller blocks. Stiffeners were cleaned and primed by the same method as the substrate blanks. The stiffeners were assembled with close-out tubes into a subassembly by holding the parts on the master tool while installing the fasteners. The stiffener subassembly was then bonded with gap filling epoxy adhesive to the back side of the substrate blank, which was vacuum chucked to its proper contour on the master tool. After curing, the frame side was painted with 2-part polyurethane paint. The reflector side primed surface was lightly sanded in preparation for film application. Film application was by the 3M "wet application" method which involved positioning the film on the wetted surface and squeegying out the trapped water and air bubbles. Figure 6 is a photograph displaying the front and rear sides of the completed test panels.

TEST PROGRAM

Coupon Testing

Coupon tests were performed early in the program to aid the selection of materials and dimensions used in the design and to provide optical data needed in the performance analyses. Table 2 lists the tests, their purposes, and the results.

The selected materials and processes resulted in reflective surfaces exhibiting 85% spectral reflectance and a 1σ specular reflectance of 1.5 mrad. The .76 mm thick substrate survived hailstone impact without damage. Preliminary temperature/humidity tests indicated a potential problem with the 3M YS91A film, which has since been resolved by minor process modifications by 3M.

Panel Testing

The two test panels were subjected to both point source and sun source optical testing. The first test involved the use of a point source and a target collocated in a plane at a distance from the test panel equal to the radius of curvature. The test setup was aligned to project the image formed by the test panel onto the target. An aperture series, lenses, and detector located at the target plane were used to quantify the angular scattering of light rays resulting from panel surface errors. Figure 7 shows the optical equipment and configuration.

The test panel was moved toward and away from the target plane while observing the image size until the smallest diameter was observed. This established the radius of curvature. Next, apertures of 2 mrad through 16 mrad in diameter were successively placed in front of the image at the target plane while the response of a photovoltaic detector was observed and recorded. This process was repeated several times to allow statistical data treatment. The response data were normalized to the full open aperture (16 mrad) and tabulated.

27

Test results for each panel, SN7 and SN10 are plotted on the intercept factor graph shown in Figure 8 for the purpose of comparison with the analytical panel simulation. In this simulation, a one mrad source at infinity, hemispherical reflectance, specularity, and orange peel from coupon tests and zero pointing error were assumed. The solid lines are 1σ surface errors of 1, 2, and 3 mrad. The dashed lines are test data. It is apparent from the graph that the surface error for both panels is between 1 and 2 mrad. Additional analyses estimate the errors to be 1.4 and 1.5 mrad for SN7 and SN10, respectively.

The sun source test was performed as an alternate approach to measuring the image size and distribution and to measure peak fluxes. Figure 9 is a photograph of the outdoor setup, which included a target board, water-cooled radiometer, digital voltmeter readout, and a manually guided test panel support. Not shown in the photograph were a 35 mm camera and an Eppley 5° normal incidence pyrheliometer (NIP).

Measurements were made by aiming the panel at the radiometer and carefully moving the image about until the peak flux was located. The image was then moved horizontally across the radiometer in one inch increments, reading the response at each increment, thereby obtaining an intensity distribution scan. Direct insolation readings were taken with the NIP and 35 mm photos were taken during the same time period.

Data from the radiometer scans and optical densitometer measurements of positive transparencies made from the 35 mm negatives indicated that negligible energy existed outside a 6 inch diameter circle. This is in close agreement with the point source data after accounting for geometry differences between the two experiments. Peak fluxes for the measurements were 101 suns for SN7 and 99.5 suns for SN10. This compares with 103 suns derived analytically from intercept factor curves.

PROGRAM CONCLUSIONS

This study has met its general objective of developing a rigid panel concept that utilizes a thin film reflective surface for application to a low-cost point-focusing solar concentrator. It shows that a thin film reflective surface is acceptable for use on solar concentrators, including 1500°F applications. Additionally, it shows that a formed steel sheet substrate is a good choice for concentrator panels. The panel was shown to have good optical properties, acceptable forming tolerances, environmentally resistant substrate and stiffeners, and adaptability to low to mass production rates. The final estimates for the reflector panel material costs indicate a price of approximately \$16/m^2.

Table 1. Concept Evaluation and Ranking

Concept	Weight lb/m^2	Material cost 4/m^2	Manufacturing complexity +	Technical risk +	BBEC mils/kW$_{th}$-h	= Ranking
Stiffened steel skin	21.3	11.73	Low	Low	3.7	1 (Selected)
Stiffened steel clad plastic core laminate	15.6	12.06	Moderate	Moderate	3.9	2
Stiffened steel clad WFHB core laminate	17.7	11.86	Moderate to high	Moderate	3.8	3
Aluminum clad/ paper honeycomb sandwich	11.8	15.05	High	High	4.8	5
Steel clad/paper honeycomb sandwich	14.9	14.98	High	High	4.8	4
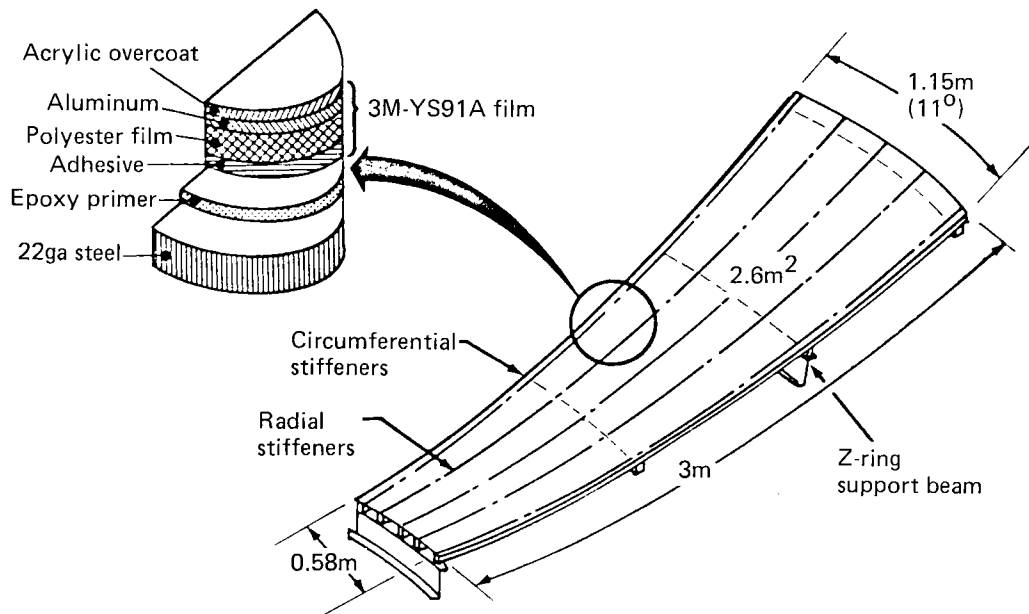
Figure 1. Outer Reflector Gore Concept
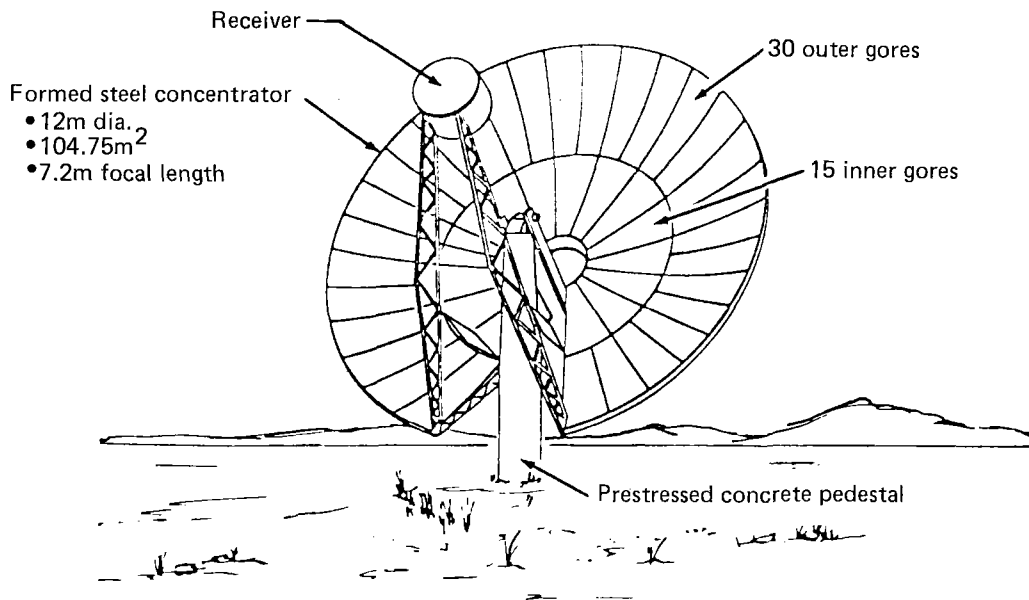
Figure 2. Thin Film Concentrator Conceptual Design

Thin film concentrator
receiver temperature = 815°C (1500°F)
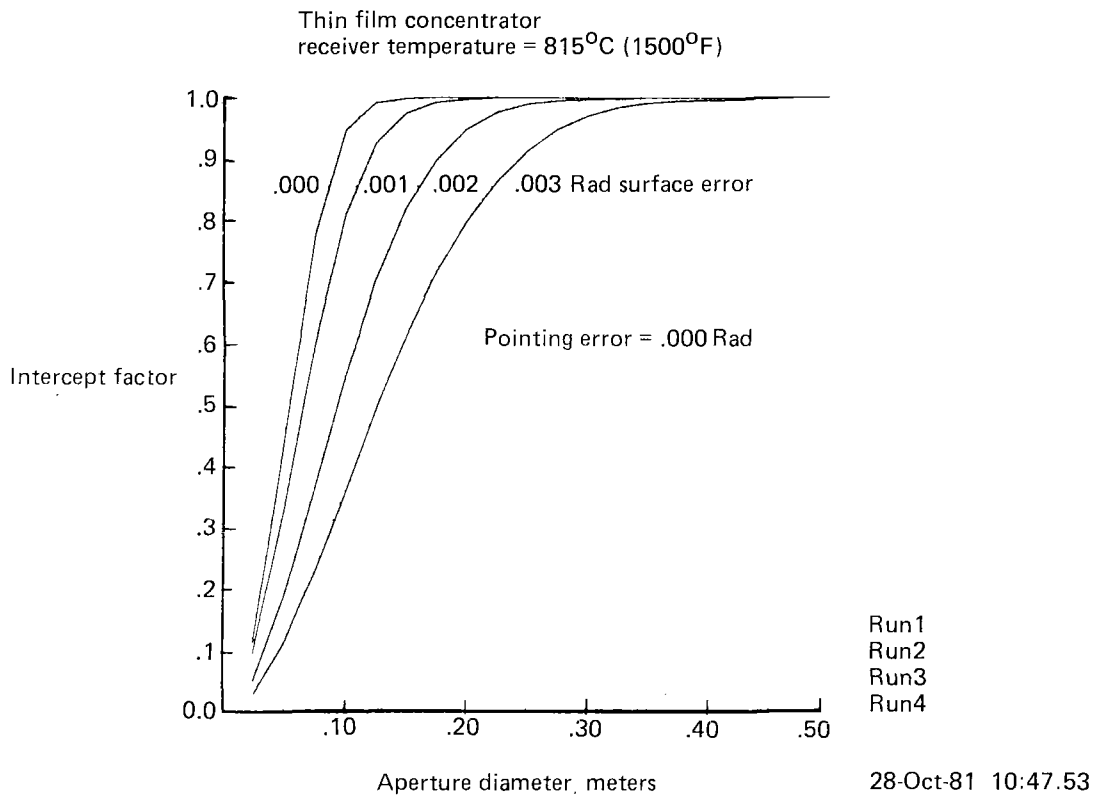
Figure 3. Intercept Factor Curve 815°C (1500°F)
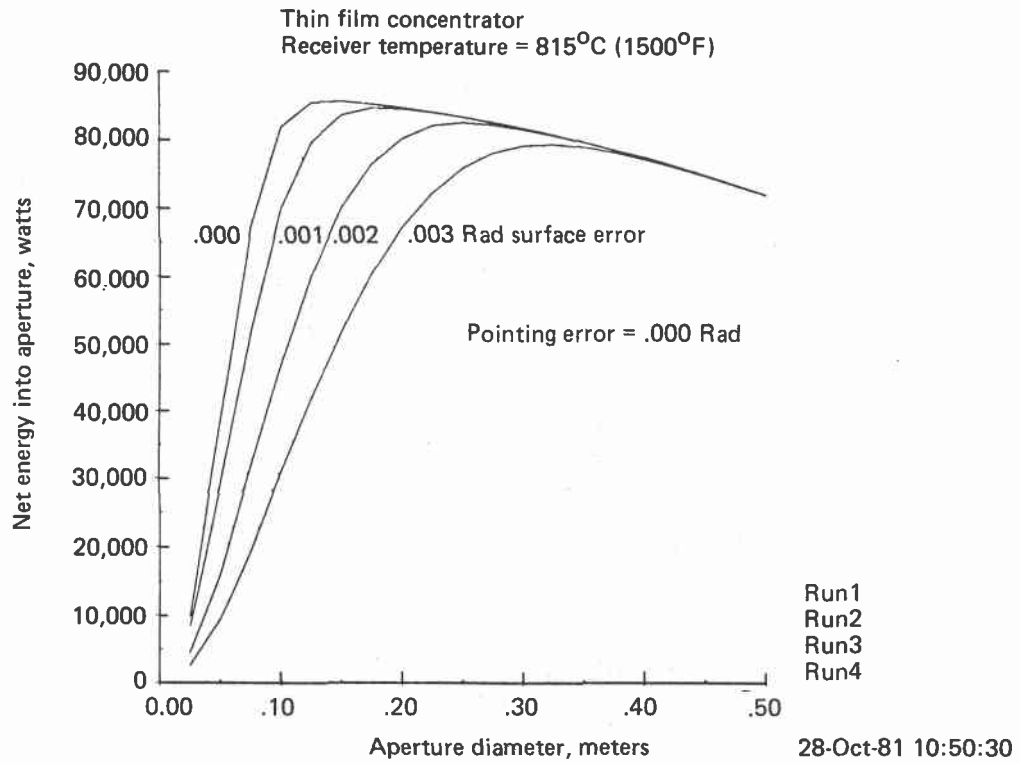
Figure 4. Net Energy Curve 815°C (1500°F)

- Basic components
  - Reflective film
  - Steel sheet 22 gage, ASTM-A620
  - Hat section stiffeners
  - Tube end stiffeners
  - Structural adhesive

- Reflective area
  - 0.4m^2 (4.3 ft^2)

- Assembly weight
  - 11.0 lbs calculated
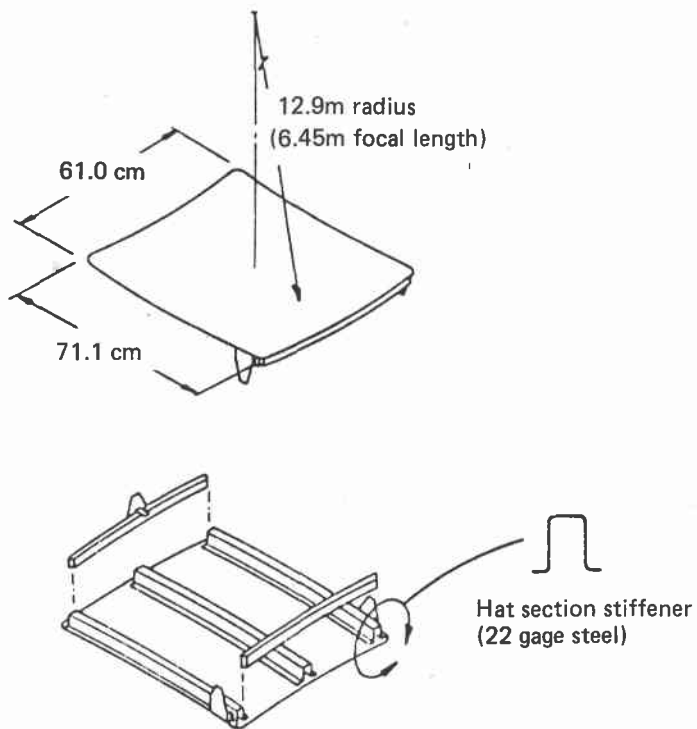
Figure 5. Test Panel

31
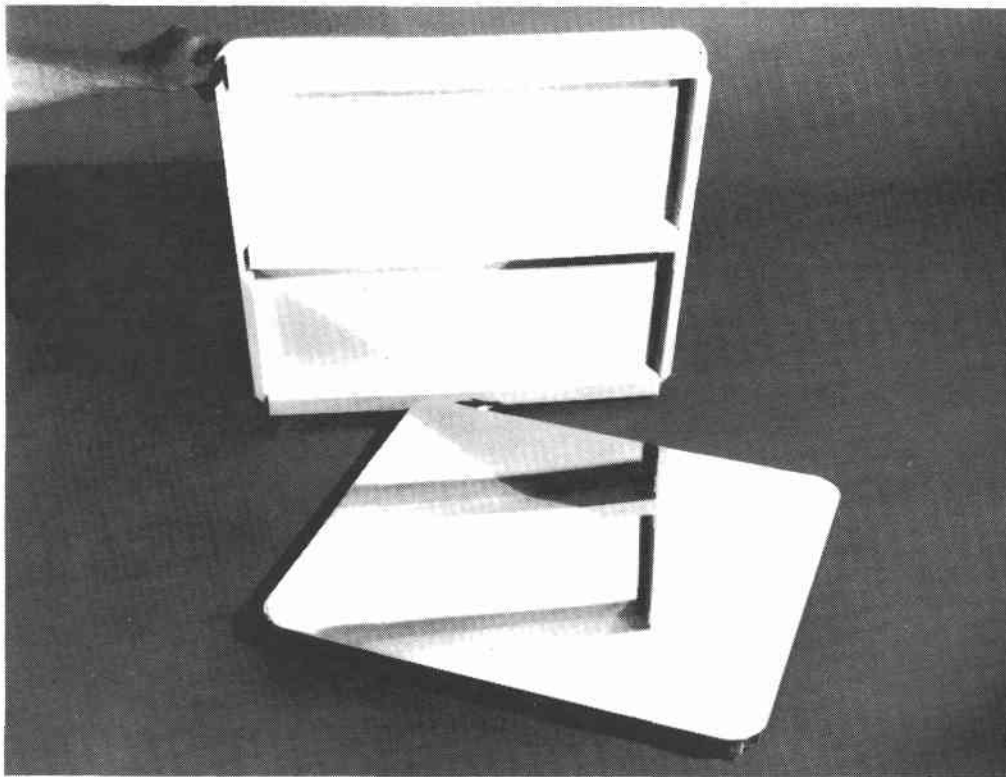
Figure 6. Test Panels S/N 7 and S/N 10

Table 2. Coupon Development Testing

Test	Purpose	Results	
		Initial concept	Preliminary design
Spectral reflectance Air mass 2, 29 mrad)	Coupon screening Optical performance analysis	84%	85%
Specular reflectance (1σ half angle aperture), mrad		1.4 - 1.8	1.5
Reflector figure (1σ area slope error), mrad		.3 - .5	.3 - .4
Substrate surface roughness (RMS - micro-inches)	Substrate design drawings Specifications	29	11
Hailstone impact (1 inch diameter at 70 ft/sec)	Verify substrate thickness	0.03 inch marginal	
	Determine film damage	No film damage	
	Design specifications compliance	Requires assessment	
Temperature extremes Soak at -30°C, +50°C	Determine temperature effects	Surface pebbling at +50°C	

32
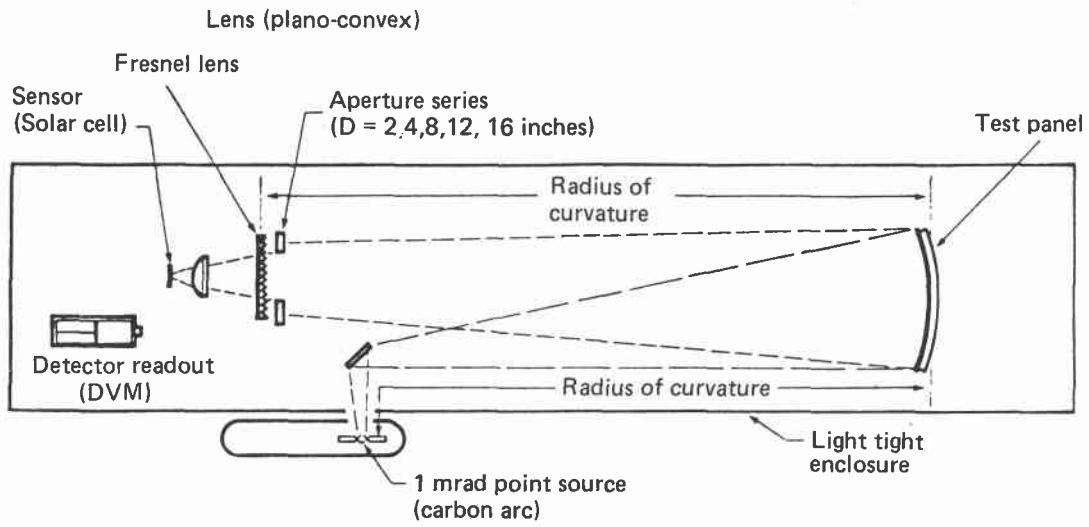
Figure 7. Point Source Panel Evaluation Apparatus
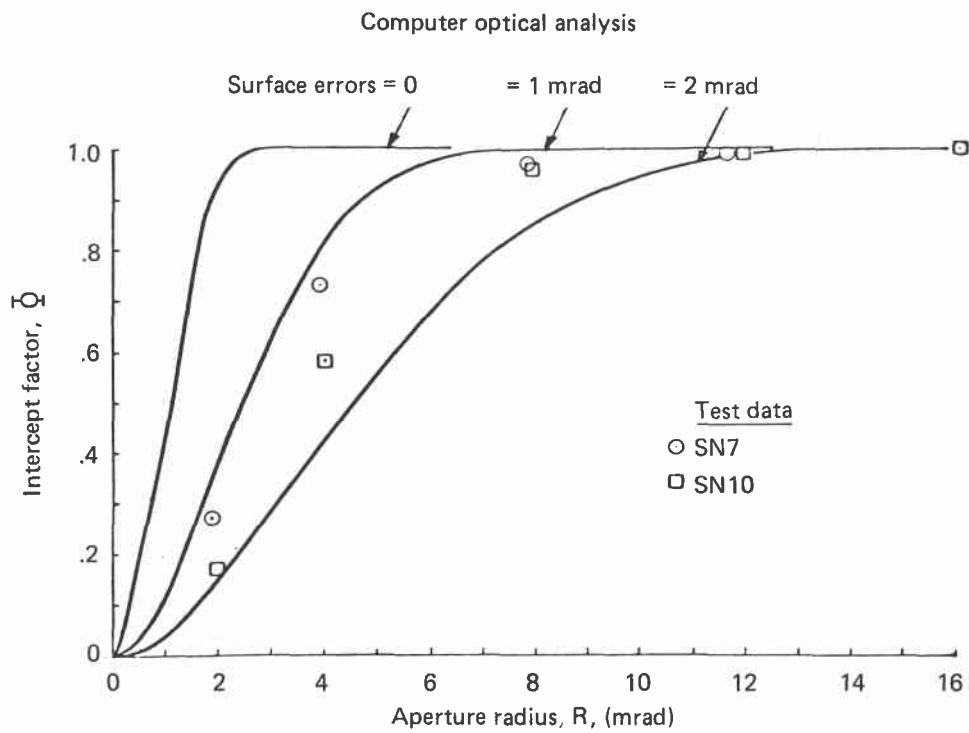
Figure 8. Test Results — Analysis Comparison
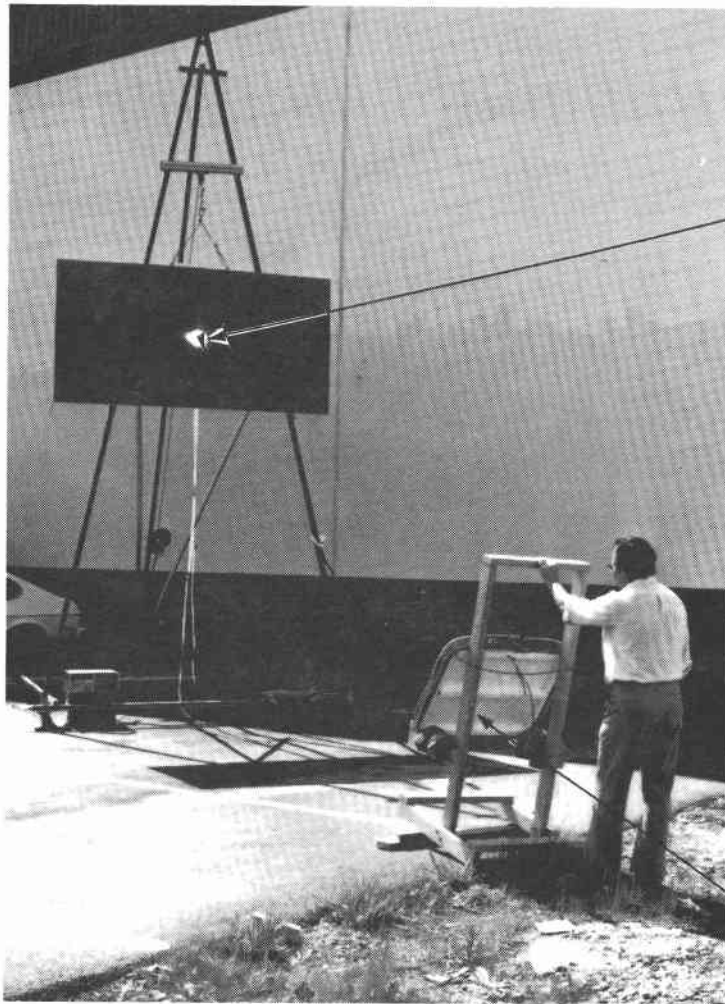
Figure 9. Sunlight Test Apparatus

A Transmittance-Optimized, Point-Focus Fresnel Lens Solar Concentrator

M.J. O'Neill, V.R. Goldberg, D.B. Muzzy

E-Systems, Inc.

Energy Technology Center

P.O. Box 226118

Dallas, Texas 75266

INTRODUCTION

E-Systems is currently developing a point-focus Fresnel lens solar concentrator for high-temperature solar thermal energy system applications. The concentrator utilizes a transmittance-optimized, short-focal-length, dome-shaped refractive Fresnel lens as the optical element. This unique, patented (Ref. 1) concentrator combines both excellent optical performance and a large tolerance for manufacturing, deflection, and tracking errors.

Under Jet Propulsion Laboratory (JPL) funding, E-Systems has completed the conceptual design of an 11-meter diameter concentrator which should provide an overall collector efficiency of about 70% at an 815°C (1500°F) receiver operating temperature and a 1500X geometric concentration ratio (lens aperture area/receiver aperture area).

In the following paragraphs, a review of the Fresnel concentrator development program will be presented, including a description of the concentrator, a summary of its expected performance, results of optical and thermal analyses of the collector, a discussion of manufacturing methods for making the large lens, and an update on the current status and future plans of the development program.

CONCENTRATOR DESCRIPTION

The point-focus lens concentrator is shown in Figure 1 and described in Table 1. The optical element is a convex, dome-shaped, acrylic Fresnel lens. The dome consists of ten conical-segment rings, which are each flat in the radial direction and curved in the circumferential direction. The rim angle of the lens (from optical axis to outermost prism) is 45 degrees. Each of the conical-segment rings is about 61 cm wide, with a smooth outer surface and a prismatic inner surface. The lens is made of uv-stabilized acrylic plastic, about 2.4 mm thick. Steel space-frame structure is

employed for both the basic concentrator and the pedestal. Reinforced concrete is used for the foundation. The tracking system provides full two-axis sun-tracking and inverted (lens-down) stowage. The Fresnel concentrator will be adaptable to a wide variety of receivers currently under development by JPL and others. The air volume between lens and receiver is enclosed with a thin aluminum conical shroud to minimize dirt and moisture accumulation on the inner surface of the lens. A slight pressurization of this air volume may be desirable for dust infiltration prevention. The total concentrator weight is about 13,000 pounds (13 pounds per square foot of aperture).

CONCENTRATOR PERFORMANCE SUMMARY

The point-focus Fresnel concentrator performance is summarized in Table 2 for two cases of practical importance. The first case corresponds to a high-temperature receiver which would be required for a Brayton or Stirling engine application. For this case, a 1500X geometric concentration ratio is utilized (corresponding to a receiver aperture diameter of 0.28 meter). After treating reflection/absorption losses in the acrylic lens, 90% of the sunlight is transmitted. Of this transmitted sunlight, about 92% is contained within the limited 0.28 meter receiver aperture circle, i.e., 92% is the receiver intercept factor. About 6% of the lens aperture is blocked by structure; thus the blocking/shading factor is 94%. After all of these loss mechanisms are considered, the overall optical efficiency is 78%. Still considering Case I, this 78% optical efficiency for an 11 meter diameter concentrator (aperture area = 95 m^2) corresponds to a black-body receiver energy absorption rate of 59 kw (thermal) under a direct insolation of 800 w/m^2. Assuming an 815°C receiver temperature, the black body thermal radiation loss will be 5 kw (thermal). Thus the net collector output will be 54 kw (thermal), corresponding to a 71% overall collector efficiency.

For the second case in Table 2, a lower temperature receiver is assumed, corresponding to a Rankine engine application. For this lower temperature, a lower geometric concentration ratio (500X) provides better overall collector performance. After considering the same loss factors described above, the concentrator optical efficiency is 83%, this higher value being attributable to a better receiver intercept factor for the larger receiver aperture diameter (0.49 meter). After subtracting the

2 kw (thermal) black-body radiation loss corresponding to a receiver temperature of 371°C, the net collector output will be 61 kw (thermal), equivalent to an overall collector efficiency of 80%.

CONCENTRATOR ANALYSIS

Figure 2 is a schematic of a point-focus Fresnel lens concentrator, showing three possible lens contours (of an infinite set) which could be used on the concentrator. These possible lens designs all have smooth exterior surfaces and prismatic inner surfaces. Of this infinite set of lens possibilities, E-Systems has selected a convex, non-spherical-contour lens, in which each prism transmits direct solar rays with equal angles of incidence and excidence, as shown in Figure 3. This incidence/excidence symmetry (also called the minimum deviation condition) provides each prism with the lowest possible reflection losses, and thereby the highest possible transmittance, for that prism's light deviation (turning) angle, as proven rigorously in Reference 1. In addition to maximal transmittance, this minimum-deviation-prism lens also provides a maximal tolerance for lens contour errors (slope errors), an improved tolerance for lens manufacturing errors (prism angular errors and rounded prism peaks), and a smaller solar image size (including finite solar disk angular diameter and chromatic aberration effects), when compared to previous flat and spherical contour lenses. The optical performance superiority of the new lens is fully described in Reference 2. Perhaps the most important attribute of the new transmittance-optimized lens is its high slope error tolerance, which allows a substantial relaxation of the support structure stiffness requirements, and thus a significant reduction in weight and cost of the concentrator. Compared to a reflective concentrator (e.g., a 45 degree rim angle parabolic dish), the Fresnel lens concentrator is more than 100 times more tolerant of radial slope errors and 8 times more tolerant of circumferential slope errors.

Optical analyses of the transmittance-optimized lens concentrator have been completed. These analyses are based upon cone optics, i.e., the theoretical mapping of the conical bundles of radiation which originate at the solar disk, which are incident upon the lens outer surface, and which form elliptical images in the focal plane, as shown in Figures 2 and 4. Because of dispersion (chromatic aberration), the solar images of different wavelengths are spread across the focal plane as shown in Figure 4. For any

fixed receiver aperture diameter and any particular prism in the lens, the design wavelength can be selected to minimize the energy missing the receiver aperture, and thus to maximize the intercept factor. Thus the lens can be tailored for a particular design concentration ratio by properly varying the design wavelength for the various prisms comprising the lens. Once this lens design tailoring is completed, the radiant flux profile in the focal plane can be calculated by integrating over all contributing portions of the lens (treating the local lens transmittance), and over all contributing wavelengths, to define the total radiant flux concentration at each point in the focal plane. Results of such a flux profile calculation for several design concentration ratios are shown in Figure 5. The radiant flux is normalized by the one-sun direct solar flux incident on the lens, while the radial position in the focal plane is normalized by the lens aperture radius, for the results shown in Figure 5. Note that for the 1500X design geometric concentration ratio lens, the peak radiant flux at the center of the focal plane is about 15,300 suns. Also note that, for the same 1500X-tailored lens, very little radiant energy misses a receiver circle with a normalized radius (ρ/R) of 26 x 10^{-3}, which corresponds to a 1500X geometric concentration ratio.

The flux profiles of Figure 5 can be integrated over various size receiver circles to define the overall energy interception rate for various geometric concentration ratios. The results of such an integration are shown in Figure 6, wherein the intercepted energy rate has been normalized by the energy rate incident on the lens outer surface; thus the effective transmittance (optical efficiency) is shown as a function of geometric concentration ratio for lenses tailored for four different geometric concentration ratios. As one should expect, the 500X-tailored lens is the most efficient of the four lenses at 500X, the 1000X-tailored lens is the best of the four at 1000X, etc. Note that for low concentration ratios, all lenses converge in transmittance value to about 91%, which corresponds to the aperture-integrated-average lens transmittance after treating reflection losses for all regions of the lens. More importantly, note that the 1500X-tailored lens provides about an 84% optical efficiency for a 1500X application. The results of Figure 6 do not include absorption losses within the thin acrylic lens, which are expected to be 1-2%, based upon measurements for similar acrylic Fresnel lenses. Thus, the basic lens transmittance has been reduced by one percent from the values in Figure 6

to the values in Table 2, to roughly account for this absorption loss. Also, the results in Figure 6 do not include structural blocking/shading losses, although this 6% loss has been included in Table 2.

The optical results presented above can be combined with a black body receiver thermal radiation loss calculation to define collector efficiency. A parametric study of colletor efficiency for various lens design concentration ratios, various actual concentration ratios, and various receiver operating temperatures, has been completed. The results of this study are shown in Figure 7. [These results do not include structural blocking/ shading losses (a 94% factor) or acrylic absorption losses (a 99% factor); thus the collector efficiencies shown are higher than will actually be achieved in practice, by as much as 6% in collector efficiency. However, these additional losses have been treated in Table 2.]

It is interesting to note in Figure 7 that there is an optimal concentration ratio for each receiver temperature, this maximum collector efficiency point corresponding to the best tradeoff of optical efficiency and heat loss. Note that for the 1500X-tailored lens and for a receiver temperature of 815°C (1500°F), the highest collector efficiency corresponds to about a 1500X actual concentration ratio; the peak collector efficiency at this optimal point is about 77%. When blocking/shading losses and acrylic absorption losses are subtracted from this peak efficiency, the overall collector efficiency is reduced to 71%, as previously presented in Table 2. Based upon the results of Figure 7, the 1500X-tailored lens was selected as the best lens of the four considered for use over a wide range of concentration ratios and receiver temperatures.

LENS MANUFACTURING METHODS

Based upon an analysis of potential lens manufacturing methods, the best long-range mass-production method is probably extrusion-embossing, using conical rollers to directly produce the conical-segment rings shown previously in Figure 1. A schematic of this production technique is shown in Figure 8. Since this production technique will require further development, a more proven lens production method will be used in the near-term. This technique utilizes a parquet of linear lens elements to approximate the desired conical geometry, as shown in Figure 9. The performance degradation due to the parquet approximation is very small, e.g., about 1% for 4 inch wide parquet segments used in a 1500X concentration ratio application. The linear lens parquet elements will be solvent-bonded to a thin sheet of

acrylic plastic to form a one-piece panel. Both the mass production of linear lens elements and the lamination methodology have been used by E-Systems for the past three years on a linear Fresnel solar collector, with excellent results (Reference 3).

CURRENT STATUS

E-Systems has completed the conceptual design of the Fresnel concentrator, and the optical/thermal analyses of its performance. Based upon its predicted high performance and its low mass-production cost potential (due to its error tolerances and light weight), the Fresnel concentrator concept shows excellent promise for high-temperature, point-focus, solar thermal power system applications. Currently, the main thrust of the development program is to fabricate and test prototype lens panels (as shown in Figure 9) to verify the expected optical performance levels of the lens. These prototype panels should be completed and ready for JPL testing in early 1982. If the test results confirm performance levels in close agreement with theoretical predictions, the next step in the development program should be the fabrication and testing of a full-scale prototype concentrator.

REFERENCES

1. O'Neill, M.J., "Solar Concentrator and Energy Collection System," U.S. Patent No. 4,069,812, 24 January 1978.
2. O'Neill, M.J., "A Unique New Fresnel Lens Solar Concentrator," Silver Jubilee Congress of the International Solar Energy Society, Atlanta, Georgia, May 1979.
3. O'Neill, M.J. and R.A. Waller, "Analytical/Experimental Study of the Optical Performance of a Transmittance-Optimized Linear Fresnel Lens Solar Concentrator," Annual Meeting of the International Solar Energy Society, Phoenix, Arizona, June 1980.

FIGURES AND TABLES

Figures 1 through 9 and Tables 1 and 2 are located on the pages following this text.

E-SYSTEMS

Energy Technology Center

POINT FOCUS
FRESNEL LENS CONCENTRATOR

LENS/RECEIVER ASSY

MAIN RING BEAM

ELEVATION AXIS

PEDESTAL ASSY

SHROUD

RECEIVER MOUNTING RING

AZIMUTH DRIVE

CONCRETE FOUNDATION/TRACK

ELEVATION DRIVE

AZIMUTH TURNTABLE BEARING
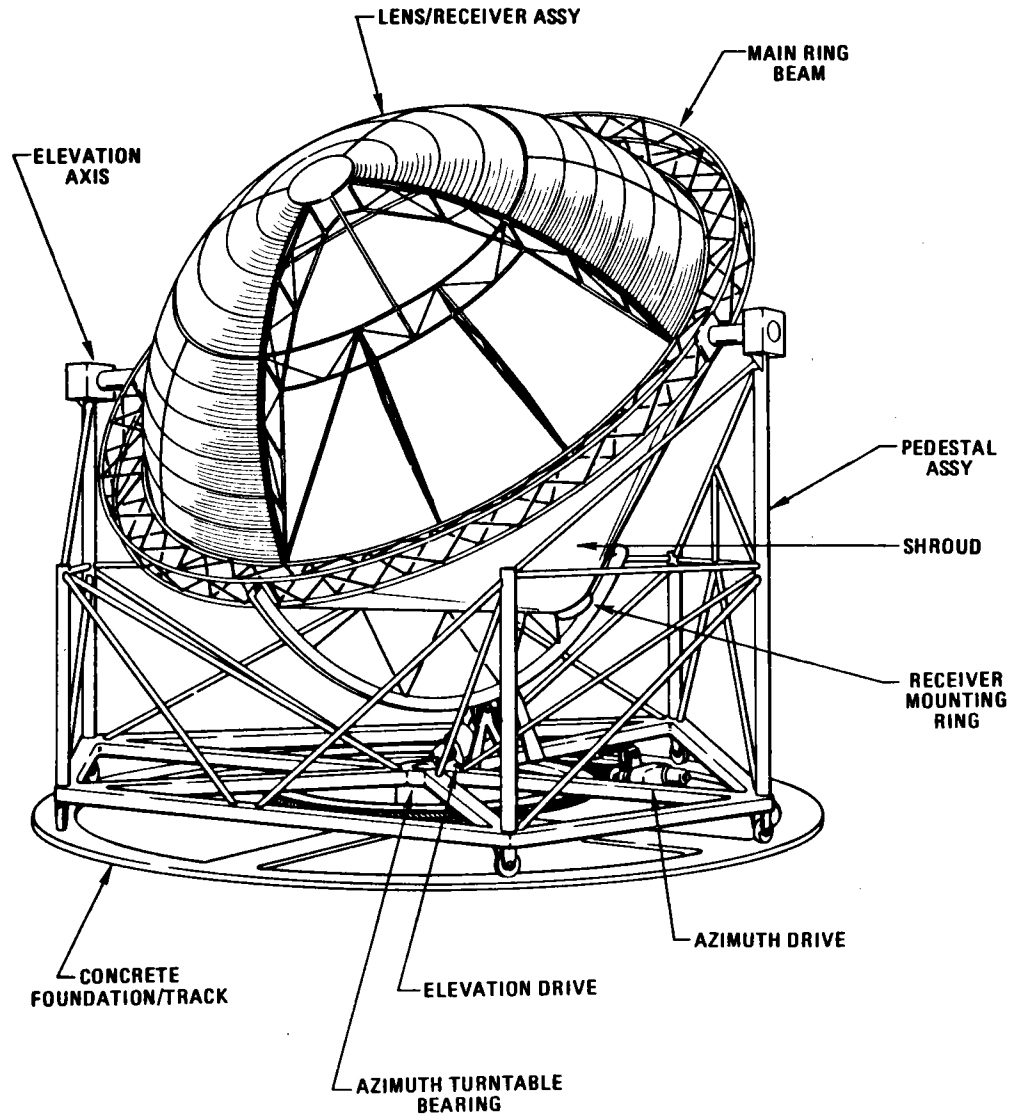
TABLE 1

E-SYSTEMS
Energy Technology Center

RECOMMENDED SYSTEM DESCRIPTION

- **PHYSICAL**

  CONCENTRATOR APERTURE DIAMETER .... 11M (36 FT.)
  CONCENTRATOR RIM ANGLE .... 45 DEGREES
  OVERALL COLLECTOR WEIGHT .... 13,000 POUNDS (EXCLUSIVE OF RECEIVER)

- **LENS PANELS**

  REFRACTIVE MATERIAL .... ACRYLIC (2.4 MM NOMINAL)
  PANEL CONSTRUCTION .... BONDED CONICAL SEGMENT PANELS
  DUST PROTECTION .... PRESSURIZED INTERIOR (BETWEEN LENS AND
  SHROUD)

- **LENS/RECEIVER ASSEMBLY**

  LENS SUPPORT STRUCTURE .... STRUCTURAL STEEL SPACE FRAME WITH MAIN RING
  BEAM, 12 RADIAL BEAMS, AND INTERMEDIATE
  SUPPORTS.
  RECEIVER SUPPORT STRUCTURE .... BIPOD AND SWAY BRACES, WITH PRESSURIZED
  SHROUD

- **PEDESTAL (ALIDADE)**

  AXIS CONFIGURATION .... EL OVER AZ, WHEEL TRACK
  CONSTRUCTION .... STRUCTRUAL STEEL SPACE FRAME

- **FOUNDATION**

  TRACK .... CIRCULAR REINFORCED CONCRETE RING
  AZIMUTH AXIS .... CONCRETE PIER FOR AZ BEARING MOUNT.
  CONCRETE BEAMS INTEGRATING PIER AND RING
  TOTAL CONCRETE 7CU. YDS.

- **DRIVES AND TRACKING**

  AZIMUTH RANGE .... ±180 DEGREES
  AZIMUTH DRIVE .... CABLE WINCH, POSITIVE ACTION
  MAX. AZIMUTH VELOCITY TO STOW .... 2,000 DEG/HOUR
  AZIMUTH MOTOR .... AC SYNCHRONOUS STEPPER, 1800 IN-OZ @ 72 RPM
  ELEVATION RANGE .... ±90 DEGREES
  ELEVATION DRIVE .... CABLE WINCH, POSITIVE ACTION
  MAX. ELEVATION VELOCITY TO STOW .... 2,000 DEG/HOUR
  ELEVATION MOTOR .... 1800 IN-OZ @ 72 RPM, AC SYNCHRONOUS STEPPER

- **RECEIVER**

  WEIGHT (JPL DEFINED) .... 705 POUNDS

TABLE 2

E-SYSTEMS
Energy Technology Center

SYSTEM PERFORMANCE SUMMARY

- **OPTICAL PERFORMANCE**

	CASE I	CASE II
GEOMETRIC CONCENTRATION RATIO	1500	500
LENS TRANSMITTANCE	90%	90%
RECEIVER INTERCEPT FACTOR	92%	99%
BLOCKING/SHADING FACTOR	94%	94%
OVERALL OPTICAL EFFICIENCY	78%	83%

- **THERMAL PERFORMANCE** (@ 800 WATTS/M² INSOLATION)

RECEIVER CAVITY TEMP	815°C (1500°F)	371°C (700°F)
RECEIVER RADIATION THERMAL LOSS	5 KW (THERMAL)	2KW (THERMAL)
COLLECTOR NET OUTPUT	54 KW (THERMAL)	61 KW (THERMAL)
COLLECTOR OVERALL EFFICIENCY	71%	80%
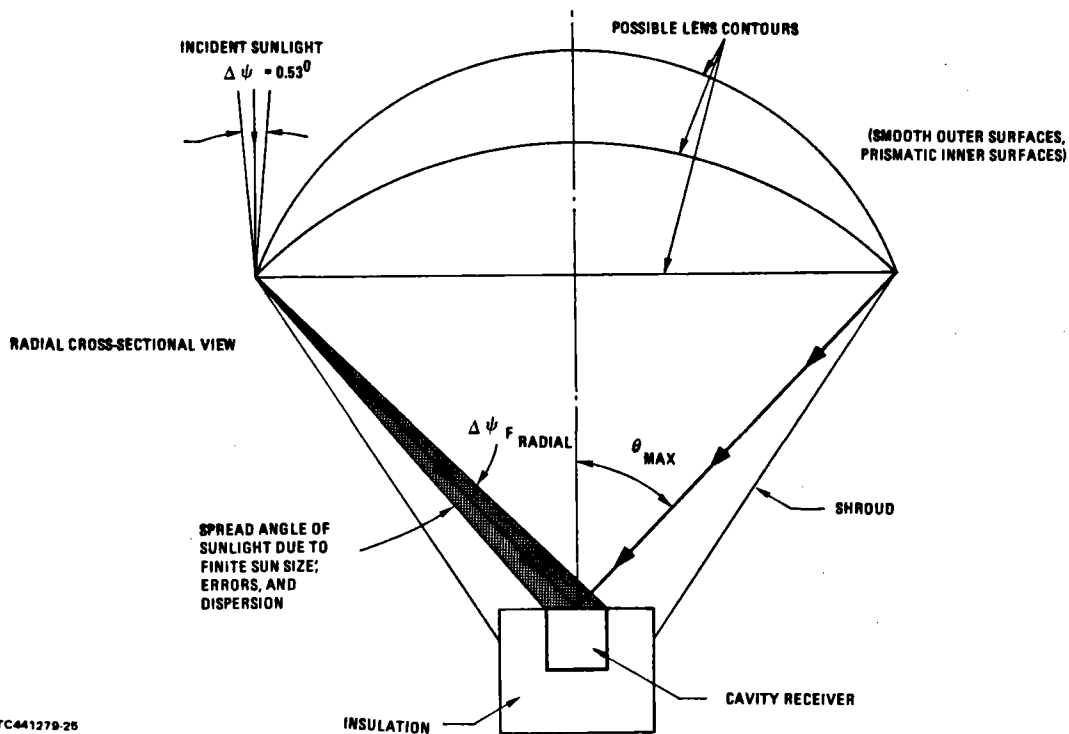
ETC441279-25

FIGURE 2 *INFINITE FAMILY OF LENS CONTOURS FOR SAME RIM ANGLE CONCENTRATOR*

FIGURE 3

PRISM FACE OVER-EXTENSION
TO MINIMIZE OPTICAL LOSSES

SMOOTH OUTER
LENS SURFACE—

LENS

INCIDENT LIGHT

LIGHT

LIGHT
SHADOW
LIGHT
SHADOW
LIGHT
SHADOW
LIGHT
SHADOW
LIGHT
SHADOW

LEAVING
LIGHT
TOWARD
FOCUS

LENS

BLUNT TIPS ON PRISMS
DUE TO MANUFACTURING

RECEIVER CAVITY
APERTURE

INFRARED IMAGE

DESIGN WAVELENGTH
IMAGE

ULTRAVIOLET IMAGE

PRISM ANGLE
ERRORS OR
RADIAL SLOPE
ERRORS MOVE
IMAGES LONGI-
TUDINALLY

ENERGY
MISSING
RECEIVER

ENERGY
MISSING
RECEIVER

CIRCUMFERENTIAL SLOPE
ERRORS MOVE IMAGES
TRANSVERSELY

ELLIPTICAL IMAGE
DUE TO 0.53° CONE
OF LIGHT FROM SUN
INTERCEPTING FOCAL
PLANE AT NON-NORMAL
INCIDENCE ANGLE

LONG CHAIN OF IMAGES CAUSED
BY DISPERSION (CHROMATIC ABERRATION)

ETC441279-20

FIGURE 4   TYPICAL IMAGE PATTERN PRODUCED BY DIFFERENTIAL
ELEMENT OF LENS SHOWING EFFECTS OF DISPERSION
AND ERRORS – NOT TO SCALE

FIGURE 5 FLUX PROFILES FOR OPTIMAL 45° RIM ANGLE LENSES

E-SYSTEMS
Energy Technology Center

ETC590380-183
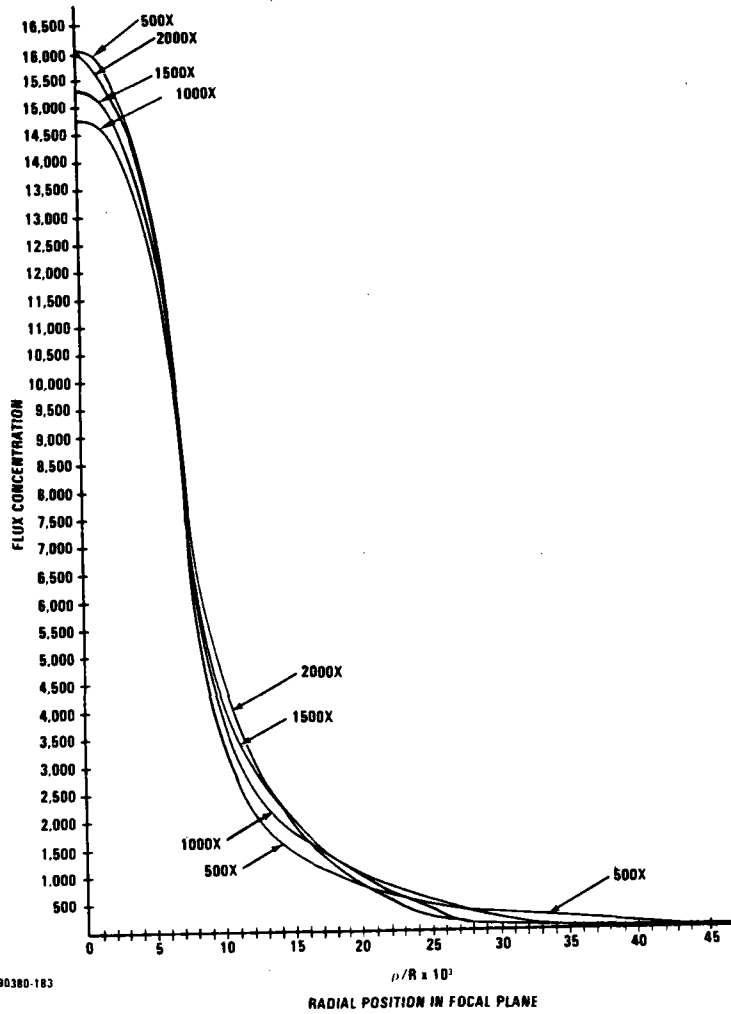
FIGURE 6 EFFECTIVE TRANSMITTANCE/GEOMETRIC CONCENTRATION RATIO FOR 45° RIM ANGLE

E-SYSTEMS
Energy Technology Center

500X - 89.50%
1000X - 86.80%
1500X - 83.50%
2000X - 80.50%

ETC590380-191

45
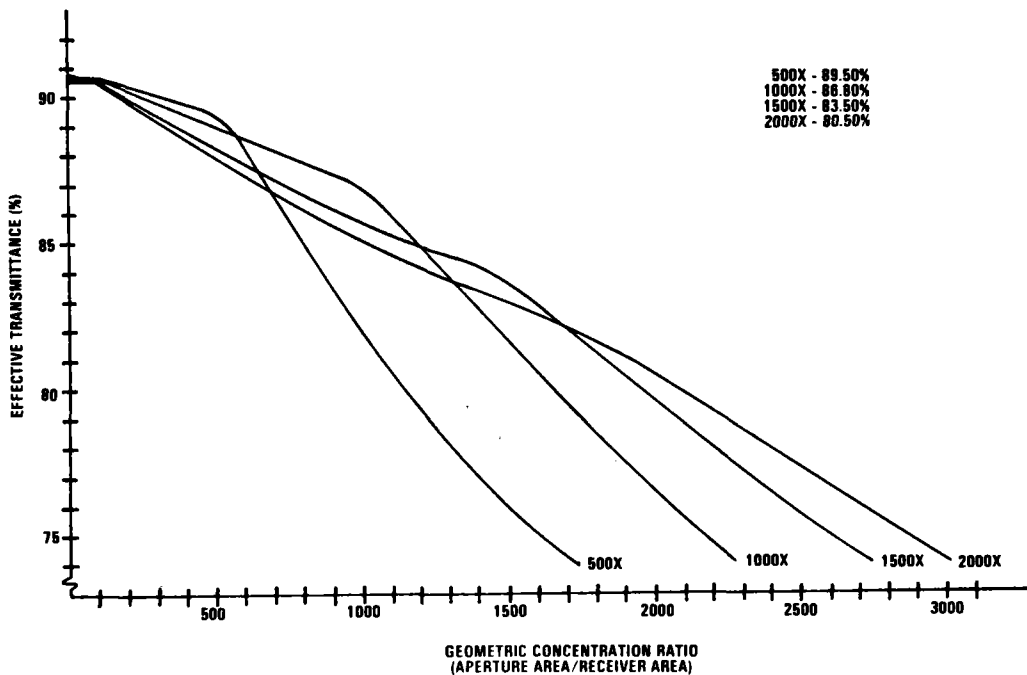
FIGURE 7

COLLECTOR EFFICIENCY FOR
45° RIM ANGLE LENSES

E-SYSTEMS
Energy Technology Center

EXTRUDER

TAPERED
DIE LIPS

HOT ACRYLIC
EXTRUDATE

SMOOTH ROLL
(CONICAL)

PRISMATIC ROLL
(CONICAL)

CONICAL SEGMENT
WITH ANNULAR PRISMS
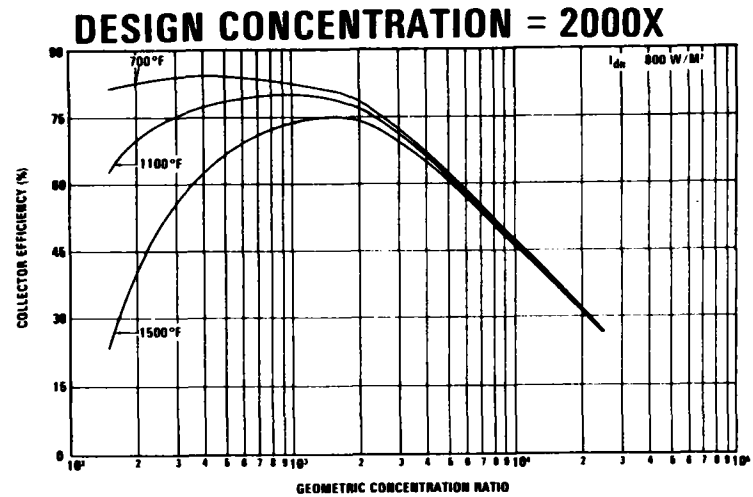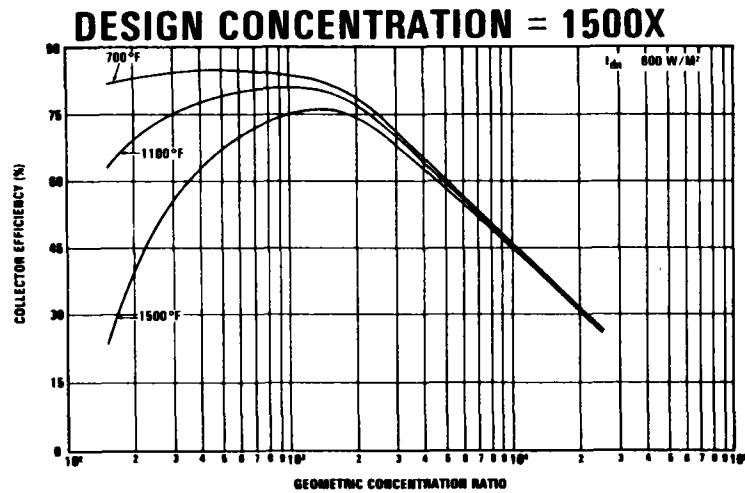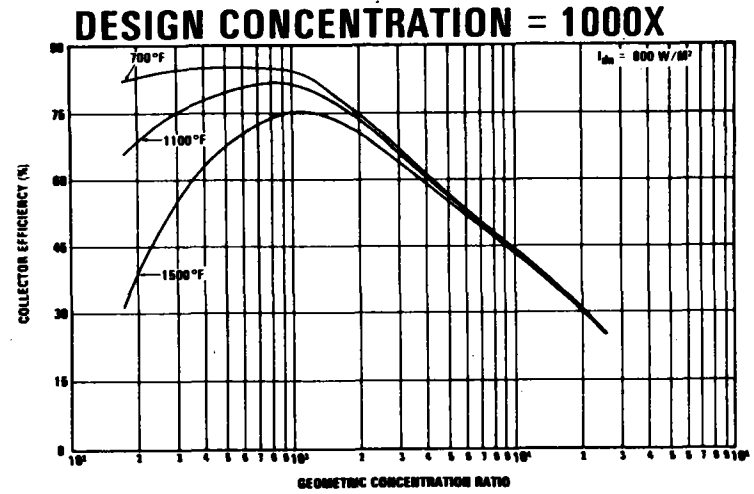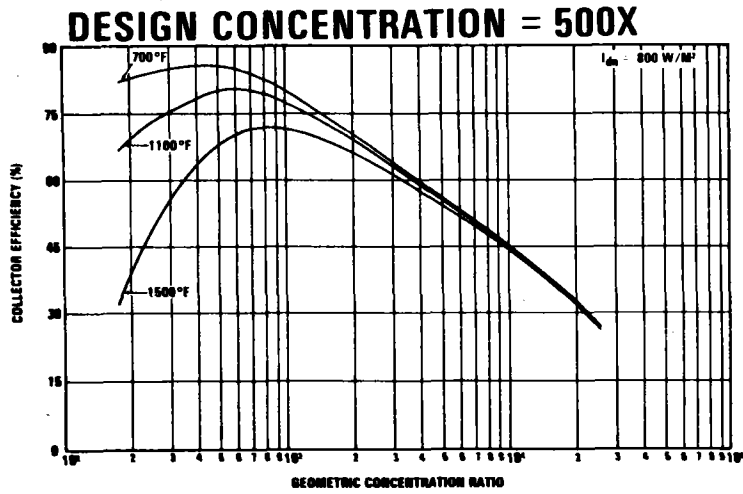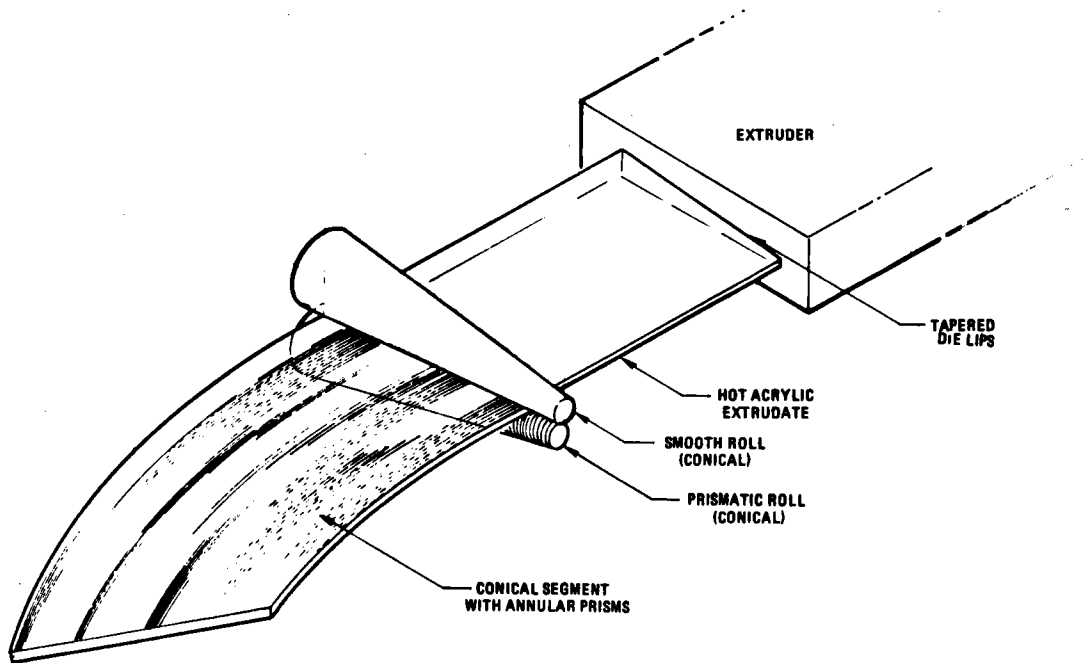
·FIGURE 8

ETC441279-22

*POTENTIAL MASS PRODUCTION OF CONICAL SEGMENTS BY
EXTRUSION/EMBOSSING PROCESS*

DOME IS SIMULATED WITH
CONICAL SEGMENTS TO
ELIMINATE COMPOUND
CURVATURE

UNFOLDED CONICAL
SEGMENTS ARE FLAT
TO ALLOW FLAT LENS
PANEL MANUFACTURE

CONICAL SEGMENT IS
SUBDIVIDED INTO
MANAGEABLE SIZE
PANELS

NOT TO SCALE

PANEL IS SUBDIVIDED
INTO SMALL PARQUET
ELEMENTS WITH LINEAR
PRISMS TO ALLOW TOOL-
MAKING.
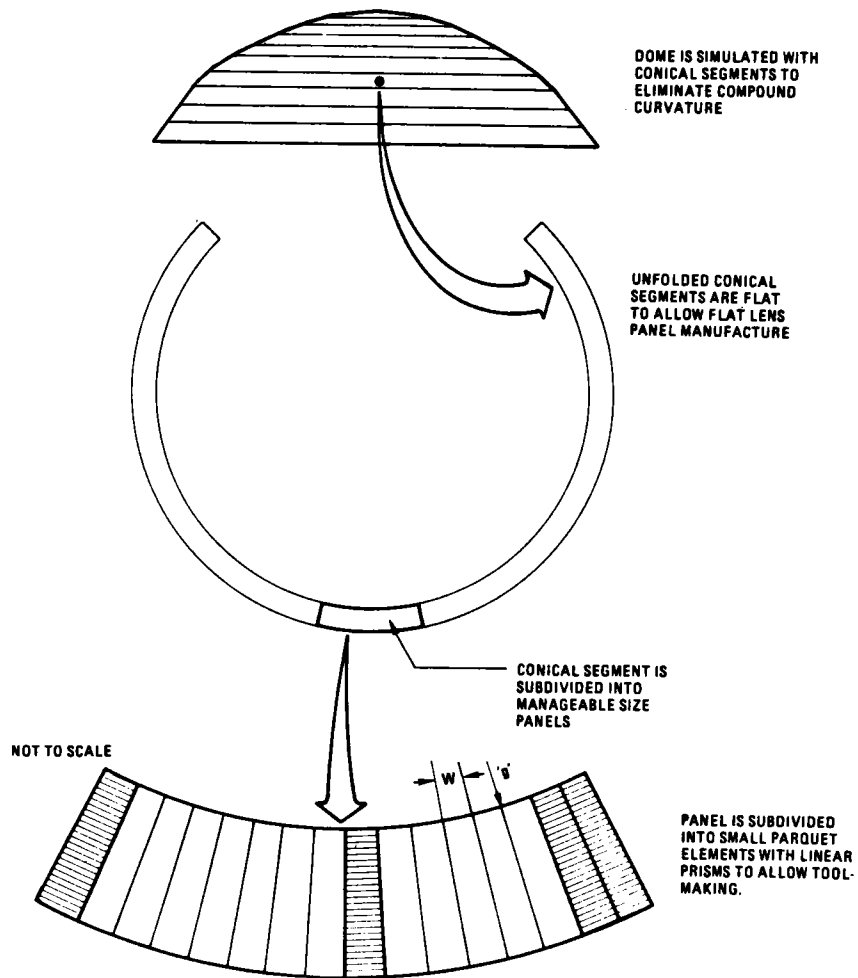
ETC441279 21

FIGURE 9   *GEOMETRY INVOLVED IN USING FLAT LINEAR FRESNEL
LENS ELEMENTS TO MAKE DOME POINT FOCUS LENS*

47

The Small Community Solar
Thermal Power Experiment

Taras Kiceniuk*

From its beginning the Small Community Solar Thermal Experiment has responded
to the changing emphasis in the area of solar energy as perceived by the
nations policy makers and by those responsible for implementing those
policies. Originally conceived as a five megawatt plant, the proposed
experimental plant was scaled down to one megawatt when it was decided that
the smaller facility provided a valid model at lower cost.

In the interest of further cost reduction, and with awareness of the increased
national emphasis on the development of high risk but potentially high-payoff
technology and on the decreasing role assigned to commercial demonstrations,
the plant size has been further reduced to 250 kilowatts. Although this
reduction in size may result in a less visible and less impressive facility,
the original technical aims of the experiment will still be achieved. Because
of the modular nature of the parabolic dish, distributed-generation, Rankine
system, changes in plant size have only a secondary effect on plant design.
The basic power module, comprising concentrator, receiver, engine, and
alternator, is independent of total plant size. Increasing the size of the
plant requires increasing only the number of individual power modules making
up the plant. The central control system has also been designed and
fabricated to deal with a varying number of power modules. Each power module
contains enough of its own required computer and control subsystems to perform
those tasks -- such as concentrator tracking and turbine operation -- which
can best be handled autonomously at each module.

Only the central power conditioning system which converts the rectified output
of the individual alternators into 3 phase 60 Hertz power for distribution is
influenced by plant size in that it must match the power output of the
combined modules. Even here the module concept is emphasized in that the
power conditioning can be accomplished by several intermediate sized
converters, each servicing a number of modules.

---

*Member of technical staff, Jet Propulsion Laboratory, Pasadena, California.

Another benefit of the modular parabolic dish scheme is that fully automated operation is virtually intrinsic to its conception. The autonomous modules are sent only top level commands and instructions like "start up" and "shut down" or information which is shared in common, such as ephemeris data. Of necessity, all other functions are independent and each unit is self sufficient and provided with many safeguards to shut down a given module in the event of anomalous behavior. The central facility which services the many modules consists of a modern computer programmed to command and integrate them in conformity with a predetermined operating strategy and in response to changing weather conditions.

The prime systems contract for the design of the Small Community Experiment was awarded to the Ford Aerospace and Communications Corporation (FACC) in December 1979. The contractor was required to conduct preliminary design, component and subsystem development, subsystem and system level verification testing, and detailed design. FACC was also asked to complete the plans for specific site preparation and for the procurement of plant hardware.

Because of projected delays in the delivery of the General Electric 12 Meter Concentrator, which was earmarked for the power module, and because of the reduction in funding , FACC was directed to concentrate its effort to complete the power conversion assembly and the control subsystems and to suspend further work on the design of a specific plant. To these ends it was decided to maintain a strict schedule for the development and integration of the power conversion assembly (PCA) and to test that unit in the solar mode on the Test Bed Concentrator (TBC) at JPL's Parabolic Dish Test Site (PDTS). This test will subject the PCA, including all of the control and energy transport subsystems related to module operation, to conditions very similar to those which will exist on the concentrator planned for deployment in the 250 KW multimodule plant.

The current status of the hardware being assembled for the PCA test on the Test Bed Concentrator (TBC) is as follows:

(1) The original mounting ring of the TBC has been replaced by a larger one designed to accept the complete Organic Rankine PCA package.

(2) The mirror facets of the TBC have been adjusted to provide a flux distribution which closely matches the one predicted for the General Electric designed 12 Meter Concentrator with a mean slope error of about 4 milliradians.

(3) The Ford computerized control system has been installed at the Parabolic Dish Test Site so that the power conversion function can be controlled as it will be in the experimental 250 KW plant.

(4) The PCA has been tested and the performance mapped in FACC's test facility at Newport Beach. This facility has the capability of supplying radiant heat flux to the receiver at power levels equal to the maximum which will be provided by the concentrator on a clear sunny day. The facility is also equipped with complete power, temperature, and pressure data measuring and recording equipment. As soon as these tests are complete, the PCA will be shipped to the Parabolic Dish Test site where it will be assembled on the Test Bed Concentrator.

The experience gained with the PCA as a result of these tests will be used to refine and update the design to insure its successful and reliable operation, first in the module design verification test of a single complete module and later in the 250 KW experimental plant. Further tests will also be conducted on this updated PCA to insure that the levels of reliability and performance will meet the requirements of a commercial plant. The module design verification test, scheduled for late 1982, will also be carried out at the PDTS, but it will be performed using the 12 Meter dish, designed by General Electric and fabricated by FACC. This test will validate all aspects of the module's operation: sun acquisition and tracking, PCA control, emergency procedures, and selected plant operational features.

The status of the site-related activities has also been affected by funding restrictions with selection of the site (from the present list of six semi-finalists) delayed by DOE pending firm commitment of the funding for the Experiment. Upon selection of the six candidate sites over a year ago, it was determined that a 250 KW experiment was generally perceived by the site participants to be acceptable, though less desirable than a 1 MWe plant, and

that a plant less than 250 kW would lack the impact and visibility which they regarded as necessary to secure the commitment of resources, cooperation, and support from their communities. The final selection of the plant site by DOE is required before the specific plant design can proceed, therefore the site selection date is now a primary determinant of the date for plant startup.

DEVELOPMENT STATUS OF THE

SMALL COMMUNITY SOLAR POWER SYSTEM

R. L. Pons

Aeronutronic Division

Ford Aerospace & Communications Corporation

Newport Beach, CA 92663

ABSTRACT

This paper presents the development status and test results for the
Small Community Solar Thermal Power Experiment (SCSE Program). Current
activities on the Phase II power module development effort are presented
with emphasis on the receiver, the plant control subsystem and the energy
transport subsystem. Detailed presentation of test results for the Barber-
Nichols Organic Rankine power conversion subsystem are given in a companion
paper.

INTRODUCTION

Ford Aerospace is currently completing the second phase of development of the
system under contract to JPL. The effort comprises the development and
integration of a single prototype power module consisting of a parabolic dish
concentrator, a power conversion assembly (PCA), a multiple-module plant
control subsystem (ETS). The PCA is shown in Figure 1 and consists of a FACC-
developed cavity receiver coupled to an organic Rankine cycle (ORC) engine-
alternator unit defined as the power conversion subsystem (PCS); the PCA is
mounted at the focus of a parabolic dish concentrator. At a solar insolation
of 1000 W/m^2 and ambient temperature of 28°C (82°F), the power module produces
approximately 20 kW of 3-phase, 3 kHz ac power, depending on the concentrator
employed. A ground-mounted rectifier converts the ac power to 600 volt dc
power, which is transported to the central collection site where it is supplied
directly to the common dc bus which collects the power from all modules in the
plant.

Development/qualification testing of the PCS has been completed successfully
by Barber-Nichols in Colorado and the unit has been shipped to the FACC
facility for mating to the receiver and all-up, solar-simulated performance
verification testing. Upon successful completion of these tests, the PCA
and associated ETS/plant control subsystem hardware will be shipped to the
JPL-Parabolic Dish Test Site (PDTS) at Edwards AFB for system-level solar
tests of a complete power module. Initial testing will take place on
the existing 11 m. diameter Test Bed Concentrator (TBC) since the JPL-
sponsored Low Cost Concentrator will not be available for testing for several
months. The plant control subsystem can accommodate other concentrators and
several candidates may be available for testing in 1982.

The following paragraphs describe and summarize the development status of
various Small Community System components.

POWER CONVERSION SUBSYSTEM

The ORC-PCS is a regenerative, hermetically-sealed system with a single-stage axial flow turbine direct-coupled to a high speed permanent magnet alternator (PMA). Toluene is the working fluid at a maximum temperature of 400°C (750°F) and maximum pressure of 4.52 MPa (656 psia). The unit is shown in Figure 2.

The air-cooled condenser is configured in a cylindrical shape surrounding the regenerator and the turbine/alternator/feedpump assembly. This results in a very compact PCS, measuring 1.1 m (44 in) in diameter by 1.5 m (60 in) in length. The cooling fan is driven at variable speed in order to minimize. parasitic losses and maintain high part-load efficiency. PCS weight is approximately 335 kg (740 lbs).

A vapor throttling valve at the exit of the receiver maintains nearly constant turbine inlet temperature by controlling the mass flow rate of the working fluid to compensate for variations in solar flux level. The valve is a pintle-type valve operated by a hydraulic actuator which is powered by high pressure working fluid. Valve command signals are keyed to temperature sensors at the receiver outlet.

Further details of the system hardware and initial results of development and qualification tests on the PCS at the Barber-Nichols facility are separately described in a companion paper.

Design Analysis Results

Analysis results were obtained for the receiver using a 25 element cavity model. The distribution of net absorbed flux is compared to the incident flux in Figure 8 . The corresponding copper shell and fluid temperature profiles are shown in Figure 9 for the design limit input power. It is characteristic of the design that the core temperature profiles are not strongly dependent on input thermal power. This is due to the selected PCA control method which modulates the toluene flow to maintain a nominally constant receiver outlet temperature for the toluene. Slight temperature profile shifts will occur with varying toluene pressure in the receiver, but these too are minor since the primary throttle valve for the toluene flow control is down-stream of the receiver.

Finally, the receiver thermal efficiency is shown in Figure 10 as a function of direct, normal insolation. At the rated value of 1000 w/m^2, the efficiency (ratio of power delivered to the toluene/power input to the cavity) is greater than 97 percent. (as shown later, measured results are about 0.2% higher).

Predicted stresses for the stainless steel tubing and copper shell are well below allowable yield strengths. The tubing calculations were made in accordance with the ASME codes, and included stresses due to differential thermal expansion between the tubing and the shell. The principal shell stress is in the cylindrical portion and is induced by the non-linearity in the axial temperature profile. The long-term creep strength of the shell is the most important criteria and led to selection of a magnesium-zirconium-chromium alloy of copper. Stresses in the core support struts due to core thermal expansion were also estimated and were found to be less than one-half the material's allowable yield strength.

The design objective for the aperture plate was to provide a stable, long-life aperture lip in normal sun acquisition, track, and detrack operations of the collector. Maintaining the proper aperture diameter is necessary to minimize reflection, reradiation, and convection losses from the receiver cavity. Steady heating of the lip will occur due to imperfect focusing of the concentrated solar beam, and due to collector pointing errors. Transient face heating will occur as the beam traverses the aperture plate during sun acquisition and detrack.

A review of available materials candidates led to rejection of heat-sink and ablative concepts in favor of a radiatively cooled design. In this approach the lip heating is accommodated by outward radial conduction through a metal shell and re-radiation from the face to ambient. Transient heating of the face is accommodated by the limited heat capacity of the shell.

The lip heating model is shown schematically in Figure 11. The primary tradeoff results included (1) selection of copper for the plate in preference to aluminum, (2) selection of a high emittance coating for the plate face, and (3) maximizing plate thickness in preference to extending its diameter (for a given plate weight). The copper ring at the aperture lip was sized to pro-vide adequate circumferential conductance for a peak lip heating rate of twice the circumferential average. The plate thickness was selected to limit the transient temperature rise to 50°C for a 2 deg/s collector slew rate. The resultant lip heating capability of the concept is shown in

RECEIVER

The EE-1 ORC receiver has been thoroughly tested at the Ford Aerospace facility in Newport Beach; it has met or exceeded all specified design requirements. A cutaway sketch of the receiver is shown in Figure 3 . The receiver has been designed for a life of 30 years. The design concept is a direct-heated, once through, monotube toluene boiler operating at both sub- and super-critical pressure. The cavity is formed by a cylindrical copper shell and backwall, with stainless steel tubing brazed to the outer surfaces. This core is supported by eight struts, insulated with high-temperature mineral wool, and enclosed with a weather-proof aluminum casing. The cavity aperture is formed by a copper plate and lip ring.

The receiver has been designed for a life of 30 years. Design requirements for the receiver include input thermal power up to 95 kW_t, toluene flow from 0.9 to 9.1 kg/min, nominal toluene outlet temperature and pressure of 399°C (750°F) and 5862 kPa (850 psia) respectively, maximum weight of 272 kg (600 lb), and a maximum toluene pressure drop of 448 kPa (65 psi).

Hardware

The principal receiver components are the core assembly, support structure, insulation, casing and aperture plate. The core (Figure 4) consists of a cylindrical barrel and a flat backwall. The cavity interior dimensions are 0.61 m (24 in) in diameter by 0.48 in. (19 in) deep. These copper pieces have grooves machined in their outside surfaces to match a helical coil and a spiral coil, each of 347 stainless steel tubing. The tubing, with 1.59 cm (0.625 in) outside diameter and 0.89 mm (0.035 in) wall thickness, is brazed to the copper shell to assure good thermal contact. The core weighs 147 kg (325 lb). It is protected from corrosion in air by a nickel plating. The cavity interior surface is painted black to obtain a 0.95 solar absorptivity.

The core support structure (Figures 5 and 6) features a circumferential band around the core at its center-of-mass. Four struts tie this "belly band" to the main support ring of the receiver which is in turn attached to four mounting rails on the PCA structure (not shown). These central struts provide complete lateral support for the core. Axial and pitch/yaw support is provided by four struts running from the cylinder/backwall junction out to the main support ring. The eight struts are length-adjustable and are pinned at each end to accommodate thermal expansion of the core relative to the support ring.

The complete receiver assembly is shown in Figure 7 . The insulation surrounding the core is a low-density, refractory ceramic wool. Outer casing segments are formed from aluminum sheet and provide a structural tie-in of the aperture plate to the support ring.

The aperture plate is made of 3.2 mm (0.125 in) copper sheet, with a copper ring brazed to the sheet to form the aperture lip. The aperture diameter is 37.95 cm (14.95 in), providing a concentration ratio of 1000 for the collector. A stainless steel cone runs from the aperture lip to the forward edge of the core shell. The aperture plate assembly is nickel plated for corrosion protection and is painted black on its exterior face to maximize its thermal emittance.

Figure 12 for varying concentration ratio, collector surface slope error, and a nominal collector pointing error. Although the nominal collector surface slope error is 3 mrad without exceeding 400°C lip temperature at the 1000/1 concentration ratio, the predicted lip temperature for nominal collector performance is less than 200°C.

A detailed thermo-structural analysis of the aperture plate revealed the desirability of a toroidal surface for the plate. Analysis results are summarized in Figure 13 for the selected plate profile with a 25.4 cm meridional radius of curvature. The maximum predicted stress is 38 ksi, indicating local plastic yielding. However, the peak local strain is only 0.2 percent, and the fatigue life will exceed 2000 such local cycles. Also shown in Figure are the stresses for the nominal plate thermal profile, and these are well below the yield strength.

Test Results

A closed toluene loop test system (Figure 14) was fabricated to provide the same fluid input/output characteristics as the ORC engine, which was under-going parallel development at Barber-Nichols. In addition to the piping network, control panels and instrumentation, a special electrical heater was designed and fabricated to simulate the solar input to the cavity receiver (Figure 15).

The thermal/structure testing of the receiver has been successfully completed completed. These tests included various start-ups, shutdowns, low and high power steady-state and transient operation. These tests were initially planned to be performed at the supercritical pressures for which the receiver was designed. However, the receiver was also tested at subcritical pressures due to change to subcritical conditions under low to medium power levels brought about by the lower turbine/alternator/pump speed of the ORC.

The receiver tests were performed during the qualification and the earlier development tests. These tests were divided into the following series:

- Receiver core structural test
- Thermal/structural proof test
- Performance verification test
- Thermal survival test

Some of the salient results are presented in the following paragraphs.

1) Receiver Core Structural Test

This test was performed to verify the structural integrity of the core and to confirm that the tubing was leak-free for various internal pressures at ambient temperature conditions. The core was first leak checked at low pressure (100 psig) followed by pressurization to the 1630 psig proof pressure level for 30 minutes. This was followed by a leak check at the maximum working pressure of 850 psi and finally a vacuum leak check at 0.5 psig. Visual inspection of the core after testing revealed no deformation or structural damage. The assembly of the receiver was then completed and installed in the facility.

2) Thermal/Structural Proof Test

This test was performed to verify the structural integrity of the assembled receiver (less aperture plate) at elevated temperatures. The receiver was subjected to the maximum heater power, toluene flow rate and pressure capabilities of the test loop.

The receiver performed very well at the maximum operating conditions. Figures 16 through 20 present results from this test. As shown in Figure 16, the cavity heater reached the desired (maximum) steady-state operating power of ~ 100 kW after a few minutes operating time. Figure 17 presents the receiver core temperature response to the simulated solar power. Temperature histories are presented at four locations on the front (cylindrical) portion of the core and at two locations near the center of the core end plate. Once the average core temperature reached ~ 600°F the toluene flow rate (Figure 16) was increased and then varied to maintain the toluene outlet temperature shown in Figure 18. The toluene inlet temperature at the receiver as well as the inlet and outlet pressures are also presented in this figure. Figure 19 presents the temperature history for several locations on the receiver. These locations include the maximum core temperature at the center of the backwall (the flux sensor) as well as the support rods, outer shell and ambient temperature. The maximum core temperature ranged from about 850°F to 900°F throughout the Thermal/Structural Proof Test. The maximum temperature for the lateral and axial support rods were approximately 450°F and 350°F, respectively. The maximum outer shell temperature was approximately 120°F.

Figure 20 presents the receiver core temperature profile for the Thermal/Structural Proof Test at the same steady-state time as the previous figure. This figure presents the actual copper temperatures along the external surface of the receiver core as measured by thermocouples. The excellent agreement of the predicted temperature profile is shown in the figure.

The copper core temperature was 475°F at the front of the receiver (cylindrical section aperture end). This was 100°F higher than the entering toluene fluid. The core temperature increased roughly 10°F per inch in the cylindrical section of the receiver. The core temperature at the cylindrical and backwall interface was approximately 700°F and was 770°F at the toluene outlet location. The maximum core temperature was located at the center of the flux sensor and was 875°F.

Investigation of this temperature profile as well as many others during the tests did not reveal any local "hot spots" along the receiver core. The ability of the copper core to conduct heat away from any localized sections of poor heat transfer (if they should exist for some reason) virtually precludes the development of "hot spots".

3) Performance Verification Test

Steady-state thermal performance tests were completed during a number of major test runs. Table I summarizes some of the salient operating conditions for each of the steady-state runs. As shown, the receiver core was operated over a wide range of conditions (supercritical, subcritical, low power, high power) while maintaining the required ~ 400°F inlet and ~ 750°F outlet toluene temperatures. An evaluation of the losses in the receiver and heater

58

(heater power less fluid power out, last column in Table I) indicates the values at the higher power levels are greater than anticipated. (Originally estimated at about 0.5 kW loss through the receiver insulation and ~ 5 kW in the heater.) It now appears that the loss through the back and sides of the heater is larger than expected.

Numerous transient test runs were made during periods between the steady-state test runs. These transient cases were performed to investigate the receiver response characteristics while operating at supercritical and at subcritical conditions (i.e., with two-phase flow). Both the liquid and vapor control valves were operated to vary the receiver operating pressure and the toluene flow rate. In addition, the Barber-Nichols vapor flow control valve was utilized for many of the transient tests in conjunction with the other test parameters. Figures 19 through 22 present results from a typical subcritical test run. This test consisted of three distinct operating modes: (1) cold start-up, (2) transient flow operation (3 conditions), and (3) steady state operation (3 conditions).

The cold start-up simulated the planned control logic for initial turn-on in the morning. The test was initiated with the entire system at ambient temperature. The receiver was partially filled with toluene liquid. The vapor control valve was closed until the receiver pressure reached 400 psi. The valve was then momentarily opened to relieve the pressure in the receiver. Valve modulation continued until the receiver core reached an average temperature of 600°F at which time the valve was set to a minimum flow position. When the toluene temperature at the receiver reached 750°F, the vapor valve (toluene flow) was controlled to maintain the specified temperature of 750°F.

As shown in Figure 21, the cavity heater reached the desired steady-state power level a few minutes after start-up. Figure 22 presents the receiver core temperature response of six locations to the simulated solar power. Once the average core temperature reached 600°F, the pump was turned on and the vapor valve opened to control the toluene flow rate and the exit temperature from the receiver.

Approximately 25 minutes were required from the start until the toluene exit temperature reached the 750°F steady-state operating level (Figure 21). The receiver was then operated in a transient mode (time = 20 to 65 minutes) to obtain a steady-state operating condition with the heater power, toluene flow rate, inlet and outlet temperatures and receiver pressure all essentially constant during this time period. The first steady-state time period occurred from = 65 minutes to time = 85 minutes in Figure 21 . The heater power and receiver operating pressure were then varied and a second steady-state operating condition obtained (time = 140 to 165 min.). The last steady-state mode for this typical subcritical test run plotted in Figure 21 was from time = 190 to 210 minutes.

Flow perturbations of various magnitudes and duration were investigated for the transient operating conditions. The flow rate was varied by approximately plus or minus 100 percent of the value commensurate with the heater power level. These large changes in flow resulted in the receiver outlet temperature history presented in Figure 23. As shown, the toluene exit temperature responds slowly to changes in flow. The temperature variations

behave in a very predictable manner, e.g., when the toluene flow is increased, the receiver (toluene) outlet temperature decreases, and vice versa. The entire subcritical operation was well behaved with only small temperature overshoots and undershoots caused by the intentional input perturbations.

Figure 24 presents the temperature history for several locations on the receiver assembly. The center temperature of the flux sensor rose quite rapidly during the start-up portion of the test run. After the initial transient perturbations, the sensor temperature varied between approximately 750°F and 825°F. The mid-points of the lateral and axial support rods attained their steady-state temperatures of 475°F and 375°F, respectively, after about two hours of continuous receiver operation. The outer shell temperature variation depends on location. The maximum temperature was approximately 120°F for the case plotted in Figure 24 demonstrating that the insulation does a good job of minimizing conduction heat loss.

Figure 25 presents a curve fit of the pressure drop through the receiver core as a function of toluene mass flow rate. Data were somewhat limited due to the oscillations in receiver inlet and outlet pressures as well as the toluene mass flow rate. These oscillations were caused by the diaphragm pump used in the test loop. The pressure oscillations were on the order of 5 to 10 percent of the mean system pressure downstream of the accumulator. When the system was operated at supercritical pressures, the inlet and outlet pressure variations were approximately 70 psi ($\pm$ 35 psi) and 10 psi ($\pm$ 5 psi). respectively. Thus, at any instant, the receiver inlet could be as much as 40 psi (plus the receiver pressure drop) higher than the outlet, or 40 psi (minus the receiver pressure drop) lower than the outlet pressure. The toluene vapor compressibility effectively dampened the pressure oscillations to a few percent at the receiver exit in all of the supercritical operating test cases. The measured toluene flow rate varied by a few percent at all operating conditions. This meant that the RMS pressures and flow rates had to be estimated during each test run. The pressure drop through the receiver at the maximum toluene flow rate of 18.83 lbm/min is predicted to be 38 psi. This maximum pressure drop is substantially less than the allowable value of 65 psi.

The receiver core has an integral heat flux sensor located at the center of the backwall. This sensor was provided as an independent indication of the solar power level into the receiver. This information can be utilized (if necessary) by the control system, to determine the receiver energy balance, etc.

The predicted receiver efficiency* shown previously in Figure 10 is within 0.2% of the data obtained from the tests. The revised values are 97.2 and 97.6 percent for the rated and maximum power levels, respectively. This slight efficiency increase is attributed to lower predicted temperatures for the receiver cavity. The lower mean effective cavity temperatures are a direct result of the observed toluene convective heat transfer coefficiencts being a factor of two greater than those used during the design performance predictions. Table II presents a brief summary of the computed receiver losses and effective cavity temperatures at rated and maximum power.

---

*Based upon the absorbed power to the toluene working fluid divided by the incident power passing through the receiver aperture.

4) Thermal Survival Test

The thermal survival test was performed to verify the high-temperature structural integrity of the receiver. This test was initiated by applying moderate thermal input power to the dry receiver core until it reached a maximum temperature of 1000°F. The thermal power was then adjusted to maintain this temperature for approximately 15 minutes. The cavity heater was then removed, permitting the receiver to cool at its natural cooldown rate. Figure 26 presents the receiver core temperature history for the thermal survival test. Also shown are the temperature histories for the cavity heater, support rods outer shell and ambient air. The lateral and axial support rods reached maximum temperatures of 760°F and 510°F, respectively. The maximum outer shell temperature was approximately 100°F. The support rods and outer shell did not reached their equilibrium (steady-state) temperatures during this test. This was a result of the very low conductive heat loss through the support rods and insulation blanket. The maximum support rod temperatures in this test was 150°F to 200°F higher than the maximum steady-state temperatures measured during normal operating conditions. This demonstrated the integrity of the support rods when subjected to a maximum over temperature condition corresponding to the specified survival value. The entire receiver went through the thermal survival environment with no observed problems.

Conclusions

The testing of the SCSE receiver has been successfully completed. The demonstrated performance of this unit exceeded the design predictions for all operating modes. A summary of the salient test results is given below:

- The receiver efficiency was verified as 97.2 percent.

- The maximum pressure drop through the receiver core was verified to be 38 psi, considerably less than the allowable maximum of 65 psi.

- The measured receiver core temperatures were lower than those predicted by the design analysis due to higher than predicted convective heat transfer to the toluene working fluid. The result is an overall receiver efficiency that is greater than the design predictions.

- The receiver was successfully operated in all possible modes including:

    - cold and warm start-ups

    - steady-state and transient flow conditions

    - low, medium and high power levels

    - subcritical and supercritical pressures

- Although the receiver was designed to operate only at supercritical pressures, its performance was excellent during both supercritical and subcritical conditions. Comparable performance was measured for the supercritical and subcritical modes. (Subcritical conditions are a result of wider-than-planned turbine/alternator/pump speed range under low to moderate power levels.)

- Local "hot spots" were not observed at any of the numerous instrument locations on the development or qualification receiver cores.

- The receiver core and toluene outlet temperatures were easily controlled, stable and well behaved.

- Inspection of the receiver upon completion of the tests did not reveal any structural deformation or deficiencies.

- The integral flux sensor performed as expected and provided sufficient temperature resolution.

The receiver performed extremely well during all of the various test modes. No design deficiencies were found, and it was concluded that the basic receiver design meets or exceeds all of the performance requirements for the Small Community application and is a very forgiving design.

PLANT CONTROL SUBSYSTEM

The plant control subsystem has been designed for automatic, totally remote
(unattended) operation. Manual control capability will be provided for
installation, check-out, testing and maintenance. General functions are
1) automatic/manual control of all plant subsystems, 2) coordinated sequencing
of plant subsystems for all operating modes, 3) failure protection and
4) status monitoring.

Operating Principle

The plant control system is shown schematically in Figure 27. The computer
hierarchy is designed to make each power module relatively self-sufficient
by providing it with its own processor which is called the Remote Control
Interface Assembly (RCIA). The RCIA is capable of controlling all of the
functions of that power module, including concentrator control, closed-loop
control of the vapor valve, start-up and shutdown procedures, and the col-
lection and monitoring of data.

The overall plant operation is under the supervision of the Master Power
Controller (MPC), which is located at the central power collection site.
The MPC provides the operator interface and controls the overall plant
operation by sending high-level mode commands to each RCIA.

The system is designed to operate the plant with high efficiency under
continuously varying solar energy input. It is simple in concept and provides
totally stable operation in all modes. There are three elements of the con-
cept, as follows:

1) Concentrator Control

Concentrator control typically consists of 2-axis tracking and associated
sequencing, e.g. start-up, shutdown, emergency de-track, etc. The essential
feature of this tracking concept is its dual operation, i.e., 1) coarse
tracking via computer-stored ephemeris data and concentrator angular position
sensors and 2) fine tracking via auto-nulling of optical (sun) sensor signals.
Note that the control system has been designed to interface the LCC although
other concentrator tracking systems can be easily accommodated.

2) Fluid Control

The fluid control loop (Figure 28) operates the coupled receiver and ORC
engine to make certain that 1) the net thermal energy absorbed by the

63

receiver is transmitted to the engine in concert with the time-varying solar
energy input, and 2) high part-load efficiency is achieved. These requirements
are met by the engine throttle valve control. The combination of constant
turbine inlet temperature and optimum turbine speed (as discussed below)
maintains nearly constant PCS efficiency over a very wide range of solar input.

3) Turbine Speed Control

The turbine speed is maintained at or near optimum value so as to maximize
turbine/alternator overall efficiency. This is done by providing a constant-
voltage load for the individual alternators (or, equivalently, a constant
alternator output voltage is maintained) and the speed is then controlled by
the balance between the torque applied to the turbine and the torque absorbed
by the alternator. Figure 29 shows the resultant speed characteristics for
alternator parameters selected to produce a turbine speed which maximizes
overall efficiency. The constant-voltage load is produced by the inverter,
which incorporates an active circuit that senses its input voltage and varies
its duty cycle so that the effective input impedance is varied in order to
draw the current required to keep the alternator output voltage constant.
With multiple power conversion units connected to the inverter in a parallel
electric circuit, as shown in Figure 30, the voltage across each alternator
terminal is the same and is determined by the equivalent impedance can thus
be varied to maintain constant voltage despite continuously varying solar
input. Power output variations among one or more engines are thus represented
by current variations in the electrical circuit. Individual alternator field
control is thus avoided and all power units are controlled by the central
inverter. The dynamics of the speed control are dominated by a first-order
response to a step change in input power with a time constant of about one
second. The voltage control loop of the inverter has a bandwidth of about
6 Hz--well above the speed control dynamic frequency.

Mode Control

The overall control pf plant functions is organized in a hierarchal modular
form as shown in Figure 31. The plant is designed to operate autonomously
without operator intervention, or to respond to high-level operator requests.
The logic related to overall plant autonomy is referred to as plant automoding
and is contained within the MPC. The MPC controls all power modules in the
plant by sending high-level mode commands to the RCIA at each power module
over the serial data link. Typical power module modes which are commanded
by the MPC are: power on, power off, power standby, and emergency shutdown.

The power module modes are received by the RCIA for that module and broken
down into sequences for the concentrator and the PCA. The concentrator is
thereby caused to go to one of the modes described above. The PCA modes
include detailed sequential procedures to start the engine, shut it down, and
monitor its operation to detect and take action on anomalies. Normal mode
includes implementation of the vapor valve control law.

For programmatic reasons due largely to the requirement for interfacing
with the TBC at the Edwards AFB test site, the software to achieve plant
automoding has been deferred to the next phase of the program.

Hardware Implementation

1) MPC

As shown in Figure 32, the control hardware is implemented as a distributed control system with one central Master Power Controller (MPC) and with a local Remote Control Interface Assembly (RCIA) at each power module.

The MPC is configured around a Data General Nova 4/X Minicomputer. The unit includes 64K words of MOS semiconductor memory and a 6.25 M work Winchester disk. Operator interfaces are provided via a CRT display with keyboard and a printer as shown in Figure 33. Interface cards are provided for A/D, D/A conversions, discrete I/O, and serial digital data links. A magnetic tape recorder provides a vehicle for data recording. In addition, a modem is provided to connect a remote terminal by telephone or hard line so the operator may be at a remote site such as a central utility dispatch office. In the automoding mode, the operator allows the plant to operate autonomously, generating power when adequate solar insolation is present and when the grid is available to accept it.

In addition, the operator has a number of manual and test mode options available to him. In this way, the operator may power the plant up or shut it down by simple instructions from a keyboard, or may similarly control the operation of individual power modules. The operator also has control over the collection and display of data from the plant.

Even though the MPC could be implemented with a custom designed microprocessor, it utilizes a commercial mini-computer customized in-house to the EE-1 requirements. This offers improved peripheral support, and good high-level languages and operating systems.

2) RCIA

A microprocessor-based RCIA, located at the base of each concentrator, has been designed to meet a wide (-25 to +49°C) operating temperature range, and to minimize production cost (55 are required in each plant).

Figure 34 shows a photograph of the RCIA enclosure and various components. The NEMA Type 4 enclosure is rain-tight and dust-tight. All circuitry is contained on ten printed circuit cards which plug into the card cage for low maintenance. Interconnections between the RCIA cards are accomplished via the STD BUS developed by Pro-Log Corporation. This makes available pre-fabricated boards for test interface purposes.

Provisions are made via a test connector on the RCIA enclosure to attach an external test keyboard/display unit. This unit when used in conjunction with monitor routines contained on an RCIA EPROM can be utilized to read memory, write memory, manipulate CPU registers, and set program breakpoints. When used along with special purpose imbedded test routines, the unit can be used to test RCIA hardware both during fabrication and in the field.

Software

The control software consists of the Master Operational Program (MOP) which resides in the MPC and the Remote Operation Program (ROP) which resides in the RCIA.

The MOP operates within the framework of the Data General Real-time Disk Operating System (RDOS) while the MOP executive provides the real-time control and module sequencing. Since the modules execute at different rates, the executive is designed to utilize a multitasking technique in which module executions are interleaved according to time slot and priority to most efficiently utilize CPU computation time. The data link interface module controls the command/response protocol on the data link to the RCIA. Modules are provided to service input data from the weather station, ETS, and the keyboard. Data input by these modules is converted to engineering units by the data base format module and stored in memory. This data base is utilized to perform the power and energy computations, and to derive data for magnetic tape recording and CRT display. A typical CRT display format is shown in Figure 35. The Built-In-Test (BIT) module provides the means to simulate normal MPC inputs to allow system checkout.

Each RCIA has a resident ROP program. Operation of the ROP is controlled by the ROP executive. The executive is a special purpose, multitasking controller operating from real-time inputs generated by a 50 Hz timer interrupt. The Data Input modules read data from the MPC data link, A/D converter, and the input registers. The Mode Control Module determines overall power module modes while the PCA Control module involves engine sequence logic. The Throttle Valve Position Control module implements the control law for the fluid temperature loop. The Fault Detection module involves the monitoring of out-of-tolerance input conditions and unallowed system states. In the event these occur, a warning flag is sent to the MPC. If the fault is of a critical nature, steps are immediately taken in the RCIA to shut down the power module. The Output Format module translates the data base into the ASCII hexidecimal format for transmission to the MPC. The Concentrator Control module performs concentrator mode and position control functions. In addition, modules are provided for Built-In-Test and real-time debugging from the MPC CRT.

The microprocessor utilized on the CPU card is a Z80 which is an industry standard multiple-sourced part. The program instructions to be executed and the constants to be utilized in computations are resident in the 16K word programmable read-only-memory (PROM). The microprocessor utilizes 6K words of semiconductor random access memory (RAM) for intermediate computations (scratchpad) and variable data storage. A clock generator provides a real-time reference for system operation and is used to establish the main computation cycle time of one second. Analog data signal conditioning for the engine is accomplished at the focal point and sent via 4-20 ma current loops to minimize signal degradation from the focal point to the RCIA which is 20 meters (65 feet) away. All of these data are multiplexed and analog-to-digital converted at the RCIA. The RCIA also provides analog outputs via digital-to-analog converters and discrete interfaces to floating relay contacts to maintain ground isolation.

3) Data Link

The serial digital data link between the MPC and the various RCIA's utilizes
a character oriented serial digital format. This format consists of successive
characters consisting of a start bit, ASCII coded data, a parity bit for error
checking, and a stop bit. Binary data numbers are broken into two four-bit
portions, each one represented by a hexidecimal code (0-F), and transmitted
as two ASCII characters. Data is communicated as groups of characters called
frames. Each frame consists of an opening control character, RCIA number,
character count, command, data checksum, and a closing character.

The types of MPC commands and RCIA responses that occur in the system include
the following:

a) Data request in which the MPC is expecting a data response.

b) Command only/test in which no data is expected, but a system or
    test initiation is issued. The RCIA responds with only an
    acknowledgement.

c) Invalid MPC/RCIA transmission in which the RCIA receives a bad
    transmission and sends back a negative response with only an
    acknowledgement.

d) Broadcast which is utilized to command all modules simultaneously.
    This will be utilized for commands such as concentrator stow in
    conditions of high wind, etc. No RCIA response is allowed to a
    broadcast transmission.

The data link protocol selection was made to yield flexibility and minimize
implementation risk. The character oriented approach with ASCII coding
permits the use of conventional equipment for testing purposes. Data to be
transmitted is within the 9600 baud rate practical limit of character-
oriented protocols.

The ROP has been developed utilizing a Tektronix 8002 development system
shown in Figure 36 . This system facilitates program development by offering
operator interfaces, storage, editing, macro-assembling, and high-level
languages. In addition, the system includes an in-circuit emulator probe and
trace to allow monitoring of bus activity and CPU registers during real-time
program execution. Also shown in the figure is a PCA simulator box developed
for software debugging and system checkout. The simulator supplies switches
to provide discrete inputs, lights to display discrete outputs, analog signal
sources, and an active filter network to simulate the engine flow control
loop characteristics. In addition, a micro-terminal box was utilized to allow
the data link to be exercised without the MPC.

ENERGY TRANSPORT SUBSYSTEM (ETS)

The ETS is comprised of 1) a conventional dc electric system which inter-
connects each power module, 2) central static dc-to-ac inverter(s) for power
conditioning and voltage/load control and, 3) associated equipments for grid
interfacing and synchronization. The system is designed to operate at

600 volts dc, interfacing with a 4800 volt (typical) utility distribution line. Facility power is used to drive the individual concentrators, PCS accessories and the control room; an uninterruptable power supply (UPS) is provided for power when the grid is out and self-generated power is not sufficient to operate the system. A load bank is also provided to dissipate excess energy during grid out/concentrator de-track operation. The major benefit of the dc approach is that is permits the speed of the ORC engines to be varied with the change in solar insolation in order to achieve high part-load efficiency and hence high annualized performance. In addition, the use of the central inverter for voltage/load control eliminates any need for individual field control of the alternators, as discussed below. Also, grid synchronization in frequency and phase is simplified since an ac system would require synchronization of each engine whereas this system is accommodated at the central point of grid contact.

The sinewave inverter is a bridge type SCR power switching regulator. It consists of a QUASIsquare wave inverter and a filter which forms the output waveform; Figure 37 is a picture of the actual hardware, which has successfully completed all qualification testing. The inverter is a self-commutating type unit. Capacitors and inductors are used for commutation of the SCR's and an AC filter is provided consisting of a series element and shunt LC networks.

The square wave output of the inverter is fed into a filter element. There is also a resonant LC circuit which resonates at three times the output frequency of the inverter, minimizing the third harmonic output voltage. Resonant circuits are also used to reduce the fifth harmonic and the seventh harmonic. The square wave inverter and the AC filter are combined to provide a sinewave output. The utility voltage is sampled and fed back, through an isolation transformer, to the control circuit thereby synchronizing the inverter circuits with the utility line. The input voltage is sampled and fed to the control circuits to provide a constant input voltage regardless of input current. This results in providing the proper load on the ORC turbine; appropriate status signals are provided to the MPC.

CONCLUSIONS

Tests conducted to date show all elements of the Small Community Solar Thermal Power System to be performing quite well and should continue to do so when operated on the TBC at the Edwards AFB test site. Note further that the completely autonomous plant control subsystem should have very broad applications, regardless of the type of heat engine or point focus concentrator employed.
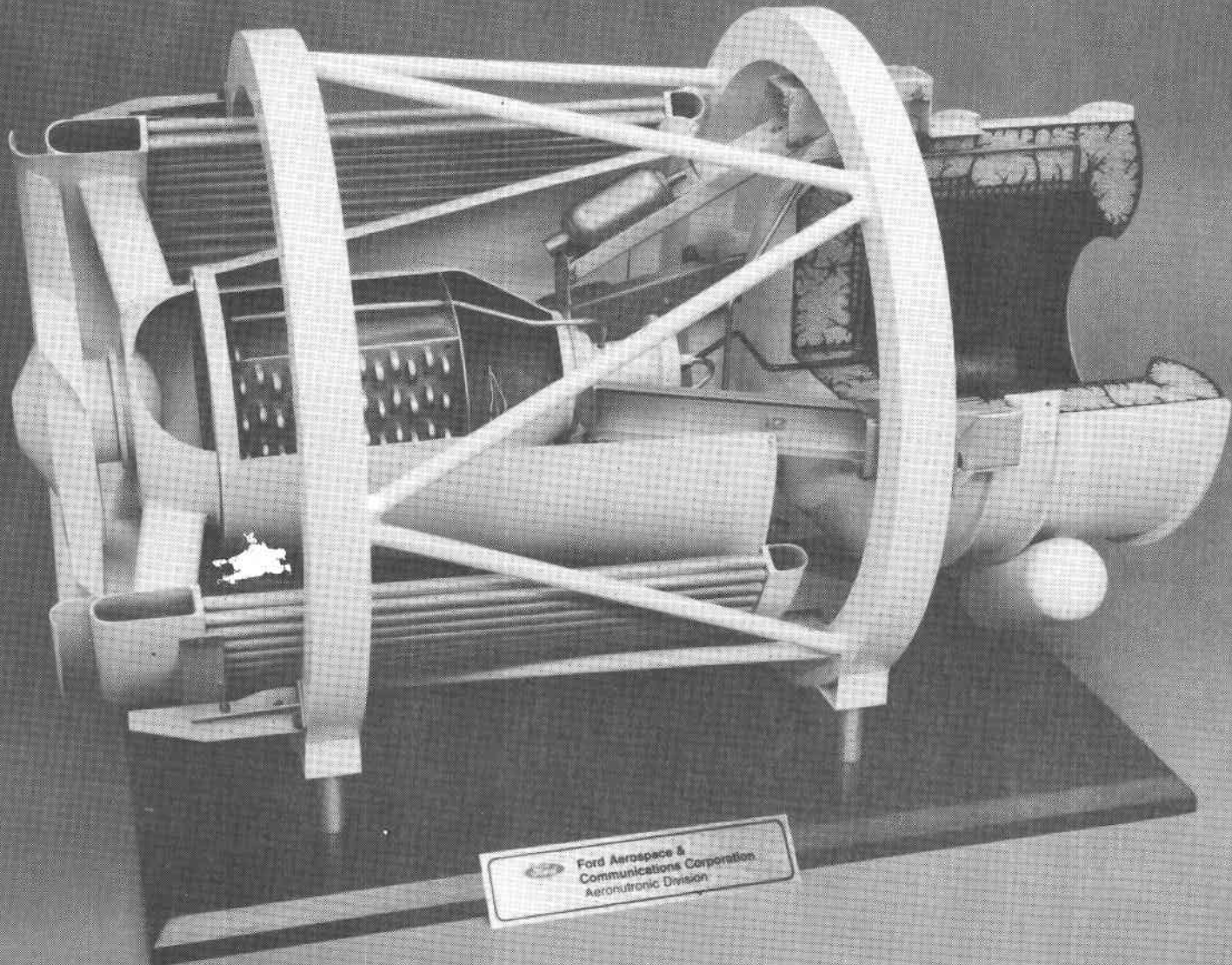
FIGURE 1. ENGINEERING MOCK-UP OF POWER CONVERSION ASSEMBLY (PCA)
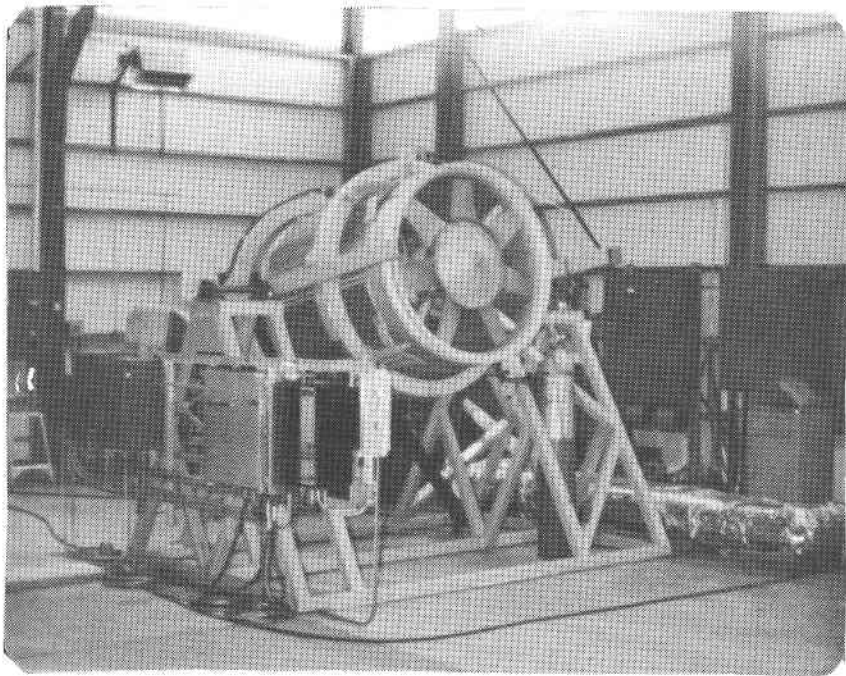
FIGURE 2.   ORC POWER CONVERSION SUBSYSTEM (PCS) UNDER TEST AT BARBER-NICHOLS
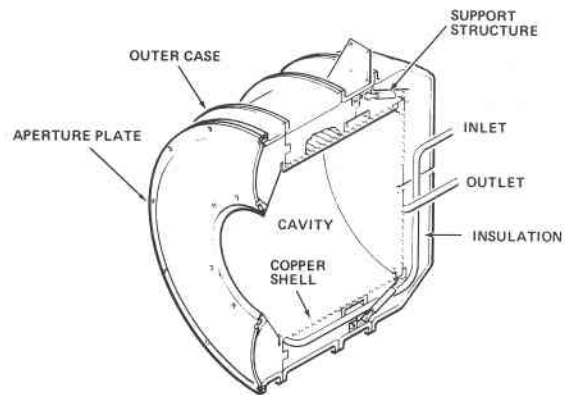
FIGURE 3.   CUT-AWAY VIEW OF RECEIVER ASSEMBLY
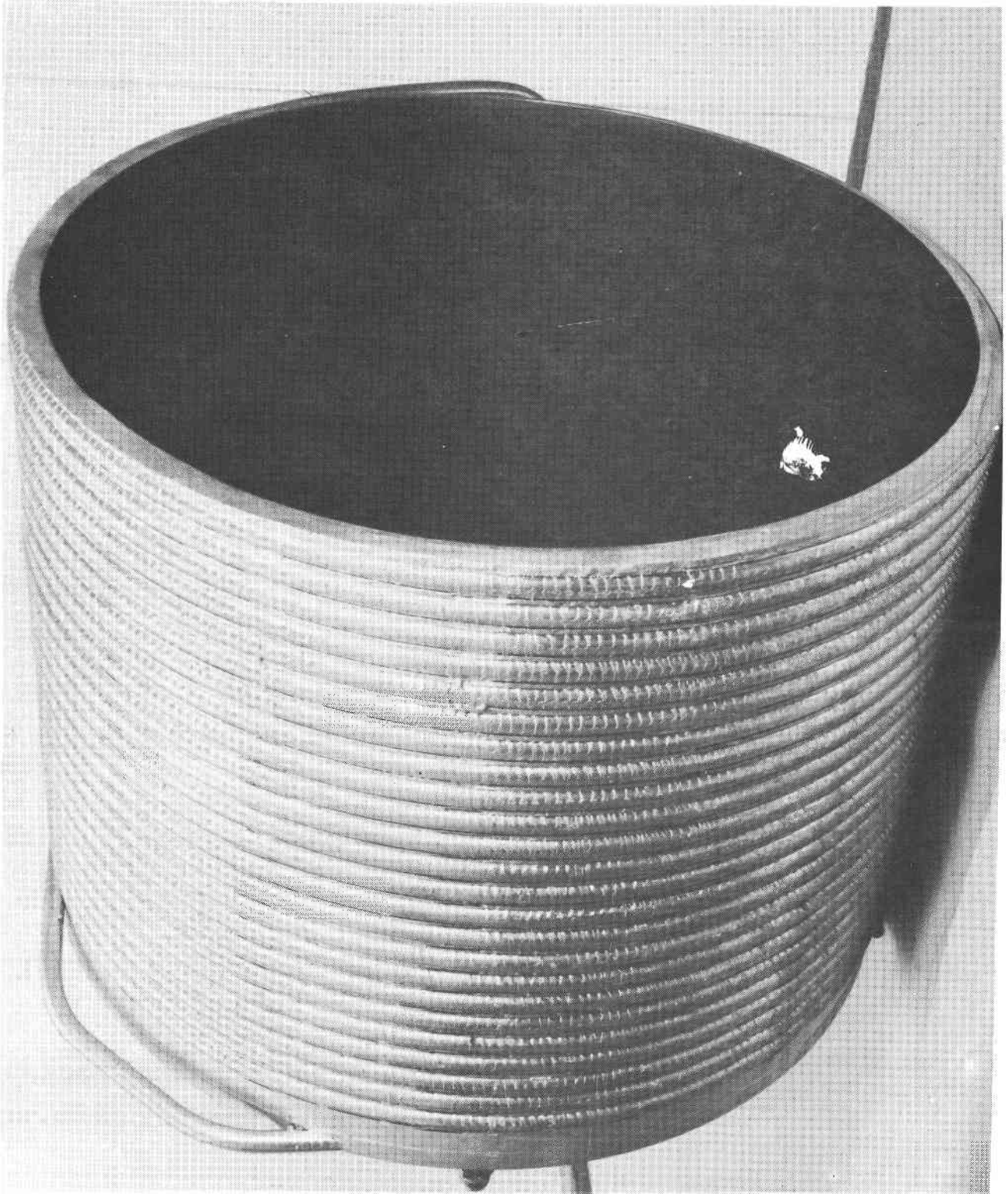
FIGURE 4. ORC RECEIVER CORE SHOWING BRAISED STAINLESS STEEL TUBING
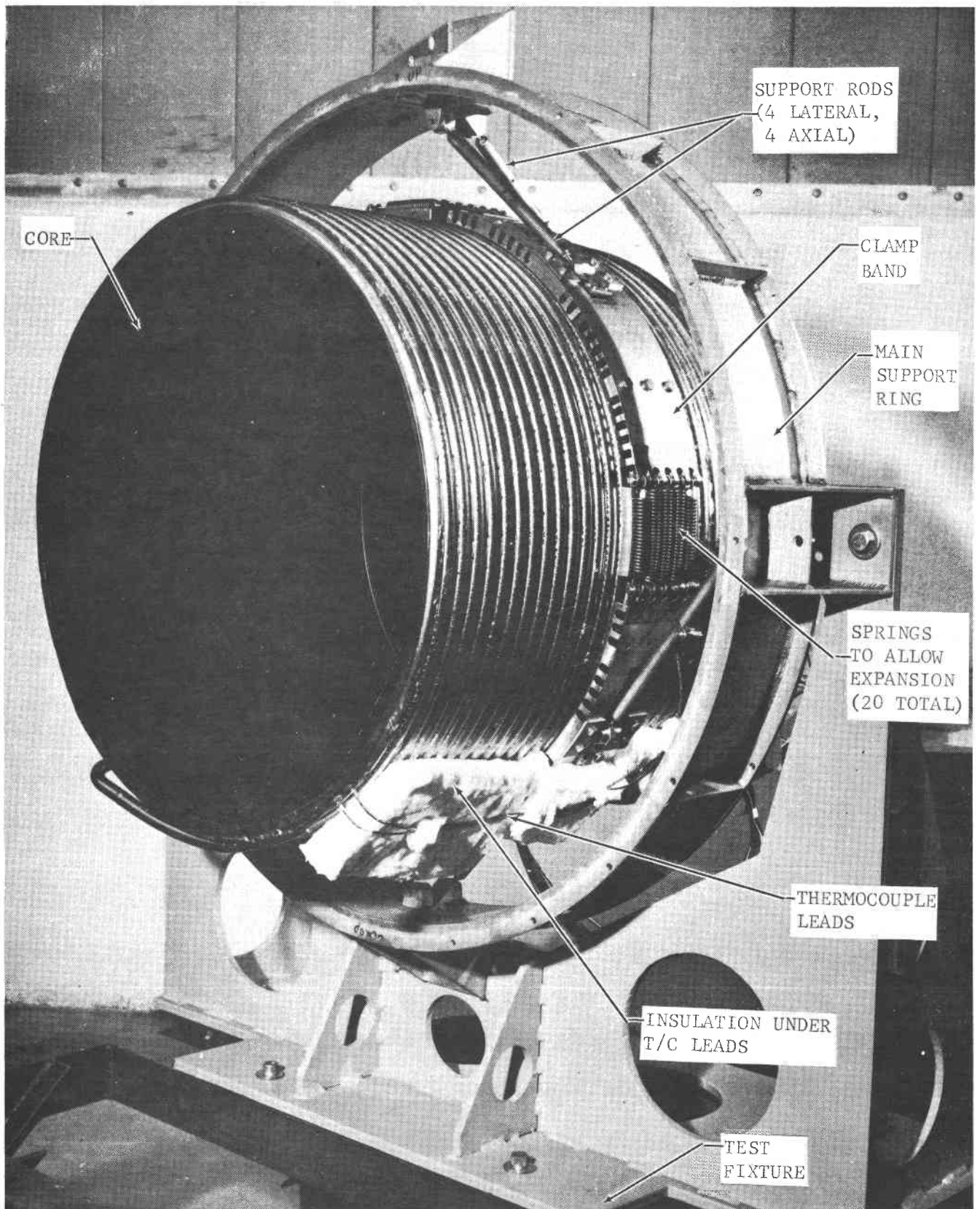
FIGURE 5.   FRONT VIEW OF RECEIVER WITH INSULATION AND APERTURE PLATE REMOVED, SHOWING SUPPORT STRUCTURE.
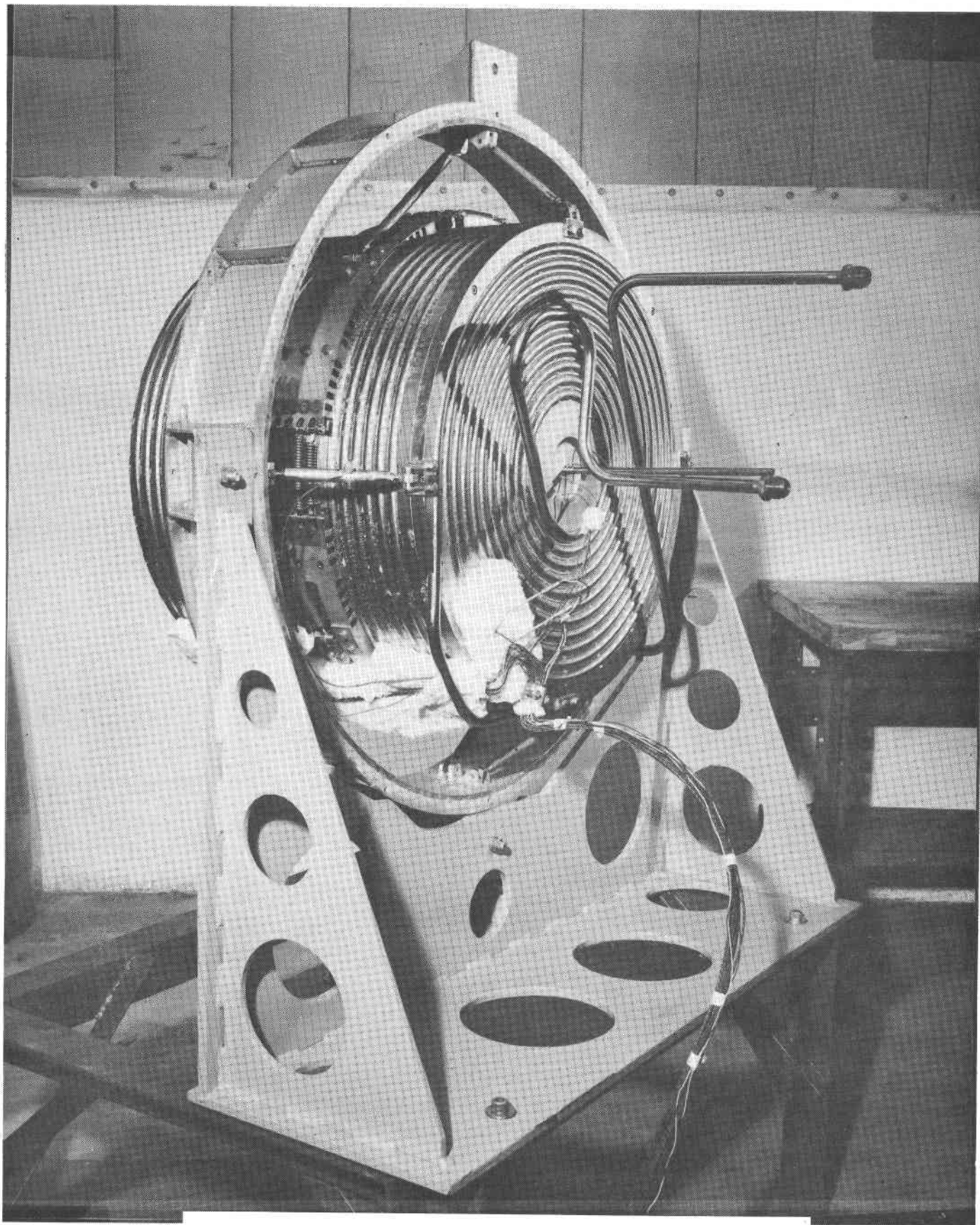
FIGURE 6. REAR VIEW OF RECEIVER CORE AND SUPPORT STRUCTURE

74
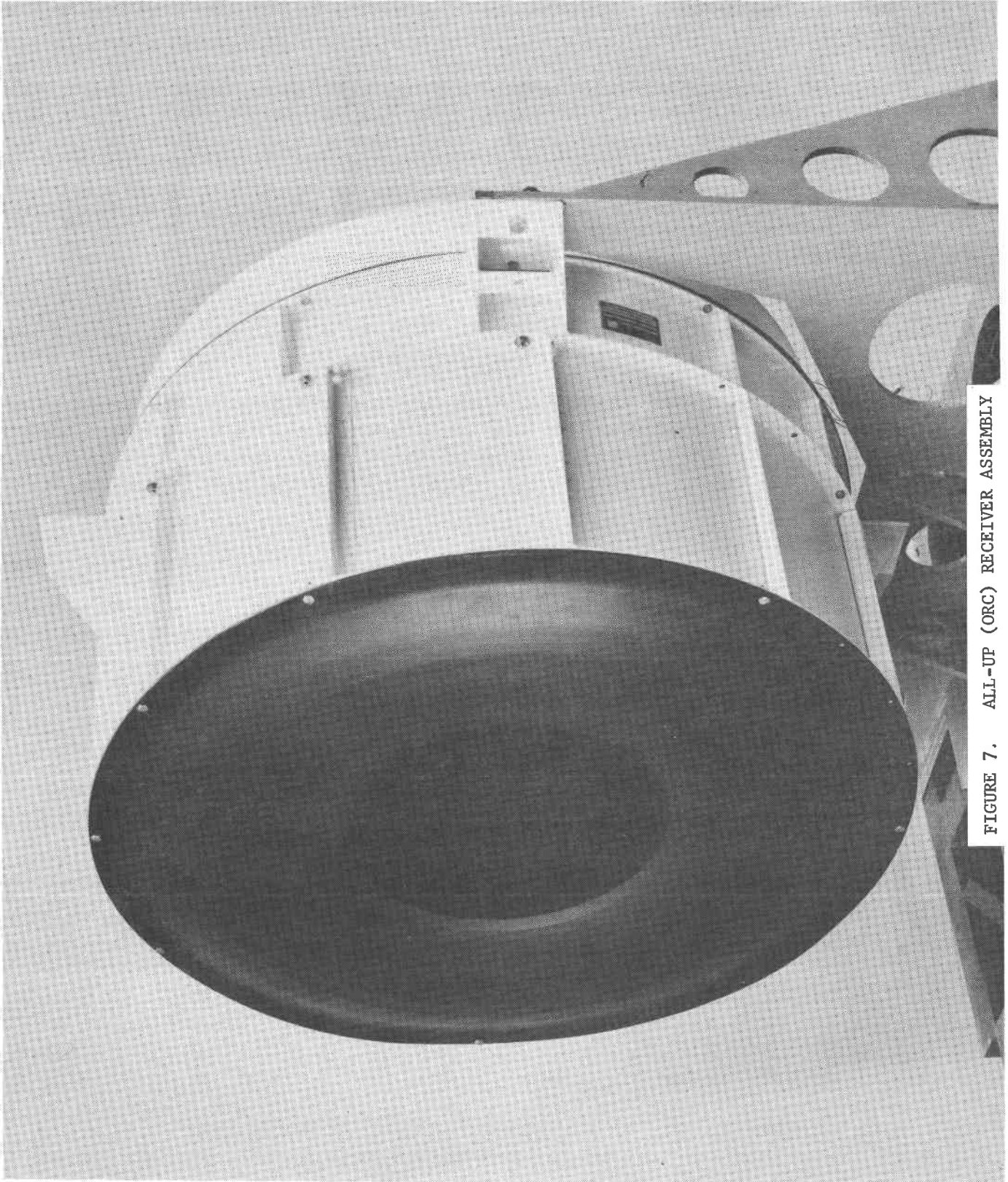
FIGURE 7. ALL-UP (ORC) RECEIVER ASSEMBLY
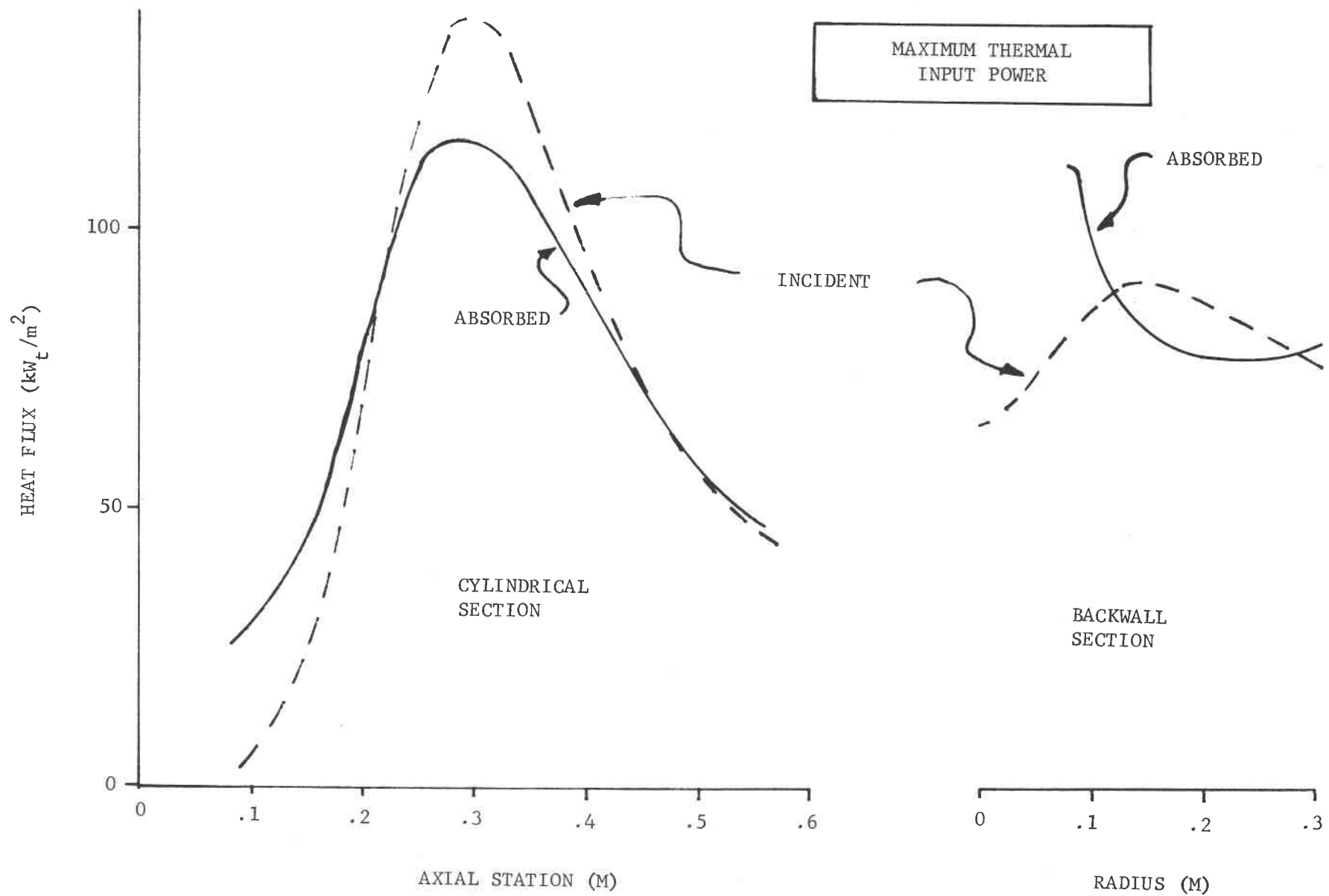
FIGURE 8. PREDICTED CAVITY THERMAL FLUX DISTRIBUTIONS
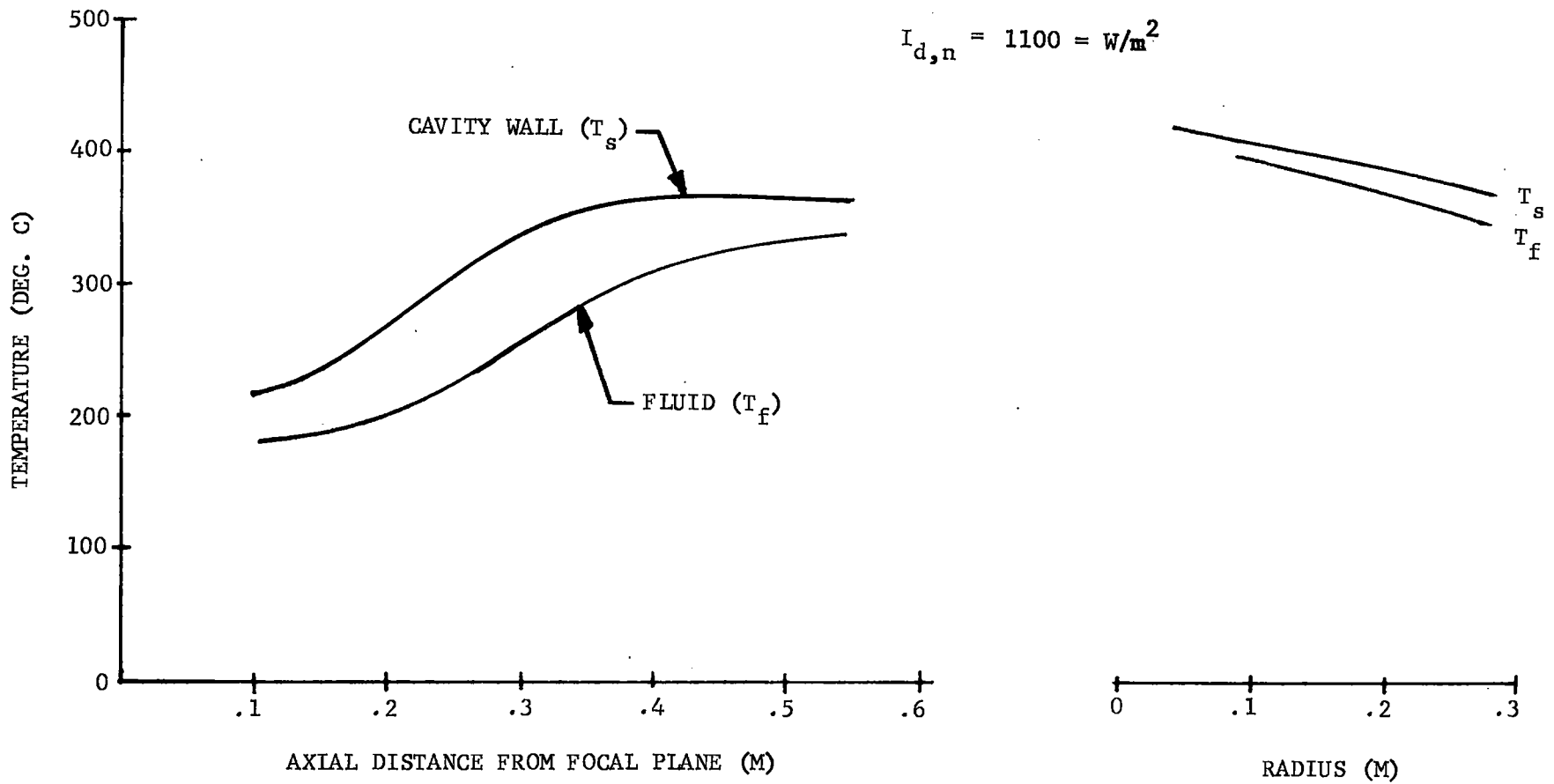
FIGURE 9. PREDICTED COPPER SHELL AND FLUID TEMP: PROFILES AT MAXIMUM
DESIGN CONDITIONS
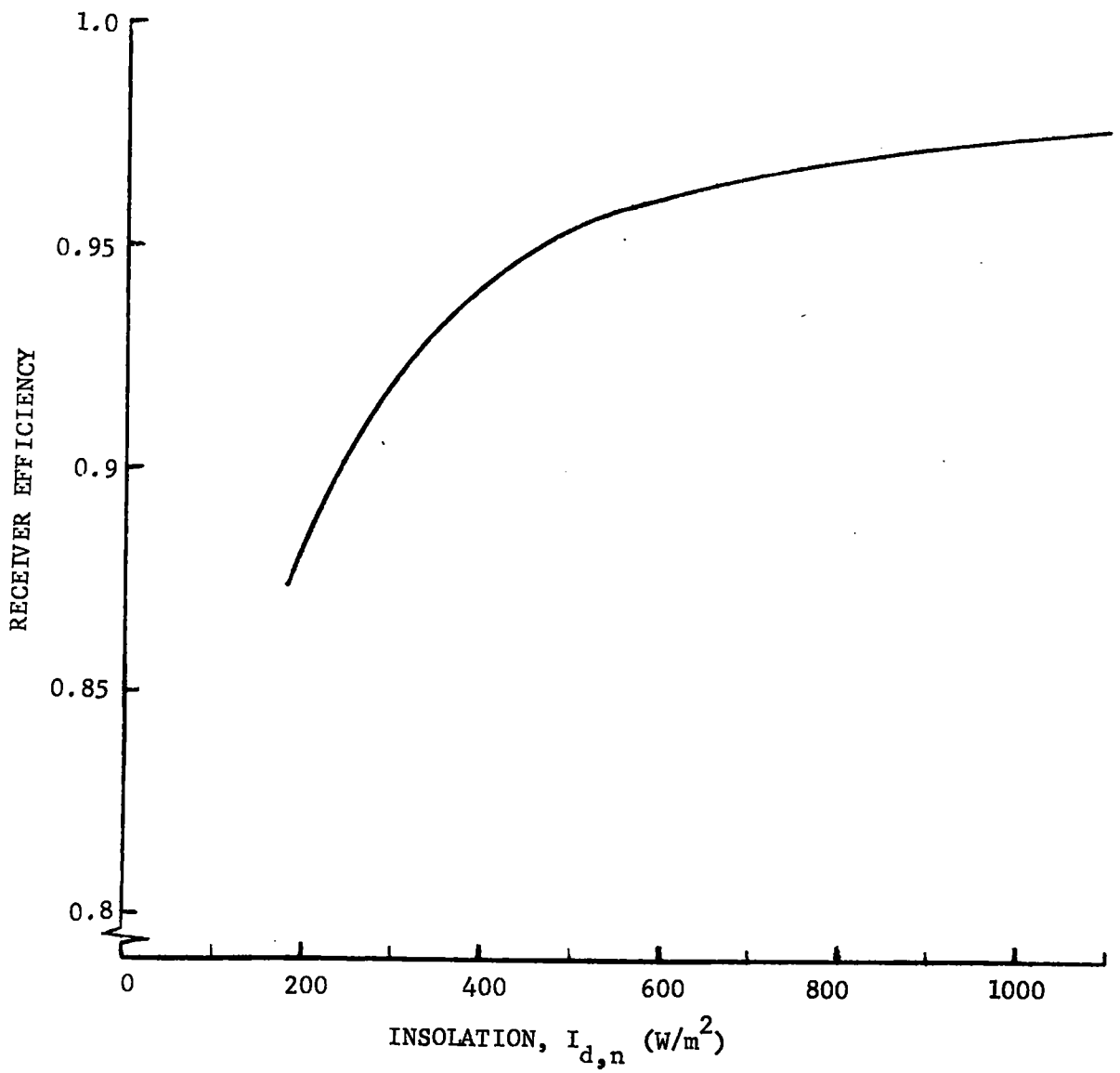
FIGURE 10.   PREDICTED RECEIVER EFFICIENCY

GAUSSIAN FLUX DISTRIBUTION

$3\sigma_{PTG}$

LIP RING

δ SHELL

a, ϵ

SHELL

FOCAL PLANE

CAVITY INSULATION

D_{PLATE}

D_{AP}

RECEIVER AXIS
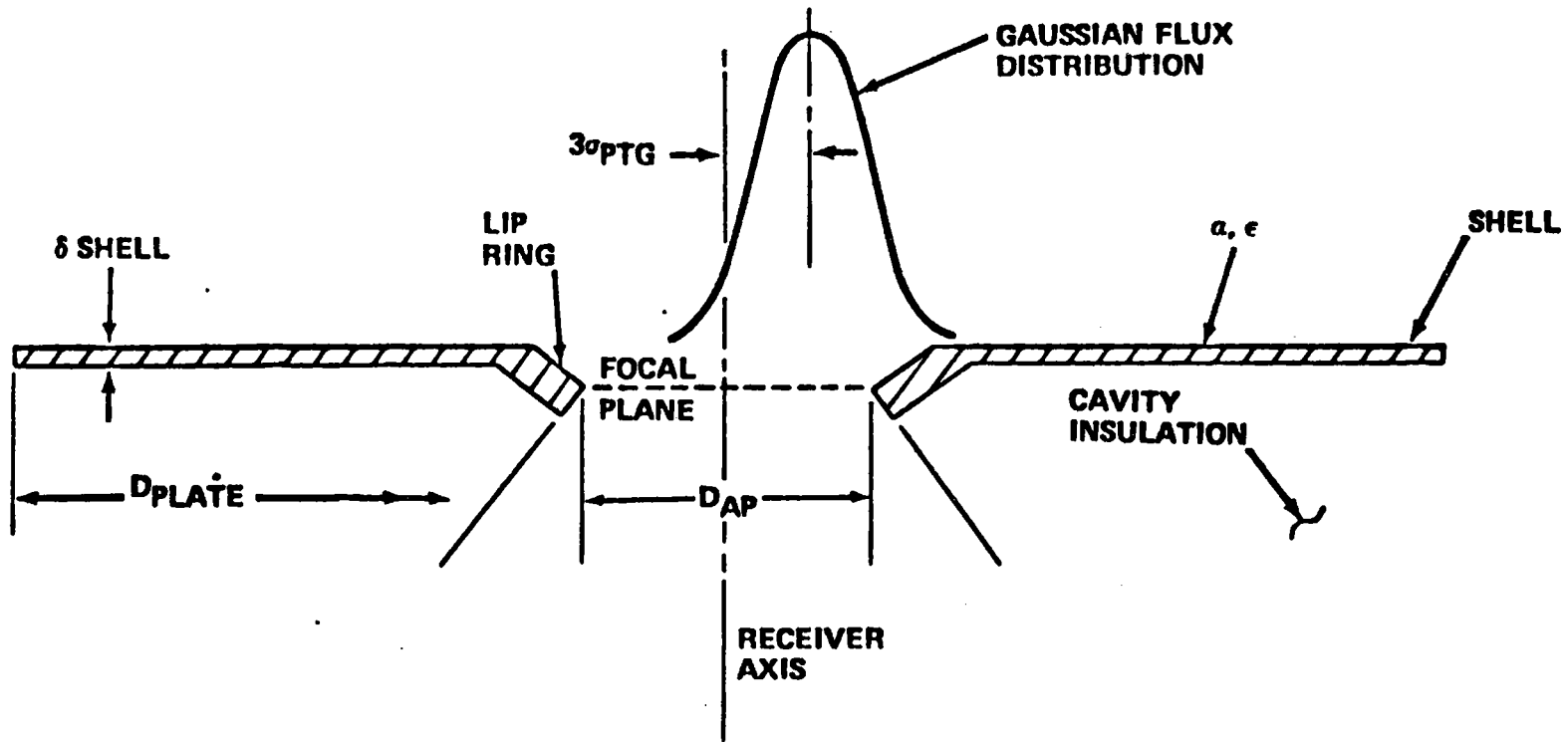
DESIGN LIMIT CONDITIONS

$I_{D,N} = 1100 \ W/M^2$ $T_{AMB} = 28^\circ C$

$\rho_{DISH} = 0.82$ $K_{DUST} = 1.0$ $K_{BLOCK} = 0.932$

$\sigma_{SUN} = 2.176 \ MR$ $\sigma_{SPEC} = 0.62 \ MR$

FIGURE 11.   DIAGRAM OF APERTURE LIP HEATING MODEL.
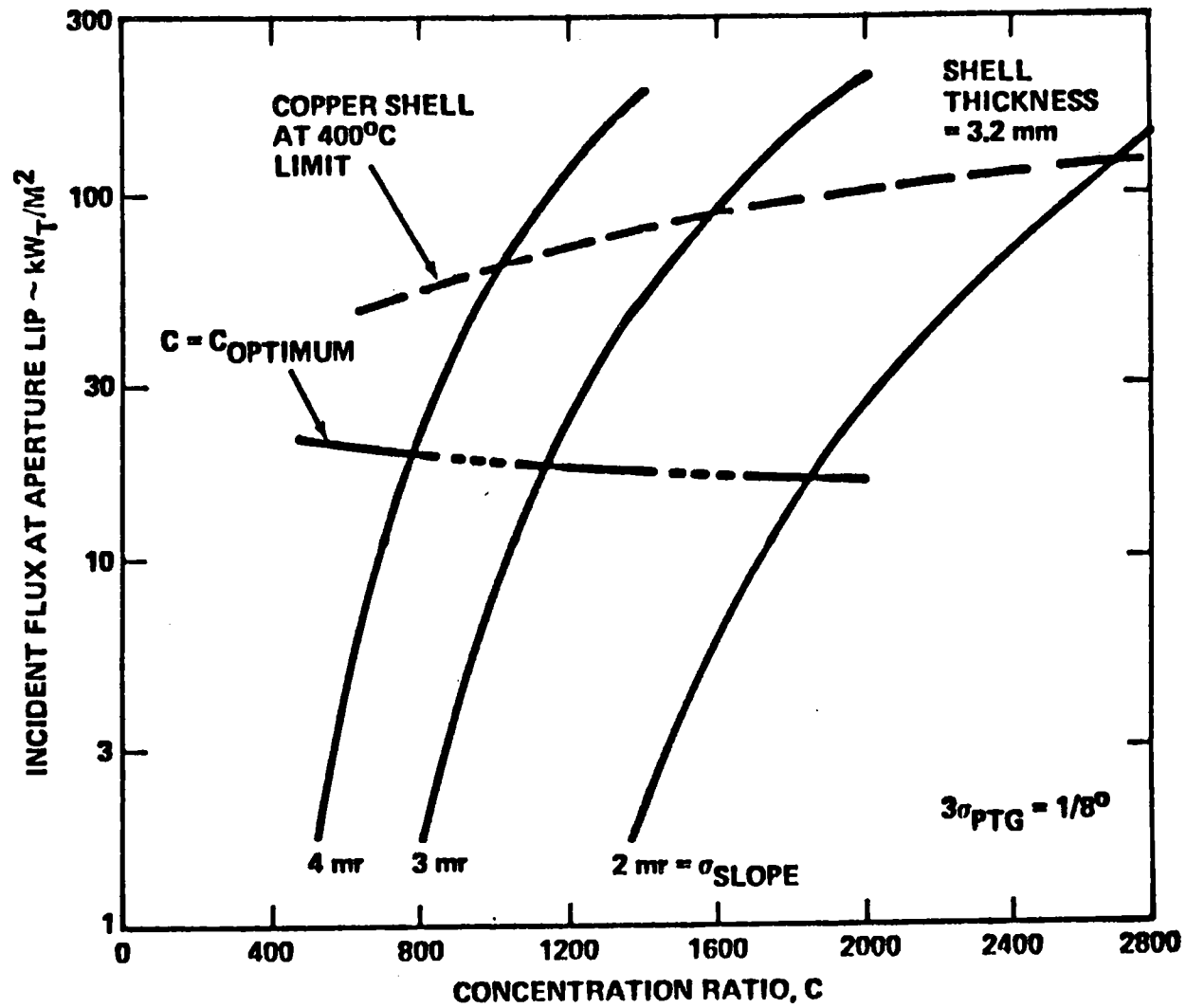
FIGURE 12. LIP HEATING CAPABILITIES FOR COPPER SHELL APERTURE PLATE

FIGURE 13.   THERMAL STRESSES IN THE APERTURE PLATE UNDER TWO OPERATIONAL
ENVIRONMENTS
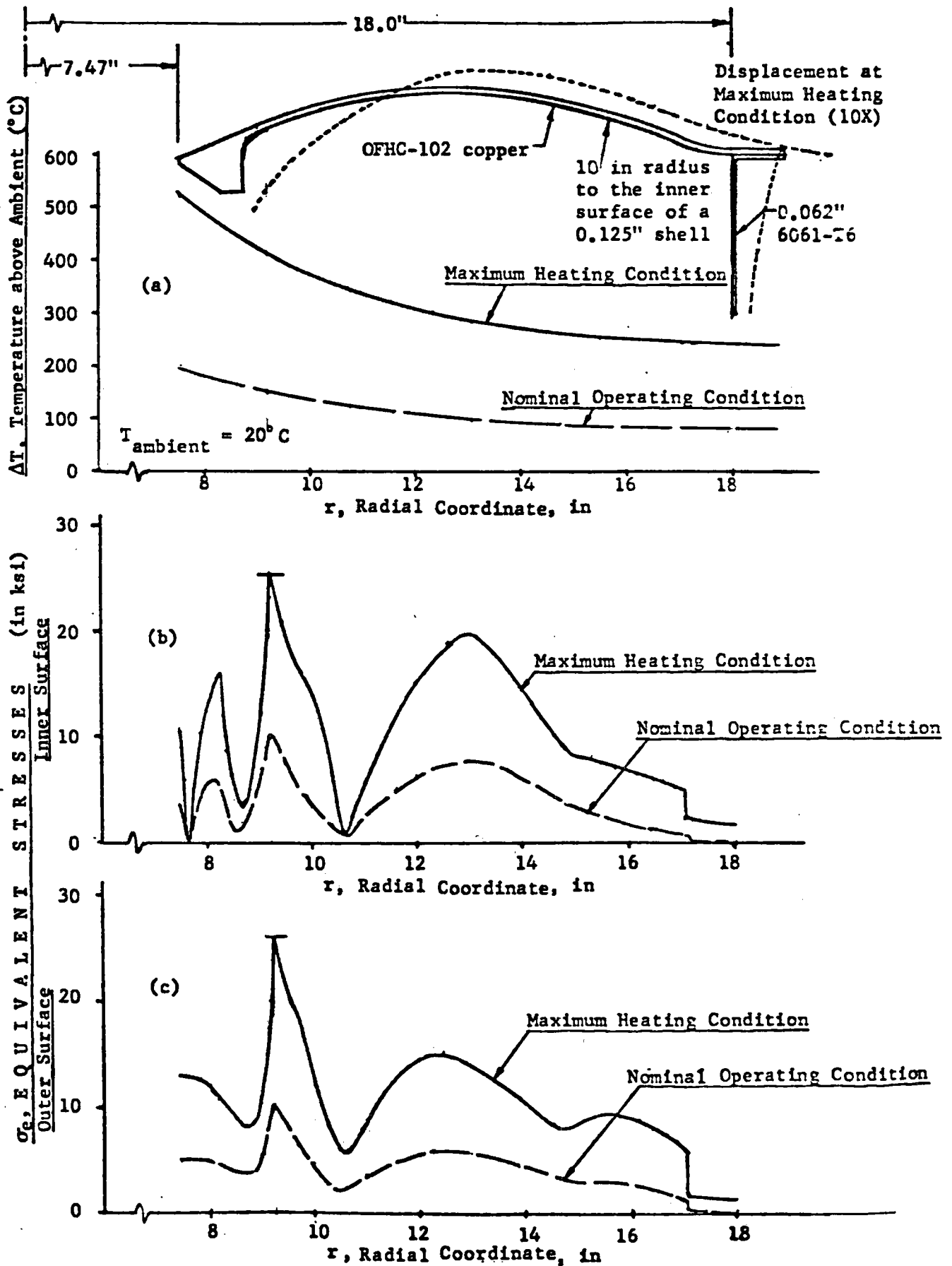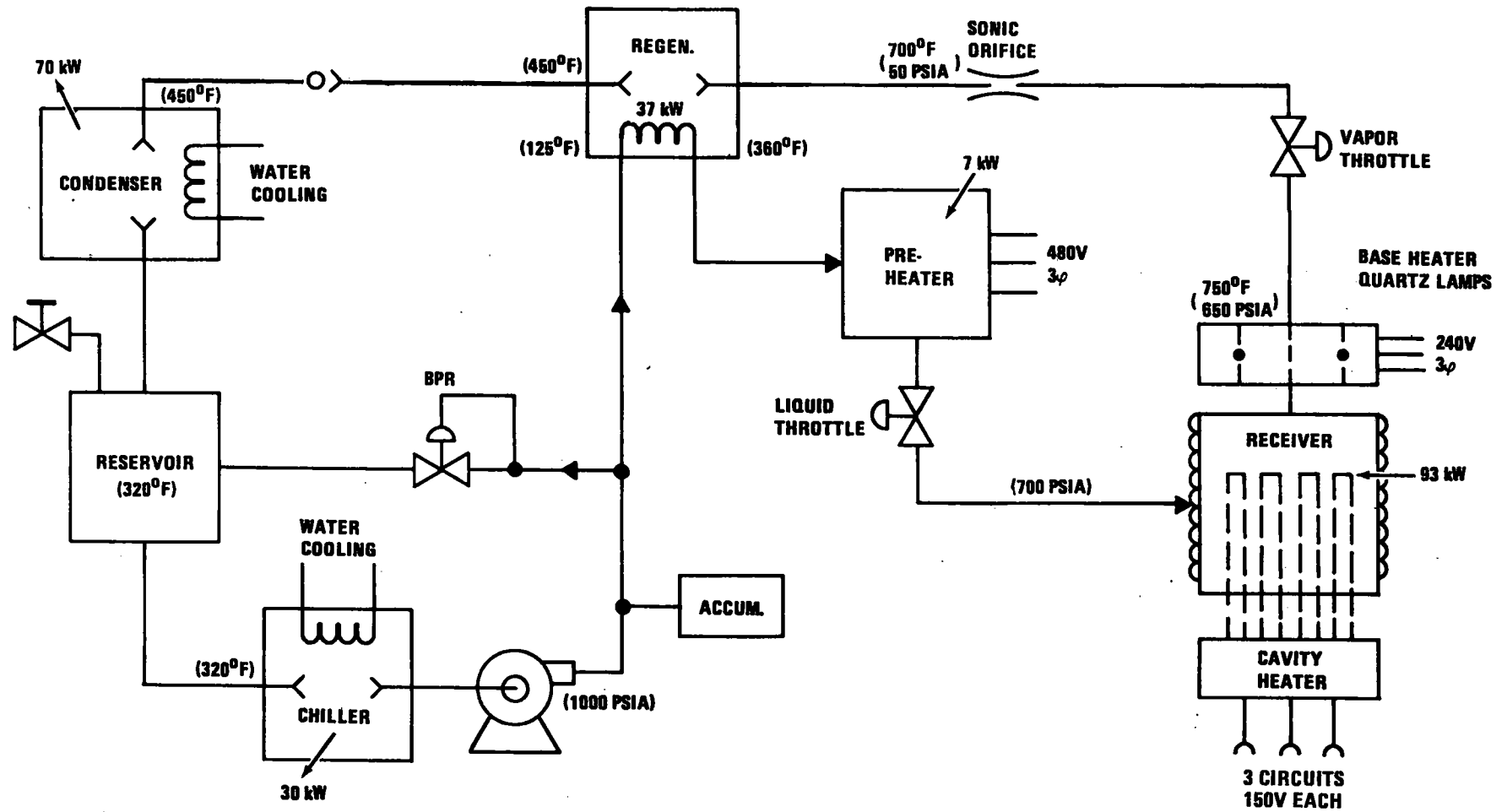
FIGURE 14. ORC RECEIVER TEST LOOP
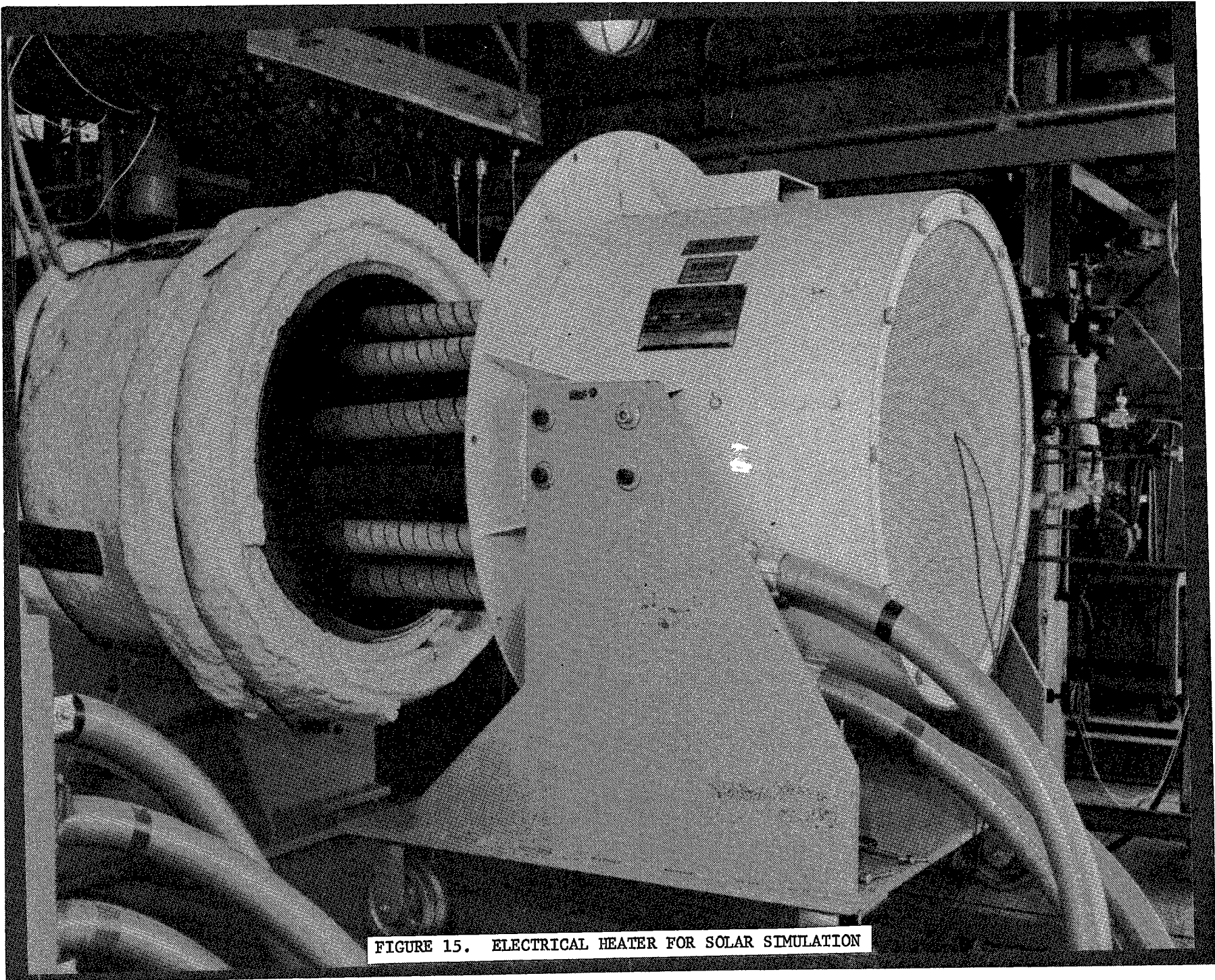
FIGURE 15.   ELECTRICAL HEATER FOR SOLAR SIMULATION

83
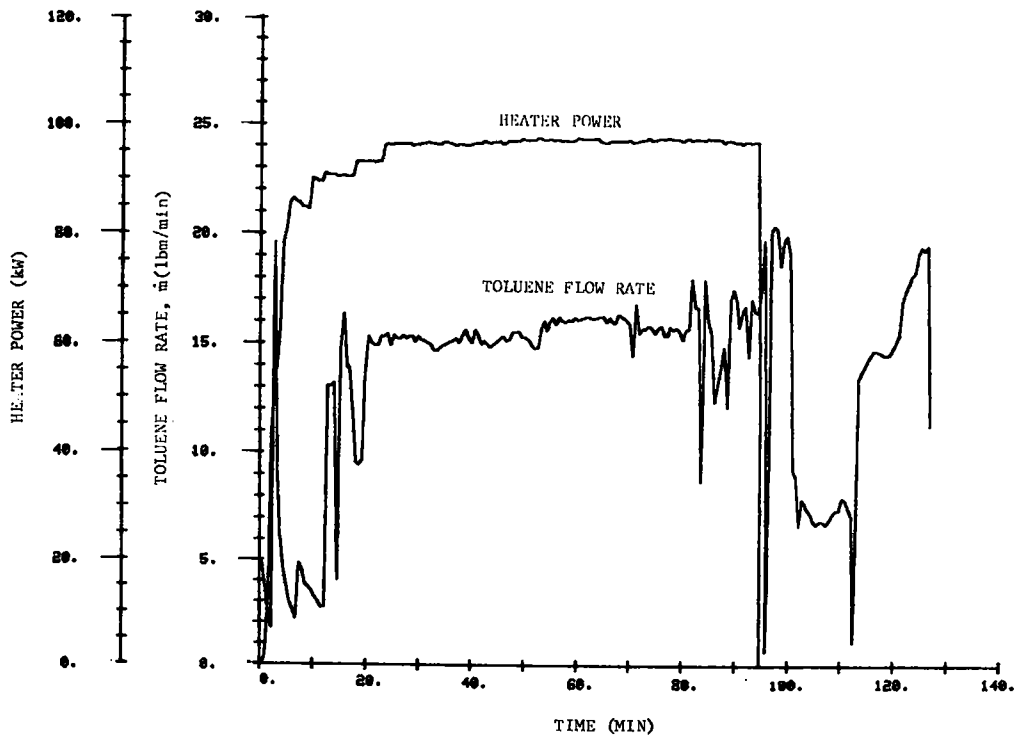
FIGURE 16. CAVITY HEATER POWER AND TOLUENE FLOW RATE HISTORIES DURING THE THERMAL/STRUCTURAL PROOF TEST
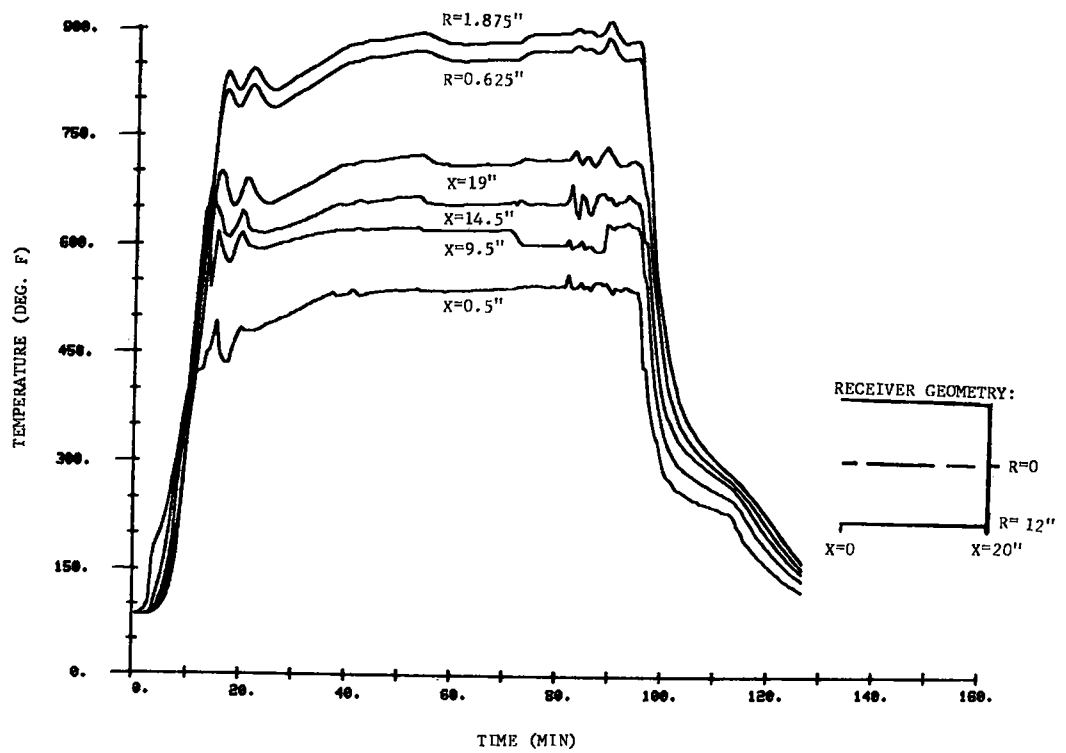
FIGURE 17. RECEIVER CORE TEMPERATURE HISTORY DURING THE THERMAL/STRUCTURAL PROOF TEST

84
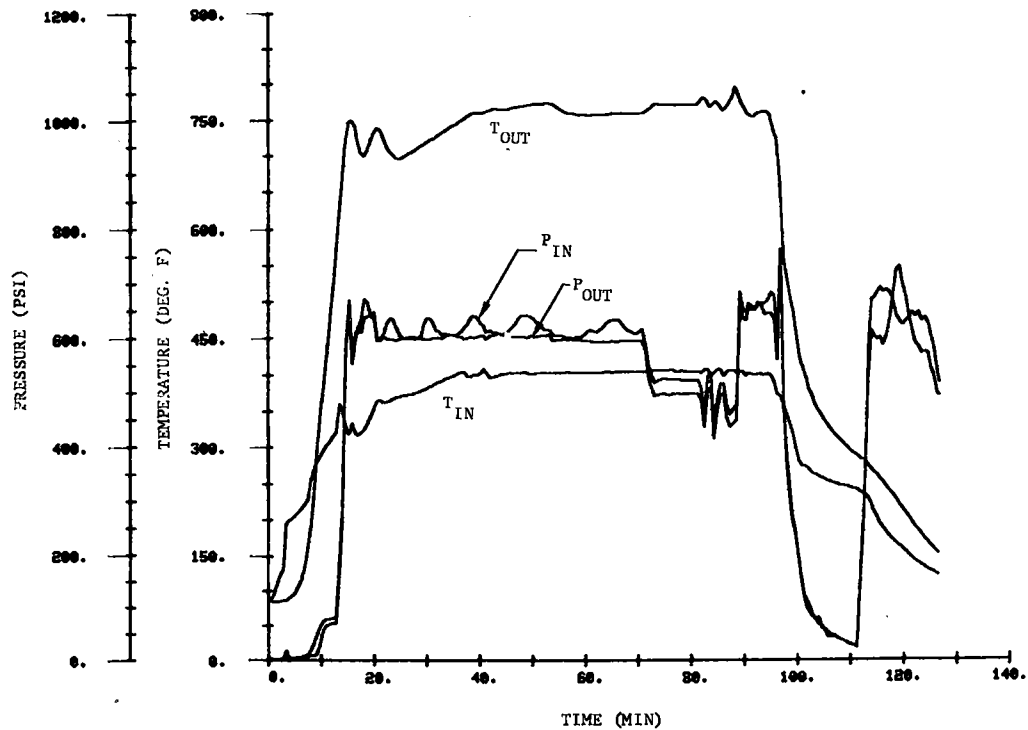
FIGURE 18. TOLUENE TEMPERATURE AND PRESSURE HISTORIES AT THE RECEIVER INLET
AND OUTLET DURING THE THERMAL/STRUCTURAL PROOF TEST
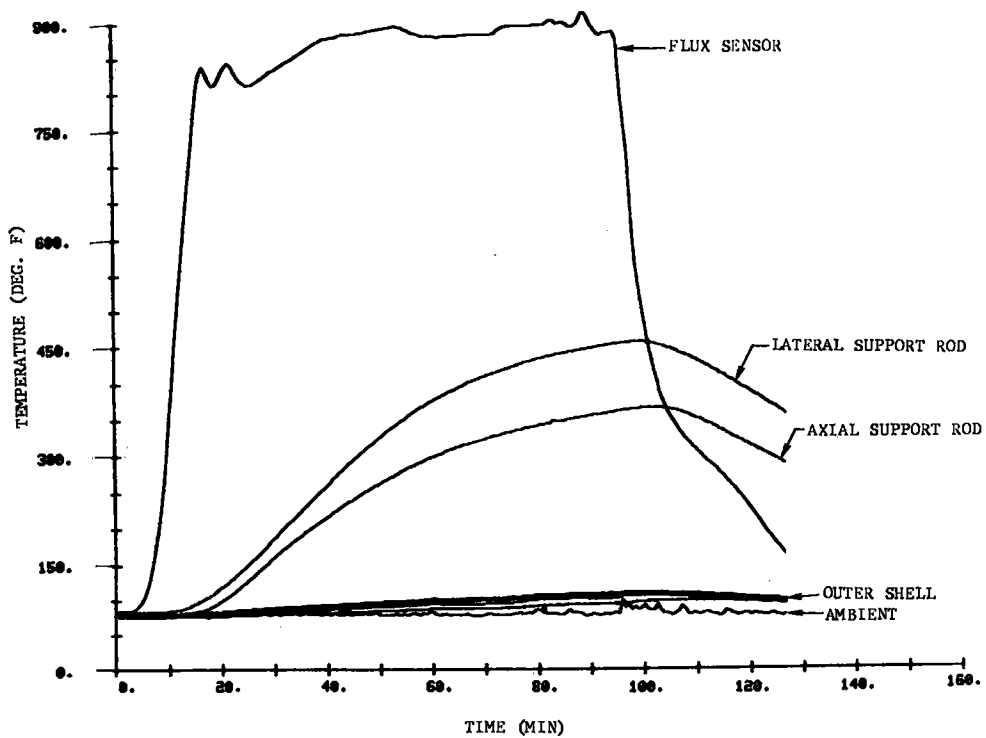
FIGURE 19. TEMPERATURE HISTORIES FOR SELECTED LOCATIONS ON THE RECEIVER
ASSEMBLY DURING THE THERMAL/STRUCTURAL PROOF TEST
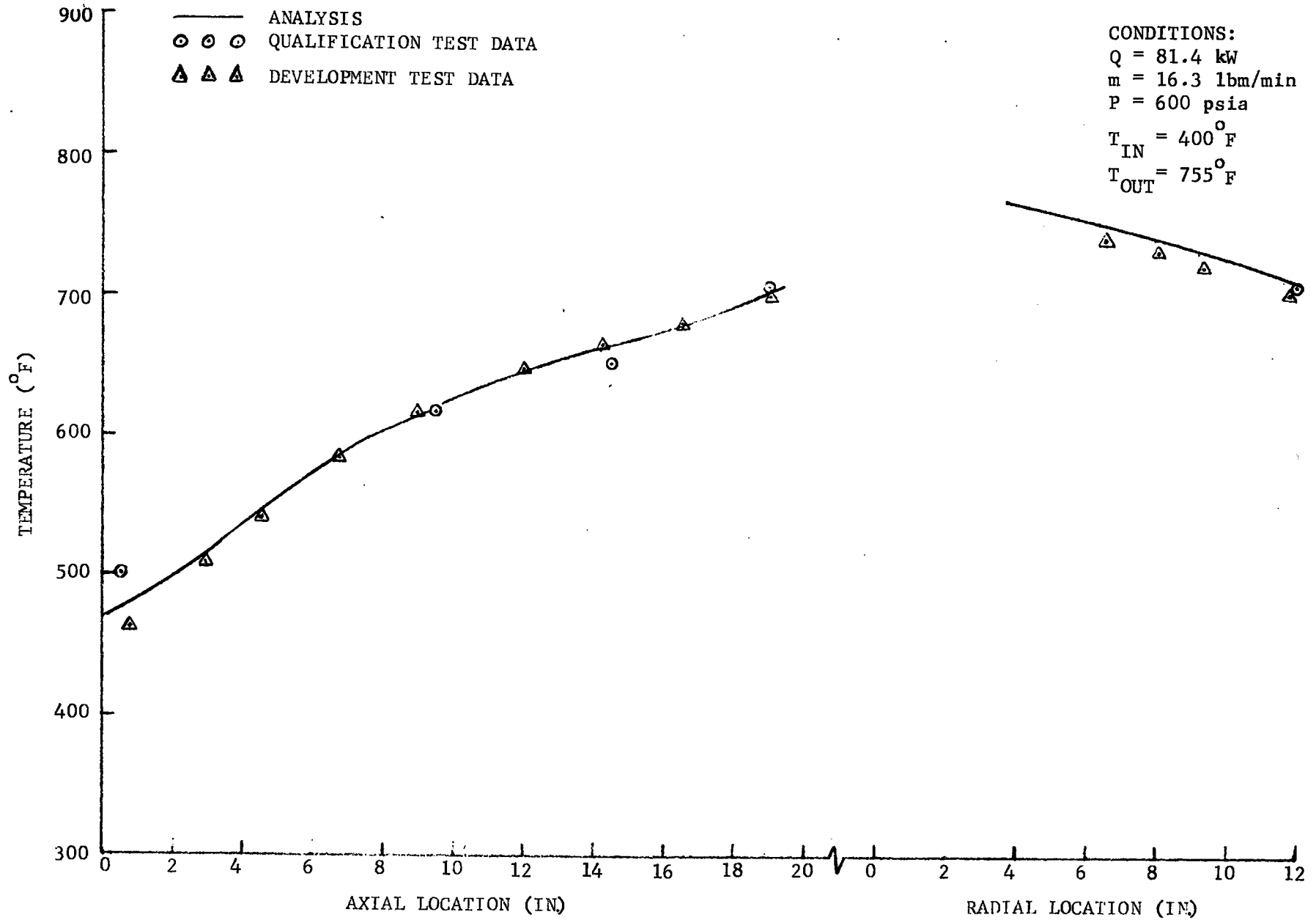
FIGURE 20. COMPARISON OF MEASURED AND PREDICTED RECEIVER CORE TEMPERATURE PROFILES
FOR THE THERMAL/STRUCTURAL PROOF TEST

TABLE I. OPERATING CONDITIONS FOR THE PERFORMANCE VERIFICATION TESTS

SS RUN	CAVITY HEATER PWR (kW)	TOLUENE FLOW RATE (LBM/MIN)	RECEIVER CONDITIONS			PWR TO FLUID* (kW)	HEAT LOSS (kW)
			PRESSURE (PSI)	TEMP AT INLET ($^\circ$F)	TEMP AT OUTLET ($^\circ$F)		
1	16.0	3.0	465	400	735	14.8	1.2
2	32.0	6.0	733	399	754	29.0	3.0
3	35.0	6.4	620	400	750	31.6	3.4
4	35.0	5.9	450	401	746	29.6	5.4
5	35.5	6.1	570	404	741	29.6	5.9
6	38.0	6.5	660	404	755	31.9	6.1
7	38.5	6.3	485	405	755	31.7	6.8
8	51.5	8.3	580	403	758	41.8	9.7
9	61.0	12.0	630	405	745	57.5	3.5
10	64.0	12.1	660	406	749	58.4	5.6
11	96.5	15.5	610	401	757	77.6	18.9
12	96.5	15.6	510	403	767	80.7	15.8
13	97.0	16.3	600	400	755	81.4	15.6

*COMPUTED FROM TOLUENE FLOW RATE AND ENTHALPY.
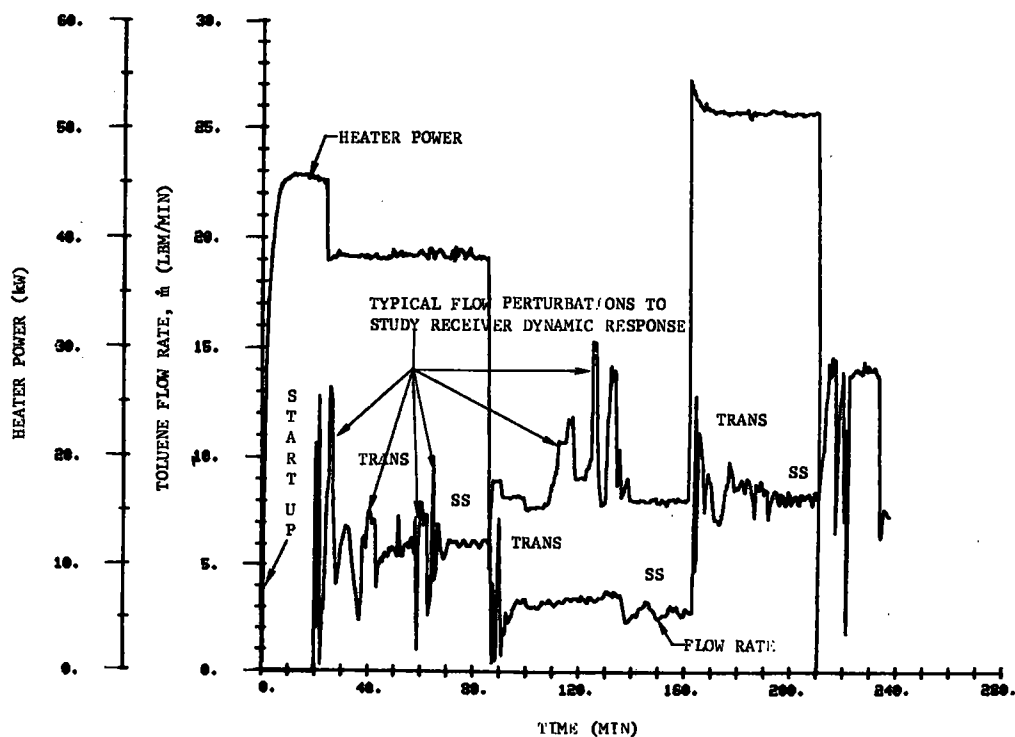
FIGURE 21. CAVITY HEATER POWER AND TOLUENE FLOW RATE HISTORIES DURING A TYPICAL QUALIFICATION TEST
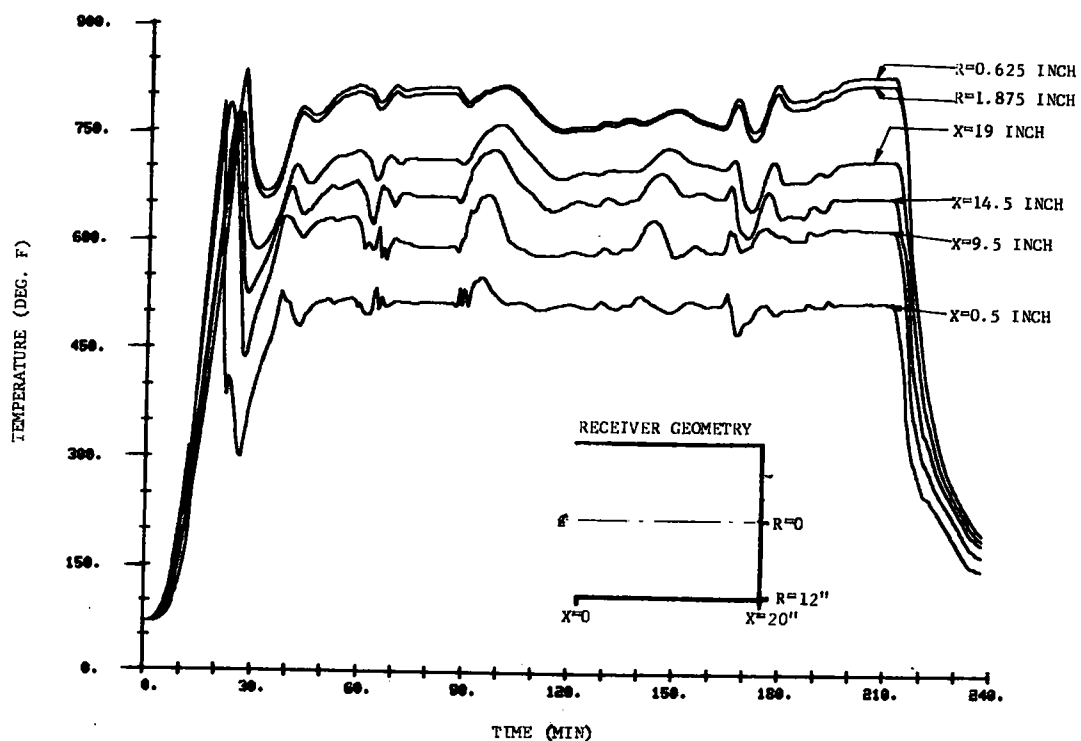
FIGURE 22. RECEIVER CORE TEMPERATURE HISTORY DURING A TYPICAL QUALIFICATION TEST

88
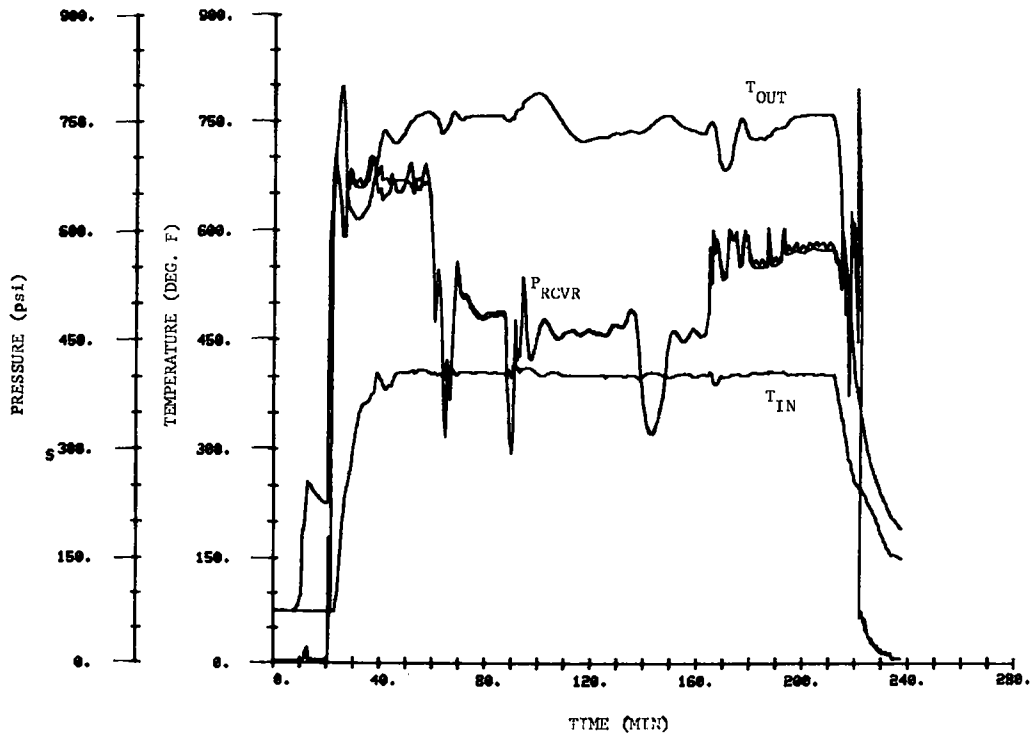
FIGURE 23. TOLUENE TEMPERATURE AND PRESSURE HISTORIES AT THE RECEIVER INLET
AND OUTLET DURING A TYPICAL QUALIFICATION TEST
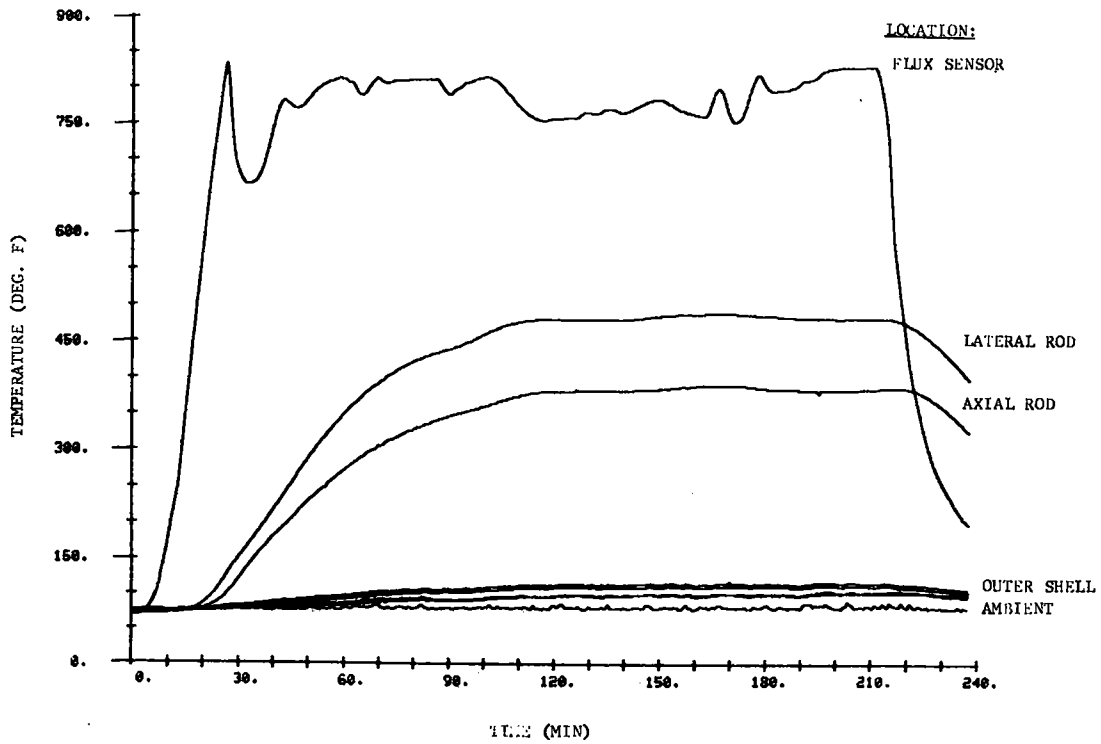
FIGURE 24. TEMPERATURE HISTORIES FOR SEVERAL SELECTED LOCATIONS ON THE
RECEIVER ASSEMBLY DURING A TYPICAL QUALIFICATION TEST
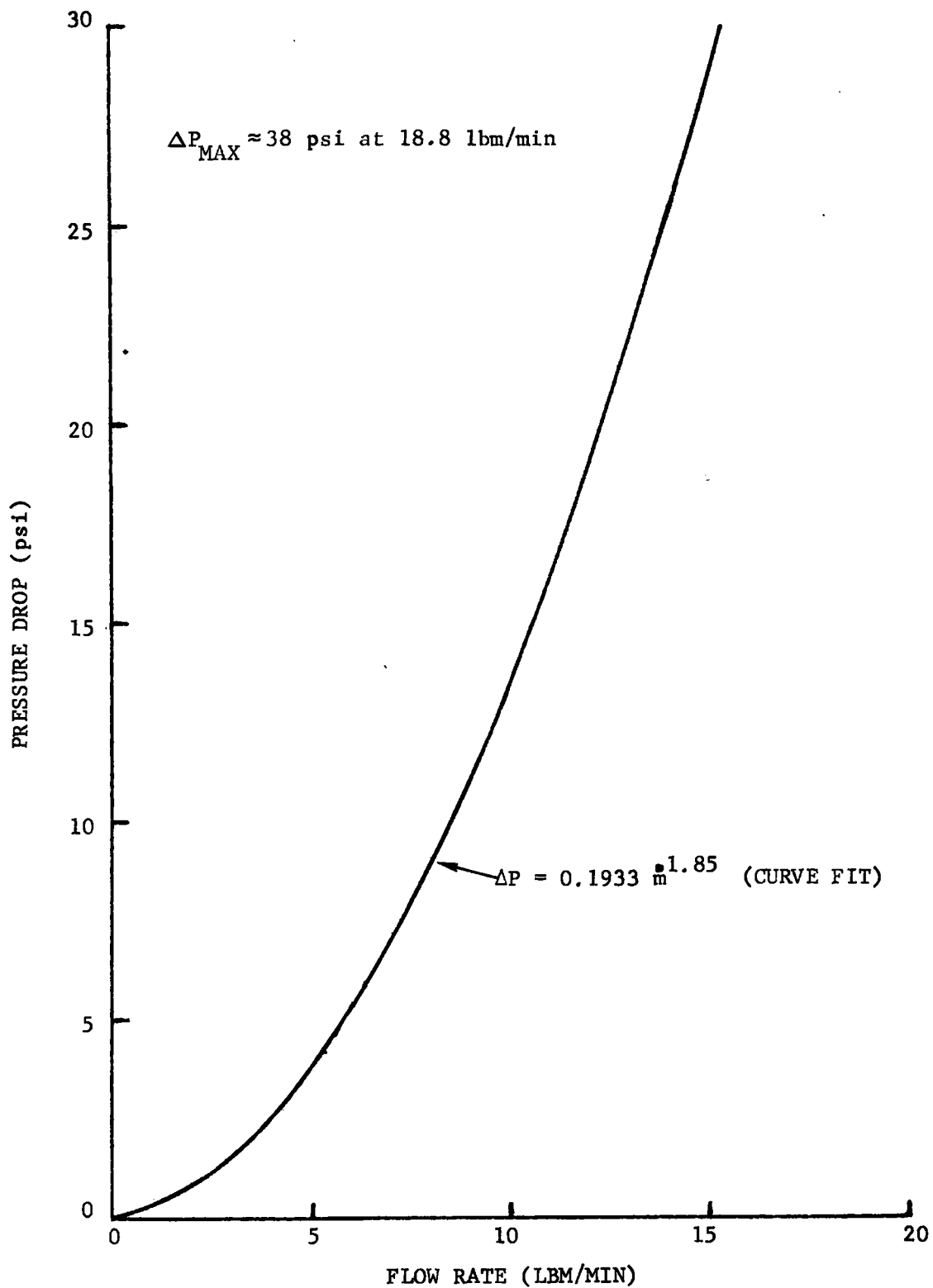
FIGURE 25. PRESSURE DROP THROUGH THE RECEIVER CORE AS A
FUNCTION OF TOLUENE FLOW RATE

90

TABLE II. RECEIVER PERFORMANCE PREDICTIONS

Power Level	Receiver Efficiency (%)	Mean Effective Cavity Temperature (°F)	Reradi- ation Losses (kW)	Con- vection Losses (kW)	Con- duction Losses (kW)	Reflec- tion Losses (kW)
Rated[1]	97.2	648	0.975	0.570	0.294	0.326
Maximum[2]	97.6	658	1.009	0.580	0.295	0.389

CONDITIONS:

   Solar Absorptivity = 0.95
   IR Emissivity = 0.93
   Convective Heat Transfer Coefficient = 16 $W/m^2 - °C$
   Insulation Conductivity = 0.058 $W/m - °C$
   Ambient Temperature = 82°F

Notes:
[1] Rated Power = 77 kW
[2] Maximum Power = 93 kW
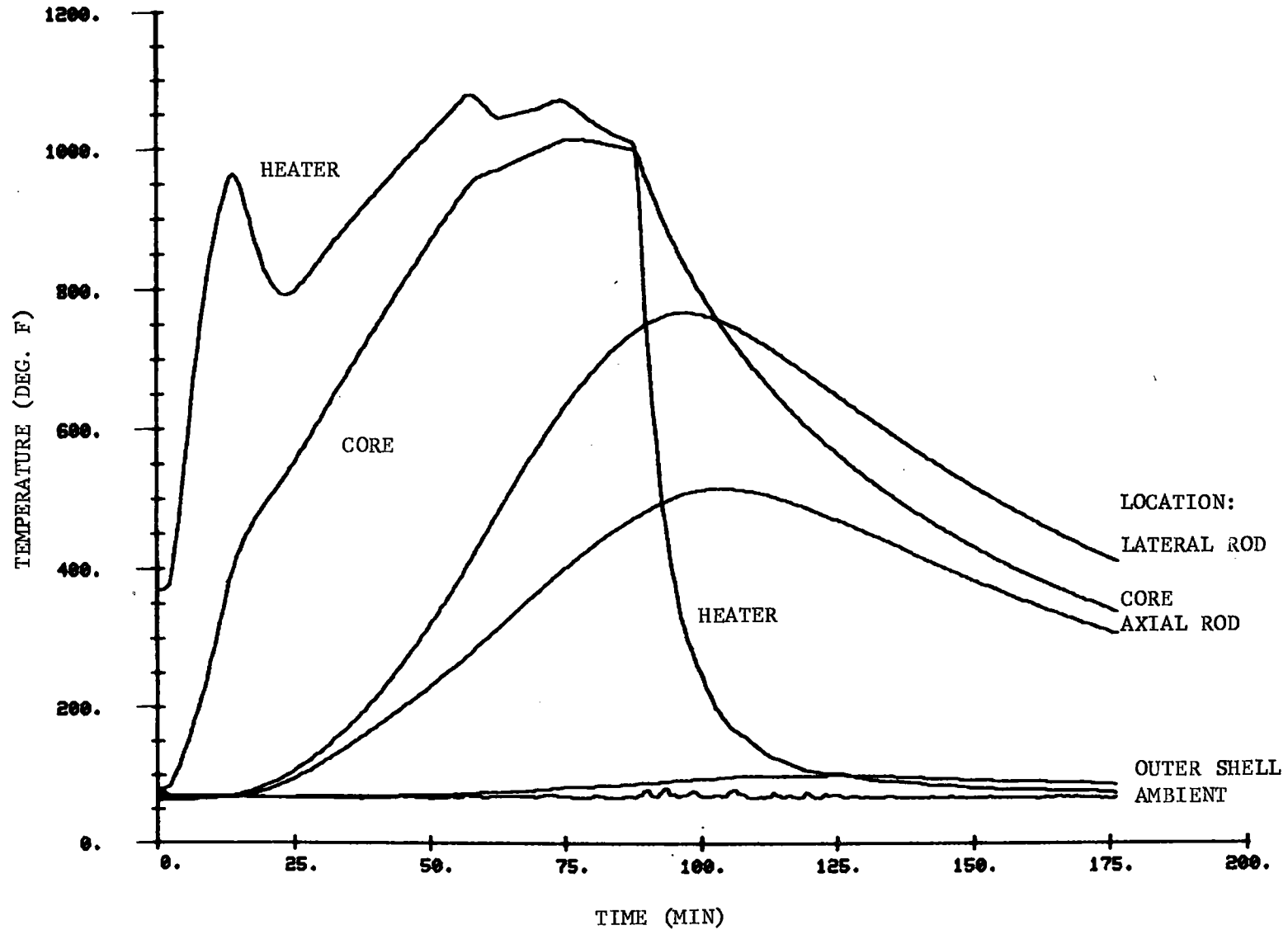
FIGURE 26. TEMPERATURE HISTORY OF HEATER AND RECEIVER DURING THERMAL SURVIVAL TEST
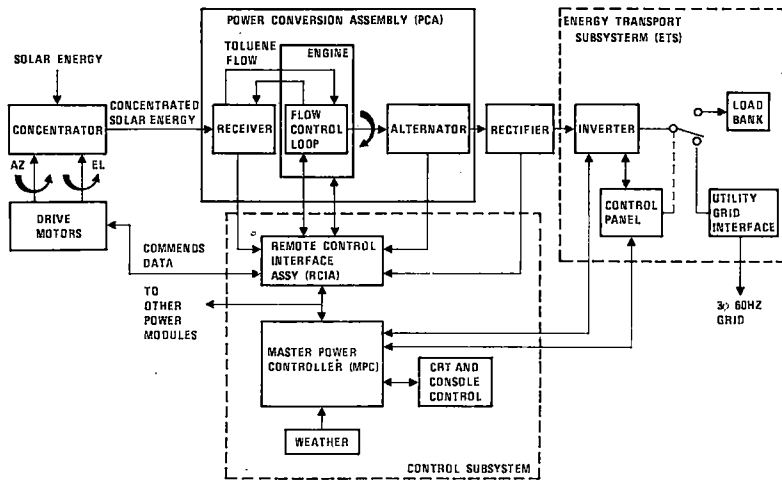
FIGURE 27.   PLANT CONTROL SUBSYSTEM BLOCK DIAGRAM
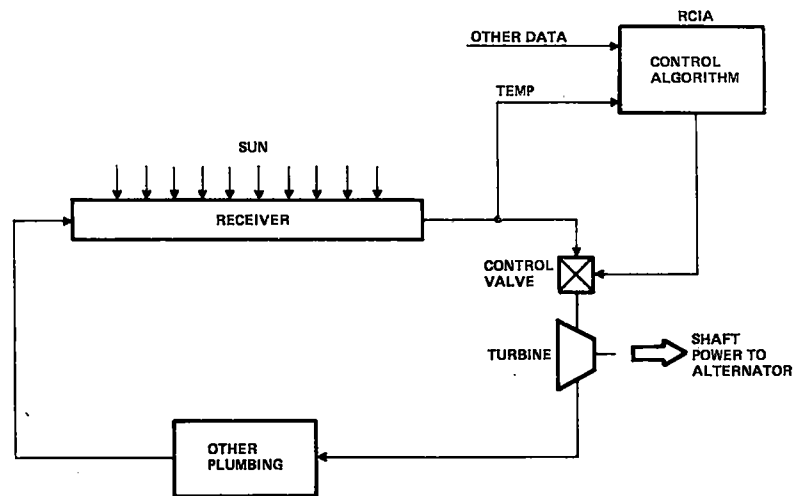
FIGURE 28.   SIMPLIFIED MODEL OF FLUID FLOW CONTROL LOOP
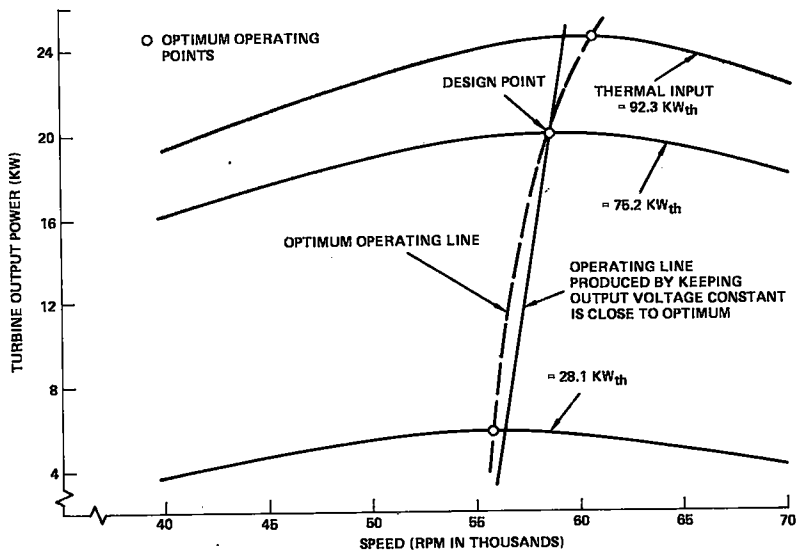
FIGURE 29.   TURBINE/ALTERNATOR OPERATING CHARACTERISTICS

93
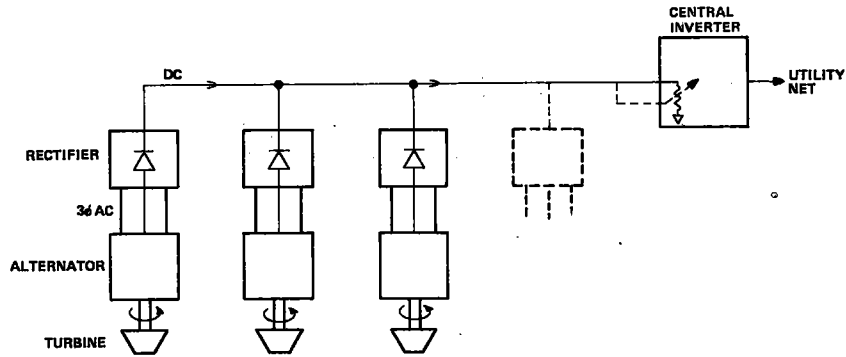
FIGURE 30. CENTRAL INVERTER DRIVEN BY MULTIPLE ALTERNATORS
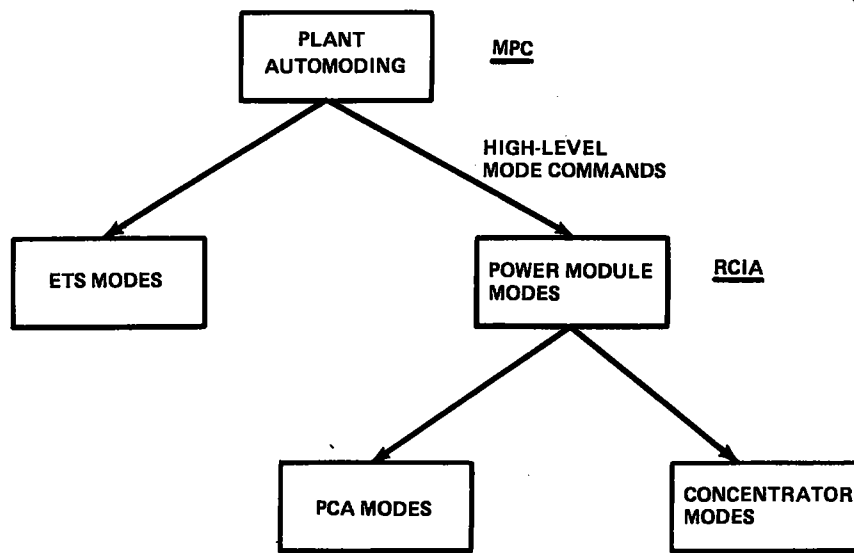
FIGURE 31. PLANT MODING HIERARCHY
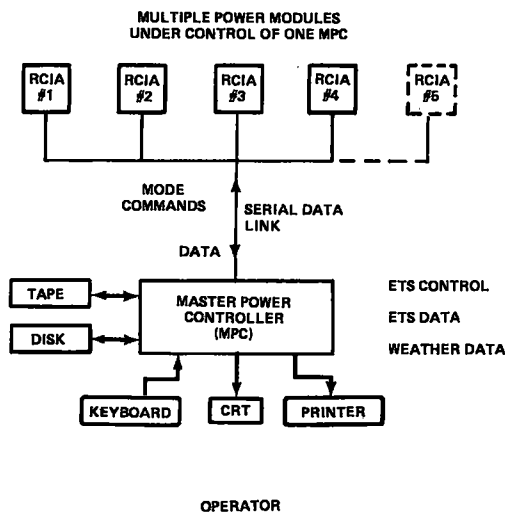
FIGURE 32. MULTIPLE POWER MODULE CENTRAL HARDWARE CONFIGURATION
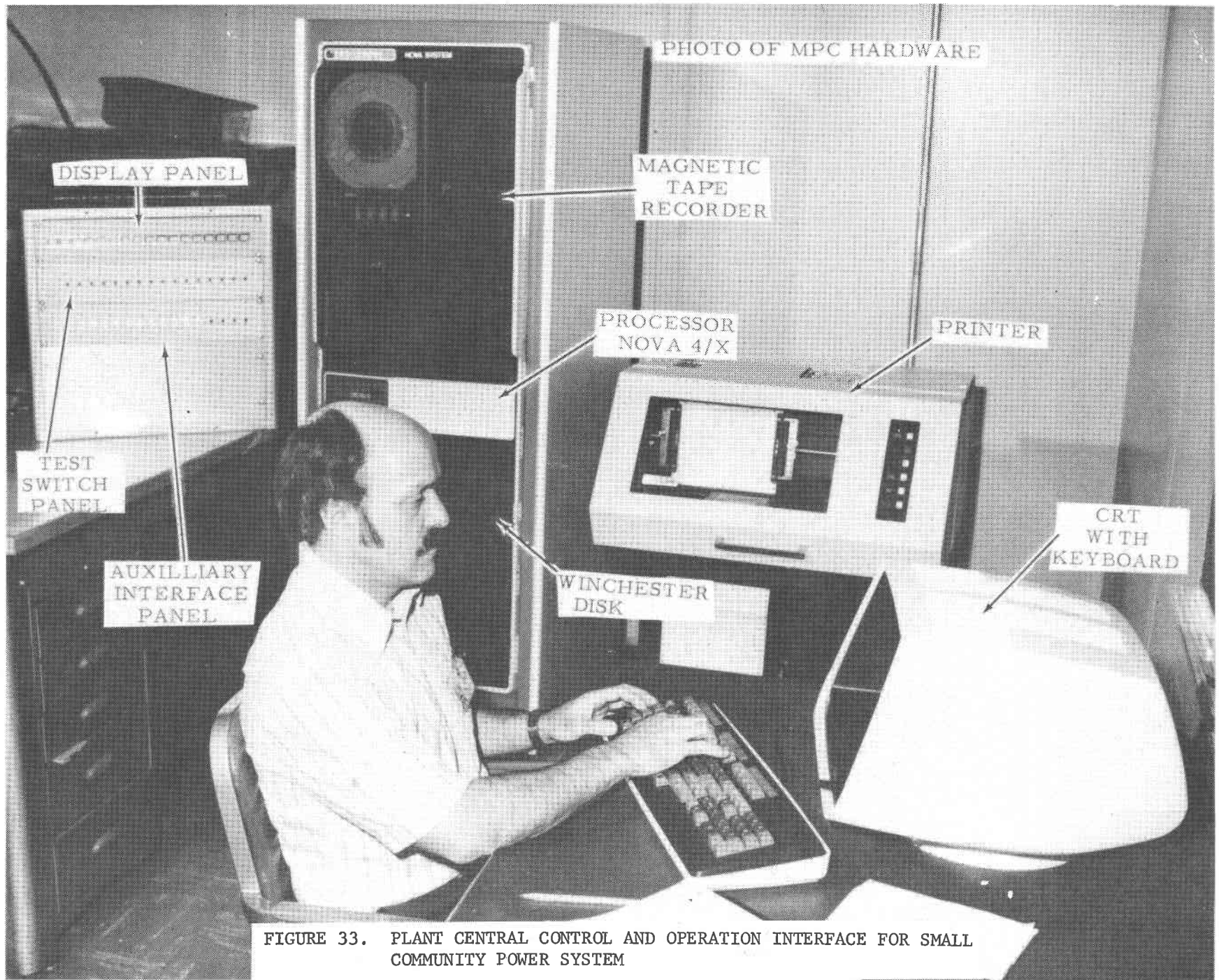
FIGURE 33. PLANT CENTRAL CONTROL AND OPERATION INTERFACE FOR SMALL COMMUNITY POWER SYSTEM

+24V PWR SUPPLY

±12V PWR SUPPLY

+5V PWR SUPPLY

CARD CASE

CIRCUIT CARDS

FLAT RIBBON CABLE

TRANSITION CABLE ASSEMBLIES

61 X 76 X 31 cm (24" X 30" X 12") NEMA ENCLOSURE

I/O INTERFACE CONNECTORS
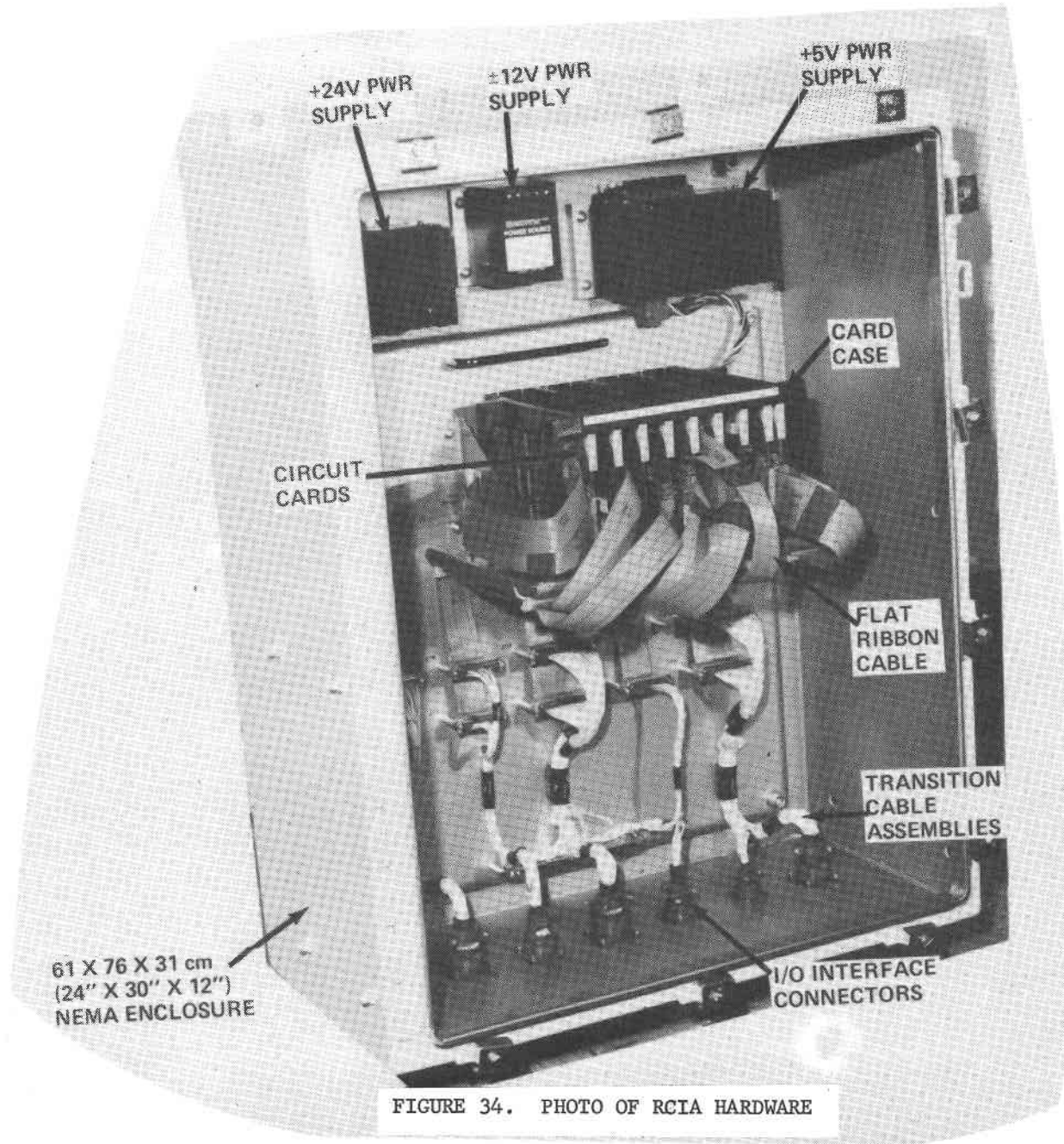
FIGURE 34. PHOTO OF RCIA HARDWARE

```
DATE:  06/21/81  FACC SMALL COMMUNITY SOLAR EXPERIMENT

TIME:  13:47:05                                      DISPLAY: 1

                        POWER (kW)          ENERGY (kWH)
                     THEOR     MEAS        THEOR     MEAS

TOTAL SOLAR                    XXX.X                 XXX.X

RECEIVER IN                    XXX.X                 XXX.X

RECEIVER OUT         XXX.X     XXX.X        XXX.X    XXX.X

RECTIFIER OUT        XXX.X     XXX.X        XXX.X    XXX.X

INVERTER OUT         XXX.X     XXX.X        XXX.X    XXX.X



                        MODE/STATUS SUMMARY

PCA MODE:  NORMAL                     ETS MODE: PWR TO UTIL

LCC MODE:  SLEW                       POWER:    XXX.X

FAULT STATUS: PCA CRITICAL/TURBINE OVERSPEED
```

FIGURE 35.   TYPICAL CRT OUTPUT DISPLAY
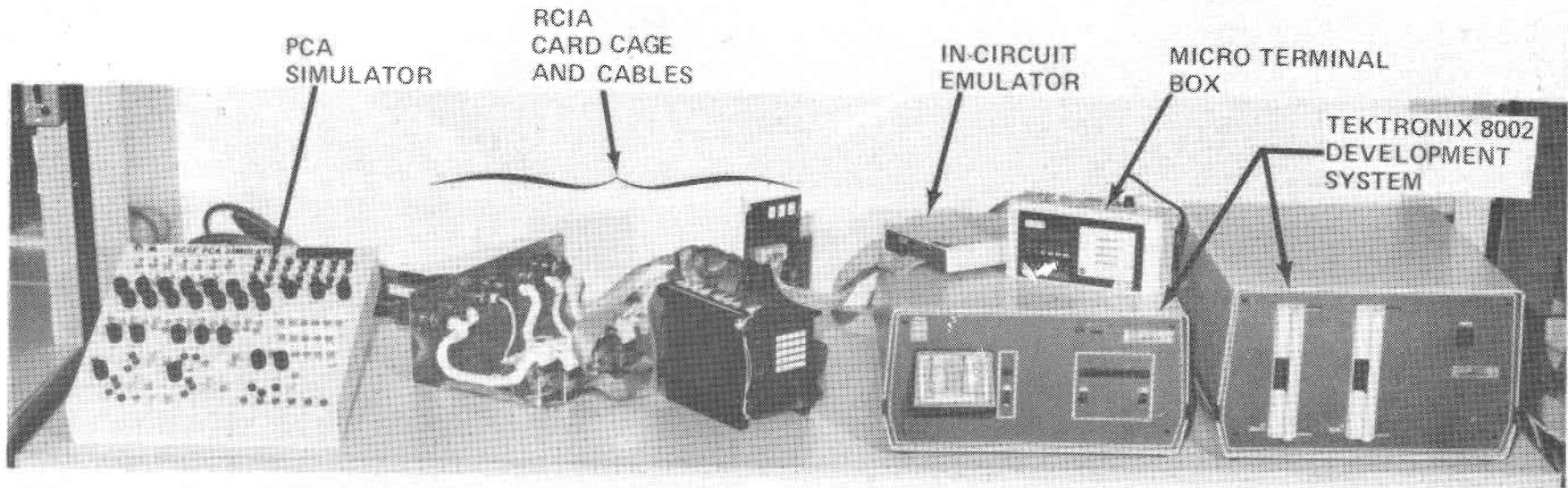
FIGURE 36.   RCIA HARDWARE/SOFTWARE INTEGRATION TEST SETUP
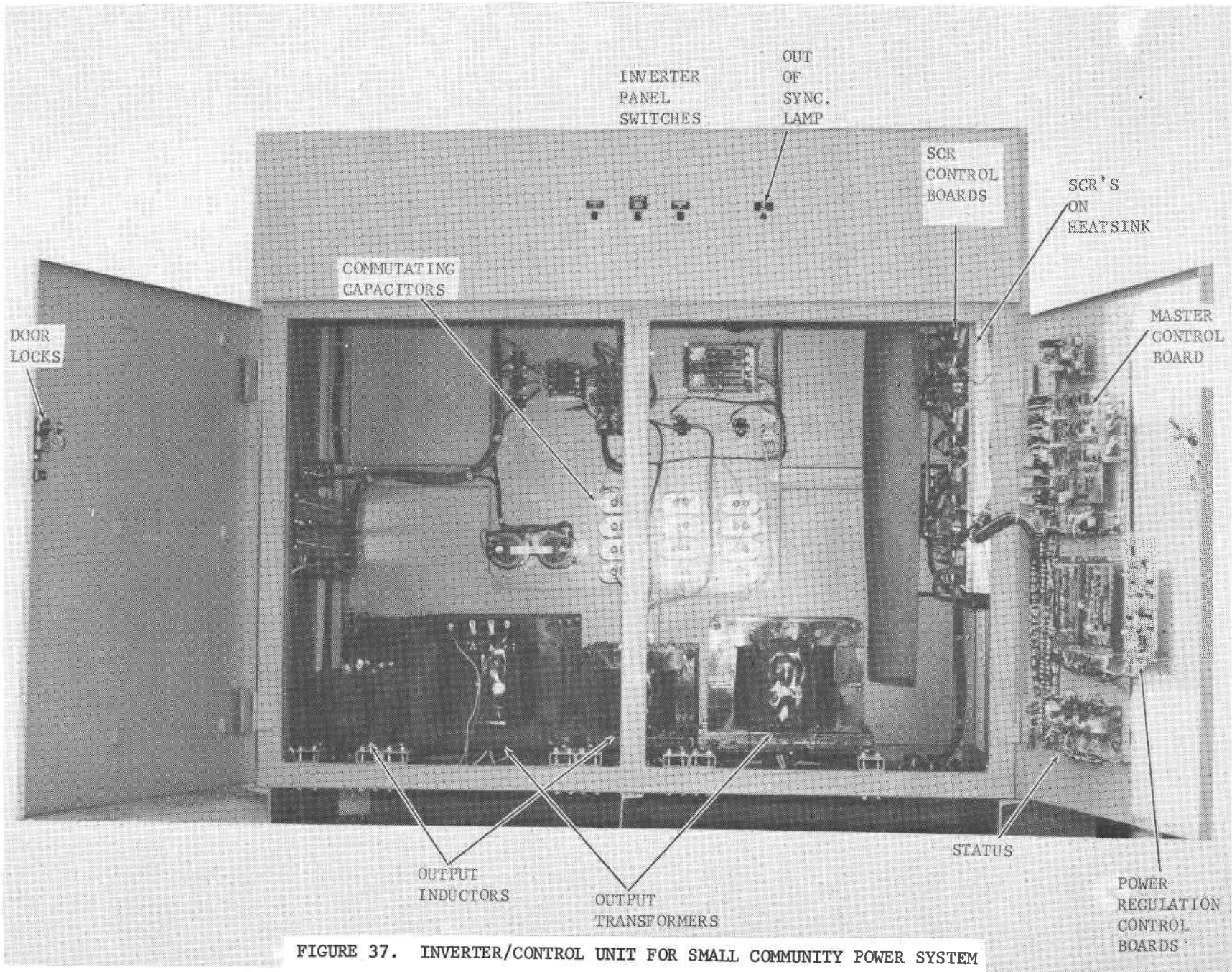
FIGURE 37. INVERTER/CONTROL UNIT FOR SMALL COMMUNITY POWER SYSTEM

ORGANIC RANKINE POWER CONVERSION SUBSYSTEM DEVELOPMENT
FOR THE SMALL COMMUNITY SOLAR THERMAL POWER SYSTEM

R. E. Barber

Barber-Nichols Engineering Co.

Arvada, Colorado

F. P. Boda

Ford Aerospace & Communications Corp. (FACC)

Newport Beach, Calif.

ABSTRACT

This paper describes the development and preliminary test results for an air-cooled, hermetically-sealed 20 kW_e organic Rankine (ORC) cycle engine/alternator unit for use with Point Focussing Distributed Receiver (PFDR) solar thermal power systems. 750°F toluene is the working fluid and the system features a high speed, single-stage axial flow turbine direct-coupled to a Permanent Magnet Alternator (PMA). Good performance has been achieved with the unit in preliminary tests at Barber-Nichols Engineering Company, the developer of the Power Conversion Subsystem (PCS), and testing is continuing at Ford Aerospace and the JPL test site.

INTRODUCTION

In April, 1980, Barber-Nichols Engineering Company was awarded a contract by Ford Aerospace for the development of a quiet, compact and efficient prototype PCS for incorporation in the Small Community Solar Power System under development by Ford for JPL. The PCS is comprised of an air-cooled hermetically-sealed ORC engine with a direct-coupled, high speed PMA supplied by Simmonds Precision Inc. of Norwich, NY. The PCS is designed to be coupled to a Ford developed cavity receiver and installed at the focus of a parabolic dish concentrator. These units constitute a solar power module with a nominal 20 kW_e power output (at 1000 W/m^2 solar insolation). Multiple modules can be easily interconnected to form a complete solar power plant of up to 10 MW_e depending on the desired application.

The PCS supplies 3-phase, high frequency ac power to a ground-mounted rectifier for conversion to 500 v. dc power; the dc output of each solar power module is centrally collected in a common bus and inverted to ac for interfacing with a utility grid network. The PCS design represents state-of-the-art Rankine cycle technology, however it possesses several unique features which benefit its application to this type of solar thermal PFDR system. For example, it is the first successful hermetic high-speed turbine/alternator/pump configuration of this size to be operated on toluene-lubricated hydrodynamic fluid film bearings which contribute to the long life expectancy of the system. The system is designed to operate in both the supercritical and subcritical pressure regimes

which contributes to the completely stable operation of the coupled receiver/ PCS unit. A corollary element of this operational stability is the development by Barber-Nichols of a high temperature toluene vapor flow control valve. The valve provides analog modulation of the working fluid mass flow rate to insure timely heat removal from the receiver regardless of solar insolation level and with simultaneous maintenance of virtually constant turbine inlet temperature. The latter feature increases system performance at reduced input power levels (part load).

The PCS has successfully completed qualification testing at Barber-Nichols and has been shipped to Ford Aerospace for mating with the receiver and further testing. By December of 1981, it is expected that the complete Power Conversion Assembly (PCS plus receiver) will be installed on the Test Bed Concentrator at the JPL Parabolic Dish Test Site, Edwards AFB, California.

DESIGN REQUIREMENTS

The design requirements for the PCS are summarized in Table 1. The maximum weight limitation is a major influence on subsystem design. Together with the external envelope restrictions, it results in a very compact design for both the air-cooled condenser and the regenerator. This places major emphasis on careful trade-off analysis of the major system components. An additional challenge exists in the desire for high performance in a very small power package, particularly with regard to the PMA. This required a major development effort, since there was no available high-speed PMA with either the desired power capacity or efficiency.

SUBSYSTEM DESCRIPTION

A cutaway view of the Power Conversion Subsystem is illustrated in Figure 1. The PCS schematic layout is shown in Figure 2 which includes the interface with the FACC-designed local controller, i.e. the Remote Control Interface Assembly (RCIA). The companion P-H diagram for toluene is shown in Figure 3. The circled numerals 1 through 7 correspond to the state points shown on the schematic. Figures 4 through 13 show the various PCS components; salient features of these components are as follows.

Turbine/Alternator/Pump (TAP) Assembly

The shrouded, single-stage, axial turbine is a supersonic design with 30° symmetrical impulse blading, a maximum design pressure ratio of 325 and a predicted maximum efficiency of 74%. It is a full admission unit with 10 nozzles. The turbine wheel is fabricated from Inconel 718 with a tip diameter of 125 mm (4.92 ins) and a blade height of 10.7 mm (0.42 ins). Each of the 110 blades are electrochemically milled on an ECM machine developed by Barber-Nichols. Turbine speed varies over the range of 45,000 to 60,000 rpm as a function of input power.

The PMA employs 6 Samarium-Cobalt magnets on the rotor with a 9-tooth copper-wound, laminated iron stator. The complete alternator is 72 mm (2.8 ins) OD and 127 mm (5 ins) long, producing 3-phase 3000 Hz ac power at 60,000 rpm with a predicted 95% peak efficiency.

102

The feed pump is a radial flow, partial emission, centrifugal type
with a predicted 27% peak efficiency. The pump is designed to supply
full system flow of 544 kg/hr (1200 lb/hr) and peak pressure of 5.9 MPa
(855 psi).

The entire TAP rotating unit is supported on two hydrodynamic tilting
pad bearings, each comprised of 3 radial shoes with the working fluid
(toluene) functioning as the lubricant. There are two hydrodynamic flat-
pad thrust bearings with aligning supports. The bearing material is
52100 steel, with an overlay of tin-antimony babbitt plating.

Regenerator

The regenerator is a conventional fin-tube cross counterflow configuration
which was made as large as possible within weight limitations since cycle
studies show an optimum performance point occurring above the maximum
allowable weight. It is constructed of stainless steel tubing with
brazed-on aluminum fins.

Condenser

The air-cooled condenser consists of 369 finned aluminum tubes in parallel,
arranged in 3 concentric layers. Cooling air at a maximum rate of 212 m^3/min
(7500 cfm) is drawn in axially by the two speed fan and exhausted radially
outward across the condenser tubes.

Control Valve

The vapor flow control valve is a pintle-type valve operated by a hydraulic
actuator which is powered by high pressure working fluid. Valve command
signals are keyed to temperature sensors located in the receiver.

Additional Components

A hotwell, a start pump, boost pump and overspeed brake are also provided.
The overspeed brake was also supplied by Simmonds Precision. In the event
of loss of control or electrical load, the brake brings the TAP to a dead
stop in approximately 6 seconds by shorting out the PMA and closing the
vapor control valve. Hermetic sealing is accomplished by welding where-
ever possible and the use of double "0" ring seals because the design uses
no external dynamic seals, potential leakage of air or moisture into the
unit is avoided and long life of the working fluid is ensured.

PRELIMINARY TEST RESULTS

The PCS test program started with component-level development tests of the boost and start pumps, turbine bearings, regenerator, condenser, fan, flow control valve, alternator, rectifier and brake.

Following the completion of PCS assembly, the entire unit was subjected to extensive functional testing at the Barber-Nichols facility in Arvada, Colorado. This PCS development testing utilized an electrically-heated facility boiler to vaporize the toluene working fluid. The functional development testing of the prototype PCS resulted in certain minor design modifications to the bearing, dimensions, bearing materials, turbine wheel processing and electrical components.

Qualification testing of the deliverable prototype PCS was completed in early October 1981. A variable attitude test rig was used to demonstrate operation of the unit at elevation angles of 5°, 45° and 90° above the horizon. Performance was mapped across input power ranges of zero to 94 kW thermal, uncontrolled ambient temperatures of 69 to 101° F, turbine speeds of 45,000 to 60,000 rpm and dc output voltages of 400 to 650 volts. In operation, the PCS is smooth, quiet and very stable. Qualification testing also demonstrated that the unit is precisely controllable, safe, leaktight and structurally sound.

The Barber-Nichols-designed flow control valve performed flawlessly, providing accurate flow-rate metering of 750° F toluene vapor and absolute shutoff capability. The overspeed brake also worked rapidly and reliably, as did all the other failsafe protective features.

On the basis of preliminary data, the prototype PCS has achieved good efficiency (23.5% overall cycle efficiency), but further improvements are possible with modifications to turbine, alternator and heat exchanger hardware. The PCS cycle efficiency value used here is based on net dc electrical power out (after accounting for PCS parasitic power) divided by thermal input power from the boiler.

CONCLUSIONS

The design, development, fabrication and testing of the first solar-powered organic Rankine cycle Power Conversion Subsystem of this type was accomplished in a span of 18 months from conception to delivery. Preliminary test results indicate that this prototype unit promises safe, reliable operation and good efficiency with the potential for future improvements. Further integrated testing of the unit will be performed at Ford and then at the JPL Parabolic Dish Test Site in December 1981. The concept of a dish-mounted organic Rankine turbo-alternator is no longer a paper study, but is becoming a demonstrated reality.

ACKNOWLEDGEMENT

The authors wish to acknowledge that success of this program was due to the contributions and support provided by Bill Nesmith, Engine Coordinator at the Jet Propulsion Lab and the following Barber-Nichols Engineering Co.

personnel during the analysis, design, fabrication and test phases:

Ralph W. Blakemore, Senior Project Engineer;
Jere Sobotka, Senior Project Technician;
Robert G. Olander, Technical Director;
Tim Penney, Senior Engineer;
Gary Frey, Senior Technician;
Art Hutter, Lead Machinist

TABLE 1

PCS REQUIREMENTS AND DESCRIPTION

● POWER CONVERSION SUBSYSTEM INCLUDES:

  --ORGANIC RANKINE CYCLE ENGINE WITH DIRECT COUPLED
    ALTERNATOR

  --CONDENSER, REGENERATOR, VALVES, FILTERS, PLUMBING

  --PUMPS (BOOST, FEED, START) AND FAN

  --RECTIFIER, BRAKE CONTROL AND ELECTRICAL BOXES

  --SAFETY AND PROTECTIVE FUNCTIONS

● APPROX 20 KWe AT RATED 75.6 KWt INPUT (1000 W/m^2 SOLAR FLUX)

● APPROX 25 KWe AT PEAK 92.4 KWt INPUT (1100 W/m^2 SOLAR FLUX)

● OPERATE 5° to 90° ELEVATION, STOW AT MINUS 90°

● MAX SPACE ENVELOPE ~ 1.12 m (44") DIA x 1.52 m (60") LONG

● MAX WEIGHT AT FOCUS = 390 Kg (860 LBS)

● 500 VOLT D-C OUTPUT TO FACC INVERTER

● SOLAR RECEIVER (BOILER) OUTLET TEMPERATURE IS 399°C (750°F)

● WORKING FLUID IS TOLUENE IN HERMETICALLY SEALED LOOP

● MINIMUM REQUIRED SUBSYSTEM EFFICIENCY AT RATED POWER = 24%
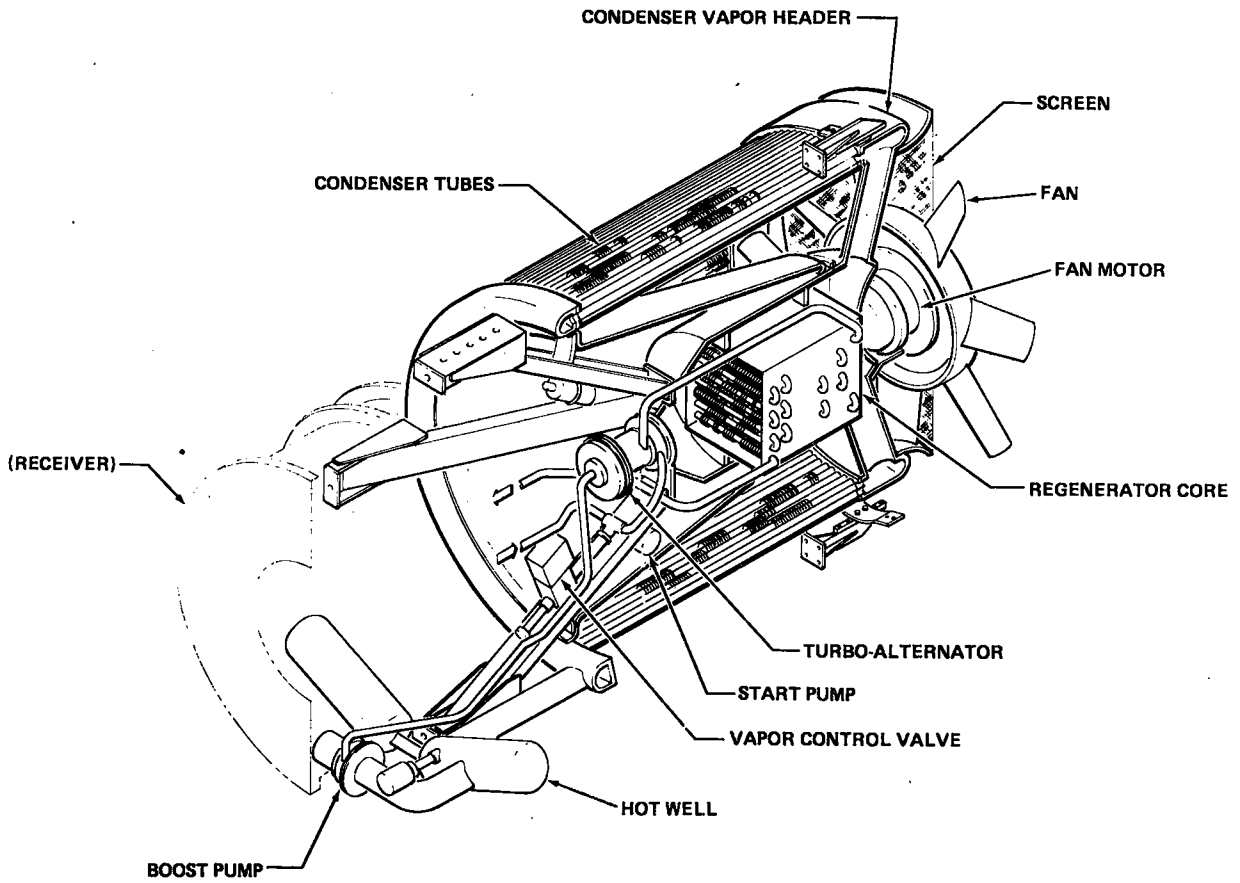
FIGURE 1.   CUTAWAY VIEW OF POWER CONVERSION SUBASSEMBLY
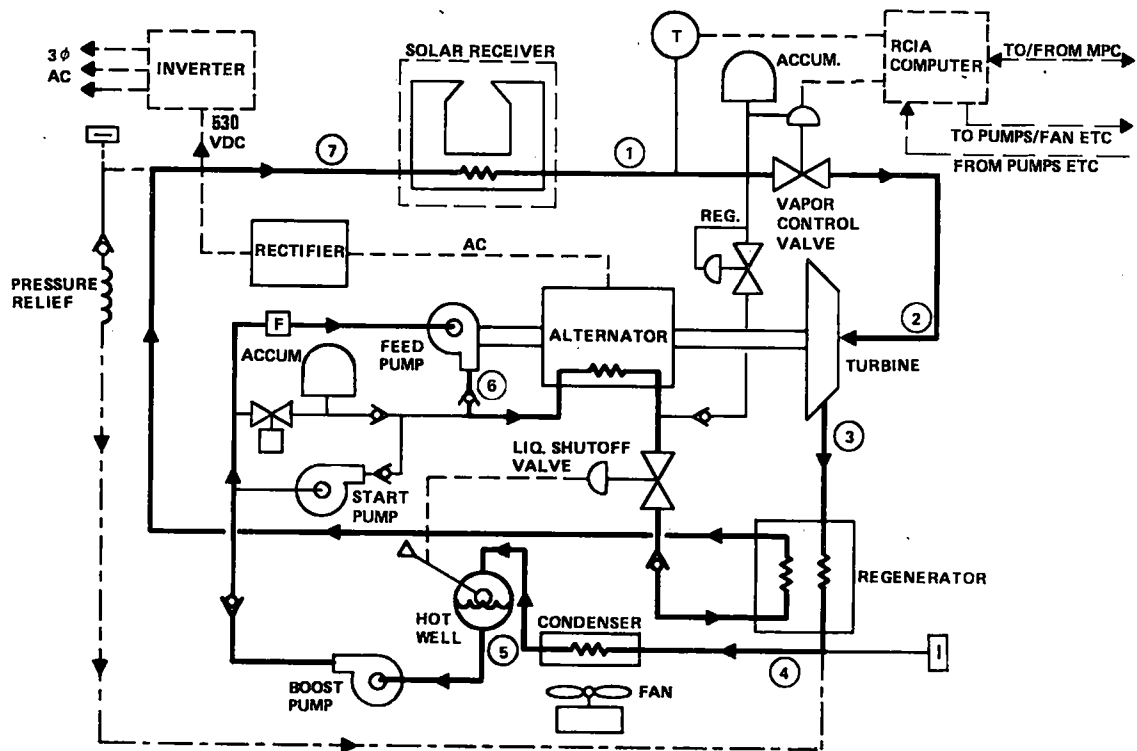
FIGURE 2.   POWER CONVERSION SUBSYSTEM (PCS) SCHEMATIC
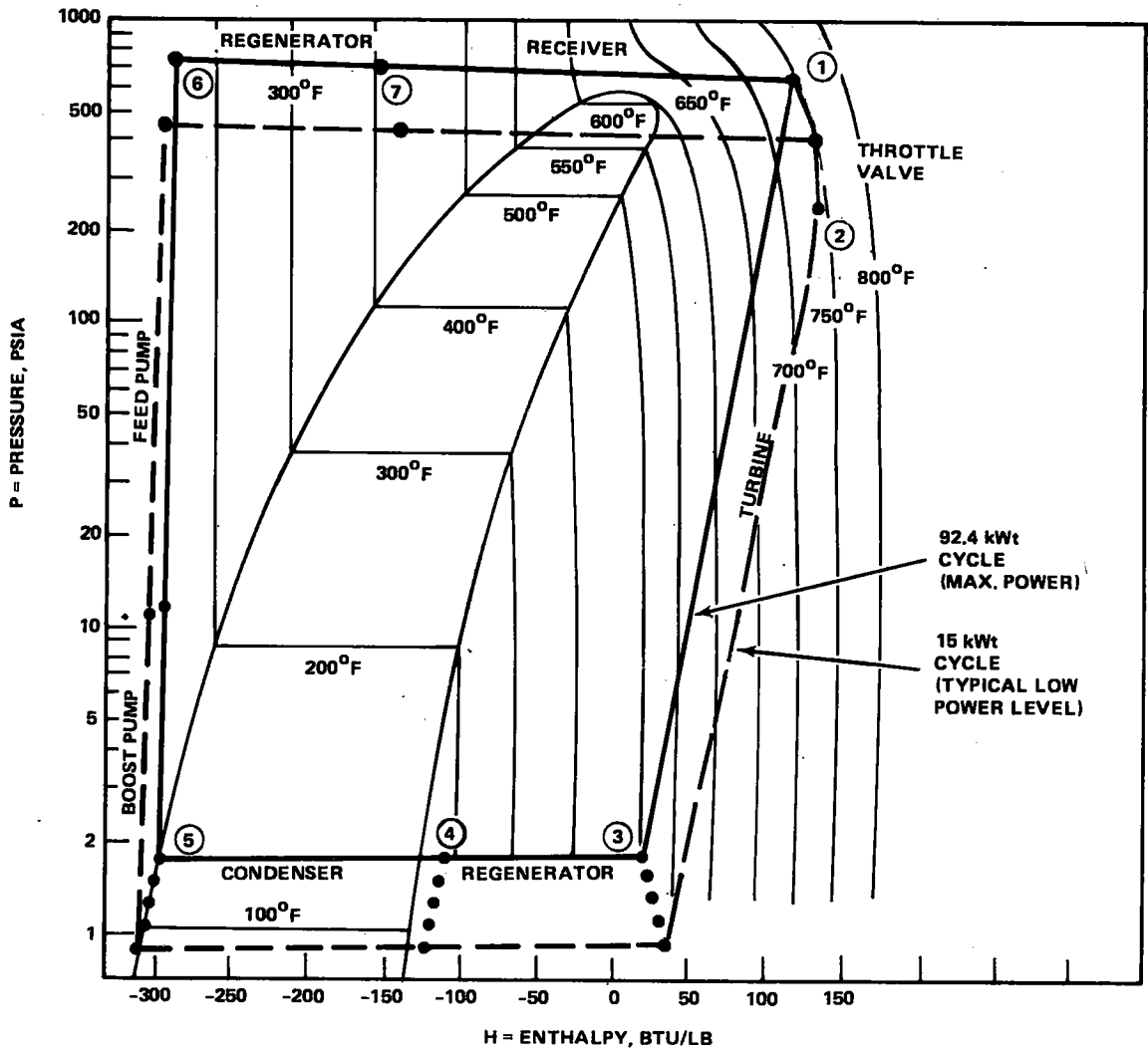
FIGURE 3. TOLUENE P-H DIAGRAM WITH PCS STATE POINTS

FIGURE 4. CUTAWAY MODEL OF TURBO ALTERNATOR

SUPERHEATED TOLUENE VAPOR IN

HIGH PRESS LIQUID TOLUENE OUT

VAPOR MANIFOLD

TURBINE NOZZLE

TILTING-PAD RADIAL BEARINGS

TURBINE WHEEL

GIMBALLED HYDRODYNAMIC THRUST BEARING

LIQUID TOLUENE IN

ALTERNATOR STATOR WINDINGS

FEED PUMP

COOLING JACKET

ALTERNATOR ROTOR
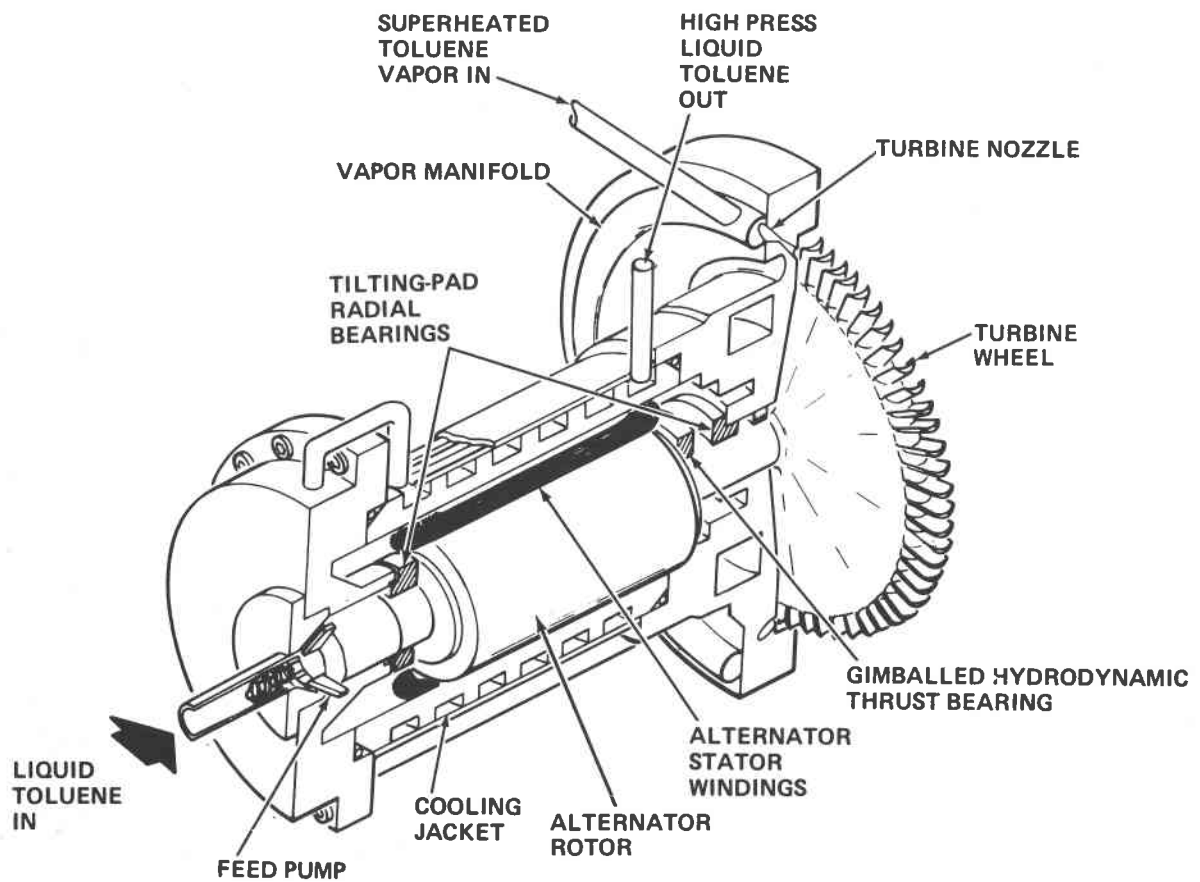
FIGURE 5. TURBINE-ALTERNATOR-PUMP (TAP)
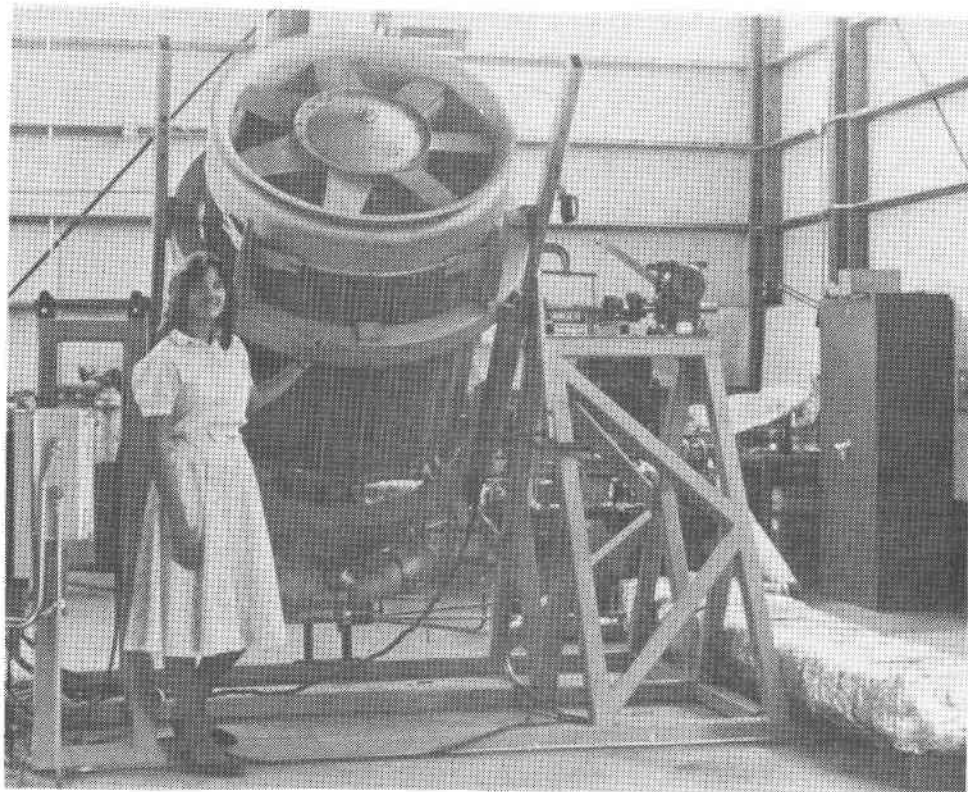
FIGURE 6. PCS IN TEST RIG AT 45° ELEVATION ANGLE
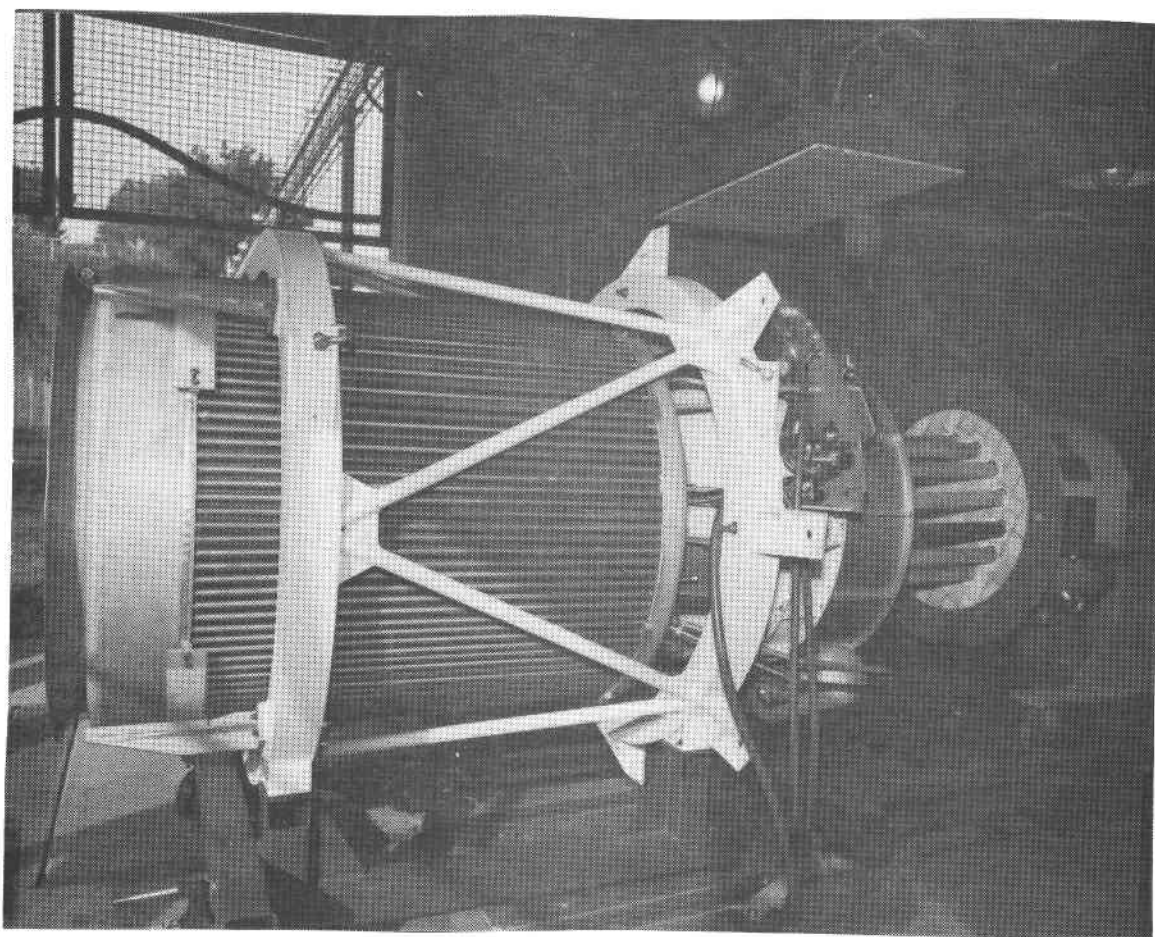
FIGURE 7. PCS, RECEIVER AND TEST HEATER AT 5° IN FORD TEST CELL
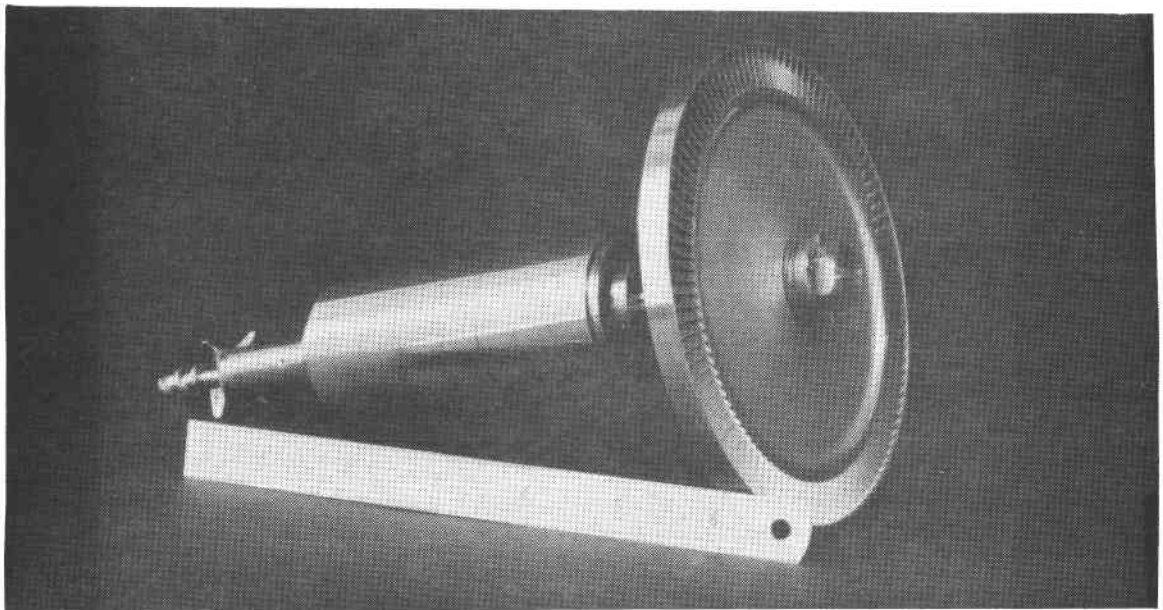
FIGURE 8. ROTATING SHAFT WITH PUMP, ALTERNATOR AND TURBINE WHEEL
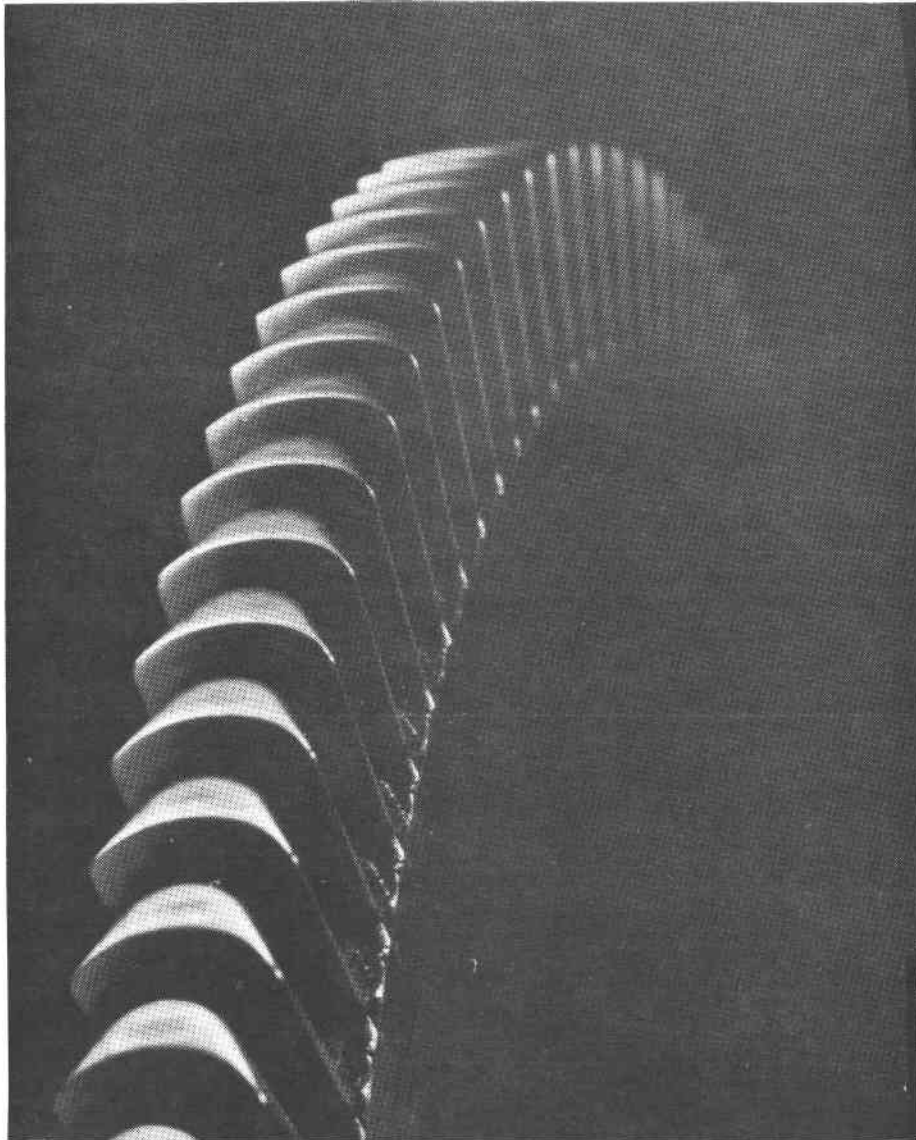
FIGURE 9. BLADE PROFILE OF ELECTROCHEMICALLY MILLED TURBINE WHEEL
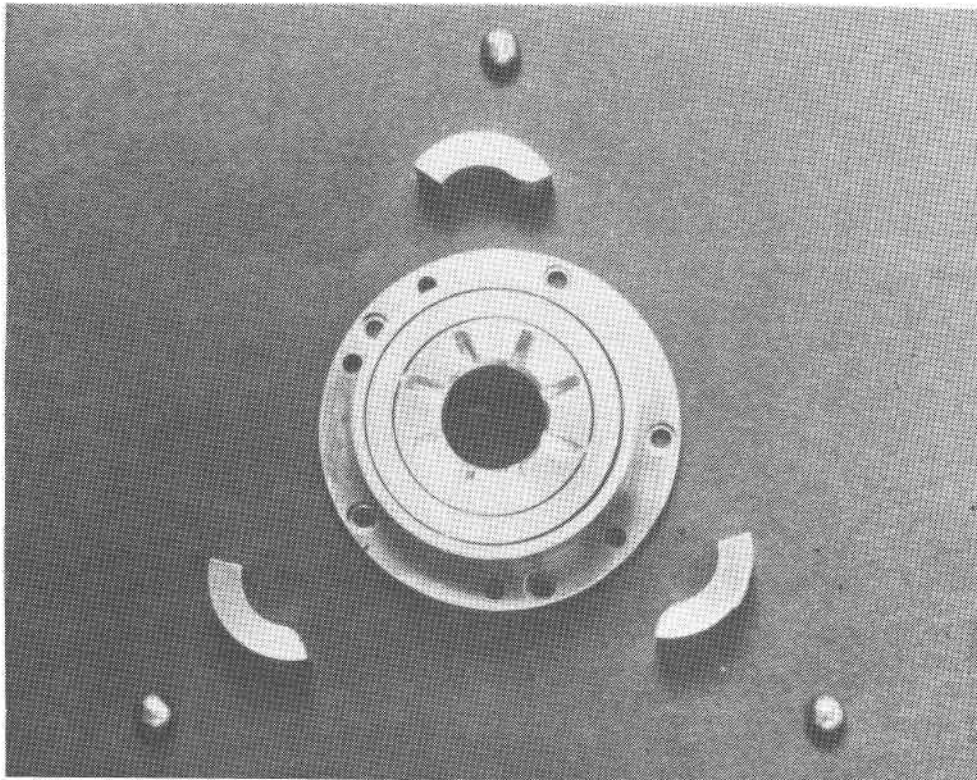
FIGURE 10.   HYDRODYNAMIC THRUST BEARING AND TILTING-PAD RADIAL BEARING SHOES
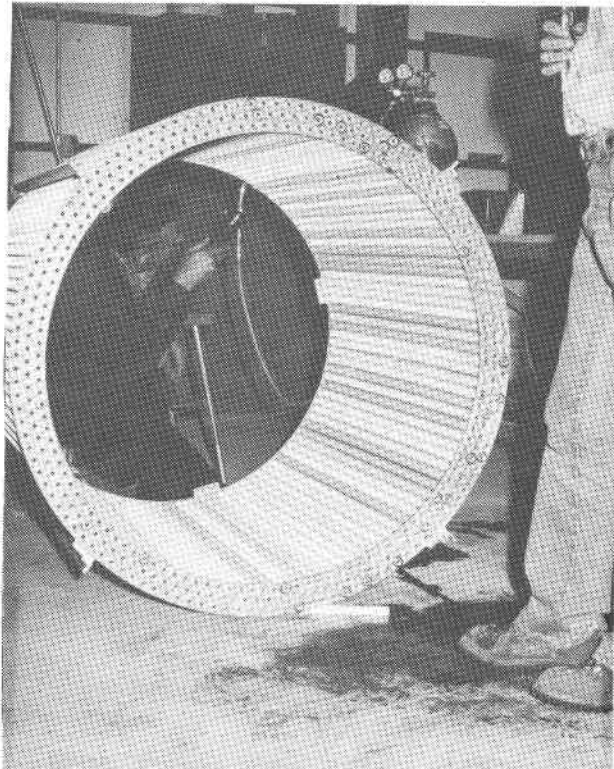
FIGURE 11.   CYLINDRICAL, AIR-COOLED CONDENSER CORE
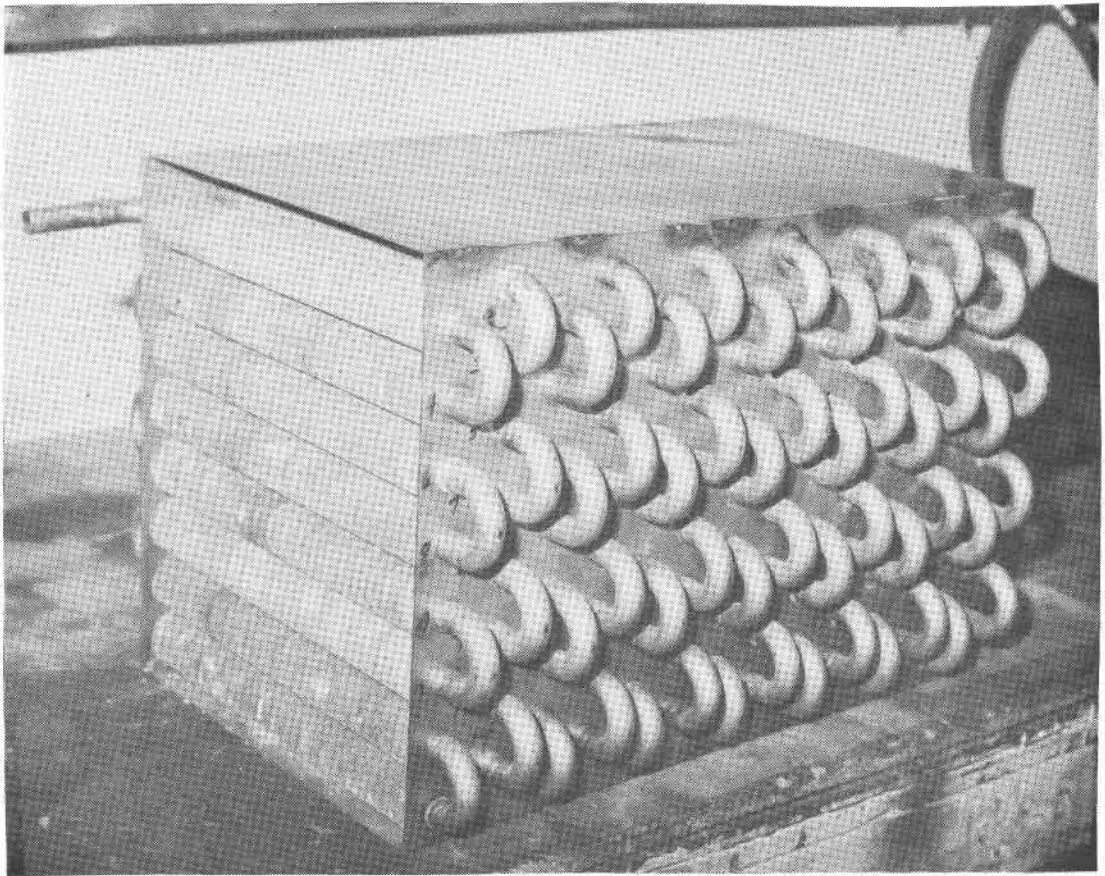
FIGURE 12. REGENERATOR CORE
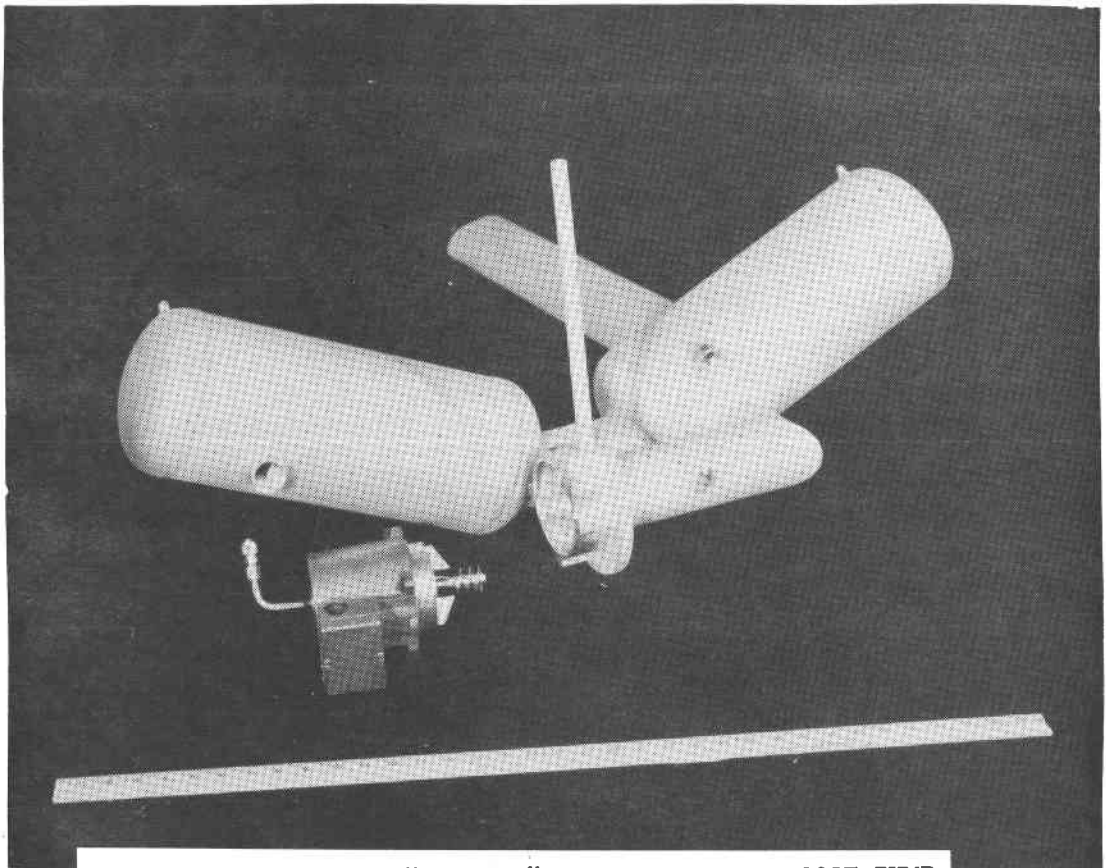
FIGURE 13. ALUMINUM "HOTWELL" RESERVOIRS AND BOOST PUMP

VERIFICATION TESTING OF THE PKI COLLECTOR AT
SANDIA NATIONAL LABORATORIES, ALBUQUERQUE, NEW MEXICO

J. S. Hauger and S. L. Pond
Applied Concepts Corporation
P.O. Box 2760, Reston, VA 22090

ABSTRACT

Verification testing of the PKI collector was undertaken prior to its operation as part of an industrial process heat plant at Capitol Concrete Products in Topeka, Kansas. Testing was performed at a control plant installed at Sandia National Laboratory, Albuquerque, New Mexico (SNLA).

Testing was conducted as per Applied Concepts' Technical Report J02-03-81 "Verification Test Plan," in two phases to test short-term system performance characteristics and to validate system design, manufacture, and installation through operability testing.

Early results show that plant performance is even better than anticipated and far in excess of test criteria. Overall plant efficiencies of 65 to 80 percent were typical during hours of good insolation. A number of flaws and imperfections have been detected during operability testing, the most important being a problem in elevation drive alignment due to a manufacturing error. All problems were corrected as they occurred and the plant, with over 40 hours of operation, is currently continuing operability testing in a wholly-automatic mode.

BACKGROUND

Applied Concepts Corporation is responsible to JPL for the design and implementation of a Thermal System Engineering Experiment to be carried out at Capitol Concrete Products in Topeka, Kansas. The experiment will test the technical and operational feasibility of employing a PKI collector in an industrial process heat application and environment. An experiment control plant will be operated at SNLA. Further information on the PKI system and on plant evaluation at Capitol Concrete have been presented in other papers to this conference.

Before placing and operating a test plant at the industrial site, it was desirable and wise to verify the performance and operability of the system in the laboratory environment. This was particularly true because of the incorporation into the first PKI production model of certain engineering improvements, based on lessons learned with the fifth generation prototype and which required testing and validation of concept at the system or plant level.

The experiment control plant installed at SNLA was the appropriate vehicle for verification testing.

a. Test Procedures

1. General

A full report of testing procedures is presented in Applied Concepts' Technical Report J02-03-81, "Verification Test Plan," dated October 13, 1981.

Conceptually, verification testing was divided into two phases. A one-week performance test would verify that the plant could produce the desired energy product (100% saturated steam at 30 to 60 psig) at or above certain output and efficiency levels, on an instantaneous or short-term basis. A three-week operability test would then monitor plant operation over a longer period to detect, analyze, and correct defects in system design manufacture and installation, prior to operations at the industrial site. In practice, the two test phases were run simultaneously. This means that as a series of minor problems became apparent during performance testing, they were evaluated and corrected on-the-spot, while further testing continued.

b. Performance Testing

1. Variables

The independent variable for performance testing is that of plant steam quality. 100 percent saturated steam is assured by a steam separator in the output line, with output pressure operator controlled to 30 to 60 psig. Plant thermal power output is calculated according to the equation:

$$PO = \frac{(\Delta FM_2 - \Delta FM_3)(\bar{h}_{T4} - \bar{h}_{T2})}{T}$$

where

PO	=	plant output (BTU/hr.)
ΔFM_2	=	feedwater input (gallons)
ΔFM_3	=	condensate removed from output (gallons)
$\bar{h}_{T4}$	=	enthalpy of saturated steam at average output temp. (BTU/gal.)
$\bar{h}_{T2}$	=	enthalpy of input water (BTU/gal.)
T	=	elapsed time of operation

Average plant efficiency is calculated according to the equation:

$$APE = \frac{PO}{\bar{N} \cdot A \cdot C} \times 100$$

where

APE	=	average plant efficiency (percent)
PO	=	plant output (BTU/hr.)
$\bar{N}$	=	average normal incidence pyrheliometer reading (kW/m^2)
A	=	collector area (80.3m^2)
C	=	conversion factor = 3,412 BTU/kW hr.

Plant parasitic power consumption is calculated according to the equation

$$PPP = \frac{C \div \Delta P}{T \cdot PO} \times 100$$

116

where   PPP = plant parasitic losses (percent)

          ΔP   = change in kW hour meter over elapsed time

          PO   = plant output (BTU/hr.)

          T   = elapsed time (hr.)

          C   = conversion factor = 3412 BTU/kW hr.

In addition, a plant performance envelope definition which compares output and efficiency to insolation will be conducted.

b. Criteria

A successful performance test was defined to be not less than 10 hours of direct normal insolation with operation and valid data acquisition, with an output of not less than 100,000 BTU/hr., an average total plant efficiency of not less than 50 percent, and a parasitic power consumption not greater than 2 percent.

c. Operability Testing

1. Variables and Criteria

Operability testing, in addition to the performance variables identified above, will measure the plant forced outage rate. For the purposes of operability testing, this is defined as the hours of non-availability when insolation exceeds 0.6 kW/m^2, divided by the total number of such hours. A successful verification test was defined to be a three-week period during which the forced outage rate is less than 0.25.

More important than the additional measure of outage, however, is the "shake-down" aspect of operability testing in which problems in design, manufacture, or installation are indentified and corrected.

TEST RESULTS

At the time of preparation of this paper, only preliminary results are available. Operability testing has aided in the identification and correction of these problems:

(1) **Boiler manufacture:** A head gasket whose temperature rating was only 180°F was employed by the component manufacturer. Gasket has been replaced.

(2) **Level switch fouling:** High and low-level switches in the boiler have very short service life due to fouling. A cleaning step was added to the manufacture process and filters and scavenger magnets were employed.

(3) **Elevation drive shaft misalignment:** It was learned that the angular alignment of drive shafts must be within a tolerance of ± 1%. Due to a manufacturing error, some

117

alignments were proper within only $\pm$ 5°. Mirror adjustment plates capable of absorbing a greater misalignment were fabricated and installed.

Performance testing has exceeded the criteria established before the test. With greater than forty hours of operation, average hourly plant efficiencies have ranged from the low sixties during periods of low insolation and before correction of the elevation drive problem, to as high as 80 percent during high insolation (950 watts/m²) and after correction of drive misalignment. (See Figure 1 for some point values).

More detailed results will be represented during the oral presentation in Atlanta.

Figure 1.
Plant Output and Efficiency Data Points for
Production of 40 psi Steam

Date	Insolation (kW/m²)	Output (BTU/hr.)	Overall Plant Efficiency
10/29	0.85	150	.65
10/29	0.99	200	.73
11/09	0.96	222	.84
11/09	0.94	210	.81
11/09	0.90	192	.78
11/10	0.98	217	.81
11/10	0.98	205	.77

PKI SOLAR THERMAL PLANT EVALUATION AT
CAPITOL CONCRETE PRODUCTS, TOPEKA, KANSAS

J. S. Hauger   D. N. Borton
Applied Concepts Corporation   and   Power Kinetics, Inc.
P.O. Box 2760, Reston, VA 22090   110 8th St., Troy, N.Y. 12181

ABSTRACT

Applied Concepts Corporation is supporting JPL in the structure and implementation of a system feasibility test to determine the technical and operational feasibility of using the PKI collector to provide industrial process heat. The test is of a PKI system in an industrial test bed plant at Capitol Concrete Products in Topeka, Kansas, with an experiment control at Sandia National Laboratories, Albuquerque (SNLA).

Plant evaluation will occur during a year-long period of industrial utilization. It will include performance testing, operability testing, and system failure analysis. Performance data will be recorded by a PKI designed data acquisition system. Reporting will be completed monthly, with results presented as per standard SERI format. User, community, and environmental inputs will be recorded in logs, journals, and files maintained by Capitol Concrete, with assistance from The University of Kansas Research Center and the Kansas Energy Office. Applied Concepts' and PKI's engineering staff will be responsible to diagnose and correct any plant failures.

Plant installation, start-up, and evaluation, are anticipated for late November, 1981. The data acquisition system and reporting methods have been tested during verification testing at SNLA.

BACKGROUND

In January, 1981, Applied Concepts Corporation, as the result of a competitive procurement, undertook to support JPL through the planning and implementation of a "Thermal System Engineering Experiment." Together with our partner and principal subcontractor, Power Kinetics, Inc., we are now in the process of placing a point focussing solar thermal energy plant in an industrial application and environment, in order to test the technical and operational feasibility of the system in its present state of development.

The solar energy plant to be the test bed for the PKI collector was designed by Applied Concepts. It consists of a single, PKI module, platform mounted at Capitol Concrete Products in Topeka, Kansas. The plant will deliver 170 pounds per hour of 30 to 60 psi steam, at an existing, natural gas fired boiler which is used to pressurize two autoclaves for the curing of concrete masonry blocks.

Solar plant operation and maintenance will be the responsibility of the industrial user. Plant operation is designed to be completely automatic. The collector will provide up to 5 percent of the total load when hours of insolation and production coincide. It will be used to maintain boiler temperature, i.e., for boiler preheat, during any hour when sunlight is available and the autoclaves are not up, e.g., during weekends and product loading and unloading.

The Capitol Concrete experiment will be conducted over the course of one year. In order to more fully understand the differential impacts of plant operation in an industrial environment, an experiment control plant will be operated at Sandia National Laboratory in Albuquerque, New Mexico, in parallel with the industrial plant. Whereas the industrial installation was chosen to be representative of those conditions under which solar process heat plants must operate to be a viable commercial technology, the control plant is representative of the most favorable conditions, i.e., high insolation, a unique environment, and the availability of high technology skills.

EVALUATION OBJECTIVES AND METHODS

JPL has established nine experiment objectives which can be met through plant evaluation. The objectives can be associated with three evaluative methods.

a. Performance Testing

1. Objectives

(1) Verify that the PKI collector system can produce usable thermal energy from solar radiation.

(2) Determine to what extent the experimental plant contributes to meeting the user's energy requirements.

(3) Characterize plant performance as a function of insolation, weather, operations, and environmental factors.

(4) Provide accurate input to performance, cost, and energy/economics impact models.

2. Methods

Performance data will be gathered by a PKI designed instrumentation package and data acquisition system (DAS). The DAS includes a normal incidence pyrheliometer, thermocouples, an electric watt meter, and pressure transducers, whose millivolt signals are collected by a Fluke Model 2200 B Data Logger. The Fluke corrects the thermocouples, records data on hard copy paper tape, and when requested by an Apple II Plus computer, sends the data across an RS 232 communication link to the Apple for CRT display and storage on 5¼ inch magnetic diskettes. The Apple also receives and records collector status data from the system controller and data from two flowmeters, measuring feedwater input and condensate recovery from a steam separator in the output line.

In addition, at the control plant, a load measurement experiment is being conducted in which two orthogonal horizontal strain guages measure the transverse forces on the concentrator frame. Concurrently, wind speed and direction are measured and collected by an A/D converter in the Apple.

Data recorded during operation at Sandia and at Capitol Concrete will be forwarded weekly to PKI where it will be processed and forwarded to Applied Concepts Corpration. Reporting format for performance data will be that specified by SERI in "Monthly Reporting Requirements for Solar Industrial Process Heat Field Tests" (MR-632-714, September 1980).

b. **Operability Testing**

1. **Objectives**

   (1) Identify and quantify the impacts of operating the plant on the daily operations activities of user personnel and on user/manning requirements at Capitol Concrete Products.

   (2) Identify the impact, if any, of the installation and operation of the plant on the local environment.

   (3) Identify the impact, if any, of the installation and operation of the PKI collector system on potential acceptance of commercial units by local officials.

2. **Methods**

   The primary method for collecting information on user, community, and environmental inputs, will be the maintenance of logs and journals. These will include a user's Operation and Maintenance Log as specified in Applied Concepts' Technical Report J02-02-81, "Operations, Maintenance, Safety and Spare Parts Plan," dated October 14, 1981, a Visitors Log, a Media File, and a Letter File. The University of Kansas Center for Research and the Kansas Energy Office will assist Capitol Concrete in these reporting tasks and will forward their analyses to Applied Concepts on a monthly basis.

c. **System Failure Analysis**

1. **Objectives**

   (1) Understand the failure modes of the PKI collector system.

   (2) Provide feedback to the system level hardware and software procedures.

2. **Methods**

   Applied Concepts and PKI will respond to JPL requests for assistance, within 24 hours of notification of a plant failure at SNLA or Capitol Concrete Products. A Plant Failure Log and Outage Report format have been established to document the diagnosis and correction of failures together with an analysis of safety implications of each failure.

3. **Progress to Date**

   As of the writing of this report, installation of the plant is underway in Topeka, while verification testing is being completed in Albuquerque. The DAS at SNLA has been operated and the first data disk delivered for analysis to PKI.

   It is anticipated that checkout of the Topeka installation will be completed by November 24, weather permitting. Plant evaluation will begin shortly thereafter. Any available results will be reported orally in Atlanta.

RECENT TESTS ON THE
CARTER SMALL RECIPROCATING
STEAM ENGINES

T. Kiceniuk

W. Wingenbach

RECENT TESTS ON THE
CARTER SMALL RECIPROCATING STEAM ENGINES

INTRODUCTION

Although the reciprocating steam expander still commands the enthusiastic support of a small group of loyal advocates, there are few applications where the qualities of the reciprocating piston steam engine have enabled it to hold its own or to win out over other kinds of heat engine. Two promising areas, both incidently for small engines, are pollution-free automotive applications and solar thermal power generation. The Carter engines (Figures 1 and 2) were designed and built precisely to address these opportunities (1) (2).*

The Carter engines differ from the traditional small piston driven steam engines in the following ways:

(1) The engines operate at high speed, typically around 4000 RPM. In automotive application this means that the engine must be used in conjunction with an automobile transmission for shifting gears. For solar use, the operating speed range is ideally suited to the requirements of a two pole, 60 Hz alternator, which also serves as a flywheel if directly coupled to the engine.

(2) The engines employ (Figure 3) a simple, but highly effective inlet valve actuation mechanism, the so-called "bash valve". The steam inlet valve consists of a small conical button made from Tungsten Carbide which sits over the steam inlet port in the cylinder head (the head also comprises the high pressure steam chest). A coil spring fashioned from high temperature resistant Rene 41 insures that the valve remains seated when in the closed position. The valve is opened to admit steam by being lifted off its seat through the action of a small Stellite post mounted on the top of the piston which contacts the hollow conical underside of the valve as the piston nears the top of its stroke. This simple, effective mechanism has been exhaustively tested on the bench and in the engine and is capable of withstanding both the high temperatures and the repeated stresses to which it is subjected. The velocity of the piston at the moment of contact with the stationary valve is less than 15 fps, even at 3600 RPM. The exhaust steam is discharged through a conventional annular port located in the cylinder at the lower end of the piston travel.

(3) The inventory of working fluid is minimal, the amount of distilled water used is approximately equal in volume to the displacement volume of the cylinders. In the automotive version of the engine, the working fluid is heated in a single finned tube which surrounds the fuel-fired combustion zone in the steam generator. The small size and quantity of the tubing means that relatively expensive materials having the correct properties can be employed without incurring serious cost penalty, and also that safety risks are small.

---

*Numbers in parentheses refer to references in back of report.
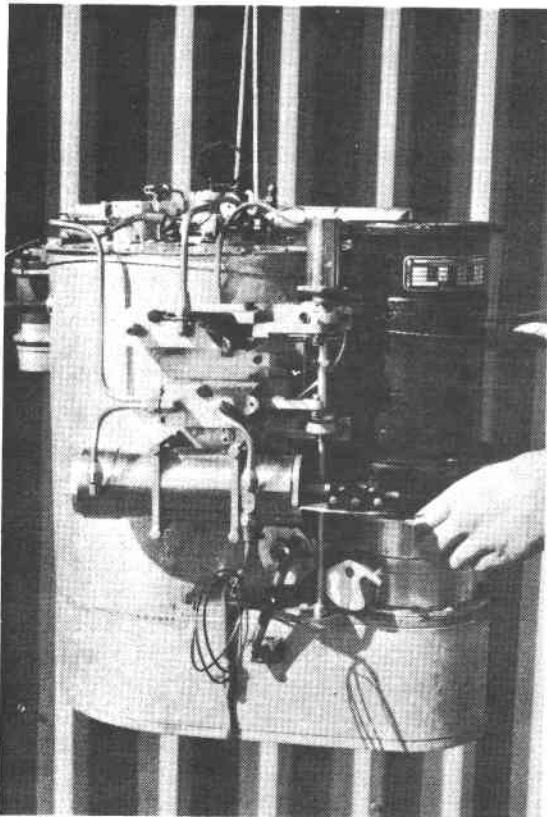
STEAM GENERATOR
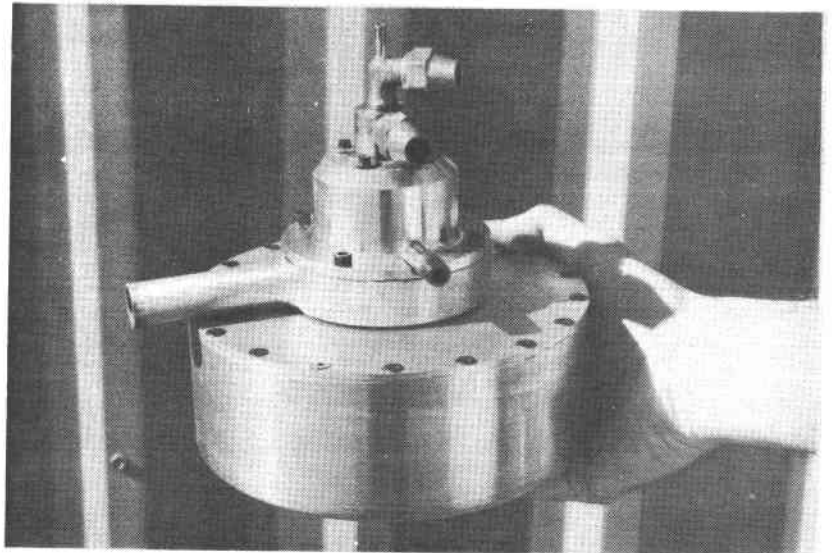
OIL-WATER SEPARATOR
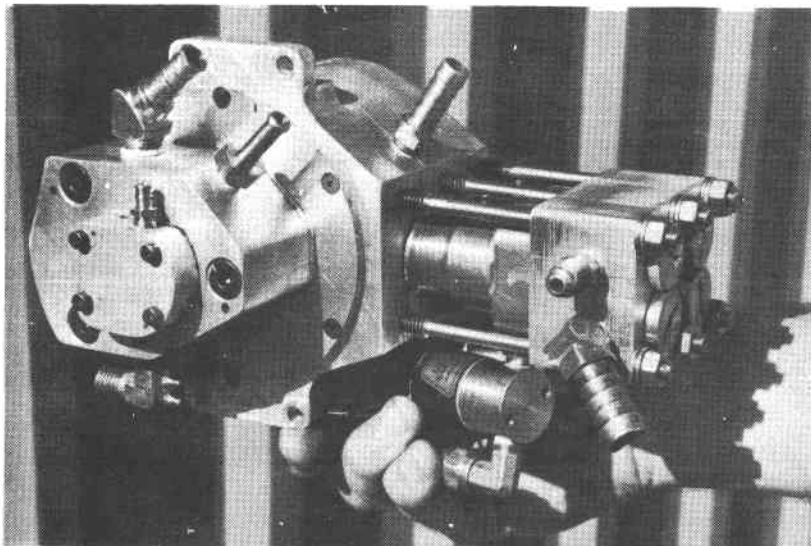
WATER PUMP
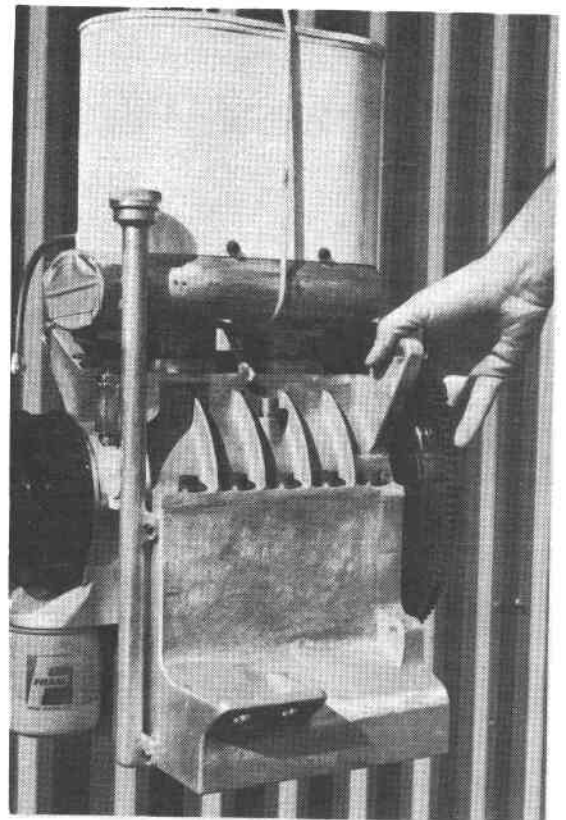
EXPANDER

Figure 1. Jay Carter Two Cylinder Paratransit
Vehicle Steam Engine.
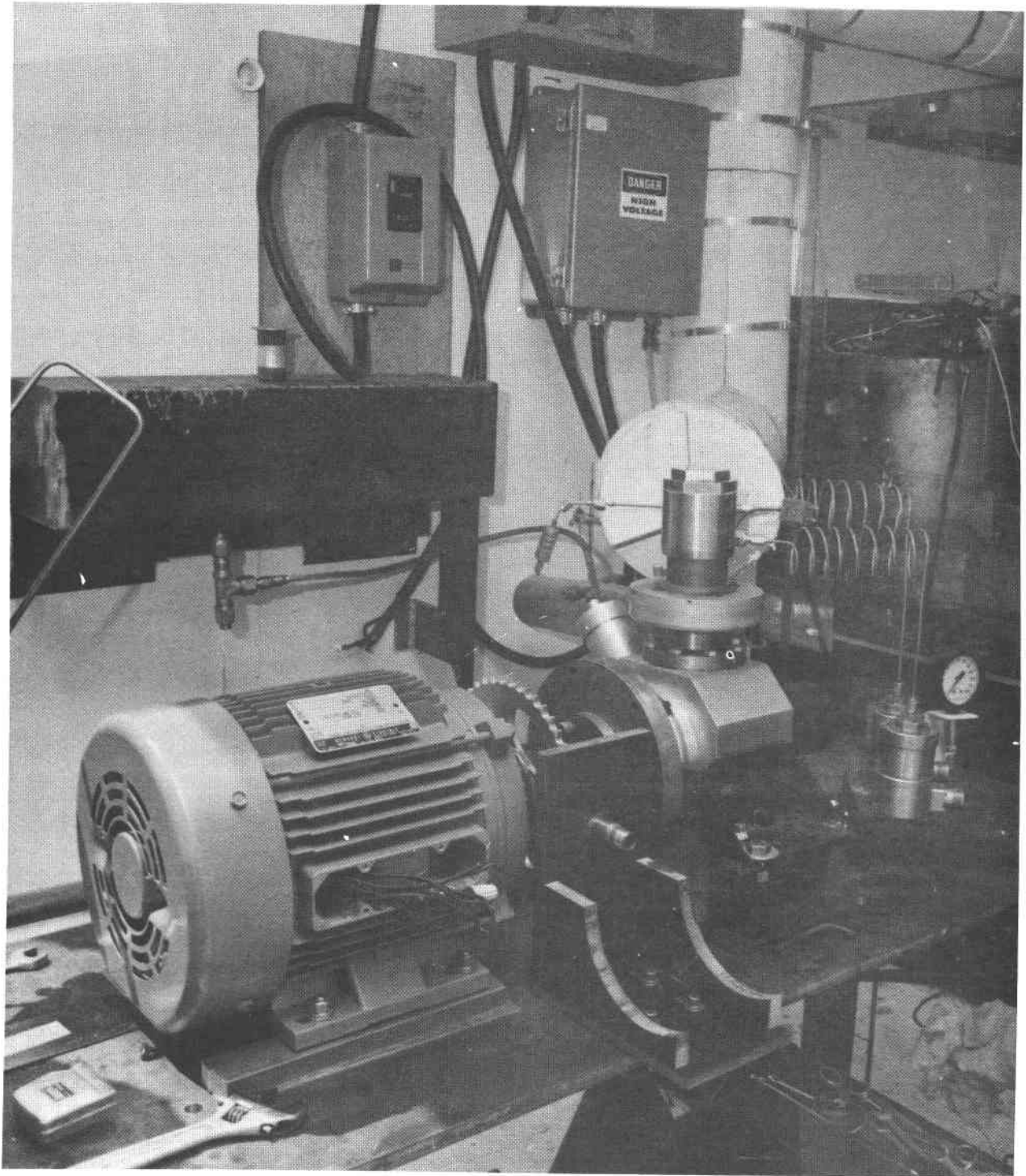
Figure 2. Jay Carter Single Cylinder Developmental
Prototype Automobile Steam Engine

316 L CASTING

STEAM IN

170 ATM
2500 PSI
677° C
(1250° F)

HOLLOW INCONEL O-RING

RENE 41

CARBIDE

STELLITE

TRIBALOY 400
CYLINDER LINER

NEEDLE BEARING

4130   DUCTILE IRON   4130

VITON
O-RINGS

8620

AL EXHAUST

AL CRANKCASE

OIL FILTER

EXPANDER
32 KG
(70 LBS)

4130 CASTING
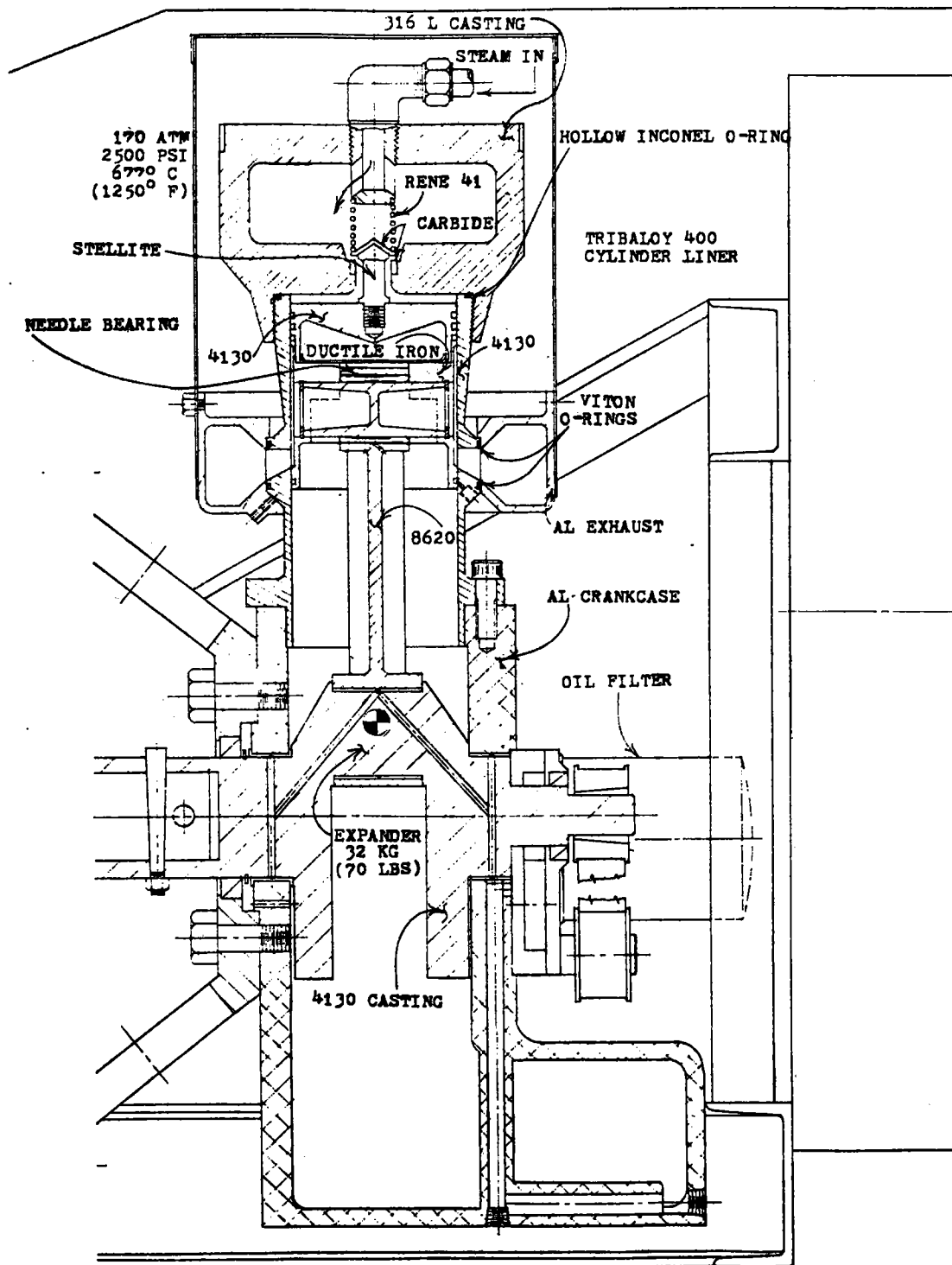
Figure 3. Expander Layout

127

(4) A regenerator is located ahead of the condenser to preheat the working fluid on its return to the steam boiler.

In common with other piston steam expanders, the Carter engines employ pistons, piston rings, cranks, feedwater pumps, bearings, etc. Lubrication is a potential problem, as in all steam engines, in that degradation of the lubricating oil due to high operating temperatures must be guarded against and the oil must be separated from the water before the water is circulated back to the boiler to be vaporized.

The specification for both the single cylinder and two cylinder Carter expanders are shown in Table 1. Only these specifications and data relating to the expander and its accessories and to the induction alternators mounted on each engine are discussed in this paper, since the characteristics of the fuel-fired boiler were not considered relevant to this study. Details of the complete automotive engine are given in Reference 2.

BACKGROUND OF THIS STUDY

Steam has been historically the most popular and successful working fluid for use in solar thermal power system engines (3), and was therefore a natural candidate for study in the JPL parabolic dish project. Under the technical direction of NASA Lewis Research Center (LeRC), concept definition studies were undertaken by Sundstrand Corporation (4), Foster Miller (5), and Jay Carter (6). Due to subsequent funding limitations the intended second phase of these contracts was never implemented. As a result, no new hardware was developed, although some effort did continue with other funding.

Table 1. Carter Steam Engines Specifications

Model: Paratransit Vehicle Engine
Type: Two-cylinder, single acting uniflow
Bore: 2.5 in.
Stroke: 3 in.
Displacement: 29.54 in^3
Expansion Ratios: 10:1
                    14.4:1
Speed: 3600 RPM
Nominal Power Rating: 23.09 HP (at 1000°F, 10:1 Expansion ratio)

Model: Automotive Developmental Prototype Engine
Type: Single-cylinder, single-acting uniflow
Bore: 2 in.
Stroke: 2.5 in.
Displacement: 7.85 in3
Expansion Ratio: 11.6 to 1
Speed: 1800 RPM
Nominal Power Rating: 8 SHP

128

When the Small Community Solar Thermal Power Experiment (SCSE) entered its second phase, a determination was made to use the Rankine Cycle in the Experiment instead of either the Stirling or Brayton Cycles. To implement that decision JPL, with the help of LeRC, formed a study team to look into the problem of the readiness of the Rankine engine. Although the organic Rankine cycle (ORC) was selected as the preferred technology for SCSE, it was recognized that no engine was an "off-the-shelf" item and that the performance and reliability data which existed for any small Rankine power plant was speculative. At the same time it was deemed desirable to consider possible backup engine technologies in the event that the ORC was not successful. Because the Jay Carter Paratransit vehicle engine already existed, but had not been run, it was decided to obtain firm performance data on this engine. Ford Aerospace and Communications Corporation (FACC) was asked to supplement their development of the ORC (which was being done through Barber-Nichols Engineering) through of a small performance study and testing contract with Jay Carter Enterprises. These tests were then performed on the Jay Carter Paratransit Vehicle Engine at the West Coast Facility of Jay Carter Enterprises under the direction of W. Wingenbach.

After successful completion of a test on the fuel-fired engine, where three-phase electric power was fed into the Santa Barbara distribution grid of Southern California Edison Co., the engine was shipped to the JPL Parabolic Dish Site. There it was operated in the solar-only mode, using steam generated by the Test Bed Concentrator (TBC).

About the same time that these tests were being conducted it was determined that a backup engine for the ongoing Omnium-G system tests was desirable. Since the original single cylinder Carter developmental engine was still in existence (Figure 2), this unit was modified and refurbished and also run on steam generated by the TBC.

FUEL FIRED TESTS OF THE CARTER PARATRANSIT VEHICLE ENGINE

OBJECTIVE

The objective of the project was to test an existing Jay Carter Enterprises (JCE) steam engine so as to characterize its performance under conditions similar to those which would be encountered in the Small Community Solar Thermal Power Experiment and to compare the results with performance predicted by computer simulations of the engine.

The existing two cylinder steam engine was developed as an automobile (Paratransit Vehicle) engine (Ref. 1). The engine has a displacement of 30 cubic inches, is designed to operate at 1050 deg.F and develops up to 90 horsepower. Although the Carter steam engines were and still are considered to be the highest performing automotive steam engines ever built (2), development work was shifted in 1976 from steam engines to other energy sources, namely wind generators.

In 1979, JCE received a contract from the National Aeronautics and Space Administration (NASA) to conduct a concept definition study to characterize a JCE design steam engine as part of a 15 KWe Solar Electric Power System. A branch office was established in Santa Barbara, California for the purpose of conducting the study and of renewing development of steam engines for various applications. Results of the study are reported in Reference 6.

The automobile engine, which had been sitting idle since 1976, was transported to Santa Barbara along with available testing equipment for the purpose of conducting tests and performing engine evaluation.

TEST PROCEDURE

The engine test system consisted of the expander, steam generator, feedwater pump assembly, alternator assembly, condenser assembly, and control system. The engine, along with a control panel, was located in a small building while the fuel supply and the condenser assembly were located outside. Utilities for the building included single and three-phase 240 volt AC power. A 25 HP three-phase induction motor was installed to absorb steam engine output and was used in conjunction with efficiency calibration curves supplied by the manufacturer to calculate the engine output. A three-phase watt-hour meter was used to measure the electrical power generated. All power absorbing accessories were driven by separate instrumented electric motors. Non-power absorbing units simulating the physical presence of automotive accessories were mounted to the engine and belt driven. To reduce engine vibration a counterbalance shaft was driven by the same belt and in the same manner as was employed in the automobile installation. A single-phase watt-hour meter was used to measure the power supplied to the feedwater pump assembly.

A flow diagram for the engine is shown in Figure 4. Flow is from a water storage tank or a measuring burette, through the feedwater pump and feedwater preheater to the steam generator. Water flow rate is controlled by feedback from temperature sensing at several places in the steam generator. Steam flows from the generator through a throttle valve into the expander where it is expanded to obtain mechanical power. During expansion, oil is injected into the steam in the region of piston ring travel. The expanded steam flows out of an exhaust manifold through the feedwater preheater (regenerator) and into the condenser. The condensate returns through a centrifuge which separates water and oil; water being returned to the water tank and the oil to the engine.

Tests were conducted over a range of values of thermal input and steam temperature. Thermal input was controlled by the flow rate of diesel oil supplied to the steam generator, while temperature was controlled by adjustment of the water control system. Power was absorbed by the three-phase induction alternator which was connected to the Southern California Edison (SCE) power grid.*

Thermocouples were used to measure steam inlet temperature (T1) and feedwater temperature (TFW). Pressure gauges were used to obtain steam inlet pressure (P1) and feedwater pressure (PFW). Mass flow was obtained by timing flow out of the water burette after diverting the returning feed water. Generated power and accessory power were obtained by timing the turning rates of the watt-hour meters.

---

*This power was purchased by Southern California Edison as part of a buy-back provision of the Public Utilities Regulatory Policies Act (PURPA).

SEPARATOR

STEAM GENERATOR

WATER PUMP

THROTTLE VALVE

PRE-HEATER

INDUCTION GENERATOR

EXPANDER

CONDENSER

CONDENSATE PUMP

OIL RETURN
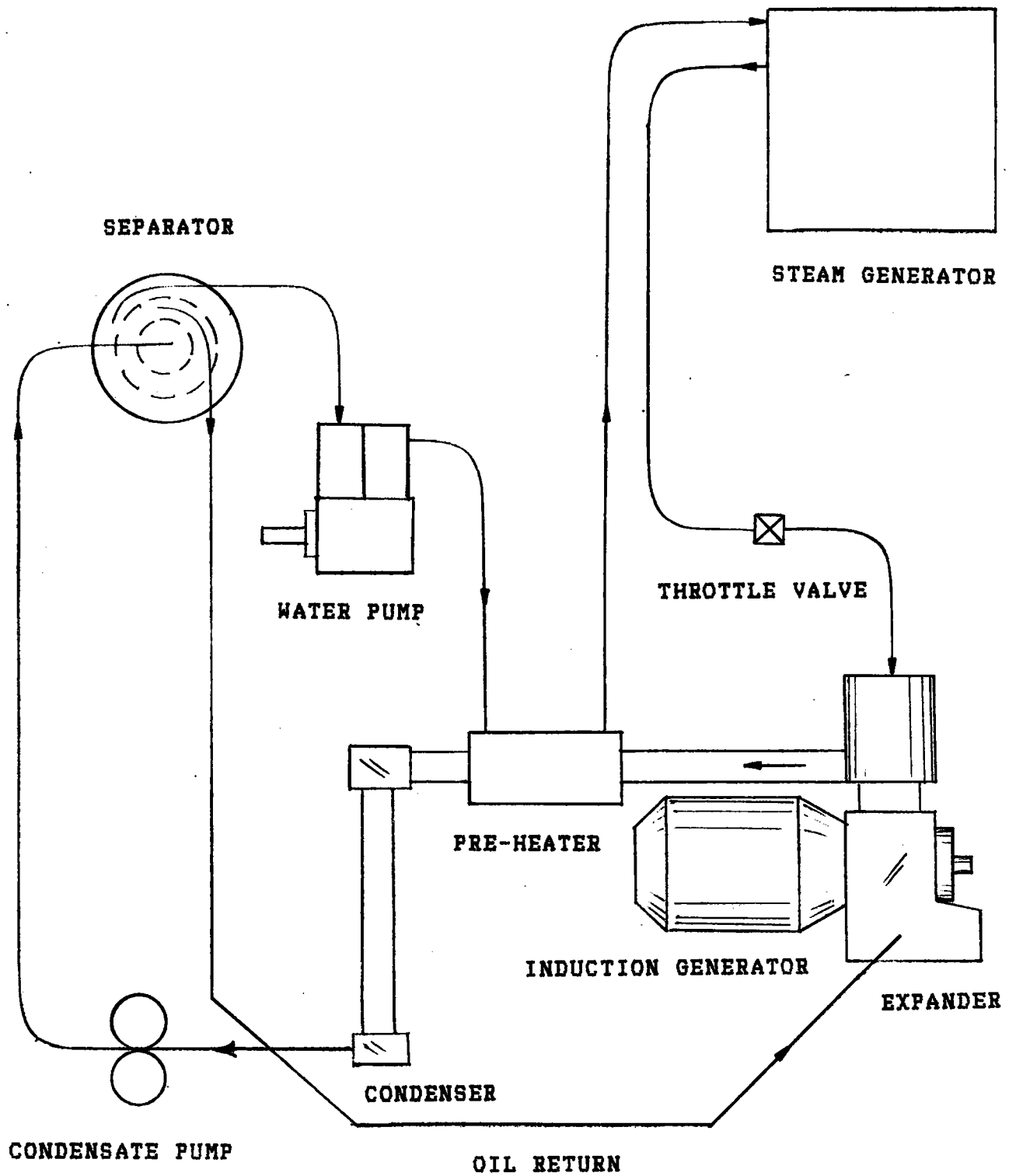
Figure 4. Steam Engine Flow Diagram.

131

Table 2. Engine Simulation

ENGINE TYPE	SIMPLE	ENGINE SPEED	3600. RPM
THERMAL INPUT	80. KW	STEAM TEMPERATURE	1000. DEG.F
IDEAL CYCLE EFF	0.250	CONDENSING TEMP.	212. DEG.F
NO. OF CYLINDERS	2	EXPANSION RATIO	10.0/1
CYLINDER DIAMETER	2.500 IN.	DISPLACEMENT	29.452 CU.IN.
FRICTION LOSS	1.90 HP	THERMAL LOSS	1.81 HP

THERM	POW	NSHP	ACP	P1	H1	P2	H2	QW	TFW	EG	EX	EHE	EPC
80.00	15.7	22.9	0.58	1192.	1499.	63.	1194.	211.	233.	92.0	86.3	21.2	19.5
71.12	13.7	19.9	0.47	1132.	1501.	59.	1198.	187.	237.	92.0	84.6	20.9	19.2
62.24	11.7	17.1	0.37	1038.	1504.	54.	1203.	164.	242.	92.0	82.5	20.5	18.9
53.36	9.9	14.3	0.29	979.	1506.	51.	1209.	142.	247.	92.9	79.8	19.9	18.5
44.48	7.8	11.4	0.23	956.	1506.	50.	1218.	119.	255.	92.1	75.7	18.9	17.5
35.60	5.7	8.2	0.16	873.	1509.	45.	1233.	95.	269.	92.8	69.3	17.3	16.1

WHERE:
THERM=THERMAL INPUT-KW
NSHP=NET SHAFT POWER-HP
P1=INLET PRESSURE-PSIA
P2=EXHAUST PRESSURE-PSIA
QW=MASS FLOW RATE-LB/HR
EG=GENERATOR EFFICIENCY-%
EHE=HEAT ENGINE EFFICIENCY-%

POW=ELECTRIC OUTPUT-KWe
ACP=ACCESSORY POWER-HP
H1=INLET ENTHALPY-BTU/LB
H2=EXHAUST ENTHALPY-BTU/LB
TFW=FEEDWATER TEMP.-DEG.F
EX=EXPANDER EFFICIENCY-%
EPC=POWER CONVERSION EFFICIENCY-%

Table 3. Results of Test Series No. 1--10/1 Expansion Ratio

TEMPERATURE--1000.DEG.F

THERM	POW	GPOW	ACP	P1	H1	TFW	PFW	HFW	HNET	QW	EPC
78.58	15.42	15.71	0.29	1000.	1502.	215.	1200.	184.	1318.	204.	19.6
64.99	11.29	11.78	0.19	750.	1510.	215.	950.	183.	1327.	167.	17.8
52.83	8.49	8.63	0.14	660.	1512.	205.	800.	179.	1333.	135.	16.1

WHERE:
THERM=THERMAL INPUT-KW
GPOW=GROSS ELECTRIC POWER-KWe
P1=INLET PRESSURE-PSIA
TFW=FEEDWATER TEMP.-DEG.F
HFW=FEEDWATER ENTHALPY-BTU/LB
QW=MASS FLOW RATE-LB/HR

POW=ELECTRIC OUTPUT-KWe
ACP=ACCESSORY POWER-KWe
H1=INLET ENTHALPY-BTU/LB
PFW=FEEDWATER PRESSURE-PSIA
HNET=NET ENTHALPY-BTU/LB
EPC=POWER CONVERSION EFFICIENCY-%
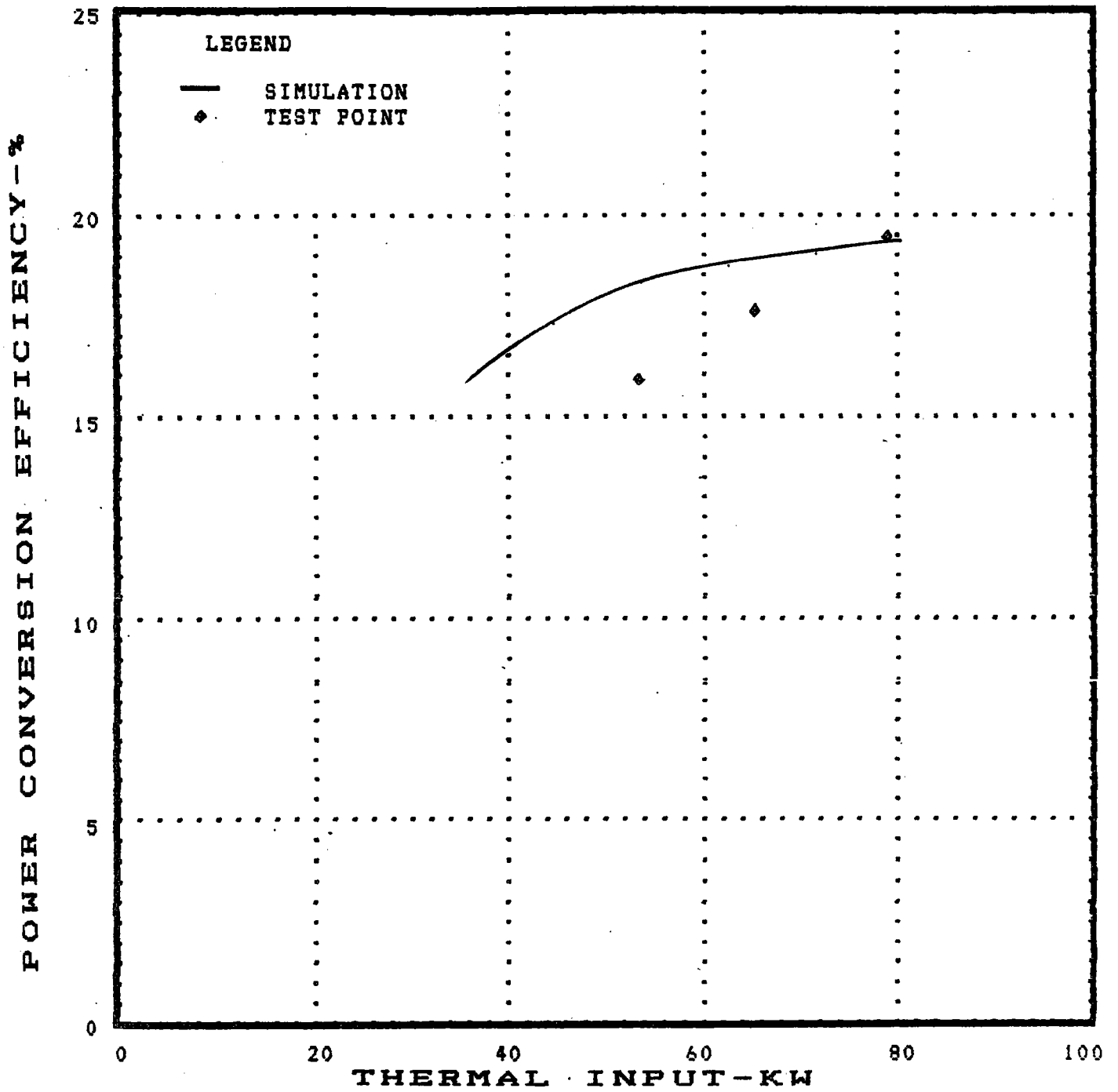
FIGURE 5.   TEST SERIES #1--1000 DEG.F

DOCUMENT TRANSMITTAL

JET PROPULSION LABORATORY
California Institute of Technology
4800 Oak Grove Dr. / Pasadena, CA 91109

TO: Sandia National Livermore Lab.

Box 969

Livermore, CA 94550

Attn: Dick Caputo

DATE SENT: 3/31/83

No. OF COPIES: 1

REQUESTED BY: Self

REFERENCE: Telecon w/Tah

REPORT No. 5105-118

TITLE: Parabolic Dish Solar Thermal Power Annual Program

Review Proceedings (December 8-10, 1981)

AUTHOR/ORIGINATOR

REPORT DATE:

CONTRACT:

REMARKS: Enclosed is the document you requested.

APPROVED BY: A. M. Pearson

PREPARED BY: Tah Nelson

JPL 2788 R 12/81

SOLAR DATA CENTER
(213) 577-9519 OR 9520

TABLE 4. ENGINE SIMULATION--10/1 EXPANSION RATIO

TEMPERATURE--1050 DEG.F

THERM	POW	NSHP	ACP	P1	H1	P2	H2	QW	TFW	EG	EX	EHE	EPC
80.00	16.1	23.5	0.58	1214.	1527.	63.	1209.	208.	247.	92.0	86.4	21.9	20.2
71.12	14.1	20.6	0.48	1157.	1529.	60.	1213.	185.	251.	92.0	84.7	21.6	19.9
62.24	12.1	17.6	0.38	1100.	1530.	57.	1218.	162.	255.	92.0	82.6	21.2	19.5
53.36	10.1	14.6	0.30	1038.	1532.	54.	1225.	139.	262.	92.9	79.7	20.5	19.0
44.48	8.1	11.8	0.23	977.	1534.	51.	1234.	118.	270.	92.1	75.9	19.6	18.0
35.60	5.9	8.5	0.16	946.	1535.	49.	1249.	94.	283.	92.8	69.5	17.9	16.6
26.72	3.7	5.4	0.11	817.	1538.	42.	1278.	72.	309.	91.1	59.1	15.0	13.7

TEMPERATURE--950 DEG.F

THERM	POW	NSHP	ACP	P1	H1	P2	H2	QW	TFW	EG	EX	EHE	EPC
80.00	15.1	22.0	0.56	1144.	1471.	62.	1179.	213.	220.	92.0	86.2	20.5	18.8
71.12	13.2	19.2	0.45	1071.	1474.	58.	1183.	189.	224.	92.0	84.5	20.2	18.6
62.24	11.3	16.6	0.36	979.	1477.	53.	1188.	166.	228.	92.0	82.4	19.8	18.3
53.36	9.5	13.7	0.27	887.	1480.	47.	1195.	142.	234.	92.9	79.4	19.3	17.9
44.48	7.6	11.1	0.20	796.	1483.	42.	1204.	120.	242.	92.1	75.7	18.5	17.0
35.60	5.6	8.0	0.13	701.	1486.	36.	1219.	96.	256.	92.8	69.3	16.9	15.7
26.72	3.4	5.0	0.08	598.	1489.	31.	1246.	73.	280.	91.1	58.5	14.1	12.8

TEMPERATURE--850 DEG.F

THERM	POW	NSHP	ACP	P1	H1	P2	H2	QW	TFW	EG	EX	EHE	EPC
80.00	13.9	20.3	0.54	1096.	1414.	63.	1149.	219.	193.	92.0	85.8	18.8	17.3
71.12	12.2	17.8	0.42	1009.	1418.	58.	1154.	194.	197.	92.0	84.1	18.6	17.2
62.24	10.4	15.2	0.34	965.	1419.	55.	1158.	169.	201.	92.0	81.9	18.2	16.8
53.36	8.7	12.6	0.27	874.	1423.	49.	1165.	145.	207.	92.9	78.9	17.7	16.4
44.48	7.0	10.2	0.20	785.	1427.	43.	1173.	123.	215.	92.1	75.1	16.9	15.6
35.60	5.1	7.3	0.13	691.	1431.	38.	1187.	98.	228.	92.8	68.4	15.5	14.3
26.72	3.1	4.5	0.08	590.	1435.	32.	1213.	74.	250.	91.8	57.3	12.7	11.7

TEMPERATURE--750 DEG.F

THERM	POW	NSHP	ACP	P1	H1	P2	H2	QW	TFW	EG	EX	EHE	EPC
80.00	12.7	18.6	0.50	1009.	1360.	61.	1121.	224.	168.	92.0	85.4	17.2	15.9
71.12	11.0	16.1	0.41	947.	1363.	57.	1125.	198.	172.	92.0	83.6	16.9	15.6
62.24	9.5	13.9	0.32	901.	1365.	54.	1129.	174.	175.	92.0	81.3	16.6	15.3
53.36	7.9	11.5	0.25	815.	1369.	48.	1136.	148.	181.	92.9	78.2	16.1	15.0
44.48	6.3	9.2	0.19	742.	1373.	43.	1143.	126.	188.	92.1	74.3	15.4	14.2
35.60	4.7	6.8	0.12	659.	1377.	37.	1156.	101.	199.	92.6	68.0	14.1	13.1
26.72	2.8	4.1	0.08	569.	1381.	32.	1179.	76.	220.	91.8	56.3	11.4	10.5

TABLE 5. RESULTS OF TEST SERIES #2--10/1 EXPANSION RATIO

TEMPERATURE--1050.DEG.F

THERM	POW	GPOW	ACP	P1	H1	TFW	PFW	HFW	HNET	QW	EPC
69.56	12.76	13.03	0.03	950.	1539.	195.	1100.	166.	1373.	173.	18.3
54.68	9.10	9.29	0.19	700.	1545.	195.	850.	165.	1380.	135.	16.6
36.39	5.12	5.25	0.13	525.	1550.	205.	600.	174.	1376.	90.	14.1
25.13	2.07	2.14	0.07	450.	1552.	235.	550.	205.	1347.	64.	8.2

TEMPERATURE-- 950.DEG.F

THERM	POW	GPOW	ACP	P1	H1	TFW	PFW	HFW	HNET	QW	EPC
64.55	11.32	11.65	0.33	875.	1484.	205.	1050.	175.	1309.	168.	17.5
54.59	8.31	8.50	0.19	650.	1491.	195.	800.	65.	1326.	141.	15.2
37.96	4.53	4.67	0.14	525.	1495.	205.	650.	175.	1320.	98.	11.9
22.85	1.79	1.85	0.06	425.	1499.	235.	550.	205.	1294.	60.	7.8

TEMPERATURE-- 850.DEG.F

THERM	POW	GPOW	ACP	P1	H1	TFW	PFW	HFW	HNET	QW	EPC
75.61	12.97	13.29	0.32	800.	1430.	215.	1000.	185.	1245.	207.	17.1
56.51	8.71	8.92	0.21	610.	1438.	215.	800.	185.	1253.	154.	15.4
38.19	4.36	4.49	0.13	450.	1444.	205.	600.	174.	1270.	103.	11.4
22.18	1.40	1.45	0.05	350.	1448.	225.	450.	194.	1254.	60.	6.3

TEMPERATURE-- 750.DEG.F

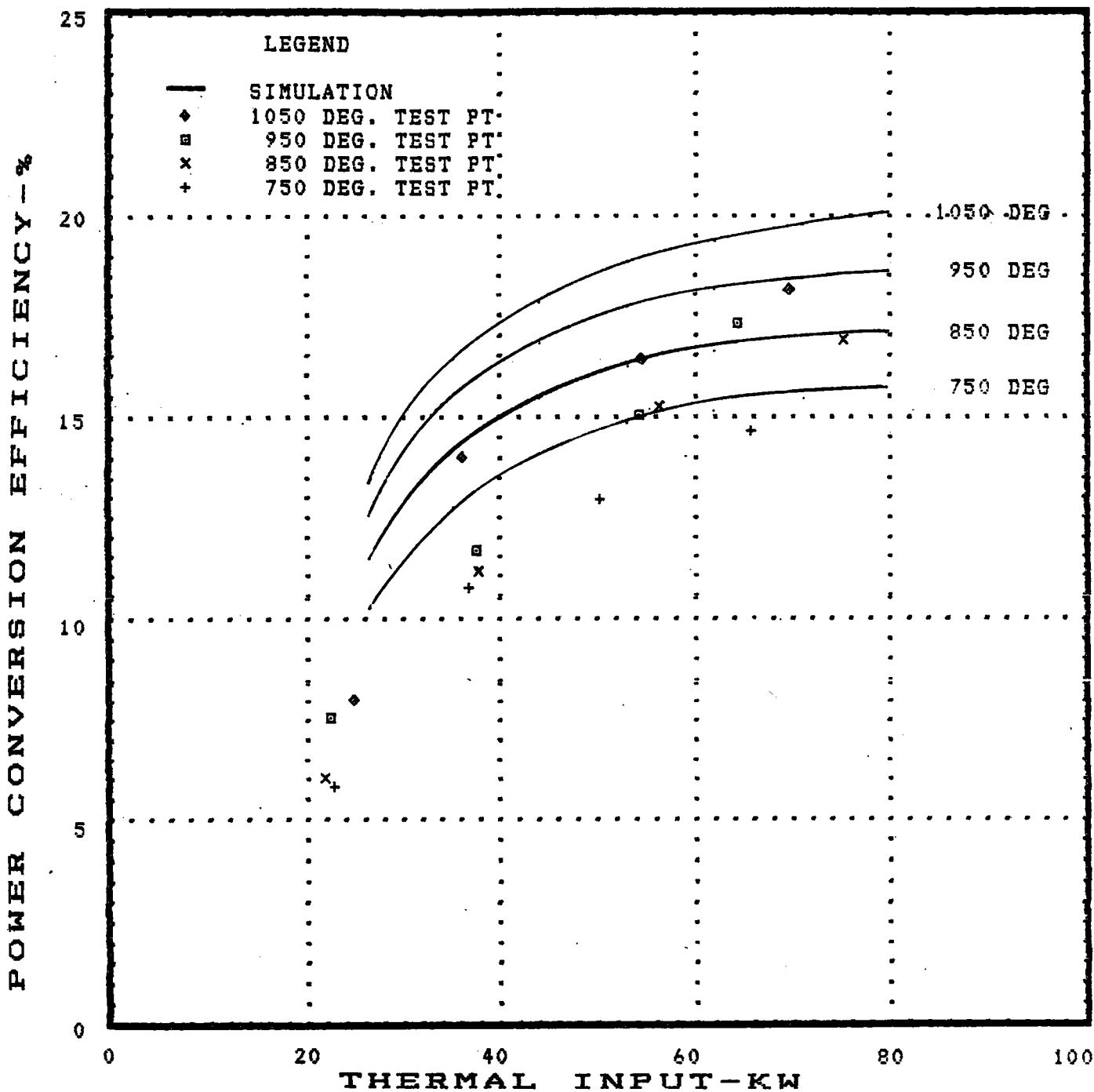| THERM	POW	GPOW	ACP	P1	H1	TFW	PFW	HFW	HNET	QW	EPC
66.02	9.78	10.07	0.29	775.	1373.	205.	950.	175.	1198.	188.	14.8
50.57	6.71	6.94	0.23	700.	1377.	225.	850.	195.	1182.	146.	13.3
37.21	4.09	4.23	0.14	450.	1390.	205.	600.	174.	1216.	105.	11.0
23.11	1.41	1.46	0.05	350.	1395.	225.	450.	194.	1201.	66.	6.1

FIGURE 6. TEST SERIES #2--10/1 EXPANSION RATIO

TABLE 6. ENGINE SIMULATION--14.4/1 EXPANSION RATIO

TEMPERATURE--1050 DEG.F

THERM	POW	NSHP	ACP	P1	H1	P2	H2	QW	TFW	EG	EX	EHE	EPC
80.00	17.0	24.9	0.77	1796.	1511.	63.	1169.	205.	212.	92.0	87.1	23.2	21.3
71.12	14.9	21.8	0.63	1697.	1514.	59.	1174.	182.	215.	92.0	85.5	22.9	21.1
62.24	12.8	18.7	0.51	1633.	1516.	56.	1179.	160.	220.	92.0	83.5	22.5	20.7
53.36	10.8	15.6	0.42	1561.	1518.	54.	1186.	137.	226.	92.9	80.8	21.8	20.3
44.48	8.7	12.7	0.30	1409.	1522.	48.	1195.	116.	235.	92.1	77.3	21.1	19.4
35.60	6.6	9.5	0.21	1175.	1528.	40.	1212.	93.	250.	92.8	71.8	19.8	18.4
26.72	4.3	6.3	0.11	940.	1535.	31.	1239.	72.	274.	91.1	62.8	17.3	15.8
17.84	1.3	1.9	0.05	626.	1543.	21.	1343.	50.	368.	91.0	34.5	8.3	7.5

TEMPERATURE--950 DEG.F

THERM	POW	NSHP	ACP	P1	H1	P2	H2	QW	TFW	EG	EX	EHE	EPC
80.00	15.9	23.1	0.73	1671.	1452.	62.	1140.	210.	185.	92.0	86.8	21.6	19.8
71.12	13.9	20.3	0.60	1595.	1455.	59.	1144.	187.	189.	92.0	85.3	21.3	19.6
62.24	12.1	17.6	0.48	1441.	1460.	53.	1150.	164.	194.	92.0	83.3	21.1	19.4
53.36	10.2	14.8	0.36	1282.	1466.	47.	1158.	141.	201.	92.9	80.7	20.6	19.1
44.48	8.2	12.0	0.25	1126.	1472.	40.	1168.	118.	210.	92.1	77.1	19.9	18.3
35.60	6.1	8.9	0.17	959.	1477.	34.	1183.	95.	224.	92.8	71.4	18.6	17.2
26.72	4.0	5.8	0.11	794.	1483.	27.	1208.	73.	247.	91.1	62.1	16.1	14.7
17.84	1.2	1.8	0.06	584.	1490.	20.	1305.	51.	334.	91.0	33.5	7.4	6.7

TEMPERATURE--850 DEG.F

THERM	POW	NSHP	ACP	P1	H1	P2	H2	QW	TFW	EG	EX	EHE	EPC
80.00	14.6	21.3	0.69	1543.	1393.	61.	1109.	215.	157.	92.0	86.5	19.9	18.3
71.12	13.0	18.9	0.57	1486.	1396.	59.	1113.	193.	161.	92.0	85.0	19.7	18.2
62.24	11.2	16.3	0.46	1366.	1401.	54.	1119.	168.	166.	92.0	82.9	19.4	17.9
53.36	9.4	13.6	0.35	1218.	1408.	47.	1127.	144.	174.	92.9	80.3	19.0	17.7
44.48	7.6	11.0	0.24	1073.	1415.	41.	1138.	121.	183.	92.1	76.6	18.4	16.9
35.60	5.6	8.2	0.17	917.	1422.	34.	1152.	97.	196.	92.8	70.8	17.1	15.8
26.72	3.6	5.3	0.10	763.	1428.	28.	1177.	74.	218.	91.1	61.0	14.7	13.4

TEMPERATURE--750 DEG.F

THERM	POW	NSHP	ACP	P1	H1	P2	H2	QW	TFW	EG	EX	EHE	EPC
80.00	13.5	19.6	0.65	1424.	1336.	60.	1080.	221.	131.	92.0	86.2	18.3	16.8
71.12	11.8	17.3	0.54	1363.	1340.	57.	1084.	196.	135.	92.0	84.5	18.1	16.6
62.24	10.2	14.9	0.44	1279.	1345.	53.	1090.	172.	140.	92.0	82.4	17.8	16.4
53.36	8.6	12.5	0.33	1147.	1352.	47.	1098.	147.	148.	92.9	79.7	17.4	16.1
44.48	6.9	10.1	0.23	1015.	1359.	41.	1108.	124.	157.	92.1	76.0	16.8	15.4
35.60	5.1	7.4	0.15	870.	1367.	34.	1123.	99.	169.	92.8	69.9	15.5	14.4
26.72	3.2	4.7	0.10	729.	1374.	28.	1146.	75.	191.	91.1	59.7	13.2	12.0

TABLE 7.   RESULTS OF TEST SERIES #3--14.4/1 EXPANSION RATIO

TEMPERATURE--1050.DEG.F

THERM	POW	GPOW	ACP	P1	H1	TFW	PFW	HFW	HNET	QW	EPC
87.31	15.53	16.30	0.77	2400.	1497.	235.	2500.	209.	1288.	232.	17.8
63.83	10.99	11.39	0.40	1450.	1525.	215.	150.	187.	1338.	163.	17.2
39.26	5.42	5.60	0.18	850.	1541.	25.	950.	195.	1346.	100.	13.8
23.93	1.95	2.04	0.09	625.	1547.	215.	700.	185.	1362.	60.	8.1

TEMPERATURE-- 950.DEG.F

THERM	POW	GPOW	ACP	P1	H1	TFW	PFW	HFW	HNET	QW	EPC
86.98	14.87	15.66	0.79	2300.	1433.	225.	2400.	198.	1235.	241.	17.0
63.75	10.41	10.78	0.37	1350.	1468.	215.	1500.	186.	1282.	170.	16.3
39.97	5.19	5.38	0.19	850.	1485.	225.	950.	195.	1290.	106.	13.0
23.52	1.68	1.77	0.09	600.	1493.	215.	700.	185.	1308.	61.	7.1

TEMPERATURE-- 850.DEG.F

THERM	POW	GPOW	ACP	P1	H1	TFW	PFW	HFW	HNET	QW	EPC
85.04	14.39	15.20	0.81	2175.	1367.	215.	2300.	188.	1179.	246.	16.9
65.84	10.82	11.22	4.00	130.	1408.	225.	1450.	196.	1212.	186.	16.4
39.53	5.07	5.26	0.19	800.	1430.	225.	900.	195.	1235.	109.	12.8
26.89	2.32	2.39	0.07	650.	1436.	215.	725.	185.	1251.	73.	8.6

TEMPERATURE-- 750.DEG.F

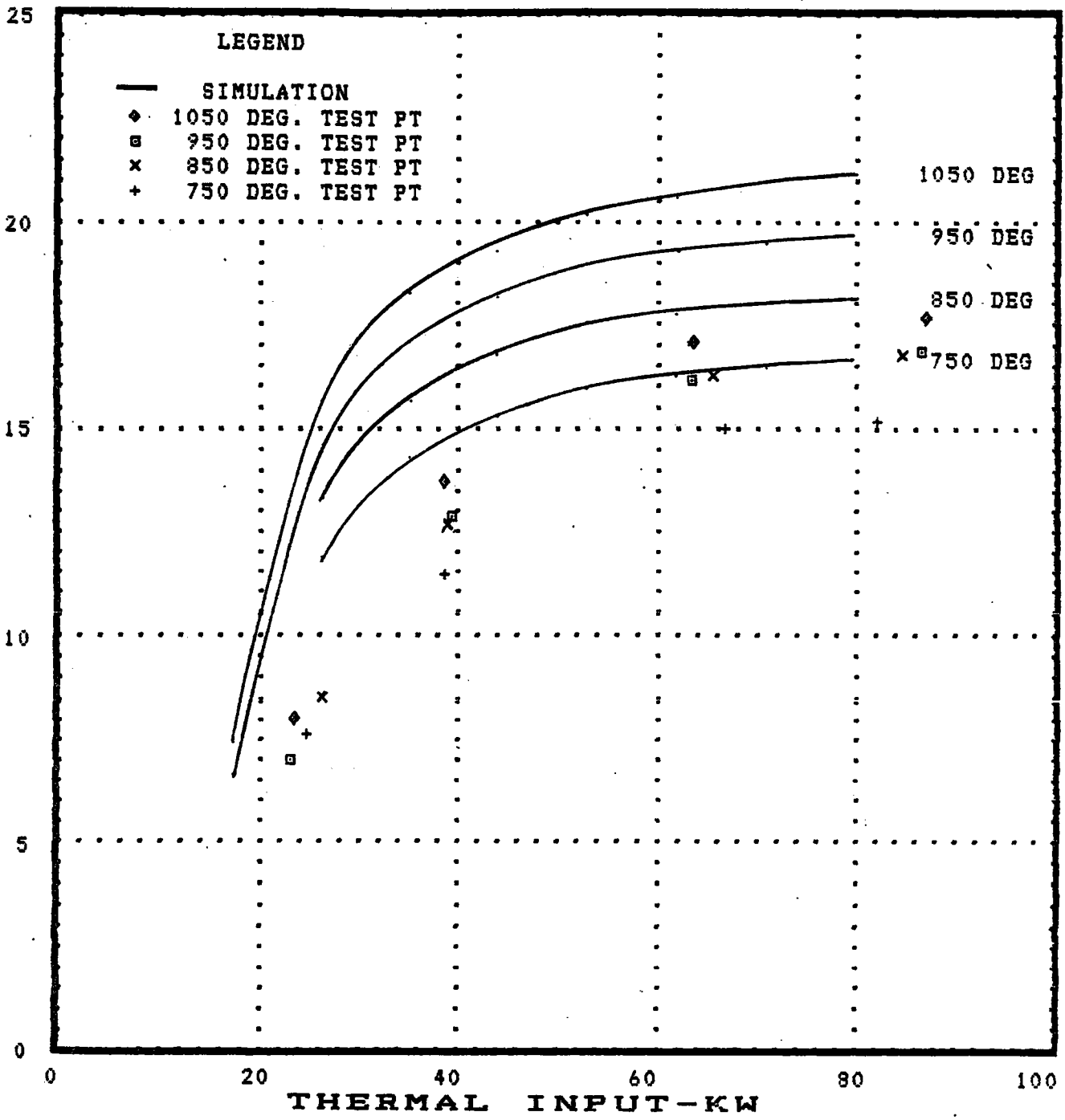| THERM	POW	GPOW	ACP	P1	H1	TFW	PFW	HFW	HNET	QW	EPC
82.51	12.63	13.33	0.70	1800.	1310.	205.	1950.	177.	1133.	249.	15.3
67.27	10.16	10.56	0.40	127.	1344.	225.	1400.	196.	1148.	200.	15.1
39.15	4.55	4.73	0.18	725.	1376.	225.	850.	195.	1181.	113.	11.6
25.10	1.92	2.01	0.09	600.	1382.	215.	700.	185.	1197.	72.	7.7

Figure 7. Test Series No. 3--14.4/1 Expansion Ratio

Tests were conducted at the original expansion ratio (ER) of 10 to 1 and at a modified ER of 14.4 to 1. Computer simulation of the engine predicted a slightly improved efficiency at a higher ER. The change in ER was affected on the engine by placing a metal filler in the clearance volume i.e., the volume which fills with high pressure steam prior to expansion.

Difficulties were encountered in getting the engine ready for testing. Some of these were related to the long dormancy of the engine while others were related to undocumented development work that had been going on at the time of cessation of steam engine work at JCE.

TEST RESULTS

Three test series were conducted. These were:

1) Preliminary testing at the original expansion ratio (ER) of 10/1.
2) Testing at ER of 10/1.
3) Testing at ER of 14.4/1.

Test series No. 1 was conducted at a steam inlet temperature of 1000 deg.F. Table 2 gives results of a computer simulation of the engine at this condition while Table 3 gives test results. Figure 5 combines the simulation and test results.

Between test series No. 1 and No. 2, the steam admission valves and valve springs were replaced due to breakage of the springs. The insulation around the cylinders was also changed from asbestos to fiberglass. Tables 4 and 5 and Figure 6 give results for test series No. 2. Between test series No. 2 and No. 3, fillers were placed in the cylinder clearance volume to change the ER from 10/1 to 14.4/1. Tables 6 and 7 and Figure 7 give results for test series No. 3.

The anticipated effect of inlet steam temperature and power level variations are confirmed by test results. However, the resulting values were usually lower than expected with the difference between observed and expected results becoming more pronounced as testing continued. Even the increase in expansion ratio for test series No. 3, which was expected to increase efficiency, in some cases actually resulted in lower observed efficiency.

Some observations were made of the condition of the engine and installation during and after testing:

> The cast aluminum exhaust manifold was leaking oil, water, and steam during the tests. Efforts to correct the problem were unsuccessful with the result that insulation around the cylinders became less effective as it absorbed oil and water as testing progressed. Post-test examination of the manifold revealed pits which apparently penetrated the wall of the casting and allowed exhaust steam, along with lubricating oil, to escape.

> Post-test examination of the blow-down valve showed signs of leaking of high temperature steam. The purpose of the blow-down valve is to allow purging the cylinders of steam condensate prior to running the engine. The plumbing on the cylinder side of the valve contains steam at high pressure and high temperature and a leak in this location has a pronounced effect on engine efficiency. The valve is located where it is difficult to see and the smoke and steam resulting from the exhaust manifold leak obscured the steam leak at the blow-down valve.

Post test examination of the simulated automobile air conditioning compressor revealed a defective bearing. This bearing had been checked and found to be operable prior to testing. It had evidently deteriorated during testing and was absorbing a significant amount of engine power by the time testing was completed.

Prior to initiation of tests, a check of steam admission valve lift indicated a valve lift of .040 inch. A post-test check showed a slight decrease in this parameter . There is a 5/8 inch diameter single valve per cylinder. Previous engines had used two 3/4 inch valves per cylinder with .070 inch lift. The effect of this significant decrease in valve opening from previous engines is observed during high mass flow when steam pressure in the steam chest is much higher than expected from computer simulations, indicating probable choking of the steam flow. The effect on efficiency is not known but it is probably detrimental.

CONCLUSIONS

Engine performance was generally satisfactory. The effect of temperature and power level variations was demonstrated. Engine efficiency was considered good although lower than projected by computer simulations. The effect of change in expansion ratio was not demonstrated because of engine deterioration during testing.

The discrepancy between expected and observed performance as well as the deterioration in engine performance is probably due to engine defects revealed by post-test inspection. The expander used in this test program had never been operated before and consequently, the defects had not been previously observed. Correction of these defects would very likely produce an engine with performance equal to that predicted by computer simulations.

SUMMARY

The Jay Carter Enterprises Paratransit Vehicle steam engine was tested over a range of conditions which might be experienced by the power converter subsystem of the Small Community Solar Thermal Power Experiment.

Some difficulties were encountered getting the engine ready for testing. These difficulties were related to the five year dormancy of the entire system and to incomplete development work that had been going on at the time of cessation of steam engine work at JCE.

Other difficulties were encountered during testing. These were related to the fact that the particular expander being tested had never been run before and possessed some manufacturing defects. Nevertheless, the engine was operated successfully and results of testing do verify results of computer simulations of the engine in regard to the effect of temperature and power level variations. Engine efficiency was good but generally lower than expected and performance dropped as testing continued. The effect of change in expansion ratio was not demonstrated because of deterioration in engine performance. Post-test inspection revealed numerous correctable defects which were believed to be responsible for these observed shortcomings.

Engine performance was generally satisfactory and further testing after correction of defects should produce results in agreement with computer simulation results.

SOLAR TESTS ON THE CARTER SYSTEM ENGINES

Each of the Carter engines was tested using steam generated in the Garrett Steam receiver mounted on the TBC (Figure 8). For these experiments a mobile steel enclosure was erected at the base of the TBC and insulated steam lines were led from the steam receiver down the dish structure and to the engines within the enclosure. Because of the anticipated thermal losses associated with the long steam lines, the temperature and pressure of the incoming steam were measured at a point just ahead of the engine. The particulars for instrumenting and operating the two engines differed, and data from both were subject to considerable uncertainty because there was insufficient time or resources to develop refined control and instrumentation systems.

Three-phase, 240 Volt, induction motors were used as alternators, feeding power to the SCE grid as a means of absorbing the power developed by the steam engines. These off-the-shelf units were calibrated beforehand. The 25 HP motor, driven by the larger engine demonstrates efficiency above 92% whereas the 5 HP motor from the smaller single cylinder engine peaked at 82%. When connected to the line these motors serve as starter motors for the steam engines, running them at near synchronous speed. As the steam engines begin to deliver net torque to the motors their speed rises above the synchronous value and electric power is generated which feeds into the grid. Both units operated successfully to deliver useful power. A summary of results obtained with the two engines used in the solar mode are presented in Table 8.

Table 8.

ENGINE: Paratransit Vehicle Engine

Inlet Steam: 815°F at 876 psig; 10 kWe power output
921°F at 1563 psig; 6.46 KWe power output
Condenser Exhaust

Engine Efficiency: 18% (including alternator)

ENGINE: Developmental Prototype Engine

Inlet Steam: 730°F at 840 psig; 1.557 KWe power output

Atmospheric Exhaust

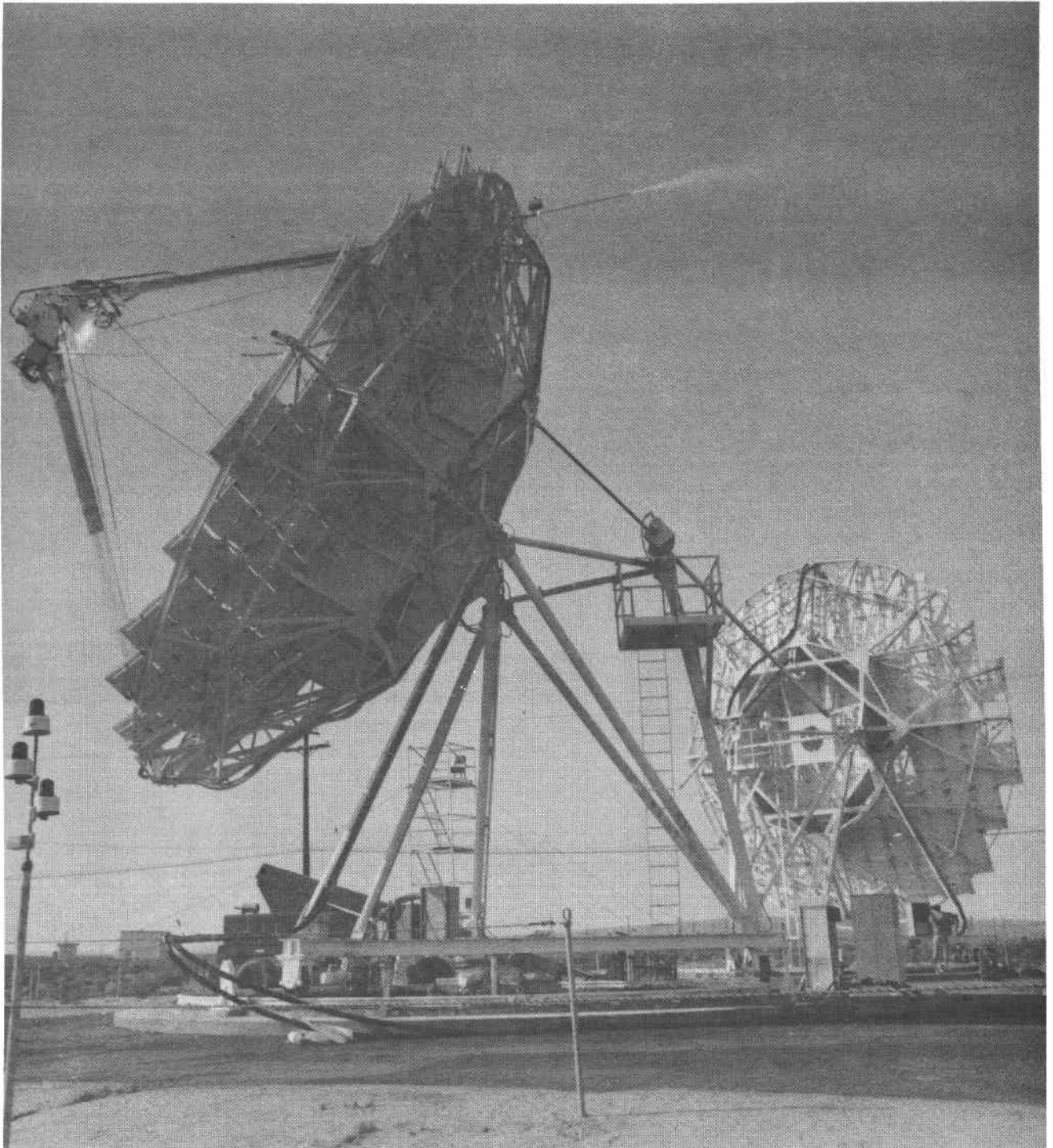Engine Efficiency: 12% (including alternator)

Figure 8. Garrett Receiver Mounted on Test Bed
Concentrator at PDTS. Steam is Being
Vented to the Atmosphere.

REFERENCES

1. J. W. Carter and W. J. Wingenbach, "The Carter System-Preliminary Test Results of Second Generation Steam Engine." Paper 760341 presented at SAE Automotive Engineering Congress and Exposition, Detroit, February 1976.

2. S. Luchter and R. Renner, "An Assessment of the Technology of Rankine Engines for Automobiles." Final Report ERDA-77-54, UC-96, April 1977.

3. A. B. Meinel and M. P. Meinel, "Applied Solar Energy", Addison-Wesley Publishing Company.

4. T. Bland, "Is kWe (Nominal) Solar Thermal Electric Power Conversion Concept Definition Study - Steam Rankine Turbine Study". Report DOE/NASA/0061-79/1, NASA CR-159589, AER 1713, October 1979.

5. H. Fuller, et. al., "15 kWe (Nominal) Solar Thermal Electric Power Conversion Concept Definition Study - Steam Reciprocator System". Report DOE/NASA/0062-79/1, NASA CR-159590, June 1979.

6. W. Wingenbach and J. Carter, "15 kWe (Nominal) Solar Thermal - Electric Power Conversion Concept Definition Study - Steam Rankine Reciprocator System." Final Report DOE/NASA/0063-79/1, NASA CR-159591, June 1979.

400-kW$_e$ High-Efficiency Steam Turbine
For Industrial Cogeneration

H.M. Leibowitz

Mechanical Technology Incorporated
968 Albany-Shaker Road
Latham, New York 12110

ACKNOWLEDGMENTS

ABSTRACT

An advanced state-of-the-art steam turbine-generator has been developed by Mechanical Technology Incorporated (MTI) to serve as the power conversion subsystem for the Department of Energy/Sandia National Laboratories' Solar Total-Energy Project (STEP) in Shenandoah, Georgia. The turbine-generator, which is designed to provide 400-kW$_e$ net electrical power, represents the largest turbine-generator that has thus far been built specifically for commercial solar-powered cogeneration.

The controls for the turbine-generator incorporate a multiple, partial-arc entry to provide efficient off-design performance, as well as an extraction control scheme to permit extraction flow regulation while maintaining 110-psig pressure. Normal turbine operation is achieved while synchronized to a local utility and in a stand-alone mode. In both cases, the turbine-generator features automatic load control as well as remote start-up and shutdown capability.

A four-stage, axial steam turbine rotates on a 42,450-rpm pinion to drive an 1,800-rpm synchronous generator through a double-reduction gearbox. At the inlet throttle condition of 720°F, 700 psig, the turbine is designed to produce 400 kW$_e$ and 2,249 lb/hr of 110-psig extraction steam while consuming 8,591 lb/hr of steam at the inlet throttle. In addition, the 6-psig exhaust steam is designed for use in an absorption chiller to provide 164 tons of plant air conditioning. The back-pressure turbine includes two high-pressure and two low-pressure stages separated by the 110-psig extraction port.

Tests totaling 200 hours were conducted at MTI to confirm the integrity of the turbine's mechanical structure and control function. Performance tests resulted in a measured inlet throttle flow of 8,450 lb/hr near design conditions. The successful completion of all structural, control and performance tests has produced a turbine-generator uniquely qualified for industrial cogeneration applications in the 500-hp class.

The turbine-generator was shipped to Shenandoah, Georgia, on September 1, 1981 for installation at the Bleyle knitwear mill. It is expected that the unit will be put into service by December, 1981.

1.0 INTRODUCTION

In our current struggle to reduce U.S. dependence on foreign oil, we have all come to recognize the obvious benefit of improving the efficiency of today's energy conversion machinery. At today's energy prices, even a modest increase of a few points in efficiency provides a fast return to offset the capital cost premium associated with more advanced, efficient equipment. It is not uncommon to achieve payback periods of less than two years, particularly when oil is the fuel consumed.

Likewise, but less obvious to most, the argument for high efficiency is just as keen when dealing with renewable energy sources where the "fuel" cost is actually nil. For these renewable energy technologies such as solar, wind, ocean thermal and geothermal, the incremental improvement in efficiency translates directly to a commensurate cost reduction in the energy-gathering equipment. Normally, the renewable resources contain a much lower energy flux than do the conventional fossil fuels; as a result, the conversion equipment required to produce usable thermal energy is quite large and expensive. For example, the cost of generated power in a solar thermal energy system is directly tied to the size of the collector field, which, in most cases, is more than 50% of the total system cost. Consequently, there is an enormous payoff associated with optimizing the turbine-generator efficiency at almost any price. As a case in point, consider a system whose total price is $10,000/kW, of which the collection system costs is $5,000/kW. Increasing the turbine's efficiency by 10% reduces the overall system cost to $9,500/kW$_e$ because 10% fewer collectors are required, all else remaining the same. Hence, a 1-MW system can then be built for one-half million dollars less than one employing a less efficient turbine. This also suggests that an additional one-half million dollars could be spent for the more efficient turbine without affecting the overall economics of the system.

It was precisely this rationale that spawned the development of the high-performance turbine-generator for the Shenandoah project. A performance optimization strategy produced the turbine's unique design features that are described herein. The manner in which this design strategy was implemented is the subject of this paper.

2.0   THE PROBLEM STATEMENT AT SHENANDOAH

The turbine's duty cycle at Shenandoah and its performance criteria imposed a specification that was not offered commercially in the 400-kW$_e$ size range. As a result, an unconventional design strategy was required. Some of the major items within the specification were:

- Total energy supplier: electric power, steam extraction, absorption cooling
- Optimum efficiency: design point to 50% electric load
- Automatic and remote start-up and shutdown
- Automatic load following
- Stand-alone and synchronous operation
- Automatic extraction pressure control
- 60 Hz ± .3 Hz frequency quality maintained during electric and thermal load transients.

While the specification as a whole may appear somewhat aggressive, the most difficult requirement was the premium placed on the turbine's efficiency. As previously indicated, turbine efficiency exerts enormous leverage on total system cost by directly impacting the size of the collection field, which is by far the costliest component in the system. As a matter of fact, the commercialization of solar thermal power generation is being paced by collector/receiver costs, particularly for high-temperature systems such as the parabolic dish and heliostat/power tower configurations.

2.1   Design Strategy

The high-efficiency goal affected the turbine design in two ways. In comparison to conventional designs, considerably higher rotational speeds were required, and a partial-admission, axial machine was necessitated to achieve high part-load performance.

Recognizing that the poor performance, relatively speaking, of conventional steam turbines in the 500-hp class is due to poor aerodynamic matching between the blade speed and gas velocity, the design strategy became clear; increase the

rotational speed and, in so doing, increase the blade speed to achieve the optimum expansion efficiencies. The N_s versus D_s correlation shown in Figure 1 clearly indicates this strategy. By increasing the specific speed, N_s from the 5 to 15 range to an N_s in excess of 50 increases the expansion efficiency by 20 to 30 points.
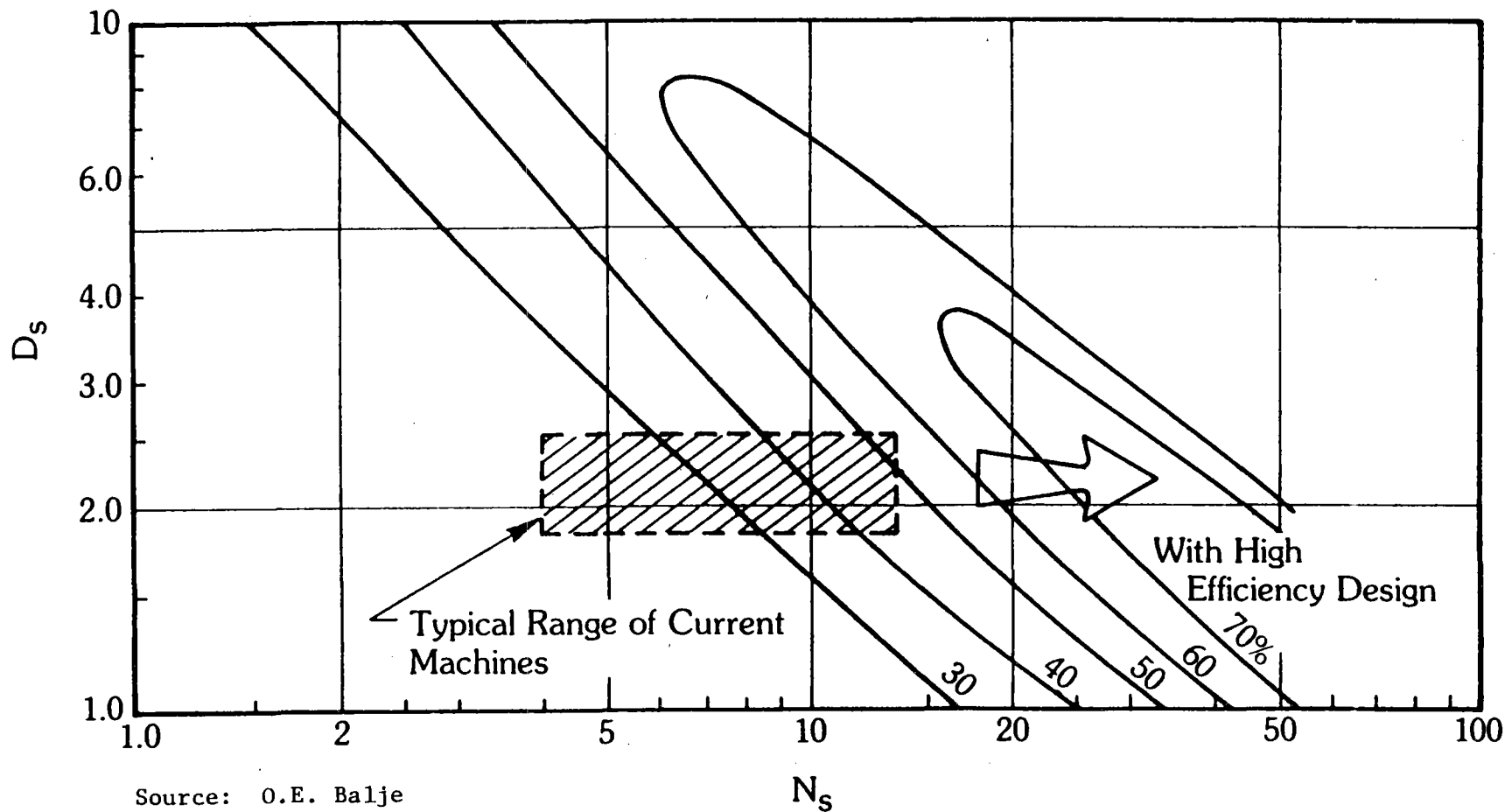
The "cost" associated with adopting this strategy is high speed. The 600-hp turbine built for Shenandoah rotates at a pinion speed of 42,450 rpm, which is significantly higher than the 3,600- to 12,000-rpm machines that typify most commercial designs. High speed requires high reduction gearing and its inherent parasitic losses and, equally as important, the technical acumen to address multi-critical, flexible shaft rotors. Where these skills are not present or otherwise not used, high speed is viewed as a limiting factor to the turbine's availability/reliability. The fact of the matter is that well-designed, high-speed turbomachines have proven as reliable as their low-speed, inefficient counterparts. In a recent study[1] of 280 high-speed turbocompressors operating at speeds to 52,000 rpm, their availability was calculated at .9997, based on an excess of three-million operating hours. The subject turbine is similar in design to those surveyed.

---

[1]Leibowitz, H.M., Rochow, K.H., and Bryant, T.E., "The Reliability of High-Speed Turbomachinery: A Survey of Single-Stage Centrifugal Compressors, June 1980, MTI 80TR34, unpublished.

N = rpm
H_A = Head, ft, Adiabatic
V_E = Volume, cfs, Exhaust
D = Diameter, ft

$$N_s = \frac{N\sqrt{V_E}}{H_A^{3/4}} \qquad D_s = \frac{D\,H_A^{1/4}}{\sqrt{V_E}}$$

Typical Range of Current Machines

With High Efficiency Design

70%
60
50
40
30

Source: O.E. Balje

N_s

Fig. 1 $N_s D_s$ Diagram for Single-Stage, Partial-Admission Axial Turbines

3.0 TURBINE DESIGN

3.1 Aerothermal

A four-stage, partial-admission axial turbine was selected for its high design point and part-load performance capability. As shown in the cross section, Figure 2, the turbine consists of a high-pressure section and a low-pressure section separated by an extraction port (not shown). Favorable part-load performance is incorporated in the design by a 6, 2, 2 partial-admission strategy. At full throttle, 10 nozzle partitions extending over a 180° arc are open. The number of open partitions drops to 8 for 75% load and then to 6 for 50% load.

The blading is of the impulse variety with nozzle heights ranging from .25 to .56 inch, first stage and last stage, respectively. Wheel diameters, at the pitch section, vary from 3.85 to 4.16 inches. The specific speed, N_s, and specific diameter, D_s, for each stage are plotted in Figure 3, which predicts isentropic efficiencies in the 70% range, based on Balje's correlation[2].

Using MTI-derived design correlations, the thermodynamic state points of the expansion process were calculated and are presented graphically in Figure 4. The enthalpies represented by points A, B, C, and D reflect a high-pressure turbine efficiency of 65% and a low-pressure turbine efficiency of 73%. Accounting for the reheat effect associated with the extraction steam at point C and the 55/45 flow split between the high- and low-pressure turbines, the overall aerodynamic efficiency is predicted to be 68%.

---

[2] Balje, D.E., "A Study in Design Criteria and Matching Turbomachines: Part A - Similarity Relations and Design Criteria for Turbines," _Journal of Engineering for Power_, January 1962.
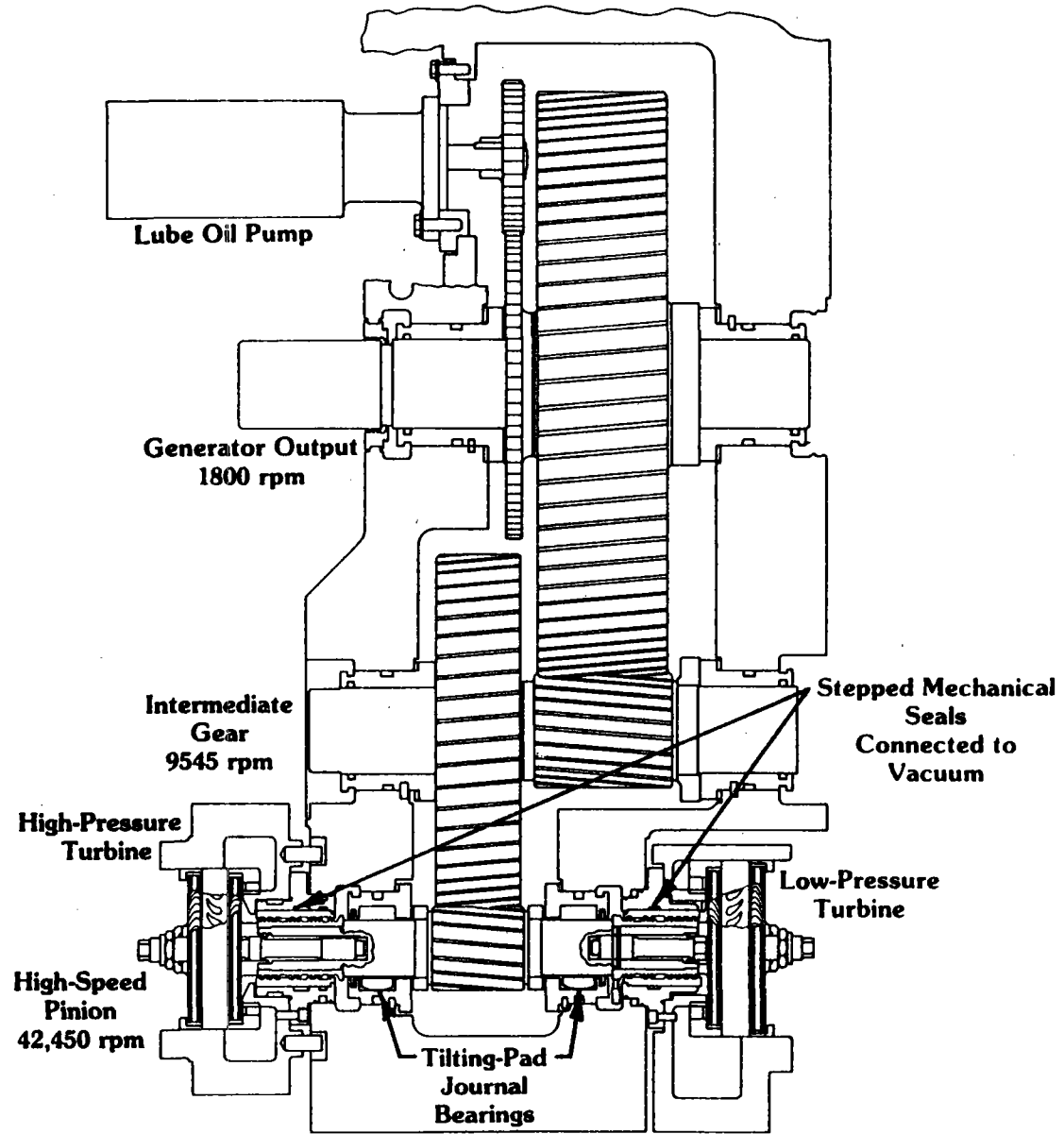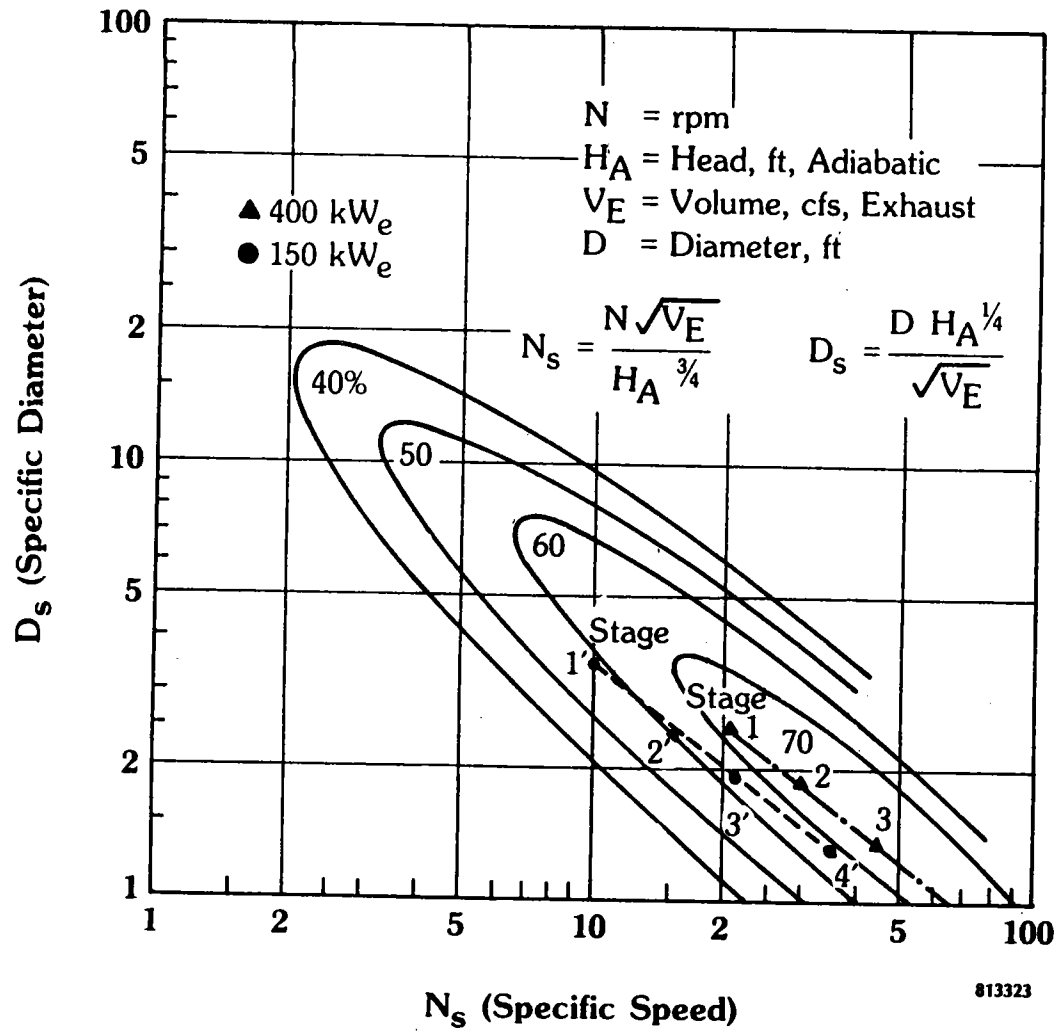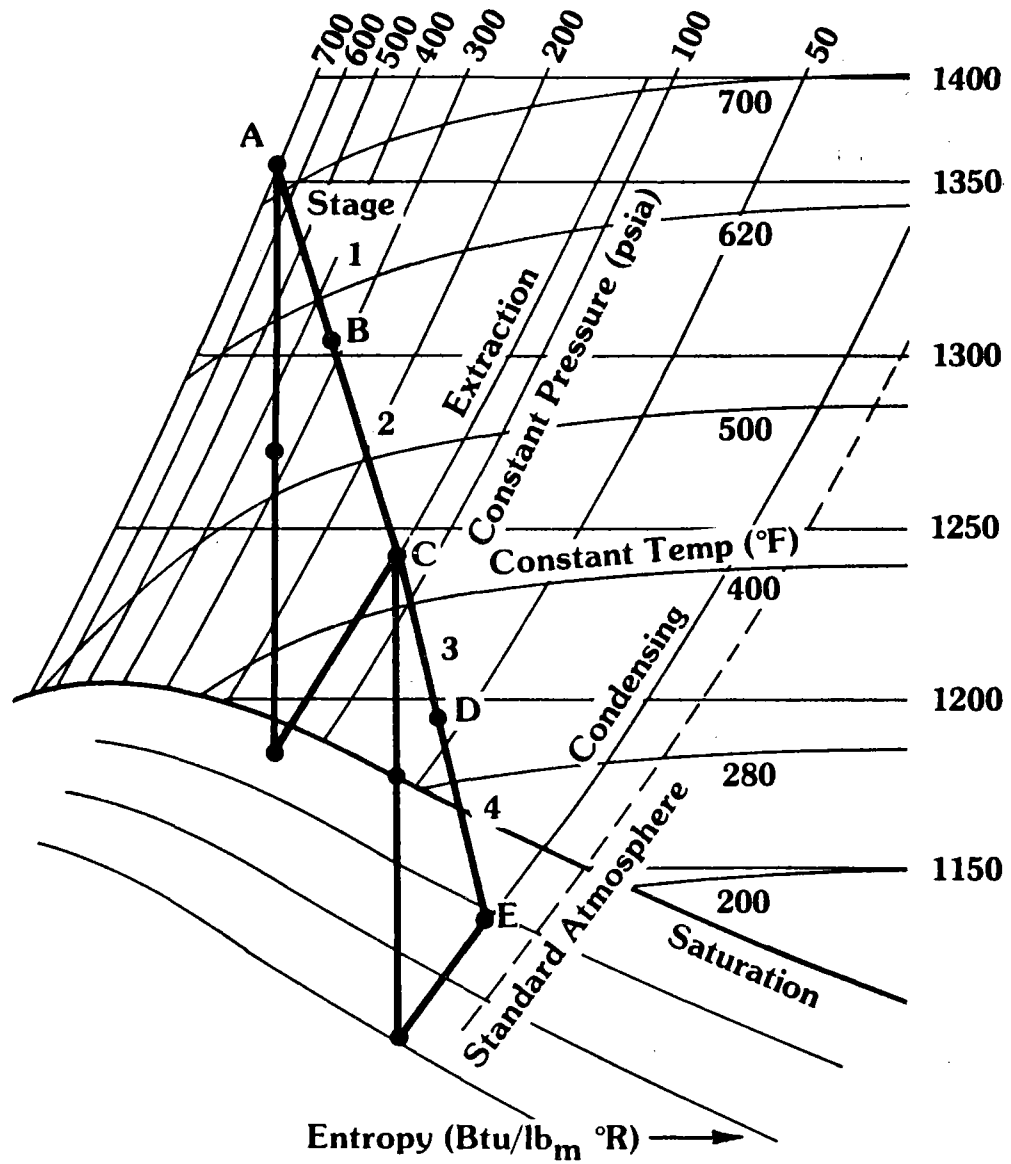
Fig. 2 Turbine/Gearbox Cross Section

Fig. 3 Predicted Aerodynamic Performance
(Source: O.E. Balje)

State Point	T (°F)	P (psia)	H (Btu/lb)
A	720	715	1356
B	580	335	1273
C	438	125	1244
D	325	58	1195
E	230	20	1135

813320

Fig. 4 Expansion Thermodynamic State Points

3.2 Mechanical

The turbine/gearbox mechanical design is generically similar to a large family of high-speed, integrally geared, overhung rotor turbomachines that have been built by MTI over the past 10 years. The selected gearbox is a 23.6:1 double-reduction design that has successfully operated in a similar application. The first step-down occurs at a gear ratio of 4.44:1 from the 42,450-rpm pinion to the 9,545-rpm intermediate shaft. The second ratio to the 1,800- rpm shaft is 5.3:1. Overall, the mechanical efficiency of the gearbox and turbine bearing system is estimated at 92%, based on empirical data from the previous application.

The high-speed pinion is overhung on both sides, and supported by two, five-element, geometrically preloaded, pivoted-pad journal bearings with forward and reverse thrust capability. The bearings on the 9,545-rpm intermediate shaft and 1,800-rpm output shaft are conventional, fixed-pad, cylindrical bearings. A power take-off gear set, rotating at 3,600 rpm, drives an integral oil pump. The turbine, gearbox, and generator are all mounted on a common base plate that also contains the lube oil sump; hence, an integrated, compact system results.

The pinion was integrally machined into the turbine rotor using AISI 9310 steel. The blades and nozzle partitions were electric discharge machined (EDM) from 17-4 PH stainless steel bar stock. The rotor assembly is shown in Figure 5. Each wheel has a shroud that was brazed in place after the EDM operation. Following machining, the wheels were overspeed tested to 53,000 rpm, which represents 125% of design speed.

The rotor seal (Figure 6) uses a stepped labyrinth, in conjunction with buffer air and a vacuum port arrangement, on each side of the rotor. The 6-psig buffer air vents through the gearbox and through the vacuum port, where a vacuum source pulls the leakage steam and air together and disposes it overboard. In addition, high-pressure steam is transferred from the high- to the low-pressure turbine through an interconnecting pipe. This leakage steam combines with the low-pressure turbine steam for additional expansion through the last stage.
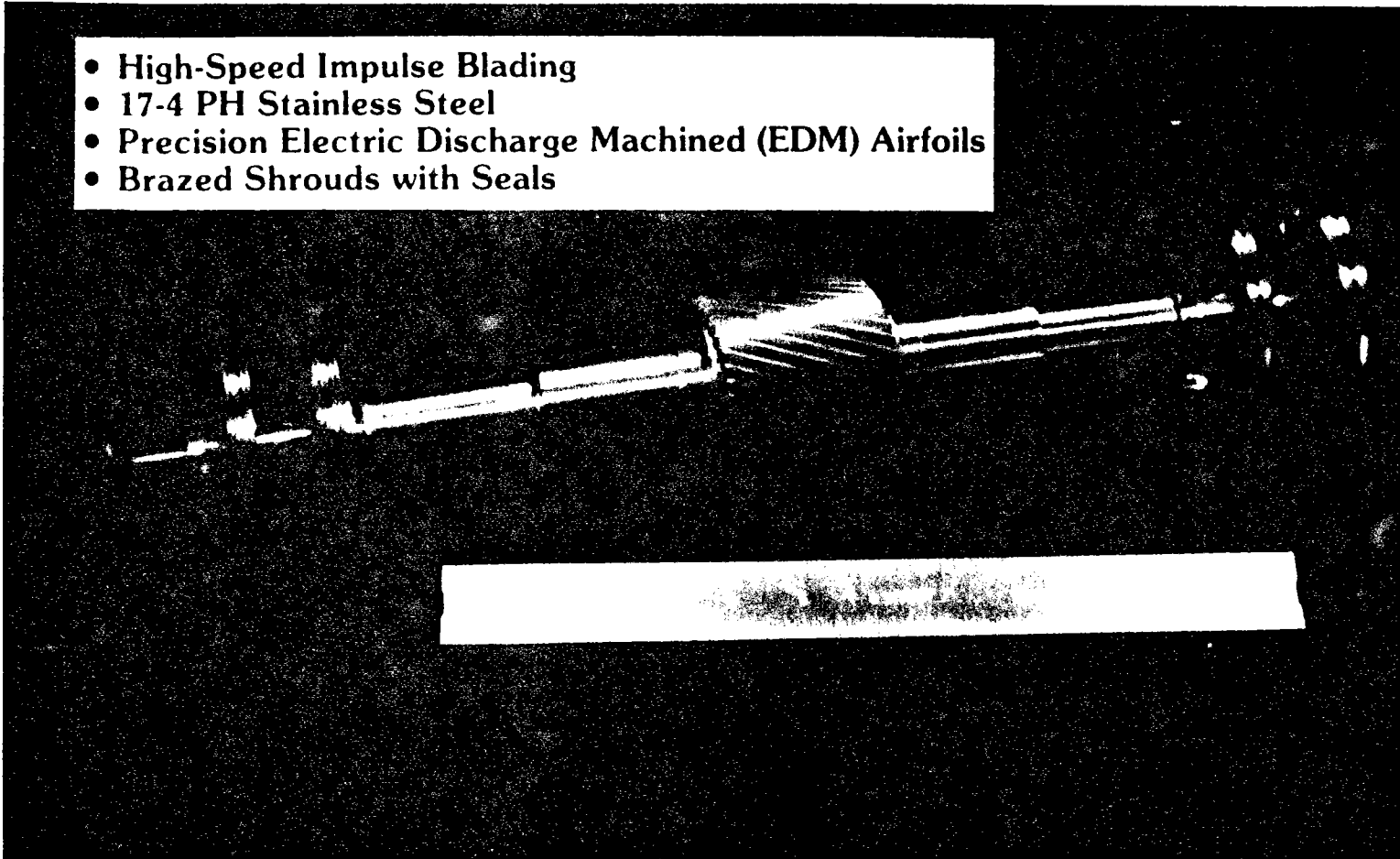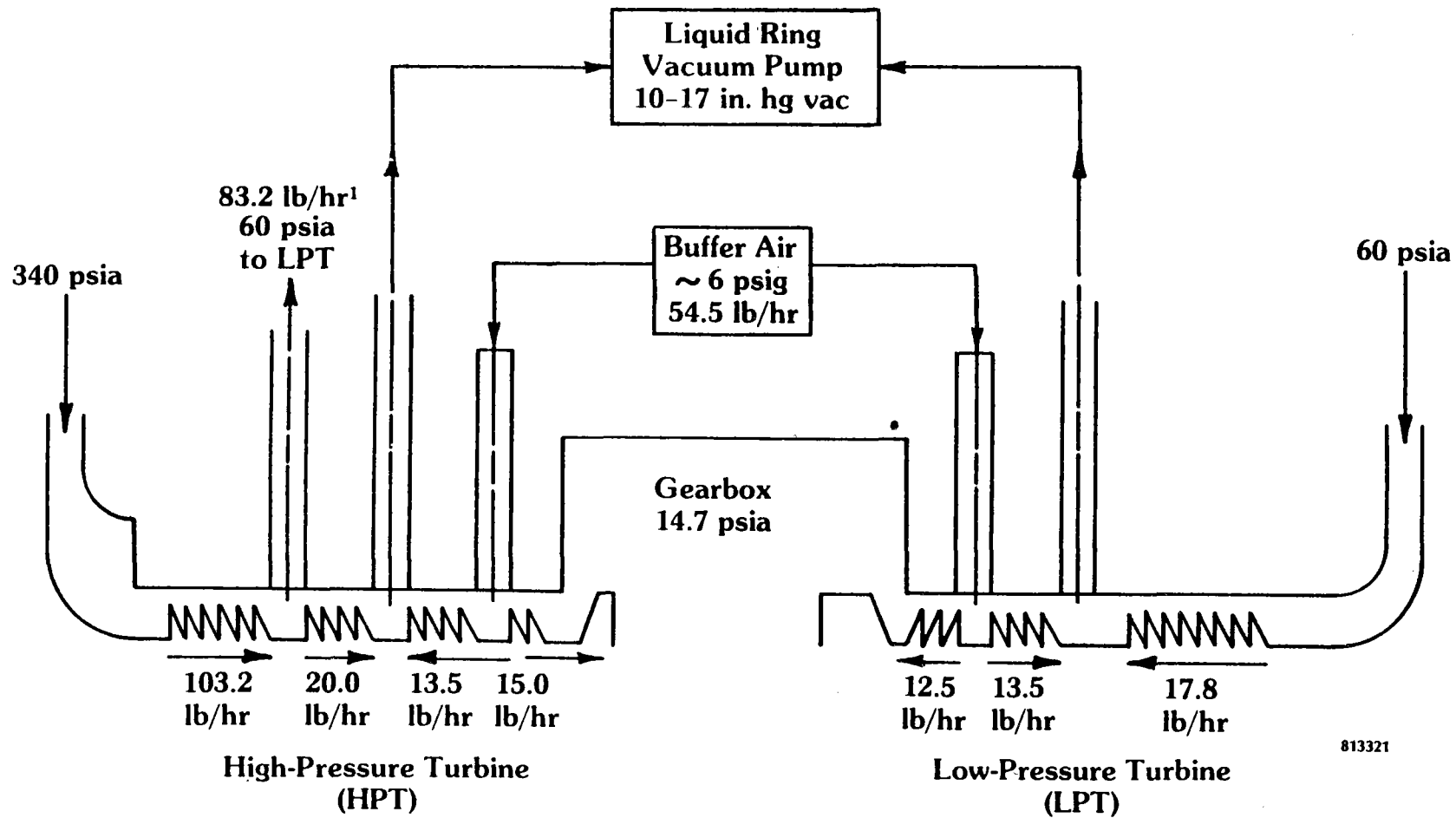
- High-Speed Impulse Blading
- 17-4 PH Stainless Steel
- Precision Electric Discharge Machined (EDM) Airfoils
- Brazed Shrouds with Seals

Fig. 5 High-Speed Rotor Assembly

Fig. 6 Turbine Seal Schematic

The turbine, which is designed with a double overhung flexible rotor, operates above the first and second lateral natural frequencies and below the third, which is a torsional mode. As shown on the critical speed map, Figure 7, the margin between the second critical and the design speed is roughly 10,000 rpm. At the same time, the 42,450-rpm operating speed falls below the third critical by approximately 10,000 rpm as well.

3.3 Rankine-Cycle Performance

The turbine-generator, operating within the Rankine cycle, is designed to produce 400-kW$_e$ net electrical output at an inlet throttle flow of 8,591 lb/hr at 700 psig, 720°F; the exhaust steam pressure is 6 psig. Between the high- and low-pressure turbine sections, 2,244 lb/hr of steam is extracted at 110 psig. At these conditions (excluding solar collection system losses), the Rankine cycle's overall thermal efficiency is 15.2% (see Figure 8). Predictions made for off-design operation are presented in Table 1. Using the partial-admission strategy, the steam rate at 50% load (200 kW$_e$) increases to 25.25 lb/kWh, which is only 15% more than the 21.48 lb/kWh steam rate predicted for the 400-kW$_e$ design point.

3.4 Control System

The problem statement imposed by the turbine control system requirements represented a challenge that was second only to the high-performance requirements of the power conversion system. The Shenandoah turbine, as an industrial cogenerator, was stipulated to operate (1) in a stand-alone mode when providing Bleyle's total energy demand and (2) in a synchronized mode in order to cogenerate with Georgia Power Company, the local utility. In addition, all operation was to be automatically responsive to electrical and thermal load changes, the latter imposed as a 110 psig ± 5 psig requirement at the extraction port. Start-up and shutdown were to be automatic and remotely controlled.

As indicated earlier, good part-load performance is achieved via a partial-admission schedule. To accomplish this, two nonmodulating, high-pressure arc valves are actuated at discrete power levels corresponding to the 200- and 300-kW$_e$ load conditions. In other words, all valves are wide open
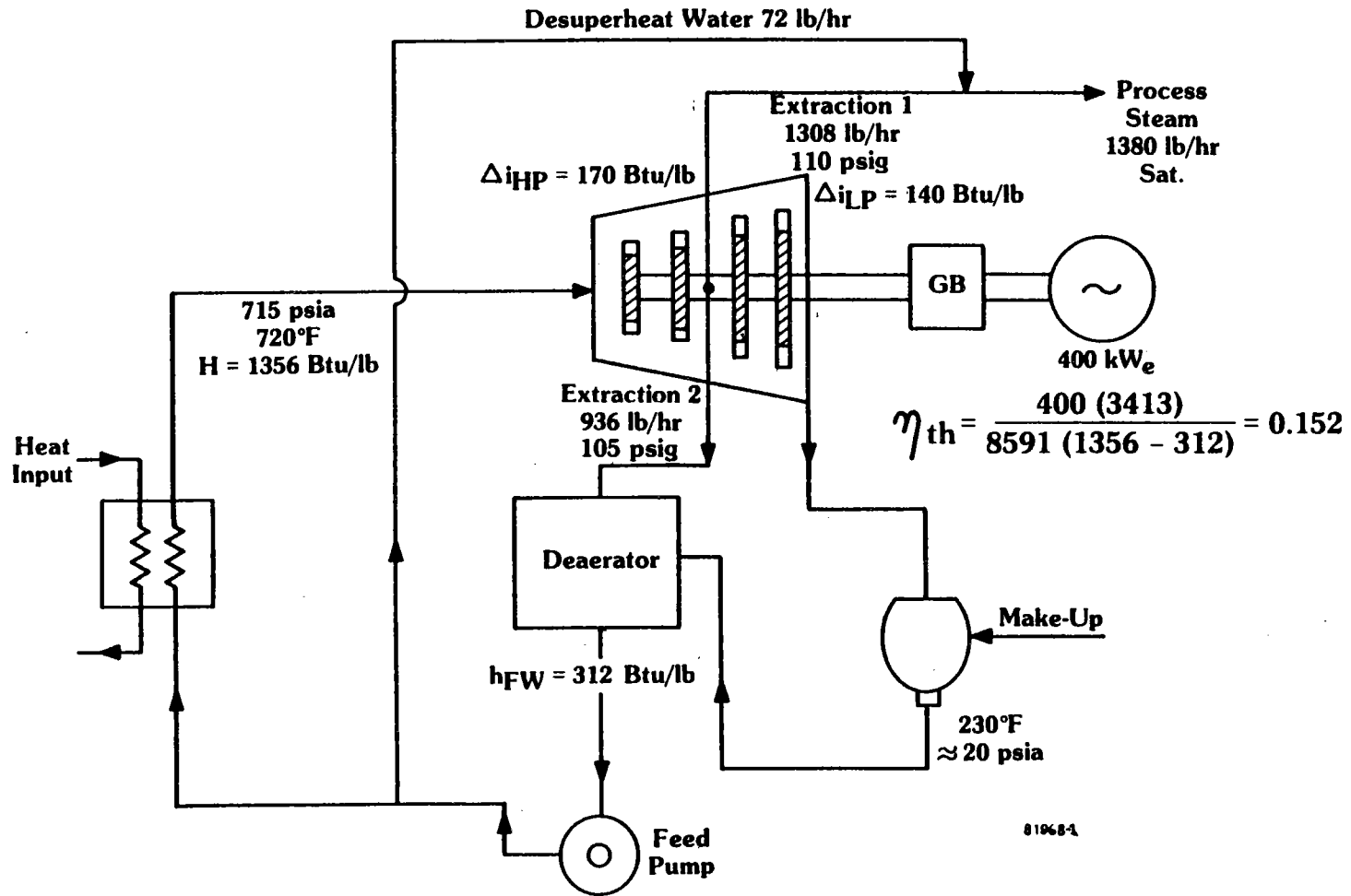
161
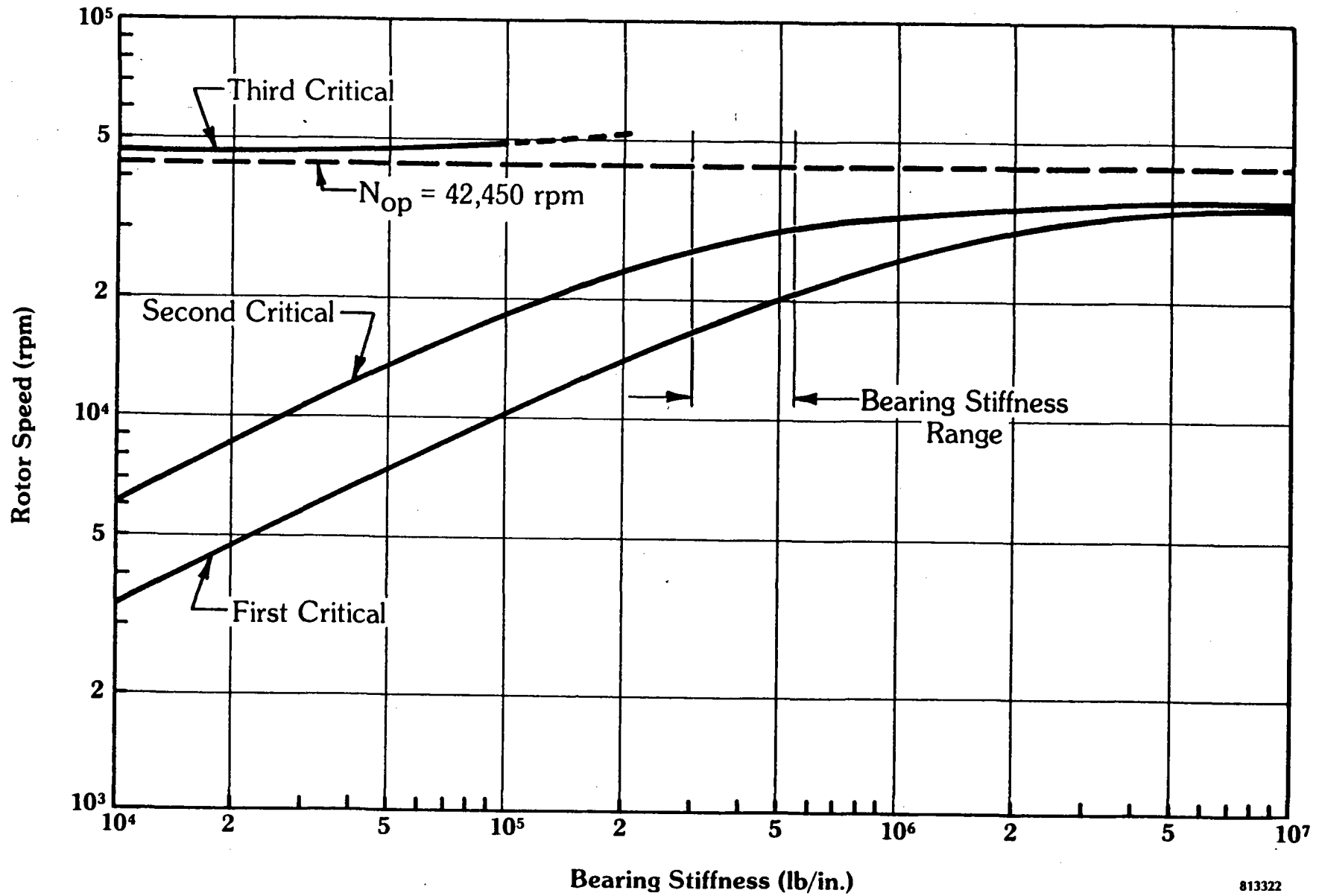
Fig. 7   High-Speed Pinion Critical Speed Analysis

162

813322

Fig. 8 Turbine Subsystem Steam Utilization

TABLE 1

STEAM TURBINE PERFORMANCE SUMMARY

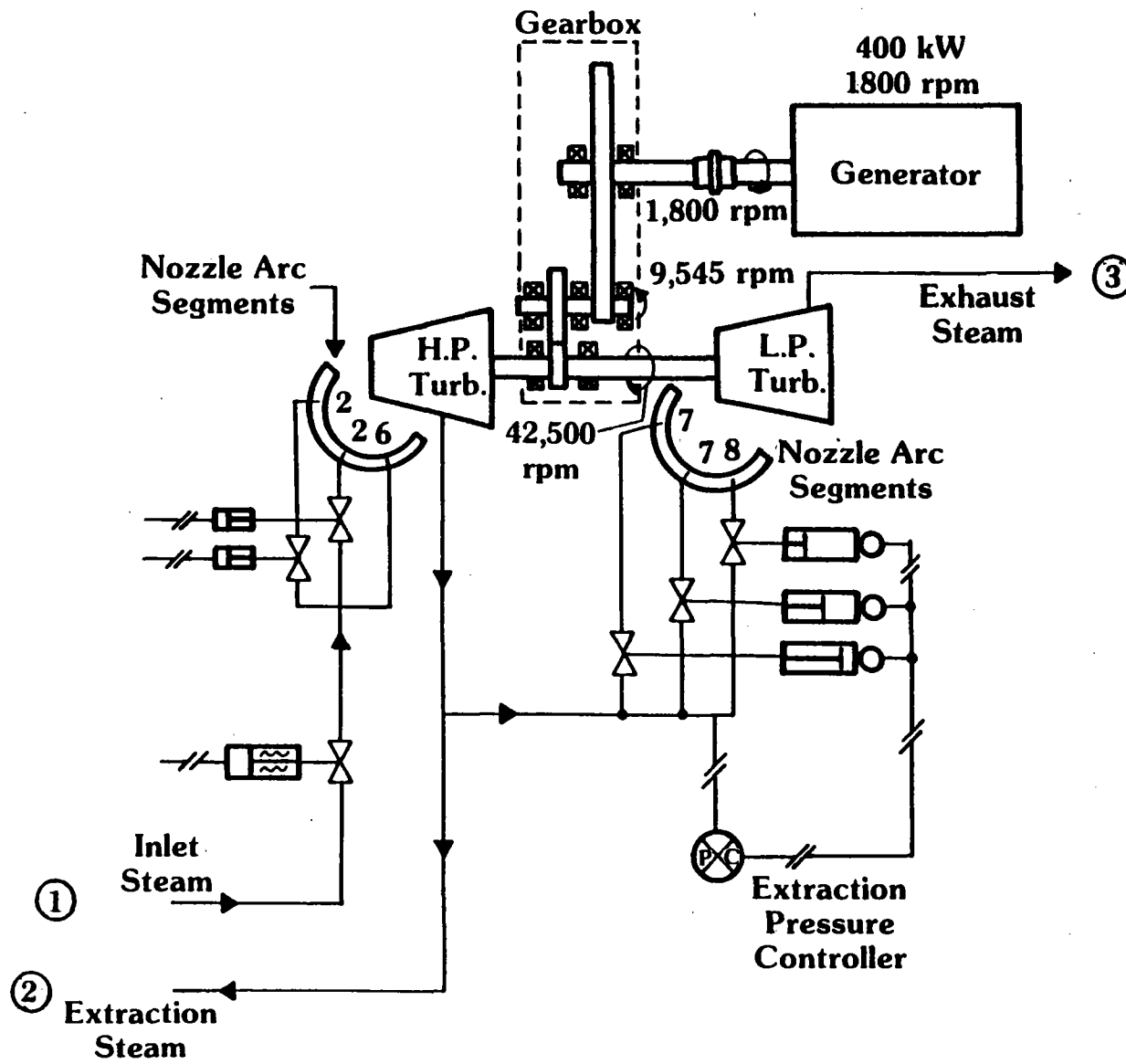|	Design		
Electrical Output (kW)	400	300	200
Process Steam Flow (lb/hr)	1380	1380	1380
Throttle Pressure (psig)	700	700	700
Throttle Temperature (°F)	720	720	720
Enthalpy at Inlet (Btu/lb)	1356	1356	1356
Extraction Pressure (psig)	110	110	110
Deaerator Pressure (psig)	105	105	105
Throttle Flow (lb/hr)/(% Design)	8591/100%	6897/80%	5049/59%
*Extraction to Process (lb/hr)	1308	1304	1298
Extraction to Deaerator (lb/hr)	936	749	546
Condenser Flow (lb/hr)/(% Design)	6347/100%	4844/76%	3205/51%
Total Extraction (lb/hr)	2244	2053	1844
Enthalpy at Extraction (Btu/lb)	1244	1248	1253
**Steam Rate (lb/kW-hr)	21.5	23.0	25.2

*Differs somewhat from process steam flow by amount of desuperheat water flow added after extraction.
**Based on inlet throttle flow and extraction conditions indicated above.

164

at 400 kW_e. At 300 kW_e, one valve is closed and, at 200 kW_e, both valves are closed. Any set point between these load conditions is achieved by throttling the main inlet valve.

At the extraction station, the control is more elaborate. Three fully modulating, pressure-controlled valves are employed to maintain the extraction pressure at 110 psig ± 5 psig throughout the entire operating range; i.e., for all power settings and all extraction flow conditions. In all cases, the three extraction valves, ~~including~~ two high-pressure arc valves and ~~a~~ the main throttle valve, operate in unison, automatically, to achieve any turbine map setting (see Figure 9).

Synchronous Operation. The generator operates at a constant 1,800 rpm when synchronized to the utility. During this mode of operation, the generator load is controlled by the operation of the load-sensing, motor-operated potentiometer. As the load increases, an electrical signal from the potentiometer is increased and sensed by the governor control which causes the latter to increase. This signal is then transmitted to the inlet throttle valve for subsequent actuation, increasing the turbine flow and, correspondingly, the generator ~~load~~. output.

Stand-Alone Operation. During stand-alone operation, the generator speed is referenced to the rated speed set point of the governor. A change in electric load or extraction flow causes the inlet servo control valve to modulate to compensate for the change, thus ensuring speed control and stability of the turbine-generator. Under both stand-alone and synchronous operation, the extraction pressure control and high-pressure arc valve control are operational.

Fig. 9 High-Performance Steam Turbine Industrial Cogeneration

4.0 MECHANICAL TESTING

To confirm the mechanical design, the turbine was accelerated to 42,450 rpm with the generator unloaded and on manual speed control. A high-speed field balance was required to negotiate the second critical at approximately 32,000 prm. Balancing was necessitated because of the flexible shaft design which, at frequencies approaching the second lateral, caused the rotor to bend and the plane of unbalance to shift. Initially, test weights were placed on the two outboard wheels in order to determine balance. Final balancing was achieved by the material removal technique. As shown in Figure 10, the maximum displacement was measured to be within .4 mils (peak to peak) at the design speed. Subsequently, the response while accelerating through the second critical was essentially eliminated.

In addition to the vibration survey the bearings were also monitored. Surprisingly, the highest temperatures were recorded on the intermediate speed shaft where the maximum readings were 180°F. On the high-speed pinion, the bearing temperatures all remained below 170°F. These temperatures were recorded at a 400-kW$_e$ generator load. Unloaded, the bearing temperatures were approximately 10-15°F lower. In any event, these temperatures were well within the operating limit of 200°F.

Mechanical testing concluded with the successful check-out of the electrical and mechanical overspeed trips, whose trigger points were set at 105% and 107% of speed, respectively. In addition, the inlet stop valve closure time was measured to be within 2×10^{-3} sec.
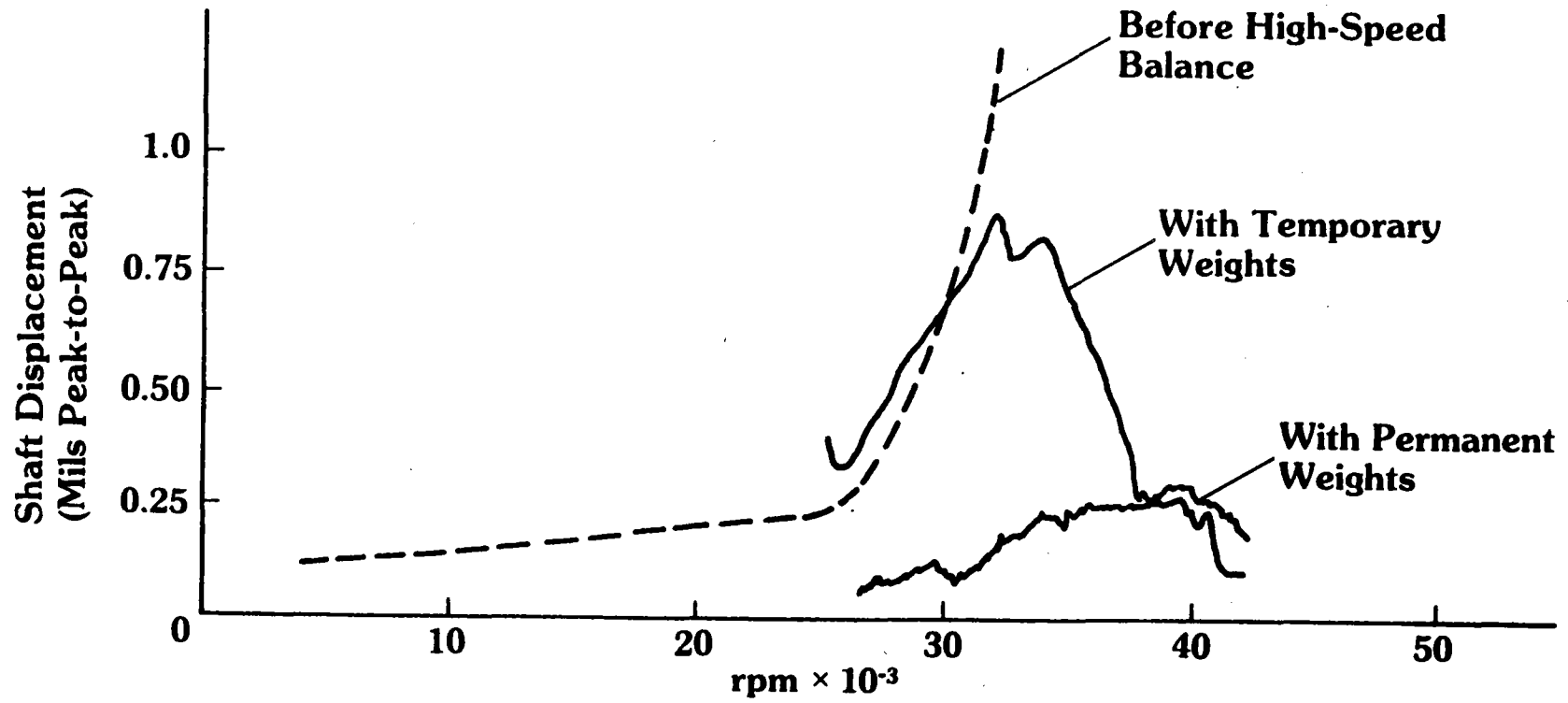
Fig. 10 High-Speed Pinion Operation

5.0 PERFORMANCE CALIBRATIONS

5.1 Steady-State, Design Throttle Testing

Following the mechanical tests, performance calibrations were conducted at 200, 300, and 400 kW$_e$ at three extraction flow rates for each power setting. The turbine operated at a nominal setting of 700/720/ 20; i.e., 700 psig, 720°F at the inlet and 20 psia back pressure. As shown in Figure 11, the measured throttle flows, when corrected to reflect the design extraction flow, were slightly higher than predicted. At the 400-kW$_e$ setting, approximately 2% or 200 lb/hr of additional flow was required. This penalty increased to 5% or 250 lb/hr at the 200 kW$_e$ setting. Overall, the turbine's mechanical efficiency, reflecting all but the generator losses, was measured at 61%, three points below the design goal of 64%.

At the 700/720/20 setting with the inlet valves fully open, the generator output reached only 390 kW$_e$; the 10-kW$_e$ shortfall was caused by a combination of higher losses, as cited above, as well as a nozzle area insufficient to pass the additional flow required to compensate for said losses. Consequently, the throttle conditions were raised to 720 psig/745°F in order to achieve the desired 400 kW$_e$. At this setting, the throttle flow was 8450 lb/hr, based on the average of 13 data points taken approximately 5-10 minutes apart using standard ASME flow meter practice. These data and the 700/720 throttle data are presented in Figure 11.

5.1.1 Losses

In an attempt to determine the loss mechanism(s) that caused the higher than predicted steam rates, aerodynamic efficiencies were calculated using measured pressures and temperatures across each steam chest. For the high-pressure and low-pressure turbines, efficiencies measured 65 and 67%, respectively. The high-pressure section operated as designed, but the low-pressure turbine was six points low; i.e., 67% versus 73%. Overall, the aerodynamic efficiency was 66%, two points lower than the design value. Lower interstage velocity energy recov-
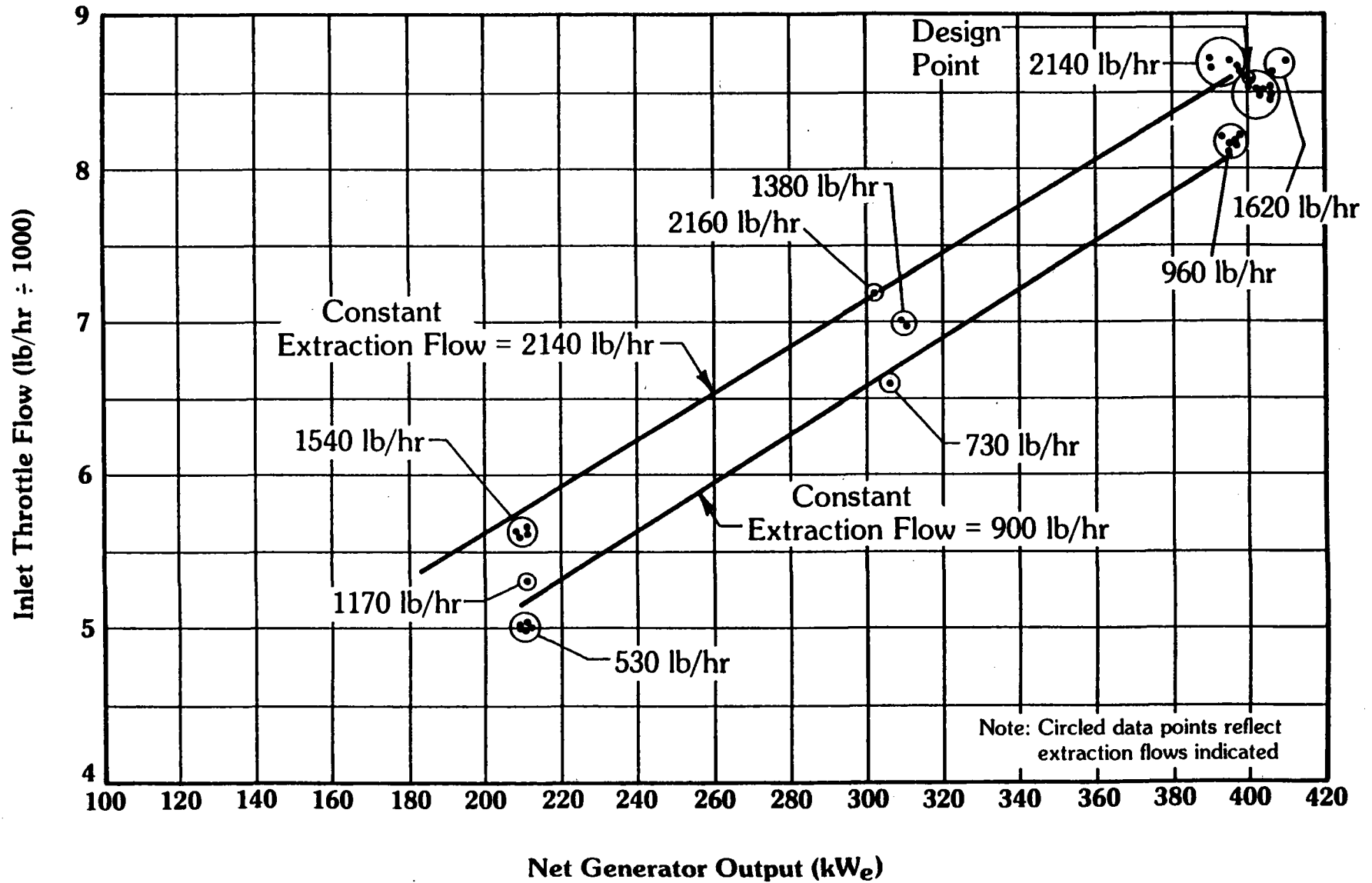
Fig. 11 Steam Turbine Performance Summary

ery and higher aspect ratio losses in the low-pressure stages are suspected to have caused this aerodynamic penalty.

In addition to the aerodynamic loss mechanisms cited, additional losses resulted from labyrinth and tip seal clearances that were larger than designed. Instead of a nominal .003-in. radial clearance, the as-manufactured parts were assembled with a .005-in. radial clearance. It was estimated that this added clearance consumed an additional 100 lb/hr of steam.

Although it was not possible to empirically quantify the extent of each loss mechanism, it is generally belived that some combination of the aerodynamic losses cited and seal leakage losses were responsible for the slightly higher than predicted steam rates.

## 5.2 Transient Testing

5.2.1 Thermal Load Response

The turbine's demonstrated response to instantaneous changes in electrical and thermal loads is presented in Figures 12 through 14. At electric loads of 100, 200, 300 and 375 kW_e, the extraction flow was changed by approximately 1000 lb/hr at rates varying from 1000 lb/hr/sec to in excess of 6000 lb/hr/sec; the steeper rate corresponding to the greater generator loads. The corresponding change in the electrical output frequency (normally 60 Hz) measured .45 Hz at 100 kW_e and gradually became lower as the load increased; i.e., to .3 Hz at 375 kW_e. See Figures 12 and 13, which were measured during the most severe transient -- as the extraction valve was closed. During valve opening, the frequency deviation decreased to less than .1 Hz for all load settings.

In all cases except when the extraction valve is closed at the 100-kW_e load, the transient response was better than the design goal of ± .3 Hz deviation. Generally speaking, the response was more sensitive to closing the extraction valve than to opening it; this was no doubt due, in most part, to the faster valve response in the case of the former, where the steam pressure accelerates closure
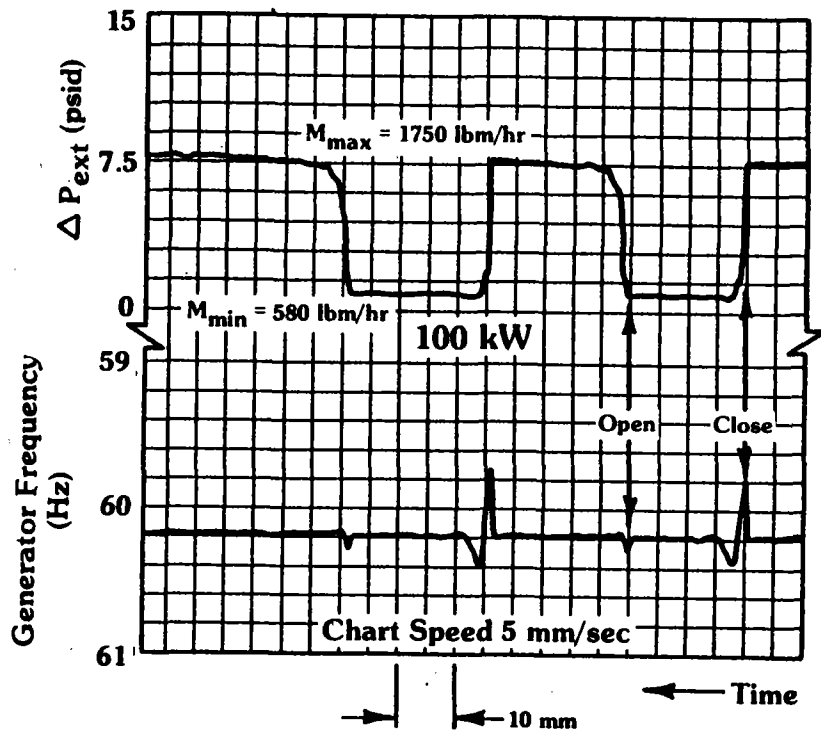
171
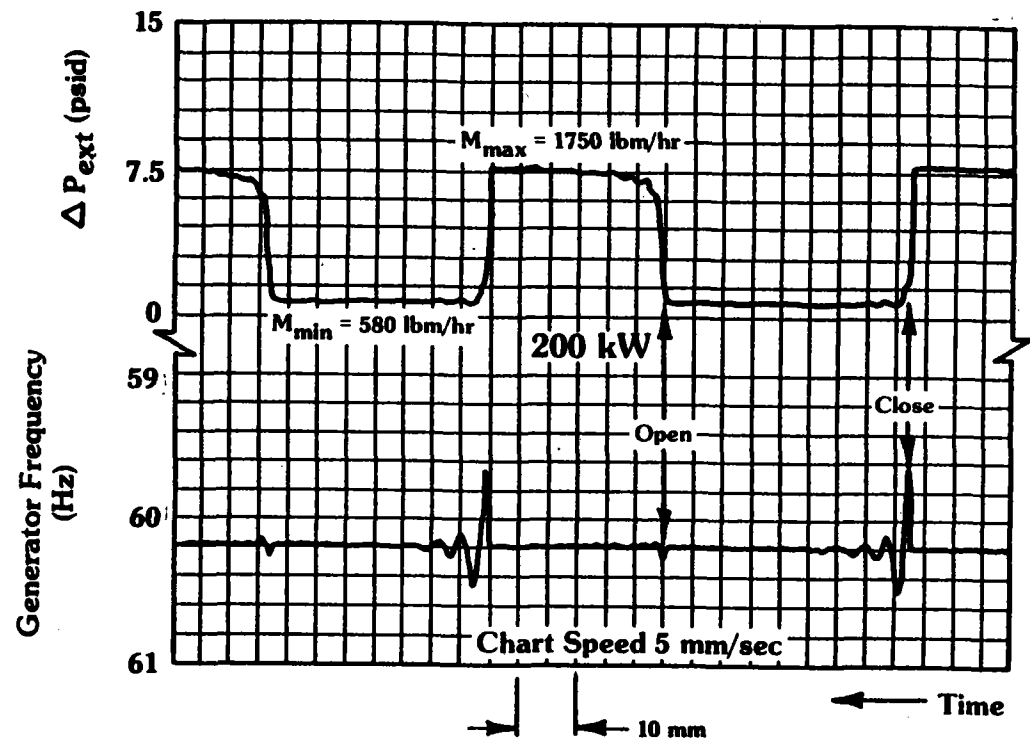
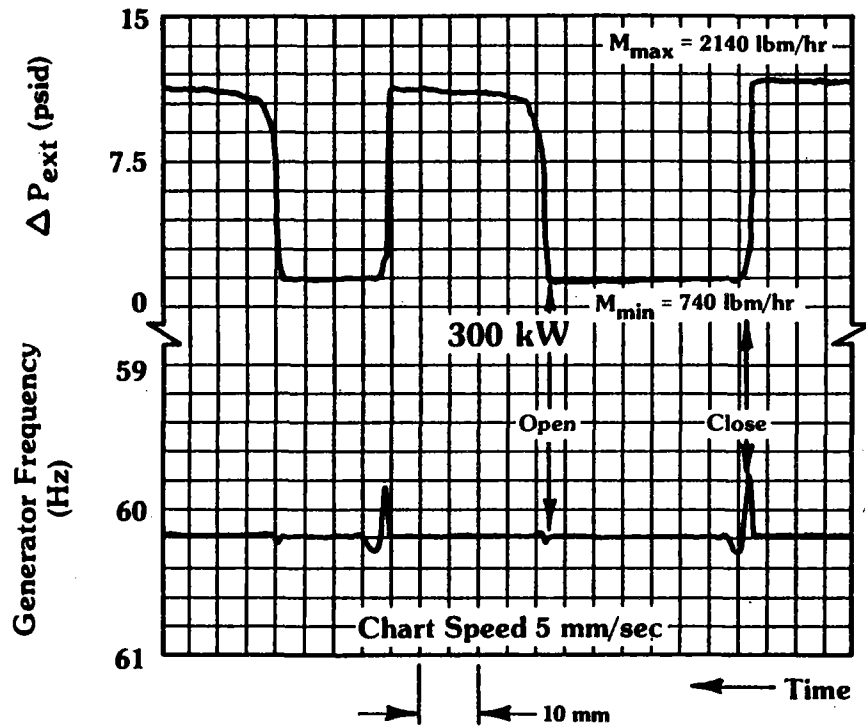Fig. 12 Frequency Response to Thermal Load (100 kW and 200 kW)

813192

Fig. 13 Frequency Response to Thermal Load (300 kW and 400 kW)

300 kW

P_{in} = 700 psig
T_{in} = 730°F
P_{ext} = 113 psig
T_{ext} = 450°F
$P_{exhaust}$ = 6.1 psig
Extraction Flow:
  M_{min} = 740 lbm/hr
  M_{max} = 2140 lbm/hr

375 kW
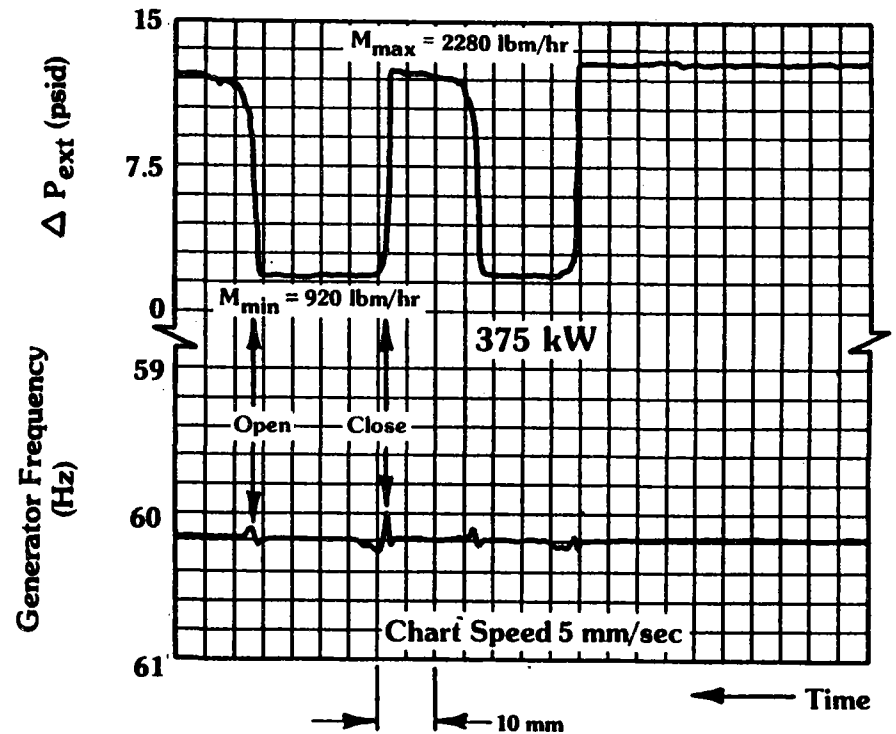
P_{in} = 700 psig
T_{in} = 721°F
P_{ext} = 114 psig
T_{ext} = 438°F
$P_{exhaust}$ = 6.1 psig
Extraction Flow:
  M_{min} = 920 lbm/hr
  M_{max} = 2280 lb/hr

813193

and, conversely, delays opening. The effect of generator load was to improve the response as the load increased.

5.2.2 Electrical Load Response

Holding the extraction flow constant at the 720 psig/700°F throttle setting, the electrical load was instantaneously changed in 25-kW$_e$ increments from 100 to 350 kW$_e$. The results are plotted in Figure 14, which indicates that the frequency deviation varied from approximately .5 to .3 Hz as the electric load was increased. This is consistent with the thermal load tests; i.e., improved response at higher loads.

These same tests were repeated during load shedding; i.e., from 350 kW$_e$ down to 100 kW$_e$. The response was slightly better with frequency deviations of .2 to .4 Hz observed. Again, the response was better at higher loads.

Fig. 14 Frequency Responses to Electric Load
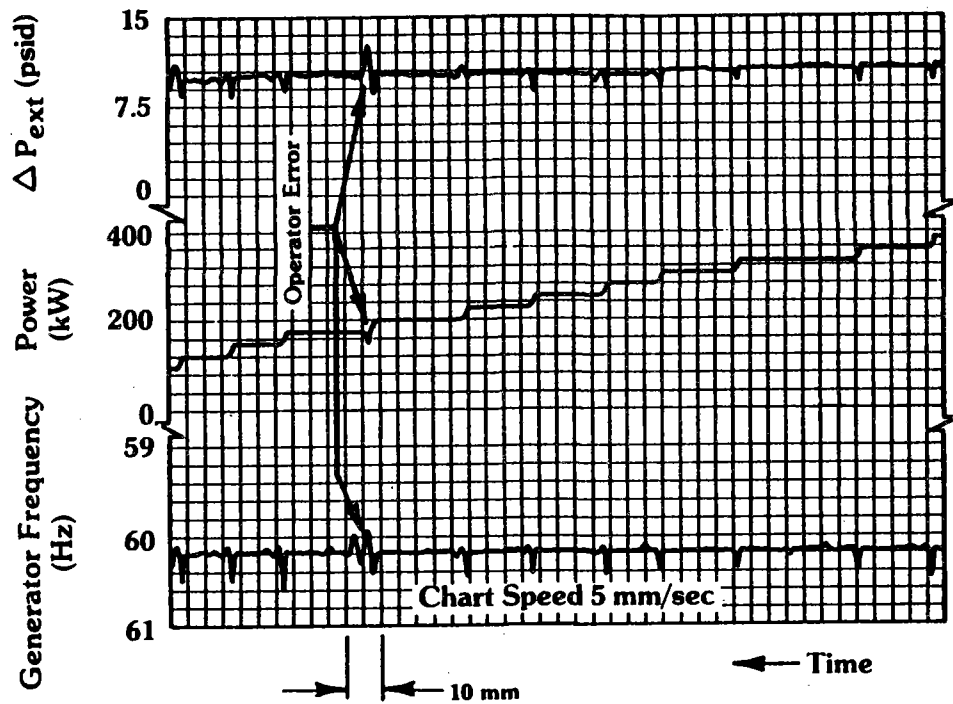
Decreasing Loads

P_{in} = 707 psig
T_{in} = 714°F
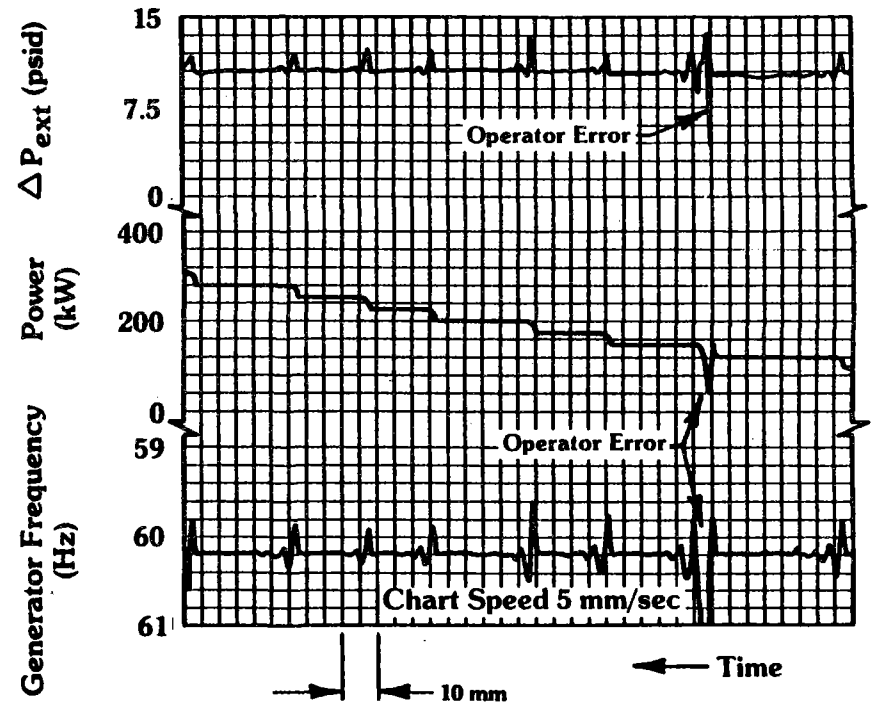
Increasing Loads

P_{in} = 700 psig
T_{in} = 729°F

6.0 CONCLUSIONS

The operational success achieved by the subject turbine-generator has estab-
lished the state of the art in industrial cogeneration equipment in the under
1-MW class. The ability to generate power in both synchronous and stand-alone
modes, and the stable and immediate response to thermal- and electric-load tran-
sients, respresent an overall cogeneration system capability that is unique to
the industry.

Within the system itself, the conversion efficiency of the turbine is approxi-
mately 12-15% better than that offered by conventional, multi-stage turbines in
the 500-hp range, notwithstanding the subject turbine's slight performance pen-
alty as compared to design values (see Figure 15). Moreover, the improvement
cited in this comparison includes the admission and extraction throttle losses
for the subject turbine, but not for the conventional equipment, which do not
offer these extraction features. On an equivalent basis, then, the performance
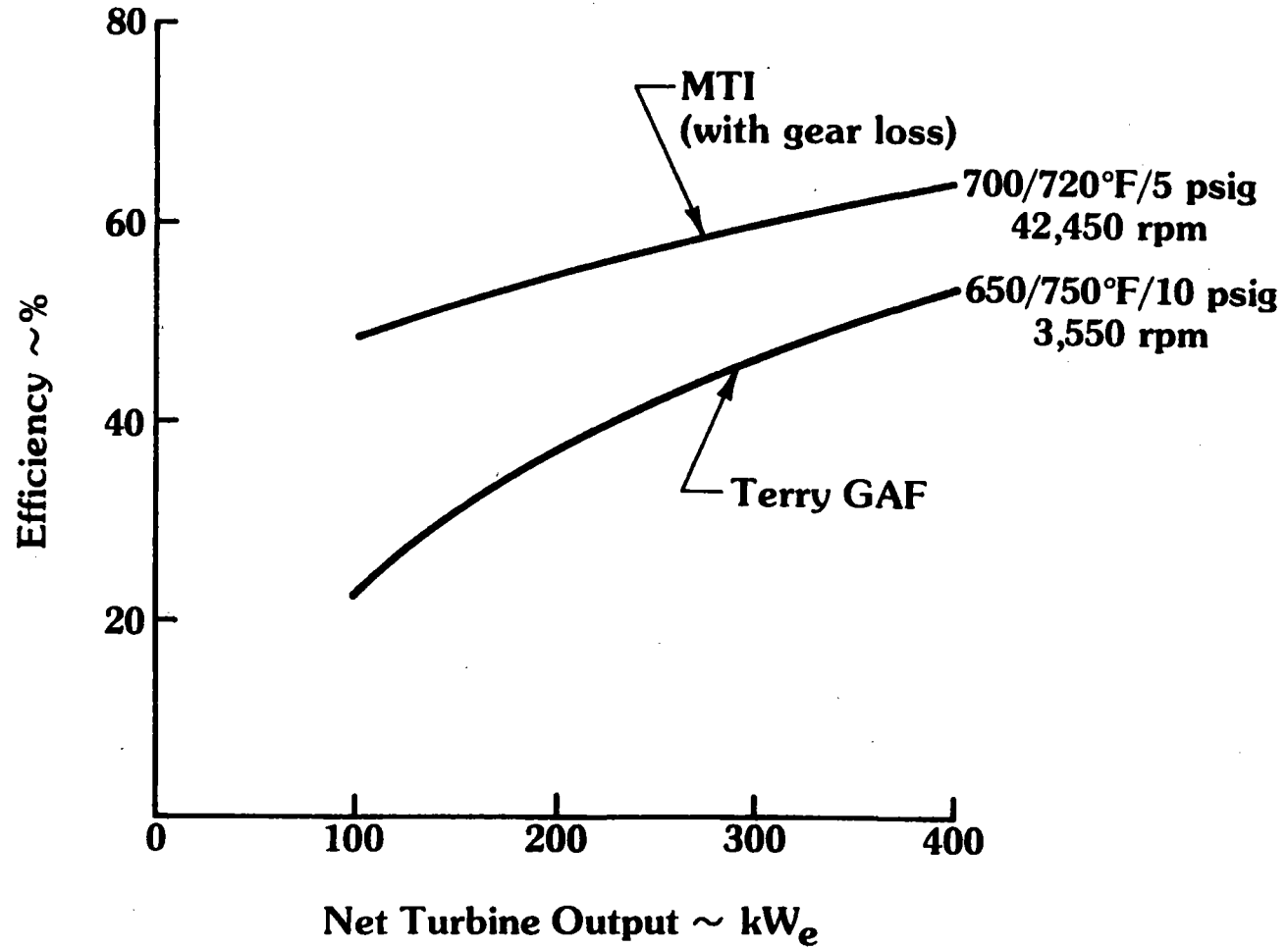improvement increases to 15-20% over conventional turbine-generator sets.

Fig. 15   Axial Steam Turbine Performance Comparison

MODIFICATIONS AND TESTING OF A 4-95
STIRLING ENGINE FOR SOLAR APPLICATIONS

H.G. Nelving
KB United Stirling (Sweden) AB & Co

W.H. Percival
United Stirling, Inc.

INTRODUCTION

United Stirling of Sweden (USSw) has been under contract by the Jet Propulsion Laboratory since September 1980 to modify a model USSw 4-95 engine, connected to a 25 kW induction alternator, for use with a solar thermal parabolic dish electric module. The hybrid type solar receiver (DSSR) was developed by Fairchild Industries and integrated with the engine by the Advanco Corporation. Power-plant testing was to take place at JPL/Edwards on a Test Bed Concentrator (TBC). A description of the 4-95 engine and the in-house program at United Stirling was given in the USSw paper presented at the JPL Dish Solar Thermal Annual Review at Pasadena, in January 1981. Also presented in the paper was the first phase testing of the 4-95 engine, connected to a dynamometer, with heat supplied by a liquid fuel combustor normally installed on the engine. It is shown in figure 1. The model 4-95 has also served as the baseline engine in the DOE/NASA Automotive Stirling Engine (ASE) program.

The purpose of this paper is to describe the modifications and testing of the standard USSw 4-95 Stirling engine, which were required for the solar application while operating in the inverted position. Power was absorbed by a GE induction alternator connected to the utility grid.

Also included in this paper are the results from recent testing of another 4-95 solar engine at the DOE/Georgia Tech solar site, sponsored by United Stirling. It was done in parallel with the JPL-DSSR testing at Edwards for the purpose of comparing performance of two USSw designed solar-only receivers, which were based on the standard 4-95 involute heat exchanger.

SOLAR ENGINE MODIFICATIONS

After completion of the dynamometer testing, modifications to the lubrication system for inverted operation were started. Design and fabrications were done in cooperation with Ricardo of England with whom USSw has a cooperative agreement. Modifications included machining numerous holes and slots to form oil drain passages in the crankcase bulkheads and the gas compressor housing. The goal was to provide adequate oil drain by gravity alone. This was achieved in static tests made at Ricardo with the crankcase inverted as well as horizontal. To further assure "dry sump" operation under dynamic conditions, an external scavenging pump was installed, driven from one of the crankshafts. The external pressure lubrication pump was fitted adjacent to the scavenge pump. An external oil drain tank was installed below the lowest (under all orientations) drainage point and connected to seven crankcase outlets by short pipes.

A view of the external tank and drain system is shown in figure 2.

The principal unknown during the design phase was the effect of oil flooding on the piston rod sliding seals (termed by USSw, the PL seal). Since the PL seals are normally in the "upper" part of the crankcase and, therefore, continuously drained, it was believed they might be incapable of pumping outward against the additional head of oil which might occur with the engine inverted, thereby contaminating the engine working spaces with lubricant.

The light weight (aluminum frame) 25 kW GE alternator was integrated with the 4-95 engine by design and fabrication of an aluminum alloy intercasing to match the two interfaces. The two shafts were connected by a flexible coupling. The intercasing can be seen in figure 2.

Integration of the engine/alternator unit to the Edwards TBC mounting ring was made by fabricating a steel frame of square tubes which forms the interface between the mounting ring bolt circle and the engine/alternator mounts. For testing at United Stirling's laboratory, the main frame was attached to a secondary mounting frame having a horizontal axis to allow rotation of the powerplant for inverted operation. The powerplant and frame assemblies can be seen in figures 2 and 3.

ENGINE TESTING

Engine testing was done with helium working gas, as specified by JPL. At all times the load was carried by the alternator connected to the local grid. Since Swedish frequency is 50 Hz, the engine was running at 1500 rpm under all load conditions. The engine was started by running the alternator as an induction motor, using a tapped transformer at reduced voltage to increase time to reach 1500 rpm to about 7 seconds, in order to moderate bearing loading at low speeds. The engine was initially tested in the inverted position, with the combustor in place, to study the oil flow distribution and the PL seal operation. Minor problems with oil flow were solved by increasing the drainage pipe area. Initial running while inverted gave some indication of a PL seal problem, with oil contamination in one cylinder. However, on examination of the seal, it was found to be improperly manufactured. After replacing it, no further oil problems were encountered during the entire laboratory test program operating between horizontal and inverted positions.

After 130 hours of initial testing, the engine was performance tested for 25 hours, followed by 175 hours of endurance running. The engine was disassembled for inspection at 100 hours and after the endurance run. No problems were encountered. Further check-out tests and demonstration runs resulted in a total of 350 hours of successful operation under simulated solar dish orientation. Incidently, the gasoline combustion system appeared to function properly in all positions, and the induction alternator operated as expected. Its efficiency was outstanding -- 92-93 percent. United Stirling has learned that near future designs can be expected to approach 95 percent.

ENGINE PERFORMANCE

The measured performance at 1500 rpm for various levels of working gas mean pressure, which is proportional to load, is shown in figure 4. Maximum power was 22 kW electrical output, at an overall efficiency of 31.5 percent. The average temperature of the involute heater tubes (outer wall) was 720 °C and average cooling water temperature was 50 °C. Auxiliaries driven by the engine included the lubricant and scavenge pumps and the helium compressor. Based on an alternator efficiency of 93% and a burner efficiency of 89%, the "solar" thermal efficiency is calculated to equal 38 percent (net heat to solar heat exchanger and shaft power output).

It is estimated that efficiency at 1800 rpm is nearly identical to that at 1500 rpm, and the maximum power is 20% higher. Performance inverted was found to be the same as measured when running upright, as was expected.

After completion of testing in Sweden, the powerplant was shipped to Edwards, California in June 1981 for integration with the DSSR and installation on the Test Bed Concentrator. Reports on the Edwards' testing are given by JPL and Advanco.

UNITED STIRLING TESTING AT GEORGIA TECH

On the campus of Georgia Tech is a solar installation known at the DOE Advanced Components Test Facility (ACTF), consisting of a field of 550, 3 foot diameter, mirrors. By means of mechanical shaft and cable drives, the mirrors track the sun and focus concentrated solar flux at the lower level of a tower platform 70 feet above the ground.

As a result of discussions which began in January 1981, between USSw and the ACTF management, USSw contracted to test a 4-95 engine/generator package nearly identical to the one at Edwards. The program was intended to parallel the JPL program and provide additional experience with solar-only receivers, in contrast to the hybrid type used with the engine at Edwards. The initial program included computer modeling and an optical analysis of several USSw receiver designs. By definition, a Stirling receiver includes the engine heat exchanger (receiver body) and the optical cavity surrounding the receiver body. The cavity consists of a sheet metal cylinder with internal insulation and a ceramic aperture plate. Two different heat exchangers, somewhat resembling the standard 4-95 involute heater, were constructed, as well as several receiver cavities incorporating different types of insulation and reflecting surfaces.

Some initial testing was done in August with the standard involute heater, shown in figure 5, to verify operation and the automatic temperature control. Working gas was hydrogen. Testing was resumed in November, with the new receiver body installed. The outside diameter was increased to 15.75 inches compared to 11.25 inches for the standard involute heater. Several changes were made to the receiver. The aperture was opened to a full 16 inches,

which is the maximum possible, and the engine was lowered in its tower frame until the conical heater surface was substantially at the focal plane. In addition, the Georgia Tech personnel continued to realign the mirror field for the solar declination, which had not been done since August. With much improved weather, 15 hours of running was achieved over the weekend. Maximum power was 12 kW. The best run was made on November 18, after completion of the mirror alignment. Maximum power was 18.5 kW to the grid, with an average of 18 kW between noon and 1 p.m.. This can be seen in the accompanying chart, figure 6, of power vs. time. The power improvement was achieved as the facility operators learned to optimize the hour angle setting by observing the heater temperatures, as can be seen on the chart of temperature vs. time, figure 7. The engine was operating with automatic temperature control, holding the average at about 720 °C.

On the weekend of November 21, the engine was operated with the second of the two new heater designs. Maximum power achieved was 16.5 kW, at about the same insolation level as on November 18. Since the principal goals of the program had been met, the engine was removed from the tower.

Three major achievements were realized from these tests, in addition to the record electrical power output:

1) Solar heat exchangers were tested for the first time under sunlight intensities roughly equal to those from a parabolic dish concentrator.

2) Two new solar-only heaters were tested successfully in a running engine. Although having somewhat greater dead volume than the standard heater, it did not appear to seriously reduce power or efficiency. No malfunction or leakage occurred.

3) The 4-95 solarized engine has proven itself in the solar environment. It performed as designed without requiring maintenance to the basic Stirling cycle.
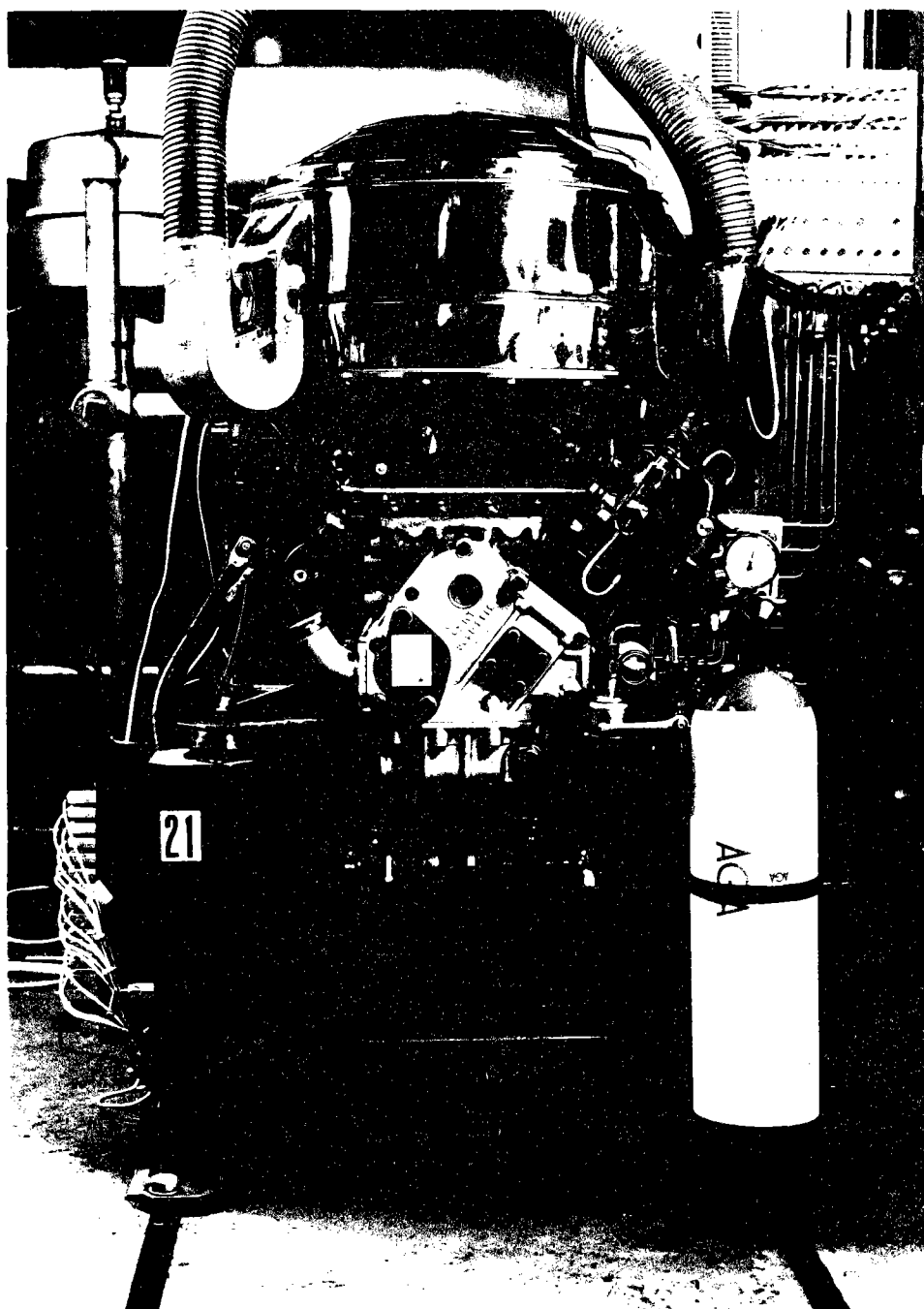
FIGURE 1 -- 4-95 ENGINE ON DYNAMOMETER
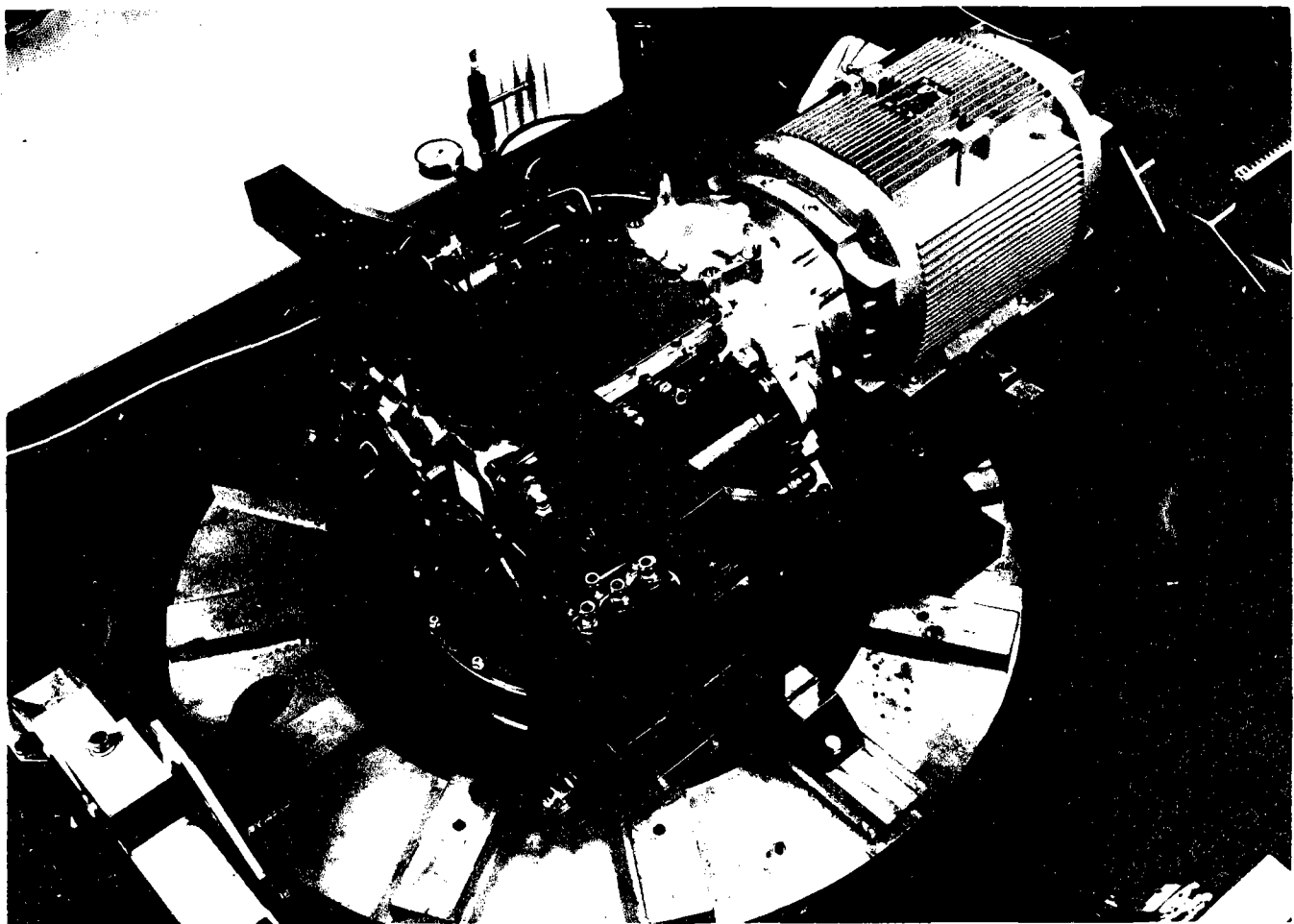
FIGURE 2 -- 4-95 ENGINE INVERTED WITH ALTERNATOR
AND MOUNTING FRAMES
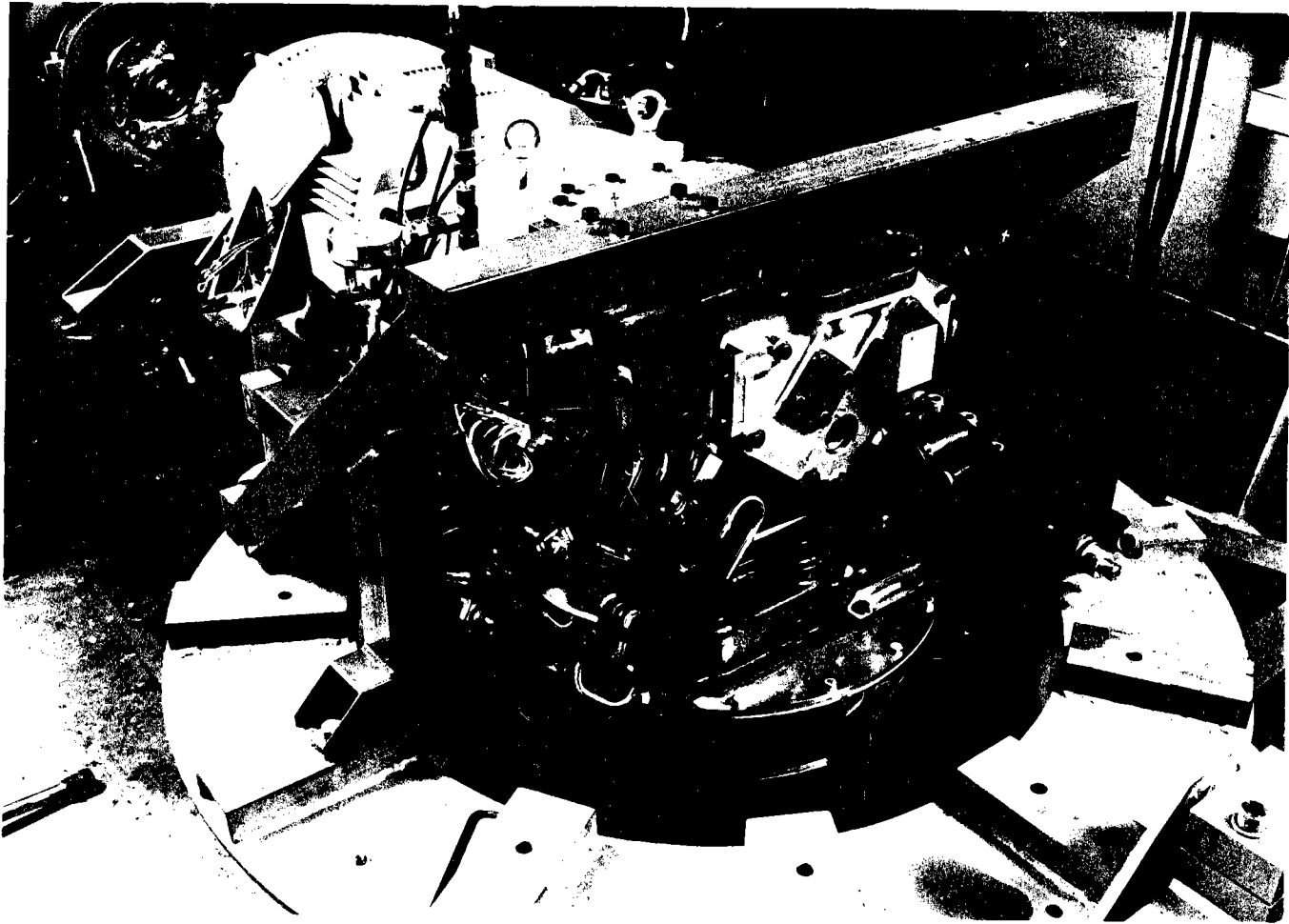
FIGURE 3 -- 4-95 ENGINE INVERTED WITH COMBUSTOR
AND TBC MOUNTING RING

PERFORMANCE
SOLAR STIRLING ENGINE 4-95-021

1500 RPM, HELIUM

Y-axis: POWER kW, EFFICIENCY % ($\frac{Electrical\ Power\ Out}{Fuel\ In}$)

X-axis: MEAN PRESSURE MPa

Efficiency
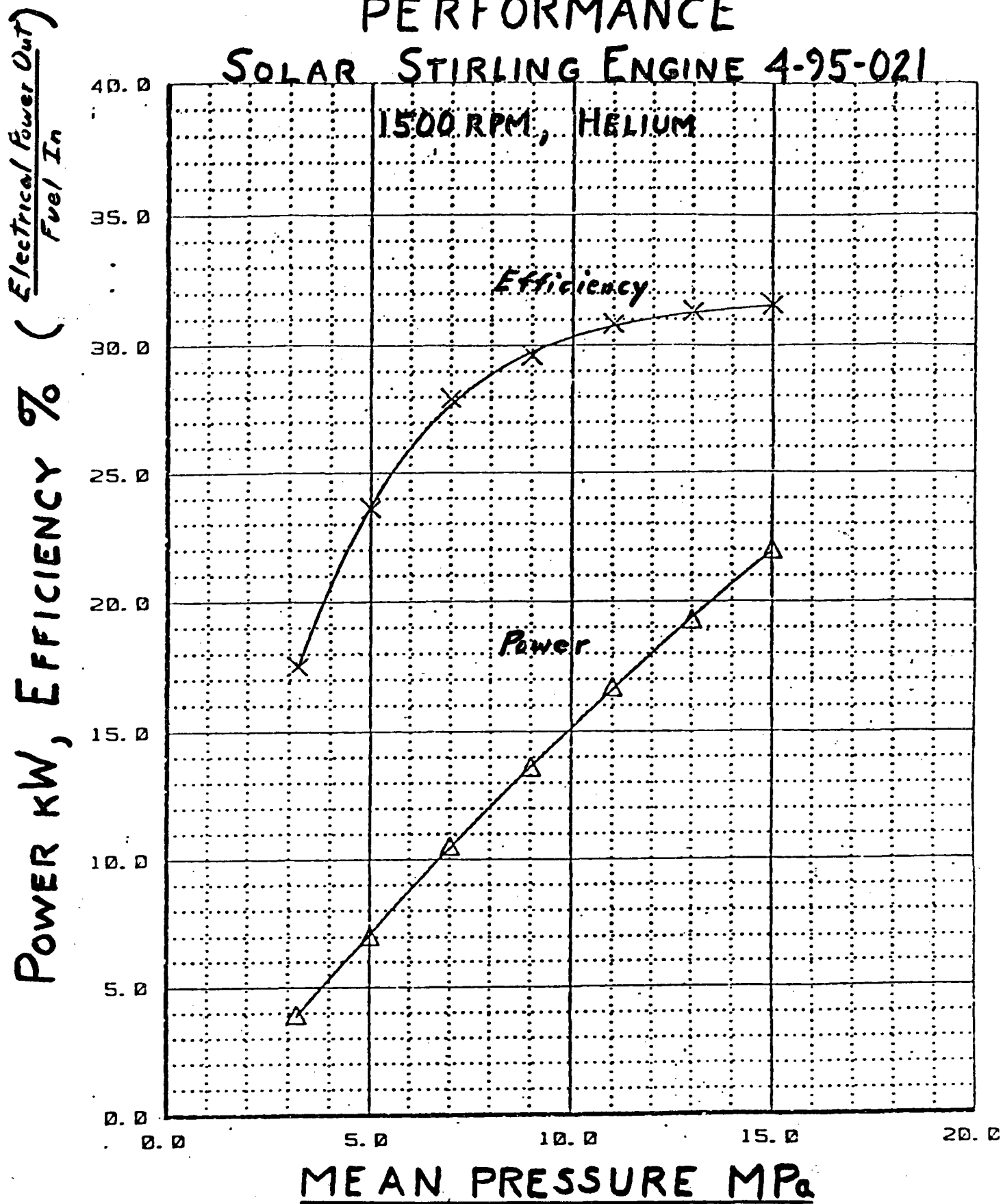
Power

FIGURE 4

FIGURE 5 -- 4-95 STANDARD INVOLUTE HEAT EXCHANGER

UNITED STIRLING 18-NOV-81

SENSOR | UNITS
POWER 1 | KW
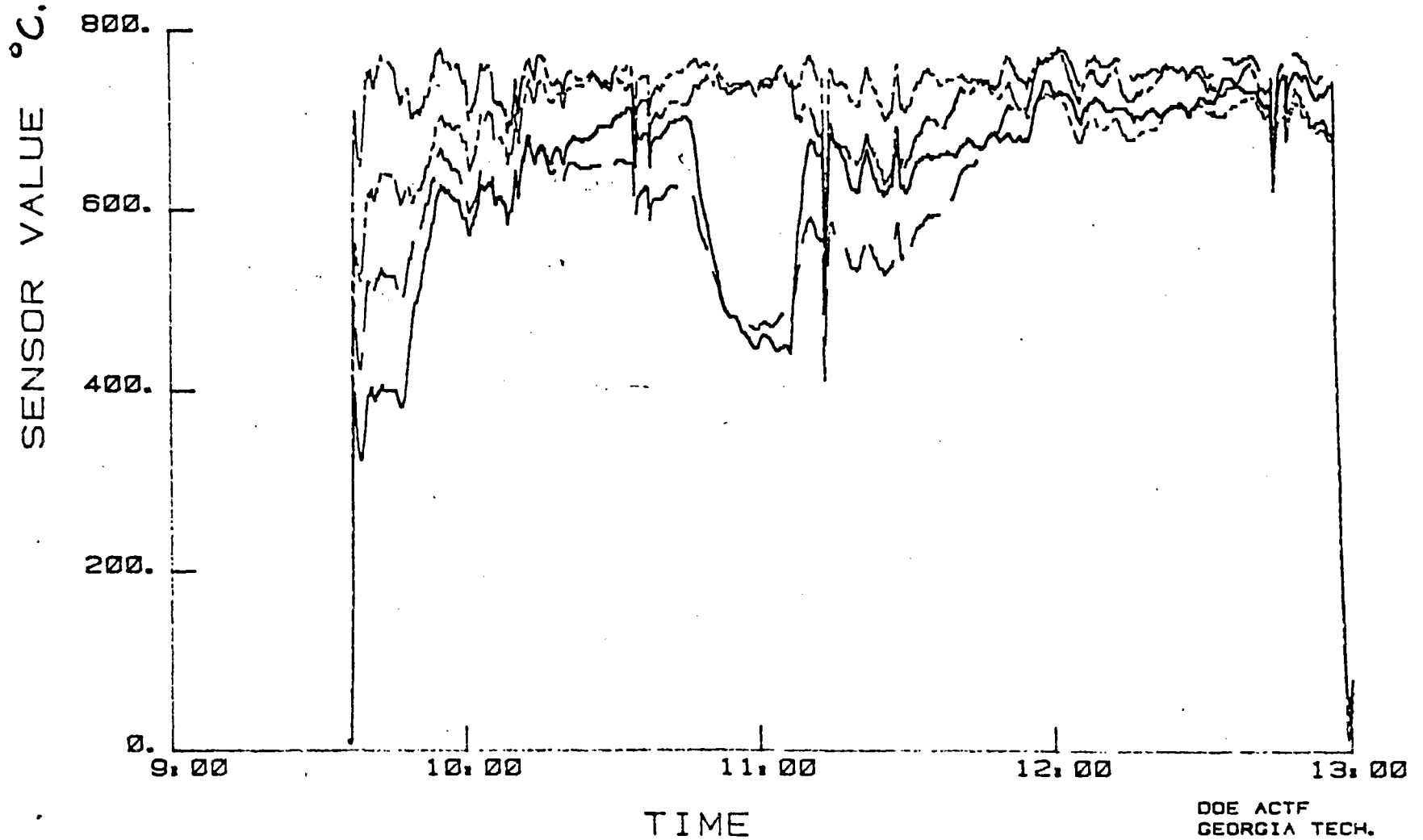
DOE ACTF
GEORGIA TECH.

TIME

FIGURE 6

FIGURE 7

DISH STIRLING SYSTEM INTEGRATION AND TEST PROGRESS REPORT

R. A. HAGLUND, VICE PRESIDENT

ADVANCO CORPORATION, El Segundo, California

Abstract

Advanco Coporation under contract to the Jet Propulsion laboratory with support from United Stirling, Sweden, Solar Turbines International, San Diego, California and the General Electric Company, Schenectady, New York, each working under separate contracts to the Jet Propulsion Laboratory, have carried out and completed the integration and check-out of the complete Dish Solar Stirling Thermal Power System at JPL's Parabolic Dish Test Site at Edwards Air Force Base, California. The test program to demonstrate t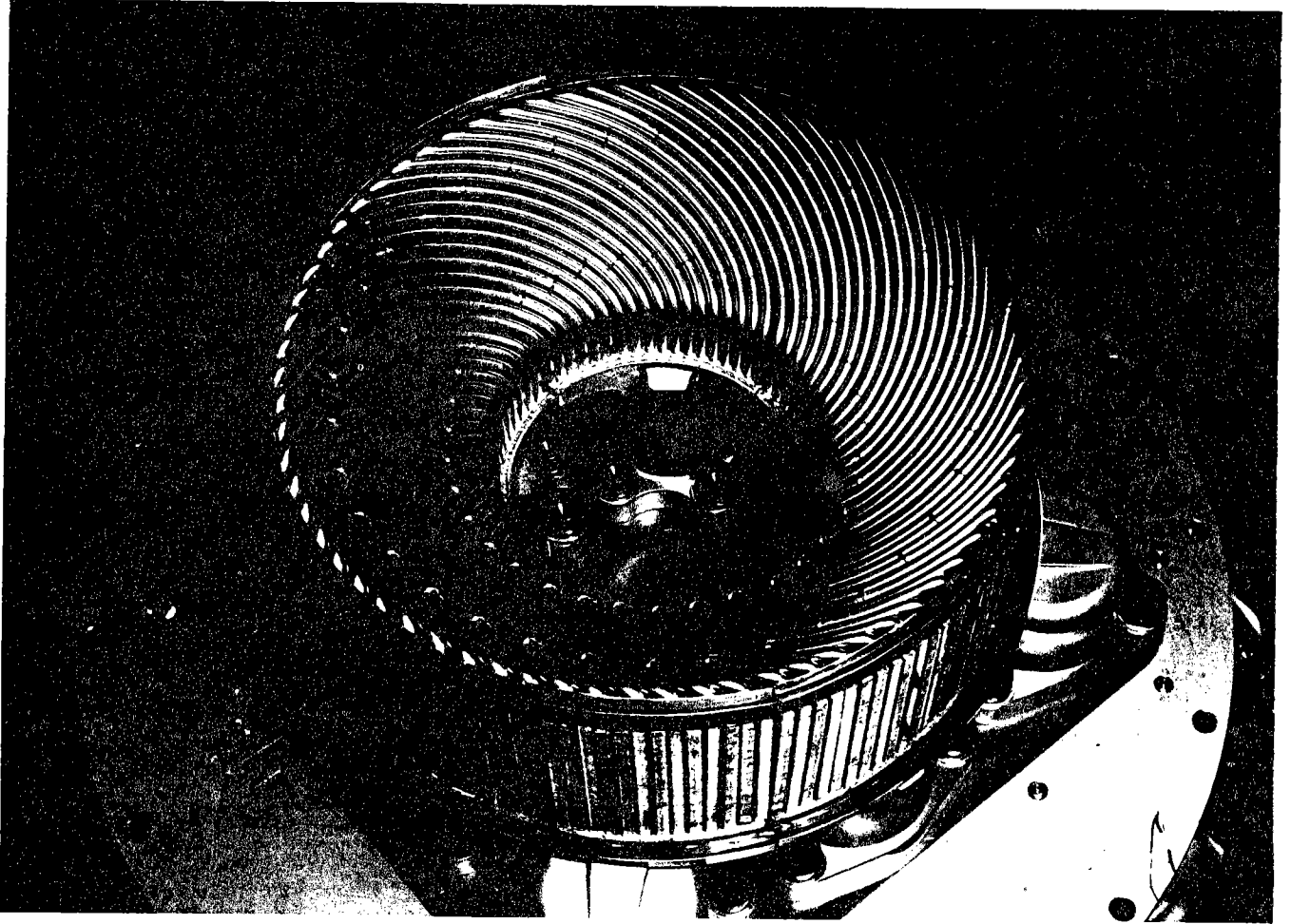his full-up Dish Stirling Solar Thermal Electric System is well under way and the preliminary results of the tests conducted thus far are presented. The results are very encouraging and show promise of high performance and efficiency. The outstanding performance and durability of the 4-95 Stirling engine has been the highlight of this 6 month integration and test activity. Exposure to severe heat, dust, sand and wind during the summer months and heavy rains, high winds, including sand storms and freezing cold in recent months has not affected the engine or the receiver in any noticable manner.

Integration

The Dish Stirling Solar Thermal Electric System is comprised of the following major components and susystems.
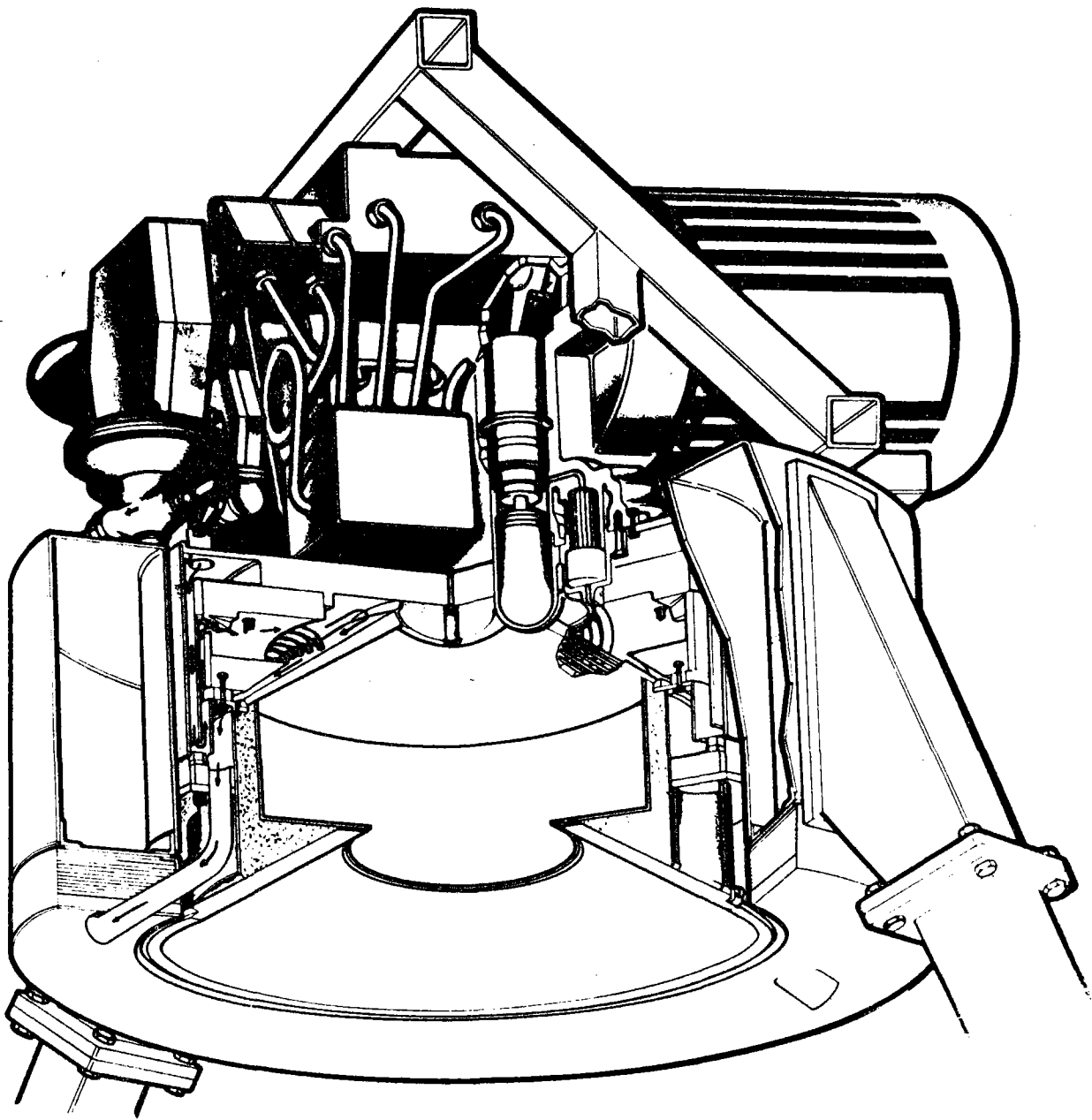
Figure 2. DSSR and 4-95 Engine/Alternator

o   JPL Test Bed Concentrator No. 2

o   United Stirling 4-95 Stirling engine

o   Fairchild direct coupled Hybrid Dish Stirling Solar Receiver

o   General Electric 25KVA induction Alternator

o   General Electric Utility Interface and Substation Unit

o   Advanco Dish Stirling System Control Console

The complete full-up Dish Stirling Solar Thermal Electric System when operating "on-sun" is illustrated in Figure 1. The basic features of the 4-95 Stirling engine, the 25 KVA induction alternator and the hybrid Dish Solar Stirling Receiver are shown in Figure 2a and 2b. The Dish Stirling System Control Console is shown in Figure 3.

A single line schematic diagram of the electric system contained within the Utility Interface and Substation Unit is shown in Figure 4.

The closed loop cooling water system including air-cooled radiator can be seen in Figure 1.

Test Program

A number of component and subsystem tests were conducted prior to the integration activity. A separate engine test program to prove the design of the dry oil sump lubrication system to permit operation of the engine in the inverted position was conducted by United Stirling in Sweden. A hybrid receiver combustion and heat thransfer development test program was conducted jointly by JPL, Fairchild and the Institute of Gas Technology prior to delivery of the receiver to JPL for integration with the 4-95 engine.
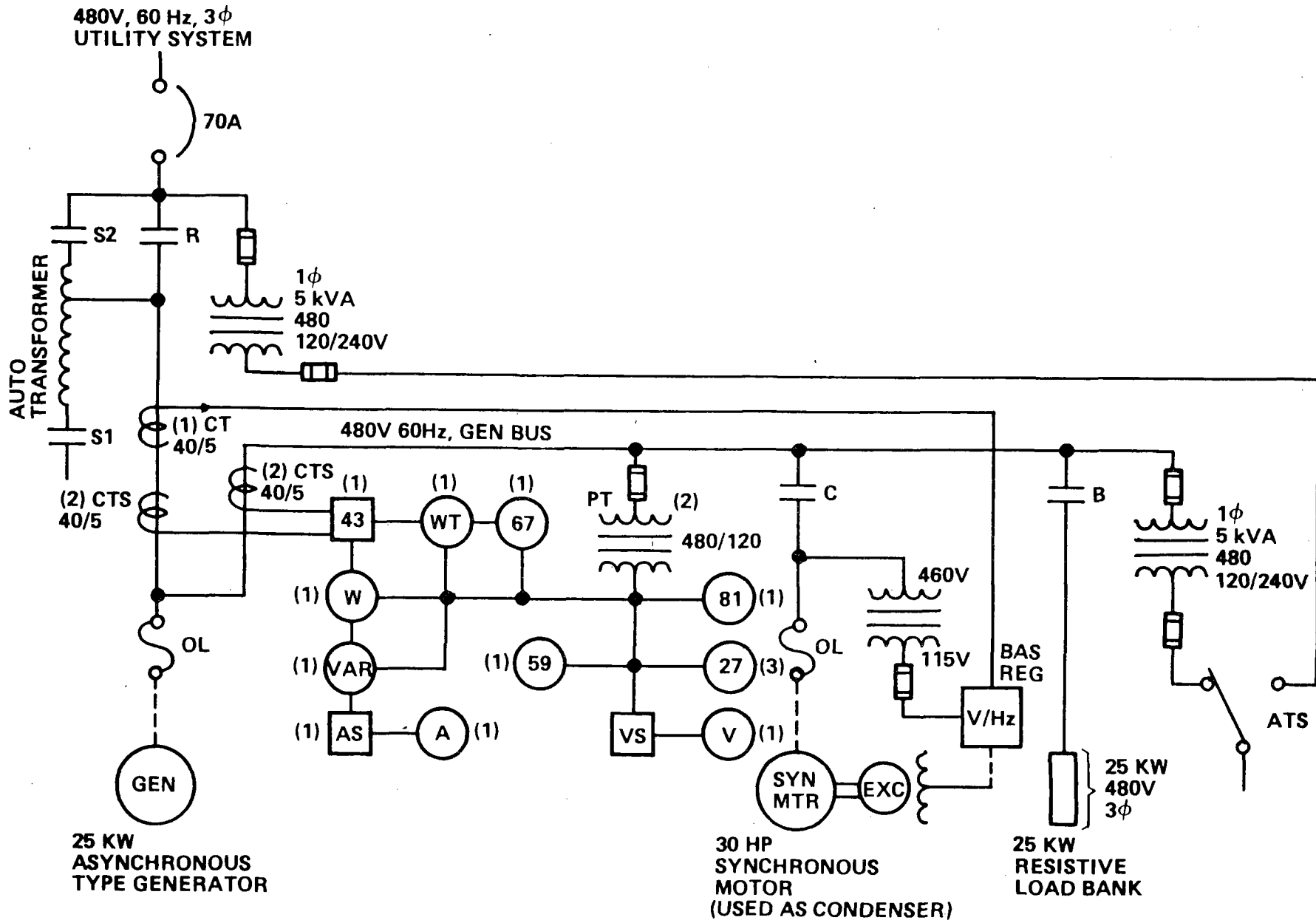
Figure 4. Electrical Schematic Diagram

Integration tests with the hybrid receiver, the 4-95 engine, the Utility Interface and Substation Unit and the Dish Stirling Control Console were conducted on the precursor pad at JPL's Parabolic Dish Test Site prior to integration with the JPL Test Bed Concentrator. Assembly and check-out of the full-up Dish Stirling Solar Thermal Electric System was completed on October 2, 1981. A matrix of the progressive sequences of test conditions starting at low power and ultimately reaching full power at the maximum design pressures and temperature is shown in Figure 5.

PERCENT FACETS (ACTIVE)	HEATER TUBE TEMPERATURE ($^{\circ}$C)	ENGINE MEAN WORKING PRESSURE (MPA)
0	650	7
25	720	9
50	770	11
80	(820)	(13)
		(15)

To achieve the initial low level of solar heat input (i.e., 25 percent active mirror facets) the non-active mirror facets were masked as shown schematically in Figure 6. The masking pattern that was developed by computer analysis to assure the optimum solar flux pattern. The computer analysis was confirmed by flux mapping and cold water calorimeter tests.
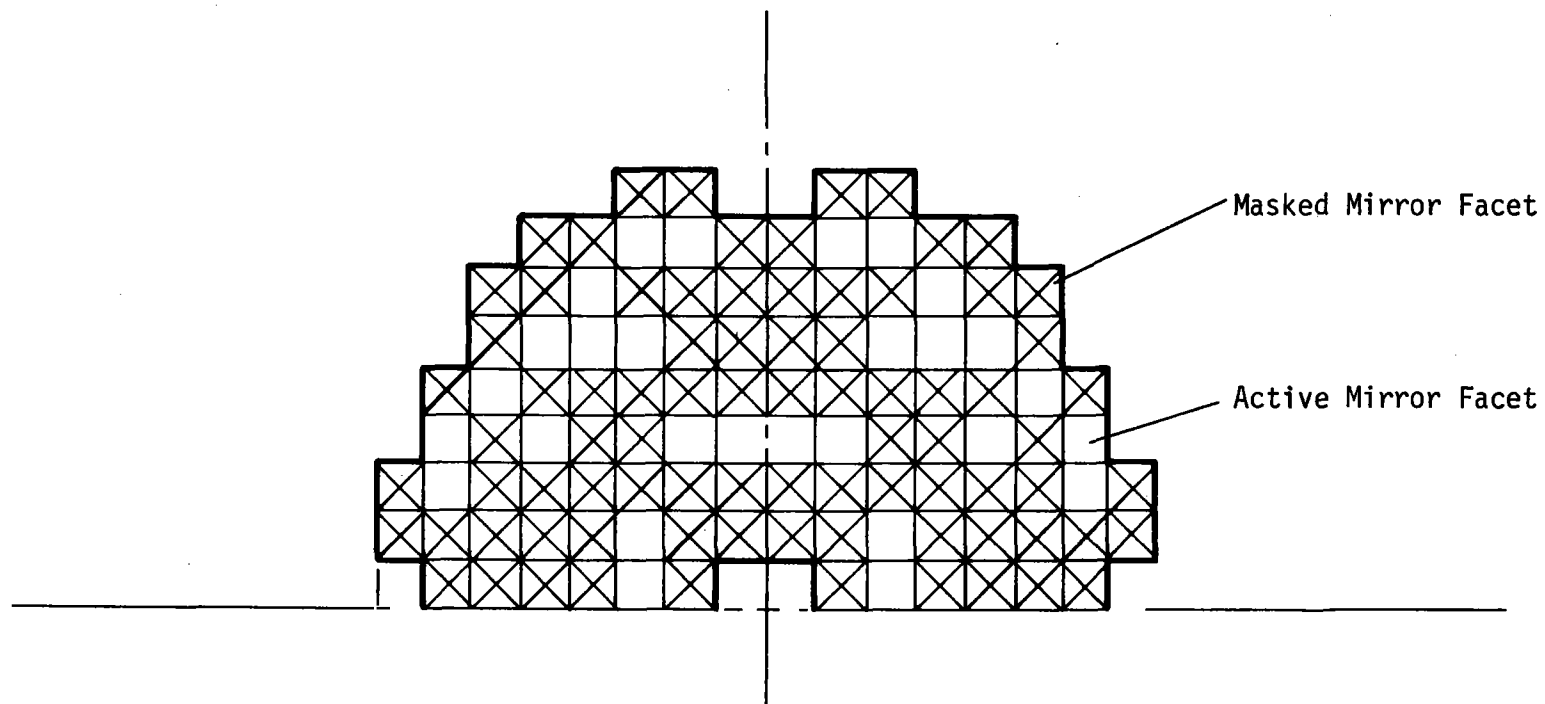
Figure 6.   25% Mirrors

The test results obtained at the various pressure and temperature conditions with 25 percent and 50 percent active mirrors facets are shown in Figures 7 and 8 respectively. By coincidence, the opportunity arose that allowed observation of engine/receiver transient performance during rapidly changing cloud cover conditions. As shown in Figure 9, the engine output remained essentially constant while the insolation level changed dramatically and suddenly. The combustion system provided thermal buffer energy as required to maintain constant engine speed and power output. Low power tests in the "solar only" mode (i.e. on sun with the combustor off) have been successful. Such additional tests at high power are planned.

FIGURE 7. 25% ACTIVE FACETS

ENGINE MEAN PRESS (MPa)	HEATER TUBE TEMP ($^{\circ}$C)	ALTERNATOR OUTPUT (KWe)
7	650	8.0
	720	9.5
	770	11.0
9	650	9.7
	720	11.4
	770	13.0
11	650	14.0
	720	13.0
	770	15.3

FIGURE 8.50% ACTIVE FACETS

ENGINE MEAN PRESS (MPa)	HEATER TUBE TEMP (^oC)	ALTERNATOR OUTPUT (KWe)
7	650 720 770	
9	650 720 770	
11	650 720 770	
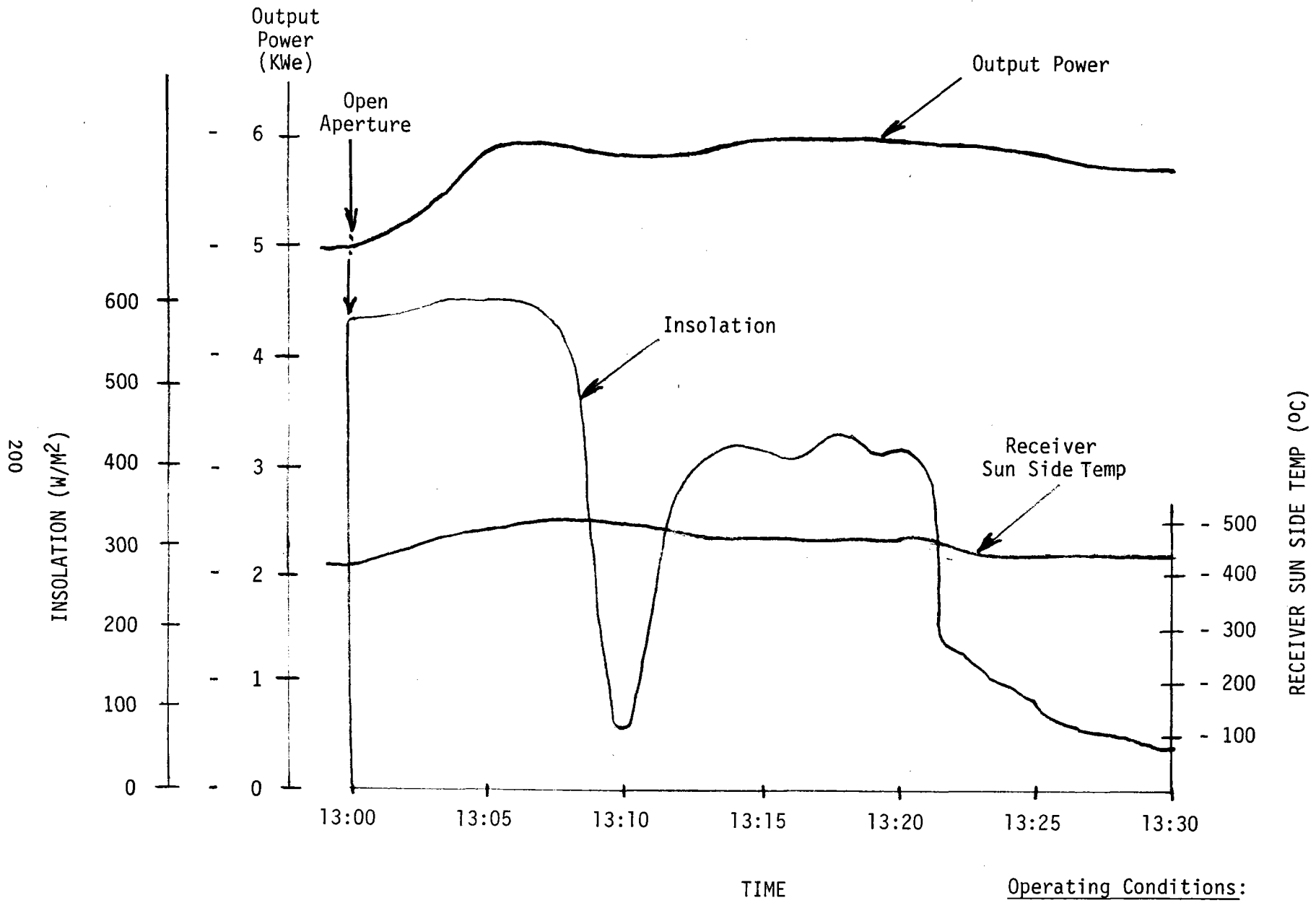
FIGURE 9 TRANSIENT PERFORMANCE

Operating Conditions:
Engine Press. 7MPa
Heater Tubes 650°C
25% Active Facets

COMMERCIALIZATION OF PARABOLIC DISH SYSTEMS

BYRON WASHOM

ADVANCO CORPORATION, EL SEGUNDO, CALIFORNIA

Recent federal tax and regulatory legislation has provided a short term market window for renewable energy technologies. A number of entrepreneurial firms in the small hydroelectric and wind technology areas have taken advantage of these 'supply side economic' incentives and signed multi-megawatt contracts for the manufacture of their hardware and sale of its electrical or thermal output. These same federal tax and regulatory policies are available to the parabolic dish technology. Although the lack of comparable life cycle testing and low capital cost makes parabolic dishes a less attracive investment opportunity when compared to wind and small hydroelectric, dishes remain attractive when compared to other venture capital investment opportunities in general. This paper discusses a case for the parabolic dish technology, and it notes the specific areas in need of technical or economic improvement.

The Public Utility Regulatory Policy Act (PURPA) of 1978 provided that a small power producer generating from renewable energy sources would be exempt from the Public Utilities Holding Act if the size is less than 80 MW_e and any fossil fuel consumption is less than 25%. This in effect created the opportunity for venture capitalist to establish 80 MW solar generating projects and sell electricity either to local utilities or other customers without being subject to the impossible federal bureaucracy of being a public utility. This new legal

entity provides a middle-man between the hardware manufacturers and the risk averse public utilities and the cost averse Public Utility Commissions. Furthermore, PURPA established the basis and price by which the utilities must purchase the electricity and the basis for establishing the price is known as the Fuel Avoidance Cost (FAC) and it is escalated quarterly. The FAC may include fuel operations and maintenance, reduced transmission losses, opportunities to sell power to other utilities, load management, avoided or retired capital, and reduced reserve margin requirements due to higher system reliability.

The Energy Tax Act of 1978 (P.L. 95-618) and the Crude Oil Windfall Tax Act of 1980 (P.L. 96-223) provide a supplemental investment tax credit of 15% for special energy property installed prior to December 31, 1985. Solar thermal technologies are now classified as special energy property. Thus, a purchaser of solar thermal property would be eligible for the regular 10% business investment tax credit and a 15% energy tax credit on the basis of the capital cost. This is particularly advantageous to parabolic dish technologies where the initial capital cost is extremely high and the operational cost is relatively low. Utlities by the way are ineligible for these energy tax credits; thus, venture capital groups now have a decisive advantage over utilities in financing renewable energy projects.

The Economic Recovery Act of 1981 (P.L. 97-34) created the Accelerated Cost Recovery System for property placed in service after 1980. Generally, the statutory recovery periods for depreciation are now shorter than the most recently published ADR class lifes. It is believed that most solar thermal technologies will fall into the five year or ten year depreciation schedule and be subject to depreciation by the 'straight line' depreciation method.

The Energy Recovery Tax Act of 1981 provided for exemption of the 'at-risk' provision for special energy property. Previously a private investor could only take, for tax purposes, a cummulative deduction from his income up to the amount of money he has at risk in the venture. No further losses may be deducted until such time as the investment begins to show net positive taxable income. Exemption of special energy property encourages the risk capitalist to increase the leveraging (i.e., the debt to equity ratio) of his project by securing the maximum amount of non-recourse debt. This admittedly is difficult with solar equipment projects not providing the required collateral to the lender because of doubtful resale value, but it does remove a potential barrier and it offers creativity of securing of the debt by parties other than the owner (i.e., manufacturers warranties, insurance guarantees, take-or-pay purchase guarantees by the utilities).

Let's review the federal regulatory and tax laws stated thus far and investigate where they are leading capital investment in renewable tecnologies. PURPA provided a means for entrepreneurial companies to enter into 80 MW Purchase Power Agreements with public utilities and receive a fair price according to the provisions of the Fuel Avoidance Costs Clause. These same entrepreneurial companies are encouraged to make capital investment in renewable energy technologies by being granted a supplemental 15% energy tax credit and being exempted from the 'at risk provision' which allows greater leveraging of the project. The Accelerated Cost Recovery System provides a more rapid depreciation schedule than previously available. Therefore, Congress has provided for significant up-front tax benefits to accrue to investors in solar energy equipment who under optimal conditions receive payback of their original equity investments within the first year via tax benefits.

This paper's enthusiasm for the present tax and regulatory provisions is not without it's risks to all parties involved, for there are many. This is clearly not a place for the risk averse. The energy tax credits require that the property be installed and operating by December 31, 1985; thereafter abscence of this most significant incentive reduces the selling price depending on the projects debt to equity ratio, by more than 50%. It is also questionable as to the maximum number of fully integrated parabolic dish systems that can be fully tested, manufactured and installed prior to the 1986 deadline. The source of the borrowed funds in a highly leverged project will look for an iron clad source of debt servicing regardless of the profitability and performance of the project which will require significant recourse loans on the part of the owner, performance warranties from the manufactuers and possibly take or pay contracts from the utilities. Lesser issues deal with stabilization of fossil fuel prices, reduction of the maximum income tax rate on individuals and land and transmission line availability.

As many of you are aware the U.S. Treasury Department feinted an attempt at repealing the energy tax credits this year. Congress expressed their continued suport of these incentives by circulating resolutions in both the House and Senate that strongly advised the Administration against any possible proposals. In what must be regarded as solar energy's finest hourly politically, 64 Senators and 264 Congressmen co-sponsored the resolution. The Administration has subsequently withdrawn the move to repeal the tax credits.

In conclusion, this paper documents the alternative to the federal budget outlays for the commercialization of solar energy technologies by creating solar management companies/limited partnerships to take maximum advantage of existing supply side economic incentives. This opportunity can only be exercised once a sufficient research, development and demonstration phases of a program has been successfully completed. Upon completion, those manufacturers in conjunction with venture capitalist are provided a clear investment opportunity where the high risks are compensated with attractive economic returns. Wind, parabolic trough, photovoltaic, small scale hydroelectric and alcohol fuel projects are fully utilizing this approach, and the parabolic dish systems have every opportunity to do the same.

A POINT FOCUSING COLLECTOR FOR AN
INTEGRATED WATER/POWER COMPLEX

H. ZEWEN, G. SCHMIDT, S. MOUSTAFA

MESSERSCHMITT-BOELKOW-BLOHM
P.O. Box 801169
D-8000 MUNICH 80

KUWAIT INSTITUTE FOR SCIENTIFIC RESEARCH
P.O. Box 24885
KUWAIT

1.0   Introduction and Objectives

Messerschmitt-Boelkow-Blohm and the Kuwait Institute for Scientific Research
developed together a point focusing parabolic dish, which is in its actual
configuration able to deliver process heat for the temperature range between
150 and 500 ° C. This point focusing parabolic dish was identified as the
most promising solar collector for small solar thermal power stations (1).
The first collector module was tested at the Solar Energy Experiment Station
of KISR in 1979. In the meantime 56 dishes have been assembled in 100 KW_{el}/
500 KW_{th} food/water/power complex, which is in operation in the Kuwait desert
region of Sulaibyah (2).

This paper identifies the utilization potential of the point focusing para-
bolic dish, summarizes its main design parameters, reports on the collectors
performance tests and describes the utilization of the collector as primary
energy source in a food/water/power complex.

2.0   Utilization Potential

2.1   Process Heat Generation

The production of process heat seems to be one of the most promising applic-
ations of solar utilization in a near future. A simple system consisting out
of small collector field, a heat storage and a heat transfer system is able
to deliver thermal energy for a temperature range up to 500 ° C, where
industrial process heat is requested for industrial applications as

- food industry (cooling, drying, pasteurizing)
- textile industry
- paper industry
- concrete and ceramic industries
- steam for injection into oil fields
- breweries
- alcohol production.

To produce process heat for these industrial applications concentrating
collectors are needed with concentration ratios between 50 and 300. In order
to keep capital and operating cost low use must be made of effective solar
collectors with efficiencies of higher than 60 to 70 %. Figure 1 shows that

the parabolic dish is the only collector, where the efficiency drops slowly
with increasing temperature. In the Mediterrean and North African Region
actually 20 % of the total oil demand is needed for process heat, represent-
ing a big marketing potential for near term energy utilization.

2.2 Electricity Generation

The most challenging application for the use of solar energy is the electri-
city production by small solar systems for agricultural communities in remote
areas, far away from an existing grid. The power level ranges from 50 KW
through several hundred KW up to about 1 MW.

High concentrating collectors as the parabolic dish are able to be operated
with upper process temperatures of 300 ^{o} C to 500 ^{o} C and lead therefore to
power station efficiencies of 10 to 15 % overall efficiency. Figure 2 shows
the typical schematic design of a solar farm with parabolic dishes, where
the collector field is coupled via a thermal storage to an Organic Rankine
Cycle as energy conversion system.

All known farm systems, which are under development or already in operation
are based on the two loop principle, where the absorber is operated with a
fluid in the liquid state. The absorber of the parabolic dish, presented
in this paper, is designed in such a manner that a phase change from liquid
to vapor can take place in the absorber so that a single loop system is
feasable, which is with respect to economy much more attractive than a two
loop system.

Solar farm systems using parabolic dishes in combination with gasturbines
or stirling engines are expected to be in an efficiency range of 20 % to
25 %, that is the same range of large tower systems operating from 500 ^{o} C
to 1200 ^{o} C (4).

2.3 Cogeneration

Solar farm systems working with high concentrating point focusing collectors
can be operated with a lower process temperature, high enough to supply
sufficient process heat for a lot of applications, e.g. brackish and sea
water desalination, domestic hot water, cooling etc. Cogeneration plants

of this type serve therefore as the main source of electrical and thermal energy for integrated food/water/power complexes supporting small agricultural communities in remote areas. For such settlements all the energy required for food production, purification of water and electric power needs can be taken from the sun. Today the cost of solar produced energy is rather high when compared to energy generated from fossil fuel. However, for remote areas far away from existing grids, the cost of solar produced energy by cogeneration plants may become acceptable earlier.

The desalination of water in the Arabian Gulf area is extremely expensive. In Kuwait, the consumer has to pay today US$ 3,2 per 1000 Gallons of desalted water (a government subsidized price). The real production costs are much higher, therefore the desalination of water with the waste heat of solar cogeneration plants seems to be an attractive concept (5).

3.0   Development of a Parabolic Dish Collector

3.1   Main Design Parameters

For the design of a parabolic dish collector two parameters are of main importance:

- the rim angle α_R of the mirror contour
- the concentration ratio (aperture area to absorber area)

The rim angle affects the surface area of the collector, as a function of the aperture area. Figure 3 shows the effect of the rim angle, in which the ratio of mirror area to aperture increases rapidly when the rim angle is increased. Figure 4 shows the energy collected by a certain aperture as a function of the rim angle. Due to decreasing optical performance of the mirror areas near the edge of the paraboloid, the effectivity related to the aperture levels out when the rim angle is increased beyond 130 ^{o}.

The energy collected, related to the mirror area, therefore has an optimum in the range of α_R = 90 ÷ 110 ^{o} , depending slightly on the mirror surface properties.

Optimizing the concentration ratio of a paraboloid collector needs detailed knowledge on optical and thermal losses as function of the absorber size.

210

Before entering this optimization procedure the type and shape of receiver must be defined. Surface receiver and cavity receiver both are candidate types for the paraboloid collector.

The cavity receiver requires a considerably larger focus length for the paraboloid than the surface receiver, thereby increasing the requirements for contour accuracy, mechanical support stiffness and tracking.

The surface absorber allows for a very small focus length and is comparable in efficiency as long as its surface reflectivity can be kept down by coatings.
Up to 750 K several coatings are available with small reflectivity and very small degradation rate. Therefore the surface receiver was selected as a baseline concept for applications up to 750 K. Figure 5 summarizes the optimization of concentration ratio using a spherically shaped surface absorber in the focus of the paraboloid.

The calculation of the absorber intercept factor was based on detailed laser measurements and a computer calculation using these results. For the technology applied for the mirror surface and a spherically shaped surface absorber the optimum concentration ratio is in the range of 200.

3.2   Basic Design Concept

The design of the parabolic dish collector which is shown in Figure 6 was based on detailed configuration studies. Its main features can be summarized as follows:

Tracking: polar mounted hour axis using a computer guided
                  control for following the daily path of the sun.

Reflector dish: Six sectors of sandwich structure, plated with small
                  black silvered flat glass mirrors each 30 x 30 mm in
                  size and 0,9 mm thick, are bolted together to form
                  the paraboloid contour.

Absorber: The spherically shaped absorber is built from copper
                  (Fig. 7). The sphere is formed by a shell of 20 mm
                  thickness, at the outer surface of which a spiral

211

channel is machined which afterwards is coated
with a 3 mm copper layer by electrodeposition.
It is highly insensitive to local peaks in heat
flux distribution. This allows to keep the
absorber in a fixed position, while the reflector
is moving around the focus. Thereby flexible hot
lines are avoided and the absorber can be connec-
ted to the field piping system by well insulated
stainless steel tubes.
Mechanical rigidity and life duration capability
of the copper structure are proven up to a tempe-
rature of 750 K. So the temperature limits of
absorber structure, optical coating and the heat
transfer fluid are nearly identical and corre-
sponding to the optimum performance temperature
range of the system.

3.3 Technical Data for the Point Focusing Parabolic Dish

Concentration ratio	200
Intercept factor	0.94
Ground cover area	5 x 5 m
Height	6 m
Wind speed (op./emerg.)	50/130 km/h
Thermal power	13,5 KW
Aperture area	18,3 m^2
Concentrator diameter	5 m
Concentrator material	reinforced plastic
Mirror	0.9 mm facets
Rim angle	102 $^\circ$
Absorber diameter	170 mm
Absorption	0.92
Tracking	Microprocessor-controlled

3.4 Collector Performance

Initial testing of heat transfer behaviour was conducted on the absorber using a fossil heat source, during its early stages of development, for simulation of the heat flux imposed on the absorber surface. These tests were necessary to compare several energy transfer fluids like Diphyl (Dowtherm A), Marlotherm S and Santotherm 66, which are applicable for two loop systems. During these heat transfer tests, the superiority of Diphyl was confirmed with respect to circulation pump power required, Table 1.

Detailed environmental testing was also performed on optical surface coatings for the copper absorber. The coating can be replaced at the site without disassembly of the absorber. The subsequent heat treatment procedure can be performed during operation also.

The efficiency of the collector may be obtained from the relation:

$$\eta = R \times F \times \alpha - \frac{\varepsilon \times \sigma \left(\frac{T_1^4 + T_2^4}{2} - T_0^4\right) + K \left(\frac{T_1 + T_2}{2} - T_0\right)}{I \times C}$$

where

R = Reflectivity

F = Intercept factor

α = Absorber absorptance

ε = Absorber emittance

σ = 5.67×10^{-8} $(W/m^2 K^4)$

T_1 = Absorber inlet temperature $(^{\circ}K)$

T_2 = Absorber outlet temperature $(^{\circ}K)$

T_0 = Ambient temperature $(^{\circ}K)$

I = Incident radiation (W/m^2)

A_p = Aperture area (m^2)

A_A = Absorber area (m^2)

C = Concentration ratio = A_p/A_A

K = 20 $W/m^2 k$ (experimental value)

The first collector module was installed and tested at KISR in October 1979; The testing continued during 1980 to study the performance and the reliability of the collector. Figures 8 to 10 show typical performance runs for different operation temperatures from T = 250 $^{\circ}$ C to T = 450 $^{\circ}$ C.

As already mentioned the actual absorber is covered with a non selective coating, which has an emittance of 0.85, due to the reason that easy maintenance during operation had priority over higher efficiencies. Figure 11 indicates the potential improvement of the collector performance if the actual emittance of 0.85 is decreased to 0.10.

All mechanical and optical inaccuracies are summarized by the collector intercept factor, which is in the range of 0,92 to 0,95. This value in conjunction with the concentration ratio of 200 may illustrate the development status achieved with this collector.

The inherent capabilities for increasing the concentration ratio and temperature may be demonstrated by Figure 12 which shows, that the thermal output is completely insensitive to tracking inaccuracy within a range of $\pm$ 0,25 ^{o}.

During the last year, tests had been performed for single loop systems using the spherical absorber for the direct generation of superheated steam. Steam generation tests up to 500 ^{o} C indicate already, that this absorber concept can easily be adapted also for the use in single loop systems.

Because the paraboloid collector developed principally can also be used for high temperature cavity receivers, some predevelopment effort was also spent on receiver concepts being capable of withstanding temperatures up to 1000 ^{o} C.

4.0   Application Example

A collector field consisting of 56 point focusing parabolic dishes is operated since June 1981 in Kuwait in an integrated solar complex, whereby the rejected thermal energy of the organic Rankine energy conversion system can be effectively utilized, so that cogeneration of 100 KW electric power and 500 KW thermal power is available.

Figure 13 shows the collector field, where all dishes are assembled in parallel and the collected energy is delivered to a thermal storage having a capacity of 700 KWh.

From the 1000 KW of direct normal radiation received by the collector field,

728 KW are absorbed by the collectors and 670 KW are delivered to the heat exchanger of the energy conversion system. The energy conversion process is presented in Figure 14, and it should be pointed out that the solar power station was designed from the very beginning with special regard to a subsequent utilization in an application program for electrical and thermal users. The lower process temperature is on a sufficient high level to be usable for thermal applications.

The first users of the power station require electric energy. Accordingly to the net electric output the station provides sufficient electric power for:

- pumping brackish water from approximately 70 m depth to a reservoir located at ground level

- distribution of brackish water for irrigation of an area of about 2 ha used for agriculture

- to drive a reverse osmosis desalination unit delivering potable water

- to power the air conditioning systems of several mobil homes

- to power a data acquisition system and a small workshop.

The plant also includes several large greenhouses equipped with passive and active evaporative cooling systems for desert operational conditions, trickle irrigation systems, automatic moisture monitoring and irrigation control.

After the first phase of operational tests, the air cooled condenser will be replaced by a water cooled condenser so that the rejected heat from the plant itself can be fed to a low temperature store from where all anticipated thermal users are supplied. Most of the thermal energy will be supplied for water desalination, because the Multistage Flash desalination represents an ideal user of the waste thermal energy and allows for studying the various scenarios for solar energy utilization of such users in a solar system, where the thermal varies during the day (5). In a MSF desalination system sea - or, in this case, brackish water is heated. The heated brine may then be fed into a series of chambers (stages) with decreasing pressure. The hot brine evaporates and the produced steam condenses around the cooler condensing tubes at the top of each stage chamber. In each stage the condensing water preheats the brackish/sea water feed. Whereas in a simple distillation

process 600 Kcal of heat yields one liter of fresh water, the MSF process has the potential of multiplying this yield many folds.

The residual amount of the rejected heat from the power plant's condenser will be used for the supply of domestic hot water.

5.0   Economic Considerations

A great effort has been spent in the last years in many countries for the direct use of solar energy for industrial, agricultural and domestic purposes. The progress achieved is evident.

Nevertheless, it is obvious, that solar plants are still far away from energy costs that are tolerable under economic aspects, and that a considerable effort will be necessary in the future to achieve this goal.

The dominating factors for cost reduction are

- increase of system performance and efficiency as far as possible in order to minimize the solar collector area which is the cost leading item of such plants

- decrease of production cost by cost minimizing design and serial production for solar collectors.

Solar power stations, which can be operated with a high system performance and efficiency have a good chance to be compatible with fossil energy sources in a near future. With respect to process heat production, parabolic dish collectors can be operated in systems having an overall efficiency of 60 to 70 %. In areas with a high solar insolation, as it is the fact for all Mediterrean areas this kind of collector can supply an average daily amount of 6.5 KWh/m^2. A small collector field, as it was represented in the previous chapter, is capable to deliver approximately 1 ton of high quality steam per hour at a temperature level of 450 ^{o} C. Cost analyses comparing small fossil fired plants with solar heated plants of the same dimension show that the solar station will be compatible with an oil fired plant in the next five years.

References

(1) Conceptual Design of Solar Thermal Power Plants (100 W - 10 MW),
Dr. P. Zahn, Messerschmitt-Boelkow-Blohm, Space Division, 8000 Munich 80

(2) Moustafa S., H. Zewen, 1979. A distributed Receiver Solar Thermal Power
Plant. Annual Research Report No. ISSN-0250-4065, Kuwait Institute for
Scientific Research.

(3) Future Development Trends of Point Focusing Collector Farm Systems.
G. Schmidt, P. Schmid, H. Zewen, S. Moustafa, Messerschmitt-Boelkow-
Blohm, P.O.Box 801169, 8000 Munich 80

(4) Concentrating Systems for Small Solar Power Stations. J. Feustel,
O. Mayrhofer, Workshop on concentrators for Solar Energy Applications,
Heverlee Belgium, 1978

(5) A Cogeneration distributed receiver solar power plant. S. Moustafa
et al., Kuwait Institute for Scientific Research, Kuwait.

(6) Organic Rankine Cycles for the conversion of waste heat and solar heat
into mechanical energy. A.P. Corneille, S. Haaf, Linde, Cologne.
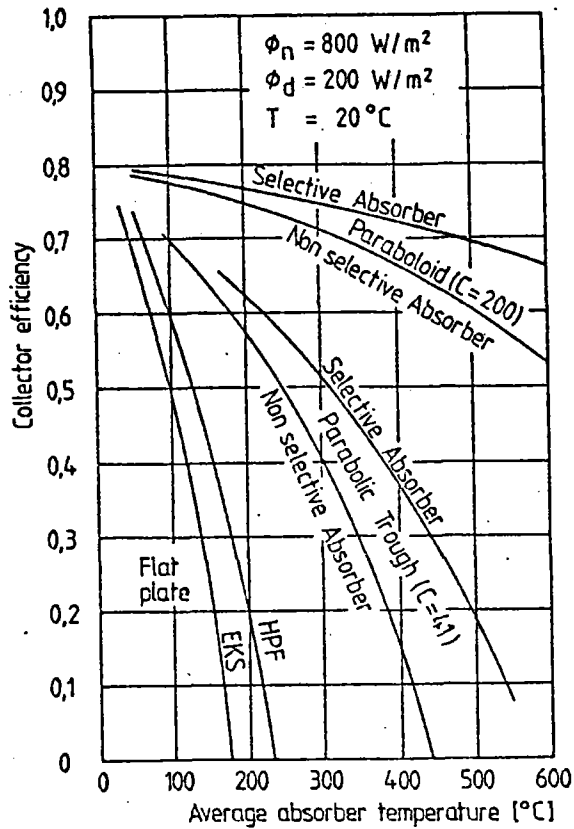
Fig. 1   Influence of Collector Concept
          on Collector Efficiency

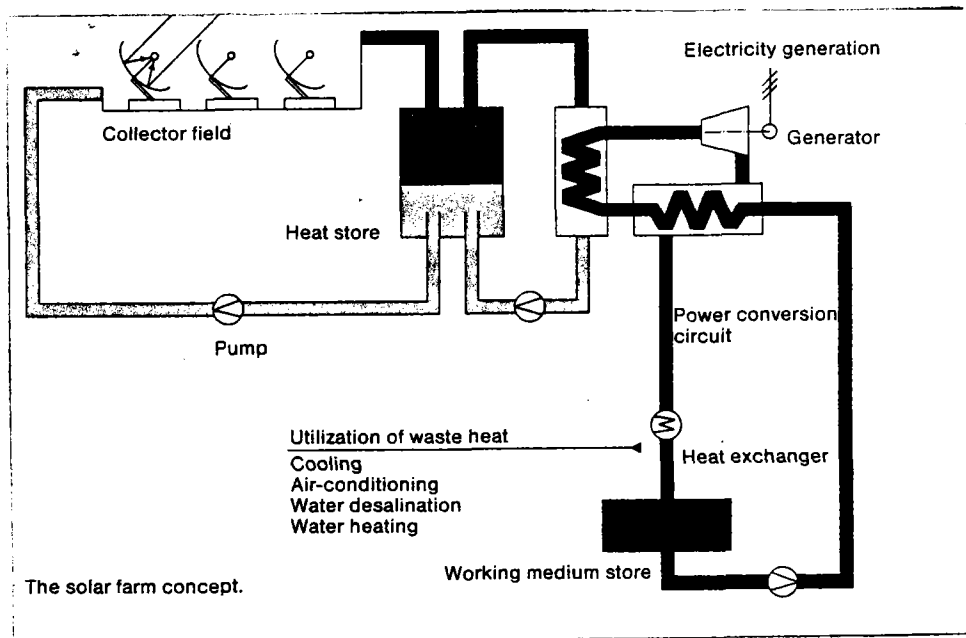The solar farm concept.

Fig. 2   Schematic Design of a Solar Farm
          System with Parabolic Dishes
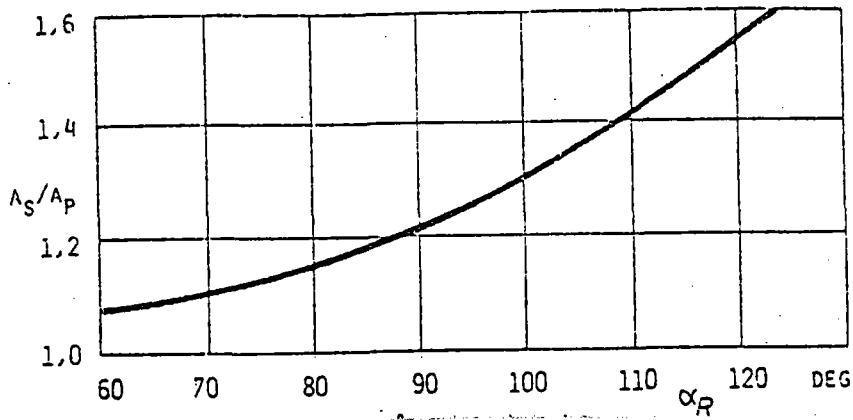
Fig. 3   Ratio of Mirror Surface Area to
          Aperture Area vs. Rim Angle
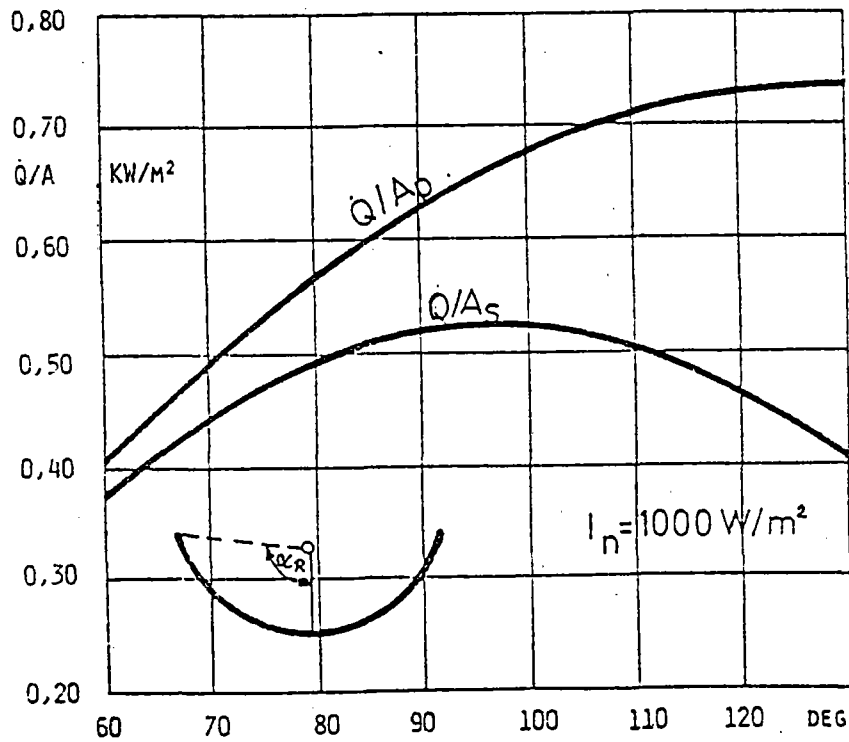
Fig. 4   Rim Angle Optimization
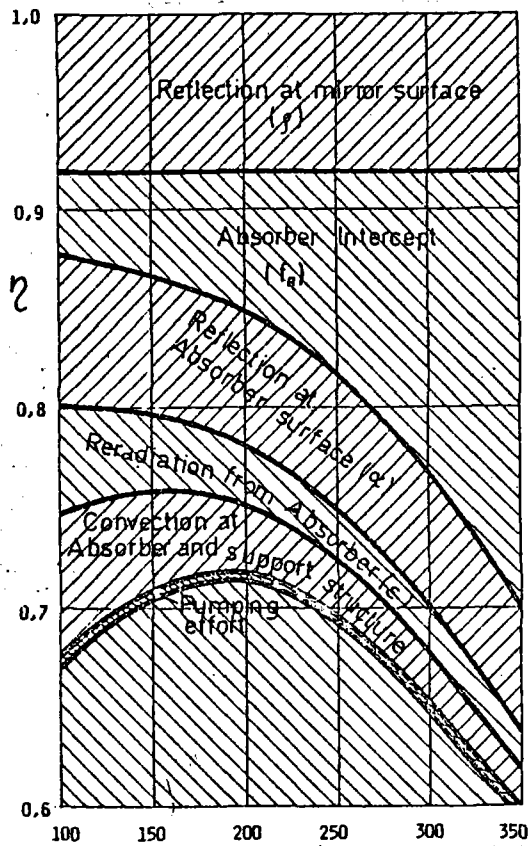
Fig. 5 Loss Budget of a
Parabolic Dish
Collector

Fig. 6 Point Focusing
Parabolic Dish

Fig. 7 Spherical Absorber
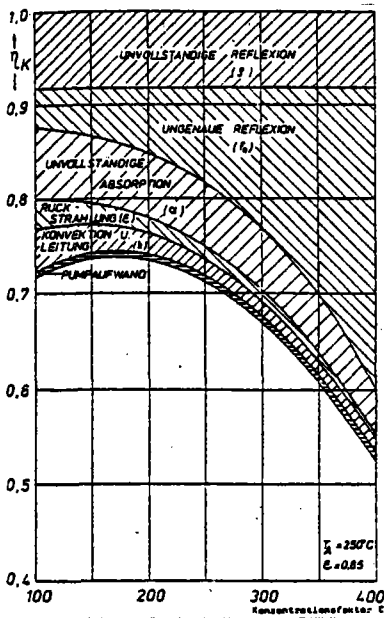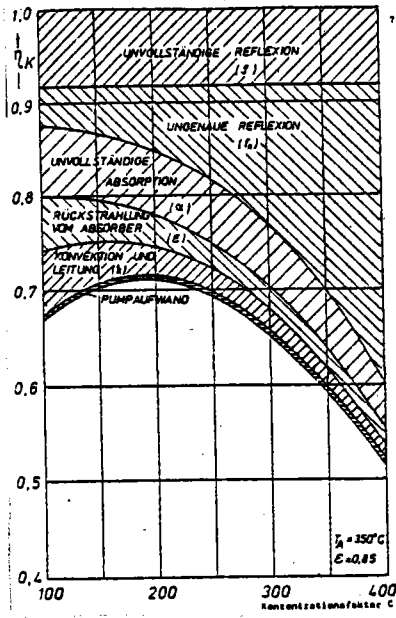
Fig. 8 (T = 250 °C)   Fig. 9 (T = 350 °C)   Fig. 10 (t = 450 °C)
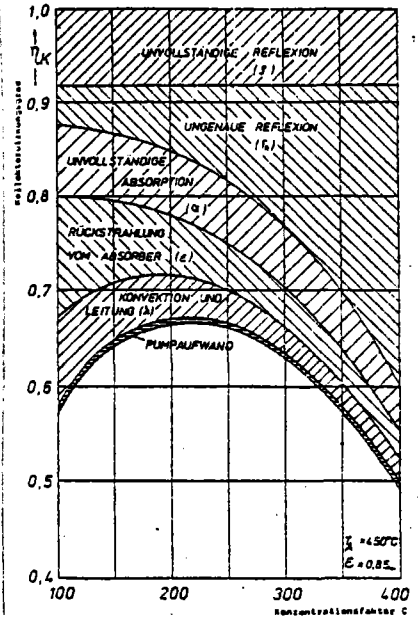
Paraboloid Collector Efficiency for 3 Absorber Temperatures
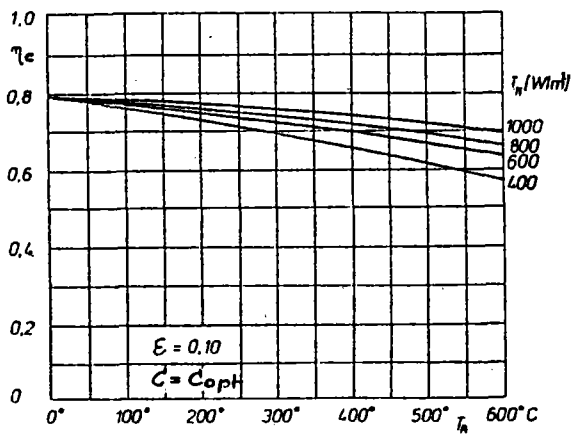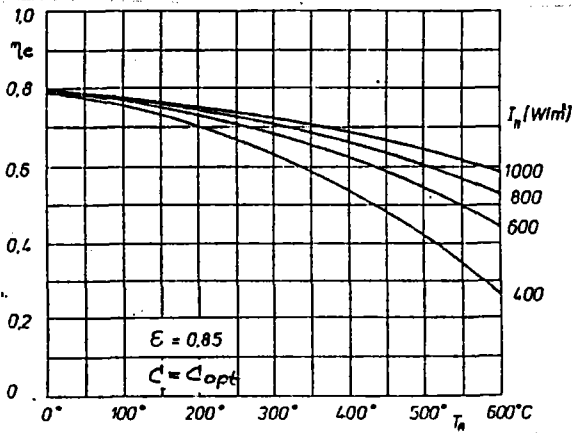
Fig. 11   Collector Efficiency us.
          Absorber Temperature.
          Influence of Irradiance
          and Emittance ·   221
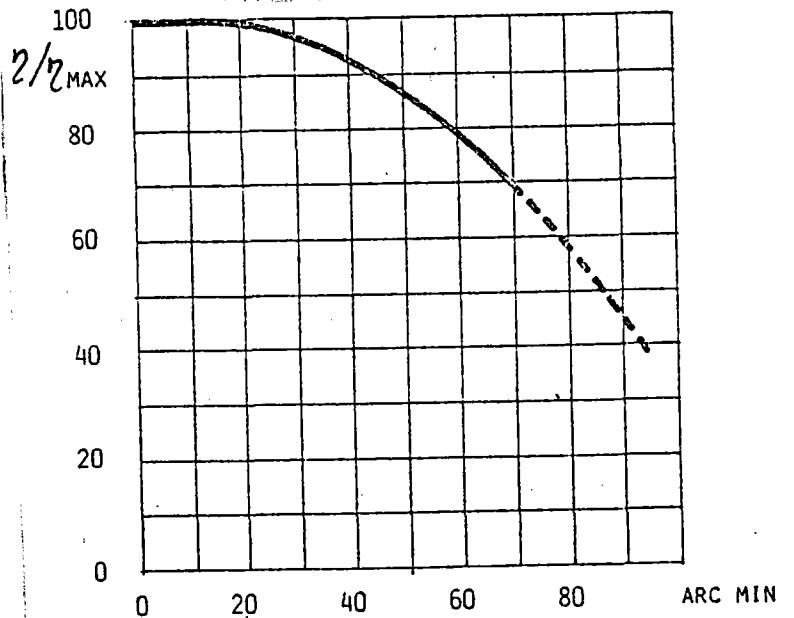
Fig. 12   Tracking Accuracy
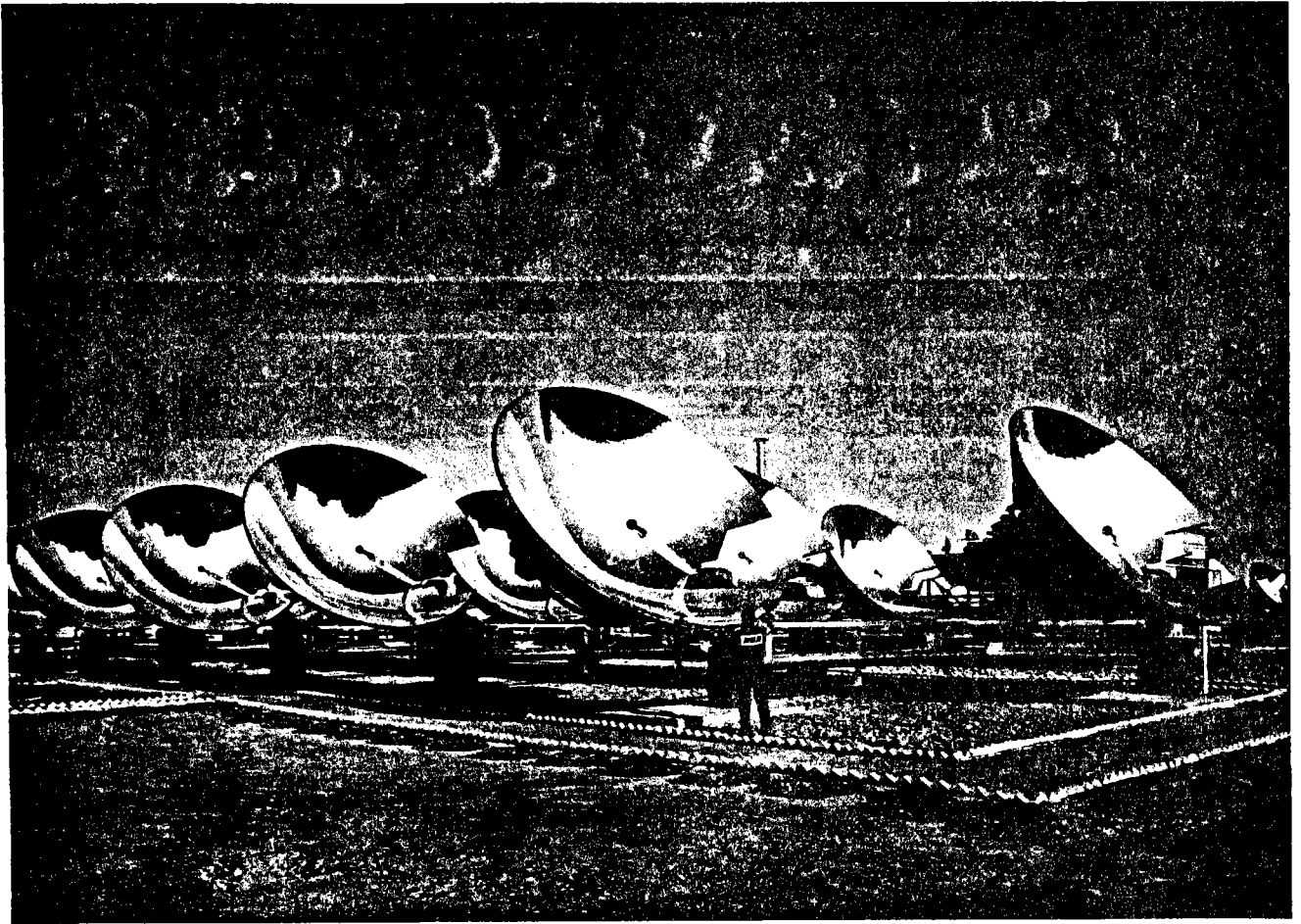
Fig. 13   Parabolic Dish Collector Field
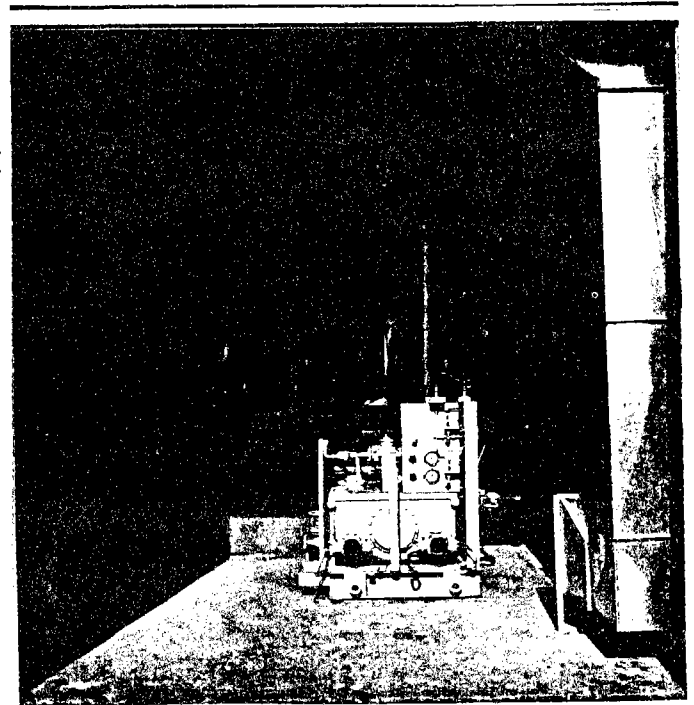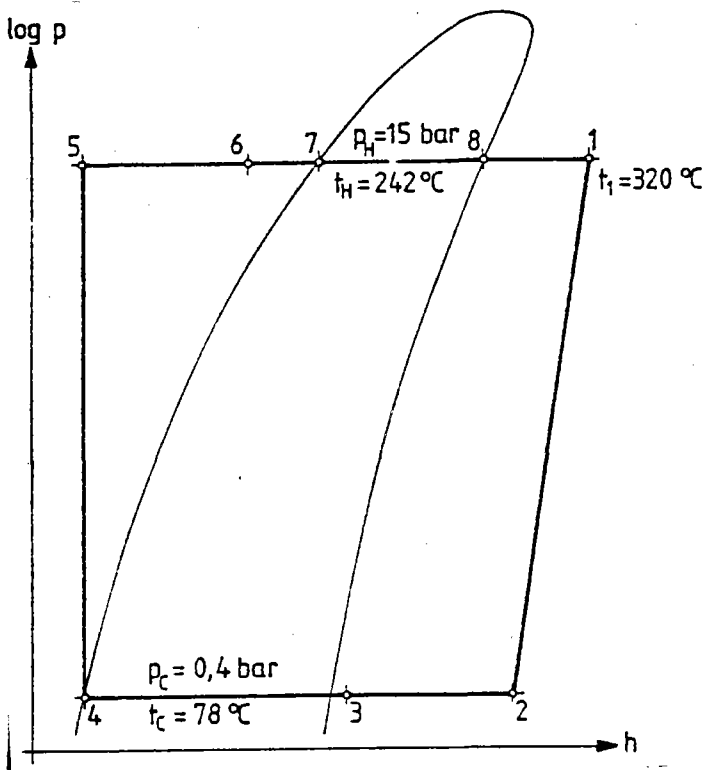
Fig. 14   Organic Rankine Cycle: Log p, h Diagram and view into
           the Turbine Hall

Fluid	viscosity 10^6 m²/s	conductivity W/mK	density Kg/m³	specific heat J/gK	Relative pump power %
Caloria HT 43	0,70	0,114	689	2,80	23,7
Syltherm B	0,50	0,118	680	2,03	19,7
Santotherm 66	0,44	0,108	785	2,78	13,0
Marlotherm S	0,51	0,102	834	2,55	18,3
Diphyl (Dowtherm A)	0,25	0,097	818	2,26	7,5
Gilotherm OMD	0,39	0,113	852	2,39	10,5
Hitec	1,76	0,603	1870	1,56	7,7

Table 1: Comparison of energy transfer fluids in terms of circulation pump power relative to the energy transfered (Absorber inlet temperature 240° C, absorber outlet temperature 350° C; fluid properties at 290° C; peak heat flux 25 W/cm²)

THE FRENCH THERMO-HELIO-ELECTRICITY-KW

PARABOLIC DISH PROGRAM

Michel Audibert

George Peri

Department d' Heliophysique Marseille, France

THE FRENCH THERMO-HELIO-ELECTRICITY-KW (THEK) PARABOLIC DISH PROGRAM

Among the several research and prototype development programs which were started by Centre National de la Recherche Scientifique (CNRS) in 1975, the THEK program aims to develop parabolic dish solar thermal power plants to produce thermal, mechanical, or electrical energy within the range of a few tens of thermal KW to some MW, at a temperature up to 350° C.

This program handled by Marseille Heliophysics Department involves three phases:

1) Design, construction, and experiments on two varients of laboratory prototype collectors to prove the feasibility of such collectors.

2) Based on the results of Phase 1, the aim of this phase is to start industrialization of collectors and to design, build, and experience an installation featuring 10 collectors to produce process heat.

3) Construction and implementation of demonstration collector fields to real applications.

PHASE THEK 1 (1976 - 1979)

The collector unit which has been chosen after preliminary studies is a parabolic dish made of flat elementary minor elements approximating a paraboloid of revolution. The main specifications of such a collector are:

Surface	50 m^2
Focal Length	4.8 m

Concentration Ratio	250
Tracking Accuracy	1/100 radians
Receiver	Black tube
Heat Transfer Fluid	Thermal oil
Output Temperature	325° C
Efficiency (800 W/m^2)	70%
Thermal Power	28 kW_{th}

Two varients of collectors have been constructed and experimented during Phase THEK 1. These two collectors had the same optical and thermal performances, but their structure and mechanisms were different (see figures 1 and 2).

In addition to the primary thermal loop (collector/storage tank), using thermal oil as heat transfer fluid, a secondary thermal loop was installed featuring a steam generator feeding a piston engine, itself connected to a DC generator.

The first objective has been fully attained. The prototypes allowed regulated production of thermal energy by heating a single phase heat transfer fluid up to 300° C. with an instantaneous total efficiency of nearly 70% in nominal conditions.

Tests conducted over a two-year period on these collectors served to initiate their industrial development with a greater knowledge of the subject.

PHASE THEK 2

A. Industrial Manufacture of Collectors.

To perform the first goal of Phase THEK 2 a detailed manufacturing design with cost analysis and production drawings have been made. Then, two contracts have been given by COMES (Solar Energy Commission) in 1980 to two companies* to realize two industrial prototypes each.

*BERTIN associated with CREUSOT LOIRE; The Societe de Propulsion, SEP

These four collectors are presently installed in Saint-Chamas (near Marseille) and have been running tests for two months.

The first measurements show an optical efficiency (low temperature efficiency) between 77% and 81%. The efficiency at 325° C., which is the maximum operating temperature for the thermal oil, are between 70% and 72%, as already measured on the two SEP collectors.

B. THEK 2 Experimental Power Plant.

The construction of a field featuring some ten collectors will serve to analyze the different problems raised from elementary collectors to the operational field of several tens of collectors. These problems arise at various levels and involve the following choices:
        Heat Transfer Fluid
        Heat Storage Fluid
        Fluid Collection Circuit
        Controls to be Automated
        Monitoring System
        Power Plant Management Strategy (in line with upstream
          and downstream external conditions, such as, atmospheric
          conditions, load power draw, etc.)

The design studies have been conducted in 1980 for a nominal 100 collector field to produce steam at 180° C. - 10 bars. In order to experiment the solutions adopted in these studies a 10 collector field will be installed in Saint-Chamas. The schematic of this experimental power plant is given on Figure 3. The heat transfer fluid in the collectors will be pressurized water at 260° C. - 60 bars.

The heat storage fluid, in the tank, will be saturated water at a temperature varying between 180° C. - 10 bars and 225° C. - 23.5 bars.

The steam at 180° C. - 10 bars will be obtained from the steam in the upper part of the storage tank through an expander.

COMES has issued a tender last month for the collectors and another tender will be issued by Heliphysics Department before the end of this month for the other parts of the plant. Then, the construction of the THEK 2 Experimental Power Plant will begin early in 1982, and should be completed within nine months.

PHASE THEK 3

Application of THEK collectors has already started with the construction of 11 collectors (75 m^2 each) as an auxiliary heat source for the central tower power plant THEMIS.

The first industrial applications will probably be concerned with steam production for Agro-Food industries in Southern France. Several feasibility studies are currently under way.
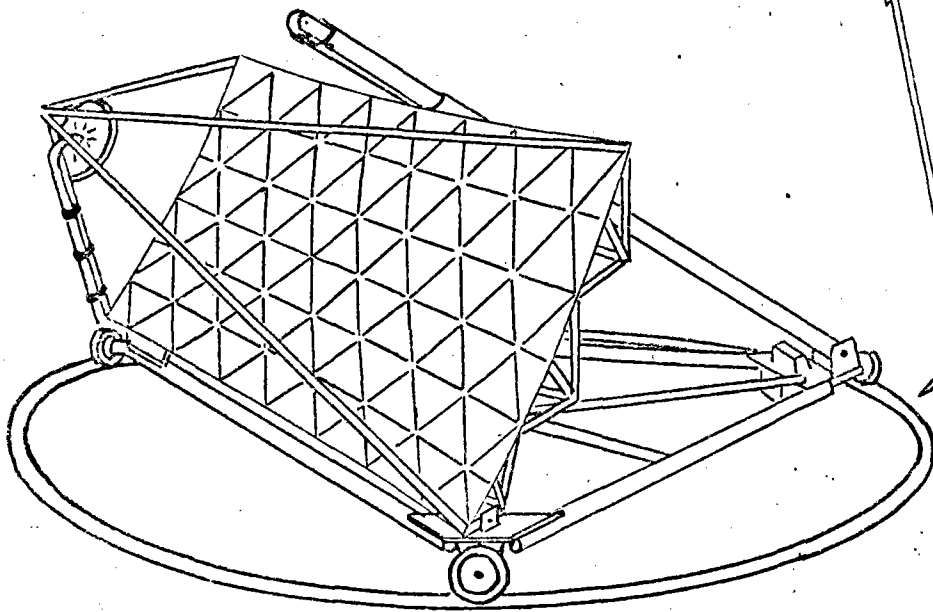
Fig.1 CAPTEUR THEK . E.T.B.
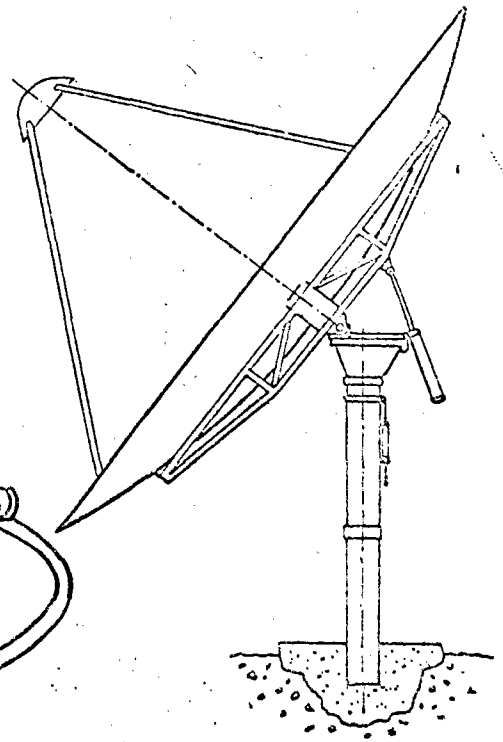
Fig 2. CAPTEUR THEK D.H.
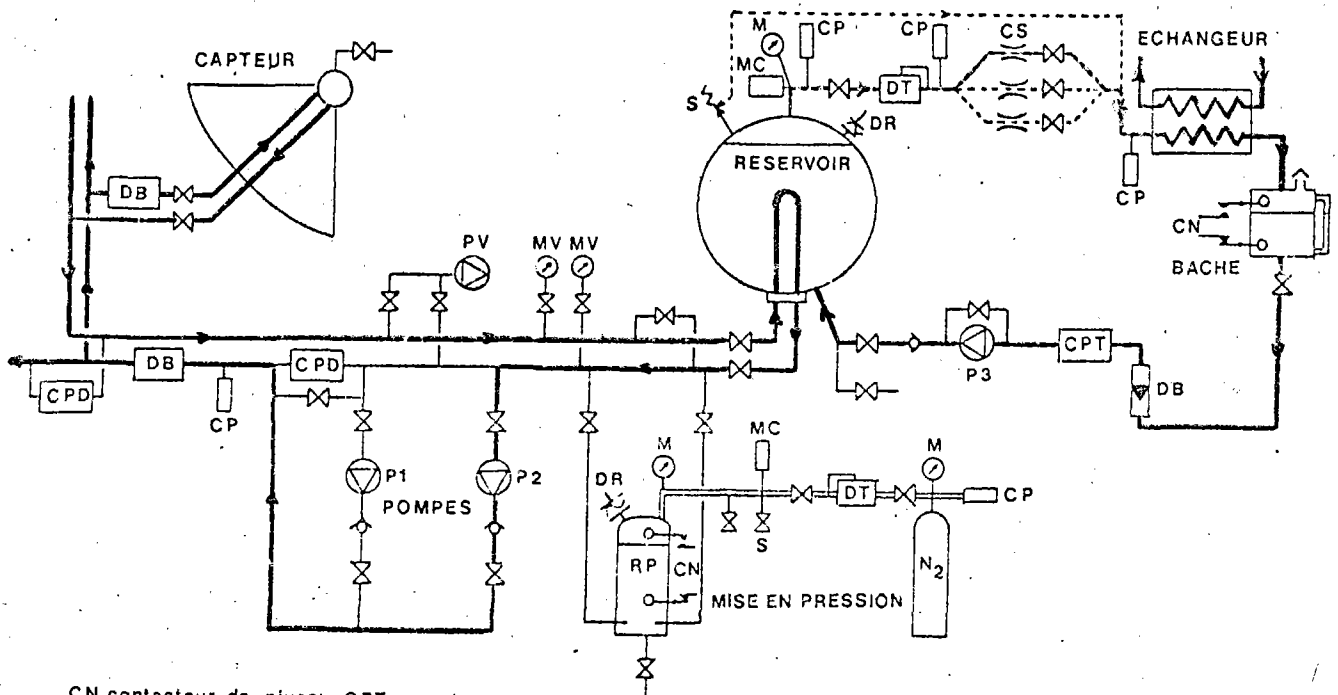
CN	contacteur de niveau	CPT	compteur				MV	manomètre à vide
CP	capteur de pression	CS	col sonique				P	pompe
CPD	capteur de pression	DB	débitmètre	DT	détendeur		PV	pompe à vide
	différentielle	DR	disque de rupture	M	manomètre		S	soupape de rupture
				MC	manocontact			

Fig.3.

Figure 4.   THEK 2 Collectors at SAINT-CHAMAS, FRANCE.

HIGH-TEMPERATURE CERAMIC HEAT EXCHANGER
ELEMENT FOR A SOLAR THERMAL RECEIVER

Hal J. Strumpf
David M. Kotchick
Murray G. Coombs

AiResearch Manufacturing Company
A Division of The Garrett Corporation
Torrance, California 90509

ABSTRACT

A study has been performed by AiResearch Manufacturing Company, a division of The Garrett Corporation, on the development of a high-temperature ceramic heat exchanger element to be integrated into a solar receiver producing heated air. A number of conceptual designs were developed for heat exchanger elements of differing configuration. These were evaluated with respect to thermal performance, pressure drop, structural integrity, and fabricability. The fabrication analysis was performed by the Norton Company, a ceramic manufacturer acting as a subcontractor to AiResearch on this study. The final design selection identified a finned ceramic shell as the most favorable concept. The shell is surrounded by a larger metallic shell. The flanges of the two shells are sealed to provide a leak-tight pressure vessel. The ceramic shell is to be fabricated by an innovative combination of slip casting the receiver walls and precision casting the heat transfer finned plates. The fins are bonded to the shell during firing. The unit is sized to produce 2150°F air at 2.7 atm pressure, with a pressure drop of about 2 percent of the inlet pressure. This size is compatible with a solar collector providing a receiver input of 85 kw(th). Fabrication of a one-half scale demonstrator ceramic receiver has been completed by Norton.

INTRODUCTION

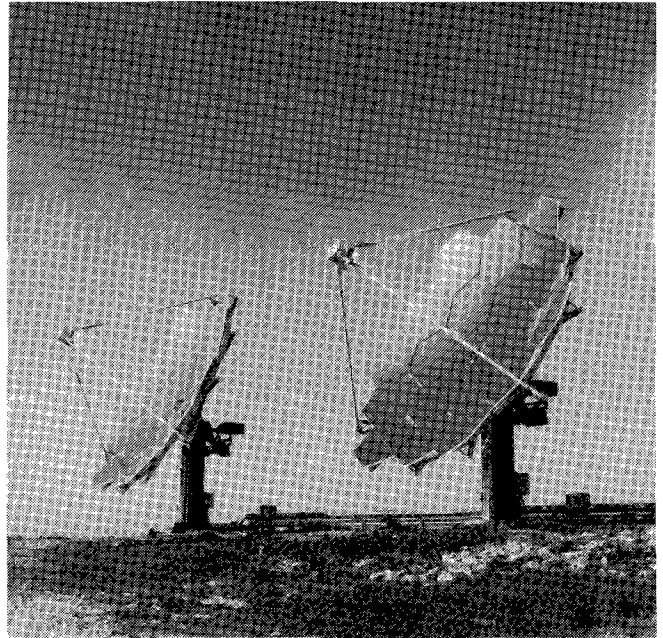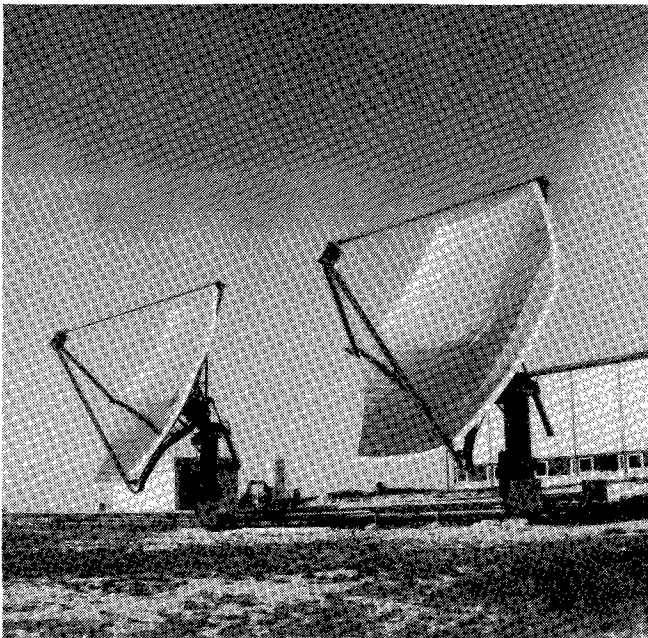A study has been performed by AiResearch Manufacturing Company, a division of The Garrett Corporation, on the development of a high-temperature ceramic heat exchanger element to be integrated into a solar receiver producing heated air. The study was funded by the Jet Propulsion Laboratory (JPL) under Contract No. 955875.

A number of conceptual designs were developed for heat exchanger elements of differing configuration. These were evaluated with respect to thermal performance, pressure drop, structural integrity, and fabricability. The fabrication analysis was performed by the Norton Company, a ceramic manufacturer acting as a subcontractor to AiResearch on this study.

The two most favorable designs were chosen for further evaluation. From this evaluation, the selected concept emerged. A detailed preliminary design and fabrication analysis was performed for this concept. In addition, a fabrication demonstration program was conducted by Norton. The outline of the study program, divided for convenience into two tasks, is shown in Figure 1.

TASK I

TASK II
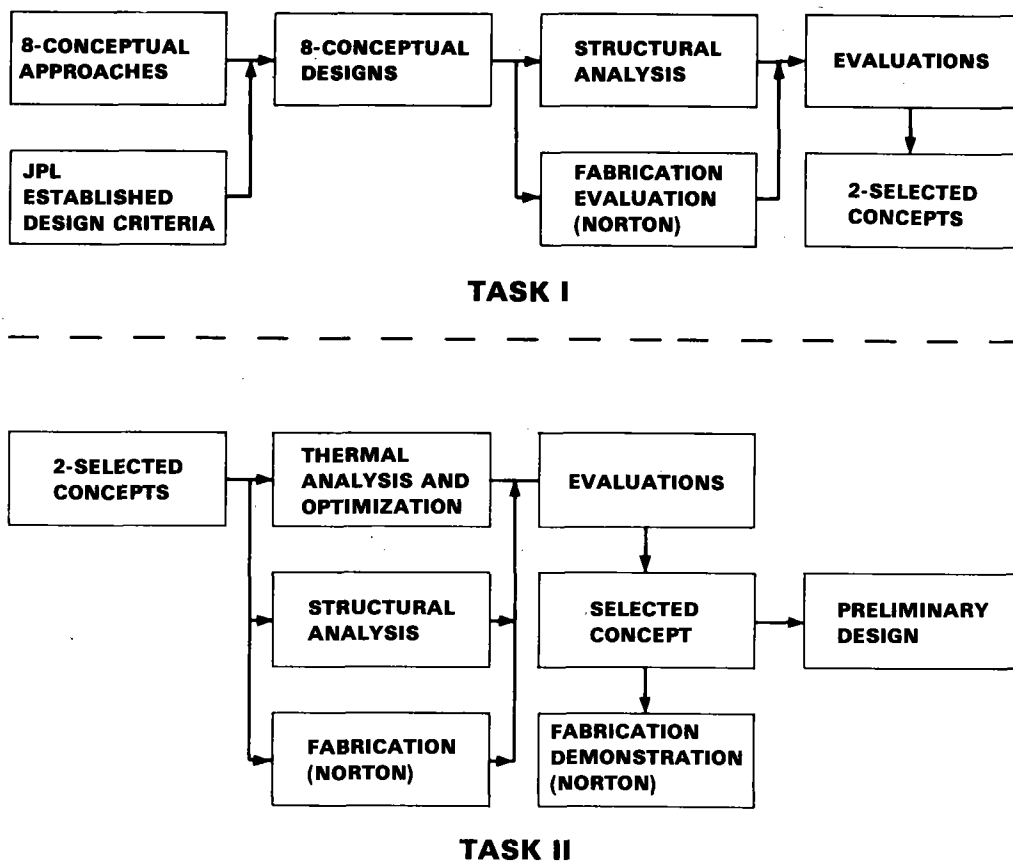
Figure 1. Program Approach

A-16638

This paper concentrates on the details of the selected design. The conceptual design study and selection process are reported elsewhere.[1]

ESTABLISHMENT OF DESIGN REQUIREMENTS

The function of the solar receiver is to absorb sunlight, using the energy to heat the working fluid (air). The sunlight is focused by a concentrator; the focal point of the concentrator is located at the receiver aperture. Figure 2 shows a conceptual concentrator and solar receiver system.

The concentrated incident solar flux is distributed on the interior walls and heat transfer surfaces of the receiver. Most of the energy is absorbed by the air; the remaining energy escapes back through the aperture or is lost from the outer surfaces of the receiver. A generalized schematic of a solar receiver is shown in Figure 3.

---

[1]A High-Performance/Low Cost Ceramic Heat Exchanger for a Solar Thermal Receiver, AiResearch Report 81-18452 (to be published).
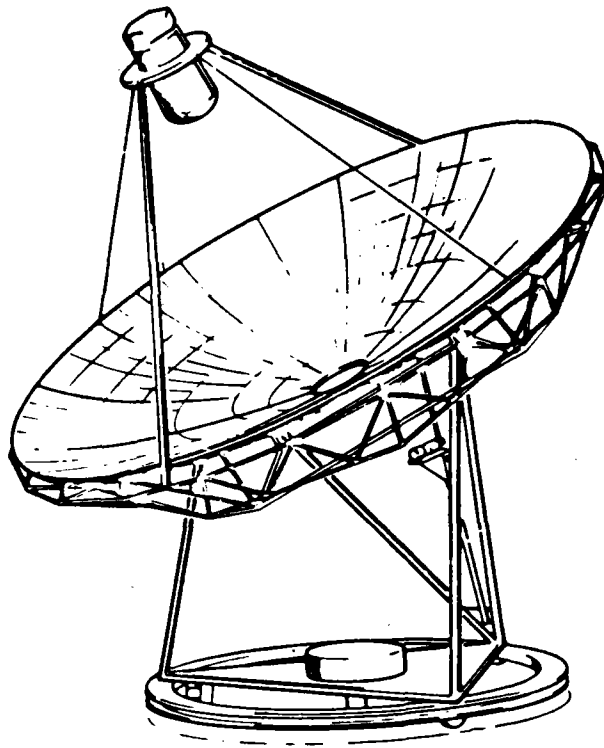
S-34158

Figure 2. Solar Collector Module

COLD
FLUID IN

INSULATION

SOLAR ENERGY
INPUT FROM
CONCENTRATOR

APERTURE

CAVITY

HOT
FLUID
OUT

FOCAL POINT OF
CONCENTRATOR

HEAT EXCHANGER
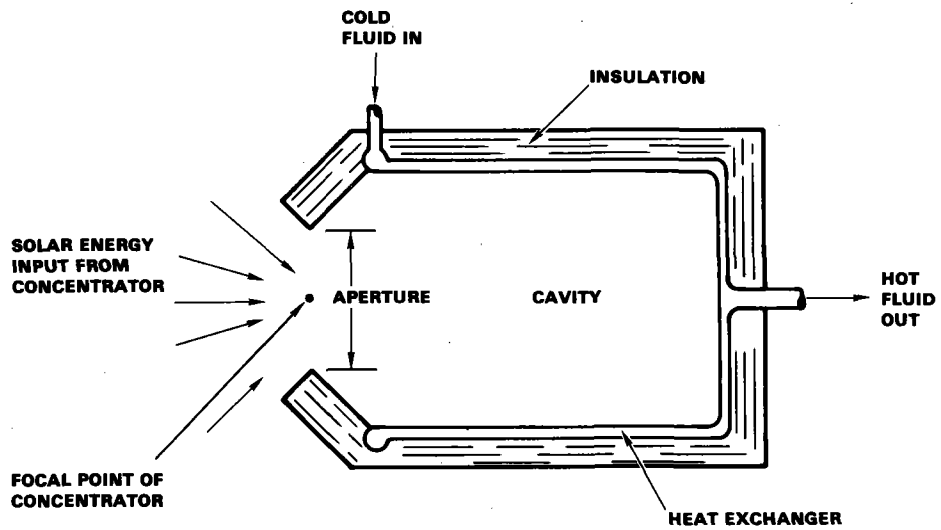
A-16955

Figure 3. Solar Receiver Schematic

The applications for the hot air produced by the ceramic solar receiver may be in the areas of electric power, fuels and chemicals, or industrial process heat. It is clear that precise design requirements cannot be developed until, at the very least, the receiver application is selected. It is necessary, however, to develop problem conditions in order to conduct the present study. A convenient and typical set of conditions is available for a power producing solarized automotive gas turbine (AGT) engine being developed by the Garrett Turbine Engine Company. This engine configuration is referred to as the Mod I. The design point for the solarized AGT receiver is given in Table 1. In order to heat the working fluid to the required temperature, a ceramic heat exchanger element is required because metallic material limits would be exceeded. The material selected for the present study, siliconized-silicon carbide manufactured by the Norton Company (NC-430), has an upper temperature limitation of around 2400°F.

JPL has specified an aperture diameter of 8 in. In order to limit incident flux spillage outside the aperture, a concentrator with a slope error of no greater than 1 mrad is required. From representative flux distribution curves for concentrators of this accuracy supplied by JPL, AiResearch flux mapping techniques were used to develop cavity wall incident flux distribution maps for the cavity sizes of interest to the present study. These techniques are described in another publication.[2] The generated incident flux distributions are symmetrical in the circumferential direction of the receiver. A typical generated flux profile is shown in Figure 4 for both incident and absorbed radiation.

TABLE 1

RECEIVER DESIGN POINT

Working fluid	Air
Outlet air temperature	2150°F
Inlet air temperature	1580°F
Inlet pressure	2.7 atm
Maximum pressure drop	4.0 percent of inlet pressure
Receiver input power	85 kw(th)

[2]Eastwood, J. C., Open Cycle Air Brayton Solar Receiver Phase I Final Report, AiResearch Report 79-15677, February 1979.
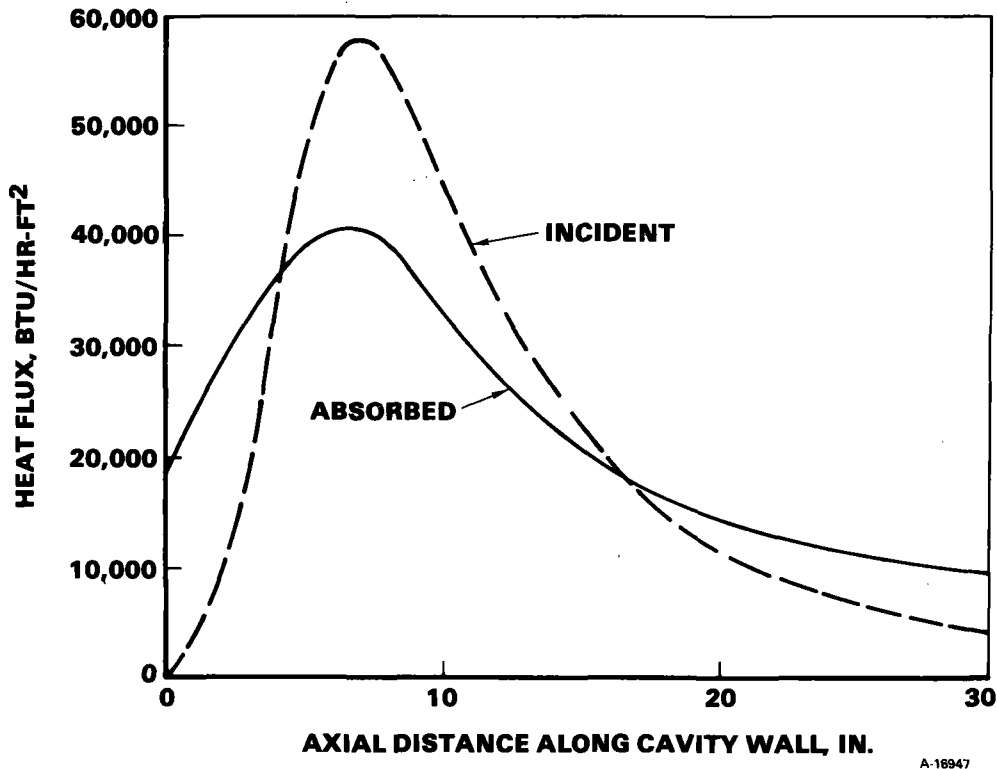
Figure 4. Typical Heat Flux Profiles

The thermal input to the working fluid is not specified. Therefore, neither the working fluid flow rate nor the desired cavity efficiency is given. The cavity efficiency is defined as the ratio of the working fluid thermal input to the specified receiver thermal input. The cavity efficiency takes into account the receiver thermal losses, including radiation and convection losses out the aperture opening and losses from the receiver outer surface. The cavity efficiency is, of course, a function of receiver geometry and temperature level.

It is desired to minimize receiver size and weight, because small size improves fabricability and enhances survival probability. In addition, small size aids in mounting and packaging of the receiver. A secondary consideration is to maximize the receiver cavity efficiency.

The receiver consists of a cylindrical main body, a flat or hemispherical closed end, a conical aperture end, and an incident radiation reflection skirt located around the aperture. The skirt helps direct any incident flux that spills over the aperture opening into the cavity. The closed end and cylindrical body of the receiver are covered with insulating material. An outer case surrounds the insulation. This is the general arrangement shown in Figure 3 (the reflector skirt is not shown, however). Figure 3 shows that the fluid inlet section is located at the aperture end, and the outlet section is at the closed end. Due to the nature of the flux distribution (see Figure 4), this arrangement has been found to yield a lower maximum wall temperature and a higher cavity efficiency than an otherwise identical receiver with opposite flow direction.

SELECTED DESIGN

Concept Definition

The selected solar receiver concept is shown in Figure 5. A cylindrical ceramic shell, with a slightly convex closed top and flanged bottom, acts as the inner wall of the receiver, absorbing the incident solar radiation. Bonded to the outer surface of the shell is a ceramic finned plate, which acts as the heat transfer surface for heating the working fluid air. Details of the finned plates are shown in Figure 6. The fins can be either plain or offset (offset fins are shown in Figure 5).

Plain fins form a series of discrete flow passages that enable hydro-dynamic and thermal development of the flow. Offset fins form interrupted flow passages with accompanying flow migration among the passages. The off-sets preclude the development of the flow by disrupting the fluid boundary layer. This results in an increase in the fluid heat transfer coefficient and pressure drop. As shown in Figure 6, the fins form an integral unit with the plate. This is different from conventional metallic plate-fin assemblies, which consist of separate fin sheets bonded to a plate.

As shown in Figure 5, the fins are in the cylindrical section of the shell. There are no fins in the top or flange regions. The outer boundary of the flow passages is defined by the insulation, which is expected to be of two types. The inner portion forming the flow passages is an air setting coating cement, which hardens to form a rigid, non-porous boundary. The outer insulation is a high temperature, blanket-type alumina-silica product. The insulation also forms the outer boundary of the outlet duct, as shown in Figure 5.

Outside the insulation is a metallic outer shell (continuing into the outlet duct region). The metallic structure is sealed to the ceramic shell using a "Flexitallic" chevron seal between the metallic and ceramic flanges. The seal consists of a spirally wound strip of metal and ceramic filler on a metallic mandrel. This type of seal is under development in another AiResearch program, Electric Power Research Institute (EPRI) Project 545-2, "High Tempera-ture Ceramic Heat Exchanger." The sealed ceramic and metallic shells form an assembly that acts as a pressure-containing vessel for the working fluid. The pressure loading acts in the direction to improve the seal. Note that the insu-lation is not pressure loaded and does not act as a structural member.

The working fluid flow path can be observed in Figure 5. Space left between the end of the fins and the ceramic flange serves as a flow distribution manifold. Fluid enters the manifold through a duct formed by the insulation, is distributed around the cylinder, and flows up through the fins. The fluid is collected at the top of the heat exchanger and exits through the outlet duct.

The distribution manifold must be sized large enough to ensure good flow distribution. Insufficient manifold flow area might cause flow starvation in the passages most distant from the inlet duct.
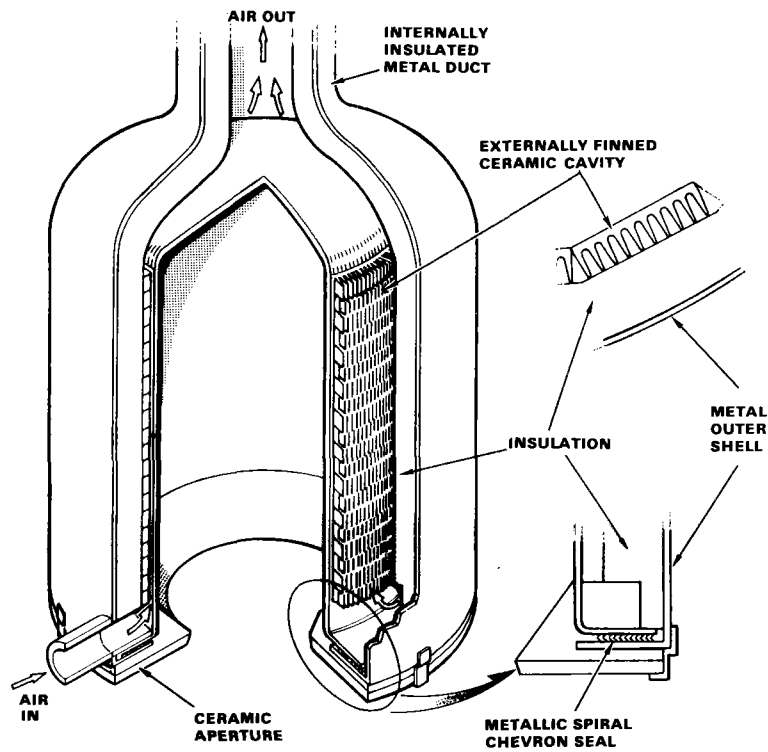
Figure 5. Ceramic Finned Shell Solar Receiver
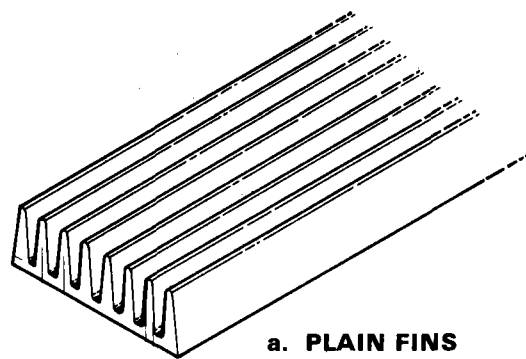
a. PLAIN FINS
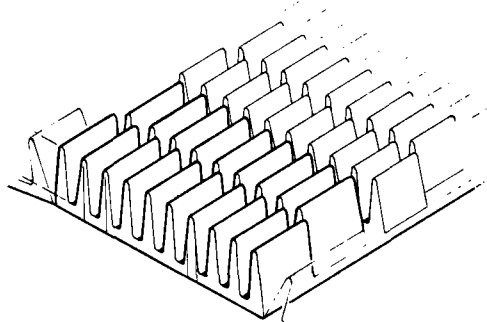
b. OFFSET FINS

Figure 6. Ceramic Finned Plates

239

Analysis and Sizing

The receiver thermal analysis was performed using the AiResearch receiver computer program, RECMDL. This program performs the required conduction, convection, radiation, and fluid stream calculations along with pressure drop calculations to predict the overall cavity efficiency and pressure losses. The program models the receiver as a finite element grid; the output includes a complete nodal temperature map of the receiver (solid and fluid). It should be mentioned that RECMDL models the receiver geometry in two dimensions--axial and radial. Hence, complete circumferential symmetry is assumed for both absorbed flux and surface temperature. This would appear to be a good assumption for an accurate mirror/collector system and uniform heat exchanger flow distribution. Although RECMDL can be used for either transient or steady-state analysis, only the steady-state mode was required for the present study, in accordance with the steady-state problem conditions of Table 1.

To meet the design point of Table 1 while maintaining all surface temperatures below 2400°F, the minimum receiver size listed in Table 2 was required. The receiver operating characteristics are also given in Table 2. The active length is the length of the fins, while the overall length includes the flange and convex top. The manifold flow area is sufficient to limit the flow maldistribution to less than 4 percent. The core pressure is well under the allowable, leaving pressure losses available for the ducts, manifold, and top region. The cavity efficiency is based on 6 in. of insulation around the entire receiver and includes all aperture and surface radiation and convection losses.

TABLE 2

RECEIVER CHARACTERISTICS

Ceramic shell ID	18 in.
Ceramic shell OD	19.3 in.
Active length	24 in.
Overall length	30.5 in.
Wall thickness	0.25 in.
Manifold flow area	9 sq in.
Fin count	5 per in.
Fin height	0.375 in.
Fin offset	0.6 in.
Fin thickness (average)	0.040 in.
Pressure drop (core only)	1.87 percent
Cavity efficiency	0.852
Maximum wall temperature	2388°F

The surface temperature map for the receiver is shown in Figure 7. The temperatures are for the inner receiver wall. The maximum temperature is at the top of the receiver, even though the maximum absorbed flux location is well down the receiver (see Figure 4) because of the absence of extended heat transfer surface (fins). In an effort to maximize the heat transfer, the velocities can be kept high by forming a narrow flow passage at the top with the insulation. The flow passage is shown schematically in Figure 8.

Based on the temperature map of Figure 7, a three-dimensional stress analysis was performed using the standard ANSYS computer code. The calculated maximum tensile stresses are presented in Table 3 for the top, cylinder, and flange sections of the receiver. The tensile stress is invariably the key stress for ceramic designs since the compression strength is much larger than the tensile strength. The stress directions are in reference to the receiver; i.e., circumferential is around the receiver, axial is along the receiver axis, and radial is outward through the receiver walls and fins. To limit the modeling effort and computer time usage, temperature gradients in the radial direction were not considered. These gradients are not expected to add significantly to the stress levels since the fins are unrestrained and free to grow in the radial direction.
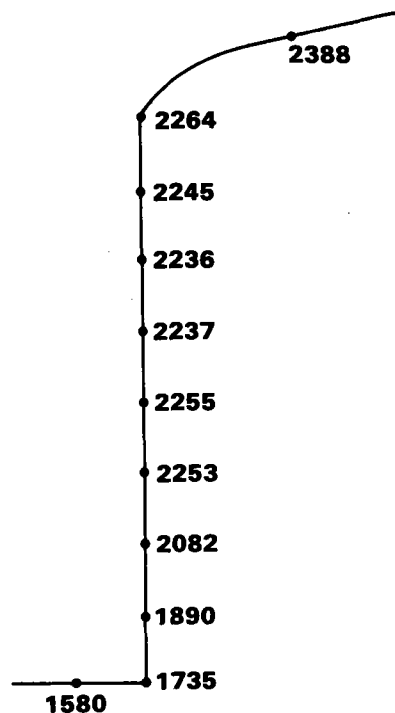
A-22353

Figure 7. Receiver Surface Temperature Map, °F
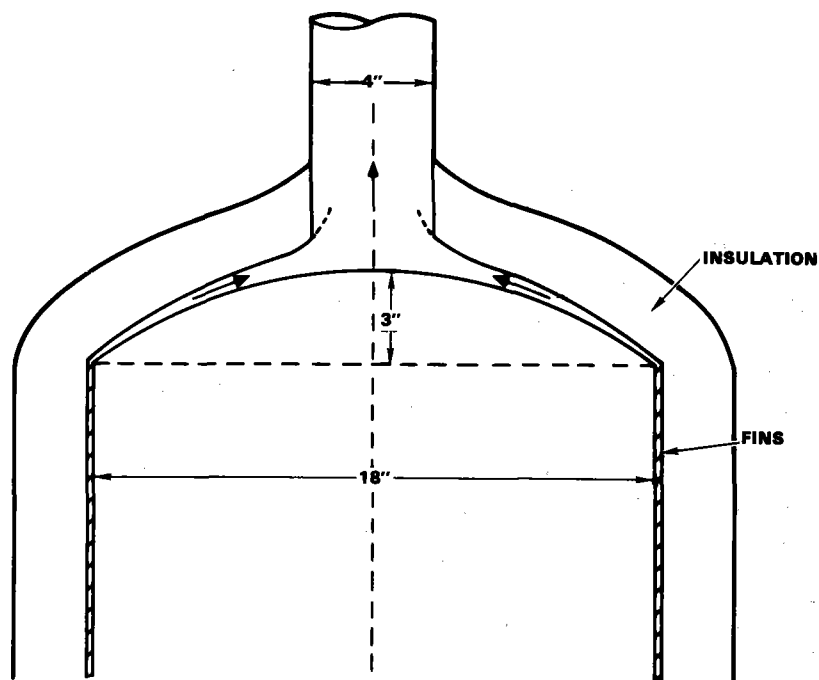
Figure 8. Receiver Top Details

TABLE 3

RECEIVER MAXIMUM TENSILE STRESSES, PSI

Section	Circumferential	Axial	Radial
Top	120	560	1800
Cylinder	5900[1]	2800[2]	1100[3]
Flange	7300	960	2700

(1) At top near dome
(2) Near center
(3) At bottom near flange

The maximum stress level is about 7300 psi in the flange region. Previous experience with the NC-430 material suggests that tensile stresses should not exceed about 8,000 to 10,000 psi for a highly reliable design. The maximum predicted stress is probably acceptable, although somewhat on the high side. As shown in Figure 7, the temperature gradient is large in the flange region. It should be possible to reduce this gradient, and the accompanying stresses, by selective insulation of the flange. Varying the flange thickness is another potential approach to reducing the stress level. Further details concerning the stress analysis, including the AiResearch probabilistic approach to ceramic design, can be found in Reference 1.

242

FABRICATION TECHNIQUE

Fabrication analysis conducted by AiResearch and the Norton Company indicated that the most desirable fabrication approach using state-of-the-art techniques was a combination of precision and slip casting. Slip casting can be explained with the aid of Figure 9. A plaster of Paris mold is constructed in the obverse shape of the desired part. A solution or slip of silicon carbide particles is poured into the mold. The ceramic part is formed by deposition of these particles as the solution is absorbed by the plaster mold. The excess slip is drained and the cast shape air dried. The resulting shrinking allows the cast to separate from the mold. Any mold curvature must be in a direction that allows for cast shrinkage and separation without any cracks forming in the casting.
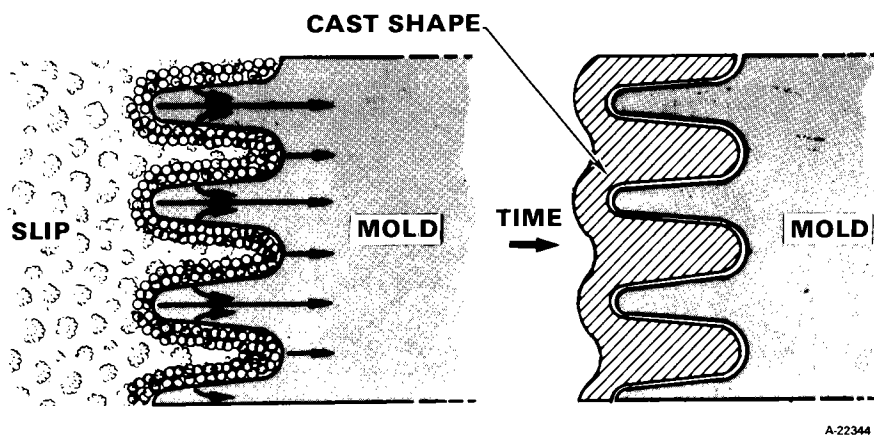
Figure 9. Slip Casting

Precision casting is recommended for highly detailed parts. As shown in Figure 10, a plastic mass of silicon carbide particles is formed into the desired shape by pressing into a mold. Air setting binders in the plastic mix rigidize the ceramic part. The mold can then be stripped away leaving the cast piece.

The proposed combination of techniques is explained with the aid of Figure 11. The ceramic shell is slip cast in two pieces, one piece for the cylinder and top sections and a separate piece for the flange. The cylindrical cross-section is not circular, however, but polygonal. This results in a series of flat facets along the cylinder outer walls. Twelve to sixteen facets are required. The facets will be slightly less defined on the inner receiver surface.

The finned plates are to be fabricated by precision casting, with the width of each plate equal to the facet width. For ease in stripping the casting from the mold (see Figure 10), the length of the plate is limited so that two or three pieces are required for each facet.
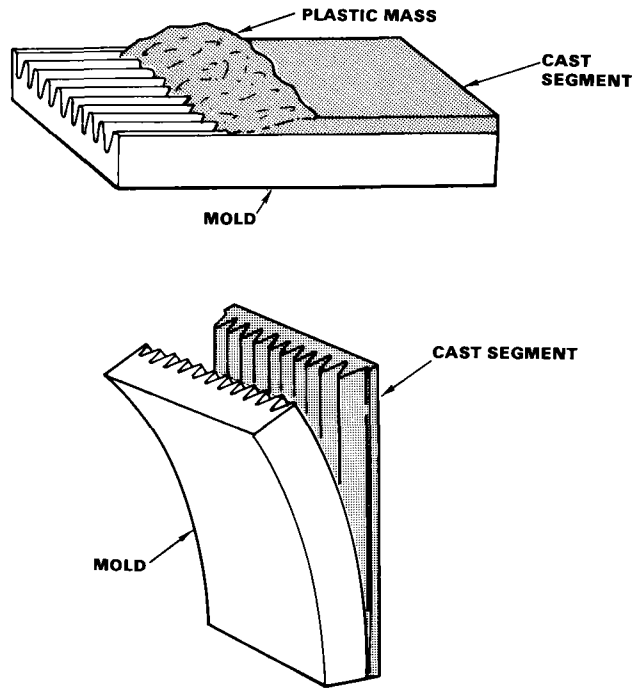
Figure 10. Precision Casting
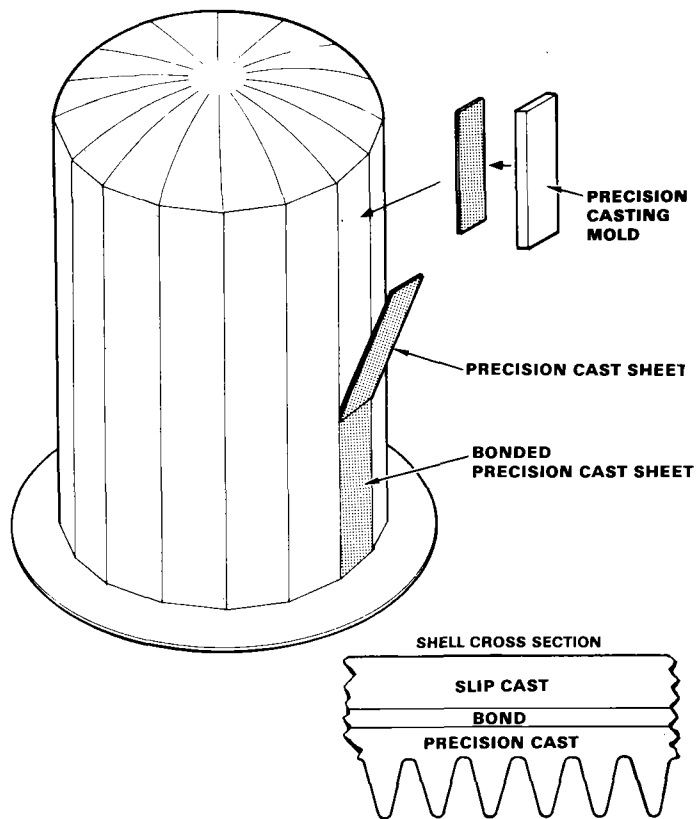
Figure 11. Fabrication Technique

244

The slip cast cylinder and flange and the precision cast finned plates are bonded together during firing in a silicon environment. The silicon is absorbed by the silicon carbide resulting in the formation of the siliconized-silicon carbide material (NC-430).

FABRICATION DEMONSTRATION

The Norton Company has fabricated a one-half scale ceramic receiver using the techniques described above. Full-size fins were used with the reduced size, sixteen-sided cylinder, as shown schematically in Figure 12. A photograph of the fabricated receiver is shown in Figure 13. The slip cast shell was fabricated in one piece, with the flange integral with the cylinder.
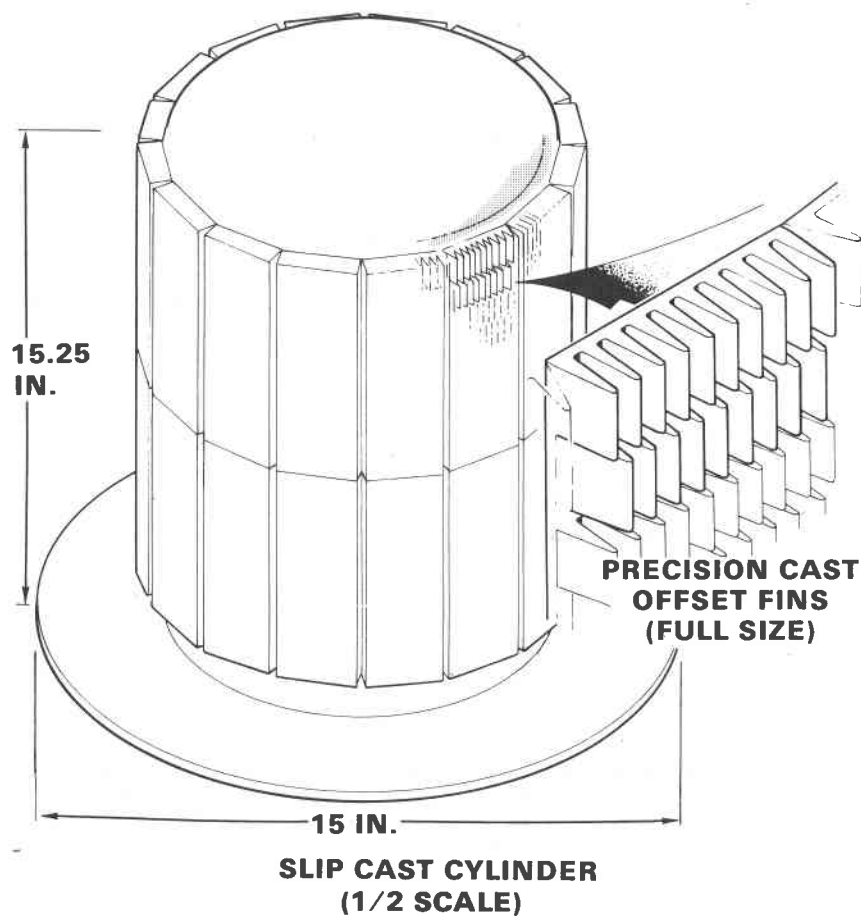
Figure 12. Fabrication Demonstration Model
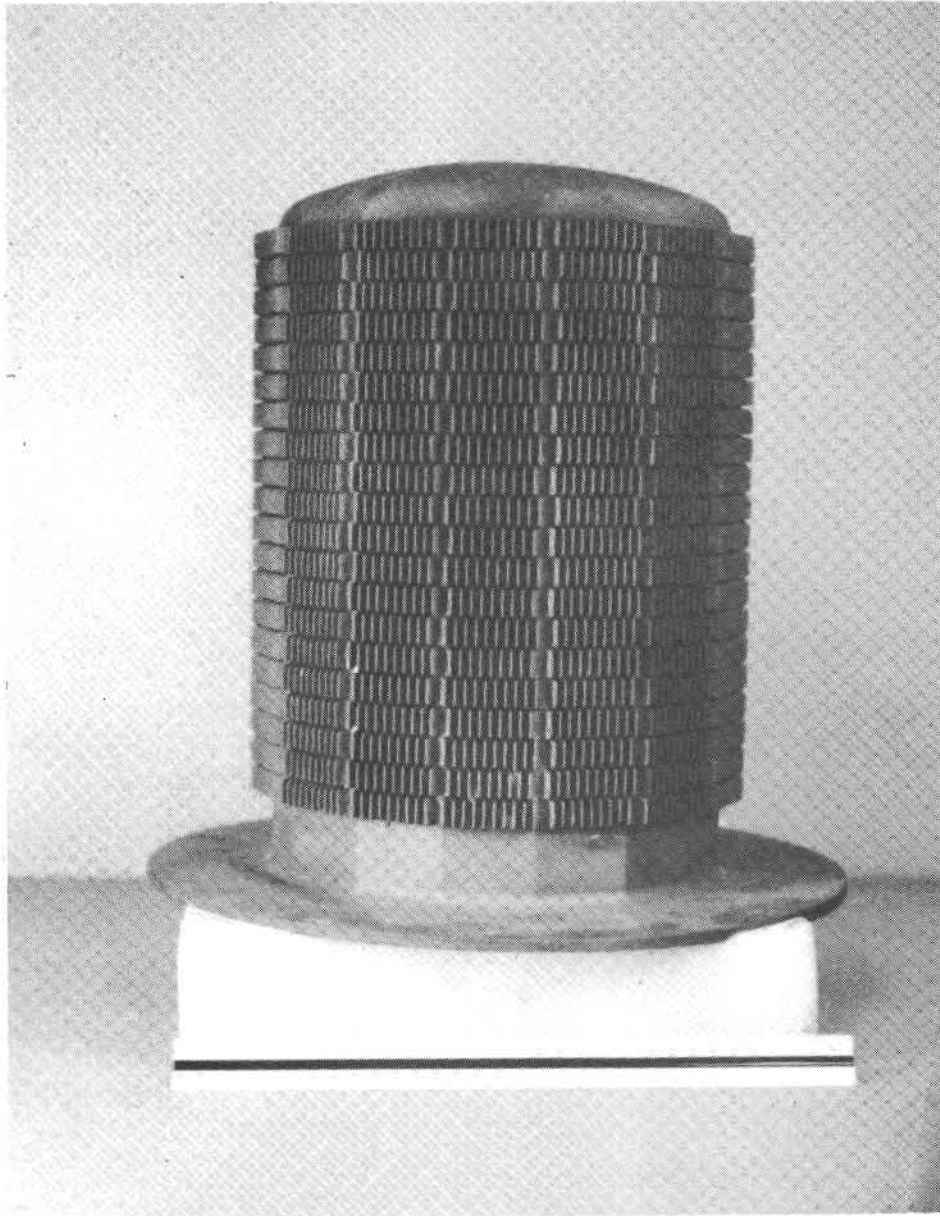
Figure 13. One-Half Scale Ceramic Receiver

CERAMIC HIGH TEMPERATURE RECEIVER

DESIGN AND TESTS

S. Bear Davis
Sanders Associates, Inc.
Nashua, NH 03061

Ceramic High Temperature Receiver
Design and Tests

During the fuel shortage of 1974, Sanders' management determined that the crisis was not simply an acute interruption of supplies, but was a significant indicator of an evolving chronic energy shortage of worldwide scope. A review of Sanders' technology showed two areas of potential applicability to energy concerns, software and high temperature ceramics. Software for energy management was already an evolving technology, but Sanders' experience with and knowledge of high temperature ceramic matrices provided a unique niche wherein we could transfer established technology to a new problem area and ultimately provide economically viable hardware to a worldwide market.

Sanders had been supplying infrared countermeasure (IRCM) systems to the military for the onboard self-defense of aircraft against heat seeking missiles. The systems use a combustion system to provide flue gas heating of a silicon carbide honeycomb matrix. The heated matrix then radiates IR energy to foil the heat seekers. Generally, the matrix operates in the IRCM systems above 1000° C, so the material, it was reasoned, could be used as a high temperature absorber of concentrated sunlight.

In the fall of 1974, Sanders built a "reduction to practice" model of the receiver and performed verification test at the .5 kW level. Since then, Sanders has been active in a number of contracts, funded by DOE, developing technology for its eventual application to commercial solar-thermal-electric conversion systems.

The High Temperature Solar Thermal Receiver, which was tested at Edwards AFB, CA during the winter of 1980-1981, evolved from technologies developed over a five year period of work. Subsequent to our "concept proof" work we were funded by NSF to build and test a 10 kW thermal receiver. This receiver was tested at the Army Solar Furnace at White Sands, NM in 1976. The receiver, shown in Figure 1, was tested successfully at 1768° F and showed thermal efficiencies of 85%. The results were sufficiently promising to lead ERDA to fund our development and test of a 250 kW receiver to measure the efficiency of an open cavity receiver atop a central tower of a heliostat field. This receiver was required to be design scalable to 10, 50, and 100MW-electric sizes to show applicability to central power tower receivers. That receiver employed rectangular silicon carbide panels and vertical stanchions to achieve scalability. The construction was shown to be fully scalable; and the receiver was operated at temperatures up to 2000° F to achieve the performance goals of the experiment during tests at the GIT advanced components test facility during the fall of 1978.
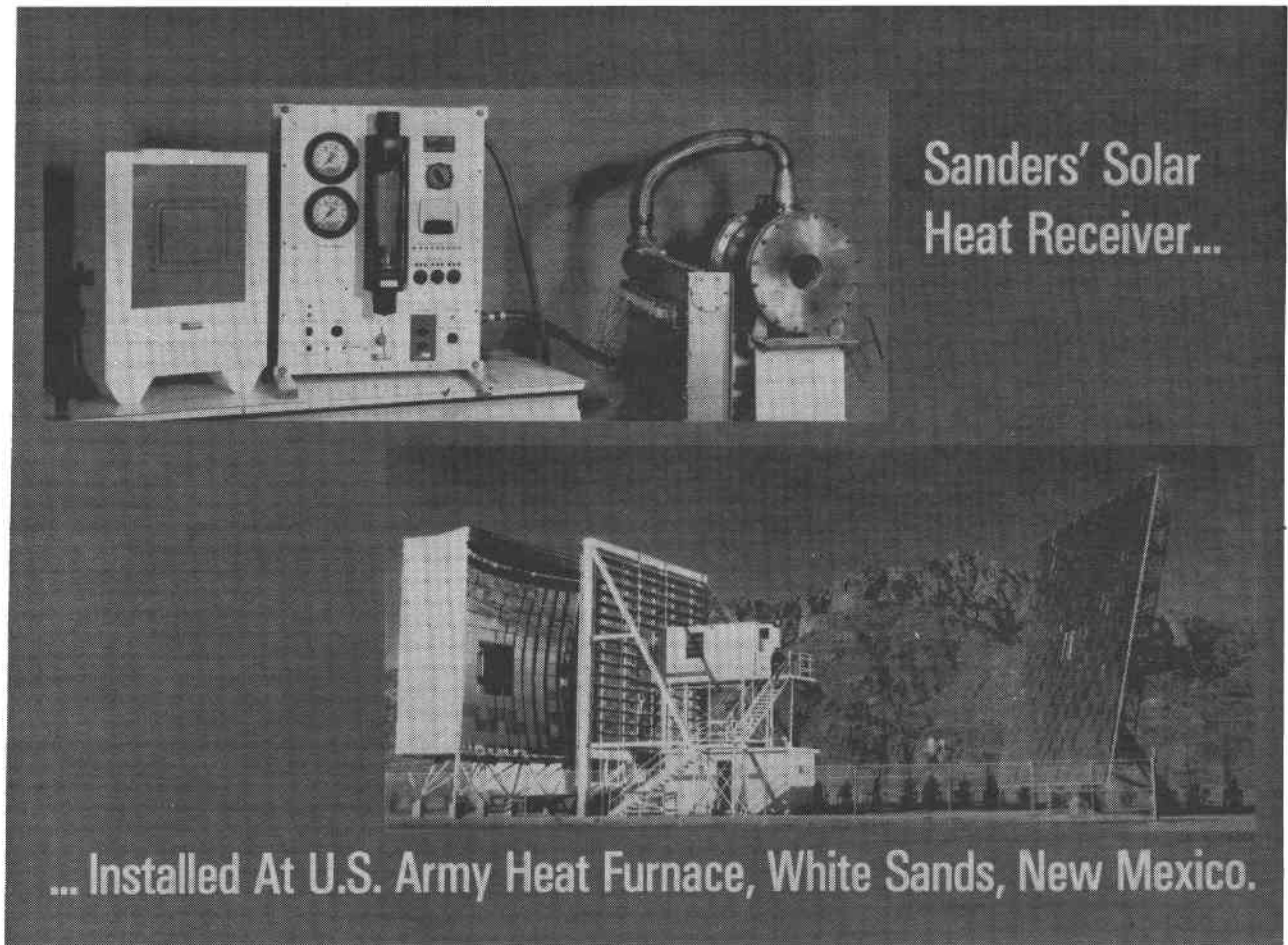
Figure 1. Installed at US Army Heat Furnace White Sands, NM

During 1979, Sanders participated in a system tradeoff study of 80 kW air brayton receivers for use on a parabolic dish concentrator. Brayton systems were shown to operate in the solar application most economically with low pressure ratios, with 80-90% recuperation of waste heat, and with turbine inlet temperatures of 1600° F and above (to approximately 2600° F). In light of these findings, Sanders was contracted by JPL to develop a design concept for a High Temperature Solar Thermal Receiver and to assess its producibility. The design was to be compatible with operation in the 2000-3000° F temperature range at pressures from 1.0 to 3.0 atm abs. That study concluded that a cost effective receiver could be built to operate at temperatures to 2600° F in the desired pressure range. The conceptual design that was developed used advanced ceramic materials as a means of achieving long life at cost effective prices.

The study contract was subsequently modified to provide for the design, fabrication, and test of a receiver during 1980. The artist's depiction of the receiver, Figure 2, shows the salient features of the Cermaic High Temperature Receiver.

The specified high operating temperatures essentially eliminated all metals from consideration for use within the receiver. Metals could have been used, but would have required active cooling and would have then represented a significant efficiency loss. Ceramics are typically considered too sensitive to thermal and mechanical shock to
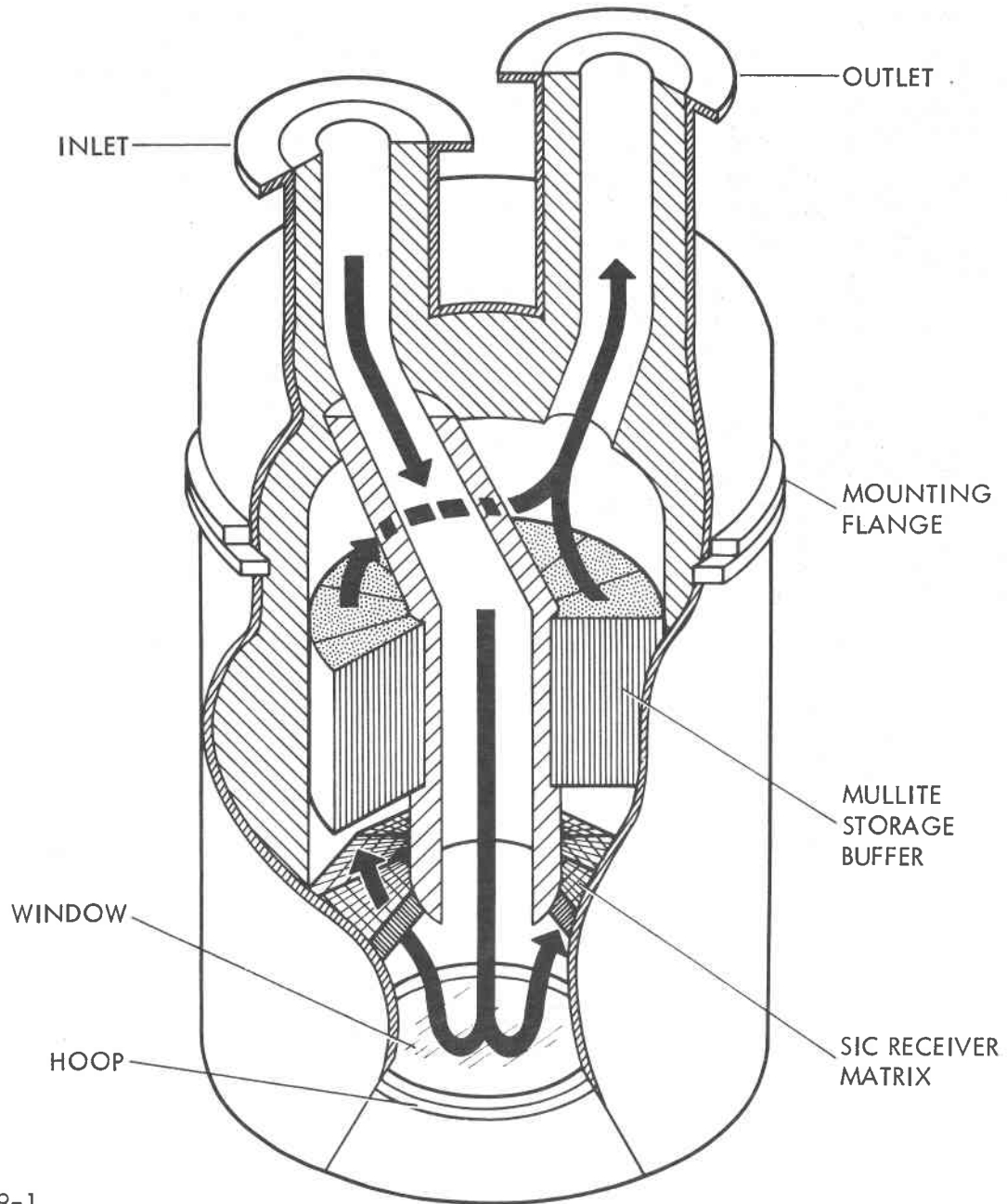
Figure 2. The High Temperature Solar Receiver Design Concept was Developed in 1970

survive the transient conditions anticipated in the solar parabolic dish environment, but can be used if carefully selected and configured. Internal structure and the thermal impedance is provided by use of a semi-rigid fibrous ceramic insulation designed for kilns. The particular material, shown in cross hatch, is a Johns-Manville product suitable for use at temperatures to 2700° F. The SiC receiver matrix is an extrusion, beveled and mitered to form a twelve sided pyramid. Orientation and sizing of the flow channels in the matrix provides for efficient, yet distributed, absorption of the solar energy necessary to achieve panel longevity. The mullite storage media provides thermal buffering to the output air. Sudden loss of solar input due to passing clouds are termination of tracking

250

results in a gradual change of receiver output temperature; the buffer limits output temperature changes to about 70° F per minute. The window is made of fused quartz and absorbs only 1% of the passing solar. IR reradiation is reduced by 30% at high operating temperatures. At lower temperatures, the IR reradiation is almost completely blocked by the window. Convective air transfer through the aperture is eliminated by the window. Finally, the window seals against the pressure load and permits use of the receiver directly in the (pressurized) brayton cycle without need for an intervening heat exchanger. When coupled with Stirling or Rankine engines, the ceramic receiver can supply power without severe transients and localized high heat fluxes which have plagued solar application of these engines.

The high temperature receiver, shown in Figure 3 during fabrication, shows the quartz aperture window and air cooled flange on the left. The preheater assembly, at the right, provided inlet air to the receiver at temperatures simulating engine regenerator exhaust temperatures. The control system developed for use in last year's test provided valuable experience in the control of a receiver operating in the hybrid mode.
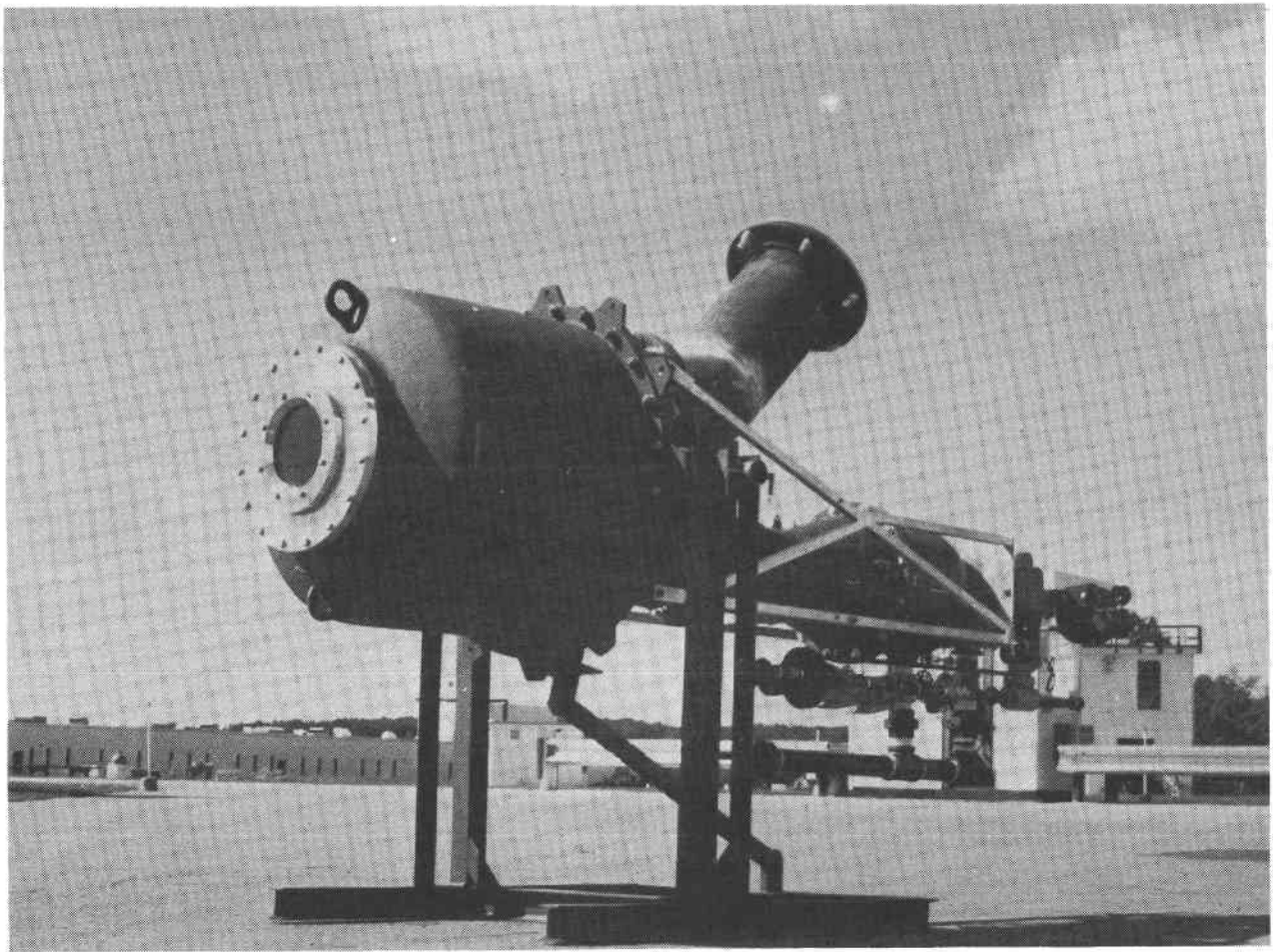

Figure 3. The HTSR and Preheater Assembly are Capable of Hybrid Operation

The High Temperature Receiver Program culminated in January 1981 with the successful test of the receiver at maximum output temperatures of 2600+° F.

Typical of the kinds of technology development engendered by DOE/JPL funding of component programs is the research and development in Silicon Carbide applications and processes. In the United States, Carborundum and Norton have research labs working on the fabrication of SiC components for chemical processes, engines, and solar receiver components. In Japan, NGK is aggressively pursuing sintered silicon carbide technology. In Germany, Anawerke is developing methods for partnership with US firms. The Sanders receivers have tracked the state of the art; our receivers have used the latest available SiC materials throughout the evolution of receiver technology. Our early receivers--.5 kW and 10 kW-- used materials based on a rolled corrugate. Those SiC matrices used in the experimental receivers were developed specifically for use in our IRCM systems and were fitted to the receiver with essentially no modification.

While this material was subject to delamination and demonstrated marginal structural integrity, it performed satisfactorily in the very harsh airborne environment with the help of a compressive clamp. The need for a compressive clamp limits use of the SiC panel to temperatures that will not destroy the clamp--about 2000° F. Potential for mass production processes to reduce panel cost is limited because significant amounts of hand labor are required to build the panels. Expected cost in production quantities is equivalent to $90./kW.

The panels used in the next generation--the 250 kW receiver--were rectangular to provide receiver scalability. Large receivers would use larger rectangular panels, more rectangular panels, or a combination of more and larger panels. Retention techniques used to hold the panels in the 240 kW receiver were completely transferable to larger receivers. The particular panels used in the 250 kW receiver werre residuals from were avoided. The scalability and manufacturing improvements of the rectangular panels offered improved cost effectiveness, but costs were projected at $60./kW in production. Marginal structural integrity of the panels again required compressive clamping with its attendant temperature limitations.

Quality assurance of the finished panels in both the 10 kW and 250 kW receivers was a potential problem area because the vendor had to rely on a subcontractor for the graphite corrugate. The results of the siliconizing process were significantly impacted by the quality of the graphite starter material.

The advanced panels used in the high temperature receiver meet commercialization requirements. These panels are manufactured by extrusion of a plasticized SiC powder. The unfired (green) panels are first beveled and mitered and then hot fired. These panels have demonstrated superior structural integrity and do not require compressive clamping. They have operated at cavity temperatures in excess of 2800° F without degradation. Design flexibility and wall uniformity permit the specification of a panel which will efficiently capture the solar flux without thermal transient problems. Finally, quality assurance is more easily achieved since the vendor produces the bulk SiC and performs all the extruding processes in-house. Production costs project at $20/kW. These panels are shown in Figure 4.

EARLY PANELS MET EXPERIMENTAL REQUIREMENTS
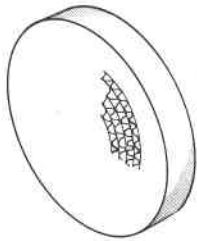
ROLLED CORRUGATE

LABOR INTENSIVE - HAND ROLL & CUT

MARGINAL INTEGRITY - DELAMINATION

TEMPERATURE LIMIT - 2000°F

SIZE LIMITED

QUALITY ASSURANCE NEEDED

PRODUCTION COST - $1K PER FT^2

IRCM HERITAGE

$90/KW

12041-2

RECTANGULAR PANELS MET SCALABILITY REQUIREMENTS
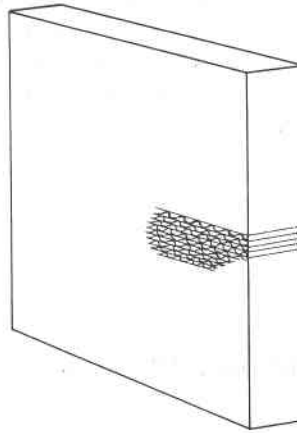
LAMINATED CORRUGATE

MARGINAL INTEGRITY

TEMPERATURE LIMIT - 2000°F

QUALITY ASSURANCE NEEDED

PRODUCTION COST - $600 PER FT^2

SALVAGE HERITAGE

$60/KW

12041-4

ADVANCED PANELS MEET COMMERCIALIZATION REQUIREMENTS
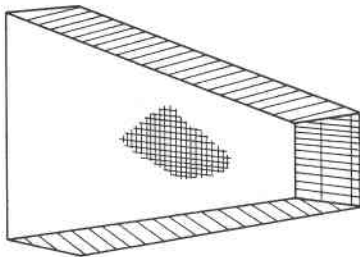
EXTRUDED SIC

DEMONSTRATED INTEGRITY

2800°F TESTED

CONSISTENT QUALITY

PRODUCTION COST $350 PER FT^2

SOLAR DESIGN

$20/KW

12041-3

ADVANCED PANELS ARE EXTRUDED FOR LOWER COST
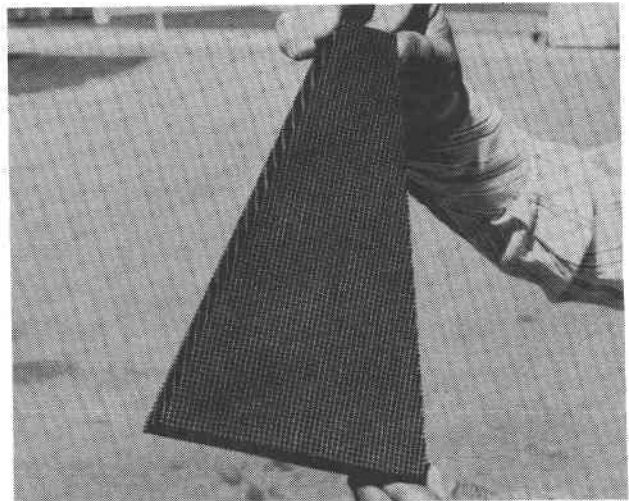
Figure 4. Solar Panels Evolve with Technology Development

Sanders Associates is now under contract with JPL to conduct a parabolic dish module engineering experiment, wherein components developed under DOE auspices will be integrated into a 20 kW electric generating system mounted on a 12-meter parabolic dish reflector.

As an adjunct to this experiment, Sanders has recently been tasked to integrate and test a power conversion assembly consisting of a Sanders receiver, a Garrett Solarized Advanced Gas Turbine (SAGT 1-A) Engine, and an induction generator aboard the Test Bed Concentrator (TBC) during July 1982. This experiment will test the receiver and development engine at output powers approaching 20 kW electric.

Valuable experience will be gained during this experiment to assess system viability and efficiency and to measure system component reliabilities. Control response and components and materials performance in the transient and steady state solar environments will provide valuable data to identify the necessary technology developments needed to develop the system technology to a point wehre commercialization is feasible. Definition of the s stem operating logic necessary to allow unattended operation is an important goal of this experiment. Manual input of system control commands, based on predetermined environmental (insolation and meteorological) conditions, will be attempted to simulated unattended operation if preliminary tests progress satisfactorily.

HTSR MODIFICATIONS ENHANCE SYSTEM CONFIGURATION

APERTURE	8" ADAPTABLE TO 14"
STORAGE	NOT REQUIRED
FLOW GALLERIES	INCREASED FLOW AREA
FACIA SHIELDING	PASSIVE
INSULATION	MOLDED & STABILIZED
VESSEL	REDUCED WEIGHT COMPROMISE
INTERFACING	2 COLLECTORS, 2 ENGINES

Figure 5. HTSR Modifications Enhance System Configuration

The Solar receiver design tested at PDTS last winter will be modified for this test to enhance the system configuration, as shown in figure 5. The aperture will be adaptable for 8" to 14" diameter to allow use with the TBC concentrator at high efficiency or with the Parabolic Dish Concentrators (PDC-1 or PDC-2) with their characteristically lower concentration ratios. The (mullite) thermal storage media will be removed--experience has shown it is not needed in this application--to lighten the reciever.

The receiver (pressure) vessel will be redesigned wehre possible to reduce its weight where possible. Flow gallery cross sections will be enlarged to accommodate the SAGT 1-A mass flow requirements. Passive shielding for the receiver will be pursued to increase overall system reliability. Advanced insulation fabrication methods will be used to reduce labor costs and to improve insulation resistance to erosion. Finally, provisions will be made to interface the receiver with other engines by designing interchangeable inlet and outlet duct flanges.
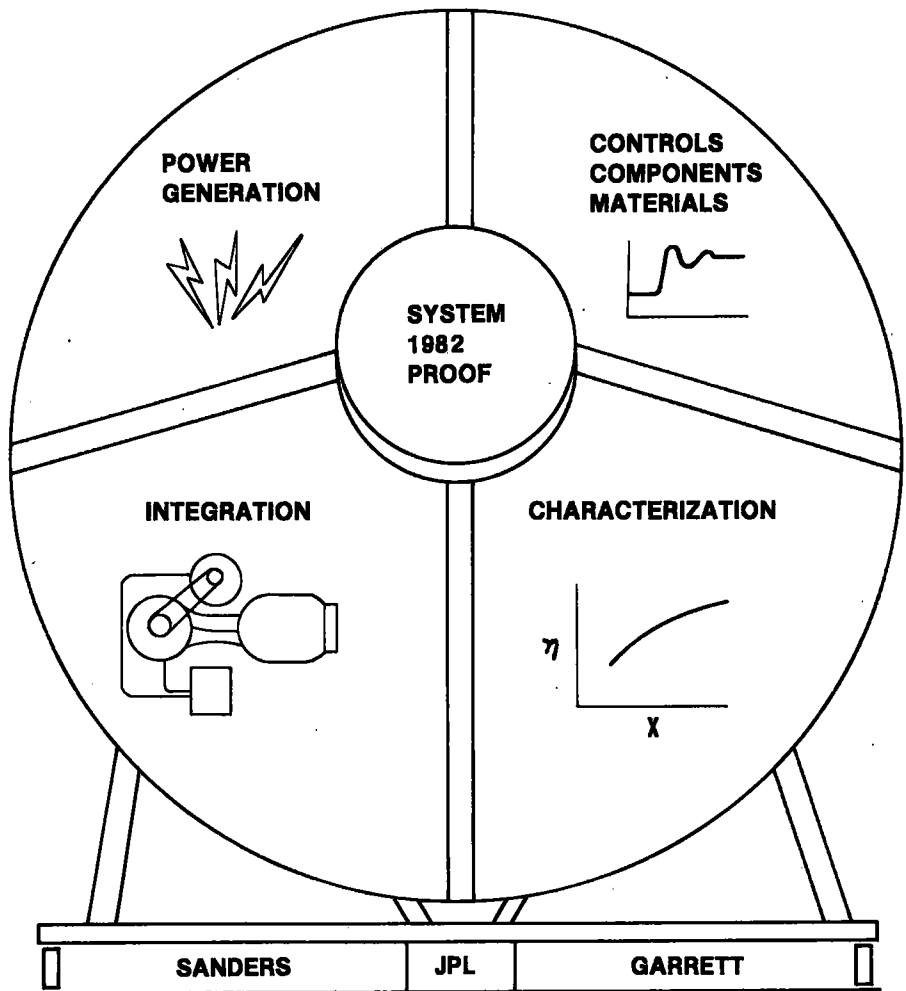
Figure 6. Test is Vital Milestone on Path to Commercialization

The SAGT 1-A power conversion assembly (PCA) test is a vital task, important to the overall solar program. The key to success is minimum (amortized) cost per kilowatt-hour of power generated. Brayton engines possess characteristics that provide significant system cost advantages over other types of engines. They have few moving parts and often exhibit operating lives over 50,000 hours (versus fewer than 3,000 hour for most other engines); they operate with high thermodynamic efficiency thereby reducing required collector areas; they are mass produced thereby reducing price; and they are light thereby reducing required support structures.

The test is important, then, because it will put one such system on line in a measurable display of progress, will demonstrate the rapidly approaching availability of solar electric power, and will encourage continuing support for the final technological advances needed to make these systems generally available to an energy dependent world.

255

GARRETT SOLAR BRAYTON
ENGINE/GENERATOR STATUS

31-4372   December 8, 1981

Prepared by: B. Anson/RJH

Approved by: _C. J. Bishop_

C. J. Bishop, Supervisor,
Documentation & Data Management

Bruce Anson for

R. A. Rackley, SAGT Project
Manager

GARRETT TURBINE ENGINE COMPANY
A DIVISION OF THE GARRETT CORPORATION
PHOENIX, ARIZONA

257

GARRETT SOLAR BRAYTON ENGINE/GENERATOR STATUS

ABSTRACT

The solar advanced gas turbine (SAGT-1) is being developed by the Garrett Turbine Engine Company, (hereinafter referred to as Garrett) under DOE/JPL/NASA Contract DEN3-181 for use in a Brayton cycle power conversion module. The engine is derived from the advanced gas turbine (AGT101) now being developed by Garrett and Ford Motor Company for automotive use under DOE/NASA Contract DEN3-167. The SAGT Program is presently funded for the design, fabrication and test of one engine at Garrett's Phoenix facility. The engine when mated with a solar receiver is called a power conversion module (PCU). The PCU is scheduled to be tested on JPL's test bed concentrator under a follow-on phase of the program. Approximately 20 kw of electrical power will be generated.

GARRETT SOLAR BRAYTON
ENGINE/GENERATOR STATUS

1.0 INTRODUCTION

A solar powered version of an advanced gas turbine is being developed by Garrett under DOE/JPL/NASA sponsorship and direction. This involves the design fabrication and test of a small regenerated Brayton cycle engine designated SAGT-1. Another effort currently under consideration involves mating the SAGT-1 engine with a solar receiver for tests on the JPL Test Bed Concentrator. This configuration would include an electrical generator on the output power shaft and is designated the SAGT-1A (Figure 1). The intended purpose of the SAGT-1A is to provide an early field demonstration of the capability of solar power to provide electric power output from a Brayton cycle engine.

This paper provides a report on the SAGT-1 phase of the program. Items addressed are the SAGT-1 design, progress of the AGT101 advanced gas turbine (DOE/NASA Contract DEN3-167) from which the SAGT-1 is derived, and predicted SAGT-1 performance. The potential SAGT-1A program also is described.

Figure 1.   SAGT-1A.

260
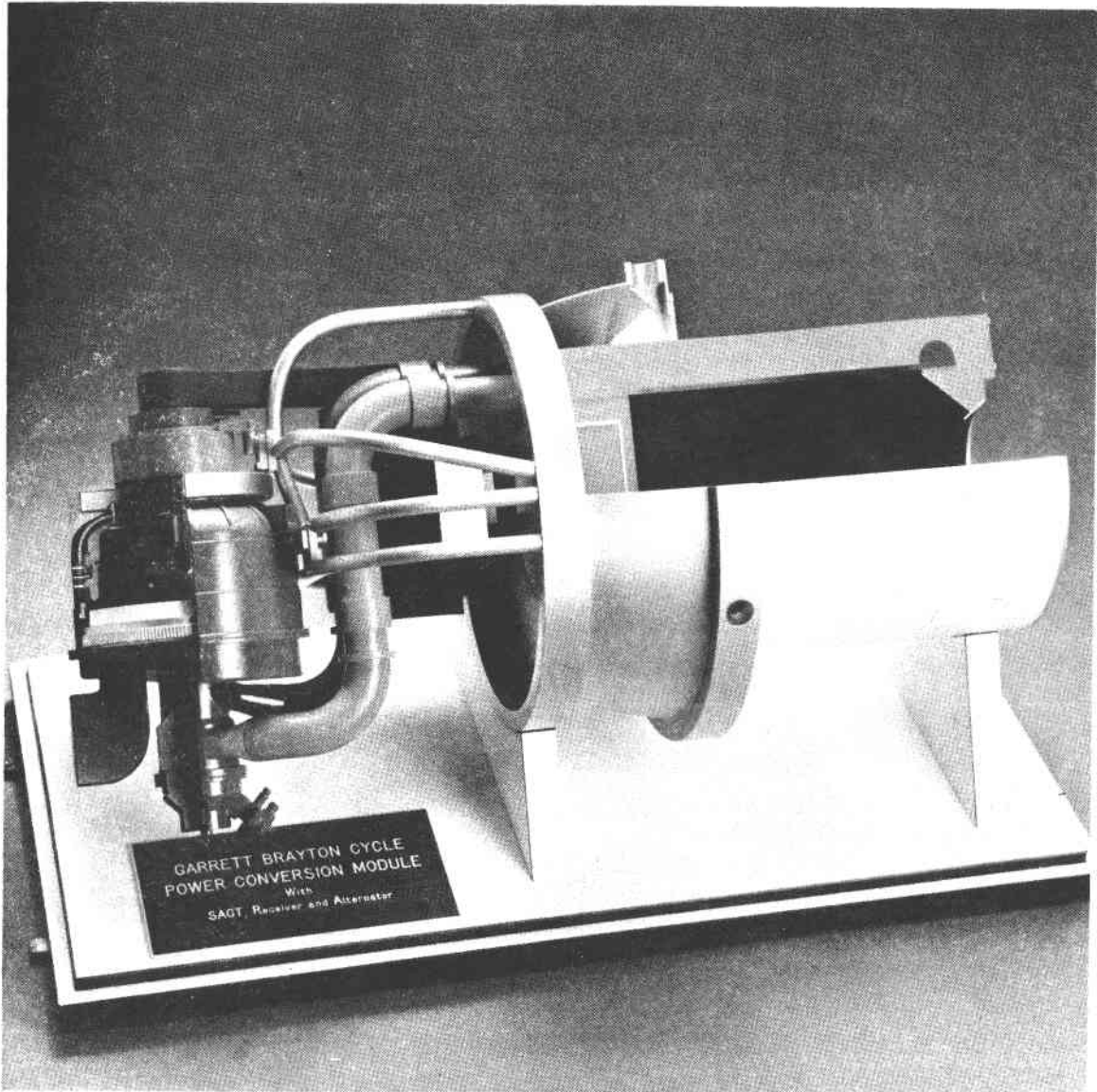
2.0 SAGT-1 DESIGN

The SAGT Engine (Figure 2) utilizes the automotive AGT101 power section with only minor modifications to allow for operation with the external solar heat source. The SAGT also is capable of operation on fossil fuel with the existing combustor.

As is evident, the AGT101 is used nearly in entirety. This is of prime importance because it allows the SAGT program to take full advantage of the extensive AGT101 development effort. The AGT101 is planned for automotive usage; this offers a mass production cost potential that will enhance SAGT applications to the solar market. Since the SAGT program is so closely attuned to the AGT101 program, a brief description and status of the AGT program is presented in Section 3.0.
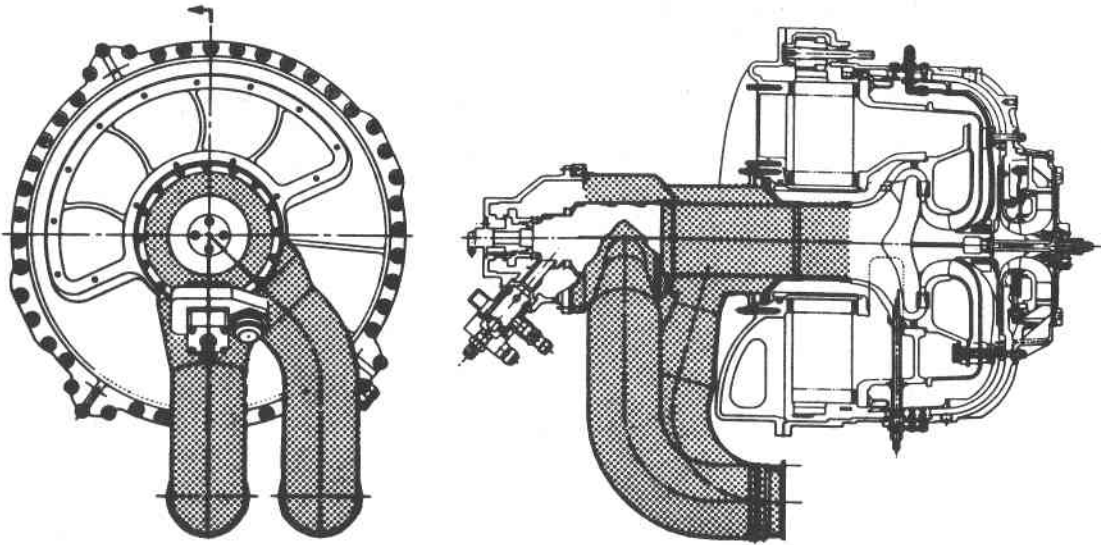
HARDWARE PECULIAR TO SAGT

HARDWARE COMMON TO AGT101 MOD 1

Figure 2.   SAGT Power Section.

3.0 AGT101 STATUS

The AGT101 is being developed by Garrett and Ford and leading ceramic contractors under DOE/NASA sponsorship. The program was initiated October 1, 1979 as a powertrain development program for automotive usage. However, the program has been retargeted toward an engine development program as a result of budget constraints. It is anticipated that the engine development will be competed at the end of FY85.

The AGT101 is a regenerated single-shaft engine. Ceramics are extensively used in the engine hot-flow-path section. The engine, as shown in Figure 3, is flat rated at 100 horsepower, with a maximum operating speed of 100,000 rpm, a turbine inlet temperature of 2500°F, and a minimum specific fuel consumption (SFC) of less than 0.3. The single-shaft rotating group is composed of a turbine, compressor, and output gear supported by an air-lubricated, foil-journal bearing and an oil-lubricated ball bearing.

Ambient air enters the engine through variable inlet guide vanes and passes through a single-stage compressor. The compressed air is routed around the full engine perimeter to the high pressure side of the ceramic rotary regenerator. This feature provides increased thermal efficiency by minimizing heat loss from hotter interior components. The partially heated air passes through the regenerator core, where it is further heated prior to entering the combustor. Fuel is added and combustion takes place. Hot gas exits the combustor at a maximum temperature of 2500°F (full power) and then expands through the turbine. The hot turbine exhaust gases heat the regenerator core and then are exhausted from the engine at a temperature of 520°F.

Ceramics (Figure 4) are used extensively in the engine to allow high turbine inlet temperature (without cooling) which provides the

Figure 3. AGT101 Engine.

REGENERATOR SHIELD

FLOW SEPARATOR HOUSING

TURBINE SHROUD

INNER DIFFUSER

TRANSITION DUCT

COMBUSTOR BAFFLE

OUTER DIFFUSER

TURBINE BACKSHROUD

TURBINE ROTOR

TURBINE STATOR

DUCT SPACERS
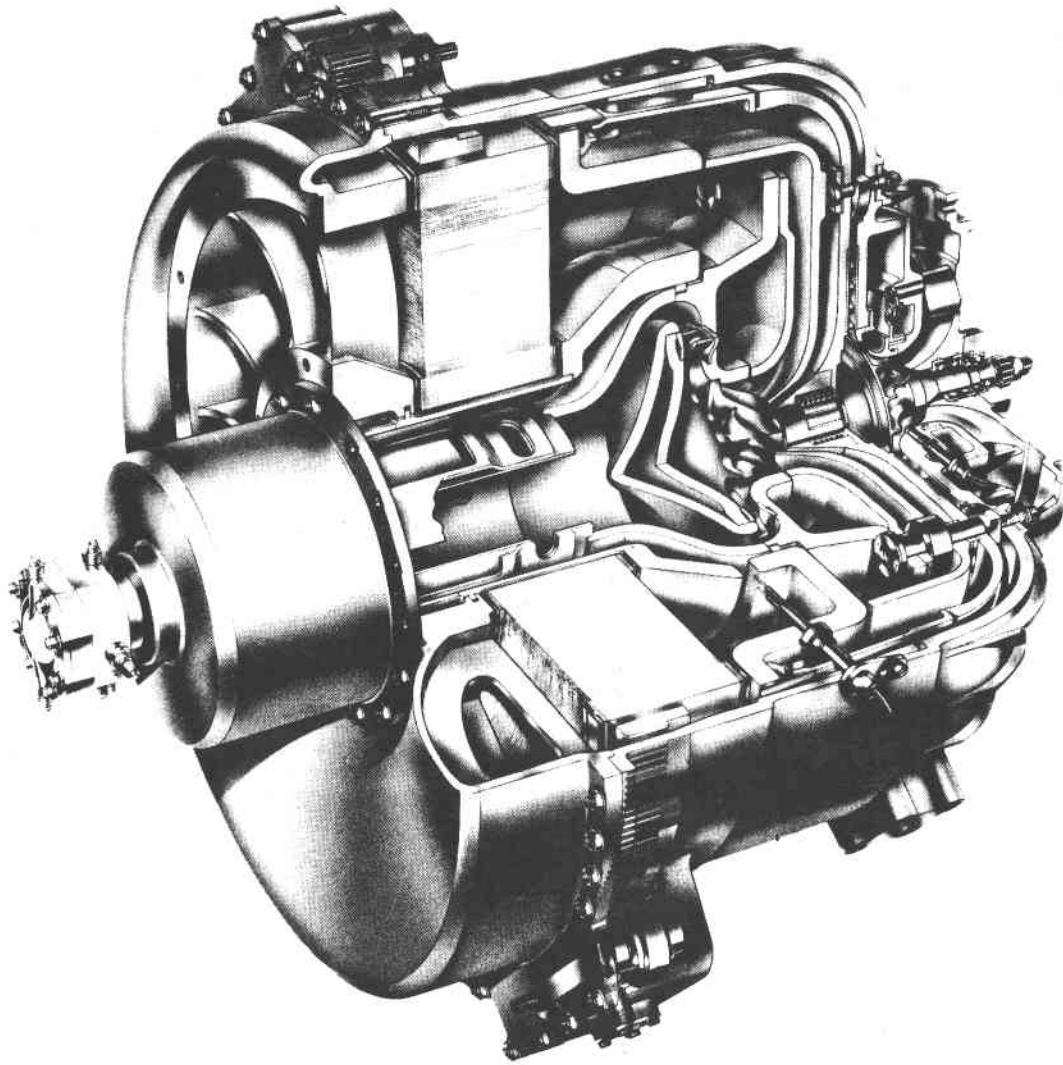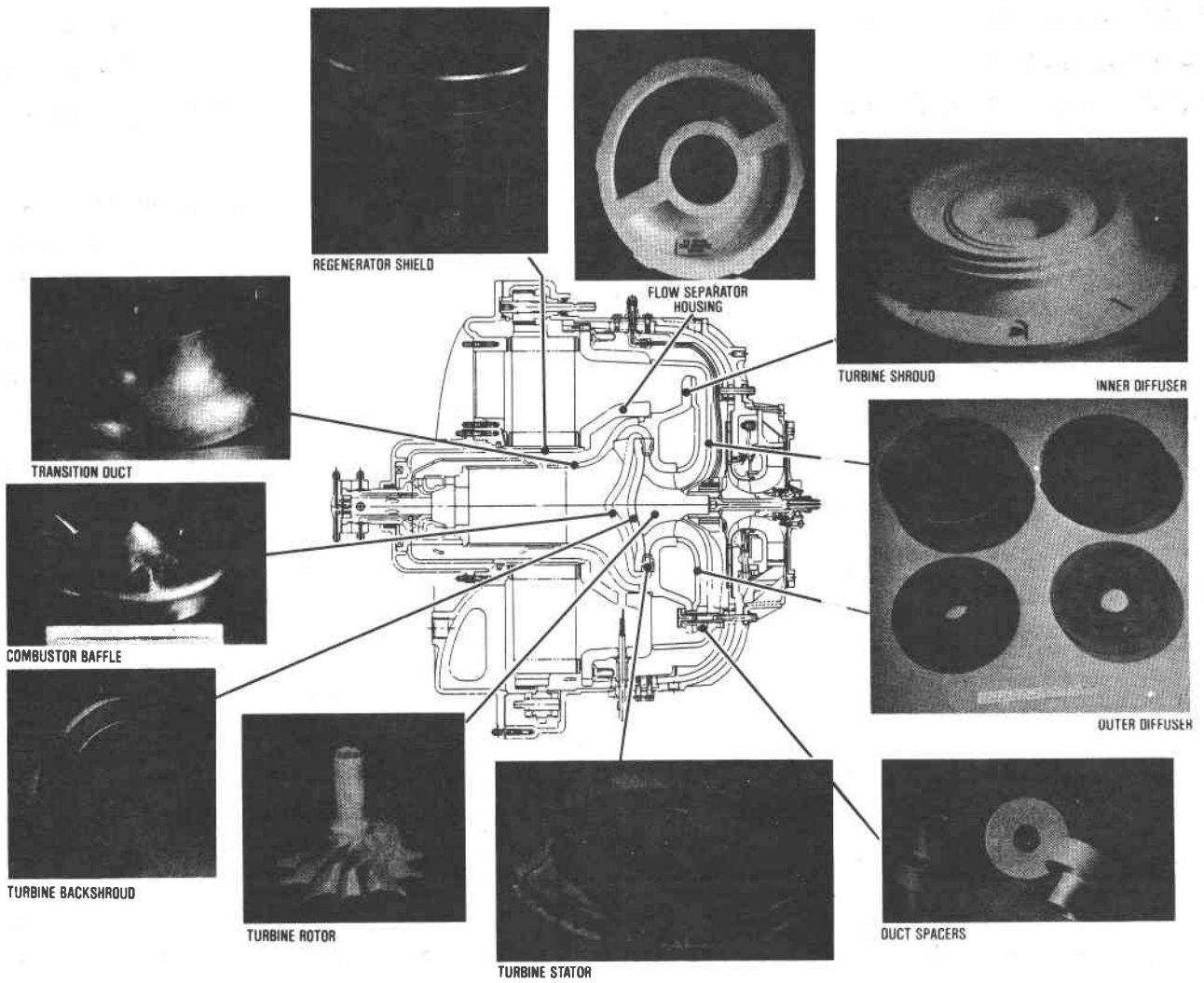
Figure 4.   AGT101 Ceramic Parts.

attendant high efficiency. In addition, ceramics offer the potential for low cost in production when net shape techniques and tooling evolve. The ingredients for ceramics are abundantly available in the United States at low cost. Thus, many of the materials used in today's gas turbines, which are expensive, come from foreign countries, and are considered strategic materials by our Government, can be replaced with ceramics. Another advantage of ceramics is light weight. Rotating parts exhibit lower inertia which enhances acceleration. A lighter engine also aids the associated vehicular fuel economy gain.

All ceramic hot section structural components are symmetrical except for one housing that separates high and low pressure regenerator flow. The symmetrical design provides a more uniform stress distribution and eases manufacturing. Individual ceramic components, shown in Figure 4, have been received from four leading United States ceramic centers [Ford, AiResearch Casting Company (ACC), Carborundum, and Corning Glass Works] and NGK in Japan. Material compositions include silicon nitride, silicon carbide and lithium aluminum silicate. Pressure screening tests have been satisfactorily completed on several parts and are in process on others.

Ceramic turbine rotor development has progressed with Ford and ACC simulated rotors successfully passing cold spin pit screening tests at speeds greater than 115,000 rpm. Both suppliers are currently developing bladed rotors. Ford recently cold-spin tested a ceramic bladed turbine rotor to 115,000 rpm.

These demonstrations constitute a significant breakthrough in ceramic development and, moreover, demonstrate the feasibility of the single-shaft gas turbine engine for automotive application. The simulated and bladed turbine rotor are shown in Figure 5.
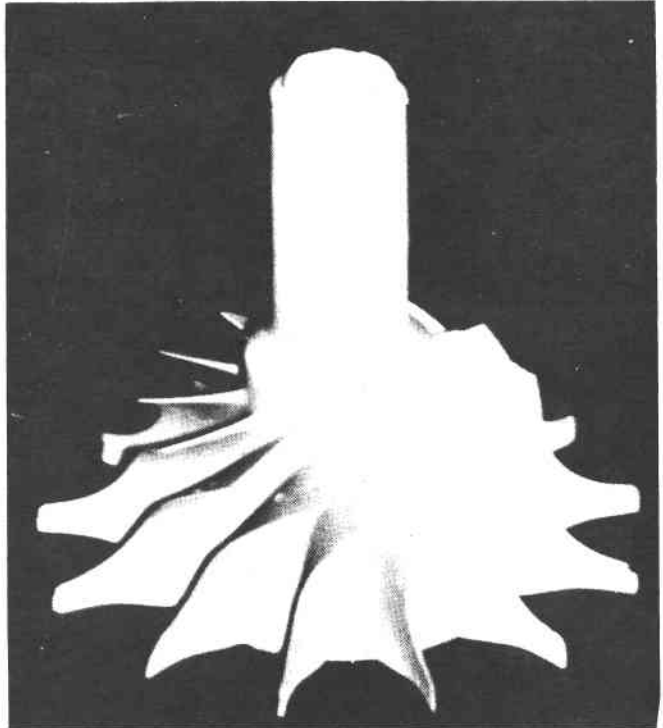
SIMULATED ROTOR   **BLADED ROTOR**

Figure 5. AGT101 Turbine Rotor Approach.

AGT101 engine development begins with an all metallic (except regenerator) 1600°F turbine inlet temperature (TIT) engine designated Mod I, Build 1. For the Mod I, Build 1 engine, which has already begun checkout tests, the aerodynamic flowpath has been fully replicated using uncooled metal castings, as shown in Figure 6. This Mod I, Build 1 engine is the basis for the SAGT-1 engine.

AGT engine development for automotive applications progresses by using ceramic hot section parts (except turbine rotor), as depicted in Figure 7, to the Mod I AGT101 (2100°F TIT) version, and finally to the Mod II engine (2500°F TIT) with ceramic turbine rotor.

AGT101 performance follows engine evolution as shown in Figure 8. As turbine inlet temperature is increased from 1600°F (Mod I, Build 1) to 2500°F (Mod II) an improved SFC is realized. In particular, the improved SFC for the Mod II is significantly better in the 10 to 30 hp range where much of the Combined Federal Driving Cycle (CFDC) simulation occurs. This results in a CFDC fuel economy of 42.8 mpg using diesel fuel in a 3000-pound vehicle.

Component development activities parallel the engine development to characterize and "quality" the components prior to engine testing. Dedicated test rigs are utilized to establish and evaluate aerothermodynamics, mechanical integrity, stress distributions due to pressure and thermal loadings. Qualified components that evolve from the component development programs, are selectively introduced into the engine development test program. Throughout the engine development an interactive component/engine feedback loop is established and maintained through planned design iterations to aid in achieving projected 1985 component/engine technology levels and overall program goals (i.e., fuel economy, acceleration, emissions, etc).
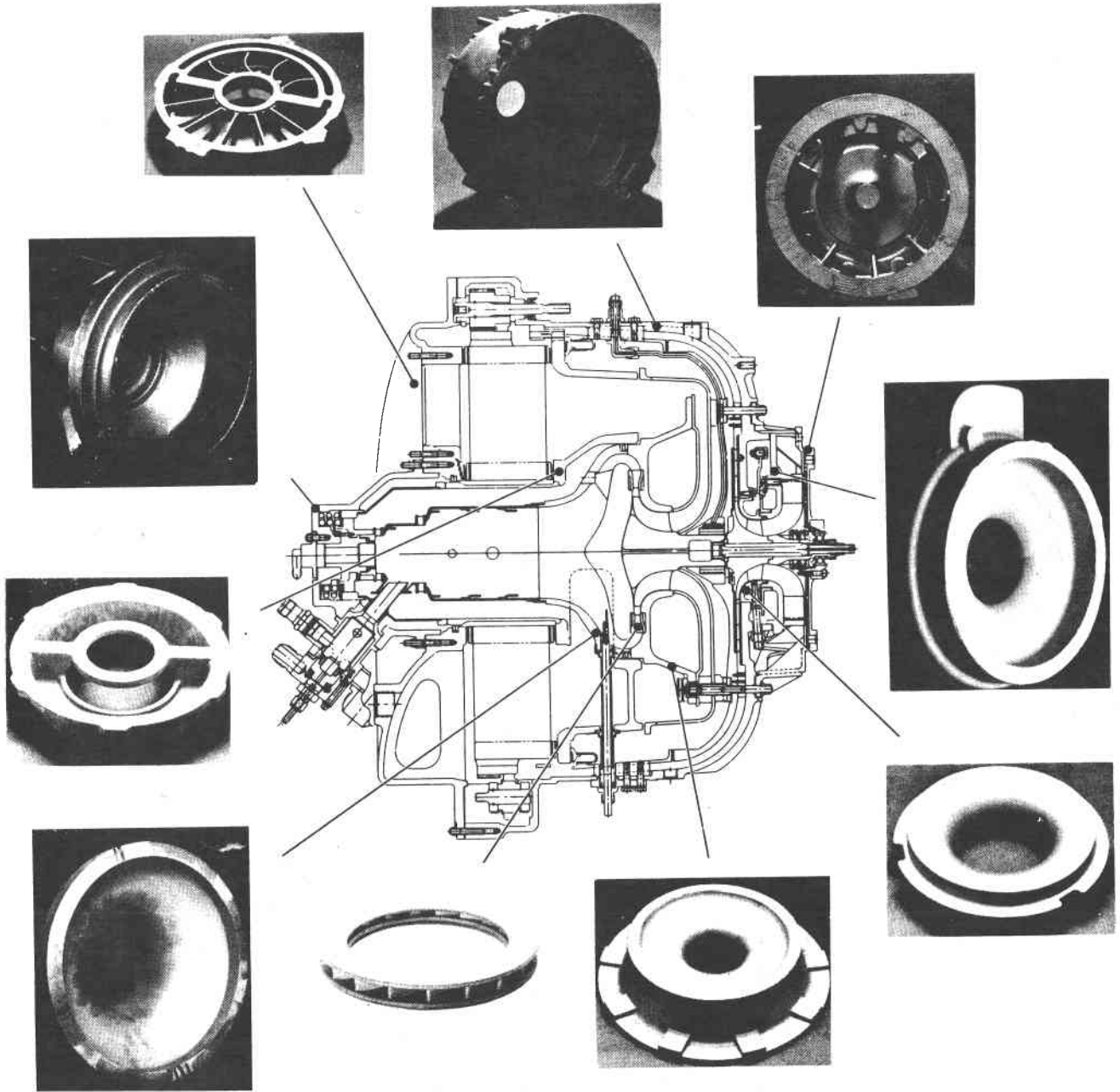
Figure 6. AGT101 Mod I, Build 1 Metal Castings.
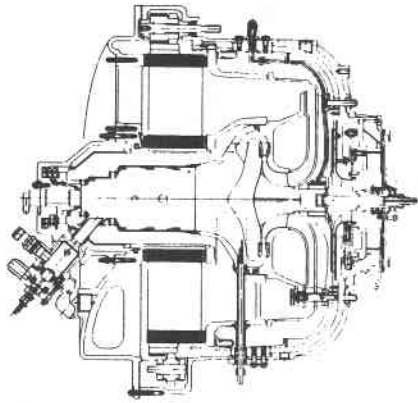
MOD I CONFIGURATION
AGT ENGINE — FIRST BUILD
1600°F TIT
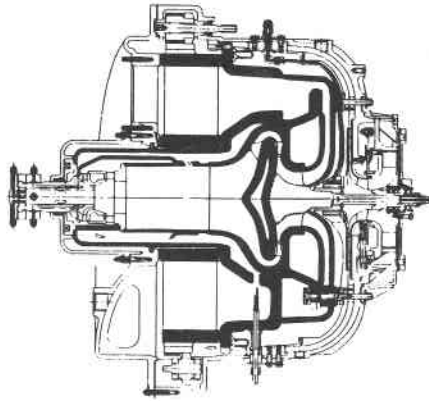
MOD I
2100°F TIT
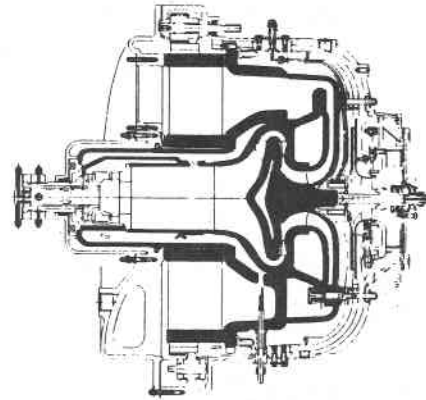
MOD II CONFIGURATION
AGT ENGINE — FINAL BUILD
2500°F TIT

CERAMIC PARTS

33-ART00265-9
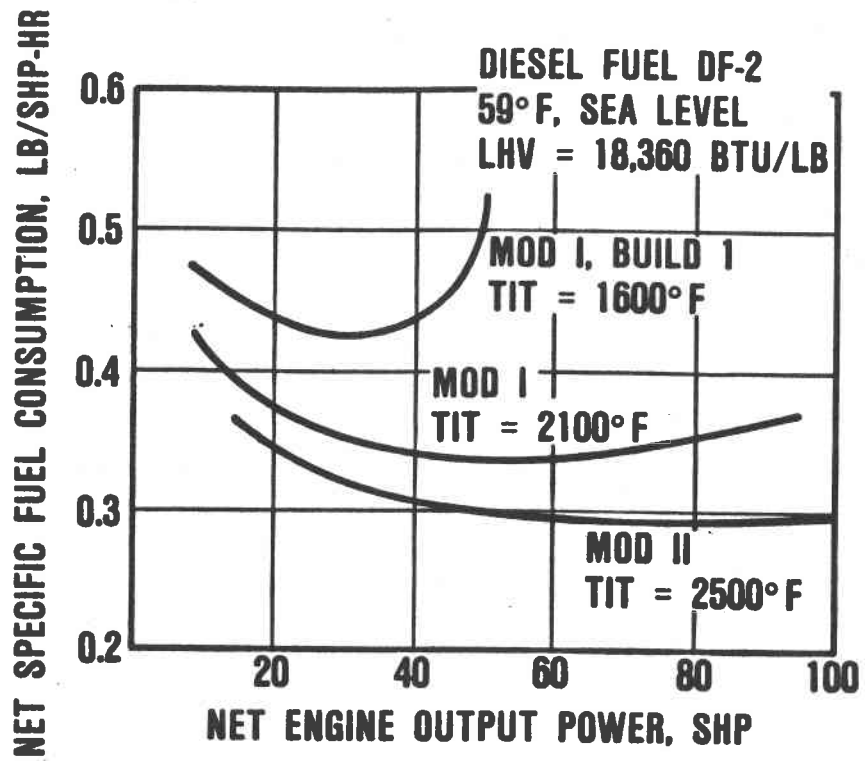
Figure 8. AGT101 Performance.

As shown in Figures 9 and 10 the first engine build has been completed. The configuration depicted is the Mod I, Build 1 engine being prepared for the first series of planned tests--cold motoring, regenerator seal breakin/glazing, and leakage evaluation. Hot and cold motoring tests have been initiated. Testing, including engine performance, will continue in 1982.

3.1 SAGT Performance

Now that the AGT has been discussed, it is appropriate to review the SAGT performance predictions; thus the predicted part load characteristics at 1500°F and 2100°F are presented in Figure 11. The SAGT-1 engine will be operated at 1500-1600°F TIT. The prediction for the 2100°F TIT SAGT show the engine growth potential with ceramic components.

It is evident in Figure 11, that engine operating temperature may be held constant for varying thermal inputs by either changing engine speed or inlet guide vane (IGV) angle. The 20-degree IGV position with variable speed offers the optimum engine efficiency over a wide range of thermal inputs. However, where engine operation is not required over a wide range of thermal insolation, there can be significant system advantages for constant speed operation.

3.2 SAGT-1A Design

As previously discussed the SAGT-1A [also called power conversion unit (PCU)] involves mating the SAGT-1 power section with a solar receiver, which then will be tested on the test-bed concentrator. The SAGT-1A configuration is shown in Figure 12. The PCU major components are:

o   SAGT-1 engine (DOE/JPL/NASA Contract DEN3-181)

o   A 60-cycle induction generator/motor

272
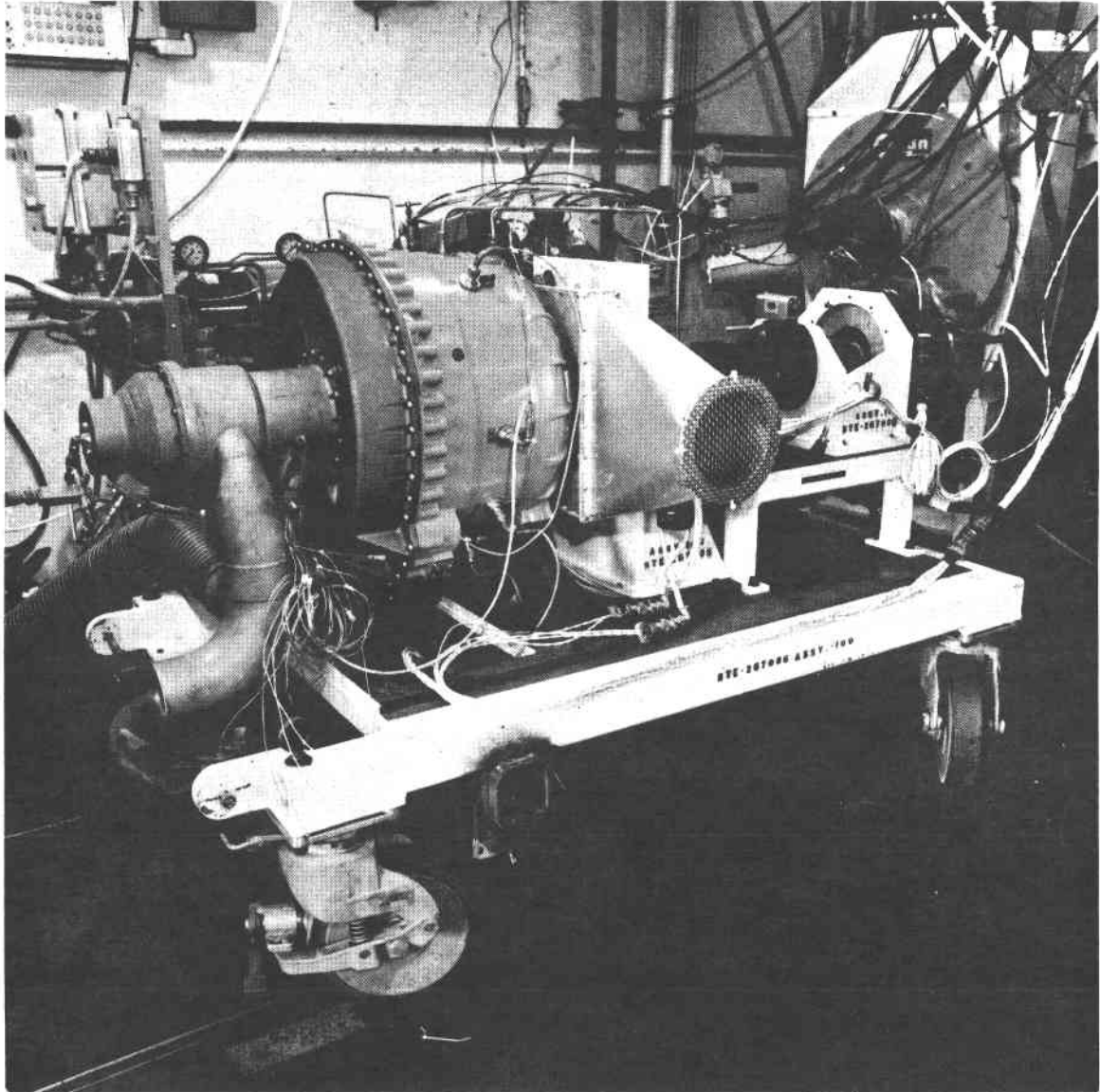
Figure 9. AGT101 Mod I, Build 1 Engine and Test.
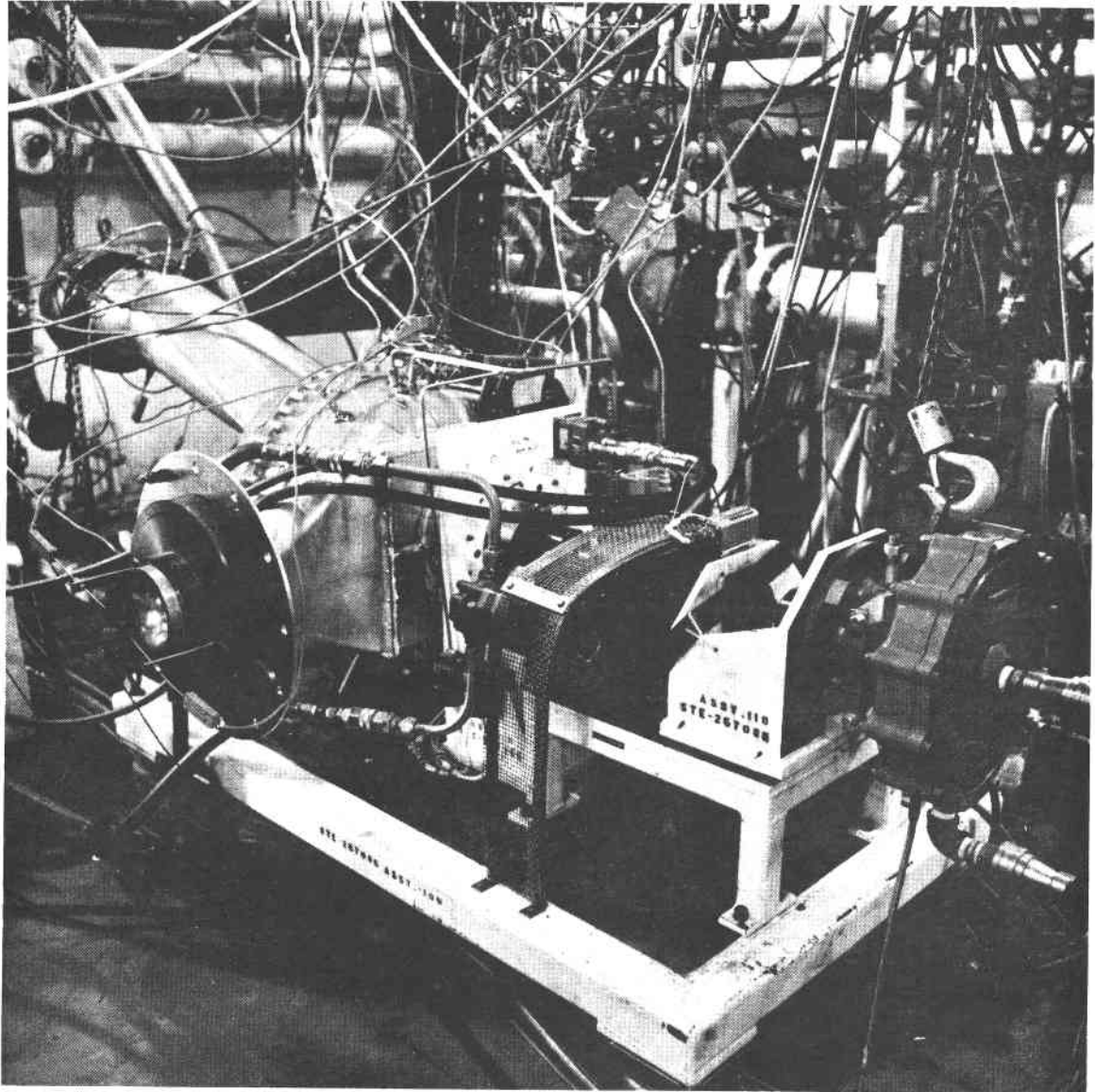
Figure 10. AGT101 Mod I, Build 1, Engine and Test.
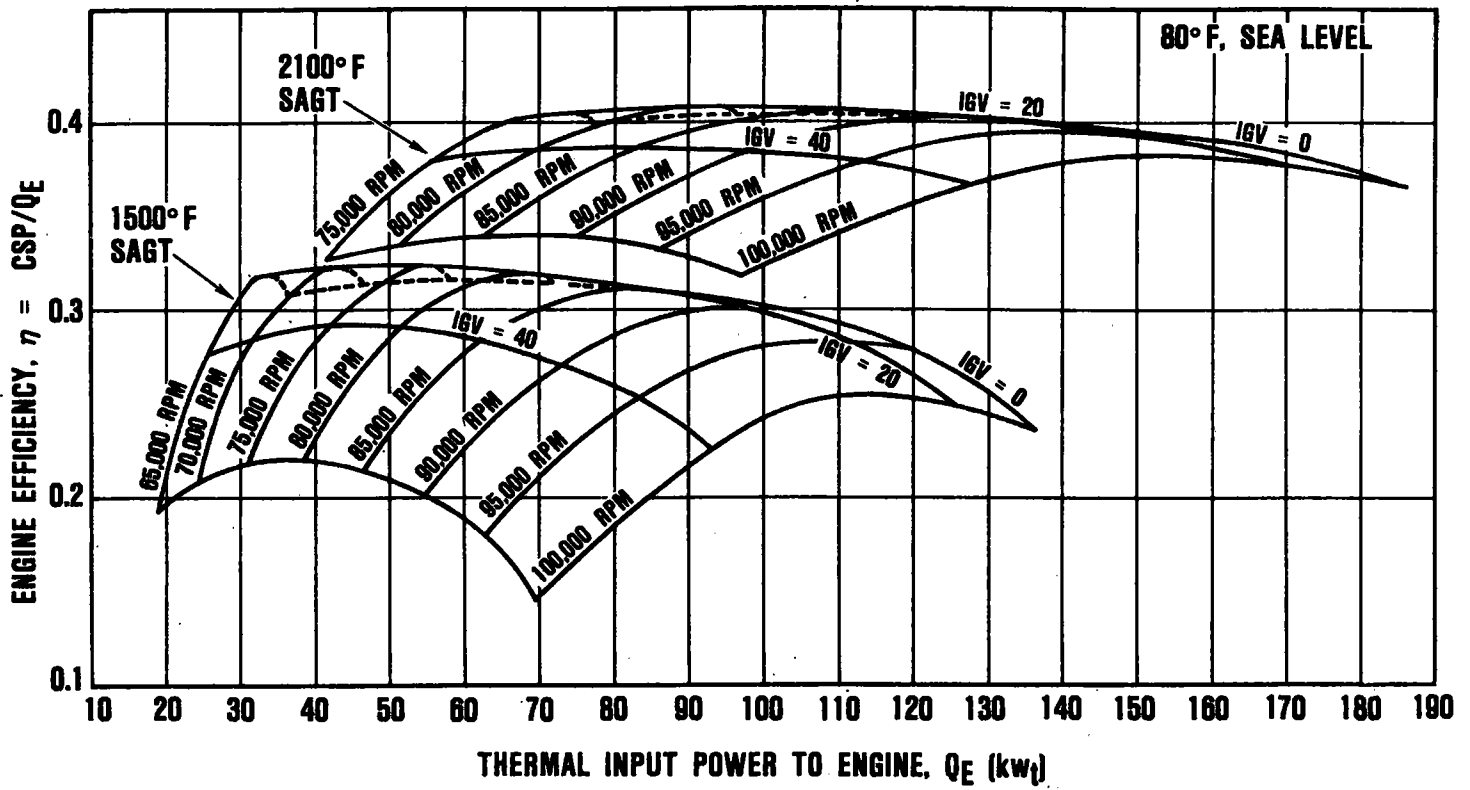
Figure 11. SAGT Growth – Speed and Turbine Inlet Temperature.
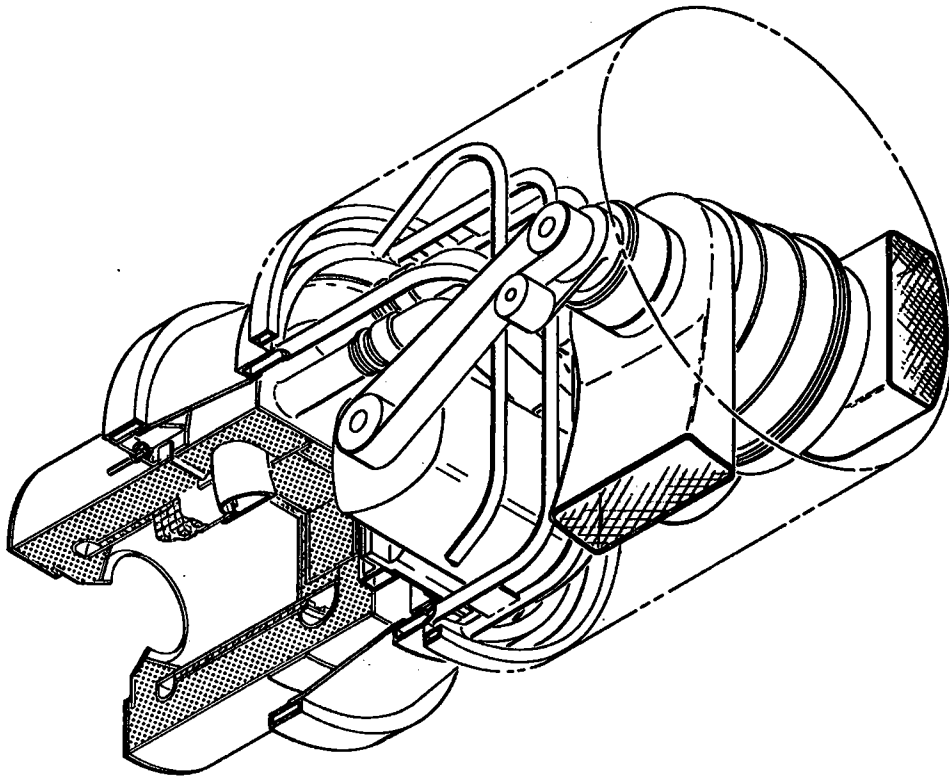
Figure 12.   SAGT-1A PCU.

o   A 38:1 reduction gearbox

o   A belt-drive system used to drive the generator

o   A solar receiver and connecting duct to the engine

o   A structure that transforms the system components into the PCU as well as mounting the unit to the parabolic dish

o   A control system

The SAGT-1A will operate at constant speed with the 60-cycle generator connected directly to the grid. TIT will be held at 1500°F as the solar thermal input varies, by the use of the variable inlet guide vanes (IGV) on the engine. Temperature will be automatically controlled by the engine control system. The engine also is capable of operation on fossil fuel in conjunction with a semi-automatic control system. Starting is accomplished by using ac grid power and the induction generator as a starter motor. The PCU will perform satisfactorily over the entire attitude operating range of the parabolic dish.

From the above description of operation, and system simplicity, the following advantages for the SAGT-1A are evident:

o   Use of the SAGT-1 without further modification minimizes the need for development

o   Use of an off-the-shelf, high-efficiency, 60-cycle generator connected directly to the ac grid, eliminates the need for a separate power conditioning unit as well as a speed/ load control for the engine

o   Provides for an early low-cost field test demonstration

3.3 SAGT-1A Program Plan

The program entails the following steps:

o   Use of existing SAGT-1 engine

o   Design, fabricate and/or procure the generator, belt-drive
     components, or control system, supporting structure and
     accessories

o   Assemble and test the PCU (engine and receiver) at Garrett

o   Deliver PCU to Parabolic Dish Test Site (PDTS)

o   Assist in checkout and test

o   Return SAGT-1 to Garrett for disassembly and inspection

Performance predictions for the power section operating at the
PDTS are shown in Figure 13. The associated PCU accessory efficien-
cies are shown in Figure 14. Combining this data, the overall peak
predicted PCU efficiency is 26 percent for a 1500°F TIT. A plot of PCU
electrical output versus thermal input is shown in Figure 15.
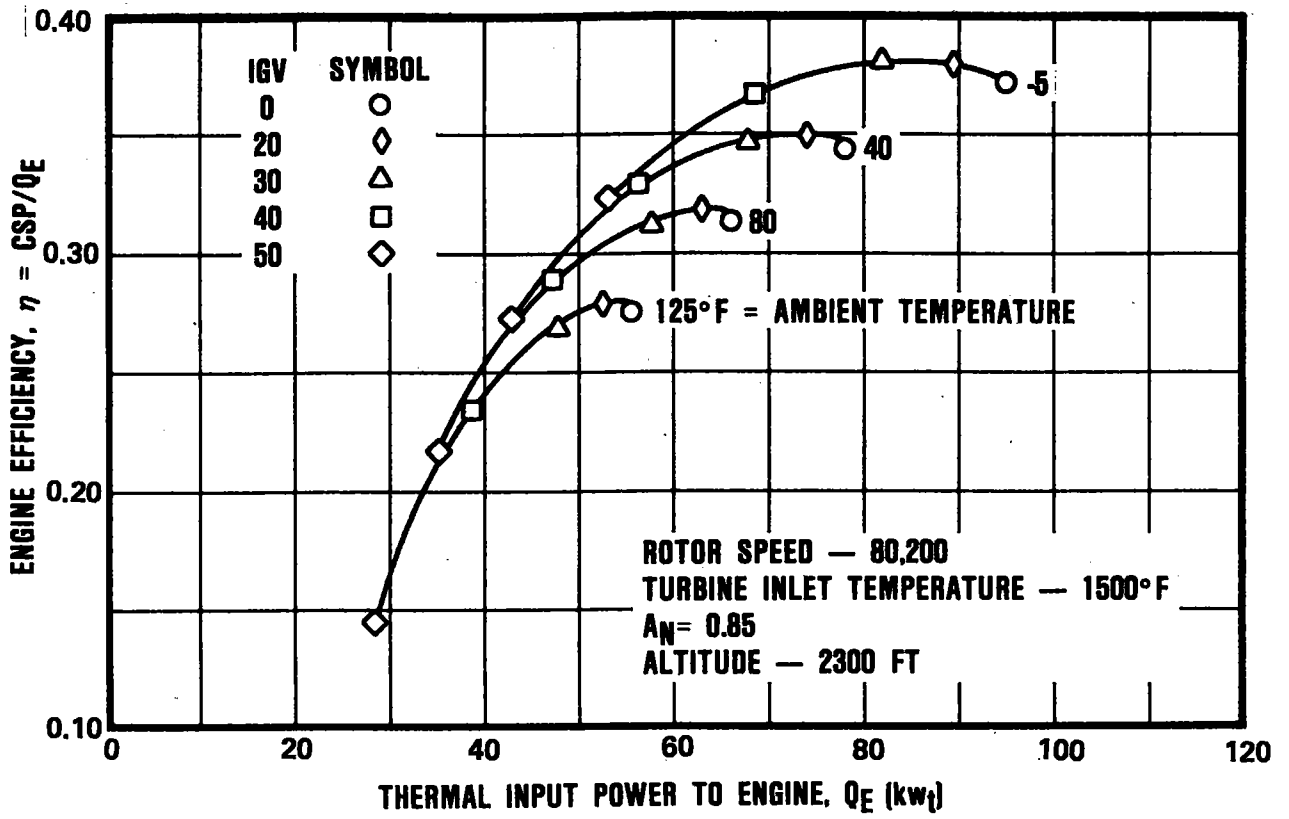
Figure 13. SAGT-1A Engine Performance.
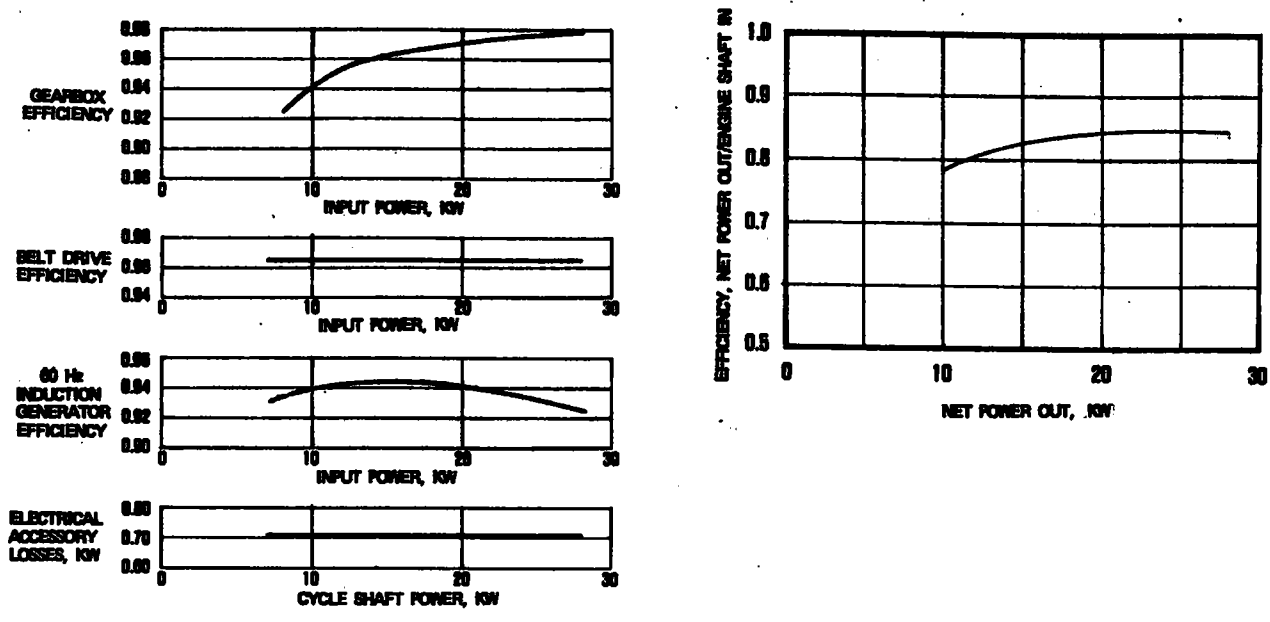
Figure 14. SAGT-1A Alternator and Accessory Performance.

ELECTRICAL POWER OUT, KW$_e$ (y-axis)

AMBIENT TEMPERATURE – 80°F
TURBINE INLET TEMPERATURE – 1500°F
ALTITUDE – 2300 FT

THERMAL INPUT POWER TO ENGINE, Q$_E$(KW$_t$) (x-axis)
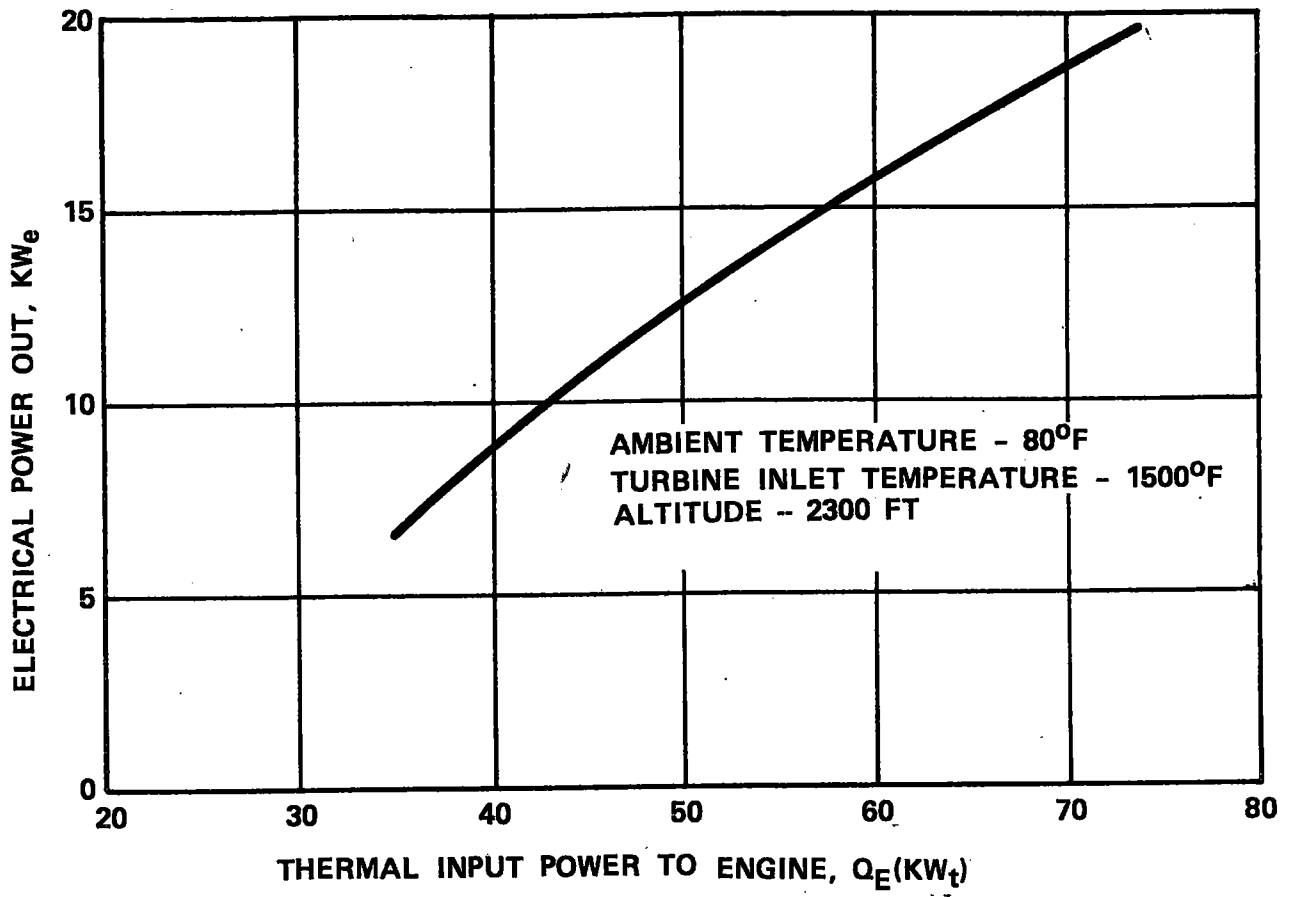
Figure 15.   SAGT–1A PCU Performance.

4.0 SUMMARY

The SAGT-1 design and fabrication is now complete with testing scheduled in January 1982. Progress on the AGT101, from which the SAGT is derived, has proceeded satisfactorily. Mod I, Build 1 component rig performance tests have been completed for the compressor, turbine, combustor, and are continuing for the rotor dynamics and regenerator. The first AGT101 engine testing is underway. Ceramic development has been very encouraging on the static structures and rotor.

The SAGT-1A program presently is being formulated. It is targeted to perform tests in mid-1982.

Ceramic development on the AGT program offer increased engine efficiency for the future, with attendant increases in electrical power output capability. This offers attractive options for future solar applications.

APPLICATION OF THE SUBATMOSPHERIC ENGINE TO SOLAR THERMAL POWER

INTRODUCTION

A natural gas-fired Brayton engine is being developed under the joint sponsorship of the Gas Research Institute, the Department of Energy, and AIResearch and is intended to be the prime mover for a 10-ton commercial heat pump. This engine has many attractive features that make it an ideal candidate for solar thermal-power generation applications.

The unique feature of this engine is its subatmospheric mode of operation. It operates between atmospheric pressure and a partial vacuum. This means that heat is added to the cycle at atmospheric pressure; this permits the receiver to be unpressurized, greatly simplifying its design and cost.

Other features include:

● Designed for high production (10,000 units per year)

● High efficiency due to recuperation (up to 30 percent engine efficiency)

● Long life without maintenance

● Suitable for hybrid fuel/solar operation

● No liquids required on tracking assembly (insensitive to gravity)

Six engines are being manufactured under the current heat pump development program. The next phase, to start in January 1982, will involve 10 additional engines for field test. Pilot production is scheduled to begin in 1984; thus prototype and production engines could readily be made available for use in solar thermal-power projects.

SYSTEM DESCRIPTION

This engine is suitable for mounting at the focal point of a two-axis tracking parabolic dish as illustrated in Figure 1. When combined with a 7-meter dish and an appropriate receiver, the engine will be capable of an 8-kw electrical output. The output of the alternator is high frequency ac, which can be used directly or rectified to dc. Systems can be operated independently or connected with other modules via a common dc bus to provide any desired amount of power.

Engine/Alternator

The basic engine being developed under the GRI/DOE contract is designed to utilize natural gas at low pressure (several inches of water) without the need for a gas compressor. In the subatmospheric configuration, heat is supplied at atmospheric pressure rather than at higher pressures as in conventional gas turbine engines. The basic gas-fired engine is easily converted to a solar

SINK HEAT EXCHANGER

COOLING FAN

TURBO MACHINE

REFLECTOR PANELS

RECEIVER

PM ALTERNATOR

RECUPERATOR PLENUM

SUPPORT POST
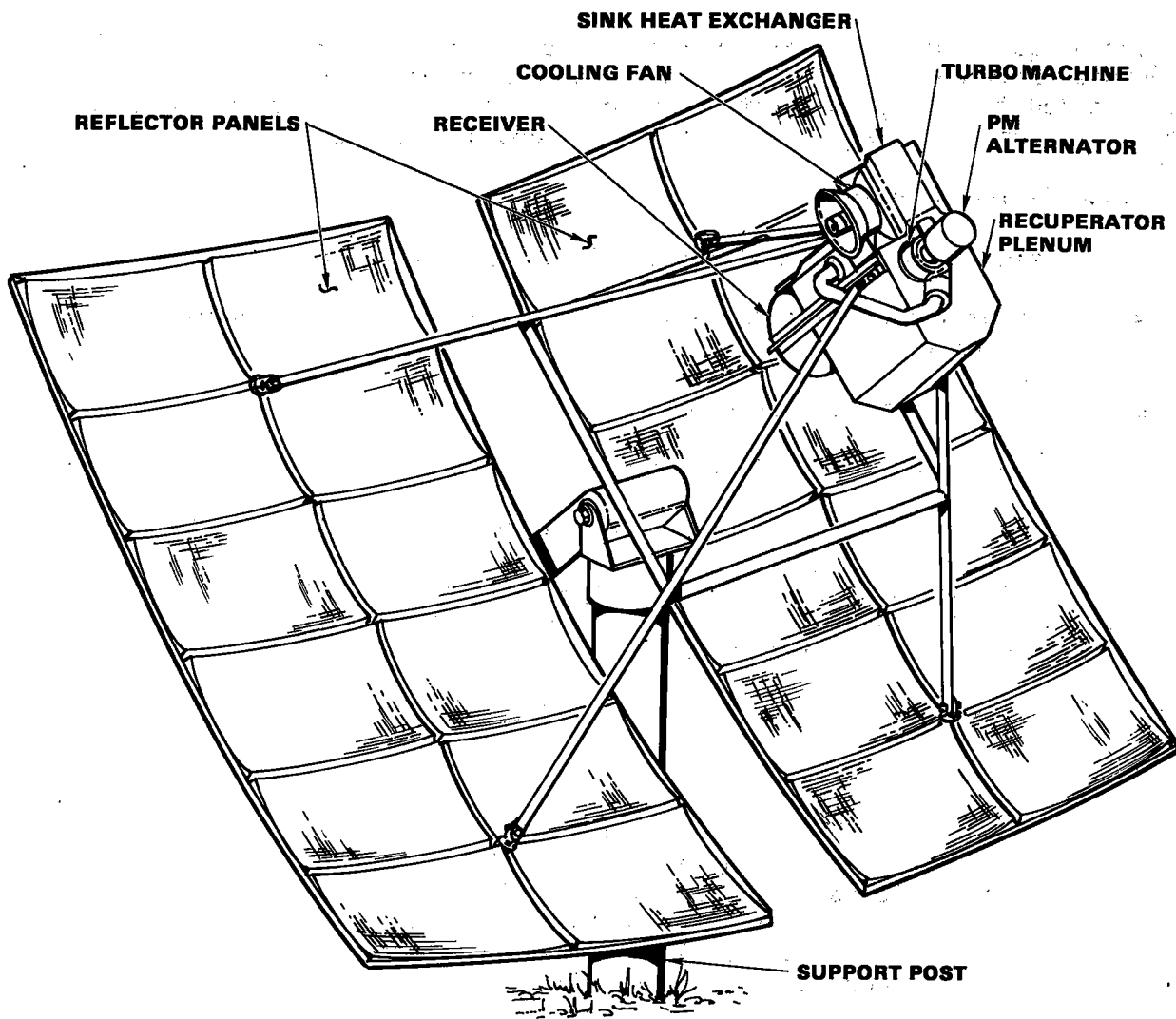
A-22861

Figure 1. Solar Brayton Engine

284

engine by connecting a solar receiver between the regenerator outlet and the combustor as shown in Figure 2. The combustor is eliminated for pure solar applications or retained for solar hybrid applications.

In the solar mode, the engine operates as a "closed" Brayton-cycle engine referenced to ambient pressure through the open receiver. There is essentially no flow into, or out of, the system except through the receiver aperture as the system heats up or cools down.

Hot air at about 1200°F from the regenerator flows into the receiver where it is heated by solar energy to 1600°F. It then expands through the turbine to a partial vacuum of about 6 psia. As it expands, it is cooled and produces shaft horsepower. Part of this shaft horsepower drives the Brayton compressor, and the remainder is available to drive the alternator. Turbine exhaust air is further cooled in the regenerator and then in the sink heat exchanger, where its temperature is reduced to near ambient.

This air, which is still at subatmospheric pressure, is now compressed to slightly above atmospheric pressure by the Brayton compressor. It is then heated in the regenerator, thus recovering energy from the turbine exhaust and completing the circuit back to the receiver.

In the hybrid mode, makeup air for combustion is drawn in through the receiver aperture and discharged through the vent.

Turbocompressor

The Brayton turbocompressor shown in Figure 3 has been designed for long maintenance-free life. It incorporates many of the design features found in automotive turbochargers, thus having potential for extremely low production costs. The unit consists of a cast single-stage radial turbine and a single-stage radial compressor. These are bolted back-to-back to the shaft to form the rotating assembly. The shaft is supported on unique foil air bearings developed by The Garrett Corporation. The bearings use ambient air as both the coolant and the lubricant, and are entirely self-acting (hydrodynamic).

The turbine wheel is of high-temperature cast alloy, and the compressor wheel is cast steel. Cast turbine and compressor scrolls, a turbine nozzle, a compressor diffuser, a thermal shield, and a compressor inlet housing complete the drive design.

The design arrangement draws cooling air over the bearings into the compressor inlet housing. A labyrinth seal keeps the bearings essentially at ambient atmospheric pressure. A thermal shield between the turbine and compressor wheels, plus other thermal design features, minimize thermal leakage.

Recuperator

The high-temperature recuperator is constructed from a formed tube sheet of nitride-dispersion-strengthened, 400-series, stainless steel. Its counter-flow configuration provides an effectiveness of 0.90.
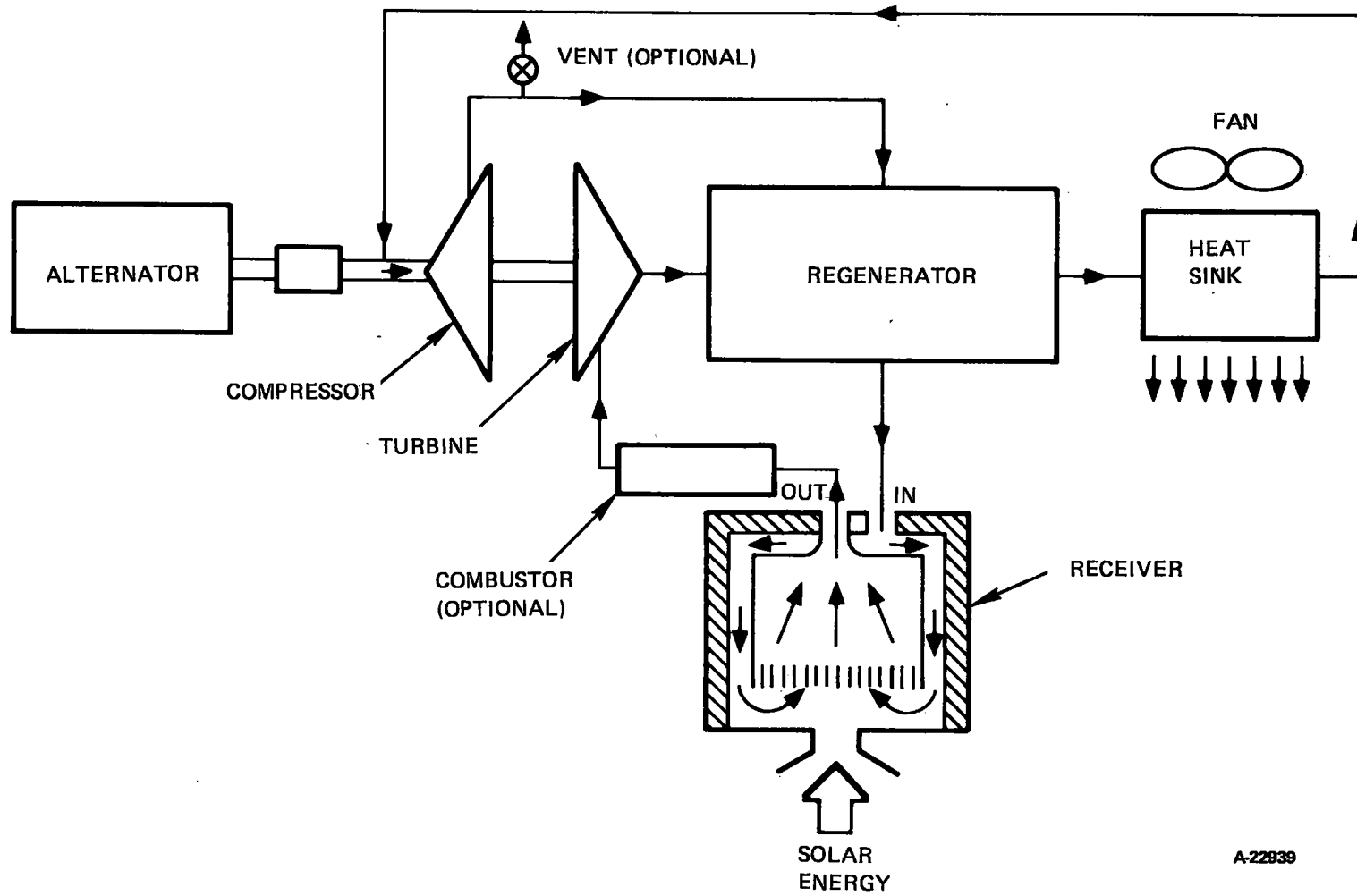
Figure 2. Engine Schematic Diagram for Solar Conversion
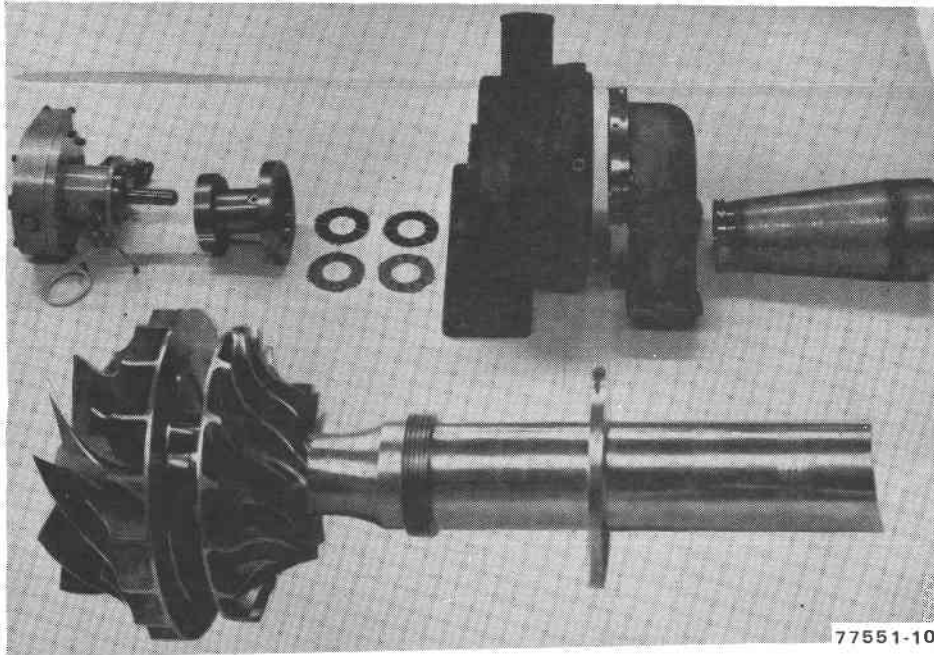
HOUSING AND BEARINGS

ROTATING ASSEMBLY

77551-10

HOUSING
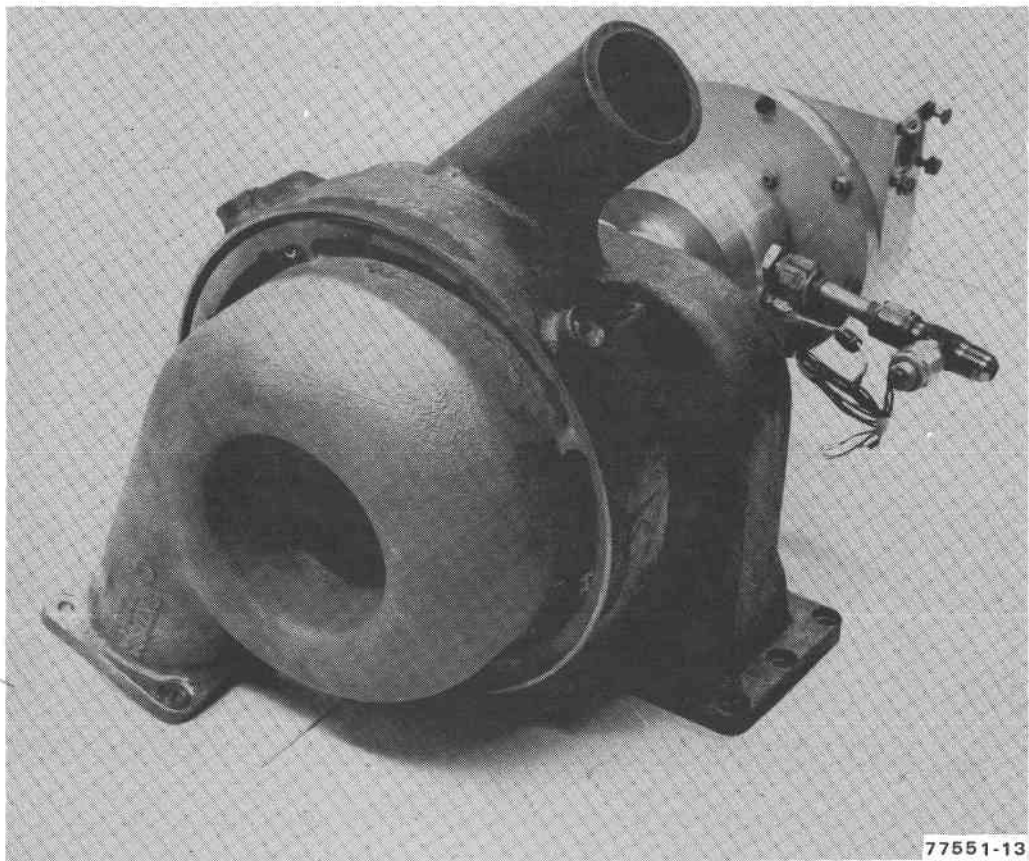
77551-13

Figure 3. Turbocompressor

287

The core consists of alternate layers of gas and air fins. The development unit is shown in Figure 4. Air enters a plenum and is distributed by turning fins into the central counterflow section of the core, where most of the recuperation takes place. After leaving the counterflow section, air flows through additional turning fins and out of the return air plenums. Gas enters at the return air end and passes through the core in a counterflow direction. High-performance rectangular strip fins are used in the counterflow section in both the air and gas passages.

Both the air and gas fins are brazed to the tube sheets with a high-temperature, nickel-base braze alloy. Brazing maximizes heat transfer and makes the entire core an integral structural assembly capable of withstanding high pressures and temperatures without external support. This type of design is used by AiResearch in its large industrial regenerators.

LOW COST, HIGH EFFECTIVENESS
AND DURABILITY ACHIEVED BY

COUNTERFLOW
FORMED TUBE SHEETS
INTEGRAL MANIFOLDS
OFFSET FINS
NICKEL BRAZED CONSTRUCTION

83884-2

HOT PASSAGE
TYPICAL 76 PLACES

COLD PASSAGE
TYPICAL 75 PLACES

FLOW
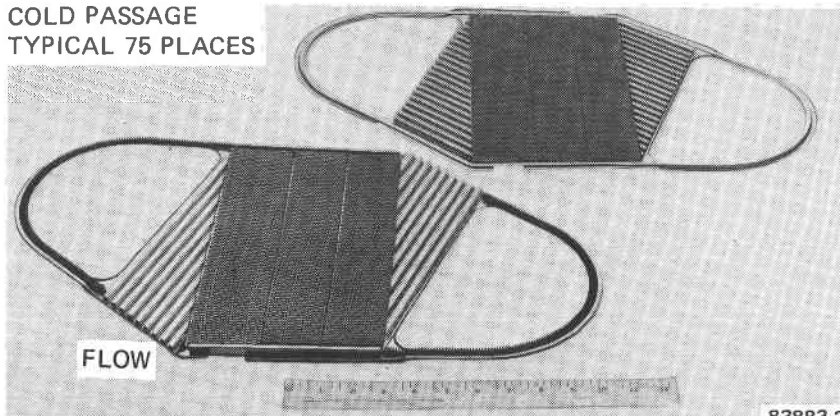
83883-2

Figure 4. Recuperator

Alternator

The alternator, shown in Figure 5, was developed as a dynamometer to load the engine in the heat pump program. It is a two-pole permanent magnet, brushless design utilizing samarium cobalt magnets. It has been demonstrated in test to have an efficiency of over 94 percent. This unit also incorporates foil air bearings of similar design to those used in the turbocompressor. All cooling of the alternator is done with ambient air.

The alternator housing is bolted to the turbocompressor housing. The rotating assemblies are connected via a permanent magnet coupling. Thus the alternator rotates at the same speed as the turbocompressor. This simple design precludes the need for a gearbox with its attendant lubrication system complexity and maintenance requirements. All system lubrication and cooling is provided by ambient air.

Receiver

Undoubtedly the greatest benefit of a subatmospheric cycle utilized in a solar system is that it permits use of an atmospheric receiver, thus greatly simplifying the design requirements for this critical component.

Figure 6 depicts an atmospheric receiver design prepared by Sanders Associates for use with the AiResearch subatmospheric engine. Air enters the receiver at 1200°F. It is distributed around an annular passage and flows into the main open cavity of the receiver. It then passes through the active heat transfer element, a disc of silicon-carbide honeycomb. The heated air is collected and exits the receiver at 1600°F.

As can be seen from the figure, the design is extremely simple. Nothing has to be sealed, there are no pressures to contain, and parts may be allowed to float during thermal expansion and contraction. Thus no mechanical or thermal stresses are imposed in operation. This results in a lightweight unit with low-cost materials.

Since the unit is operating well below the temperature limits of the silicon carbide, it is insensitive to "hot spots" caused by unanticipated variations in solar flux distribution.

ENGINE PERFORMANCE AND DEVELOPMENT STATUS

All major components have successfully completed component development. They have been assembled into a fully integrated preproduction engine (shown in Figure 7). System development is proceeding satisfactorily. Final system performance based on component test calibrations is predicted to be as shown in Figures 8 and 9. The engine efficiency at the design point of 1600°F turbine inlet temperature is predicted to be 30 percent with a power output of 8 kw.
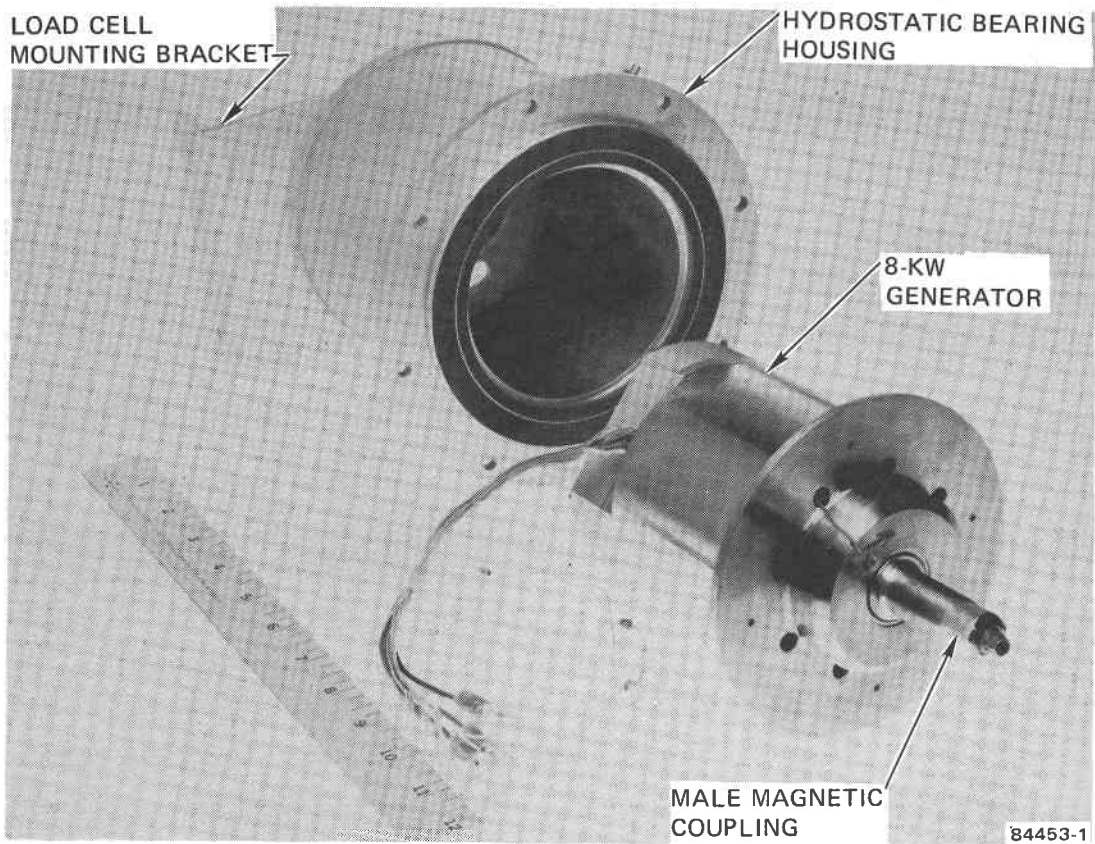
Figure 5. Alternator
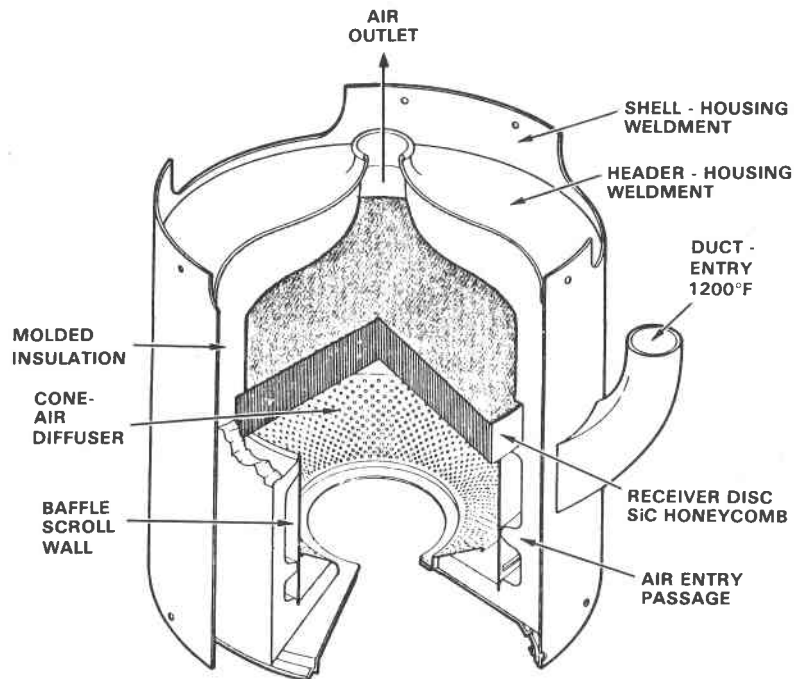
Figure 6. Sanders Atmospheric Receiver Design

GAS CONTROL VALVES

FRESH AIR BYPASS VALVE

TEST INSTRUMENTATION

BRAYTON COMPRESSOR DISCHARGE DUCT

DYNAMOMETER

85091-7
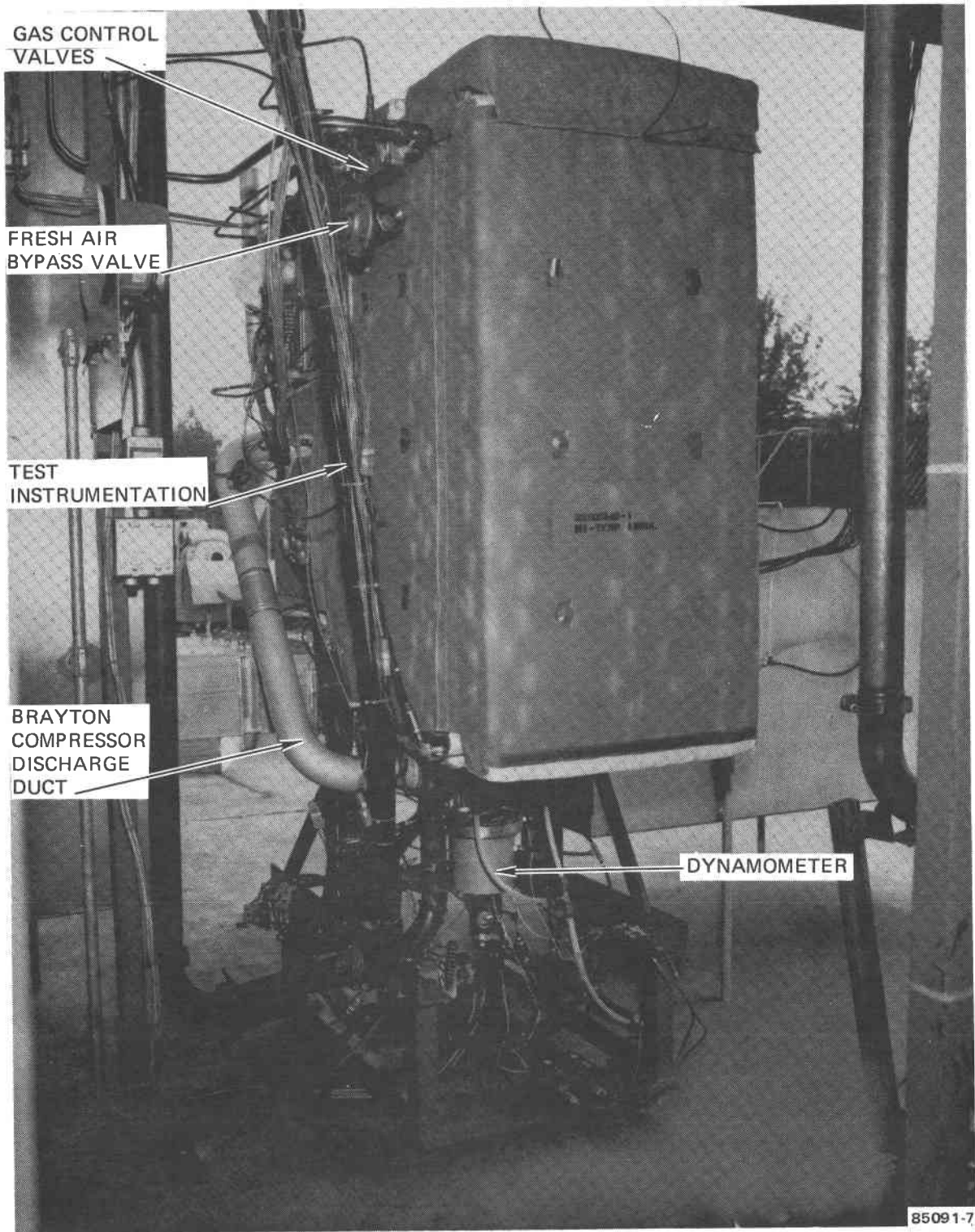
Figure 7.   Preproduction Engine
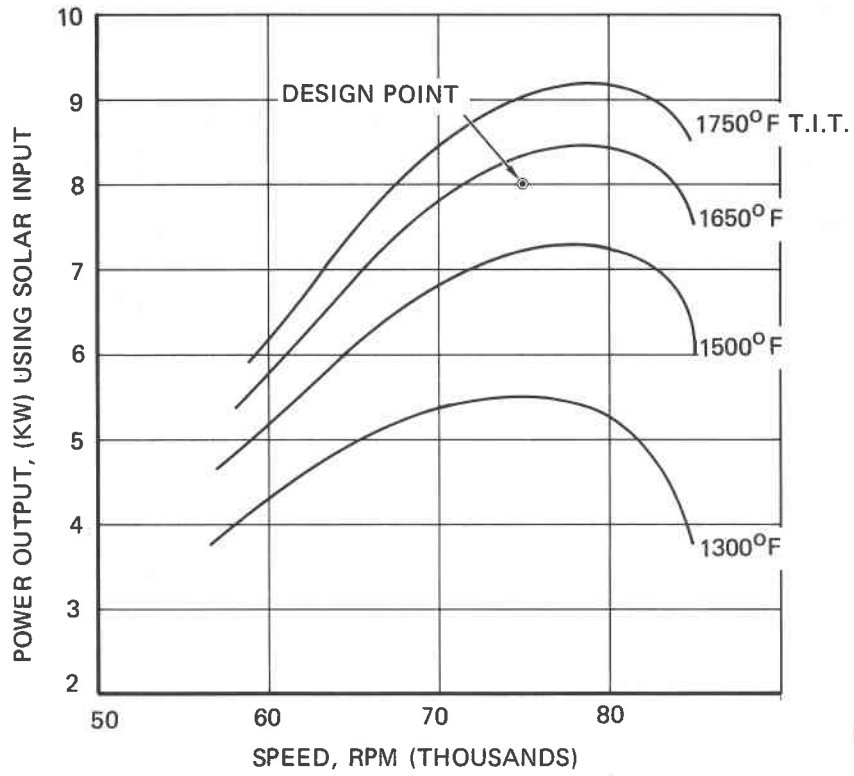
291

Figure 8. Performance Map
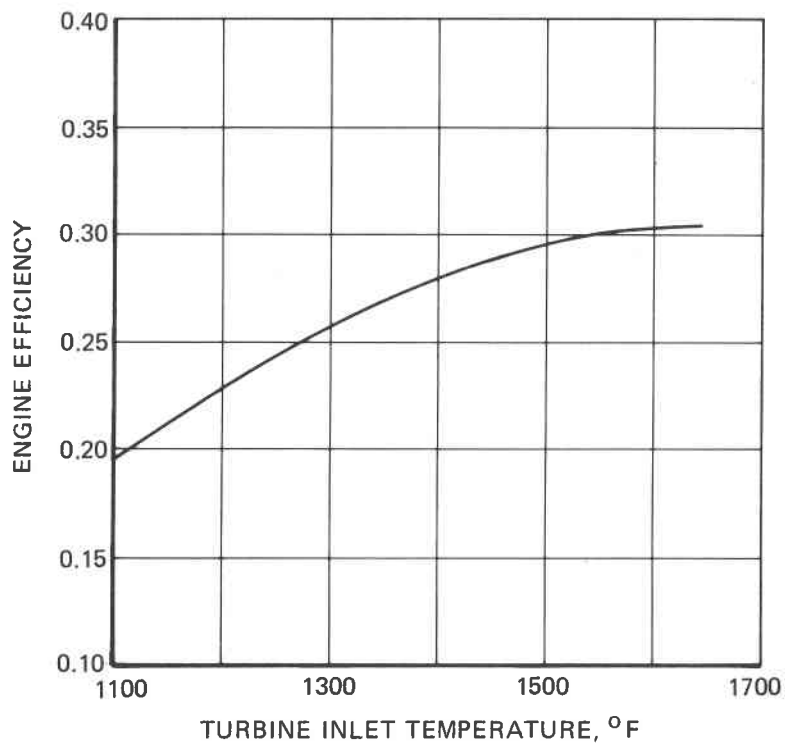
Figure 9. Predicted Engine Efficiency

Under the present contract, six prototype engines are being built and tested, including one for extended endurance testing. In a follow-on contract to be started in January 1982, 10 additional engines will be manufactured and installed in gas-fired heat pumps. These heat pumps will be installed on commercial buildings around the country and operated in a field test program. Preproduction and full production are scheduled to start in 1984 and 1985, respectively. An annual engine production rate of between 5000 and 10,000 units is projected for heat pump applications alone. Other uses for the engine such as solar thermal-power generation would increase this production rate.

POTENTIAL BENEFITS

FROM A

SUCCESSFUL SOLAR THERMAL PROGRAM

K. L. Terasawa and W. R. Gates

Jet Propulsion Laboratory

STES BENEFITS ANALYSIS

Introduction: The Private and Social Benefits of Solar Thermal Energy Systems

The 1973 Arab oil embargo focused attention on the precarious nature of the U.S. energy market which had developed a heavy reliance on imported petroleum and natural gas. This gave rise to widespread political and public support for a national energy policy designed to solve the "energy crisis" in a manner consistent with the overall objectives for the U.S. economy. The resulting energy policy stresses reducing the demand for petroleum imports primarily through two mechanisms: energy conservation in the near-term augmented by the development of a broad range of alternative domestic energy technologies in the mid- to long-term. Solar Thermal Energy Systems (STES) constitute one of these domestic energy alternatives.

STES will provide cost competitive energy alternatives for deployment in a wide range of applications. The impact on the domestic energy market resulting from the development and installation of an innovative energy technology such as STES is depicted in Figure 1. In this diagram, hypothetical energy demand and supply curves representing two situations have been pictured: before and after the development of STES. In the absence of an STES option, the intersection of the supply and demand curves indicates that domestic energy consumption from conventional sources will equal Q_0. The introduction of STES will shift the energy supply curve as shown, indicating that the total supply of energy will increase when a new energy technology becomes available. The magnitude of this shift, for alternative energy price levels, depends on the cost of producing STES. In this stylized illustration, STES is not economically competitive when energy prices are low. Therefore, the supply curve does not shift in the low price region. If high energy prices prevail, however, STES becomes competitive and the supply curve shifts outward by an amount equivalent to the quantity of STES forthcoming at each corresponding energy price level. The intersection of the demand curves with the new energy supply indicates that domestic energy consumption will increase from Q_0 to Q_N. At this level of total consumption, Q_C indicates the level of energy supply from conventional sources, while the quantity between Q_C and Q_N represents the energy supplied by STES. Furthermore, the price of energy, as indicated by the vertical axis, is higher in the initial situation than it is after the deployment of economically competitive solar thermal energy systems.

The net result, in the simplified illustration provided by Figure 1, is that the development of cost competitive energy alternatives such as STES can be expected to increase total energy supplies and domestic consumption while reducing the quantity of energy supplied from conventional sources. The increase in energy consumption results because STES secures a level of market penetration which more than compensates for the reduction in consumption from conventional sources. Furthermore, while STES is expected to displace a variety of fuel types, the primary impact will be on the most expensive alternative fuel, petroleum.

There are a variety of benefits which can be attributed to the development and deployment of STES. More specifically, the benefits accruing from the installation of cost competitive STES can be divided into two broad categories: benefits which are reflected in market transactions, and impacts which are not. The primary benefit in the first category is the savings in energy related

costs realized as electric utilities, industrial, and agricultural sectors replace conventional generating capacity with economically competitive STES. The value of this benefit is represented by the shaded area in Figure 1. Secondary benefits in this category include considerations such as net changes in employment levels and the affect of lower energy costs on other sectors of the domestic economy. The second category of impacts, which are not captured through the pricing mechanism or market transactions, include positive environmental impacts, as well as increases in the levels of national security, economic stability, and competition in the domestic energy market. Potential benefits in this second category could be quite significant, however, they are quite difficult to quantify and often excluded from consideration.

Solar Thermal Electric Systems: A Complement to Coal and Nuclear Technologies

As outlined previously, an excessive reliance on imported petroleum is frequently perceived as the characteristic leading to the "energy crisis" of 1973. In the electric utility industry, for example, generating capacities prior to 1973 included a high proportion of petroleum-fired technologies for use in base, intermediate, and peaking applications. As a result of the 1973 Arab oil embargo, a variety of federal policies were implemented in an effort to reduce the use of petroleum as a fuel source. Conservation has been encouraged to lower electricity consumption in general and alternative domestic energy technologies are being developed to replace petroleum based systems. Coal and nuclear technologies have been particularly successful in displacing petroleum technologies in base load applications.

The impact of these measures is depicted in Figure 2 which shows the projected electric utility consumption of fuel by type from 1980 to 2000. In this figure it is evident that coal and nuclear systems are expected to account for an increasing portion of electric power generation, while the share attributable to petroleum and natural gas is expected to decrease. This shift in generation mix results from the economically driven replacement of petroleum and gas fired base and intermediate load capacity by coal and nuclear capacity. In the year 2000, this transition is virtually complete. The remaining petroleum and gas consumption represents peak load applications. Further petroleum displacement by nuclear and coal systems is likely to be economically prohibitive due to the technical difficulties encountered in using coal and nuclear energy in peaking applications. Thus, if further reductions in petroleum usage are desired, they must be secured through the deployment of some other domestic energy technology.

Solar energy systems, including STES, offer the opportunity for additional economic displacement of petroleum as a fuel type in electric power generation. Due to the low start-up and shut-down costs of solar energy technologies, combined with the high correlation between peak electricity demand and peak insolation in the southern and southwestern regions of the U.S., solar energy provides a potential means for the economic displacement of petroleum used to satisfy peak load electrical demands. Nuclear and coal based systems encounter significant technological difficulties in attempting to supply this portion of the demand for electricity. Thus solar energy systems complement nuclear and coal fired technologies by displacing petroleum in usages for which nuclear

and/or coal substitution are infeasible or economically prohibitive. Further-more, the development of solar energy systems provide a hedge against the possibility that coal and nuclear will experience limited future utilization due to unforeseen technological, environmental, or political problems.

Thus, solar energy represents an important element in the national effort to develop a broad range of domestic energy alternatives. Solar energy systems complement other technologies, such as nuclear and coal-fired capacity, thereby encouraging additional cost-effective displacements of imported petroleum which would not be feasible in the absence of a solar option. As such, the development of solar energy contributes to the national objective of reducing the U.S. dependence on imported petroleum. In addition to displacing imported petroleum, the economic, environmental, and political benefits outlined previously will all characterize the deployment of solar energy systems in electric utility applications.

STES: A Range of Applications Serving a Variety of Economic Sectors

Federal, energy-related R&D programs in the post-1973 period have concentrated primarily on developing alternative technologies to be used in the generation of electricity. Figure 3, however, indicates that the electric utility industry directly accounted for less than ten percent of the U.S. petroleum consumption in 1980. This share is projected to decrease over time, becoming less than two percent by 2000. As a result, significant progress towards displacing imported petroleum requires programs which address the household and commercial sector, the industrial sector, and the transportation sector in addition to the electric utility sector. Primary emphasis in the development of coal and nuclear technologies, however, centers on the use of these resources in the generation of electricity. Similarly, many solar energy technologies, including photovoltaics and wind systems, produce electricity as their primary output. Thus, progress toward the national objective of cost-competitive displacements of imported petroleum requires development efforts on technologies suitable for a wide range of applications in sectors other than the electric utility industry.

Solar thermal energy systems represent such a technology. Solar thermal energy provides a renewable domestic source of power which can be used to generate electricity, heat, or as a total energy system capable of providing both electric and thermal power. Therefore, STES can be employed in a variety of sectors including electric utilities, industries requiring thermal power, and agricultural applications. STES can also be used to produce transportable fuels and chemical feedstocks. Furthermore, solar thermal energy can be supplied through systems ranging in size from tens of kilowatts to hundreds of megawatts. Since STES is highly modular, it is possible to maintain more optimally sized system generating capacities in the face of increasingly uncertain demand growth than is the case for large, centralized generating systems. Similarly, modularity enables users to operate and add additional capacity simultaneously. These characteristics provide STES flexibility with respect to system size requirements and range of application, enabling STES to satisfy many categories of energy demand.

Alternative solar thermal conversion processes exhibit varying degrees of technical and commercial readiness. Some systems, notably water and space heating, have virtually completed the R&D process and represent near-term technologies. Other systems, such as solar thermal electric technologies, will require additional R&D before becoming available for introduction in mid- or long-term markets. Therefore, solar thermal technologies are capable of providing cost competitive systems for both near-term and long-term deployment. This consideration, combined with the flexibility in size and range of applications discussed above, render STES an important element in the federal energy program. STES complements coal and nuclear technologies in electric utility applications and addresses additional market sectors which are not amenable to coal and nuclear technologies or other types of solar energy systems. Thus, STES provides the potential for cost-competitive displacements of imported petroleum in a variety of applications.

The Demand for STES in Electric Utility Applications

As of this point, the discussion here has outlined the rationale for developing solar energy technologies as a supplement to coal and nuclear systems. Furthermore, due to the wide range of potential applications, it has established STES as an important solar energy option. It is now necessary to discuss the net benefits expected from utilizing STES in each potential application. Examination of the net benefits accruing from each STES application can be used to determine the desirability of federal participation in the development of STES. Similarly, since the expected net benefits are equal to the value of using STES minus the cost of producing these systems, benefit assessment will also indicate the system costs required to ensure that STES provides an economically viable energy option for each alternative application. Thus, the remainder of this discussion will outline briefly the methodology used to estimate the expected net benefits attributable to the development and deployment of cost-competitive STES. Results will be presented for three major areas of STES applications: electric utilities (no storage), industrial process heat (IPH), and transportable fuels and chemical feedstocks. Due to the preliminary nature of the estimates, caution should be exercised in interpreting these numbers. These estimates are currently being refined.

The benefit estimates for electric utility applications of STES are based on work that was conducted by JPL during FY 1981. The FY 1981 activity described and evaluated the potential benefits, both private and social, attributable to the deployment of STES in 1990. This methodology was used in the 1981 Multi-Year Program Plan for the Federal Solar Thermal Energy System Program, in the STES Backup Sunset Review Document, and by the Solar Thermal Cost Goals Committee.

The value of the benefits attributable to STES depend primarily on two factors: the level of STES deployment and the value of the net benefits derived from that level of deployment. In turn, the level of deployment is determined by comparing the value of additional units of STES capacity with the costs of producing each additional unit. Theoretically speaking, as long as the value of an additional unit exceeds the costs of producing that unit, STES market penetration can be expected to increase, though actual deployment may be restricted due to manufacturing bottlenecks or inadequate consumer information. The value of each additional unit of STES capacity is referred

to as the "marginal value" of STES. Thus, benefit assessment of STES requires both estimation of the marginal value of STES and the costs of producing the systems.

The primary benefit of STES in electric utility applications is equal to the energy cost savings associated with the installation of solar energy systems. These energy cost savings include the displacement of conventional fuel and generating capacity, as well as potential savings in operations, maintenance, transmission, and distribution costs. The benefits estimated in this analysis include fuel and operation and maintenance (O&M) cost savings only. Thus, the values presented here provide conservative estimates of the benefits attributable to electric utility applications of STES. The value of fuel and O&M cost savings depends on the level of STES penetration, as well as the quantity and mix of fuel types displaced. The total energy displacement attributable to a particular solar thermal system varies with the level of insolation. As insolation increases the energy output of the solar system increases as well. In addition, while STES will displace a variety of fuels, the primary impact for low levels of penetration will be on the most expensive alternative fuel, petroleum. As the level of penetration for a particular utility increases, STES will displace increasing proportions of less expensive fuel types. Therefore, the marginal value of STES is dependent on the mix of fuels used, and will decrease as the level of penetration decreases. Furthermore, since the value of the fuels displaced depends critically on the price of each fuel type over the life of the system, it is necessary to estimate the future prices for every fuel type. Fuel price predictions are inherently uncertain. Because the value of STES is very sensitive to these estimates, a range of future values should be used, resulting in a range of expected benefits. More specifically, in this analysis three fuel price scenarios have been employed, corresponding to NEP III high, medium, and low projections for the world price of petroleum. Finally, since insolation levels, fuel use patterns, and fuel prices vary across regions of the country, marginal values should be estimated on a regional basis. Regional estimates can then be aggregated to determine the marginal value of STES to the nation as a whole.

The marginal value curves for electric utility applications of STES are depicted in Figure 4 for three fuel price scenarios. In deriving these curves, attention was restricted to fifteen high insolation states in the southern portion of the U.S., with particular emphasis on the highest insolation regions of the southwest. Individual states were grouped according to insolation level. The marginal values associated with successive additions of STES capacity were estimated for each group of states over a range of STES penetration levels. The curves for each group of states were aggregated to determine the marginal value for STES in all states included in the analysis. Thus, each horizontal segment of the curves in Figure 4 corresponds to a group of consumers that would be willing to pay the price indicated on the vertical axis for the quantity of STES capacity depicted by the width of the horizontal segment.

In addition to the three marginal value curves, Figure 4 also shows the 1990 STES cost targets. The range of costs included in these targets reflects the impact of production volume on the projected STES costs. Higher production volumes will result in lower STES costs, due to economies of scale in manufacturing. Since the marginal value curve indicates the price that potential consumers would be willing to pay for each quantity of STES capacity, the intersection of the marginal value curve with the cost curve will determine

the potential market penetration for STES. This represents the level of solar penetration which minimizes the total national cost of electricity. The market penetration consistent with this intersection point indicates that sufficient demand will exist in 1990 to capture all relevant economies of scale. Furthermore, by construction the marginal value curve depicts the value to consumers of each additional unit of STES capacity as the level of deployment increases. Therefore, the area between the marginal value curve and the cost curve for STES is equal to the total value of the energy cost savings attributable to STES. This area is also equivalent to the shaded area of the diagram in Figure 1. In other words, this area provides an estimate of one of the net benefits attributable to the development of an STES option, the potential savings in energy costs. Due to probable manufacturing bottlenecks and imperfect consumer information, actual STES market penetration is expected to fall short of the potential level indicated in Figure 4. Thus, the potential energy cost savings represent an upperbound on the actual level of benefits which will be realized by STES installations in 1990. However, if this analysis was repeated for other years, with more realistic annual sales, the cummulative penetration is expected to be on the same scale.

The Net Present Value of Solar Thermal
Electric Systems: Medium Oil Prices

Figure 5 shows the value (discounted to 1981 base year) of this potential benefit, assuming the NEP III medium oil price scenario, for a range of STES costs. Two important points should be stressed with regard to this figure. In the first place, this diagram assumes that no STES installations in electric utility applications have occurred prior to 1990. Any prior deployment would reduce the benefits realized in 1990. Of course, these earlier installations would also have a stream of associated benefits which would serve to partially or wholly offset the decrease in the benefits attributable to 1990 installations of STES. Secondly, this estimate for the net present value of 1990 STES installations assumes that the entire 1990 demand for STES is satisfied in that year. Due to manufacturing bottlenecks, capital market constraints, and imperfect consumer information, this assumption is likely to be violated in reality. This would serve to delay the realization of a portion of these benefits. The impact of this delay will depend on the value of the discount rate relative to the value of the fuel and capital cost escalation rates.

The Value of Solar Thermal Electric Systems:
R&D Success vs. Energy Prices

Figure 6 summarizes the net present value of potential energy cost savings accruing from electric utility applications of STES for three oil price scenarios and three levels of STES costs (reflecting three levels of R&D success). If R&D success is limited, resulting in STES costs in the $4000/KWe range, cost-effective installations of STES will occur only in the high energy price case. On the other hand, highly successful R&D will enable STES to penetrate the electric utility market in all three energy price scenarios. The benefits (energy cost savings) in the $4000/KWe success case range from zero to $10 billion, while the benefits in the $1400/KWe success case vary from $9 billion to $50 billion. It should be noted that the production volume can also influence the cost of STES. Thus, $4000/KWe could represent the case characterized by moderate R&D success with limited rates of production.

However, as discussed in a previous section, the size of the potential STES market indicated by the marginal value curves in Figure 4 is sufficient to capture all important economies of scale over the relevant range of STES costs. Therefore, the alternative values for STES costs can be interpreted as primarily reflecting the level of R&D success.

One important point becomes evident from examination of this table. Market penetration and energy cost savings associated with the development and deployment of STES are extremely sensitive to both future energy prices and STES costs. The outcome of R&D projects are hard to predict, especially for high risk long-term R&D projects such as the development of STES. Similarly, due to the dominant impact of OPEC on world energy prices and the unstable, unpredictable nature of OPEC pricing policies, projections of future energy prices are highly uncertain, varying over a wide range of values. Thus, the benefits of developing an STES option vary over a wide range of values, from zero to $50 billion.

Figure 6 indicates that the payoffs to investments in STES R&D will be significant in either the high fuel price scenario and/or the high R&D success case. Conversely, with limited or moderate R&D success and low or medium future energy prices, the private market benefits are small or negligible. Furthermore, the benefits in this table ignore the cost of R&D. The R&D investment required to complete the development of STES is substantial relative to the assets of most potential private investors. If these costs are deducted from the net present values given in Figure 6, many of the values actually become negative. This indicates that private investments by profit-making firms will have a negative expected rate of return in some cases. Since private industry often seeks to minimize the maximum loss, the risk of achieving negative returns in the presence of low or medium energy prices will dissuade many firms from investing in STES. Thus, private industry alone cannot be expected to fund the development of cost-competitive STES.

The objectives of society, however, differ from those of a private profit-making firm. In contrast to private firms, the social objective may be to minimize the energy related costs which must be born by energy procedures and consumers. Thus, from society's point of view, the values expressed in Figure 6 represent costs incurred by not developing an STES option. If energy prices follow the high NEP III scenario, the costs of not developing STES will be substantial (between $10 billion and $50 billion). These costs can be avoided, however, if resources are devoted to the development of STES. Since private industry is not expected to fund this R&D, federal participation in the development of solar thermal energy technologies is required to ensure that the best interests of society are served.

The Demand for STES in IPH Applications

Based on a similar methodology as employed to evaluate solar thermal electric systems, it is also possible to derive the marginal value curves for industrial process heat applications (IPH) of STES under a variety of alternative fuel price scenarios. These curves are depicted in Figure 7 for three energy price scenarios corresponding to the NEP III low, medium and high cases (system costs are expressed in terms of $/m^2$ and assume a 60% system efficiency). The range of system costs which bound the 1990 cost target for STES in IPH applications are superimposed over these curves. As with electric

utility applications, the net present value of STES for any particular system cost can be estimated by calculating the area between the marginal value curve and the horizontal line corresponding to that price level.

The marginal values for the IPH market depicted in Figure 7 reflect a more literal tax incentive structure than was used in the case of electric utilities. This change resulted from a shift in expectations that occurred during the time interval between the electric utility analysis and the IPH analysis. As such, the marginal values associated with these two sectors are not directly comparable. Within a particular market sector, however, the analysis does indicate the relative value of developing an STES option under alternative levels of R&D success and fuel price scenarios.

The Net Present Value of Solar Thermal IPH Systems: Medium Oil Prices

Figure 8 shows the relationship between R&D success, as reflected by system costs, and the net present value of STES in IPH applications assuming NEP III medium energy prices. This figure indicates that limited penetration is expected for thermal applications of STES unless R&D succeeds in reducing costs below the $300/m2 range. As prices decrease below that level, however, market penetration and expected energy cost savings increase rapidly.

The Value of Solar Thermal IPH Systems: R&D Success vs. Energy Prices

The net present value of STES in IPH applications is summarized in Figure 9 for three alternative system costs and three energy price scenarios. The values in this figure are similar to those estimated for electric utility applications. If R&D success is limited, a small market for cost-effective installations of STES will exist in the high energy price case only. On the other hand, successful R&D will enable STES to penetrate IPH markets in all three energy price scenarios. The benefits from the IPH market, however, are smaller than those estimated in conjunction with electric utilities, ranging from zero to $40 billion, depending on the level of R&D success and future energy prices.

While the absolute benefits from solar thermal electric and IPH applications cannot be directly compared, the IPH values exhibit a pattern similar to those characterizing the electric utility market. Thus, a similar set of conclusions can be drawn for STES in IPH applications. In particular, the analysis indicates that the expected net benefits of developing an STES option are significantly greater than the expected costs of completing the required R&D. Despite this fact, there is a non-trivial probability that only a limited market for cost competitive solar thermal IPH systems will exist in 1990. Due to the tendency of private industry to minimize their maximum possible losses, the risk of supporting R&D which fails to produce an economically viable system will dissuade private industry from investing in STES. Thus, federal participation in the development of STES for IPH applications is required if this technology is to be available for wide-scale deployment during this century. Federal support is necessary to ensure that society avoids the substantial energy costs which would be incurred under the high energy price scenario in the absence of a STES option.

STES in Transportable Fuel and Chemical Feedstock Applications

There are three important characteristics of solar energy which limit its market potential in electric utility and industrial process heat applications. The solar resource is diffuse, intermittent, and site specific in nature. A number of technological concepts have been proposed to overcome these limitations. In particular, the development of concentrating collectors is designed to counteract the diffuse nature of solar radiation. Similarly, thermal storage is being developed to address the intermittent availability of insolation. Electricity grids are relied on to transport solar thermal electrical power between the collection and end use sites. Unfortunately, no comparable mechanism has been devised for long distance transport of thermal energy.

Fuels and chemicals provide a concentrated form of energy which can be transported with relative ease using currently existing systems. Furthermore, fuels and chemicals can be stored, and are available on demand regardless of the time of day. Thus, fuels and chemicals can serve many energy consuming sectors of the U.S., and their use is not limited by the regional or time dependent nature of solar radiation. As such, the market potential of fuels and chemicals produced by STES far exceeds that of the electrical and IPH applications described above.

The development of production processes for transportable fuels and chemical feedstocks utilizing STES present a number of interesting challenges, and the potential payoffs are tremendous. But, due to the basic state of this R&D, it is currently impossible to identify the most promising markets or quantify the potential benefits for this application of STES. As a result, this analysis will simply mention that this potentially significant market does exist. No attempt will be made to quantify these benefits. It is important to note, however, that the nature of basic R&D, which makes it impossible to quantify the potential benefits, will also limit the level of private investment in this category of STES R&D. Thus, if progress is to be made toward developing this important application of STES, federal participation will be required.

The Social Benefits Attributable to STES:
A Qualitative Evaluation

In addition to the private market benefits of STES, as measured by the value of reductions in energy-related costs, there are a variety of important social benefits as well. These benefits are not reflected in private market transactions, making estimation of their value very difficult. As a result, they are frequently excluded from analysis. Two social benefits are depicted in Figures 11 and 12. As discussed previously, the deployment of STES in electric utility applications will result in the displacement of a variety of fuel types. Initial STES installations will primarily affect the most expensive fuel types, including petroleum and natural gas. As STES penetration increases, however, a higher proportion of total fuel displacement will be accounted for by less expensive fuel types such as coal and nuclear. Figure 11 shows the quantity of each fuel type displaced by STES as market penetration increases (i.e., system costs decrease) for three energy price scenarios. These quantities represent the actual fuel displacements expected for each combination of energy prices and STES costs, and were used in calculating the marginal value of STES. This information can be used to assess the importance

304

of a number of non-market benefits. One such benefit is the reduction in oil imports and the corresponding increase in national security attributable to the development of an STES option. As indicated in Figure 11, the total potential life-cycle oil displacement attributable to solar thermal electric systems installed in 1990 will depend on both the fuel price scenario and STES costs. In particular, for low fuel prices oil displacement will vary from zero to 11.0 quads; for medium fuel prices the range becomes zero to 9.8 quads; and with high fuel prices oil displacement ranges between 3.1 and 8.6 quads. These values correspond to average annual oil displacements of zero to .37 quads, zero to .33 quads, and .10 to .29 quads respectively. In contrast, NEP-III predicts that total oil imports will vary between 4 and 15 quads per year in 1990. Oil imports are expected to decrease over time, ranging between zero and 7 quads per year by 2000.

Another social benefit is the environmental impact associated with increases in the quantity of fossil fuel burned. Figure 12 indicates the environmental impacts corresponding to the fuel displacements listed in Figure 11. In deriving these values, assumptions must be made regarding the sulfur and heat content of the coal and petroleum being displaced by the solar thermal systems. Furthermore, these values represent the net improvement in environmental quality attributable to STES. In other words, it was assumed that the best available pollution control devices were used in 1990. The values in Figure 12 indicate the level of pollutants not removed by these pollution control devices. There are a variety of other significant non-market benefits which can be qualitatively assessed in a similar manner. Figures 11 and 12 were merely presented to call attention to these benefits, and illustrate one manner in which these important considerations can be discussed.

Summary

To summarize, this discussion has established that solar energy systems complement nuclear and coal technologies as a means of reducing the U.S. dependence on imported petroleum. Furthermore, STES represents an important category of solar energy technologies. STES can be utilized in a broad range of applications servicing a variety of economic sectors, and they can be deployed in both near-term and long-term markets. Finally, the net present value of the energy cost savings attributable to electric utility and IPH applications of STES were estimated for a variety of future energy cost scenarios and levels of R&D success. This analysis indicated that the expected net benefits of developing an STES option are significantly greater than the expected costs of completing the required R&D. In addition, transportable fuels and chemical feedstocks represent a substantial future potential market for STES. Due to the basic nature of this R&D activity, however, it is currently impossible to estimate the value of STES in these markets. Despite this fact, private investment in STES R&D is not anticipated due to the high level of uncertainty characterizing the expected payoffs, and the non-trivial probability of realizing a large negative rate of return from these investments. Thus, federal participation in STES R&D is required if this valuable solar technology is to be available for deployment during this century.

FIGURE 1

- STES WILL PROVIDE COST COMPETITIVE ENERGY ALTERNATIVES FOR
  DEPLOYMENT IN A WIDE RANGE OF APPLICATIONS
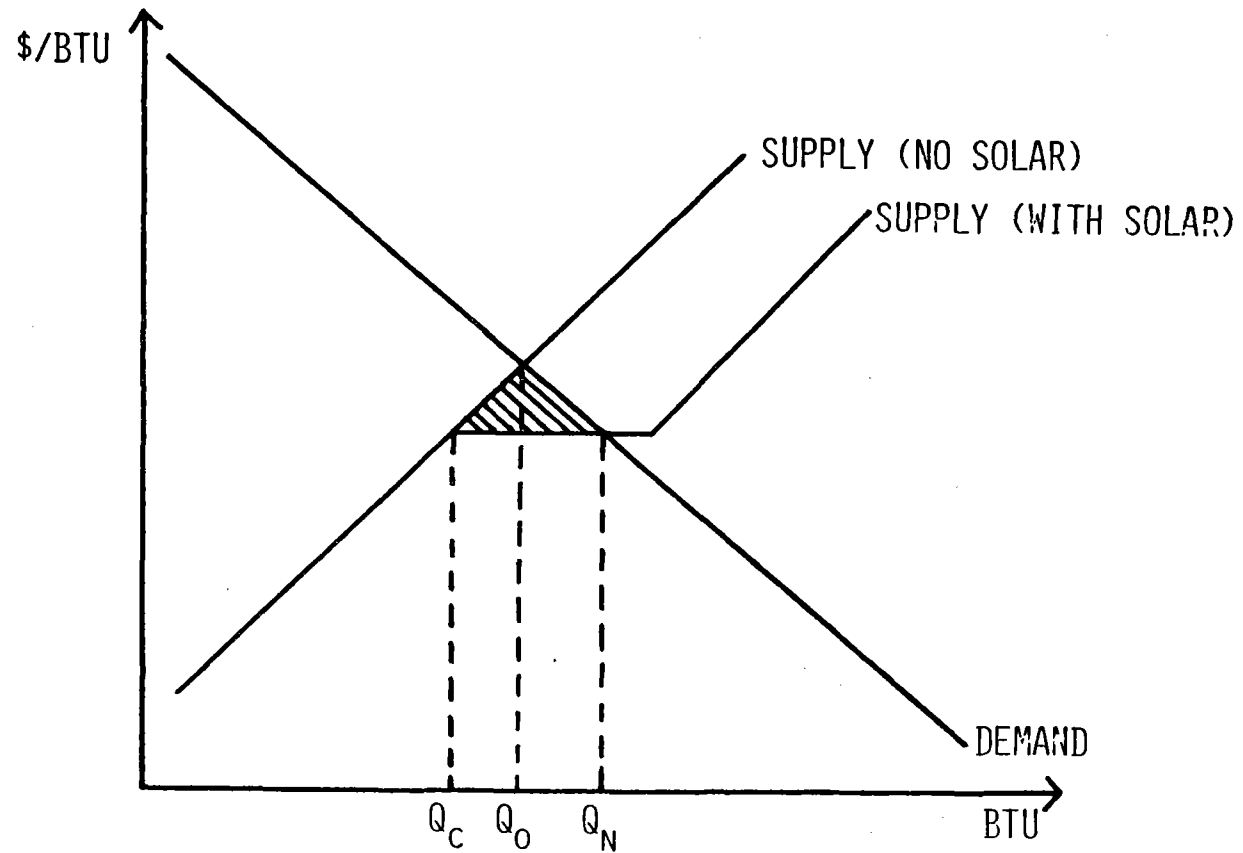
PROJECTED ELECTRIC UTILITY DEMAND FOR FUEL BY SOURCE (QUADRILLION BTU)

FIGURE 2

307
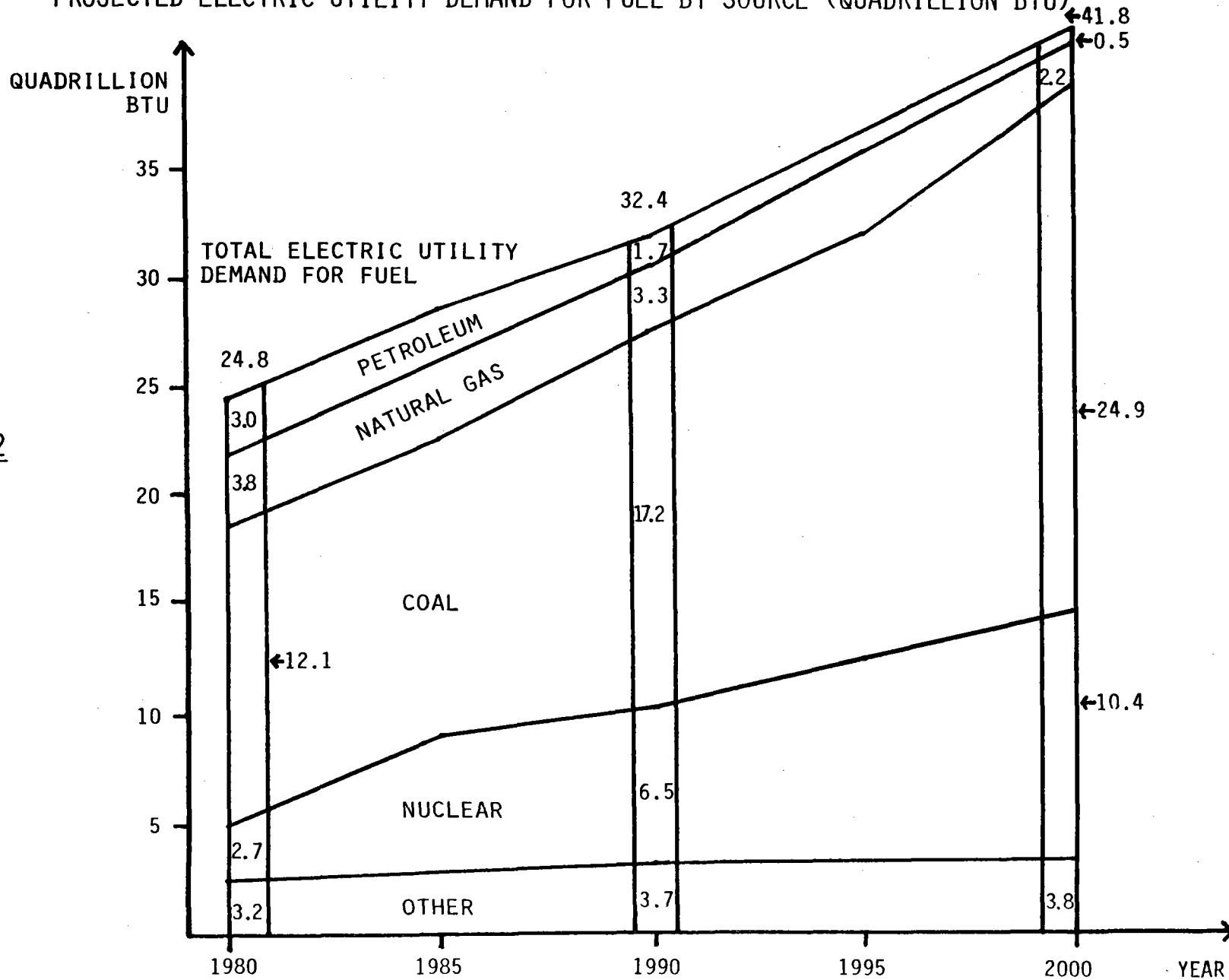
SOURCE: DATA RESOURCES, INC., ENERGY REVIEW, AUTUMN 1981, TABLE A-6, PAGE 181

PROJECTED U.S. PETROLEUM CONSUMPTION BY SECTOR (QUADRILLION BTU)
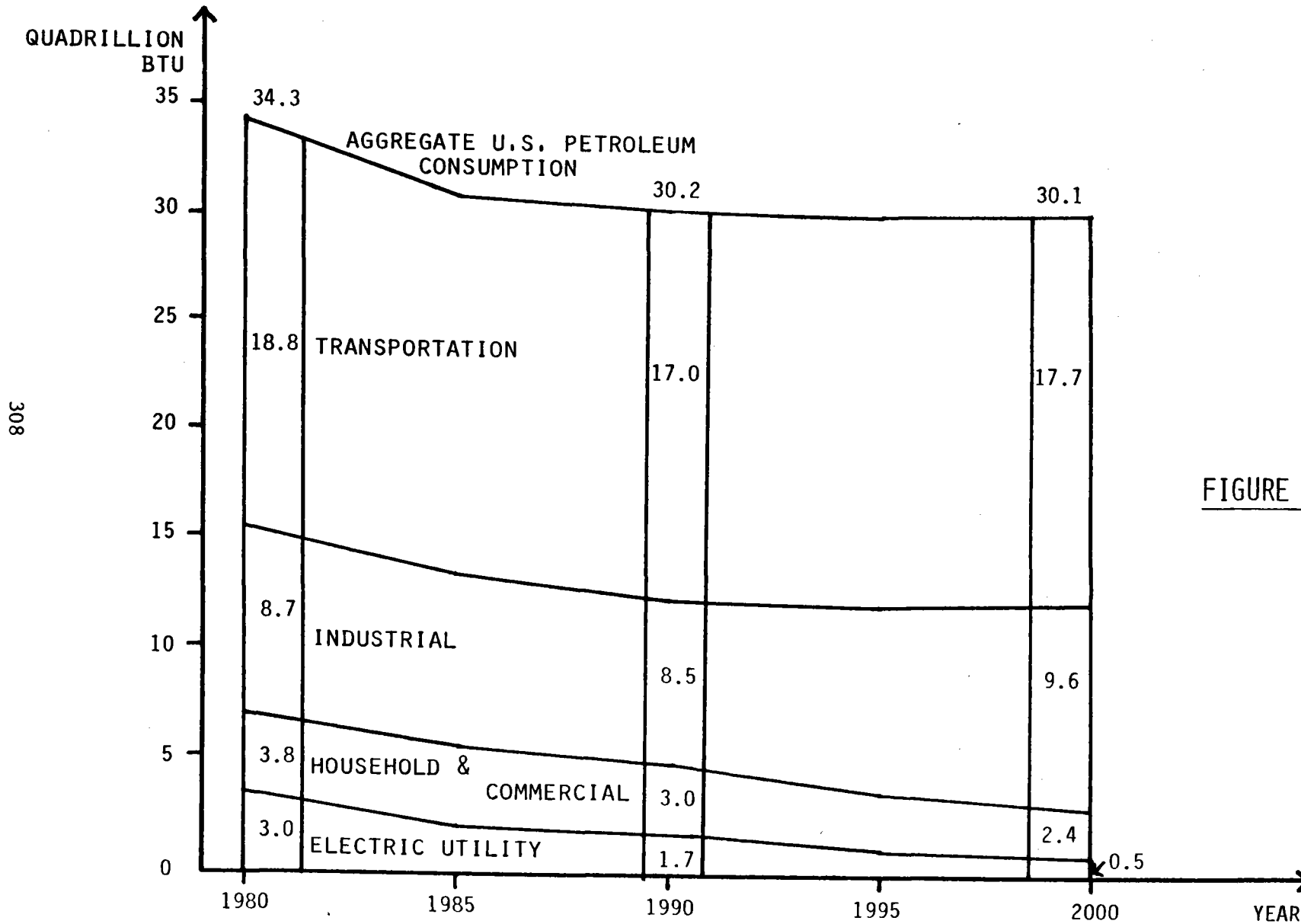
FIGURE 3

SOURCE: DATA RESOURCES, INC., ENERGY REVIEW, AUTUMN 1981, TABLE A-1, PAGE 178

FIGURE 4

MARGINAL VALUE OF SOLAR THERMAL SYSTEMS, DOLLARS PER kWe

HIGH OIL PRICES

MEDIUM OIL PRICES

(2100)

STES 1990 COST TARGET

LOW OIL PRICES

(1400)

1990 POTENTIAL AGGREGATE DEMAND FOR
SOLAR THERMAL ELECTRIC SYSTEMS, MEGAWATTS
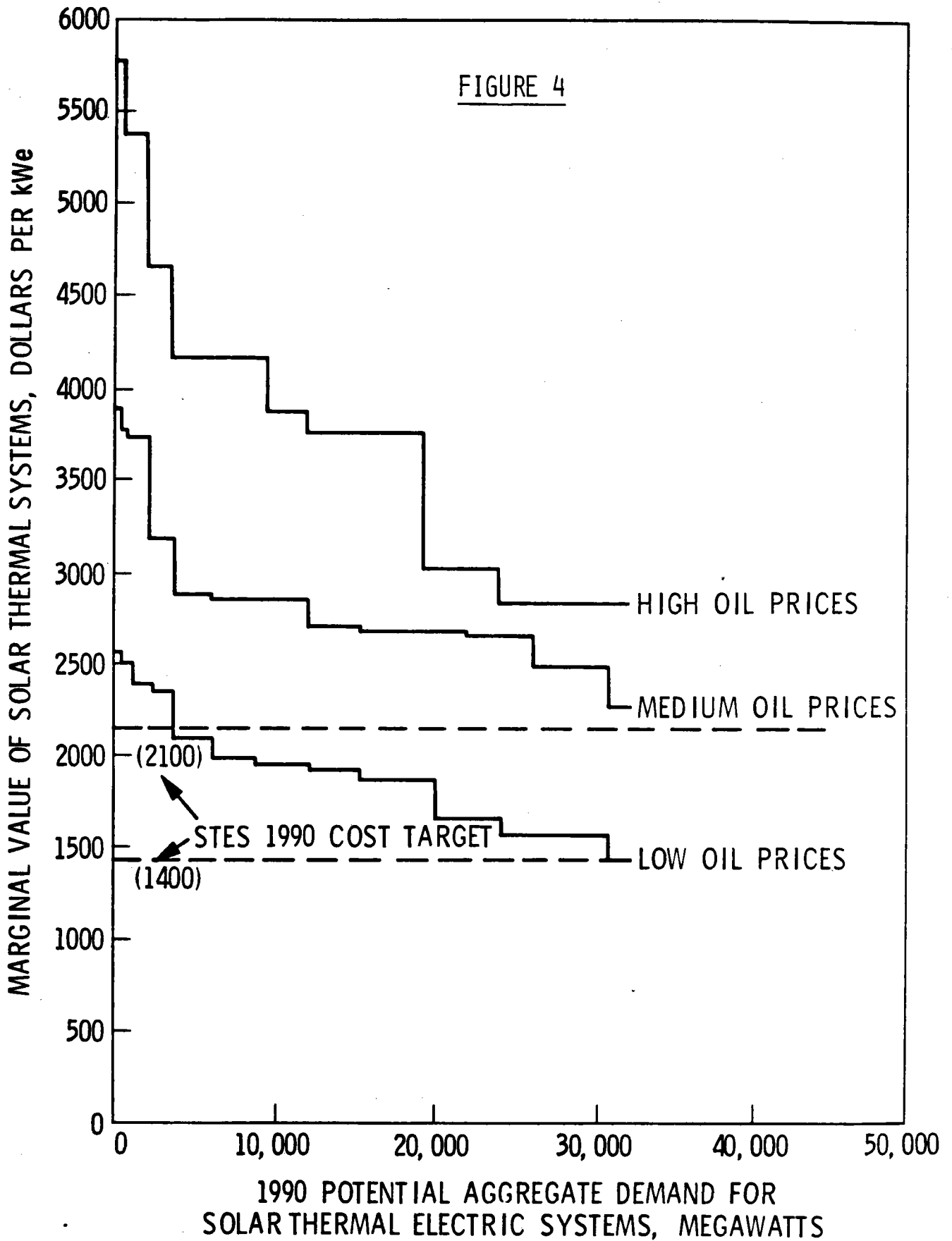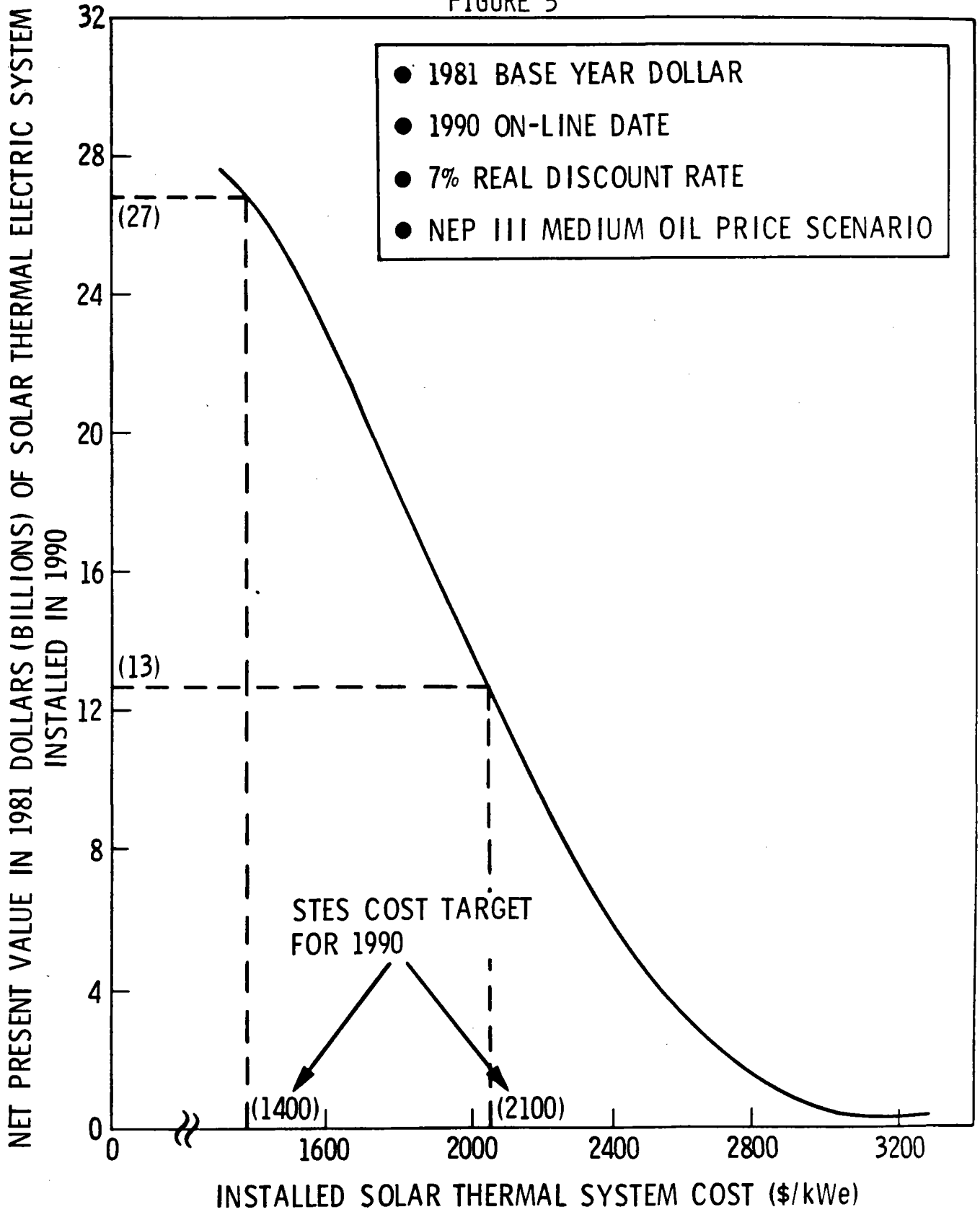
FIGURE 5

FIGURE 6

NET PRESENT VALUE IN 1981 DOLLARS (BILLIONS)
OF SOLAR THERMAL ELECTRIC SYSTEMS

STES R&D SUCCESS[2]	NEP III ENERGY PRICE SCENARIO[1]		
	LOW	MEDIUM	HIGH
$4,000/KW$_E$	0	0	10
$2,700/KW$_E$	0	2	14
$1,400/KW$_E$	9	27	50

[1] LOW, MEDIUM, HIGH REFER TO THE NEP III ENERGY SCENARIOS BASED UPON THE IMPORTED OIL PRICE OF 44, 52, 68 (1981 $/BARREL).

[2] LEVEL OF SUCCESS IS INDICATED BY THE INSTALLED SOLAR THERMAL SYSTEM COST (1981 $/KW$_E$).

FIGURE 7

1990 POTENTIAL AGGREGATE DEMAND FOR
SOLAR THERMAL IPH SYSTEMS, 10^6 M^2

312
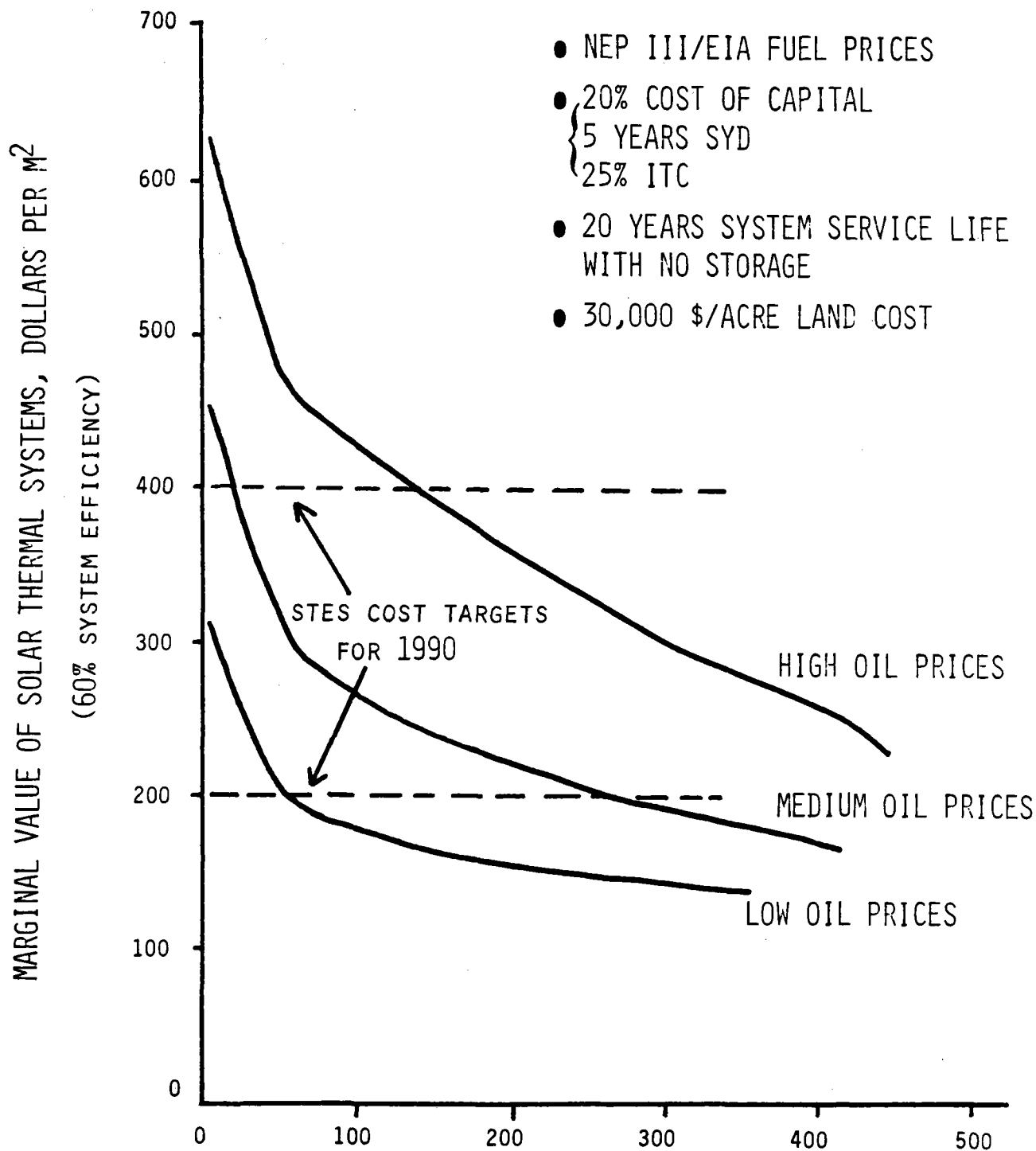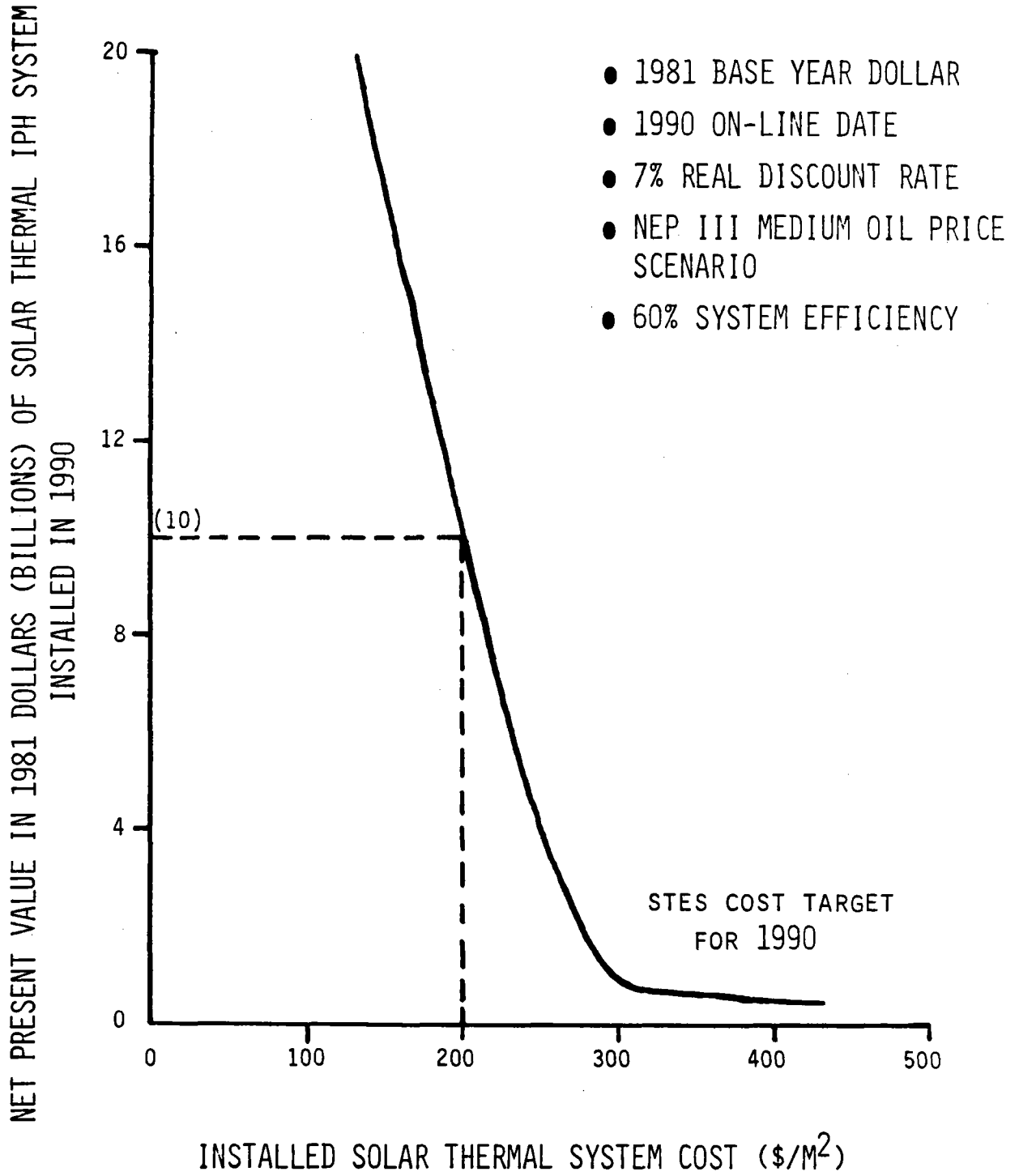
FIGURE 8

FIGURE 9

NET PRESENT VALUE IN 1981 DOLLARS (BILLIONS)
OF SOLAR THERMAL IPH SYSTEMS

STES R&D SUCCESS[2]	NEP III ENERGY PRICE SCENARIO[1]		
	LOW	MEDIUM	HIGH
$500/M^2	0	0	2
$300/M^2	0	1	17
$200/M^2	3	10	40

[1] LOW, MEDIUM, HIGH REFER TO THE NEP III ENERGY SCENARIOS BASED UPON THE IMPORTED OIL PRICE OF 44, 52, 68 (1981 $/BARREL).

[2] LEVEL OF SUCCESS IS INDICATED BY THE INSTALLED SOLAR THERMAL SYSTEM COST (1981 $/M^2 ASSUMING A 60% SYSTEM EFFICIENCY).

314

FIGURE 10

FUELS & CHEMICALS

FUEL DISPLACED BY STES

1981   Nov. 3, XXXX   YEAR
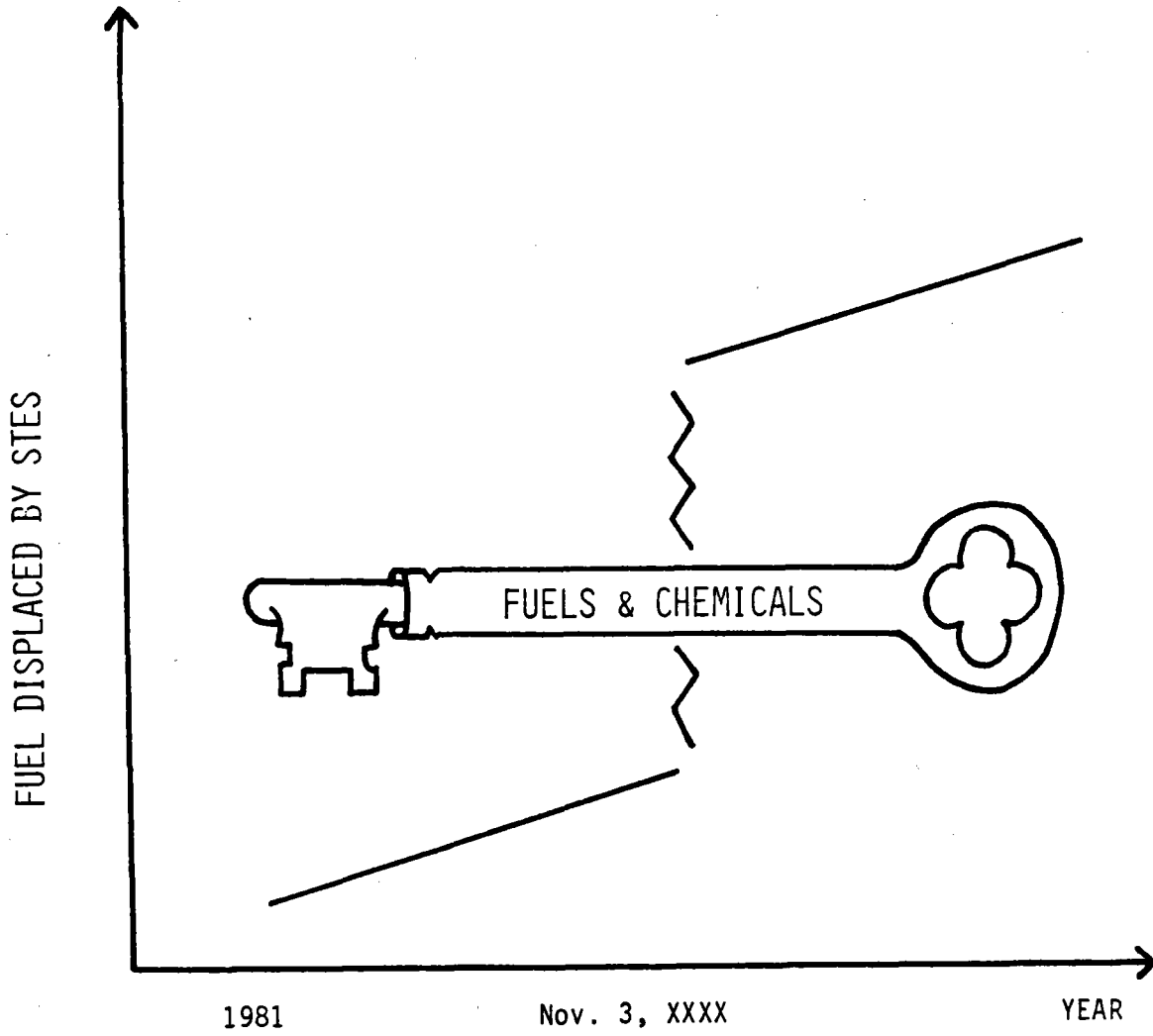
SOURCE: I.O.F.O., ANNUAL REPORT, 1982

315

FIGURE 11

STES TOTAL LIFE-CYCLE FUEL DISPLACEMENT (QUADRILLION BTU)

FUEL PRICE SCENARIO	LOW					MEDIUM					HIGH				
FUEL TYPE / STES COST ($/KW$_e$)	Nuclear	Coal	Gas	Oil	TOTAL	Nuclear	Coal	Gas	Oil	TOTAL	Nuclear	Coal	Gas	Oil	TOTAL
4000	0	0	0	0	0	0	0	0	0	0	1.2	1.0	3.2	3.1	8.5
2700	0	0	0	0	0	1.4	1.2	3.8	3.9	10.3	6.1	5.0	12.1	8.6	31.8
1400	5.0	4.7	11.8	11.0	32.5	5.4	4.7	11.9	9.8	31.8	>6.1	>5.0	>12.1	>8.6	>31.8

FIGURE 12

STES POLLUTION ABATEMENT IMPACT FOR SELECTED EFFLUENTS
(IMPROVEMENT OVER BEST AVAILABLE CONTROL TECHNOLOGY - 1990)

- LOW SULFUR COAL (.5%)
- 13,000 BTU/LB.
- PETROLEUM - .5% SULFUR

OIL PRICE SCENARIO \ EFFLUENT / STES COST($/KW$_e$)	LOW			MEDIUM			HIGH		
	CO_2 (10^6 tons/yr.)	SO_x (10^3 tons/yr.)	NO_x (10^3 tons/yr.)	CO_2 (10^6 tons/yr.)	SO_x (10^3 tons/yr.)	NO_x (10^3 tons/yr.)	CO_2 (10^6 tons/yr.)	SO_x (10^3 tons/yr.)	NO_x (10^3 tons/yr.)
4000	0	0	0	0	0	0	20	4	14
2700	0	0	0	9	2	6	75	12	50
1400	80	13	55	>75	>12	>50	>75	>12	>50

SUMMARY

- Solar energy technologies, including STES, can complement coal and nuclear systems in electric utility applications.

- STES serves a wide range of energy consumers and economic sectors.

- The expected net present value of STES in electric utility and IPH applications exceeds the cost of completing the R&D program. (The benefit/cost ratio for the Federal STES Program exceeds 30:1.)

- Transportable fuels and chemical feedstocks represent a significant long-term potential market for STES.

- Private investment in STES R&D is not anticipated.

FEDERAL PARTICIPATION IN STES R&D IS REQUIRED IF THIS VALUABLE SOLAR TECHNOLOGY IS TO BE AVAILABLE FOR DEPLOYMENT DURING THIS CENTURY.

318

CONFIGURATION SELECTION STUDY FOR ISOLATED LOADS USING PARABOLIC DISH MODULES*

W. Revere **, J. Bowyer[†], T. Fujita[†], H. Awaya[‡]
Jet Propulsion Laboratory
4800 Oak Grove Drive
Pasadena, CA 91109

Abstract

A configuration tradeoff study has been conducted to determine optimum solar thermal parabolic dish power systems for isolated load applications. The specific application of an essentially constant power demand as required for MX missile shelters is treated. Supplying a continuous level of power with high reliability is shown to require a power system comprising modular parabolic dish power units where the heat engines of the modular power units can be driven by fossil fuels as well as solar-derived heat. Since constraints on reliability result in the provision of a power generating capability that exceeds the constant demand level, efficient utilization of the power system requires battery storage. Tradeoffs regarding the optimum size of storage are investigated as a function of the number of power modules and the cost of the fossil fuel which is used to meet the demand when insolation is unavailable and storage is depleted.

Introduction

Early opportunities for implementing modular solar thermal parabolic dish systems include isolated load applications[1,2]. This paper investigates configurational tradeoffs for a particular isolated load application involving the use of parabolic dish systems to supply power for MX shelters. The basic configurational layout is shown in Fig. 1. The
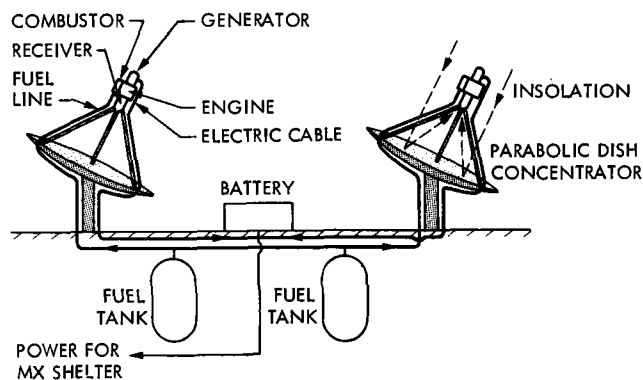
Figure 1 Parabolic Dish Power System for MX Shelter

power module comprises a two-axis tracking parabolic dish concentrator which focuses

sunlight into the aperture of a cavity receiver located at the focal point of the dish concentrator. The heat created in the receiver is used by the engine/generator assembly to produce electricity[3,4,5]. When sunlight is is available, the electrical energy from the modules (two are shown in Fig. 1 for illustrative purposes) is supplied to the MX shelter with excess energy being stored in batteries. On an annual basis, a very small amount of the excess energy is wasted when batteries are fully charged. The extra cost of batteries to capture the wasted energy is not cost-effective from an overall system optimization view-point. When insolation is unavailable and batteries are depleted, fossil fuel is used to operate the engine/generator assemblies.

From the viewpoint of selecting a configuration, there are several key tradeoffs associated with the arrangement illustrated in Fig. 1. For the high reliability required by the MX application, use of multiple units or multiple combinations of units that can meet the load requirements is considered to be a more practical and achievable approach than trying to develop a single unit that can satisfy the stringent MX reliability requirements. The multiple unit approach to reliability results in power generating capacity that exceeds the load by at least a factor of two. Effective utilization of this excess capacity requires electrical energy storage in batteries. Due to the occurence of extended periods of inclement weather, provision of a fossil fuel system is needed to meet load requirements. The alternative of providing a large solar system with long storage times is not considered to be cost effective[6]. Given the need for both battery storage and the ability to operate from fossil fuels, key configurational tradeoffs involve the size and number of dish power modules, expected reliabilities, and the split between solar and fossil fuel usage based on economic considerations oriented toward selecting the configuration with the lowest life-cycle cost.

Insolation characteristics affect the performance and economics of solar systems as shown in regional studies, where the operation of solar plants was investigated over a wide range of variations in regional insolation.[6] The proposed MX shelter-concept is to be located in the southwestern United States. For purposes of determining first-order trends, the insolation from a particular site, namely Barstow, CA, was taken to be representative of the southwestern region.

The objectives of this paper are to (1) examine the first-order effects of key configurational tradeoffs as an input to those who are considering the use of solar power for MX shelters and (2) provide general insights regarding the types of tradeoffs that are

encountered when contemplating the use of solar power for isolated load applications. In the following section, key results of the investigation are presented. Then, the three factors of power system operational modes, economic scenarios (e.g., fossil fuel price escalation rates), and solar system performance and costs are discussed in terms of their influence on the results. To provide detailed background, a summary of the analytical basis used in performing tradeoffs is provided. Finally, conclusions are drawn regarding the specific MX application as well as general insights for isolated load applications.

Key Results

Configurational variations treated in this paper are based on developmental activities that are underway in the DOE-sponsored Parabolic Dish Program [7]. The baseline dish concentrator has an 11 meter diameter. An alternative is a small ≈ 7 meter diameter dish based on adaptation of heliostats developed within the Central Receiver Program for use at the 10 MW$_e$ solar plant near Barstow, CA.

For the anticipated mid-eighties implementation of the MX missile system, engine possibilities include the Rankine, Brayton, and Stirling cycles. The Brayton engine is considered to be representative of the level of performance that could be achieved, and hence, projected Brayton cycle performance characteristics [5] are employed in this paper. The selection of the most appropriate engine for the MX involves detailed tradeoff analyses that are beyond the scope of this paper.

In the mid-eighties, improved lead-acid batteries appear to be the most likely candidate for energy storage. However, DOE-sponsored advanced battery development activities indicate that vastly improved batteries could be available in the 1990-2000 timeframe. Since these advanced batteries could be available as replacements for lead-acid batteries during the operational life of the MX system, both lead acid and advanced battery systems are analyzed. The Iron-Chromium Redox battery [8] being developed at NASA Lewis Research Center is considered to be representative of the level of improvement that could be available. Thus, its projected performance characteristics are used in this paper.

Using projected performance, cost, and reliability characteristics for solar power system components [5] and projections of fuel price relative to general inflation as determined by Data Resources Inc., [9] the above configurational variations have been investigated to delineate the most cost effective arrangements for meeting MX requirements. The primary findings are summarized as follows:

° For real fuel escalation rates ≥ - 2%/year, parabolic dish solar systems are more cost effective than a conventional fossil fuel system for the remote-site MX Application.

° For the baseline real fuel escalation of 4%/year, the most

cost-effective configurations supply a large fraction (~0.70) of the annual energy consumption from solar energy with the remainder being derived from fossil fuels.

° Modular power systems are required to meet high reliability requirements.

Reliability Requirements

Employing characteristics of first generation parabolic dish systems that are being developed for use in the mid-eighties to 1990 timeframe of the MX, the rated power output of the 11-meter dish is 23 kW$_e$ at a insolation level of 1 kW/m^2. The smaller dish (≈7-meter equivalent diameter) has a output of 10 kW$_e$ under similar conditions. Based on currently available information, a single shelter for the MX missile requires a constant 14.5 kW$_e$ on an essentially non-interrupted basis (24 hours per day for 365 days per year). Occasional excursions of one-hour duration to a power level of 21 kW$_e$, must also be accommodated. Although one 11-meter dish or two 7-meter dishes could approximately meet the peak load requirements, provision of two 11-meter dishes or three 7-meter dishes is chosen as the minimum requirement to meet the 21 kW$_e$ peak load with a comfortable margin of reserve power.

Reliability considerations cause a further increase in the number of dish power modules as shown in Fig. 2. The reliability requirements
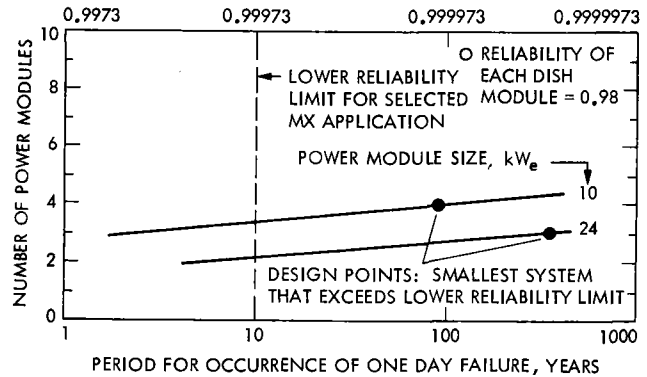
Figure 2 Reliability of Parabolic Dish Systems in Meeting MX Shelter Load Requirements

for the power supply to MX shelters is under investigation, but as a point of reference a value of about 0.9999 has been mentioned. Thus, as a lower bound figure, a value of 0.99973 corresponding to a failure of one day in ten years is used in the present study. It is seen that three 23 kW$_e$ power modules or four 10 kW$_e$ modules are required to exceed this lower reliability limit. Even if MX requirement studies indicate that still higher reliabilities are needed, the potential of achieving extremely high values for modular systems is evident from Fig. 2.

The analysis for Fig. 2 is based on a 0.98 reliability for each dish module and treats only the primary load of 14.5 kW$_e$ which is to be supplied on a continuous basis. It is expected that the need for occasional excursions to 21 kW$_e$

will have only a second-order impact on the results. The reliability of the dish module is governed by the reliability of the fossil fuel-fired power conversion system since the failure of any solar collector component (e.g., tracking assembly or receiver) can be over-ridden by using fossil fuels to generate power and meet load requirements.

For modular dish systems, the availability of power to the load is close to the value for reliability since maintenance on any given module can be scheduled to coincide with the period when that module is normally inoperative. If the system were not modular, the reliability would have to be directly reduced by scheduled maintenance to determine availability.

The ability to plumb spare engine/generator assemblies into the fossil fuel line provides an important degree of freedom in selecting optimal systems. From a reliability standpoint, these engines have the same effect as a solar dish module. Thus, if the number of power modules required to satisfy reliability requirements exceeds the number of solar modules corresponding to an optimum configuration, the reliability can be satisfied by plumbing the desired number of relatively inexpensive engine/generator assemblies into the fuel line.

Cost-Effective Configurations

Cost effective configurations are defined as those which produce the required energy at the lowest cost per unit energy, where cost includes capital equipment, fuel, and operation and maintenance (O&M). The dominant cost items are the capital costs of solar equipment and the cost of fossil fuel. As the number of solar dish modules is increased, the capital cost of solar equipment increases and the fraction of the energy derived from solar increases. The fuel costs correspondingly decrease. Thus, by varying the number of dish modules and the associated battery storage size, the cost associated with generating the required energy can be varied and the configuration with the lowest cost can be determined.

For the selected operating mode where the power system does not utilize fossil fuels until all solar-derived energy including energy from storage is depleted, the minimum energy cost for the fossil fuel hybrid system occurs when the marginal cost of energy associated with solar operation equals the marginal cost of energy during operation using fossil fuels. Defining energy costs as an annualized cost (associated with both capital and operation and maintenance) over the annual energy delivered, the marginal cost of energy is the incremental change in annualized cost over the associated incremental change in annual energy delivery.

The nomograph of Fig. 3 utilizes the equality of marginal costs of energy for the solar and fossil-fuel modes of operation to delineate optimum or cost effective hybrid con-
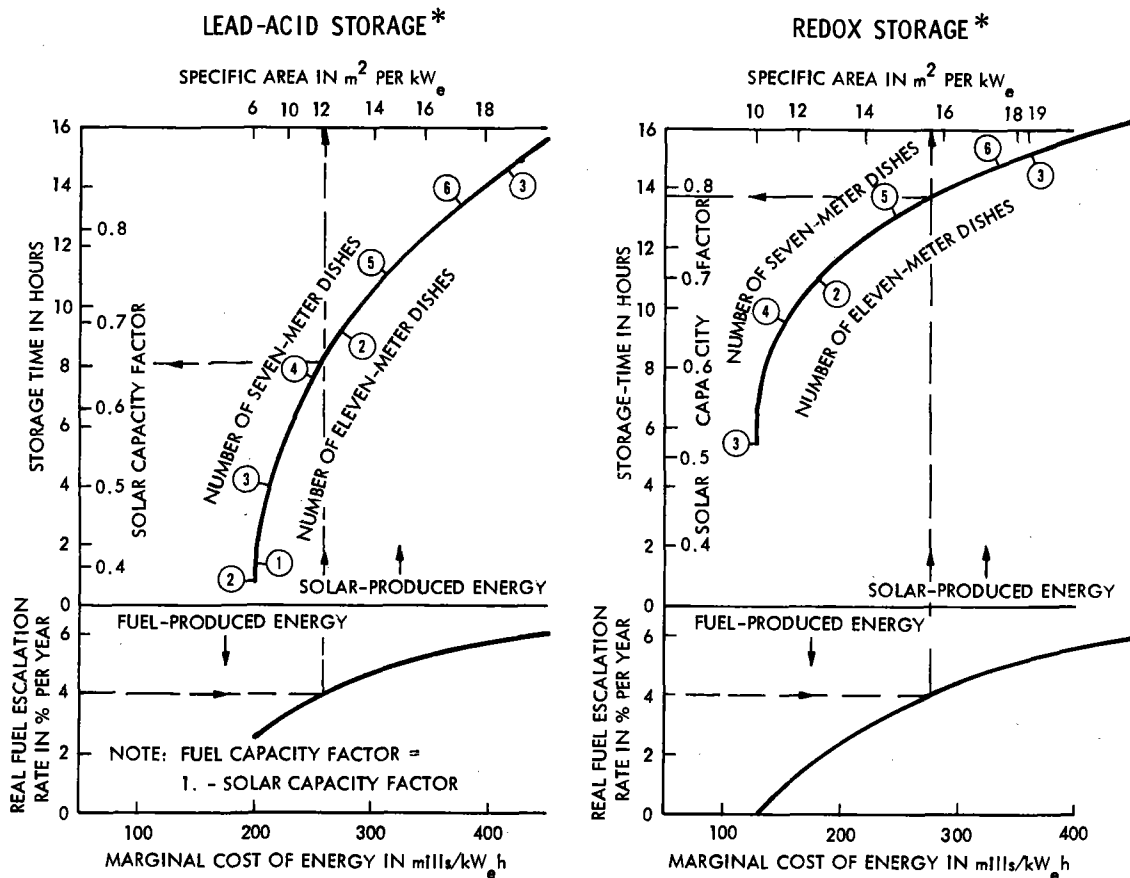
Figure 3   Nomographs for the Selection of Cost-Effective Solar/Fossil Power Systems

321

figurations. Based on DRI data[9], distillate fuel prices are $0.26/l ($1/gal) in 1981 and the nominal real fuel escalation is estimated to be ≈4% over the long-term interval encompassing the thirty year operating period of the system following startup in 1986. Thus, if one enters the nomograph at a real fuel escalation rate of 4%, the marginal cost of energy, number of dish modules, solar capacity factor, storage time, and specific area can be read from the nomograph as illustrated in Fig. 3.

The solar capacity factor is the fraction of energy derived from insolation. For the system with lead-acid battery storage, this fraction is about 0.65 whereas with Redox storage a value of nearly 0.80 is shown to be optimal. As expected, use of lower cost, advanced batteries such as Redox tends to shift the optimum configuration toward greater solar energy usage. For the essentially constant-power MX application, the fraction supplied by fossil fuels is simply unity minus the fraction from solar energy.

The bottom curves of the nomograph pertain to fuel-derived energy and are not identical for the lead-acid and Redox charts because the marginal cost is a function of the fuel capacity factor and the fuel capacity factor for the optimum configuration is different for the two cases. The cost for operation from fossil fuels includes the additional equipment (combustor, fuel tank, fuel lines, and fuel pump) to achieve fossil fuel operation, the O&M associated with this equipment, additional engine-generator O&M associated with fossil fuel operation, and fuel consumed. To determine the energy cost associated with operation from fossil fuels, these costs are annualized and divided by the annual energy generated during fossil fuel operation. Due to the inclusion of cost items other than fuel, the energy cost and the associated marginal cost are functions of capacity factor.

To obtain a larger solar capacity factor, the number of dish modules is increased along with the size of the battery. The larger number of modules generates more excess solar-derived energy which is diverted to an enlarged battery storage unit for discharge during periods when insolation is not available. The storage time is a measure of battery storage system size. It represents the time period during which a fully charged battery system can supply rated power (in this case, 14.5 kW_e). The optimal storage time for the system using lead-acid batteries is about 8 hours whereas the system employing Redox batteries requires almost 14 hours.

The specific area is defined as the total concentrator aperture area over the rated power output of the power system. For a fixed power rating, this parameter is directly proportional to the number of dishes. Since only two dish sizes of 11-meter and 7-meter equivalent diameter were selected, it is seen from Fig. 3 that the optimum configuration generally is not coincident with a finite number of dish modules. The selection of a cost-effective configuration with a finite number of either 11-meter or 7-meter diameter modules depends on the relative penalties associated with selecting either the lower or higher number of dishes which bracket the optimum value.

The effect of departing from the optimum value corresponding to the lowest energy cost for the hybrid power system is shown in Fig. 4 for both the lead-acid and Redox storage systems. The term, levelized busbar energy cost, refers to a specific discounted cash flow procedure for determining a single value for energy cost that is representative of the power system over its operating lifetime[10]. For the baseline real fuel escalation rate of 4%/year, a selection of two 11-meter dishes or four 7-meter dishes provide hybrid system energy costs that are very close to the minimum value for the system using lead-acid batteries. Use of five 7-meter dishes result in only a very slightly greater penalty whereas use of three 11-meter dishes yields a significant ≈30% increase in energy cost. For the system using Redox battery storage, use of five 7-meter dish modules is very close to the optimum while the use of either two or three 11-meter dishes results in a small ≈4% increase in energy cost.

Referring to Fig. 2, it is seen that all of the systems based on the 4%/year real fuel escalation rate meet the reliability criteria with small penalties from the optimum except for the 11-meter lead-acid storage system which uses two modules. Since use of three modules to meet reliability constraints results in a penalty of ≈30%, the most cost-effective solution would appear to be the use of a fossil-fuel-fired engine-generator unit plumbed into the fuel supply line. This unit would add only a small increase to the energy cost of the optimum two-module system while providing the desired reliability.

For real fuel escalation rates in the range of 0-4%/year, it is seen from Fig. 3 that optimum hybrid dish power systems with battery storage exist when Redox storage is used. For systems using lead-acid battery storage, solutions in the range of 0-2.5%/year are not shown since they represent departures from the ground rules pertaining to the systems presented in Fig. 3. In this low fuel escalation range for systems using lead-acid battery storage, there are essentially two solutions involving use of solar energy. First, a single 10 kW_e power module with no storage can be used. This unit would supply about 20% of the required annual energy at an energy cost of ≈86 mills/kW_e hr. The remaining energy would be supplied by fossil fuels. Since the lower-bound energy cost associated with fossil fuel operation at zero real fuel escalation rate is found to be ≈150 mills/kW_e hr, the use of a 10 kW_e module is justified from economic considerations. In fact, the real fuel escalation rate would have to drop to ≈-2% before fuel energy costs would decrease to a level equal to the energy cost from the solar module. This solution differs from those of Fig. 3 because the power level of a single 10 kW_e module is less than the system load of 14.5 kW_e and must therefore be continuously augmented by fossil fuel operation. Since about 80% of the energy is supplied by fossil fuels, the solar system serves primarily as a fuel saver whereas, for baseline systems in Figs. 3 and 4, the solar system is the primary power source.

The second solution involves either the use of a single 23 kW_e power module or two 10 kW_e modules. As seen from Fig. 3, the optimum solution employing lead-acid battery storage results
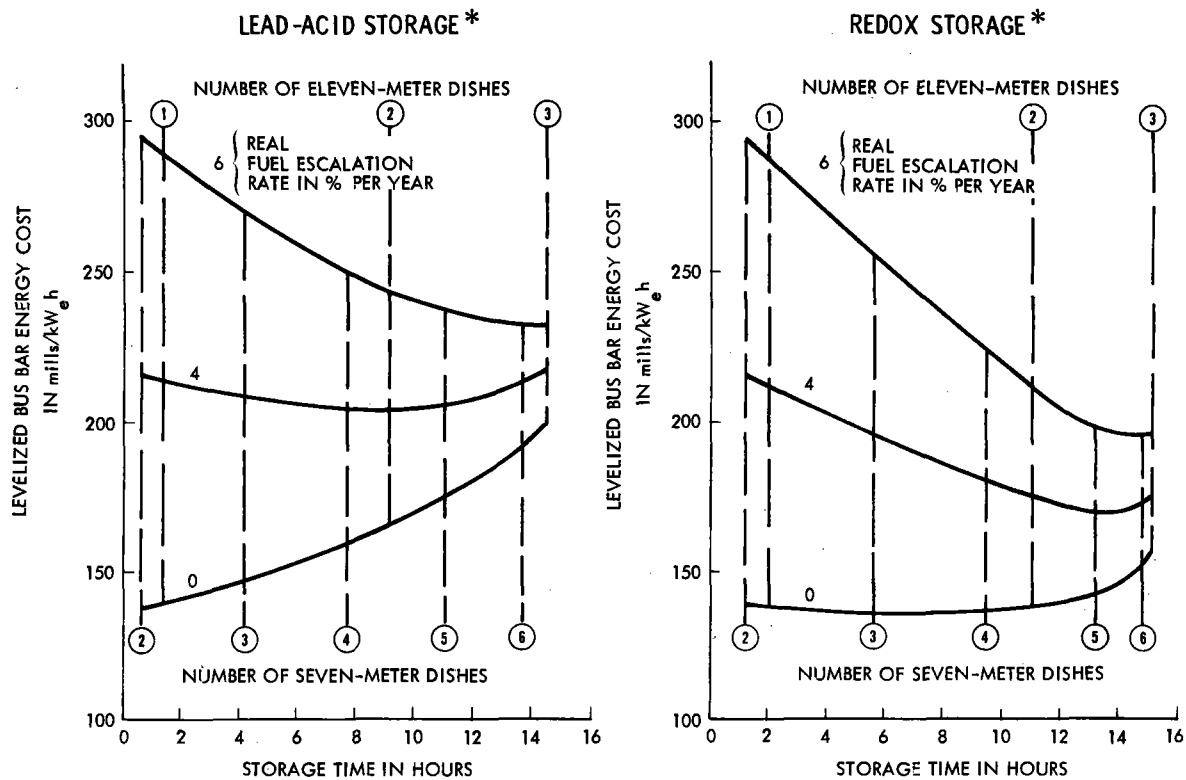
Figure 4   Energy Costs for Combined Solar/Fossil Power System

in a relatively low storage of ≈ 1 hour. For these low storage times, the elimination of battery storage results in a significant decrease in energy costs along with a relatively small decrease in energy delivery [5,6]. If the costs of battery storage were eliminated and all the energy were delivered, the energy cost could be essentially the same as the 10 kW_e module, i.e., the energy cost would be ≈ 86 mills/kW_ehr. However, since the power output exceeds the load, energy is wasted and the actual energy cost from the solar system is estimated to be ≈ 106 mills/kW_ehr. This value is below the ≈ 150 mills/kW_ehr for the zero real fuel escalation rate. Thus, use of either a single 23 kW_e power module or two 10 kW_e modules is justified on economic grounds. This solution differs from those shown by Fig. 3 since it involves a solar configuration that does not operate as stipulated to obtain the optimum solar curve presented in that figure.

The baseline case selections and tradeoffs described above are considered to be a subset of the choices facing decision makers. Variations in fuel escalation rates and the anticipated future availability of advanced battery systems such as Redox have an interactive influence on decisions and strategies. The possibility of fuel escalation rates that are higher than the baseline and the future availability of advanced batteries both tend to force decisions in the direction of higher solar usage than indicated for the lead-acid system. If fuel escalation rates are lower than the baseline, the selected baseline lead-acid system would be off-optimum in the direction of using too much solar energy. The future availability of advanced batteries would tend to compensate

and bring the system closer to the optimum.

There are clearly a number of options that can be exercised. The inherent modularity of dish systems permits the selection of options that minimize risk. For example, optimum systems using lead-acid storage as determined using baseline assumptions can be installed in 1986. If fuel escalation rates are found to be higher than the baseline, additional dish modules and batteries can be added. Also, when advanced batteries become available, the number of dish modules can be increased at the same time that the lead-acid batteries are replaced.

Comparisons with Conventional Systems

All of the curves in Fig. 4 exhibit a minimum energy cost at a finite storage time except for the curve corresponding to a zero real fuel escalation rate for the system using lead-acid battery storage. Those curves which show a minimum indicate that the hybrid solar/fossil fuel parabolic dish power system will be more economical than a conventional fossil fuel system. If the conventional fossil fuel system were less expensive, the curves would not exhibit a minimum at a finite storage time but, instead, would have their lowest values at zero storage time.

It is noted that, for baseline conditions of a 4%/year real fuel escalation rate, there is a large advantage associated with use of optimum hybrid systems as compared to conventional systems, particularly for systems which are based on the use of advanced Redox battery storage. The energy cost of conventional fossil fuel systems based on a 4%/year real fuel escalation rate is

found to be approximately 275 mills/kW$_e$hr, whereas the optimum hybrid plant with Redox storage has an energy cost of 170 mills/kW$_e$hr as shown on Fig. 4. Thus, the conventional system will have an energy cost that is about 60% greater than the optimum system using Redox batteries.

Selected Operational Modes

When considering a hybrid fossil fuel/solar power system, there are numerous strategies for operating the system. For example, the fossil combustor can be placed in series with the solar receiver so that the fossil combustor raises the temperature of the heat transfer medium leaving the receiver before it enters the engine. This has the advantage of allowing a lower solar receiver operating temperature with an associated reduction in reradiation losses while providing the high temperatures needed for efficient engine operation. There are also mixed-mode strategies where the combustor might be used even if battery storage is not depleted. Tradeoff considerations would involve factors such as extension of battery life by limiting charge-discharge cycles.

An investigation to assess optimal hybrid operating modes is beyond the scope of the present paper. Since the intent is to gain insight into the first-order tradeoffs between relative usage of solar and fossil fuels in the context of employing battery storage, a simple operating strategy which decouples the solar and fossil fuel modes of operation is adopted. This choice simplifies the analysis by allowing direct use of previous work [5,6] wherein the optimum configurations for parabolic dish solar power systems using battery storage were delinated. These optimum solar systems constitute a baseline configuration for the solar mode of operation. For the fossil fuel mode of operation, combustors, fuel tanks, fuel lines, pumps and associated controls are added. Since the modes are essentially decoupled, a relatively simple optimization criterion involving marginal costs for energy, as described previously, can be derived. Optimization of mixed-mode operating strategies would be much more complex.

Baseline Economic Scenario

The economic scenario assumed for the period from the present through the operating life of the power system has a strong influence on the optimum split between the solar and fossil fuel energy usage of a hybrid power system. Since the relevant time period is of the order of thirty years, it was decided to emphasize the use of nominal values for economic and financial parameters which are predicated on long-term trends. Baseline values used in this paper are given in Table 1.

One of the most powerful parameters which influences the results of the study is the real escalation rate for fuel. Based on a review of historical trends, there is no precedent for a long-term rate that is as high as 6%/year. Thus, this value is used as an upper bound in Figs. 3 and 4. Current trends and projection studies indicate that a value as low as a zero fuel escalation rate is unlikely, particularly over the next thirty years. The value of zero fuel escalation rate is therefore used as a lower bound.

Table 1. General Economic and Financial Parameters

Description of Parameters	Baseline Values
General Economic Conditions	
Rate of General Inflation, %/year	6[1]
Real Escalation Rate for Capital Costs, %/Year	0
Real Escalation Rate for Operating and Maintenance Costs, %/Year	1[2]
Real Escalation Rate for Fuel, %/Year	4[3]
Base Year for Costs	1981
Financial Parameters (Government Installation)	
Effective Income Tax Rate	0
Annual Miscellaneous Tax Rate and Insurance Premiums as a Fraction of Capital Investment	0
Internal Rate of Return (Discount Rate), %/Year	11[4]
First Year of Operation	1986
Plant Construction time, years	1
Economic Life of Plant, years	30

(1) A general inflation rate of 8.5% for 1981 to 1986 and of 6% for 1986 to 2016 have been derived from DRI's GNP deflator statistics (Ref. 9). Since the higher initial rate has a small effect that is considered to be within the uncertainty range of the long-term estimate, a nominal value of 6% is used.

(2) Labor-related operation and maintenance (O&M) costs have historically escalated at a faster rate that general inflation. Based on long-term trends, a value of 1% above the 6% general inflation rate is assumed.

(3) Fuel escalation rates are based on DRI data (Ref. 9) for distillate fuel costs; these costs indicate higher values than those usually projected by econometric models, the higher value of 4% is used.

(4) The rate of return of 11% nominal (5% real) corresponds to an intermediate value that is higher than the long-term trend of about 2% real escalation but lower than Office of Management and Budget (OMB) suggestions of a 10% real rate.

It is noted that financial parameters for taxes and insurance premiums are zero for Government projects such as the MX power system. These factors would tend to favor capital intensive Government projects in comparison to the private sector. However, recent changes in depreciation schedules for the private sector tend to offset this effect by similarly shifting the balance in favor of capital intensive projects. Thus, overall trends based on using financial parameters for Government projects are expected generally to hold hold for the private sector.

Parabolic Dish System Performance and Costs

The performance and cost characteristics used for parabolic dish systems in this study are based on first generation systems that will be undergoing module development testing (scheduled to start

in the latter part of CY 1981). For the selected representative module which uses a Brayton engine, the 11-meter dish produces 23 kW$_e$ at rated conditions of 1 kW/m^2 of insolation. Based on an effective reflective surface area of 92 m^2, the system efficiency is 25%, where this efficiency is defined as the net electrical energy output over the energy incident on the effective reflective surface. The engine-generator efficiency is approximately 30%. The system efficiency of the 7-meter dish is slightly lower (24%) due to the lower efficiency of the smaller engine.

Since costs are strongly influenced by production volume, the potential production levels associated with providing power for MX shelters is estimated. Based on 4200 shelters and two 11-meter dish modules per shelter, the total number of dish modules is 8400. Assuming that the modules are produced during a four-year period so that the complete MX shelter system is in operation by 1990, a production rate of ≈ 2000 modules/year is required. For the 7-meter dish module, the baseline system with lead-acid battery storage can use either 4 or 5 modules per shelter. If five modules per shelter are used, the production rate is ≈ 5000 modules/year using the basis described above.

Using the above production rates, the costs for the 11-meter and 7-meter dish modules were estimated. Although the cost breakdowns were slightly different for the two modules, the total installed costs normalized to the rated power output were found to be essentially equal for both modules. The cost breakdown for the 11-meter dish module is shown in Fig. 5. It is seen that the addition of hybridization equipment increases the installed system costs by about 8%.

The most expensive component is the parabolic dish concentrator which costs $170/m^2 in 1981 dollars. This value is based on cost volume curves [5] derived from development activities within the DOE-sponsored Parabolic Dish Program and is consistent with development objectives for first generation systems. Costs for the receiver and for the power conversion unit (consisting of the engine and alternator) have been determined in a similar manner for a production volume of ≈2000 units. In particular, an analysis of engine selling prices as a function of production volume [11] was used as the basis for estimating Brayton engine costs. In all cases, costs are expressed in 1981 dollars.

It is noted that the above capital cost estimates reflect engine cost information and concentrator mass production trends from recent studies. Basically these studies indicate costs lower than those of the earlier data used in setting project attainability-based goals can be achieved, particularly at lower mass-production volumes. For concentrators, it is believed this reduction results from a design evolution that was directed toward developing systems which would be more cost effective at lower production volumes. Also, the power system for the MX application has a lower cost than a power plant for utility applications since site preparation and substation costs are obviated.

Costs for controls and electrical transport are predicated on the use of standard components.

- MODULE: 23 kW$_e$ FROM 11 m DISH
- PRODUCTION LEVEL: ≈ 2000 modules/year
- HYBRIDIZATION EQUIPMENT INCLUDES (1) COMBUSTOR SYSTEM AT $325/MODULE, (2) FUEL PUMPS AND FUEL LINES AT $640/MODULE, (3) FUEL TANK OF 12,000 ℓ. CAPACITY CORRESPONDING TO 30% OF LOAD FROM FUEL AT $1150
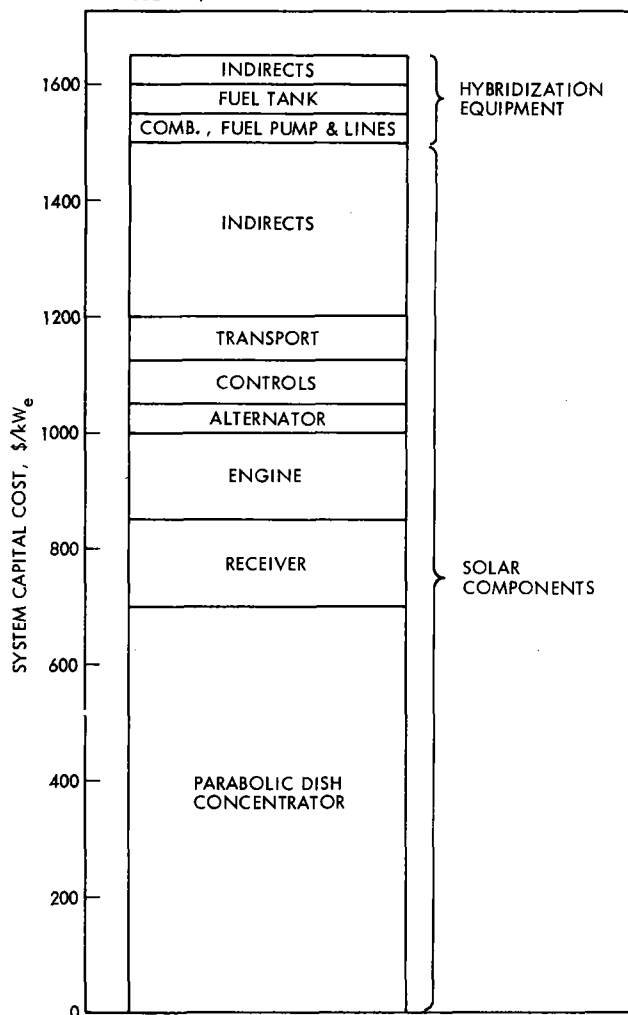
Figure 5   Installed System Cost Breakdown for Hybrid Parabolic Dish Module

Indirect costs include 5% for spares, 1.5% for shipping, and 20% for fees and contingencies. It is noted that these indirect costs constitute a substantial increase in installed capital costs of about 26%.

The cost estimates for hybridization equipment are also based on the cost of standard components. In determining fuel tank costs, it was assumed that the tank is filled every six months. If the tank were to be filled every three months, the tank costs could be halved. Since tank costs are a relatively small item, it is expected that other factors related to the logistics of operating the shelters will be the dominant considerations in determining tank size.

The direct installed capital costs used for the lead-acid and Redox battery storage systems are presented in Fig. 6 as a function of storage time. For the baseline case of 4%/year real fuel escalation rate, it is recalled from Fig. 3 that the storage times are 8 hrs and 14 hrs for the optimal
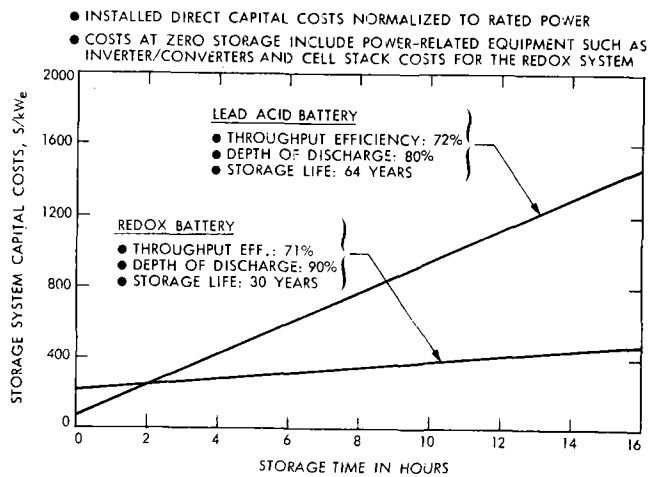
Figure 6 Direct Capital Costs for Storage Systems

systems using lead-acid and Redox batteries, respectively. In this range of storage times, the advanced Redox battery is two to three times less costly than the lead-acid system. Additionally, the Redox battery is projected to last for the thirty-year life of the power system, whereas the lead-acid battery has a 6-year life and will require four replacements during the life of the power system. This further amplifies the cost differential. These factors dominate the comparison to such an extent that slight differences in efficiencies and depth of discharge become second-order effects.

To obtain total installed battery costs, indirect costs, constituting approximately 26% of the direct costs, are included. It is important to note that the storage costs are normalized to the power system output of 14.5 kW_e for the MX application, whereas the module cost of Fig. 5 is normalized to the power output of the module (23 kW_e for the 11-meter dish module). To place the module costs of a power system on the basis of power system output, the normalized module cost from Fig. 5 must be multiplied by the power rating of the module and the number of modules and then divided by the rating of the power system. For a power system with two 11-meter modules, the cost of the modules normalized to power system output is ≈$5200/$kW_e$. The lead-acid battery with a storage time of 8 hrs adds about 20% to the system capital cost.

The operation and maintenance (O&M) costs are separately estimated for the components comprising the power system [5]. The composite effect of the operating costs and different maintenance schedules is found to be approximately 2% of the total power system and equipment costs (where indirect costs are excluded). As noted on Table 1, these labor-related charges are assumed to escalate at a real rate of 1% during the operating life of the power system. This will amplify the effects of O&M on a life-cycle basis, but initial capital expenditures are the dominant factors governing the relative economics of solar-derived power vis-a-vis use of fossil fuels.

Since it is of interest to apply the findings of this study to applications other than MX shelters, the sensitivity of the results to production

volume is investigated. In particular, the effect of reducing production volumes to a level of <500 modules/year, corresponding to a module cost of approximately $2200/$kW_e$, is shown in Fig. 7 for the
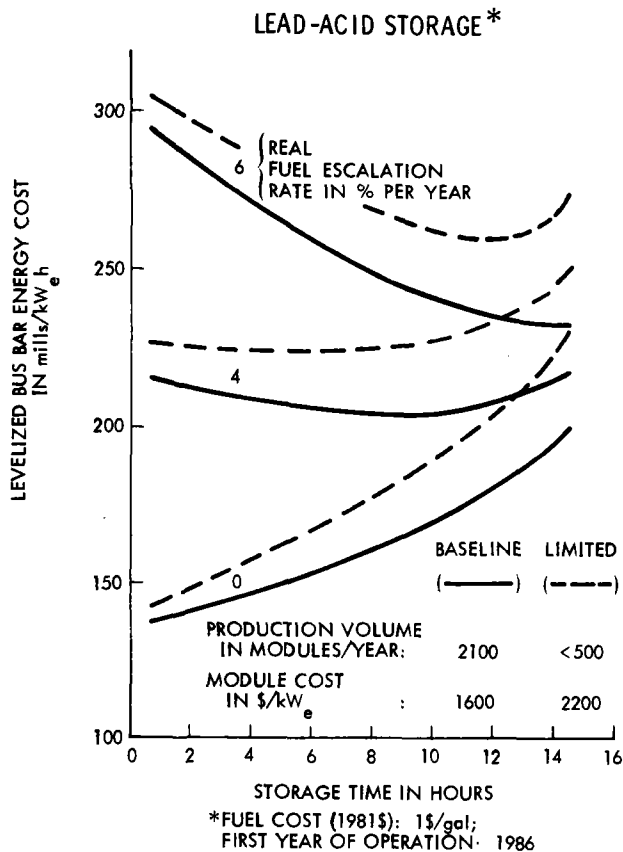
LEAD-ACID STORAGE*

Figure 7 Effect of Reduced Module Production Volume

system using lead-acid batteries. At 4%/year real fuel escalation rate, the limited-production-volume case has an optimum storage time of approximately 6 hrs as compared to 8 hrs for the baseline. Thus, even with limited production volumes, hybrid systems are shown to have economic advantages.

Analytical Basis for Configuration Tradeoffs

Certain analytical procedures used in the present papers have not been developed in the cited references. These procedures encompass reliability assessments, energy cost relations for hybrid systems, and marginal cost analyses. A brief discussion is therefore given to aid in the detailed interpretation of the results presented in Figs. 2 through 4.

In determining reliability, the role of the storage system was ignored in the interest of simplifying the analysis. This assumption results in the underestimation of the actual reliability of the system. Since each dish has hybrid capability, the probability that the dish can deliver power at any point in time is the probability that at least the hybrid option can function. The site is assumed to have an adequate supply of fuel so that the reliability of the system will only depend on the system hardware.

326

To compute the number of units, N', needed to achieve a reliability, R, the following steps are taken. First, the fewest number of units, N, to cover the load is calculated. Then, the smallest value of N' which satisfies the following conditional equation is the solution for the minimum number of power modules required to meet the specified reliability.

$$\sum_{j=N}^{N'} \binom{N'}{j} (\mu)^j (1-\mu)^{N'-j} \geq R. \tag{1}$$

The parameter μ refers to the reliability of an individual unit and the independence of unit failures is assumed so that the above binomial distribution is the appropriate model.

The levelized energy cost $\overline{EC}$ of a hybrid power plant is the annualized cost AC over the annual energy delivered E, i.e.,

$$\overline{EC} = \frac{AC}{E} = \frac{AC_s + AC_f}{E_s + E_f}, \tag{2}$$

where subscripts s and f refer to solar and fuel operation, respectively. The term AC_s is the annualized cost of solar equipment and its corresponding O&M while AC_f is the annualized cost of fossil fuel equipment and the additional O&M associated with operation using fossil fuels. The annual energy delivered during the solar and fossil modes of operation are E_s and E_f, respectively.

Defining capacity factors for solar and fossil modes of operation as $CF_s = E_s/E_{max}$ and $CF_f = E_f/E_{max}$, where E_{max} is the maximum amount of energy that the power plant could deliver if it were to operate continuously at rated power, it is found from rearrangement of Eq (2) that

$$\overline{EC} = \overline{EC}_s \left(\frac{CF_s}{CF_s + CF_f}\right) + \overline{EC}_f \left(\frac{CF_f}{CF_s + CF_f}\right). \tag{3}$$

Here, $\overline{EC}_s = AC_s/E_s$ and $\overline{EC}_f = AC_f/E_f$ are recognized as energy costs pertaining to the solar and fossil modes of operation, respectively. Also, it is noted that, for the MX-application involving essentially continuous delivery of rated power, the energy delivery $E = E_{max}$ and $CF_s + CF_f = 1$.

The separation of the energy cost for a hybrid power system into solar energy and fossil fuel contributions is readily accomplished for the selected operating strategy involving decoupled solar energy and fossil fuel modes of operation. It is seen from Eq (3) that the energy cost of the hybrid power plant is simply the weighted average of the energy cost during solar operation and the energy cost during operation using fossil fuels. The weighting factor is the fraction of energy delivered in each mode as given by the respective capacity factors.

Defining the marginal cost of energy EC' as the incremental change in annualized cost associated with an incremental change in annual energy delivery, it follows that

$$EC' = \frac{d(AC)}{dE} \tag{4}$$

Then, if the energy cost expression of Eq (2) is differentiated and rearranged, it is found that

$$EC' = EC + CF \frac{d(EC)}{d(CF)} \tag{5}$$

Thus, if the variation of energy cost with capacity factor is known, the marginal energy cost can be evaluated.

To use marginal energy costs to determine optimum hybrid plant configurations the basic hybrid relationship of Eq (3) is minimized (i.e., $d(EC)/d(CF)_s = 0$. This minimization yields,

$$EC_s' = EC_f' \tag{6}$$

This is the basic result which allowed the construction of the nomograph chart of Fig. 3.

Conclusions

Conclusions are drawn concerning the feasibility of using parabolic dish systems to supply power for MX shelters and the potential of these systems to penetrate other remote power markets. It is concluded that the use of parabolic dish systems is economically justified over a wide range of real fuel escalation rates (covering what is believed to be a reasonable uncertainty band) and that hybrid parabolic dish systems having both battery storage and the capability to use fossil fuels are a viable option for supplying power to MX shelters. Given economic parameters in the ranges considered here, the hybrid system can (1) substantially reduce costs compared to conventional fossil fuel systems, (2) decrease dependence on critical petroleum-based fuels, and (3) provide high reliability meeting or exceeding MX requirements.

Based on the specific case study of MX shelters, the potential of hybrid dish systems to penetrate remote non-grid-connected power markets has been clearly delineated. The high efficiency and inherent modularity of parabolic dish systems are key characteristics. Efficient two-axis tracking provides dish systems with the potential to generate power from solar in a more cost effective manner than conventional fossil fuel systems which use petroleum-based fuels that are projected to escalate at a real rate of 4%/year on a long term basis. Modularity allows the system to be optimally configured to meet widely varying application requirements as demonstrated by the range of possibilities examined for the MX application. Also, modularity permits the implementation of strategies that minimize risk, i.e., as suggested for the MX application, the solar energy to fossil fuel mix can be varied by adding modules in such a manner that investment risks are minimized.

Acknowledgements

References

1. Bluhm, S., "Parabolic Dish Market Assessment, First Interim Report," JPL Document No. 5105-37, Jet Propulsion Laboratory, Pasadena, CA, July 1980.

2. Truscello, V., and Williams. A. N., "Heat and Electricity from the Sun Using Parabolic Dish Collector Systems," Jet Propulsion Laboratory, Pasadena, CA, September, 1979.

3. Fujita, T.; El Gabalawi, N.; Herrera, G.; and Turner, R., "Projection of Distributed Collector Solar-Thermal Electric Power Plant Economics to Years 1990-2000," DOE/JPL-1060-77/1 (JPL Publication 77-79), Jet Propulsion Laboratory, Pasadena, CA, December, 1977.

4. Fujita, T; Manvi, R; Roschke, E.J,; El Gabalawi, N.; Herrera, G.; Kuo, T. J.; and Chen, K. H., "Techno-Economic Projections for Advanced Small Solar Thermal Electric Power Plants to Years 1990-2000" DOE/JPL-1060-78/4) (JPL Publication 79-39) Jet Propulsion Laboratory, Pasadena, CA, March, 1979.

5. Rosenberg, L., and Revere, W., "A Comparative Assessment of Solar Thermal Electric Power Plants in the 1-10 MW$_e$ Range," Document No. 5103-58, Jet Propulsion Laboratory, to be published.

6. Latta, A. F.; Bowyer, J. M; and Fujita, T., "The Effects of Regional Insolation Differences Upon Advanced Solar Thermal Electric Power Plants Performance and Energy Costs," Vol. 103, November 3, Journal of Solar Energy Engineering, American Society of Mechanical Engineers, August, 1981.

7. "Annual Technical Report, Fiscal Year 1980," DOE/JPL-1060-45, JPL Document 5105-73 (JPL Publication 81-39), prepared by Jet Propulsion Laboratory, Pasadena, CA, and NASA Lewis Research Center, Cleveland, OH, May 15, 1981.

8. Krauthamer, S., and Frank, H., "Electrochemical Energy Storage Systems for Solar Thermal Applications," DOE/JPL-1060-30, Rev. 1, (JPL Publication 79-95, Revision 1) Jet Propulsion Laboratory, Pasadena, CA, March 1980.

9. "Data Resources Inc. Spring 1981 Data Book," Data Resources Inc., Lexington, MA, 1981.

10. Doane, J., et al, "The Cost of Energy from Utility-Owned Solar Electric Systems," JPL 5040-29, ERDA/JPL-1012-76/3, Jet Propulsion Laboratory, Pasadena, CA, July, 1979.

AN ECONOMIC EVALUATION OF SOLAR ENERGY

DOUG WOOD

SOLAR STEAM, INC.
FOX ISLAND, WA 98333

An Economic Evaluation of Solar Energy

Abstract

If a solar collector collects $1,000. worth of energy per year and lasts 20 years it is not worth $20,000. The monetary value of the energy must be discounted to reflect investment alternatives for energy. Energy price changes must also be accounted for. Consumer costs and new energy costs are losing their disparity with the deregulation of energy prices. The solar dish on Fox Island is a model of solar economics. In average U.S. climate the dish will deliver 250 MBTU per year at temperatures up to 750° F. In single present worth terms the dish system cost is about $15,000 (1980$) including maintenence. The system energy value exceeds $30,000. If the money is not discounted then the energy value would exceed $63,000. The dish approach has economic advantages over other generic solar collectors. International consumer interests indicate opertunities for further development and production of solar collecting systems.

How much is a $10,000 solar collector worth? If you deposited $10,000 in an account that paid 10% interest per year, you could withdraw $1,060.79 per year for 30 years to buy energy. But, as the cost of energy increases, $1,060.79 would buy less energy each consecutive year. If energy costs increase 5% per year then you could withdraw $633 the first year, $664.65 the second year, $697.88 the third year, etc., and be able to buy the same amount of energy each year from the 30 year account. In other words, assuming energy inflates 5% per year (before inflation), and your money is discounted 10% (before inflation), then a $10,000 solar collector must deliver $633 worth of energy the first year and last 30 years to break even with investment alternatives. But, if you expect energy costs to rise 10% per year, then the collector only needs to be worth $334 the first year to break even. A solar collector is worth as much as the energy it produces in its lifetime. The precise economic figure is dependent on how much you expect energy to rise in price and how much your money is worth in your investment alternatives.

To complicate matters further, energy has two values. The consumer cost of energy ignores subsidies, regulations, and the mixing of new power with old power. $0.02/kwh for electricity in the Northwest and $1.36 per gallon of gasoline are examples of consumer costs. The other value of energy is often denoted as marginal costs, replacement costs, or new energy costs. This

figure represents the cost of finding additional energy and addresses the issues of balance of payments, inflation, and alternatives. $0.10/kwh for nuclear electricity, $40 per barrel of oil, and $7.50 per million British Thermal Units (MBTU) for deregulated natural gas represent actual social costs of energy expansion. Under Reagan's policy of deregulation consumers will be paying replacement costs for energy (excepting nuclear energy).

The current retail cost of solar collectors does not indicate the future cost of solar collectors when mass produced in a competative market. A general method of collector cost evaluation assumes that labor costs equal material costs for custom construction. Labor costs add only 33% to material costs for mass production predictions.

For ease in comparing energy systems all economic figures should be translated into "single present worth" (SPW) dollars. With money discounted 10% per year the SPW of $633 the first year is $575.45. The SPW of $664.65 the second year is $549.29. The SPW of $697.88 the third year is $524.33, etc. The sum total SPW of a system which delivered $633 worth of energy the first year, with energy prices escalating 5% per year, with money value discounted 10%, and with an economic life of 30 years, would come to $10,000 (SPW).

In another example, suppose an energy system needed a $3,000 overhaul after 10 years use. Deposit $1,156.63 in an account bearing 10% interest and in 10 years $3,000 would be available for repairs. The SPW of a $3,000 expense in 10 years

is $1,156.63 and would be added to the system cost. If a system has a salvage value of $2,000 after 30 years use, then the SPW salvage value (discounted 10%) is $114.62 and is subtracted from system cost.

Using the above evaluation criteria the following sensitivity analysis is possible for the solar dish concentrator on Fox Island. The figures are estimated to be 75% accurate in 1980 dollars.

Materials (mass produced):

Dish:

structural tubes 600'	$ 700
hubs 27, 15lbs each	450
aluminum skin .030, 1,300 sq. ft.	600
glass mirrors 1,000 sq. ft.	1,200
fastners	500
boiler and plumbing	500
controls and electronics	300
	$4,250

Dish support carriage:

post	$ 600
2 endless wenches	500
cable	250
cable rigging	200
counter weight support	500
fastners	150
	$2,600

Total materials	$ 6,850
33% for labor	2,260
installation labor at site	2,000
Total installed cost	$11,110

Collecting area	610 sqare feet
Efficiency	80%
Thermal peak power	46 kw(t) Thermal
or	160,000 BTU/hour

Annual energy value:

Seattle, WA	50,000 kwh(t) or 170 MBTU
Yuma, AZ	100,000 kwh(t) or 340 MBTU
U.S. Average Climate	75,000 kwh(t) or 256 MBTU

Concentration ratio:	120 to 1
Maximum efficient temperature:	750°F
Annual maintenance cost:	$300
Overhaul every 11 years:	$3,000
Lifetime:	30 years
Salvage value:	$2,000
Land requirements (stowage): (Parking lots offer dual purpose)	900 sq. ft.

First solution is SPW dollars:

Discount rate:	10%
Energy escalation:	5%
First cost (before tax incentives):	$11,110
Energy price:	$7.50/MBTU
System cost (SPW):	$15,243.48
System energy value (SPW): (U.S. average climate)	$30,333.37

Second solution:

Changes: energy price	$0.02/kwh
energy escalation	10%
System cost:	$15,243.47
System value:	$45,000

Third solution:

Changes: tax incentives reduce collector cost:	40%
economic life reduced to:	20 years
System cost:	$9,974.26
System value:	$30,000

Fourth solution:

Discounted payback period: (The year total energy delivered exceeds system cost)	5 years

Dish concentrators are known as point-focus concentrators. This is the only generic solar collector which does not suffer from cosine loses, i.e. dishes always face directly towards the sun. Central receivers (power towers) surrounded by acres of heliostats (mirrors) are limited by size and have costs associated with pointing error and mirror surface error. Line focus solar concentrators have been the most popular solar generic concentrator approach over the last 80 years. Line focus collectors are similar in scale and materials to point focus collectors. Line focus concentrators are trough collectors. They generally have long rectangular curved mirrors reflecting sunlight onto a long black pipe. This approach does have cosine loses and cannot get as hot as point focus. This is because line focus geometry is 10 times more critical than point focus geometry. Concentrators are not affected much by cold climate. Most concentrators are cheaper (material vs. energy) than non-concentrating collectors (flat plate collectors). Compare a 600 square foot concentrator to a 1800 square foot flat plate collector.

The generic dish will capture a significant portion of the existing solar market. It will also open new markets which demand high temperatures and/or electricity.

There are only a handful of large dish collectors in the world. The Fox Island dish was the largest in the U.S. in 1979 and is still one of the cheapest prototypes in existance

(materials vs. energy). The project experienced wide media exposure followed by a strong market response. The government of India wants two million, 24 foot diameter, electrical producing dishes in lieu of 2 nuclear power plants planned for southern India. India lacks a transmission grid. Saudi Arabia wants the dish to desalinate sea water, Sweden and Canada want the dish for district heating projects with seasonal storage. Whole towns are powered 100% year round with solar concentrators and huge underground storage tanks of water heated to $212^{O}F$. Austrailia would like the dish for isolated power production. Isreal wants to produce the dish. In the U.S. I have been approached by housing project contractors, public businesses, farmers (irrigation pumping and crop drying), alcohol producers, industry, and research facilities, all of whom wish to purchase the technology.

The Fox Island dish has features which distinguish it from other large dishes:

1. The dish forms compound curves by bending flat triangle glass mirrors into a multiplex of simple curves with stress screws.

2. The dish has a geodesic superstructure which formed an accurate shell and eliminated the need for optical adjustments.

3. The dish has tubes spanning the aperature.

4. The receiver (boiler) is externally irradiated.

5. The dish rotates up-side-down at night. (The next dish will also travel down to cup the ground for further protection.

But the next dish, a new industry, and a new source of energy will become available only if the local government and the private sector work together on the research and development of new technology. Otherwise, this technology, and other like it, will simply cease to exist. The need is real. The U.S. imports 7 million barrels of oil per day costing the U.S. $90 billion per year. Sustained solar manufacturing with gross sales of $20 billion per year would deliver the equivalent energy as imported oil and would employ 200,000 full time solar workers.

PANEL DISCUSSIONS:

INDUSTRIAL SUPPORT SECTOR REQUIREMENTS

MODERATOR:
B. Washom, President
Advanco Corporation

Panel Members
J. Wilson, Renewable Energy Institute
D. Shine, Sanders Associates
A. Shoemaker, Corning Glass Works

BYRON WASHOM:

I have arbitrarily reduced the number of speakers so that we could
spend more time to focus in on what I regard as the absolute critical
issues. I think that with my co-panel members today we will, in fact,
accomplish that. So we delve into a little bit of the details as to
the agonies of the past and the prospects for the future for, not only
this parabolic dish technology, but the industry as a whole. To begin
with, I would like to have a show of hands so we could calibrate, so to
speak, the audience that we have. If you are a member of private
industry manufacturing or service mode, would you please raise your
hand. OK. And if you are a DOE, Lab personnel or university employee,
would you please raise your hand. OK, thank you. And if you are a
member of the user community, please raise your hand. OK. As a result
of roughly I'd say 65-35 percent in two hands of the user community, I
think that's valuable that we know whether we're preaching to the choir
as to these ills or whether we're speaking to the congregation. Each
member of today's audience, I'm sure, is aware of the fundamental
change that is occurring in regarding the speed and leadership that
this nation is developing solar energy. Since our last meeting, the
Administration members have expressed their varying views and, as of
last Friday, the FY-82 Budget issue came to what I call an interim
conclusion when President Reagan signed the Energy and Water
Development Appropriations Bill. I used the term "interim conclusion"
for the last inning in this FY-82 budget is definitely not yet over.
For a recision and a deferral package can still be sent to Congress any
time, I believe, between the dates of December 15 and January 20.
Today they announced that the worsening budget deficit by the
Administration could amount to as much as one-hundred-and-nine billion
dollars, approximately twice that of the original estimate of the
present Administration. This extreme budgetary pressure will bring
what I regard as new pressures upon the bill that has not been signed.
As most of you know, the President's original request for solar thermal
in March was forty-four million dollars; it was revised downward to
thirty-two million dollars in September, but Congress went ahead and
allocated - as you heard this morning from Gerry Braun - fifty-nine
million dollars. So to say that there's a contention between the
Administration's position and the Congression is very valid. Thus, it
is premature to positively conclude that efforts in Congress to balance
or amend the Administration's position has been successful. But we can
conclude the following: First, to give credit where credit's due,
OMB's positioning, strategy, and persuasive influence over Congress
will probably be regarded in history as one of the most powerful first
year of any modern president. In spite of Mr. Stockman's recent public
and indiscrete comments in the Atlantic Monthly, OMB will, I believe,
continue to weld the same power and by no means have they exhausted
their arsenal of strategic moves. Congress has continued to be and
will continue to be solar energy's greatest supporter. There was an
unholy alliance that was created this year unlike any other previous
years. That unholy alliance was largely a credit to the Renewable
Energy Institute which you'll hear from later. But it was an unholy
alliance from the Wind Energy Association, the Photovoltaics people,
the small hydro-electric, the alcohol fuels, solar thermal, and on down

the list – where, for the first time, we realized that we had a greater
strength individually of grouping together than trying to rob Peter to
pay Paul in regards to the budget. And, finally, it was reassuring to
hear from Gerry Braun this morning that within the Solar Thermal budget
that the parabolic dish program for the first time will receive a
parity with the central receiver technology development program.
Because this is actually what could be regarded as a gracious move by
Gerry Braun, and the fact that we did have a very serious and
successful effort within the U.S. Senate to raise the appropriations
bill for parabolic dishes in the FY-82 budget to 7.9 million dollars.
I regret to report that in conference committee that Senate amendment
did not carry and so that the consequential appropriations for dishes
was reduced to the President's original request for 3.1. Now that I
have your sober attention, I would like to look forward as to what we
can now discern from the forthcoming budget picture as well as future
Administration policies.

One of the major thrusts of the Administration's solar energy policy
was to vest the burden of research, development and demonstration in
private industry and to take the remaining residual basic research and
vest that into the Federal budget. The lack of a clear delineation as
to where one ends and the other begins has created a chasm that I am
unsure is manageable in absence of a higher authority like DOE of
building the bridges between basic research and technology
development. Today we will hear about three of the dilemmas that
private industry faces, and what is needed to correct them. Our first
speaker this morning will be John Wilson from the Renewable Energy
Institute; he will followed by Dan Shine from Sanders Associates and I
will provide the comments that Art Shoemaker from Corning Glass Works
has provided us. John Wilson is the Acting Director of the Renewable
Energy Institute (REI) which is a Washington-based research institute
focusing on the development of energy from solar, wind, hydro and other
renewable sources. Prior to joining the Institute, he served as a
legislative coordinator for the solar lobby where he directed the
Washington lobbying efforts for the national membership organization
focusing on renewable energy and energy conservation. Wilson's
lobbying activities were a logistical extension of his policy and
administrative responsibilities at Center for Renewable Resources and
his active service as a key aide with the two U.S. Congressmen. Before
I turn the microphone over to him and he discusses REI and various
programs, let me make one important statement: I believe the Renewable
Energy Institute and John Wilson and his colleagues, are probably the
most important corner stones to the success of solar energy in this
country, and so I ask you to bear that in mind as you hear his comments.

JOHN WILSON
Byron is a hard act to follow. We are going to do a little back
slapping. I want to thank Byron for the invitation to come down here
today; I don't think as many of you realize how well known he is
becoming in certain circles up on Capitol Hill. Some positive, some
negative, its a difficult thing to develop that give and take attitude
and he is done it in at level that is of speed and accuracy that many

of us that have been in Washington for five to eight years have really
marveled at. This is a meeting of people who are mainly engineers and
are in the business and I'm a mechanic. I follow mechanics of Capital
Hill and the Administration, Wall Street and places that make this
industry move. To date you have programs that have been based largely
on government programs, received your funding for this that and the
other, and you've gone out and competed for awards under a certain
structure. I don't think that I'm here to tell you that's changed. It
changed quite a while ago and now you're trying to adjust. What I do
want to tell you is that the climate that's changing is not the same
everywhere. Particularly important is the fact that the climate in
Congress has not change significantly at all since the 70's when your
budget is going up highly. In fact, in many cases mainly in the
administration you've got staff and political folks as well as career
officials: people out at the Labs who have climate that they would to
retain the same way that they had years before. The only place that
the climate has really changed is in the upper pinnacles of the
administration, you've got a new group of people in our office, you got
a new group of people running the agencies and a new group of people
giving out the orders. That's where you got to spend your time; and
that's sort of why I'm here today to talk to you about the change.
Interestingly enough, Wall Street is about the same. Just before I got
on the plane this morning I had to return a call to New York, it was 6
0'clock in the morning; it was an investment banker who was about to
give a speech to 60 people on Wall Street to talk about renewable
energy. He wanted to check a couple of things and he called me at home
and woke me up at 6'0 clock. That's not unusual, there's a lot of
intresting areas and they are still putting out money. I've seen a lot
of private work going on and I think that is going to continue. The
administration changes haven't increased that at all and private
industries are moving faster, I don't think, its just slugging along.
I think thats something you need to take account of and to work with to
try to see how you can work with them to move those things in the right
direction. I told Bryon I would give you a quick overview of three
different areas, sort of looking into the crystal ball, telling you
where some things that I think are important to you are going to be
over the next couple of years: the budget, tax credits, and the Public
Utilities Regulartory Policy Act (PURPA). I will start with the latter
which is probably the most arcane to all of them.

Many of you are aware that there was a law passed by Congress which
basically deregulated the small power producer and allowed you to be
able to have a deal with your utility, if you will, so you can buy and
sell power at reasonable rates. This law is called PURPA; It was
challenged in Mississippi; A rather ornery Judge delt a fairly serious
blow to the law and its been appealed to the Supreme Court. Oral
arguments will be given around February at the earliest, and a decision
will be registered somewhere around May at the earliest. This is what
we've learned at the last few weeks from an attorney on my staff who
came from a Federal Energy Regulatory Commission who is really
knowledgeable about PURPA. He indicates that a couple of recent court
decisions relating to states-rights have changed the legal atmosphere

342

surrounding PURPA and its becoming pretty high rolling game. Nobody really knows which way the court is going to go, largely because it doesn't rotate around energy issues; it rotates around the states-rights and issues that all of us involved in solar don't really know that much about. I've got about 10 different law firms that circulate around our office looking for information, giving it back and forth; and, if any of you are particulary interested in PURPA, Section 210 or whatever, please feel free to give me a call and we will try to get you some information. One final note on that, no matter what happens with court case on PURPA, almost all the attorneys agreed that one section of the act will probably be upheld; and, that is the section that effectively deregulates the small power producer. And that is at one point that PURPA will have accomplished whether or not the rest of the act is ruled unconstitutional. That basically says that you don't have to worry if you are trying to sell some gear that the guy that buys it is going to have to end up being regulated by state PUC's.

Second, the budget. I don't think it is of any news to any of you that OMB wants solar and conservation to go to zero in 1983. The Washington Post clearly recounted an article this weekend showing all the numbers. I've had numerous conservations with people within OMB for the past four or five years and am on pretty good working terms with some of them. The fact of the matter is that they have a job to do and they have to find some money and you've got a little pittance, but it adds up, and you know which way the numbers have been going over the last couple years. I think what you need to pay some attention to, is the fact that Congress hasn't really followed that lead everytime and I'll get back to that in a second.

On the tax credits; many of you may be aware on September 24 when the President did his speech on another round of budget cuts and the new revenue enhancement, one of the things that was listed in the fact sheet that accompanied that speech and was being targeted for review by the Treasury is the energy tax credit. This may not be as important to all of you as to some particular ones who are trying to actually market some gear. But to anybody who is trying to sell something with 10% basic investment tax credit and with 15% energy investment tax credit it's awfully important. We spend a lot of time working with people who were involved, like Byron and others who are putting together deals in one industry or another. We spend even more time with lawyers and CPA's who are packaging these deals, and with their investors. And we scurried around and pulled together a fairly effective coalition, I think; in about 10 days we had 300 signatures on two resolutions, one on the Senate side and one on the House side saying don't do it. In fact it is kind of funny to note, I had two-thirds of the Senate on record and I only have one-half of the House. May be that's because we started with conservative Senators first; we got people in like Senator Wallop, we've got Senators like Senator Doyle who isn't on there, but his stance has been an awful help. We've done quite well, largely because of your efforts. It's intresting to note that the chairman of the Senate Finance Committee has a solar thermal project going up in

his back yard. I happen to know the man who owns that Concrete plant,
he's very intrested in Senator Doyle, and those connections get made.
I think we all need to keep notes of those things those, grass roots
politics are very important. Of immediate importantance, we were able
to stave off the Treasury making formal announcements and going after
the tax credits. We had meetings with Deputy Assistant Secretary,
Assistant Secretary, couple of people went into the White House one
time, and Presidents of some firms represented here went into the White
House several times with myself and with others, and had some very good
heart-to-heart talks about the fact that there were some pretty big
Companies involved in solar and they were tried of being the whipping
boy all the time; particulary on the tax credit side. The message got
heard; there were some promises made and to date, they have been kept.
Unfortunately, the Treasury staff is just as ornery and stubborn as
they were originally, they still think the tax credits are not good
sound policy. I have it on very good authority that a decision has
been made at an interim staff level meeting to proceed with elimating
tax credit at Treasury. That decision obviously will be reviewed by
the Cabinet Council. The trouble is, Treasury sits on the Cabinet
Council along with OMB and the Council of Economic Advisors; and, of
course, that means Jim Baker and that crew sit-in. What I expect to
have happen is we will get caught up in a larger wave and we'll need a
lot of money and frankly the energy tax credits are a few billions
dollars that show up on their charts, so it's not over.

The last thing I would like to touch on real fast is the fact that in
this problem, you've got an opportunity because we've never before had
the kind coalition that we have has been able to pull together
recently. I've got president's and vice presidents of large companies,
Fortunes 100's, going into the White House saying things. We've got
corporate jets coming back and forth on the issue of solar. This is
the first time I've seen it. When I worked at Solar Lobby we managed
to add a pittence of 49 million dollars to the approporation bill over
the objections of the Chairman of the House Subcommittee; and I
remember we sort of did it with some blue smoking mirrors, this time
we've been able to get some real big companies involved and that has
impressed the White House. And frankly, you got to look to the
audience and figure what you can do with them, because it doesn't
matter what you think, or what you want, or what your audience cares
about; and as far as the White House is concerned they really want to
hear from those larger companies. They had no idea you were involved
in solar, they didn't know you had a business investment and that you
had been in it for years. If I have any message to give you — it's
that you are to increase those communications in what ever way you see
fit, and get in there. To give you an idea of some of the companies
that went in: President of Boeing Engineering and Construction,
President of Acurex, Sr. Vice President of Atlantic Richfield, who is
the President of ARCO Solar Industries and also sits on my board went
in; people from the utility industries; Texaco, talking about Alcohol
fuels; a good range companies; and they listen, and they heard. Now,
what bothers me the most about this coming session this Spring is

things are going to fly real fast and furious. Tax measures will be on
top of the list because they got to raise a lot of money and Senator
Doyle has said very specifically he doesn't like all the bickering over
this little thing and that little thing and trying to come up with a
lot of money that way, it just won't work. You are talking 100 million
dollars. And Congress is more worried about the deficit that the
President is, because the House particularly, has to run for
re-election every two years. The point is that the Senators and the
Senate Finance committee will be looking at ways of raising large
amounts of money. The two ideas that this top staff thinking about
that really amount to anything are windfall profit tax on natural gas
deregulation and an old idea that has kicking around and the staff
rewrote it the other day. It's a Btu tax on energy. I sat down with
the staff and talked in great length about what they were planning to
do with the Btu tax; they really weren't sure yet. We got a lot of
work to do, because there are different ways of crafting such a tax
that could kill solar, and ways it could really enhance it, it's
relative merits versus conventional fuels; and what you need to be
certainly aware of, and I think that most of you, are is that the other
fuels have a very well healed organizations and lobbys in Washington
and they will do their best to make sure they stay on the relative
merits of their case and keep it on the top of the heap. So, I'm
suggesting to you, with your companies and organizations within your
relationships and within your associations, do the same.

Lastly, I like to raise a point. My organization is relatively new.
We opened our doors in March and we have hit the floor running. We are
the people who brought you the at-risk tax ammendment this summer.
Somebody brought it to us at the last minute, we did a little quick and
dirty work on it, and got up there and we put up an ammendment offered
by a Democrat on the Senate floor and it passed 97 to nothing. On the
economic recovery tax I had Senator Doyle, and I had the Administration
backing the thing; it took a lot of work and we had a lot of good
people working with it on it. But that's the kind of work that we like
to do. On this tax credit issue I think we have a healthy coalition
put together with Price-Waterhouse and all the big accounting firms,
some of the best energy tax lawyers in the country, the guy that wrote
McGraw-Hills new energy tax service, and my right hand lawyer who works
with us on a daily basis. What I would suggest to you is that if you
are intrested in this area you contact and spend some time with us and
we'll give as much advice as we can. I also suggest to you that you
consider getting involved in a project we are gearing up on, its an on
going tax policy project. We're a little concern that as we are moving
out of this budget area which clearly isn't shrinking-up, we've got to
quickly examine our options on the tax side. The oil industry isn't
what it is today simply because there was a lot of oil in the ground.
There is a fine network of taxing incentives that were develop over the
years and enhanced the ability of those companies to go out there and
locate, drill and bring it up, and transport it and burn it. One of
the thing in solar community or renewable energy community have to look
at is how can we look like that industry. How can we design a series

345

of tax incentives that are a range or basket-full of subsidies if you
will, that will help us just as much as oil got; that beginning
boot-strap. There's nothing magical about oil, I mean we are replacing
other fuels and that fuel replaced other fuels and so on. Our point is
we've got to do just as good a job as they did in their early formative
days, and I think we've got a couple of ingredients, but we need you.
If there is anything you can do to come along side us, we will be real
grateful. Thank you.

BYRON WASHOM

Thank you John.
The next gentleman, Dan Shine needs very little introduction to this
community. As most of you know he's Program Development Manager at the
Energy Systems Center for Sanders Associates. Since 1974, They have
been involved in a variety of high temperature receivers for both
central receiver and parabolic dish programs as well as the heat
storage system technologies. Sanders serves as systems integrator for
the Brayton dish experiment. Most notable to his introduction today is
just recently, at the Solar Energy Industries Association (SEIA) annual
meeting, Dan was elected Chairman of the Parabolic Dish committee of the
Solar Thermal Division.

DAN SHINE

The first note that I would make, I think you all owe John (Wilson) a
note of thanks, he just got three graduate credits in political science.

Byron asked me to run through one company's experience over the past
several years in solar thermal with the stress of the past year and a
half. What I will do is run through what our program history is been
at Sanders, recognizing that many of you people in industry in the
audience have been through the same thing over the past several years.
My point in doing so, is to try to highlite for you the fact that a lot
of education has to be done picking up John theme at the grass roots
level. It seem to be an attitude within the adiminstration, most
prominently publicized by Mr. Stockman and OMB, that the solar industry
and I suppose also the solar thermal industry is at the point where
market forces will take over. That simply is not true; in certain
aspects of it, you heard some presentations, this morning, such as the
PKI presentation that would indicate that are certain technologies that
are just about there, but there are severl other technologies that
still need a boost. I wish Gerry were here because I wanted to pick up
on something that he said this morning, that I would take issue with,
and I think we all should take issue with. In part of his presentation
this morning he made the statement that the govenment has, in effect,
carried the ball for the past six or seven years. I think that is
reflective of an attitude, again on the part of those people now at the
top of the heap in Washington; that is a misconception. Anyone who is

involved in a company that has been involved solar thermal over the past five years has put some of its own descretionary resources to work in this field. In our instance it probably amounts to about 20%, its in the public record. We've probably had between 5 and 6 million dollars worth of contract work with JPL, DOE or DOE San Francisco, but government money. The company, my company has also put in about 1.2 million of its own descretionary resources to carry this technology forward. And again I think that our experience has been repeated by most industries involved. I don't think that; the Stockman's the OMB's, the people in the administration realize that, they don't understand that, and its up to each Company through its Congressman or through whatever means it chooses, to get that message across. Uncle Sam, this is not been a welfare society, we've been doing our part. Cost sharing, is at 50%? is it at 20?: I don't know, but we have done our part to this point. And the misconception is that Uncle Sam has been paying from dollar one to bring this technology to a certain point. And that is not true. And it is a misconception because we have not done our jobs in educating either our Congressman or through the Parties, the Administration, as to what the realities are. In going through what our experience has been, we began in 1974 with an internally funded program. We went through a series of receivers: a 10 kilowatt thermal receiver which we tested in 1976 at White Sands, then a 250 kilowatt thermal receiver tested on the tower down here at Georgia Tech. Then, in the interim, between the '76 and the '78 test we became involved with the JPL people. We became involved in high temperature storage research and high temperature receiver research. We also built some systems; we became involved in what has been known by four different names called a parabolic dish module experiment, a military module experiment, the Yuma experiment, and Engineering Experiment 2a. Whatever you call it we have been involved. Now I site that history because I know that JPL has gone through the same agony that we've gone through. Those proposals were submitted in December 1979; the contract awards out-lasted the prisoners in Iran. It was 462 days between the time that proposals were submitted and the contract award was made. That was not in the control of the people who were bidding it, and it was not in the control of JPL. It was in the control of forces outside the principle parties involved. It is simply an illustration of what has happended in this technology, or in the attempt to develop this technology. Fortunately, for us, in keeping our system alive, or our program alive, Vince and his people managed to dig up some money to get us started in the high temperature receiver program. It was not part of the main-line program, but somehow some money was dug up. We got started and you'll hear a report on that project tomorrow. So there have been ways, but these fits and starts have hurt us and they have hurt the technology, and again, I'm sure that the experience has been repeated in any number of companies that have been involved in this program since 1976 or 1977. On our particular experience, when we first came on to contract in 1975 to the then ERDA, we built-up to a point at '76 when we had 10 full time professionals on the project. Through '79 we managed to keep between 6 and 10 people involved. As of today we have 2 people full-time and 3 or 4 part time. You loose a technology! You loose engineers to other

projects! That is happening in our instance and that is happening in other companies. You can't keep people on the dole. What is not known, perhaps, what is not known by OMB and on the hill is that it cost industry about a hundred thousand dollars a year in contracts to keep a senior engineer employed. Exclusive of hardware it cost you about a hundred thousand dollars to keep an engineer employed. And if you are going along at a hundred thousand dollars a year, it doesn't take long to figure out you're not going to get very far. The technology suffers, not one company, the technology and the Country suffer. I would hope that the message could be passed through to DOE management to OMB, again through whatever means you choose to do so, the program continuity in building on an industrial base is absoluetly essential. Once you loose a team, once you break up a team, you don't reestablish it. You can bring the same bodies back, but if there have been months hiatus in the program you just don't recover that ground. You can bring the same people back but you don't recover the ground that you lost from when the program was shut down. I know that the Labs understand that, but I'm not quite sure that everyone in DOE understands that, and I know that OMB does not understand that. Again, our mission is to educate. The message simply, sparatic funding kills industrial organizations interest in keeping a program going. You can only go to the well so often. You have a program thats going on, you're on a growth curve you're doing well, you're progressing technically, the funding shuts off you go to management saying you need a half million dollars over the next six months to keep my engineers going. Management says to you: Whats thats going to get me? If your answer is I don't know, or I think it could get us something in 1983, you're not going to get your money. And in most instances, with all due respects taking issue with what I assume was Gerry's point this morning, most of us in the industry have gone to the well, and probably can't go back again with the atmosphere being what it is. There was a statement made that small and medium size firms were willing to take a risk that there is something magical out there in that suspected market that's going to draw all these firms. I would suggest that you are not going to find a whole lot of venture capital firms that are going to want to invest money in solar thermal today, because of the status of the technology. We have brought the technology to certain point, but its not at the point where you can go off on your own and say I'm going to sell a hundred systems. There may be some exceptions, again PKI made a very good case this morning. I hope it does work out for them. But I don't think the technology and the rest of solar thermal is at the point where we can talk about a market that we're going to realize within the next two years.

One of the issues that we have discussed in the solar thermal division of SEIA is introducing a legislative initiative. Ocean thermal managed to get one, it didn't seem to do them a whole lot of good in the past couple of years. We thought that was a solution, it may still be a solution. But there is no solar thermal legislative initiative and that's one thing that we should talk about as an industry. Perhaps there must be a mandate for solar thermal. There is not one for solar applications for industry. Maybe there should be something called

solar thermal projects or a solar thermal initiative and some enabling legislation. That is lacking at the present time. Again a point that Gerry made this morning that I will take issue with personally, and I'm sure we could get involved in a debate in this, Gerry thought that the major market for parabolic dish systems would be in the small community applications. I disagree with that. I know that the people at JPL have funded a lot of studies, and we funded one on our own, that kind of said that the first market is going to be remote site power of one, two, or three systems. It's not going to be small communities. We could be wrong. But I would like to debate that kind of issue with Gerry, I don't agree with his conclusion. That may be so with the first demonstration. Demonstration is a bad word, but the first time that several units have put together, put out a hundred kilowatts or something like that may be the first time that you will see it done. But I don't think that you are going to go out and sell to a world power company a hundred kilowatts unit. I think you are going to sell ones's and two's for the first 5 to 10 years for remote site power and remote site thermal applications. My final point, and thats a point I've made and several other people have made at these kinds of meetings several times in the past, is that none of us are ever going to get anywhere until there is a working system in the field; that the tires can be kicked, and we can watch the mirrors crack, and we can watch the engines break-down. Until we understand how the whole system works, we are not going to sell any to anybody. That's another point that has to be made. Demonstration may be a dirty word, I'll have to come up with a dirty word, we'll have to come with a different word. But thats what you have to do. You have to initiate a program that is going to have you run a full-up system not for two weeks, not for 23 days, but for a year. What happens to it for over a year? What's happening now, these two weeks demonstrations are all we can afford. You need a full up system to see how it works.

BYRON WASHOM

Our final input this afternoon will be from Art Shoemaker, from Corning Glass Works, who regrets that he could not be with us today, but he asked that I pass on his comments to you. I will make them brief so that I can conclude the panel, then maybe open it up to the floor for some questions and interaction.

ART SHOEMAKER (via Byron Washom)

There is a serious issue within the parabolic dish and the solar thermal community as a whole for that matter. And that is the availability of a domestic source of thin solar glass for reflective surfaces. I beleive this morning we saw on (Bob Ponds') in ford Aerospace and Communications Corporations paper that their system efficiency for the organic Rankine unit with glass was 20% and without glass, or an alternate to glass was 16%, or approximately 20% system efficiency difference. So the importance of using glass until we have a good alternative to glass that is low cost is very critical to the overall systems efficiency. Acurex, in their presentation this

morning, I beleive, mentioned a European source of glass. Corning is a US manufacture of domestic glass, they have been involved in the solar program and the solar thermal program for a period of time. They to have suffered the same gyrations and ups and downs that Dan has just mentioned. And they have come to the same essential position that represents a delemma or option for US manufactures of solar thermal systems. They have, in essence, said to the solar thermal community: before we can dedicate one weeks production of a plant, we will need a bulk order of 1.5 million square feet of glass. For concentrators of about a thousand square feet, you can do the division as well as I can to calculate the number of dishes this represents. This would mean roughly one or two re-powering projects, two to three minor projects and a major effort in parabolic dishes. So the ability under the financial forecast to raise 1.5 million square feet of glass reflective surfaces yearly for the solar business looks remote. The other option that we have is that there is a new glass being developed, they call them "codes" at Corning, which will have chemically strengthen properties which are needed for our applications. But this glass is being developed for an alternative use, a non-energy use. And it is only under this situation that we may, luckily, achieve a domestic source of solar glass. So the point being is that, granted that there are system integrators who are having there ups and down as Dan has mentioned, but there also these subsystems suppliers who the volume of our solar business is less than one one-hundredth of one percent of their total business; and they will not make major investments until we can either a) accumulate an order, or b) by some good fortune we become a secondary product of one of their existing product lines. The alternative is to obtain foreign sources of glass; and I have nothing against foreign sources of glass other than the shipping cost, the insurance cost and the 17% import duty on glass as it enters the U.S. So this is the nature of commercializing this technology. We have to look-out, not only for the system integrator, who is responsible for putting it all together, but also these creditable subsystems suppliers, these component suppliers. Without their participation and availability, we might be, as is the case of the organic Rankine system, facing a 16% system efficiency rather that 20%. I hope I did justice to Art's comments for this meeting.

BYRON WASHOM

To conclude our formal comments I would like to make 6 points and 2 invitations.

First, as a group, and the group I refer to is industry, Labs and university people, we must maintain a momentum within the private sector that is stimulated by commercial rewards within a reasonable time period. The budget reductions may cause the premature elimination of one or more of the less promising technical parallel paths; but, it must be recognized that market-place would have done this in the future anyway.

Two, we must maintain a cadre of expertise at JPL during the transition period by which the Administration seeks to change the solar industry, and maintain this expertise into the forseeable future. Institutional shifts and programmatic authority does not guarantee that technology transfer will be accomplished ever, let alone simutaneously. Already we have witnessed a loss to the program of JPL employees that I had the greatest respect for as to the contributions to this technology.

Third, Congress has responded extremely well when industry has asked for an advocate of the technology rather than a referee amongst bickering and arguing factions within the solar energy field. I think John (Wilson's) presentation today is a good example of that. This will eventually show up into our own budget therefore we must continue to strengthen our aliances with other energy technologies. Four, we must pay equal attention to tax policy aspects of solar energy if we are ever to finance this technology in a private sector with venture capital.

Five, our technical accomplishments, particurily are field experiments, must be actively and effectively publicized. Most recently I've noticed with interest, an article on PKI, and I beleive it was in the N.Y. Times that the chairman of my board sent to me, United Stirling recently was on ABC television, and I beleive John will be quoted in the Wall Street Journal within in the next couple of days. This type of publicity not only adds to our delemma but also to our technical accomplishments and should continue to be actively publized. The final point (six) is that dealing with leadership, which must be like a vector, I beleive, whose courses unwavering in the face of increasing obstacles. Our problems this year or next are not technical, but political. Fundamentally we have not confronted technical obstructions to our progress, they have been political. Our continued leadership and our pursuit of this technological option that is capable of national energy supply, I think, will become more appreciated in the future particularly at the next energy supply disruption which I beleive is inevitable. How we can seek to implement these six different point is the subject of a meeting following this panel in the Blue Ridge A conference room. It is a Solar Thermal Industry Association meeting and no means do you need to be a member of SEIA to attend. I invite all of you; we will not be handing out membership forms, so I'm not going to put the arm you as well. We do ask to limit the meeting to industry members since we have some agenda items that need to be discussed. On your left, my right, you will see two documents, one is by SEIA on solar thermal technologies and another document is by the Renewable Energy Institute. I invite you to pick up both From the meeting this afternoon, and I guarantee you we will adjorn by the cocktail hour, we will be providing feedback to JPL in the morning with some of our decisions and resolutions from this meeting, which I beleive is a very real time response.

So, finally, let me conclude with somewhat of a joke that deals with, after all this sobering news that I've given to you, its somewhat like Custar when informed he was completly surrounded by Indians, he said: "good, now we can attack in any direction".

Let's open the floor, if you will, if there are some short comments or questions that any individuals might want to respond to.

QUESTION

Please discuss the recent Congressional hearing held at UCLA last week.

JOHN WILSON

Let me make some general comments: I don't know how many of you voted for Reagan, I suspect if you're real industry, 80% of you did; Those of you are sort of peripheral probably not, but, solar has traditionally been supported very heavily by the liberal side. I, in fact, one time worked for a California Congressman who was considered very far on the left-wing on the spectrum by most industries that I just happened to think it was a little closer to the middle, but that's a basic argument. The bottom line is that the old time supporters of solar, like (Congressmen) Dick Ottinger and Ed Markey, whom I both consider very close personal friends, can't carry the ball in this current climate. And what you need to do is supplement them with other support. Particularly the (Senator) Doyle's, particularly the (Senator) Wallop's; I consider it a major feat to get Wallops to finally support our little resolution, because he didn't want to be on there at first, because he thought maybe the administration would get mad at him. We've got to overcome it on that side, I'm very glad to see Dick Ottinger out there having those field hearings. The trouble is right now the Democrats are having field hearings around the country. It's a larger political issue, for God's sake we've got to keep it a bi-partisan issue, and if we keep it a bi-partisan issue, we won't run into the same problems as some of the other social issues will run into in the budget. Our problem is we've got to distance ourselves from some things, if we want to survive.

QUESTION - Discuss the public popularity of solar programs

JOHN WILSON

That's a point that's going to play in our favor if we know how to work it. And that is it's solar in general, renewable energy in general, happens to be one of those popular things like apple pie and motherhood. One of things that we've not yet done is gotten a good handle on that, because to translate popularity into either sales or political power or clout is an art and we don't know enough about what we don't know; we're starting an effort that will generate some information but it's going to take about a year to do it. But just what different decision makers, whether it be the public at large, people who buy energy in large amounts, think of different technologies and why they think what they think, what are their biases; and what are the barriers that are incorporated into those biases, and how do we get around them. And I think your points are very strong; advertising appeals, particularly in California, is bizarre for solar.

QUESTION

We seem to be having a lot of problems in industry, at least, that's
the impression and there's got to be something more basic than just
"the President doesn't care" or "Congress wants to abdicate" or
something else. I'd like to know, from this group, whether or not in
general we would have been better off without developing this whole
industry.

WASHOM:

He's opened it to the floor.

ANOTHER SPEAKER FROM THE FLOOR ANSWERS:

It kind of fits in with the comments I wanted to make anyway, so
I'll make them. I'd like to make some assertions that you could agree
with or not agree with and then I'd like to try to answer your
question, if I may. First, I believe that pure market forces alone
will never make a solar energy industry. Just as one piece of
evidence, Alexander built and demonstrated the steam engine in the year
100 A.D. and that didn't mean that people ran off to buy steam engines
to replace their slaves. It's on a whole cultural context. However,
pure market forces will kill it; it's necessary, but not sufficient. I
think that in the current climate that the tax incentives become
absolutely crucial because to any would-be buyer that means that in the
short-term for him, yes, it's worth buying or, no, it isn't. So I see
that as a pre-requisite. If pure market forces only will not do it,
then what does do it? The funny thing is, it was one of the biggest
liberals of all, Hubert Humphrey, that kind of got this whole thing
rolling back in 1976 with the photovoltaic initiative; that you may
remember, led to the photovoltaic FPUP, whatever that stood for, to buy
photovoltaics for the Department of Defense. Why? No logistic
problems, no fuel to feed into the engines that could go to the jets
and the ships and the tanks and everything else that keeps it all
running; in other words, solar started out as the moral equivalent of
war among liberals. It was a way, nonetheless, of beginning to provide
energy independence. And here's where I tie it into the answer to your
question. I think if this initiative had not been started in this
overall cultural climate by the fact that the OPEC hand was on the
spigot of oil and thus the government answered. We would never be
where we are today and I think if we are going to succeed in the more
conservative political climate, that it becomes necessary to remind
those conservative Senators and Congressmen who are especially
interested in issues of security, that in a very real way, the
development of solar thermal technologies are an alternative to (a) the
cutoff of energy supplies from foreign sources to which Bryon referred
and (b) the depletion, which will ultimately be the case, of those
supplies. There is the key and maybe something that can be exploited.
We would be nowhere if the government had not first become involved.

(The remainder of the question and answer period was indequately
recorded and could not be transcribed).

(Panel concluded)

Attkisson, Darryl
Planning Research Corporation
5201 Leesburg Pike, Suite 407
Falls Church, Virginia   22041

Audibert, Michel
Centre National de la
Recherche Scientifique
Department of Heliophysique
Centre de Saint - Jerome
Marseille, Cedex 4, France

Babbe, Robert
Ford Aerospace &
Communications Corporation
Aeronutronic Division
Ford Road
Newport Beach, California   92660

Barber, Robert
Barber-Nichols Engineering Company
6325 W. 55th Avenue
Arvada, Colorado   80002

Bedard, Roger
Acurex Corporation
485 Clyde Avenue
Mountain View, California   94042

Black, Stan
LaJet Energy Company
4550 Loop 322, P.O. Box 3599
Abilene, Texas   79604

Bluhm, Steve
Jet Propulsion Laboratory
4800 Oak Grove Drive, 507-228
Pasadena, California   91109

Boccardi, Crescent
Jet Propulsion Laboratory
4800 Oak Grove Drive
Pasadena, California   91109

Boda, Frank
Ford Aerospace &
Communications Corporation
Aeronutronic Division
Ford Road
Newport Beach, California   92660

Bos, Peter
Polydyne, Inc.
1230 Sharon Park Drive, Suite 61
Menlo Park, California   94025

Braun, Gerald
Department of Energy
Washington, D.C.

Bruce, V. A.
Ford Aerospace &
Communications Corporation
Ford Road
Newport Beach, California   92660

Brudner, Harvey, Dr.
Power Authority, State of New York
10 Columbus Circle
New York, New York   10019

Carley, William
Jet Propulsion Laboratory
4800 Oak Grove Drive
Pasadena, California   91109

Ceccacci, Arduino, Dr.
Servizio Italia
Salita S. Nicola Da Tolentino
Rome, Italy   00185

Chingari, Gastone, Dr.
IIT Research Institute
1825 K Street, NW, Suite 310
Washington, D.C.   20006

Cohen, Albert
Electronic Space Systems Corporation
Old Powder Mill Road
Concord, Massachusetts   01742

Custodero, Salvatore
SES
IIT Research Institute
Rome, Italy

Davis, Ab
Jet Propulsion Laboratory
4800 Oak Grove Drive
Pasadena, California 91109

Davis, S. Bear
Sanders Associates
95 Canal Street
Nashua, New Hampshire 03061

Gobbo, John Del
NASA
Washington, D.C.

Elfe, T. B.
Georgia Institute of Technology
Atlanta, Georgia 30332

Fieldhouse, Edwin
IIT Research Institute
Chicago, Illinois

Fox, Richard
WED Enterprises
1401 Flower Street
Glendale, California 91201

Frankel, Eugene
House Science & Technology Committee
B 374 Rayburn Building
Washington, D.C. 20003

Goldberg, Vernon
E-Systems
P.O. Box 226118
Dallas, Texas 75266

Goode, W. R.
Energy Division
Dixie Steel Company
P.O. Box Drawer A
Tuscaloosa, Alabama 35404

Haglund, Richard
Advanco Corporation
999 N. Sepulveda Boulevard, Suite 314
El Segundo, California 90266

Hauger, J. Scott
Applied Concepts Corporation
P.O. Box 2760
Reston, Virginia 22090

Holbeck, Herbert
Jet Propulsion Laboratory
4800 Oak Grove Drive
Pasadena, California 91109

Holgersson, Sten
United Stirling
Box 856
Malmo, Sweden S-20180

Huang, Louis
Naval Civil Engineering Laboratory
Port Hueneme, California 93043

Kasprzyk, Martin
The Carborundum Company
P.O. Box 832
Niagara Falls, New York 14302

Kiceniuk, Taras
Jet Propulsion Laboratory
4800 Oak Grove Drive
Pasadena, California 91109

Konopasek, F.
University of Manitoba
Winnipeg, Manitoba, Canada R 3T2N2

Krepchin, Ira
Foster - Miller Associates
350 Second Avenue
Waltham, Massachusetts 02154

Leibowitz, Herman
Mechanical Technology, Inc.
968 Albany Shaker Road
Latham, New York 12110

Leonard, James
Sandia National Laboratories
Albuquerque, New Mexico 87185

Livingston, Floyd
Jet Propulsion Laboratory
4800 Oak Grove Drive
Pasadena, California 91109

Lowe, Steve
Garrett Corporation
9851 Sepulveda Boulevard
Los Angeles, California 90009

Lucas, John
Jet Propulsion Laboratory
4800 Oak Grove Drive
Pasadena, California 91109

Ludtke, Norman
Pioneer Engineering &
Manufacturing Company
2500 E. Nine Mile Road
Warren, Michigan 48091

Marriott, Al
Jet Propulsion Laboratory
4800 Oak Grove Drive
Pasadena, California 91109

Marusak, Tom
Mechanical Technology, Inc.
968 Albany Shaker Road
Latham, New York 12110

McDonald, George
Airesearch Manufacturing Company
2525 W. 190th Street
Torrance, California 90509

McFarland, Cliff
Department of Energy
Washington, D.C.

Meijer, Roelf, Dr.
Stirling Thermal Motors, Inc.
2841 Boardwalk
Ann Arbor, Michigan 48104

Micheli, Carlo
AGIP Nucleare
Via Brenta 2 F
Milano, Italy

Naun, Robert
The Carborundum Company
P.O. Box 832
Niagara Falls, New York 14302

Nussdorfer, Ted
Sanders Associates
95 Canal Street
Nashua, New Hampshire 03061

Oefner, Manford
D. Swarovski
Wattens/Tivol/Austria A-6112

O'Neill, Mark
E-Systems
P.O. Box 226118
Dallas, Texas 75266

Ortegren, Lars
United Stirling, Inc.
211 The Strand
Alexandria, Virginia 22101

Overly, Peter
Acurex Corporation
485 Clyde Avenue
Mountain View, California 94042

Owen, William
Jet Propulsion Laboratory
4800 Oak Grove Drive
Pasadena, California 91109

Pappas, George
Department of Energy
Albuquerque, New Mexico

Payne, Larry
LaJet Energy Company
4550 Loop 322, P.O. Box 3599
Abilene, Texas 79604

Poell, Martin
D. Swarovski
Wattens/Tivol/Austria A-6112

Pond, Stan
Applied Concepts Corporation
P.O. Box 2760
Reston, Virginia 22090

Pons, Robert
Ford Aerospace &
Communications Corporation
Aeronutronic Division
Ford Road
Newport Beach, California 92660

Rackley, Ray
Garrett Turbine Engine Company
111 S. 34th Street
Phoenix, Arizona 85010

Reed, Tom
Luz Engineering Corporation
3940 Montclair Road
Birmingham, Alabama   35213

Rice, Mark
Power Kinetics, Inc.
110 Eighth Street
Troy, New York   12180

Rose, Thomas
ONAN
1400 73rd Avenue, NE
Minneapolis, Minnesota   55432

Ross, Don
Sanders Associates
95 Canal Street
Nashua, New Hampshire   03060

Schimmel, Walter
Sandia National Laboratories
P.O. Box 5800
Albuquerque, New Mexico   87185

Sears, Dana
ONAN
1400 73rd Avenue, NE
Minneapolis, Minnesota   55432

Sernka, R. P.
Ford Aerospace &
Communications Corporation
Aeronutronic Division
Ford Road
Newport Beach, California   92660

Shah, Jay
Chicago Bridge & Iron Company
800 Jorie Boulevard
Oakbrook, Illinois   60521

Shine, Daniel, Jr.
Sanders Associates
95 Canal Street
Nashua, New Hampshire   03061

Souva, Eugene
The Garrett Corporation
9851 Sepulveda Boulevard
Los Angeles, California   90009

Stein, Charles
Jet Propulsion Laboratory, 507-228
4800 Oak Grove Drive
Pasadena, California   91109

Stelson, Thomas Dr.
Georgia Institute of Technology
Atlanta, Georgia   30332

Strain, Edwin
Garrett Turbine Engine Company
111 S. 34th Street
Phoenix, Arizona   85010

Strieter, R. M.
D. Swarovski
2880 S. Patrick Drive
Indialantic, Florida   32903

Strumpf, Hal
Airesearch Manufacturing Company
2525 W. 190th Street
Torrance, California   90509

Suraci, Ferdinando
CNEN
Viale Regina Margherita 125
Roma, Italy   00186

Swarovski, Helmut
D. Swarovski
Ausserfeld No 9
Wattens, Austria A-6112

Truscello, Vincent, Ph.D.
Jet Propulsion Laboratory
4800 Oak Grove Drive
Pasadena, California   91109

Griethuysen, Valerie Van
United States Air Force
AFWAL/POOC
Wright Patterson Air Force Base,
Ohio   45433

Washom, Byron
Advanco Corporation
999 North Sepulveda Boulevard,
Suite 314
El Segundo, California   90266

Weisiger, Joe
Department of Energy
Albuquerque, New Mexico

Willcox, William
Rockwell International
8900 DeSoto Avenue
Canoga Park, California 91304

Wilson, John
Renewable Energy Institute
1050 17th Street, NW, Suite 1100
Washington, D.C. 20036

Wood, Doug
Solar Steam, Inc.
Box 32
Fox Island, Washington 98333

Zewen, Helmut
M S S B
800 Munich 80 Germany

Zimmerman, Donald
Boeing Engineering &
Construction Company
MS 9@/77 P.O. Box 3707
Seattle, Washington 98124